Utilising exosomes for biomarkers of Alzheimer's disease

Rhodri Gareth Thomas, BSc (Hons)

Thesis presented for the degree:

Doctor of Philosophy

September 2017

Division of Psychological Medicine and Clinical Neurosciences

School of Medicine

Cardiff University

Hadyn Ellis Building

Maindy Road

Cardiff

CF24 4HQ

Declaration

This work has not been submitted in substance for any other degree or award at this or any other university or place of learning, nor is being submitted concurrently in candidature for any degree or other award.

Signed …… (candidate) Date ……

STATEMENT 1

This thesis is being submitted in partial fulfilment of the requirements for the degree of PhD.

Signed …… (candidate) Date ……

STATEMENT 2

This thesis is the result of my own independent work/investigation, except where otherwise stated, and the thesis has not been edited by a third party beyond what is permitted by Cardiff University's Policy on the Use of Third Party Editors by Research Degree Students. Other sources are acknowledged by explicit references. The views expressed are my own.

Signed …… (candidate) Date ……

STATEMENT 3

I hereby give consent for my thesis, if accepted, to be available online in the University's Open Access repository and for inter-library loan, and for the title and summary to be made available to outside organisations.

Signed …….. (candidate) Date ……

STATEMENT 4: PREVIOUSLY APPROVED BAR ON ACCESS

I hereby give consent for my thesis, if accepted, to be available online in the University's Open Access repository and for inter-library **loans after expiry of a bar on access previously approved by the Academic Standards & Quality Committee.**

Signed …… (candidate) Date ……

Dedication

For Katie-Jayne, Heidi, Sammy and whoever else we may be blessed with in the future.

“Behold, God is [our] salvation; [we] will trust, and will not be afraid; for the Lord God is [our] strength and [our] song, and he has become [our] salvation.” Isaiah 12:2 (ESV)

Acknowledgements

I must first thank my supervisory team: Professors Aled Clayton and Julie Williams, and Doctor Rebecca Sims. I am so very appreciative of the opportunity to undertake a PhD and the support, advice and encouragement I have received. I also acknowledge the input of Doctors Elisa Majounie, Amy Gerrish and Caroline Tinsley for their supervision over the past four years and help with my application. Thank you also to Helen McKenzie who has used her English Literature skills to help me with punctuation, grammar and structure in the write-up of this thesis. I wish I could return the favour when you come to write your own!

It has been a delight to spend over six years working in the Division of Psychological Medicine and Clinical Neurosciences. I have made many friends and memories. Thank you to everyone I have had the pleasure of working with. I have also had the delight of working alongside others (past and present) in the Tumour Microenvironment group, Division of Cancer and Genetics. Again I thank everyone for their friendship and I daresay that the memories from my time with you lot are slightly more scandalous than with DPMCN!

Outside of work I have benefited so much from the fellowship I enjoy with everyone at Grace Community Church, Porthcawl. Thank you to all that I have studied the Bible with, prayed with, sung with, laughed with, cried with, camped with, shared a coffee with, shared a beer with, who has helped us move house, who has helped us renovate our house and in many other ways I have learned from. There are too many people to name individually but I think that should cover everyone.

Finally, I must acknowledge my family. I have wonderful siblings, cousins, parents, aunties, uncles and grandparents on both sides of the family. Your support, both directly and indirectly, has certainly contributed to this thesis and my overall happiness. I want to particularly acknowledge my parents, Susan and Alwyn Thomas, who have shown unwavering love and support to me throughout my life. Becoming a parent myself has made me appreciate you even more than I had before. Thank you for the sleepless nights, hospital visits, smelly nappies, birthdays, stress, worry etc. etc.! Thank you also for your front room which has housed me for numerous hours of thesis writing. My greatest thanks goes to Katie-Jayne. Words cannot fully express my gratitude to you. Your love, kindness and support are overwhelming. Thank you for believing in me for this thesis and for our future plans. Thank you for being my partner to walk through the adventure of life with. Thank you for being the impeccable mother of Heidi and Sammy. Thanks to you we are Team Thomas.

Summary

Exosomes are small, nanometre-sized, vesicles secreted by cells into the extracellular *milieu*. They have shown good potential for biomarkers of disease as they are peripherally available, and therefore non-invasively obtained, and are representative of the source cell. Discovering novel biomarkers of Alzheimer's disease is a desperate need that exosomes may address. This thesis explored the utility of RNA within exosomes for biomarkers of Alzheimer's disease.

Initially exosomes were isolated from H4 (neuroglioma) and IMR-32 (neuroblastoma) cell-lines in culture. The exosomes were thoroughly characterised and the cell-lines used to establish bulk stocks of neural-derived exosomes for downstream assay development and analyses.

As a pre-requisite of capturing neural-derived exosomes directly from biological fluids, a number of protein ligands were tested for affinity isolation of cell culture-derived exosomes. A working assay could not be developed so the direction of this thesis changed to a systems-wide approach.

A large RNA sequencing dataset was produced from RNA derived from H4 cells and exosomes. By performing whole transcriptome sequencing, novel insights into exosomal-RNA were made. It was determined that the profile of RNA within exosomes is distinct from the source cell and enriched for species that suggested that RNA was actively sorted into these vesicles.

A method was then developed for isolating exosomal-RNA from small volumes of plasma and measuring gene expression for multiple targets by quantitative polymerase chain reaction. This method was validated by showing sensitivity to small changes in exosome dose and able to detect brain-enriched gene targets.

In conclusion, RNA appears to be non-randomly sorted into exosomes and thus sensitive to the state of the source cell. A method has been developed, and validated, for isolating exosomal-RNA from small volumes of plasma. This could prove of great use in the future for discovering novel, peripherally available, biomarkers of Alzheimer's disease.

Publications

SIMS, R., VAN DER LEE, S. J., NAJ, A. C., BELLENGUEZ, C., BADARINARAYAN, N., JAKOBSDOTTIR, J., KUNKLE, B. W., BOLAND, A., RAYBOULD, R., BIS, J. C., MARTIN, E. R., GRENIER-BOLEY, B., HEILMANN-HEIMBACH, S., CHOURAKI, V., KUZMA, A. B., SLEEGERS, K., VRONSKAYA, M., RUIZ, A., GRAHAM, R. R., OLASO, R., HOFFMANN, P., GROVE, M. L., VARDARAJAN, B. N., HILTUNEN, M., NOTHEN, M. M., WHITE, C. C., HAMILTON-NELSON, K. L., EPELBAUM, J., MAIER, W., CHOI, S. H., BEECHAM, G. W., DULARY, C., HERMS, S., SMITH, A. V., FUNK, C. C., DERBOIS, C., FORSTNER, A. J., AHMAD, S., LI, H., BACQ, D., HAROLD, D., SATIZABAL, C. L., VALLADARES, O., SQUASSINA, A., THOMAS, R., BRODY, J. A., QU, L., SANCHEZ-JUAN, P., MORGAN, T., WOLTERS, F. J., ZHAO, Y., GARCIA, F. S., DENNING, N., FORNAGE, M., MALAMON, J., NARANJO, M. C. D., MAJOUNIE, E., MOSLEY, T. H., DOMBROSKI, B., WALLON, D., LUPTON, M. K., DUPUIS, J., WHITEHEAD, P., FRATIGLIONI, L., MEDWAY, C., JIAN, X., MUKHERJEE, S., KELLER, L., BROWN, K., LIN, H., CANTWELL, L. B., PANZA, F., MCGUINNESS, B., MORENO-GRAU, S., BURGESS, J. D., SOLFRIZZI, V., PROITSI, P., ADAMS, H. H., ALLEN, M., SERIPA, D., PASTOR, P., CUPPLES, L. A., PRICE, N. D., HANNEQUIN, D., FRANK-GARCIA, A., LEVY, D., CHAKRABARTY, P., CAFFARRA, P., GIEGLING, I., BEISER, A. S., GIEDRAITIS, V., HAMPEL, H., GARCIA, M. E., WANG, X., LANNFELT, L., MECOCCI, P., EIRIKSDOTTIR, G., CRANE, P. K., PASQUIER, F., BOCCARDI, V., et al. 2017. Rare coding variants in PLCG2, ABI3, and TREM2 implicate microglial-mediated innate immunity in Alzheimer's disease. *Nat Genet.* 2017 Jul 17. doi: 10.1038/ng.3916. [Epub ahead of print].

DE, M., HARRIS, M., STEVENS, A., SUSSAMS, R., HOPKINS, V., CULLIFORD, D., FULLER, J., IBBETT, P., RAYBOULD, R., THOMAS, R., PUENTER, U., TEELING, J., PERRY, V. H. & HOLMES, C. 2016. Periodontitis and Cognitive Decline in Alzheimer's Disease. PLoS One, 11, e0151081.

BUTCHART, J., BROOK, L., HOPKINS, V., TEELING, J., PUNTENER, U., CULLIFORD, D., SHARPLES, R., SHARIF, S., MCFARLANE, B., RAYBOULD, R., THOMAS, R., PASSMORE, P., PERRY, V. H. & HOLMES, C. 2015. Etanercept in Alzheimer disease: A randomized, placebo-controlled, double-blind, phase 2 trial. Neurology, 84, 2161-8.

Presentations and conferences attended

Thomas R., Majounie, E., Sims, R., Falcon-Perez, JM., Clayton, A., Williams, J. (2017). **Enrichment of non-coding RNA-species in exosomes: potential biomarkers for Alzheimer's disease** (Poster presentation). *International Society of Extracellular Vesicles, 6th Annual Meeting*. Toronto, Canada

Thomas R., Majounie, E., Sims, R., Falcon-Perez, JM., Clayton, A., Williams, J. (2016). **Exosomal RNA is biologically distinct from its source cells: next generation sequencing analysis of a neuroglioma cell-model of Alzheimer's disease** (Poster presentation)**.** *Third UK Extracellular Vesicle Forum*. Oxford, UK.

Thomas R., Majounie, E., Sims, R., Falcon-Perez, JM., Clayton, A., Williams, J. (2016). **Exosomal RNA is biologically distinct from its source cells: next generation sequencing analysis of a neuroglioma cell-model of Alzheimer's disease** (Poster presentation)**.** *Division of Psychological Medicine and Clinical Neurosciences Home Day*. Cardiff, UK.

Thomas R., Sims, R., Clayton, A., Williams, J. (2015). **Isolating RNA from exosomes for the diagnosis of Alzheimer's disease** (Poster presentation). *The 30th Annual School of Medicine and Dentistry Postgraduate Research Day*. Cardiff, UK.

Thomas R., Sims, R., Clayton, A., Williams, J. (2015). **Building an affinity capture assay to isolate neural-derived exosomes from plasma** (Poster presentation). *Alzheimer's Research UK Network Day*. Cardiff, UK.

Thomas R. **What is going on in your head?** (Oral presentation). *3-minute thesis competition – Cardiff heat (winner).* Cardiff, UK.

Grants

Neuroscience & Mental Health Research Institute Conference Travel Award (£284). Travel grant to attend Third UK Extracellular Vesicle Forum (Oxford, UK). December 2016.

Alzheimer's Research UK Network Centre Grant (£4108.73). Pump-priming award for project titled "Sequencing of RNAs extracted from exosomes".

Table of contents

List of figures

List of tables

Abbreviations

ACE	Addenbrooke’s Cognitive Examination
AD	Alzheimer's disease
ALIGATOR	Association LIst Go AnnoTatOR
ALS	Amyotrophic lateral sclerosis
ANOVA	Analysis of variance
APOE	Apolipoprotein E
APP	Amyloid precursor protein
ATCC	American Type Culture Collection
Aβ	Amyloid-β
BACE1	Beta-site amyloid precursor protein cleaving enzyme 1
BCA	Bicinchoninic acid
BSA	Bovine serum albumin
BWA	Burrows-Wheeler Aligner
cDNA	Complimentary deoxyribonucleic acid
circRNA	Circular ribonucleic acid
CNS	Central Nervous System
Cryo-EM	Cryo-electron microscopy
CSF	Cerebrospinal fluid
CT	Cycle threshold
CTF	C-terminal fragment
DNA	Deoxyribonucleic acid
dNTPs	Deoxynucleotide triphosphates
DS	Down’s syndrome
DTT	Dithiothreitol
EBV	Epstein-Barr virus
ECL	Enhanced Chemiluminescence
EDTA	Ethylenediaminetetraacetic acid
ELISA	Enzyme-linked immunosorbent assay
EM	Electron microscopy
EOAD	Early Onset Alzheimer’s disease
ESCRT	Endosomal-sorting complex required for transport
EV	Extracellular vesicle
FBS	Foetal Bovine Serum

FTD	Frontotemporal dementia
fu	Fluorescence units
gDNA	Genomic deoxyribonucleic acid
GTEx	Genotype-Tissue Expression
GWAS	Genome-wide Association Study
HD	Huntington's disease
HRP	Horse radish peroxidase
HSA	Human Serum Albumin
HSF1	Heat-shock factor-1
HSP70	Heat-shock protein 70
iPSC	Induced pluripotent stem cell
ISEV	International Society of Extracellular Vesicles
LAMP-1	Lysosome-associated membrane protein 1
LCLs	Lymphoblastoid cell-lines
lincRNA	Long intergenic non-coding ribonucleic acid
lncRNA	Long non-coding ribonucleic acid
LOAD	Late Onset Alzheimer's disease
LRP6	Low-density lipoprotein receptor-related protein 6
MA	Minus-Average
MCI	Mild Cognitive Impairment
miRNA	Micro ribonucleic acid
MMSE	Mini-Mental State Examination
mRNA	Messenger ribonucleic acid
MVB	Multivesicular body
MVE	Multivesicular endosome
ncRNA	Non-coding ribonucleic acid
NGS	Next-generation sequencing
NTA	Nanoparticle Tracking Analysis
NTC	Non-template control
P:P	Particle : protein
PBMCs	Peripheral blood monocytes
PBS	Phosphate-buffered saline
PCA	Principle Component Analysis
PCR	Polymerase chain reaction

PD	Parkinson's disease
PET	Polyethylene terephtalate
PK	Proteinase K
PMSF	Phenylmethane sulfonyl fluoride
PSEN1	Presenilin-1
PSEN2	Presenilin-2
PVDF	Polyvinylidene difluoride
qPCR	Quantitative polymerase chain reaction
RA	RNase A
REST	Repressor element 1-silencing transcription factor
RIN	Ribonucleic acid integrity
rlog	Regularised-logarithm transformation
RNA	Ribonucleic acid
RNAi	RNA interference
RNAseq	Ribonucleic acid sequencing
rRNA	Ribosomal ribonucleic acid
SA:V	Surface area : volume
SEC	Size-exclusion chromatography
SEM	Scanning electron microscopy
siRNA	Small-interfering ribonucleic acid
SNARE	Soluble NSF Attachment Protein Receptor
SNP	Single nucleotide polymorphism
SOD1	Superoxide dismutase 1
SPV	Sulfophosphovanilin
STR	Short tandem repeat
TBE	Tris-Borate-Ethylenediaminetetraacetic acid
TE	Tris-Ethylenediaminetetraacetic acid
TEM	Transmission electron microscopy
TLN	Tethered lipoplex nanoparticle
TRF	Time-resolved fluorescence
tRNA	Transfer ribonucleic acid
TRPS	Tuneable Resistive Pulse Sensing
UC	Ultra-centrifugation
UTR	Untranslated region

Chapter 1. Introduction

1.1 Alzheimer's disease

Alzheimer's disease (AD) is the most common form of dementia accounting for 60-80% of all cases (Imtiaz et al., 2014). The prevalence of dementias, including AD, is a rapidly growing, global problem. In 2001, an estimated 24.3 million people, worldwide, were suffering with dementia and it has been predicted that this will rise to 81.1 million by 2040 (Prince et al., 2013).

In the United Kingdom 850,000 individuals were living with AD in 2015 ((https://www.alzheimers.org.uk/statistics), 2015). AD is a devastating disease for the sufferer, the family members and the caregivers. There is a financial burden on the economy that outweighs stroke, heart disease and cancer (Lowin et al., 2001). The direct cost of long-term care to people with cognitive impairment was £5.4 billion in 2002 and projected to be £16.7 billion in 2031; this equates to be between 0.83-1.11% Gross Domestic Product (Comas-Herrera et al., 2007). Furthermore, an additional £11 billion was saved per year by family carers which, if included, would have resulted in a total cost of £26 billion in 2013 for dementia, in general (Prince et al., 2014).

The elderly population in the UK and Europe is escalating, with the number of over-65s being estimated to exceed 1 billion in Europe by 2020 (Murray and Lopez, 1996). Thus the cost of AD to society and to the economy will increase over the coming years.

1.1.1 History of Alzheimer's disease

The German Neurologist, Alois Alzheimer, first described a "peculiar disease of the cerebral cortex" at a meeting in Munich in 1906 (Wilkins and Brody, 1969, Alzheimer et al., 1995). His case was Auguste Deter, a housewife who was hospitalised at the age of 51 and died four and a half years later. Her symptoms included impaired memory, disorientation to time and place, persecutory delusions, auditory hallucinations and language abnormalities. General brain atrophy was observed at autopsy without macroscopic lesions but, using Bielschowsky's silver staining method, degenerating neurons with neurofibrillary tangles and senile plaques throughout the cortex were observed microscopically (Zilka and Novak, 2006).

These two observations are now considered pathological hallmarks of AD and are required for post-mortem diagnosis. In 1910, Emil Kraepelin, Alois Alzheimer's superior, designated this disorder "Alzheimer's disease" to describe the presenile form (onset prior to the age of 65). However the senile form (onset after the age of 65) has since been recognised (Blessed

et al., 1968) and often the two forms are distinguished as Early Onset Alzheimer's disease (EOAD) and Late Onset Alzheimer's disease (LOAD).

1.1.2 Symptoms of Alzheimer's disease

Cognitive symptoms

Progressive decline of memory is the classic symptom of AD (Desai and Grossberg, 2005, White and Clare, 2002). Patients typically forget recent memories, such as where they placed their keys, which progresses to difficulty in performing tasks such as making a cup of tea. Eventually, this leads to disorientation in space and time. This symptom is coupled with progressive decline of other higher functions. These include language; for example, Alois Alzheimer's original patient was unable to name a cup so instead referred to one as a "milk-pourer" (Wilkins and Brody, 1969). Eventually speech becomes repetitive, incoherent or even mute. Over time patients develop agnosia whereby they can visually perceive an object or face but are unable to correctly identify or recognise the object or person (Baudic et al., 2006, Rainville et al., 2002). Visuospatial awareness deteriorates over time with patients easily getting lost and disorientated (Mendez, 2000, Cummings and Cole, 2002); this is typically tested with the clock-drawing task (Figure 1.1) (Faison, 2005). Patients can also develop apraxia whereby simple motor tasks become difficult or impossible because ideas and thoughts cannot be translated (Desai and Grossberg, 2005, White and Clare, 2002).

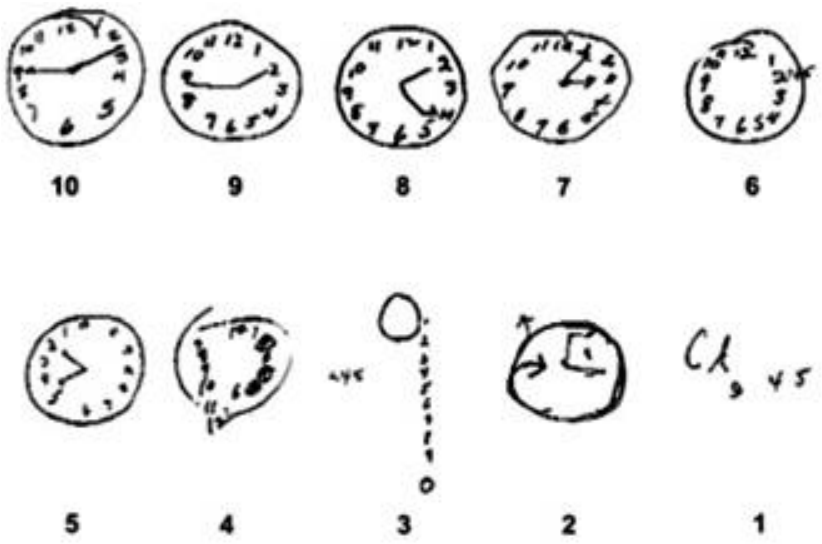

Figure 1.1: Visuospatial impairment in Alzheimer's disease causes patients to draw abnormal clocks. *This picture, collated by Faison (2005), shows that the progressive neurodegeneration in AD can lead to abnormal clock drawings as the disease becomes more severe.*

Non-cognitive symptoms

Psychotic symptoms, such as hallucinations and delusions, can occur in Alzheimer's disease (Jeste et al., 1992, Stern et al., 1994a). Hallucinations are disturbances in perception that have not occurred in reality (Behrendt, 1998). In the case of AD patients, this can be the perception that they have spoken to a friend or relative who has long been deceased. Delusions are the irrational belief that something is real despite contradictory evidence (Manschreck and Khan, 2006). Such was the case with Auguste Deter:

"Sometimes she greets the doctor as if he were a visitor […] on other occasions she screams that he wants to cut her open"

Behavioural symptoms can include: apathy, agitation, aggression, anxiety, depression, insomnia and wandering (Desai and Grossberg, 2005, White and Clare, 2002, Burns et al., 1990a, Burns et al., 1990b, Burns et al., 1990c, Burns et al., 1990d, Burns, 1992). Physical symptoms can become apparent as the disease progresses, including impairment of gait and balance, myoclonic jerks, seizures and eventually incontinence (McKhann et al., 1984, Villareal and Morris, 1999).

Disease progression

Mild cognitive impairment (MCI) is a state of impaired memory without other cognitive symptoms. It is considered a transition state prior to AD as 15% of patients with MCI go on to develop the disease within one year and up to 70% in 4–5 years (de Leon et al., 1997, Bobinski et al., 1999). However, it is possible that MCI will not develop to AD in an individual's lifetime and, likewise, someone may present AD symptoms in the clinic without prior MCI. Typically patients will live for 7-10 years (mean survival is 10.3 years) from symptom onset (Mann et al., 1992) but the range can reach up to 20 years (Bracco et al., 1994, Larson et al., 2004).

The disease progresses through three stages with defined clinical features (Mendez and Cummings, 2003). Stage I is a pre-clinical stage with a duration of 1-3 years. Symptoms include mild impairment of memory, perception, language and changes in behaviour. Stage II can span years 2-10 with more-severe impairments of memory, perception, language, motor system and more pronounced behaviour changes, including delusions in some cases. Stage III can span years 8-12 with severe cognitive deficits and speech and motor difficulties (Mendez and Cummings, 2003).

The age of disease onset varies considerably between individuals and can range from 30 to over 90 years of age. Typically disease onset is after the age of 65 accounting for 95% cases (Shastry and Giblin, 1999) and termed Late Onset Alzheimer's disease (LOAD). Both DSM-IV (Diagnostic and Statistical Manual of Mental Disorders) and NINCDS-ADRDA's (National Institute of Neurological and Communication Disorders and Stroke and the Alzheimer's disease and Related Disorders Associations) diagnostic criteria make a distinction between patients with disease onset over the age of 65 (LOAD) and those under the age of 65 (EOAD) (McKhann et al., 1984). Whilst clinical and neuropathological features overlap between these two forms, EOAD is characteristically more severe in terms of disease progression and survival time (Koss et al., 1996, Sevush et al., 1993, Villareal and Morris, 1999).

Therapeutic interventions are few and limited in their efficacy. There is no cure for AD so therapies only address the symptoms or slow the rate of decline. In the UK, drug interventions are limited to Acetyl cholinesterase inhibitors such as Donepezil, galantamine and rivastigmine. Such interventions only provide a mild benefit to cognition, behaviour and rate of decline (Desai and Grossberg, 2005, Cummings and Cole, 2002). Recently, Eli Lilly developed a drug called solanezumab; a monoclonal antibody designed to clear amyloid-β (Aβ) from the brain. It was hoped that this would be a much anticipated disease-modifying

treatment but, unfortunately, whilst evidence showed that it could clear Aβ, it was not of therapeutic benefit and failed a large phase-3 clinical trial in November 2016 (Sacks et al., 2017). As such, there has been a stagnation in new drugs becoming available and there continues to be a desperate need for new pharmaceutical therapies.

Diagnosis of Alzheimer's disease

Definitive diagnosis of AD is only possible with a *post-mortem* examination of brain tissue showing senile plaques and neurofibrillary tangles. Measurements of tau deposition can be made by evaluating the distribution of tangles across the cortical mantle and a Braak stage determined (Qian et al., 2017). At Braak stage I deposits are observed in medial temporal lobe but this can develop to Braak stage VI where this is observed across all cortical areas. The frequency of neuritic plaques can also be determined by autopsy (Qian et al., 2017). However, this can be problematic as it has been shown that 50–60% of people who do show these neuropathological hallmarks had no cognitive deficits in life (Knopman et al., 2003). During life a "probable" diagnosis of AD can be made using physical and cognitive examinations coupled with patient history. The DSM-IV (American Psychiatric Association, 1994) and NINCDS-ADRDA (McKhann et al., 1984) diagnostic criteria have been used in both research and clinical settings. It is worth noting that AD can present in the clinic very similarly, or even co-morbidly, to other dementias. Therefore the exclusion criteria of a probable AD diagnosis include concomitant cerebrovascular disease, core features of Dementia with Lewy bodies, prominent features of frontotemporal dementia or primary progressive aphasia, or evidence of other neurological disease or medication-induced cognitive changes (McKhann et al., 2011). This "probable AD" diagnosis has proved reliable and valid (O'Connor et al., 1996, Becker et al., 1994, Foy et al., 2007, Gearing et al., 1995, Holmes et al., 1999) and diagnosis of mixed dementias can be also be made.

1.1.3 Risk Factors of Alzheimer's disease

Alzheimer's disease is a complex neurodegenerative disorder. Multiple interrelated and interacting factors can contribute to disease onset and severity; factors that are both environmental and genetic (Imtiaz et al., 2014).

Environmental risk factors of Alzheimer's disease

Longitudinal studies have highlighted a number of cardiovascular risk factors in midlife which can elevate the risk of AD years later (Reijmer et al., 2012, Virta et al., 2013, Whitmer et al., 2005, Kivipelto et al., 2005). These risks include hypertension in mid and late life (Kivipelto

et al., 2001, Korf et al., 2004, Skoog et al., 1996); high levels of blood cholesterol (Kivipelto et al., 2001, van Vliet et al., 2009, Solomon et al., 2007); high body mass index (BMI) in midlife and low BMI in late life (Tolppanen et al., 2014, Whitmer et al., 2007); and Diabetes Mellitus (Tolppanen et al., 2013).

Lifestyle factors have also been implicated with AD risk. The effects of these factors include education reducing the risk of AD (Stern et al., 1994b, Ngandu et al., 2007b); physical activity in midlife reducing cardiovascular risk factors and thus AD risk (Chang et al., 2010, Sofi et al., 2011); smoking and alcohol use have provided inconsistent evidence on affecting the risk of AD but it appears that mild alcohol intake is protective whilst heavy intake is detrimental (Ngandu et al., 2007a, Piazza-Gardner et al., 2013, Panza et al., 2012, Kim et al., 2012, Sinforiani et al., 2011) and smoking has a complicated interaction with an individual's genetic background (Rusanen et al., 2010); and a healthy diet that is low in saturated fats reduces the risk of AD (Barberger-Gateau et al., 2007, Morris et al., 2003, Devore et al., 2010, Scarmeas et al., 2006).

Genetic risk factors of Alzheimer's disease

The genetic landscape of AD has changed dramatically over the last few decades (Robinson et al., 2017) (Figure 1.2). Early studies identified mutations in the amyloid precursor protein (*APP*) gene as well as proteins that are involved in the enzymatic cleavage of *APP* to toxic β-amyloid (Aβ) namely presenilin-1 (*PSEN1*) and presnilin-2 (*PSEN2*) (Tanzi and Bertram, 2005). These mutations, however, were found in familial cases of EOAD with low prevalence elsewhere. More recent advances in Genome-wide Association Studies (GWAS), sequencing and bioinformatics have begun to unveil the complex genetic architecture of the sporadic form of AD (Medway and Morgan, 2014, Jones et al., 2010, Tosto and Reitz, 2013). GWAS were able to uncover common variants with high frequency in the population that individually carried low risk. What was particularly striking about such discoveries was the implication of systems outside of the APP processing pathway such as cholesterol metabolism, immunity and endocytosis (Figure 1.2). Advances in DNA-sequencing technologies show promise of continuing these discoveries. The genetic risk factors of AD will be discussed in more detail below.

Early Onset Alzheimer's disease genetics

The *APP* gene resides on chromosome 21 and the first suggestion of an AD associated gene on this chromosome came from individuals with Down's syndrome who inherit a third copy of the chromosome. Patients with Trisomy 21 commonly develop the clinical and

neuropathological features of AD (Mann, 1988a, Mann, 1988b). Subsequently the first genetic linkage was found between a locus on 21q and autosomal dominant EOAD (St George-Hyslop et al., 1987). Later, the first point mutation on *APP* was discovered (Goate et al., 1991) followed by other mutations since found in autosomal dominant EOAD families (Weggen and Beher, 2012). *PSEN1* was implicated by genetic linkage on chromosome 14q and *PSEN2* on chromosome 1q (Sherrington et al., 1995, Van Broeckhoven et al., 1992, Levy-Lahad et al., 1995b, Levy-Lahad et al., 1995a, Rogaev et al., 1995). Thus, it emerged that *APP* and *APP*-modifying genes were implicated in EOAD. A subsequent risk gene, *ADAM10*, was identified; *ADAM10* is the major α-secretase that cleaves *APP* in amyloidogenesis (discussed in section 1.1.4) (Karch and Goate, 2015). The majority of mutations identified within these genes act in a fully penetrant, autosomal dominant manner, meaning that carriers will develop AD.

Late Onset Alzheimer's disease genetics

Linkage studies in LOAD families implicated a locus on chromosome 19 (Pericak-Vance et al., 1991) later identifying the *APOE* gene (Corder et al., 1993). The protein encoded by this gene can be one of three isoforms with unique structural features: ApoE2, ApoE3 or ApoE4 (Mahley et al., 2006). The *APOE* genotypes that encode these isoforms can be determined in a number of ways including single nucleotide polymorphism (SNP) genotyping of rs7412 and rs429358 (Butchart et al., 2015, Ide et al., 2016). Carrying the ε2 allele has a protective effect (Daw et al., 2000) whilst one or two copies of the ε4 allele confers a greater risk of AD (Robinson et al., 2017).

Since 2009, GWAS studies have dramatically changed the understanding of AD genetics. Common variants of small effect size were first found in the genes *ABCA7, BIN1, CD33, CLU, CR1, CD2AP, EPHA1, MS4A6A–MS4A4E* and *PICALM* (Lambert et al., 2009, Harold et al., 2009, Seshadri et al., 2010, Hollingworth et al., 2011, Naj et al., 2011). Subsequently, a large meta-analysis using these datasets confirmed many of the loci and uncovered others namely: *INPP5D, MEF2C, HLA-DRB5, NME8, ZCWPW1, PTK2B, CELF1, SORL1, FERMT2, SLC24A4* and *CASS4* (Lambert et al., 2013). A follow-up study identified *TRIP4* as a novel genome-wide significant locus (Ruiz et al., 2014). It is worth noting that the genes referred to may not be directly implicated in AD pathology as many of the SNPs found in association are intronic or intergenic. Therefore, these SNP associations may affect other genes at the locus and further analysis is required to determine the functional consequence. Exome studies have identified rare coding variants in *TREM2* (Guerreiro et al., 2013, Jonsson et al., 2013) and, more recently, in *PLCG2, ABI3* and again in *TREM2* (Sims et al., 2017). This evidence directly

implicates these genes as the mutations identified directly alter the protein encoded by these genes and further supports the role of microglia in AD aetiology. Whole genome sequencing analysis has identified mutations in the *APP* gene which protect against AD and cognitive decline (Jonsson et al., 2012). In summary, there are a number of risk and protective loci that have been associated with AD; from these associations, coupled with environmental risk factors, AD can be described as a complex disorder.

Additional analyses of GWAS data have unveiled a more detailed understanding of AD genetics. For example, pathway analysis using the Association LIst Go AnnoTatOR (ALIGATOR) method (Holmans et al., 2009) found the immune system and cholesterol metabolism as statistically over-represented in GWAS data (Jones et al., 2010). An additional utility of this was the development of a polygenic risk score to predict case-control status (Escott-Price et al., 2015, Escott-Price et al., 2017). Individuals carry multiple loci and this infers an aggregate risk of developing AD. The polygenic risk score is a method that assesses these aggregate genetic effects, including those that have not been associated at genome-wide significance at an individual level, to determine a person's risk of developing AD.

The advent of next-generation and third-generation sequencing platforms shows great promise in further unravelling the genetics of AD. Whole exome sequencing allows the capture of coding regions whilst whole genome sequencing allows the entirety of the genome to be sequenced. Relatively small studies have been performed but not yet to the scale of GWAS; the generation, storage and analysis of such large datasets can be computationally challenging. For example, a cohort of 928 EOAD patients and 980 controls implicated novel coding mutations in the *ABCA7* gene (De Roeck et al., 2017). In 2014 the much anticipated and far more affordable "$1000 genome" became possible (https://www.nature.com/news/technology-the-1-000-genome-1.14901). Thus, with costs being driven down rapidly the possibility of large studies, on the scale of previous GWAS studies, is drawing closer. It is likely to be of tremendous utility to match the scale of GWAS studies with the depth of data produced by these new sequencing technologies; the costs and computational challenges of next-generation sequencing means that this is not possible yet.

Understanding the underlying causal genetics of AD has, and will continue to have, far-reaching benefits. The implication of coding variants (Sims et al., 2017) and biological pathways (Jones et al., 2010) is offering new targets for therapeutic intervention. Indeed, incorporating rich genetic data into clinical trials provides better success rates in general

(Nelson et al., 2015). Particularly noteworthy is that these findings have dramatically changed the understanding of the underlying pathology of AD, as will be discussed next.

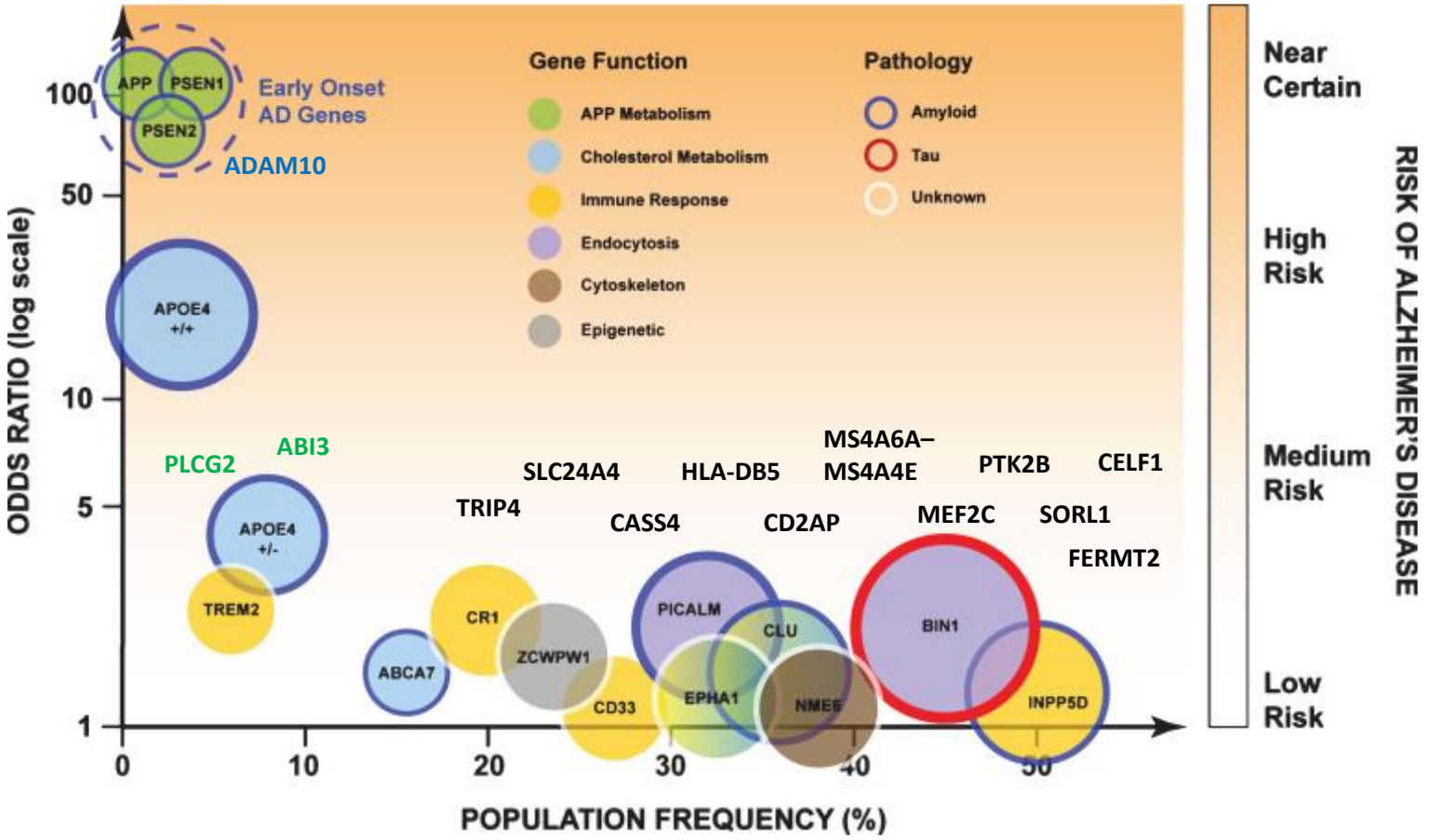

Figure 1.2: The genetic landscape of Alzheimer's disease (Robinson et al., 2017).
The familial genes APP, PSEN1 and PSEN2, carry near certain risk of developing EOAD but have low prevalence. The APOE gene carries the highest risk of sporadic AD. GWAS studies have implicated a number of common variants which individually carry low risk. Additional loci have been added in approximate positions. EOAD genes in blue text, rare coding variants in green text and common variants in black text.

1.1.4 Pathology of Alzheimer's disease

Neuropathology of Alzheimer's disease

The pathological hallmarks of AD are senile plaques and neurofibrillary tangles. Senile plaques are extracellular deposits of Aβ protein and referred to as neuritic plaques when associated with distorted neuronal cell processes. Particularly the APP cleavage products $A\beta_{40}$ and $A\beta_{42}$ (designated by their amino acid length) are fibrillary forms of Aβ found within neuritic plaques (Jarrett et al., 1993). Neuritic plaques have a core of Aβ surrounded by microglia, astrocytes and dystrophic neurites which often contain paired helical filaments (Cummings et al., 1998) (Figure 1.3).

Neurofibrillary tangles are intracellular aggregates of abnormally phosphorylated tau protein. They form paired helical filaments that can occupy the cell body of neurons; they may extend into the dendrites but are absent from axons (Cummings and Cole, 2002) (Figure 1.3). Tau filaments that undergo abnormal phosphorylation dissociate from microtubules and no longer stabilise these intracellular transport structures (Clark et al., 1997, Lee et al., 1991) and ultimately lead to cell death. In AD, plaques and tangles are predominately found in the hippocampus, entorhinal cortex and association areas of the neocortex, giving rise to the cognitive impairments observed in the clinic (Cummings, 2003). A prospective study has predicted that the process of Aβ deposition is slow and protracted, spanning over 2 decades and certainly occurring for a number of years prior to clinical manifestation (Villemagne et al., 2013).

Additional neuropathologies include amyloid angiopathy and neuronal loss. Amyloid angiopathy is principally caused by fibrillar deposits of $A\beta_{40}$ in the small arterioles, venules and capillaries of the cerebral cortex (Suzuki et al., 1994a). Neuronal loss can occur in the basal forebrain, locus coeruleus and raphe nuclei (Lantos and Cairns, 2000).

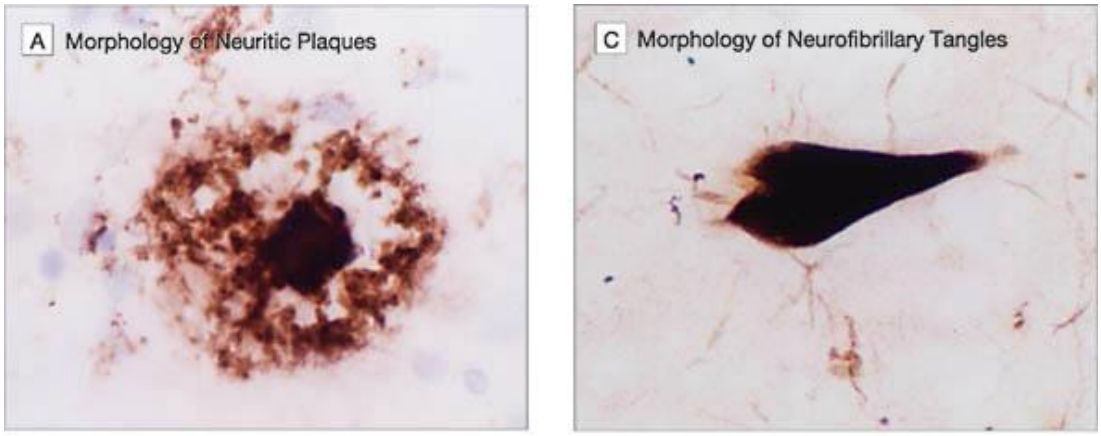

Figure 1.3: Morphology of Neuritic Plaques and Neurofibrillary Tangles (Cummings and Cole, 2002). *Neuritic plaques were labelled with a monoclonal antibody against Aß and counterstained with diaminobenzidine and hematoxylin (x2500 magnification). Neurofibrillary Tangles were visualised with Gallyas silver stain (x2500 magnification).*

Neurochemistry of Alzheimer's disease

Synaptic dysfunction precedes neuronal loss in AD (Coleman et al., 2004). As mentioned previously, neuronal loss occurs in the basal forebrain, locus coeruleus and raphe nuclei and these lead to deficits in the cholinergic, noradrenergic and serotonergic systems (Cummings and Cole, 2002). The hippocampus, substantia inominata, locus coeruleus and tempoparietal and frontal cortices have reduced levels of choline acetyltransferase (Hauw and Duyckaerts, 2001, White and Clare, 2002).

Pathogenesis of Alzheimer's disease

At a cellular level the pathogenesis of AD begins with the proteolytic cleavage of APP, a process referred to as amyloidogenesis. The *APP* transcript can undergo alternative splicing into one of eight isoforms; in particular, the isoform *APP695* is predominantly expressed in neuronal cells of the Central Nervous System (CNS) (Bayer et al., 1999). APP is a transmembrane protein that is translated in the endoplasmic reticulum, undergoes post-translational modifications in the Golgi and thereafter is transported to the plasma membrane (Kang et al., 1987, Russo et al., 2001, Shioi et al., 1992, Shioi et al., 1993, Suzuki et al., 1994b, Thinakaran et al., 1995).

APP can undergo amyloidogenic and non-amyloidogenic proteolytic cleavage (Chapman et al., 2001). Pre-dominantly non-amyloidogenic cleavage occurs in most cells via α-secretase and subsequent γ-secretase cleavage. The first proteolytic cleavage occurs between Lys16 and Leu17; it occurs in the middle of the Aβ sequence so preventing the formation of the toxic protein. A soluble APP fragment is liberated (APPsα) and the c-terminal product (α-CTF)

is cleaved by γ-secretase to the p3 peptide and APP intracellular domain (Nitsch et al., 1992, Thinakaran and Koo, 2008).

Amyloidogenic cleavage of APP is caused by initial cleavage by the β-secretase enzymes BACE1 (beta-site amyloid precursor protein cleaving enzyme 1) (Hussain et al., 1999, Lin et al., 2000, Sinha et al., 1999, Vassar et al., 1999, Yan et al., 1999). BACE1 cleaves APP at either the β site (Asp1) or β' site (Glu11) to liberate a soluble APP fragment (APPsβ) and a β-c terminal fragment (β-CTF). Subsequently γ-secretase cleaves the β-CTF to an APP intracellular domain and Aβ (Gouras et al., 1998, Thinakaran and Koo, 2008).

The convergence of BACE1 and its substrate, APP, occurs in the early endosome (Rajendran et al., 2006) where optimal pH conditions initiate amyloidogenesis (Vassar, 2001). The trafficking of these two proteins from the plasma membrane occurs by different mechanisms however. APP is internalised via clathrin-mediated endocytosis in contrast to BACE1 which is internalised via clathrin-independent endocytosis and is thus dependent on the small GTPase ARF6 (Sannerud et al., 2011). It has been shown, by *in vitro* analysis, that this convergence is not typical and that the two proteins are normally spatially segregated. APP is normally trafficked to the Golgi, but induction of neural activity in cultured hippocampal neurons altered this trafficking to endosomes instead (Das et al., 2013). Indeed, in the same study this phenomenon was reflected *in vivo* with co-localisation experiments using fractionated brain homogenates from AD patients and age-matched controls. Toxic Aβ can be expelled from the cell in soluble form (Thinakaran et al., 1996, Seubert et al., 1992, Haass et al., 1992) or via multi-vesicular bodies and secreted in exosomes (Rajendran et al., 2006, Morel et al., 2013).

There is an emerging story of non-neuronal cells contributing to the pathogenesis of AD. Microglia are the main immune cells of the brain and, in adults, microglia cycle between stable/surveillant (Nimmerjahn et al., 2005), proliferative and apoptosing forms (Gomez-Nicola and Perry, 2014, Askew and Gomez-Nicola, 2017). Microglia have been shown to be present in the brain parenchyma in increased numbers for numerous neurodegenerative disorders (Gómez-Nicola et al., 2013, Brites and Vaz, 2014, Olmos-Alonso et al., 2016). It remains under debate whether this increase is caused by infiltration of monocytes from the periphery or increased proliferation of resident microglia (Askew and Gomez-Nicola, 2017). It is also unclear, at the moment, what effect this dysregulation of the microglia population has on the pathology of the AD brain. One observation using an AD mouse-model (APP-PS1) is that microglia can exhibit a different phenotype, termed "dark microglia", that is rarely

present under normal conditions (Bisht et al., 2016). These so-called "dark microglia" appear to play a role in pathological remodelling of neuronal circuits and synapses. Another observation is that neuronal hyperactivity decreases the phagocytic potential of microglia and thus perturbs the normal dynamics of apoptosis in the diseased brain (Abiega et al., 2016). Another study demonstrated that activated microglia secrete pro-inflammatory cytokines that induce a sub-phenotype of astrocytes (Liddelow et al., 2017). This sub-phenotype loses many properties that promote neuron survival and instead induces the death of neurons and oligodendrocytes. Together, these studies suggest that microglia dysregulation can have a number of adverse effects of microglia dysregulation in AD.

Genetic evidence affirms these lines of investigation. *TREM2* is expressed amongst a "core profile" of genes in microglia (Hickman et al., 2013). It is a receptor-signalling protein that functions in microglial phagocytosis (Takahashi et al., 2005). Genetic evidence that has found AD associated variants in *TREM2* therefore implicates microglia in disease pathogenesis (Guerreiro et al., 2013, Jonsson et al., 2013, Sims et al., 2017). Thus, complimentary lines of evidence highlight that there are processes beyond the amyloid cascade that are at play in AD pathology. Following these up is vital to better understand the disease and discover new therapeutics.

1.1.5 Biomarkers of Alzheimer's disease

Clinical biomarkers of Alzheimer's disease

The clinical symptoms of AD are observed by physical and cognitive examinations, coupled with patient history, to determine a "probable AD" diagnosis (McKhann et al., 1984, McKhann et al., 2011). To compliment these assessments, five AD biomarkers have been sufficiently validated for use in the clinic (Jack and Holtzman, 2013). These can broadly be divided into two categories by what is being measured.

The first category of biomarkers are measurements of Aβ deposition. One biomarker is decreased concentrations of $A\beta_{42}$ protein in the cerebrospinal fluid (CSF) (Fagan et al., 2007, Bouwman et al., 2009, Mattsson et al., 2009, Shaw et al., 2009, Visser et al., 2009). A second biomarker uses positron emission tomography (PET), a neuroimaging technique that most commonly uses the agent carbon-11-labelled Pittsburgh compound B (^{11}C-PiB) to measure Aβ deposition by calculating uptake and retention of the tracer (Klunk et al., 2004, Drzezga, 2010, Rowe et al., 2010, Villemagne et al., 2011, Rodrigue et al., 2012, Nordberg et al., 2013). These techniques correlate well (Fagan et al., 2006, Jagust et al., 2009, Tolboom et al., 2009,

Weigand et al., 2011) and have been validated by *post mortem* examination (Strozyk et al., 2003, Ikonomovic et al., 2008, Clark et al., 2011, Fleisher et al., 2011, Sojkova et al., 2011, Tapiola et al., 2009).

The second category of biomarkers are measurements of neurodegeneration. One such biomarker is the measurement of elevated tau (total) and phosphorylated tau in patient CSF (Fagan et al., 2009, Mattsson et al., 2009, Shaw et al., 2009, Visser et al., 2009). Tau burden increases over the disease course and Braak stages can be determined at *post-mortem* examination (Qian et al., 2017). A second biomarker is the use of structural MRI to measure atrophy which is increased in AD and with Aβ burden (Hua et al., 2008, Morra et al., 2009, Desikan et al., 2009, Vemuri et al., 2009, Dickerson and Wolk, 2012). A third biomarker is hypometabolism in disease measured by [^{18}F]fluorodeoxyglucose PET imaging (Jagust et al., 2010). Again these correlate well with *post-mortem* results (Bobinski et al., 2000, Jack et al., 2002, Zarow et al., 2005, Buerger et al., 2006, Vemuri et al., 2008, Whitwell et al., 2008, Tapiola et al., 2009).

Potential peripheral biomarkers of Alzheimer's disease

To date there are no clinically-used peripheral biomarkers of AD. Yet, the invasive nature of lumbar puncture for CSF and cost of neuroimaging make this an unmet and important clinical need. There have been a number of studies of peripheral biomarkers that show potential diagnostic utility that will be discussed below.

Small RNAs found in the periphery have shown association with AD in a number of studies (Kumar and Reddy, 2016). The up-regulation and down-regulation of numerous miRNAs have been reported in whole blood (Satoh et al., 2015), serum (Geekiyanage et al., 2012, Galimberti et al., 2014, Tan et al., 2014a, Tan et al., 2014b, Dong et al., 2015) and plasma (Kumar et al., 2013). In addition to these free circulating miRNAs, it has been reported that plasma- (Lugli et al., 2015) and serum- (Cheng et al., 2014) derived exosomes carry potential miRNA biomarkers. There was, though, little consensus between these studies indicating that these biomarkers are not yet of clinical utility and further work is needed.

In addition to the miRNA carried within peripheral exosomes, the proteins that reside within exosomes have also shown promise with regard to peripheral biomarkers of disease. A proportion of Aβ can be secreted from N2a cells bound to exosomes (Rajendran et al., 2006). Exosomes can pass bi-directionally over the blood-brain barrier (Skog et al., 2008, Alvarez-Erviti et al., 2011) and thus brain-derived exosomes are present in peripheral circulation. The up-regulation and down-regulation of a number of proteins have been found to be

associated with AD including: low-density lipoprotein receptor-related protein 6 (LRP6), heat-shock factor-1 (HSF), repressor element 1-silencing transcription factor (REST), cathepsin D, lysosome-associated membrane protein 1 (LAMP-1), ubiquitin, heat-shock protein 70 (HSP70), total tau, P-T181-tau, P-S396-tau and Aβ1–42 (Goetzl et al., 2015a, Goetzl et al., 2015b, Fiandaca et al., 2015).

Longitudinal studies suggest that the damaging effects of Aβ deposition occur years prior to symptom onset (Villemagne et al., 2013), increasing the need for biomarkers that can detect AD in this pre-clinical stage. Peripheral biomarkers would be an ideal solution as they do not require an invasive lumbar puncture or costly neuroimaging. The prospect of utilising exosomes as biomarkers of AD shows promise and is the focus of this study.

1.2 Exosomes

1.2.1 History

One of the first observations of small, 40 nm diameter vesicles was in 1981 as a subpopulation of vesicles secreted from rat glioma cells (Trams et al., 1981). The term "exosome" was proposed to refer to these secreted vesicles. The mechanism by which they were secreted was unknown until two years later with the pioneering work of Clifford V. Harding and colleagues.

The landmark discovery of multivesicular endosomes (MVEs) was made by the surprising observations of transferrin receptors being internalised and trafficked in rat reticulocytes (Harding et al., 1983). At that time it was presumed that transferrin receptors were internalised and degraded in the lysosome as reticulocytes matured into erythrocytes. What Harding *et al.* observed by electron microscopy (EM), however, was that 98% of gold-labelled transferrin receptors internalised to acid phosphatase-negative compartments (Figure 1.4). The receptors localised to small vesicles, now known to be exosomes, within MVEs instead of the lysosome. Furthermore they observed the exocytosis of these small vesicles when MVEs fused with the plasma membrane (Harding et al., 1983).

Simultaneously, another research group discovered that sheep reticulocytes secreted similar vesicles that contained transferrin receptors, measured using radio-labelled antibodies (Pan and Johnstone, 1983). At the time, this group hypothesised that the mechanism of vesicle shedding was direct fusion with the plasma membrane rather than fusion of MVEs. Nevertheless, these studies complemented each other and subsequent studies further

validated the model of MVE fusion with the plasma membrane for exosome secretion (Harding et al., 1984, Pan et al., 1985).

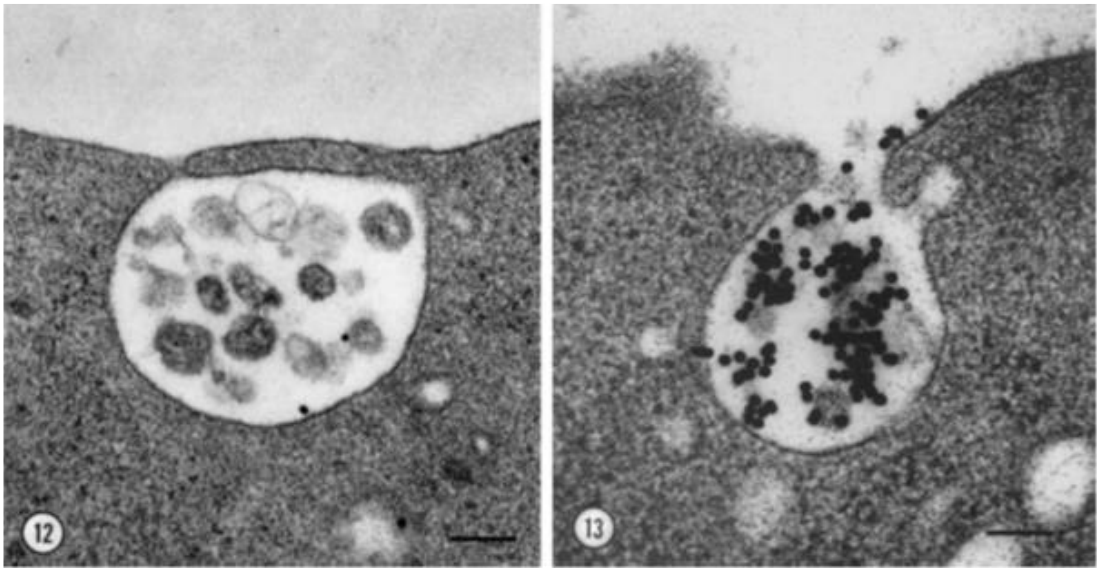

Figure 1.4: Electron micrographs of MVEs in rat reticulocytes (Harding et al., 2013).
Left – a MVE sparsely labelled with colloidal gold-transferrin. Right – MVE exocytosis by fusion with the plasma membrane. These exquisite micrographs were the first report of MVEs fusing with the plasma membrane for the secretion of exosomes. In time this phenomenon became appreciated as an important feature of vesicle trafficking, far beyond the reticulocyte-transferrin model described then.

Harding continued his work using the reticulocyte-transferrin model by investigating the mechanisms by which vesicles were released; he challenged the accepted ideas at that time that exosomes fused directly with the plasma membrane. A kinetics experiment revealed that internalised transferrin receptor was recycled down two pathways: a fast recycling pathway and a slower shedding pathway (Harding et al., 1984) (Figure 1.5). By investigating the kinetics they found that this second pathway was the major driver of reticulocyte maturation. It was the MVE-exosome pathway that Harding had uncovered a year earlier (Harding et al., 1983).

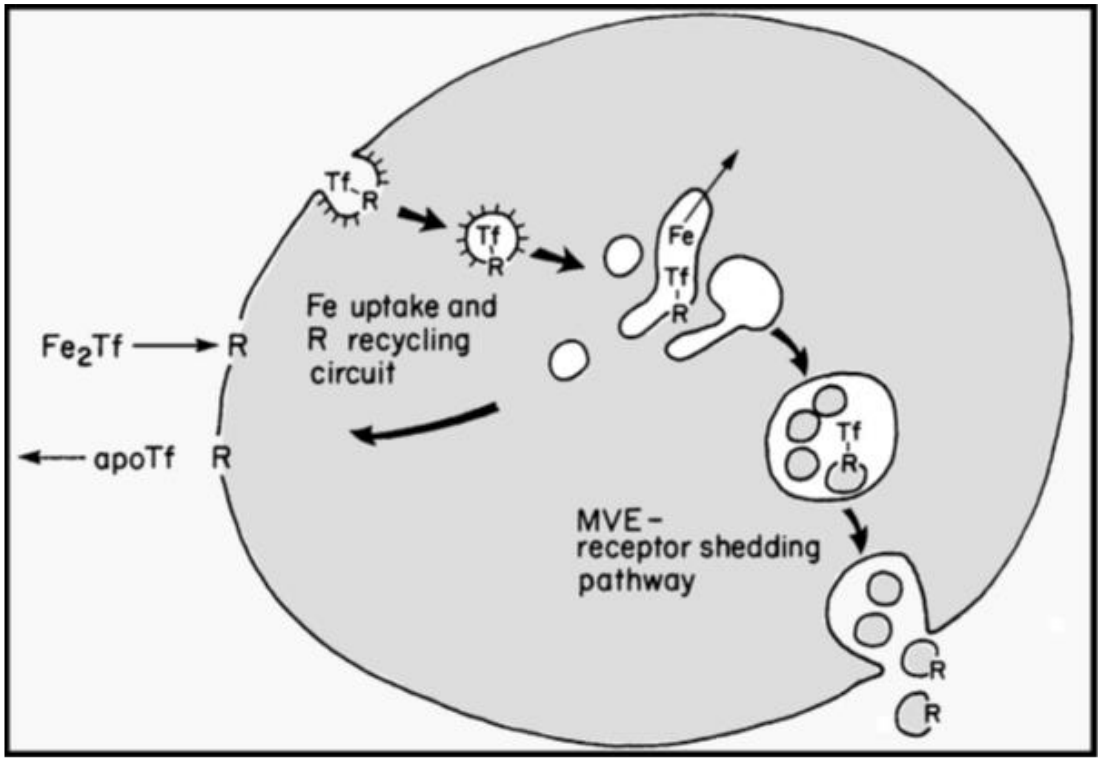

Figure 1.5: Clifford Harding's two proposed pathways of transferrin trafficking (Harding et al., 2013). *A fast recycling pathway, where transferrin is directly recycled to the plasma membrane, and a slower shedding pathway through MVEs. The kinetics of this second pathway matches that of reticulocyte maturation (Harding et al., 1984).*

More evidence emerged in later years that reinforced the existence if this pathway. Rather than molecules being recycled to the plasma membrane solely from early endocytic compartments, studies were proving that markers of the late endocytic compartments were indeed being trafficked to the plasma membrane. Some of these will be discussed below.

The lysosomal membrane glycoprotein LEP100, now more commonly referred to as LAMP-1, was found to be present in lysosomes, endosomes and the plasma membrane (Lippincott-Schwartz and Fambrough, 1987). Blocking the endo-lysosomal pathway, using chloroquine, caused 30% of LAMP-1 molecules to be redirected to clathrin-coated pits on the plasma membrane. This supported Harding's model of a distinct pathway of MVE fusion with the plasma membrane. Harding himself investigated further by looking at MHC class II-binding peptides (Harding et al., 1991). He found that these immunogenic peptides were most efficiently processed in lysosomes and then trafficked to the plasma membrane via endocytic compartments. Furthermore, MHC class II protein was found to be expressed on exosomes released from B lymphoblastoid cells and these vesicles were able to stimulate adaptive immune responses in T-cells (Raposo et al., 1996). The historical position was that exosomes were considered cell waste, however, Raposo showed a direct and immediate function of B-

cell vesicles. This was a momentous discovery that challenges the dogma that a cell is the smallest autonomous entity in biology. Thus, the phenomenon was observed and validated in cell-types beyond the original reticulocyte model.

Since this time the field of exosome and extracellular vesicle biology has dramatically grown (Harding et al., 2013, Lotvall et al., 2014) and has now developed to have wide-ranging impacts in health and disease.

1.2.2 Defining exosomes and other extracellular vesicles by their composition

Exosomes are a class of extracellular vesicle (EV) with two general defining characteristics: typically small with a diameter of 40–120 nm and originating from the endo-lysosomal pathway (El Andaloussi et al., 2013). This biogenesis differentiates them from other classes of extracellular vesicles, microvesicles and apoptopic bodies, which emanate from direct outward budding of the plasma membrane (Raposo and Stoorvogel, 2013). These other types of EVs have characteristically different size ranges of 50–1000 nm for microvesicles and 500–2000 nm for apoptopic bodies as they are not size-constrained by virtue of endosomal origin.

It is important to note that subclasses of EVs cannot be defined merely by size alone. The sizes overlap between different subclasses (Lo Cicero et al., 2015b) so that any population of EVs maybe enriched for one type but are not necessarily distinct from others (Colombo et al., 2014). It is commonplace to generalise that defined populations of EVs have been isolated using differential centrifugation. For example, it has been reported that a 2,000 x g centrifugation will isolate apoptotic bodies, a 12,200 x g centrifugation will isolate microvesicles and a 120,000 x g centrifugation will isolate exosomes (Crescitelli et al., 2013). Whilst it is convenient to make such distinctions, it is appropriate to consider these as broad definitions of EV populations.

Exosome proteins

Exosomes can be defined by their protein content. Typically, exosomes are considered enriched for the tetraspanins CD63, CD81 and CD9 (Lamparski et al., 2002, Escola et al., 1998, Heijnen et al., 1999); and components of the endosomal-sorting complex required for transport (ESCRT) machinery such as TSG101 (Stoorvogel et al., 2002) and ALIX (Roucourt et al., 2015, Stoorvogel, 2015). An unbiased proteomic analysis of exosomes was first described in 1999, using exosomes derived from mouse dendritic cells (Thery et al., 1999, Thery et al.,

2001). Many studies have since been performed with exosomes from other cell types (Mathivanan et al., 2010). These datasets have been compiled into publically available databases such as Exocarta (Mathivanan et al., 2012, Simpson et al., 2012), EVpedia (Kim et al., 2013) and Vesiclepedia (Kalra et al., 2012). Such studies have identified cell-specific exosomal proteins and others which are common across cell types. Proteins from the nucleus, mitochondria, ER and Golgi are commonly absent from exosomes, suggesting that exosomes represent a sub-proteome of the cell that particularly reflects membrane and endosomal contents (Colombo et al., 2014).

Whilst demonstrating the presence of ESCRT-related proteins, such as TSG101 and ALIX, on vesicles was once considered a definitive indicator of MVE origin, more recently ESCRT components were also identified adjacent to the plasma membrane and may also be part of micro-vesicles (Scourfield and Martin-Serrano, 2017). Accordingly, the International Society of Extracellular Vesicles (ISEV) has called for the reporting of multiple proteins as a minimal requirement in EV studies (Lotvall et al., 2014).

Proteomic analysis of other EV subtypes suggests that there is some overlap in the proteins expressed on all EVs (Turiak et al., 2011). It appears that CD9 is relatively ubiquitous across EV subtypes rather than specifically associated with MVE-derived vesicles (Bobrie et al., 2012a). In a separate study, exosomes of small size (<50 nm) were enriched for CD63, whilst larger exosomes were enriched for MHC class II (Colombo et al., 2013). The presentation of proteins on the surface of EVs is complex and highlights the heterogeneous nature of exosome preparations.

Exosome lipids

EVs, in general, are typically enriched for saturated fatty acids, sphingomyelin, phosphatidylserine, and cholesterol (Laulagnier et al., 2004, Llorente et al., 2013, Trajkovic et al., 2008, Wubbolts et al., 2003). Sphingomyelin and cholesterol, in particular, are enriched in lipid rafts, subdomains of the plasma membrane that are resistant to detergents (Ikonen, 2001). Indeed lipid raft-associated proteins are features of the exosome surface: e.g. GPI-anchored proteins and flotillins (Colombo et al., 2014).

On EVs the phospholipid phosphatidylserine is sensitive to binding by the peptide agent Annexin V (Dachary-Prigent et al., 1993). Indeed, it is commonplace to use Annexin V to block phosphatidylserine on exosomes or alter exosome secretion by altering the activity of neutral sphingomyelinase 2 or sphingomyelin synthase 2 (Yuyama et al., 2012), although N-SMase^2 inhibition is cell-type dependent and often toxic. Phosphatidylserine is situated on

the inner leaflet of the plasma membrane (Hugel et al., 2005) so its enrichment on the surface of EVs is likely to be due to the initial inward budding of vesicles prior to secretion. It has also been reported that ceramide is differentially enriched on exosomes over the course of reticulocyte maturation (Carayon et al., 2011). Thus it appears, as previously discussed for proteins, that there is a non-random sorting of lipids onto the bilayer of exosomes.

Exosome nucleic acids

The presence of RNA within EVs was first described with the horizontal transfer of messenger RNA (mRNA) from murine embryonic stem cells and human carcinomas (Ratajczak et al., 2006a, Baj-Krzyworzeka et al., 2006, Baj-Krzyworzeka et al., 2007, Ratajczak et al., 2006b) and miRNA in mast cells (Valadi et al., 2007). Indeed, mRNA from exosomes is functional: successful *in vitro* translation and *in vivo* translation in recipient cells have been reported (Valadi et al., 2007). Thus there is genuine exchange of genetic material via exosomes rather than mere random elimination of RNA from the cell.

Using electrophoretic analysis, it has been widely reported that exosomes contain little to no ribosomal RNA (rRNA), compared to cells which are replete with this species of RNA (Shelke et al., 2014). However, rRNA has been reported in apoptotic bodies and, in some cases, microvesicles (Crescitelli et al., 2013). This highlights the greater incorporation of cellular material in these larger EVs, particularly apoptotic bodies, and that it is a challenge to eliminate cellular contaminants in EV preparations.

It has been reported that specific miRNAs in plasma, such as let-7a and miR-142-3p, have been associated with EVs rather than bound to the RNA-binding protein Argonaute2 (Arroyo et al., 2011). Indeed, these targets have since been used to validate a methodology for the isolation of RNA from EVs in plasma (Enderle et al., 2015).

A particular feature of the RNA in exosomes is the protection from nuclease activity. Exosomal-RNA is encapsulated in a lipid-bounded vesicle so that it is not exposed, or susceptible, to nucleases such as RNase A (Cheng et al., 2014). It would be considered common practice to treat exosome preparations with Proteinase K and RNase A prior to extraction to ensure that intra-luminal RNAs are isolated (Shelke et al., 2014). Such protection within the vesicle makes exosomal-RNA uniquely stable and it has been reported that plasma samples, frozen at -80°C for over 12 years, can yield high-quality RNA (Enderle et al., 2015).

The profile of RNA within exosomes can be representative of the source cell (Skog et al., 2008). It has been reported that the disease-specific transcript variant, EGFRvIII, is secreted via neuroglioma exosomes and detectable in patient serum (Skog et al., 2008). The state of the source cells also determines the RNA profile of exosomes with changes shown in response to hypoxia (Li et al., 2016a, Gray et al., 2015, Yang et al., 2016) and oxidative stress (de Jong et al., 2012, Eldh et al., 2010). Thus, as discussed for proteins and lipids, the sorting of RNA into exosomes seems to be a regulated process, although this is still to be determined mechanistically.

1.2.3 Exosome biogenesis, trafficking and secretion

EM studies have since complemented Harding and colleagues observations: confirmation with another reticulocyte maturation model (Pan et al., 1985), observation of MHC class II exosomes being secreted via MVE fusion with the plasma membrane in B lymphoblastoid cells (Raposo et al., 1996) and, similarly, MHC class I and II exosomes being secreted from murine dendritic cells (Zitvogel et al., 1998), revealing structural evidence for the MVE-origin of small vesicles.

Exosomes undergo three general stages prior to secretion (Figure 1.6). Firstly, there is the biogenesis of intra-luminal vesicles within the MVE. The MVE is then trafficked to the plasma membrane and fusion results in release of exosomes into the extracellular *milieu* (Colombo et al., 2014).

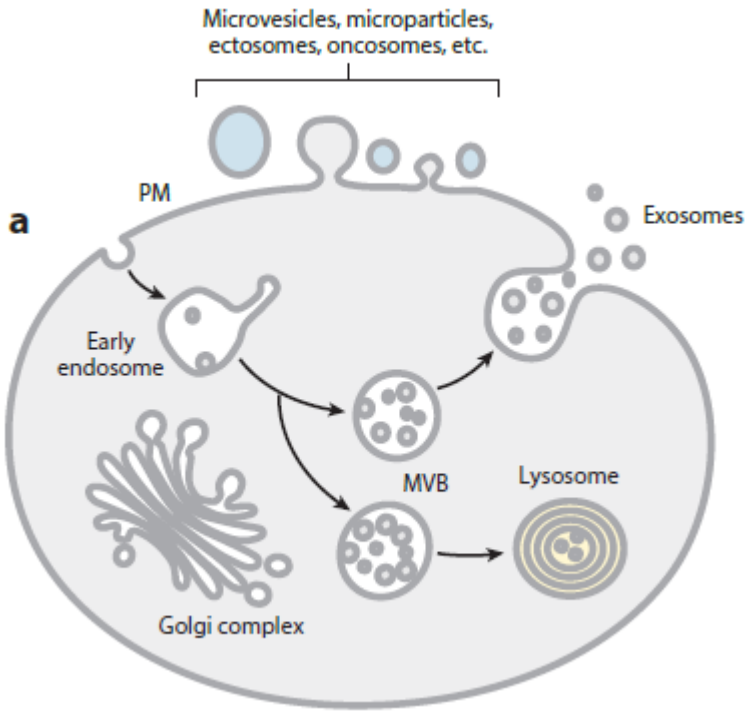

Figure 1.6: The biogenesis, trafficking and secretion of exosomes.
Exosomes arise by the biogenesis of intra-luminal vesicles in MVEs (here labelled MVB, multi-vesicular body), trafficking to the plasma membrane and fusion to release the contents. Diagram adapted from Colombo et al., 2014.

The formation of exosomes in the MVE is preceded by the sorting of proteins by the endosomal-sorting complex required for transport (ESCRT) machinery. Typically, proteins are tagged by mono-ubiquitinylation for the recruitment of ESCRT proteins (Babst, 2005, de Gassart et al., 2004). They then undergo a 3-stage process of cargo recognition/sorting to cargo concentration on the endosomal membrane to MVE vesicle formation and then into the endosomal lumen.

Due to high conservation in eukaryotes, yeast 2 hybrid assays have helped describe the numerous proteins and interactions that are involved in this process (Martin-Serrano et al., 2003, Bowers et al., 2004, von Schwedler et al., 2003). At the endosome membrane, ubiquitin-binding proteins, such as the Vps27/HRS complex or ESCRT-0, bind to clathrin to form a clathrin coat and to recruit ESCRT-I. ESCRT-I is a trimeric complex of Vps23, Vps37 and Vps28 which interacts with mono-ubiquitinylated proteins. ESCRT-I activates ESCRT-II, a trimer of Vps22, Vps36 and Vps25. ESCRT-II inititiates the formation of ESCRT-III by oligomerisation of Vps20, Vps24, Vps2 and Snf7. ESCRT-III acts by concentrating the protein cargo and recruits a number of other factors; these factors include Bro1 which in turn recruits the de-ubiquitinating enzyme Dos4, and Vps4, which dissociates the ESCRT machinery

(Figure 1.7). Proteins are then internalised into the MVE vesicles and can be trafficked to the lysosome for degradation or the plasma membrane for secretion in exosomes.

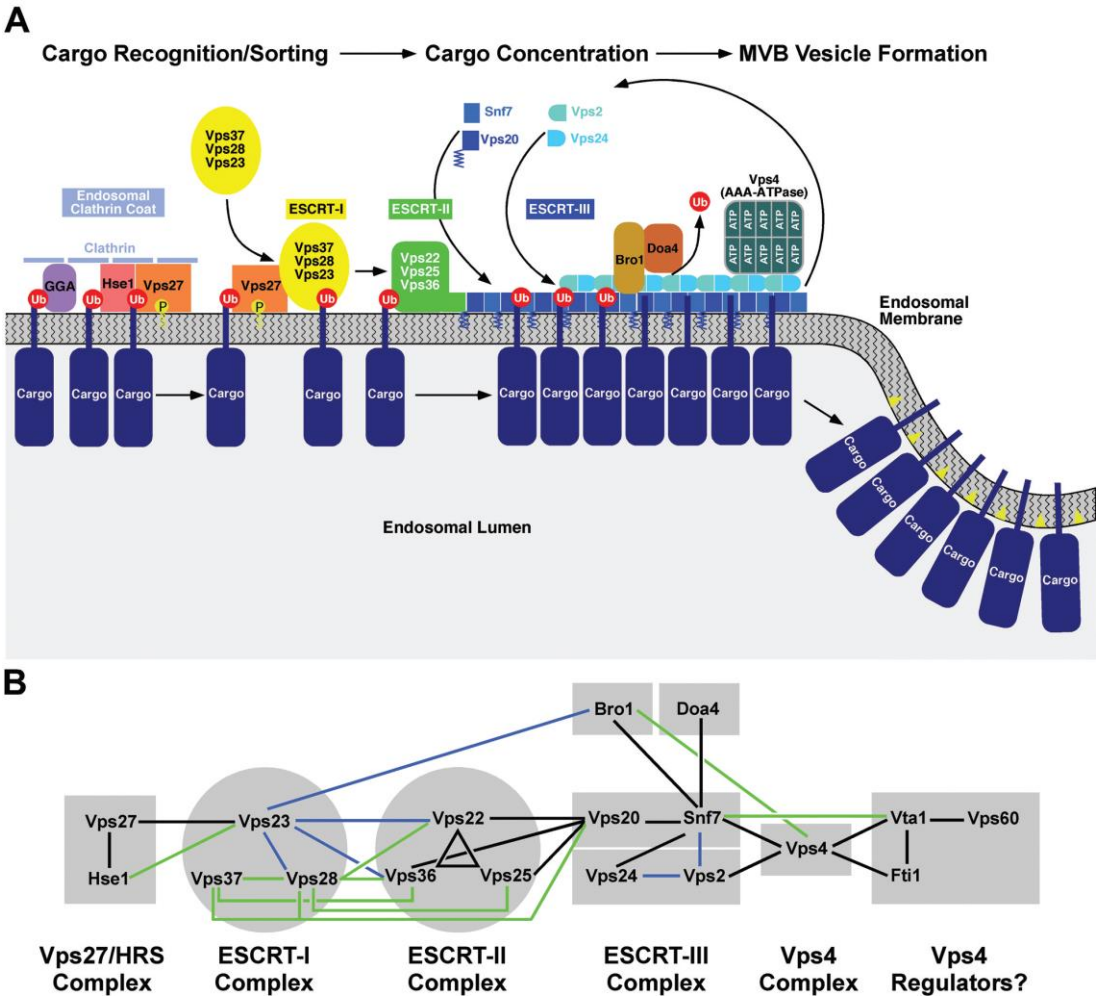

Figure 1.7: A model of protein sorting in MVE vesicles as proposed by Babst et al. (2005).
Members of the ESCRT protein family are recruited to mono-ubiquitinylated cargo proteins by the Vps27/HRS complex. Cargo protein is concentrated on the endosomal membrane prior to inward blebbing of the vesicle.

This process has been described in the context of dendritic cell (DC) maturation (van Niel et al., 2006, van Niel et al., 2008). Immature DCs tag MHC class II proteins by ubiquitination whereby it is trafficked to late endocytic compartments and subsequently degraded. In activated DCs, the ubiquitination of MHC class II is suppressed and thus the antigen is trafficked to the cell membrane for presentation on the cell surface. By mutating MHC class II to lack the ubiquitination site, MHC class II was presented at the plasma membrane regardless of activation state (van Niel et al., 2006).

A distinct pathway, independent of ESCRT, has also been described. Spontaneous invagination of vesicles into MVEs can be dependent on ceramide (Trajkovic et al., 2008). It has been proposed that this sphingolipid can promote domain-induced budding and curvature of the membrane leaflets in MVEs. This study reported that exosomes secreted by Oli-neu cells were enriched for ceramide and that inhibition of neutral sphingomyelinases caused a decrease in the number of exosome secreted. However, there may also be other processes that underlie the assembly of vesicles within MVEs that are not directly ESCRT or ceramide dependent, highlighting that vesicle biogenesis is a complex, multi-factorial process that is not fully understood.

Another study performed Nanoparticle Tracking Analysis (NTA) with the NCI-60 panel of human cancer cell-lines and cross-referenced these data with publically available transcriptomics data to find suggestive evidence of gene expression that correlates with EV secretion (Hurwitz et al., 2016). They defined the cell-types in the panel by the size of particles they secreted and found that some predominantly secrete small vesicles <150 nm diameter (typically exosomes) and others to secrete large vesicles >150 nm (typically microvesicles). They then used CellMiner to identify gene expression that correlated with these definitions (Table 1.1 & Table 1.2). As expected, different genes were enriched for each vesicle type, consistent with the different known mechanisms and location of origin. 171 of the 350 genes associated with small vesicles overlapped with large vesicle secretion. Thus, whilst there appears to be some commonality between the secretion of each vesicle type, there is certainly an element of uniqueness in the genes and pathways involved in exosome secretion.

Gene symbol	Gene name	Corr	Gene product function
CYTH3	Cytohesin 3	0.496	Guanine nucleotide exchange and phospholipid interaction; membrane trafficking
VPS41	Vacuolar protein sorting 41	0.467	Vesicle-mediated protein sorting; formation and fusion of Golgi Vesicles
NPC2	Niemann-Pick disease, type C2	0.429	Mobilizes cholesterol within the late endosome
RAB17	Member Ras oncogene family	0.408	GTPase; recruitment of effectors for vesicle formation, tethering and fusion
SNX24	Sorting nexin 24	0.390	Phosphatidylinositol binding and intracellular trafficking
SNX9	Sorting nexin 9	0.388	Involved in endocytosis and intracellular vesicle trafficking
AP1S2	Adaptor-related protein complex 1	0.388	Recruitment of clathrin to membranes and recognition of sorting signals within the cytosolic tails of transmembrane cargo molecules
ALS2	Amyotrophic lateral sclerosis 2 (juvenile)	0.383	GTPase regulator, associates with Rab5 on early endosomal compartments to mediate endosomal dynamics
ZFYVE9	Zinc finger, FYVE domain containing 9	0.372	Early endosome protein; regulates TGF-mediated signalling
RAB9A	Rab9A, member Ras oncogene Family	0.366	GTPase involved in transport of proteins between the endosomes and the trans Golgi network

Table 1.1: The top ten genes that correlate with small vesicle (<150 nm) secretion in the NCI-60 cancer cell-line panel.
CellMiner was used to find correlative gene expression (Corr) combined with Nanoparticle tracking analysis data (Hurwitz et al., 2016).

Gene symbol	Gene name	Corr	Gene product function
TLN2	Talin 2	0.512	Assembly of actin filaments; spreading and migration
AMPH	Amphiphysin	0.496	Exocytosis in synapses and certain endocrine cells; participates in membrane-associated cytoskeleton
TIAM2	T-cell lymphoma invasion and metastasis 2	0.488	Modulates the activity of Rho-like proteins and connects extracellular signals to cytoskeletal activities
CYTH3	Cytohesin 3	0.484	Regulation of protein sorting and membrane trafficking; promotes guanine nucleotide exchange on ARF1 and ARF6
TIMP2	TIMP metallopeptidase inhibitor 2	0.448	Inhibitor of the matrix metalloproteinases
ARHGDIA	Rho GDP dissociation inhibitor (GDI) α	0.437	Inhibits the disassociation of Rho family members from GDP
OPHN1	Oligophrenin 1	0.420	Stimulates GTP hydrolysis of members of the Rho family; critical for the regulation of synaptic vesicle endocytosis at presynaptic terminals
MAPK8IP1	Mitogen-activated protein kinase 8 interacting protein	0.414	May function as a regulator of vesicle transport through interactions with the JNK-signalling components and motor proteins
CD151	CD151	0.414	Tetraspanin involved in cell adhesion; may regulate integrin trafficking and/or function
SH3BP4	SH3-domain-binding protein 4	0.413	Cargo-specific control of clathrin-mediated endocytosis

Table 1.2: The top ten genes that correlate with large vesicle (>150 nm) secretion in the NCI-60 cancer cell-line panel.
CellMiner was used to find correlative gene expression (Corr) combined with Nanoparticle Tracking Analysis data (Hurwitz et al., 2016).

One of the enriched functional terms for small vesicle secretion in the Hurwitz *et al.* (2016) data was “GTPase activity” and, from direct experimental evidence, the Rab GTPases have long been implicated in MVE trafficking (Colombo et al., 2014).

The Rab family of GTPases consists of >60 members (Colombo et al., 2014). Rab11 was the first to be implicated with exosomes secretion: it showed decreased secretion of exosomes in an erythroleukemia cell-line when a dominant-negative form was expressed (Savina et al., 2002). This was later confirmed in *Drosophila melanogaster* cells (Koles et al., 2012, Beckett et al., 2013) and retinal epithelial cells (Abrami et al., 2013). Rab27a and Rab27b have both been implicated in MVE docking with the plasma membrane for exosome secretion (Ostrowski et al., 2010). The knock down of Rab27a, by RNA interference, caused enlargement of MVEs in HeLa cells suggesting a deficit in MVE processing and an accumulation of MVE content as a consequence. This has been confirmed in a number of tumour cell-lines (Bobrie et al., 2012b, Hoshino et al., 2013, Peinado et al., 2012, Webber et al., 2015). Knock down of Rab27b caused MVEs to accumulate in the perinuclear region, showing a deficit in distribution. Rab35 has been implicated in the docking and tethering of MVBs at the plasma membrane (Hsu et al., 2010). Knock down of Rab35 led to the accumulation of MVBs and decreased exosome secretion in oligodendrocytes. This was confirmed in primary oligodendrocytes (Fruhbeis et al., 2013).

It remains a challenge to dissect the roles of different Rab GTPases. It has been proposed that a subset of exosomes are secreted from late endosomes in a Rab27-dependent manner (Colombo et al., 2014). This subset are enriched for late endosome markers such as CD63, ALIX and TSG101. However, a different subset of exosomes are secreted from early endosomes in a Rab35/Rab11-dependent manner and enriched for flotillin (Colombo et al., 2014).

Another important, but less well studied, family of proteins in exosome secretion are the SNARE (Soluble NSF Attachment Protein Receptor) proteins. In general, SNAREs bind to SNAP proteins to cause membrane fusion between two surfaces (Zylbersztejn and Galli, 2011). Secretory lysosomes can fuse with the plasma membrane by SNAP-23’s association with the SNARE VAMP8 in mast cells (Puri and Roche, 2008, Tiwari et al., 2008) and VAMP7 in epithelial cells, eosinophils and neutrophils (Rao et al., 2004, Logan et al., 2006). VAMP7 appears to play a role in MVB fusion with the plasma membrane, as demonstrated by RNAi in human leukemic cells (Fader et al., 2009). Thus, the precise mechanisms and components for exosome biogenesis, intracellular trafficking and secretion are still not fully known and

appear to differently controlled dependent on the cell type being studied. This aspect requires further investigation.

1.2.4 Exosome functions

Exosomes convey signals between cells. Loaded with RNA, lipid and protein cargo they are present interstitially and in biological fluids (El Andaloussi et al., 2013). The functions of these EVs is wide and varied with implications in both health and disease.

Exosome functions in cancer

Exosomes, in general, play an intriguing and pivotal role in cancer biology (Rak and Guha, 2012, Peinado et al., 2012). This is underpinned by the capacity of cancer-derived exosomes to promote a favourable tumour niche such as the reprogramming of bone marrow progenitor cells to a pro-vasculogenic phenotype (Peinado et al., 2012). Exosomes are a route of communication between cancer and stroma cells (Camussi et al., 2011, Webber et al., 2010) and can promote tumour progression via numerous processes.

Cancer cells can be broadly defined as cells that undergo uncontrolled proliferation. To propagate this proliferation, exosomes can stimulate recipient cells. Oncogenic epidermal growth factor receptor (EGFRvIII) can be secreted from glioma cells via EVs (Al-Nedawi et al., 2008). Endothelial cells exposed to exosomes harbouring EGFRvIII will exhibit changes that support angiogenesis (Al-Nedawi et al., 2009). Simultaneously, it was demonstrated that glioma-derived exosomes deliver translatable mRNA to recipient cells; a pro-angiogenic phenotype was promoted in endothelial cells and proliferation was induced in glioma cells in a self-promoting manner (Skog et al., 2008). Thus, exosomes can encourage the hazardous proliferation of cells in cancer and reorganisation of the cancer microenvironment.

Cancer cells can communicate with the surrounding stroma via exosomes (Camussi et al., 2011, Webber et al., 2010). This was described as a novel route of communication between NCI-H460 tumour cells and fibroblasts for the transfer of the oncogenic glycoprotein EMMPRIN (Sidhu et al., 2004). Downstream this led to extracellular matrix degradation; a process that promotes tumour invasion and metastasis. Oral Squamous Carcinoma cells have been shown to secrete exosomes with altered RNA content under hypoxic conditions (Li et al., 2016a). This study particularly found that miR-21 was differentially expressed in the exosomes of hypoxic cells and that these promoted pro-metastatic behaviours when delivered to normoxic cells. Thus, exosomes provide a route for tumour cells to escape the stresses of a hypoxic environment.

Importantly, exosomes can cause cancers to escape immune response. Tumour-derived EVs have been shown to selectively inhibit proliferation and induce apoptosis in anti-tumour CD8+ T cells (Wieckowski et al., 2009). In the specific example of oral squamous cell carcinoma the Fas ligand (FasL) has been observed on EVs in patient serum (Kim et al., 2005). FasL+ exosomes promoted apoptosis via caspase-3 cascade, cytochrome-c release, reduced membrane potential in mitochondria, and reduction of TCR-zeta chain expression; overall for a reduced immune response. Also, FasL+ exosomes increase MMP9 expression and, thus, the tumour invasion potential of B16 melanoma and 3LL lung cancer cells in mice (Cai et al., 2012). Furthermore, TGF-β1 positive tumour-derived exosomes block the lymphocytic response to interleukin-2 in effector but not regulatory T-cells (Clayton et al., 2007). This included activating the function of regulatory T cells and inhibiting the cytotoxic activation of Natural Killer (NK) cells. NKG2D, an activating receptor for NK cells, is down-regulated by exosomal TGF-β1 as an additional mechanism (Clayton et al., 2008). Thus, exosomes have a variety of functions in the propagation of cancer including facilitation of uncontrolled proliferation, modulating the tumour microenvironment and evading the immune response.

Exosome functions in infectious disease

Several studies in the context of viral infections have indicated the possible manipulation of exosome pathways for propagating infectious disease. For example, in cell-models, the cell-surface receptor CCR5 can be transferred via EVs as a pre-requisite for HIV-1 infection (Mack et al., 2000). CCR5 can be transferred to deficient cells rendering them susceptible to viral invasion. More recently, the trans-activation response element (TAR) miRNA can be transported via exosomes secreted from HIV infected cells and in patient serum (Narayanan et al., 2013). Furthermore, the miRNA processing machinery, Dicer and Drosha, was found in exosomes from infected cells. Thus, the machinery required to make recipient cells more susceptible to HIV-1 infection and viral-infected cells protected from apoptosis, is housed within exosomes.

The transfer of functionally active RNAs has also been described in relation to Epstein-Barr virus (EBV). B lymphocytes infected with EBV secrete exosomes containing EBV-specific miRNAs (Pegtel et al., 2010). These exosomes caused dose-dependent repression of gene expression such as the immuno-regulatory gene *CXCL11/ITAC,* attenuating an anti-viral T-cell response.

Prions are transmissible agents that act in a comparable epidemiology to viruses. The misfolded scrapie (PrPsc) form of Prion protein (PrP) has prionogenic properties in infected

cells (Fevrier et al., 2004). Prion diseases affect the central nervous system (CNS) and it has been hypothesised that PrPsc can be acquired through the diet and be transported from peripheral tissues to the brain via exosomes. Cells infected with sheep prions release PrPsc via exosomes and these have infectious capabilities (Fevrier et al., 2004). More recently, it has been shown that neuronal cell-derived exosomes can transfer infectious PrPsc to neuronal and non-neuronal cells (and *vice versa*) (Vella et al., 2007). Furthermore, these exosomes caused Prion disease when injected into mice (Vella et al., 2007).

Thus, exosomes serve as a route for propagating infectious diseases, including viral infection and Prion disease. The internal machinery of cells can be hijacked by these hosts for the transfer of pro-infectious material.

Exosome functions in cardiovascular disease

Exosomes play a functional role in cardiovascular diseases. One study has demonstrated the therapeutic potential of exosomes secreted by hypoxic cardiac-progenitor cells after ischemia-reperfusion injury (Gray et al., 2015). Exosomes from hypoxia-treated cells showed differential expression of miRNAs and caused improved cardiac function and reduced fibrosis when used to treat a rat model of myocardial infarction. Taken further, exosomes from acute myocardial infarction patient serum were enriched for miR-30a (Yang et al., 2016). This study also found that miR-30a in exosomes was regulated by hypoxia inducible factor-1α and directly linked the regulation of autophagy in cardiomyocytes with the release of miR-30a-containing exosomes. Indeed, the presence of exosomes with biomarker potential are rapidly available in patient plasma after myocardial infarction (Deddens et al., 2016). Thus, exosomes play a pivotal role in paracrine signalling in response to cardiac injury. This has been reported more generally in an epithelial cell-model of the vasculature (de Jong et al., 2012) and a mouse mast-cell model of oxidative stress (Eldh et al., 2010).

Exosome functions in immunity

Exosomes play a role in the normal functioning of the immune system. It was first demonstrated, in 1996, that exosomes present antigens such as MHC class II for immune activation via helper T lymphocytes (Raposo et al., 1996). Indeed, this study reported that MHC class II was enriched in the MVBs of antigen presenting cells (B lymphocytes) and that the kinetics of MHC class II release suggested that exosomes were a significant route of exocytosis rather than the presumed direct fusion with the plasma membrane.

Furthermore, it has been observed that tumour-derived exosomes also present antigens which are taken up by dendritic cells and confer a T lymphocyte mediated anti-tumour

response (Wolfers et al., 2001). Taken further, tumour-derived exosomes can carry an array of known surface antigens dependent on tumour type (Baj-Krzyworzeka et al., 2006). These exosomes present antigens and contain RNA that activates an anti-tumour response by altering the biological activity of monocytes (Baj-Krzyworzeka et al., 2007). Thus, exosomes provide a route for activating and amplifying the immune system through the presentation of vesicle-surface antigens.

Exosome functions in blood coagulation

Another physiological function of exosomes is their role in the coagulation cascade. P-selectin glycoprotein ligand-1 is present on the surface of monocyte and macrophage-derived exosomes and can bind to activated platelets (Del Conde et al., 2005). This study found that exosomes fused with activated platelets in a P-selectin glycoprotein ligand-1 dependent manner and that this increased the proteolytic activity of Tissue Factor-VIIa.

Exosome functions in tissue repair

Exosomes also play a role in tissue repair. For example, exosomes derived from mesenchymal stem cells (MSCs) have been shown to decrease the risk of acute kidney injury through the inhibition of apoptosis and by stimulating the proliferation of tubular epithelial cell after ischaemia-reperfusion injury (Gatti et al., 2011). Similar protective roles have been described for MSC-derived exosomes in cardiovascular disease (Lai et al., 2011).The therapeutic potential of utilising exosomes for tissue repair, in general, has also been proposed (Ratajczak et al., 2012).

Other exosome functions

Many other functions of exosomes can be discussed including synaptic plasticity (Lachenal et al., 2011, Chivet et al., 2012), sperm maturation (Brewis and Gadella, 2010, Frenette et al., 2002, Saez et al., 2003, Sullivan et al., 2005) and as constituents of breast milk (Zonneveld et al., 2014, van Herwijnen et al., 2016). Exosomes appear to play a wide variety of functions in both health and disease.

1.2.5 Exosome purification strategies

Even over 10 years after the pioneering studies of Clifford Harding (Harding et al., 1983, Harding et al., 1984, Harding et al., 2013), studies that reported on extracellular vesicles undertook the work required to demonstrate that these were genuine exosomes by demonstrating MVB fusion in the source cell (Raposo et al., 1996). Yet the exponential growth of the field has now come to the point that, typically, the intrinsic properties of

exosomes themselves, isolated separately from the source cells, are measured and reported rather than demonstrating MVB fusion (Lotvall et al., 2014).

As discussed above, the RNA, lipids and proteins carried on exosomes play a wide variety of roles in paracrine signalling. Isolating exosomes from cell culture medium or biological fluids provides an opportunity to investigate signals secreted from a source cell prior to reaching the destination; this can be in the context of health or disease. Many purification strategies are available for the isolation of exosomes (Thery et al., 2006) and will be discussed below.

Purifying exosomes by differential ultra-centrifugation

Differential ultra-centrifugation is the process by which an exosome-containing fluid is subjected to several steps of increasing centrifugal forces (Raposo et al., 1996). It has been used as the most basic method for exosome purification for many years. In short: the first step is to centrifuge the fluid at a low centrifugal force (e.g. 300 x g for 10 min) to pellet cells and large cellular debris; the supernatant is taken into the second step with an increased centrifugal force (e.g. 2,000 x g for 20 min) that will pellet apoptotic bodies; the third step is to pellet microvesicles (e.g. 12,200 x g for 20 min); and the fourth step is to pellet exosomes (e.g. 120,000 x g for 70 min) (Crescitelli et al., 2013). Different combinations of these steps are used depending on the extracellular vesicle of interest (Figure 1.8).

In addition to the steps of increasing centrifugal force, a filtration step is often included (Thery et al., 2001, Ji et al., 2008). For example, the use of a 0.2 μm filter prior to ultra-centrifugation will aid the removal of large particles and aggregates that may be in the fluid; thus, resulting in a purer preparation of exosomes. Nevertheless, this methodology is prone to indiscriminate pelleting of proteins and small debris, in addition to the exosomes of interest. This poses a major challenge when purifying exosomes from biological fluids such as plasma. In this scenario, differential ultra-centrifugation will co-isolate high concentrations of albumin in addition to exosomes (Welton et al., 2015). Proteins, such as albumin, can produce strong signals in proteomic analyses which are likely to mask proteins of low abundance in the preparation. RNA-binding proteins, such as Argonaute (Arroyo et al., 2011) or high-density lipoproteins (Vickers et al., 2011), can also be co-isolated with this procedure. It is relatively straightforward, however, to remove such non-vesicular signals with the use of nuclease enzymes (Hill et al., 2013) and procedures are in place for doing so (Shelke et al., 2014).

Detailed methods reporting, such as rotor types and *k*-factors is a major issue in this field. The same protocol used in different laboratories can produce very different results. A recent

paper has highlighted this issue and advocate transparent reporting of methods to reduce inter-laboratory variability (Van Deun et al., 2017).

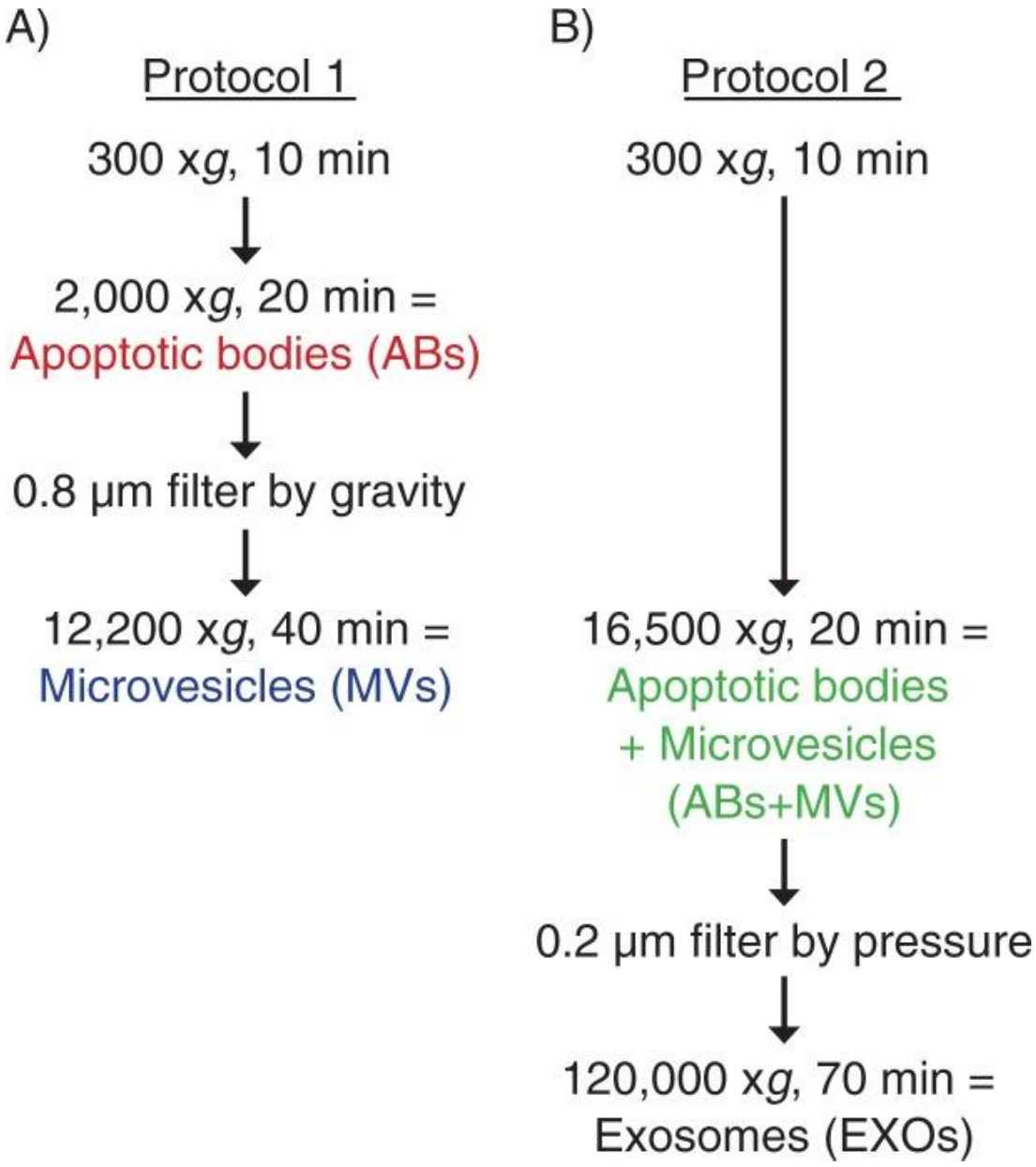

Figure 1.8: Differential ultra-centrifugation for the purification of exosomes and other extracellular vesicles.
Subsequent steps of increasing centrifugal force are applied to cell culture medium or biological fluids to isolate different species of extracellular vesicle (Crescitelli et al., 2013). These steps can be re-arranged according to the area of interest.

Purifying exosomes by continuous sucrose gradient

As opposed to differential ultra-centrifugation, which indiscriminately co-isolates exosomes with other proteins and particles, it is possible to purify exosomes based on their density using a continuous sucrose density gradient (Raposo et al., 1996). Exosomes are characteristically buoyant at a density of 1.1 – 1.2 g/ml (Escola et al., 1998, Raposo et al., 1996, Webber et al., 2014). In short, a continuous sucrose gradient using 0.2 M to 2.5 M solution is poured and overlaid, or under-laid, with a preparation of pelleted exosomes. This is then ultra-centrifuged overnight and fractions collected. Fractions can then be characterised by their density but require a wash with PBS and further ultra-centrifugation to obtain the purified exosomes.

This method is time- and labour-intensive but does provide purer preparations of exosomes than possible by ultra-centrifugation. Thus it is a useful analytical tool but, due to the intensive time and labour requirements, cannot easily be scaled up for larger studies using multiple samples. An alternative to using sucrose is the inert agent iodixanol which can provide the same range of densities as sucrose. Iodixanol gradients can separate exosomes from HIV-1 particles in human plasma and can give better resolving power (Konadu et al., 2016). However, the problem persists of this method being time- and labour-intensive.

Purifying exosomes on a 30% sucrose cushion

An alternative method which balances the ease of differential ultra-centrifugation but purifies based on the physical property of buoyant density is the 30% sucrose cushion method. This was first reported in 2002 for the isolation of exosomes from malignant ascites fluid (Andre et al., 2002). Later that year, the method was used in combination with cross-flow ultrafiltration as an FDA-approved procedure for the isolation of clinical grade exosomes from monocyte-derived dendritic cells (Lamparski et al., 2002).

This procedure involves overlaying the exosome-containing fluid on a 30% sucrose cushion made with deuterium oxide (D_2O). This cushion is a density of 1.2 g/ml so the majority of exosomes in the fluid should collect in the cushion upon ultra-centrifugation. The sucrose is collected, washed with PBS and centrifuged again. This methodology, in combination with a number of the differential centrifugation steps, has been adopted by the Clayton laboratory in Cardiff University (Clayton et al., 2004, Clayton et al., 2005, Clayton et al., 2007, Clayton et al., 2008). Thus, the sucrose cushion method provides a good compromise between differential ultra-centrifugation and a continuous density gradient.

Purifying exosomes by size exclusion chromatography

As discussed above, the co-isolation of contaminating proteins in biological fluids is a particular challenge. One method to overcome this challenge is size exclusion chromatography (Welton et al., 2015). This procedure involves running the biological fluid through a bead-containing column. Fractions are collected whereby small particles are collected first and larger particles pass through the column more slowly and are collected in subsequent fractions. This has successfully demonstrated good separation of exosomes, by proteins such as CD9 and CD81, from the contaminant human serum albumin (Welton et al., 2015). Fractions of interest can then be collected and pooled prior to ultra-centrifugation for exosome purification. This strategy is particularly useful for proteomic studies where albumin is present in such high abundance that it masks the detection of other proteins. However, it is imperfect as a single-step approach, as lipoproteins and other particulates can co-elute with exosomes. Additionally, the concentration of exosomes from enriched-fractions has been reported to be inefficient with ultra-centrifugation and precipitation of exosomes having a 5% particle recovery rate (Welton et al., 2015).

Purifying exosomes by immuno-isolation

A method that does not require ultra-centrifugation is the immuno-isolation of exosomes based on ligands on the vesicle surface. Antibodies against the ligand of interest can be loaded onto magnetic beads (Clayton et al., 2001, Wubbolts et al., 2003) or polyacrylamide beads (Mustapic et al., 2017) for the isolation of exosomes directly from cell-culture medium or biological fluids.

This method has been used to isolate exosomes based on a wide range of ligands including CD63 (Caby et al., 2005), MHC class II (Clayton et al., 2001, Wubbolts et al., 2003, Admyre et al., 2003), Her2 (Koga et al., 2005), EpCAM (Taylor et al., 2009, Rabinowits et al., 2009), NCAM and L1CAM (Goetzl et al., 2015b, Fiandaca et al., 2015, Hamlett et al., 2016, Mullins et al., 2017, Goetzl et al., 2015a, Mustapic et al., 2017).

One consideration of this method is choosing one antigen of interest. By doing so, there is pre-selection of a subset of the population of exosomes. For example, choosing a ligand, such as CD63, might pre-select for exosomes of smaller size (Colombo et al., 2013) and thus introduce a bias in the experimental design. On the other hand, it has been suggested that CD9 might be ubiquitously expressed on exosomes and other subtypes of EVs (Bobrie et al., 2012a), thus introducing an indiscriminate isolation procedure. Another consideration is the unknown factor of liberating exosomes from the bead and what effects that may have on

vesicle integrity. Furthermore, the immuno-isolation procedure may alter the functionality of the exosome. Finally, and particularly in the case of purifying from biological fluids, there is the possibility that abundant proteins, such as albumin, may reduce the efficacy of the procedure by blocking the antibody-antigen interaction or soluble variants of the target can make the method inefficient. These are caveats that require significant consideration as well as expense and suitability for upscaling.

There are many strategies for purifying exosomes from both cell-culture medium and biological fluids. These have all been used widely as they each have their own merits and will have an appeal based on the requirements of the study. For example, a continuous sucrose gradient provides highly pure exosomes for analysis at the cost of time and labour intensity. Ultra-centrifugation may provide higher exosome yields than other methodologies whereas immuno-isolation provides the selection of a population subset if a narrower research question is being asked. As such, there is no consensus for one purification strategy as better than others. Nevertheless, there are many methodologies widely accepted and readily available for the purification of exosomes.

1.3 Exosomes in Alzheimer's disease

1.3.1 Exosomes in Alzheimer's disease pathology

In 2006, the first study that directly linked exosomes with AD was published (Rajendran et al., 2006). Principally, the underlying endocytic system is utilised in amyloidogenesis for the proteolytic cleavage of APP to Aβ. The early endosome is the convergence site for APP and BACE1 to bind, followed by the trafficking of Aβ to MVBs (Rajendran et al., 2006, Morel et al., 2013). A comprehensive RNAi screen implicated a number of Rab GTPases in Aβ production (Udayar et al., 2013). In particular, Rab11 regulates the trafficking of BACE1 to the early endosome. Additionally, a cell model of amyloid metabolism has been used to further investigate these pathways (van Niel, 2016). Pigment cells have shown that APOE, in the intra-luminal vesicles and secreted exosomes, underlies the production of functional amyloid fibrils from the premelanosome protein (van Niel, 2016). Indeed, it has been shown, using and independent cell-type (N2a), that Aβ can accumulate in MVBs and be secreted via exosomes (Rajendran et al., 2006). The same study found an enrichment of exosomal protein, ALIX, around small neuritic plaques and a moderate deposition within large diffuse plaques of AD patient brain slices, compared to age-matched control. Thus, the endocytic system is implicated in the amyloidogenic processing of APP and secretion of Aβ via

exosomes. This is affirmed by genetic data which has independently implicated endocytosis in AD (Jones et al., 2010, Lambert et al., 2013, Robinson et al., 2017).

Exosomes play a number of roles in the CNS including paracrine signalling between neurons and synaptic plasticity (Lachenal et al., 2011, Chivet et al., 2012). Exosomes can also modulate the brain immune system under normal and pathological conditions (Cossetti et al., 2012). Indeed, bidirectional communication between oligodendrocytes and neurons via exosomes is important for neuronal integrity (Fruhbeis et al., 2012, Fruhbeis et al., 2013). Specifically in AD, exosomes can harbour Aβ and initiate a neuroinflammatory response (Gupta and Pulliam, 2014).

Kohei Yuyama and colleagues have investigated the interaction between Aβ on exosomes and microglia (Yuyama and Igarashi, 2017). An initial study unveiled a novel mechanism whereby neuronal exosomes can drive conformational changes in extracellular Aβ to form non-toxic fibrils (Yuyama et al., 2012). In turn, these conformational changes promoted uptake of Aβ, associated with exosomes, into microglia for degradation; it is a process that was sensitive to Annexin V and changes to sphingolipid constitution of exosomes. Thus a potential mechanism of toxic extracellular Aβ being absorbed and degraded in the brain was identified. The same group confirmed this "scavenger" role of exosomes in the brain of *APP*-transgenic mice (Yuyama et al., 2014). Intracerabral injection of neuroblastoma-derived exosomes alleviated the amyloid burden in these mice. These exosomes were highly enriched for glycosphingolipids and this was a requirement for the sequestering of Aβ. Later, it was distinguished that neuronal exosomes, rather than glial, drove this phenomenon (Yuyama et al., 2015). It has been suggested, independently, that the sequestering of Aβ on exosomes and degradation by microglia is an important process with potential therapeutic value (Tamboli et al., 2010).

The endocytic trafficking processes appear to play an important role not just in Aβ toxicity but also in tau toxicity (Rajendran and Annaert, 2012, Xiao et al., 2017). It has been shown in M1C neuroblastoma cells that tau can be secreted via exosomes and is present in association with exosomes in human CSF (Saman et al., 2012). This study particularly demonstrated that AT270+ tau was significantly enriched in early AD and suggested that this secretion pathway may be responsible for the spread of lesions. The number of microglia in the brain correlated with tau levels and another study reported, both *in vitro* and *in vivo*, that microglia can propagate the spread of tau via exosome secretion (Asai et al., 2015). Indeed, the exosome-

driven aggregation of tau can be dose-dependent, as reported in a mouse model (Polanco et al., 2016).

Thus, it appears that the endocytic system, and exosomes directly, are important factors in AD. Unsurprisingly, this is a complicated picture with numerous roles; these roles include the interaction between exosomes and microglia for the beneficial sequestering and phagocytosis of exosomal-Aβ and detrimental propagation of tau aggregation. These roles may provide future opportunities for therapeutic intervention.

1.3.2 Exosomes in Alzheimer's disease therapeutics

The intrinsic properties of exosomes may well have therapeutic potential. For example, it has been suggested that stem cell-derived exosomes exert a therapeutic effect via the delivery of their signalling cargo (Zhang et al., 2016a). More specifically, the potential of exosomes from adipose tissue-derived mesenchymal stem cells has been demonstrated by the presence of Neprilysin; an enzyme that degrades Aβ (Katsuda et al., 2015).

It has been proposed that exosomes may serve as a delivery mechanism for pharmacological agents (Cunha et al., 2016). In a murine AD model, exosomes were engineered to deliver siRNA to the brain after intra-venous injection (Alvarez-Erviti et al., 2011). Exosomes were engineered to contain an RVG peptide to specifically target neuronal cells and deliver siRNA to knockdown *BACE1*. This mechanism reduced Aβ burden in the mouse brain more effectively than standard inhibitors. Furthermore, the exosomes were derived from cultured dendritic cells from the same animal to reduce immunogenicity and thus highlighted an additional benefit of the delivery strategy (Alvarez-Erviti et al., 2011).

There is potential to use exosomes as therapeutic agents (Alvarez-Erviti et al., 2011). The biotechnological techniques to do so are being developed (Alvarez-Erviti et al., 2011) but this is far from a trivial undertaking and there seems to be a particular issue with reproducing this method of loading siRNA into exosomes. Furthermore, in the case of AD, reliable targets for therapeutic intervention still need to be identified; particularly as agents to clear Aβ have not proved successful in humans (Sacks et al., 2017).

1.3.3 Exosomes in Alzheimer's disease diagnosis

Exosomes can pass bi-directionally over the blood brain barrier, although the precise mechanisms for this are not currently understood (Skog et al., 2008, Alvarez-Erviti et al., 2011). As discussed in section 1.1.5, exosomes in peripheral circulation have the potential to

house biomarkers of relevance for CNS-diseases, such as AD (Cheng et al., 2013). Exosomal-RNA is encapsulated in a lipid-bounded vesicle which provides protection from extra-vesicular nucleases, whereas free circulating RNA is susceptible to degradation (Cheng et al., 2014).

To date, two studies have performed small RNA sequencing with peripherally-derived exosomes (Kumar and Reddy, 2016). One study isolated exosomes from 4 ml plasma to perform discovery analysis by Illumina small RNA sequencing in 35 cases and 35 controls (Lugli et al., 2015). Twenty differentially expressed miRNAs were identified, of which seven could predict case-control status with 83-89% accuracy in a machine-learning model. No replication was performed in this study (Lugli et al., 2015). A second study isolated exosomes from 1 ml serum to perform Ion Torrent small RNA sequencing in a case-control cohort of 49 individuals (Cheng et al., 2015). This study went on to replicate the sequencing by qPCR in a separate cohort of 60 individuals. Sixteen miRNAs were found to have predictive value with 87% sensitivity and 77% specificity (Cheng et al., 2015). Whilst these studies had good diagnostic utility, there was little overlap in the results (Kumar and Reddy, 2016). However, one miRNA, miR-342-3p, was down-regulated in AD across both studies.

A number of studies have investigated protein concentrations on exosomes isolated from peripheral blood but enriched for a neural source (Mustapic et al., 2017). One of these studies measured typical AD-related proteins and found total tau, P-T181-tau, P-S396-tau and Aβ1–42 significantly enriched in cases compared to controls (Fiandaca et al., 2015). Another study measured typical lysosome-related proteins and found cathepsin D, lysosome-associated membrane protein 1 and ubiquitin significantly up-regulated and heat-shock protein 70 significantly down-regulated in disease (Goetzl et al., 2015b). A third study measured the protein concentration of different cell-survival factors and found low-density lipoprotein receptor-related protein 6, heat-shock factor-1 and repressor element 1-silencing transcription factor significantly down-regulated in disease (Goetzl et al., 2015a). This methodology has not yet been applied to proteomic analysis.

It is apparent that exosomes have good potential for use in the diagnosis of AD. However, this conclusion has been made from only a handful of studies. Even so, particularly in the case of identified miRNAs (Kumar and Reddy, 2016), there is little consensus between the independent studies. As such, the utility of exosomes as peripheral biomarkers has not reached the same standards as CSF and as neuroimaging biomarkers; both of which have been verified for us in the clinic (Jack and Holtzman, 2013). Yet exosomes provide an exciting

prospect for biomarker discovery due to the availability of tissue-relevant material in the periphery.

1.4 Aim of this Study

The aim of this study was to investigate the utility of exosomes as biomarkers of Alzheimer's disease; particularly investigating the potential to discriminate health from disease by isolating and analysing the RNA content of exosomes.

To meet this aim, it was necessary to develop methods for exosome isolation from human plasma and to isolate the RNA cargo for analysis. Due to the inherent complexities of biological fluids, these methods were first established in cultured cell-lines prior to *in vivo* work. The H4 (neuroglioma) and IMR-32 (neuroblastoma) cell-lines were chosen to establish exosome stocks from a neural source (Chapter 3) for subsequent assay development (Chapter 4) and RNA analysis (Chapter 5). The analysis of gene-expression in plasma-derived exosomes was performed in a LOAD case-control cohort (Chapter 6). Therefore, the thesis aimed to answer the following questions:

1. Can bulk stocks of neural-derived exosomes be established from cell-lines?
2. Can an immuno-affinity assay be developed that can selectively isolate these neural-derived exosomes and remove exosomes from non-neural sources?
3. How does the RNA content of exosomes differ from the source cell?
4. Can a method for isolating exosomal-RNA from small volumes of patient be developed and validated for distinguishing AD cases and controls?

Chapter 2. Materials and Methods

2.1 Materials

All general reagents, unless otherwise stated, were analytical grade and purchased from Thermo Fisher Scientific UK Ltd (Loughborough, UK), Sigma-Aldrich Co. Ltd (Dorset, UK) and VWR Ltd. (Leicestershire, UK). All water was purified using a Milli-Q Biocel system (Merck, Darmstadt, Germany).

2.2 Cell strains and media

2.2.1 Mammalian strains

Cell cultures were established of two neural-based cell-lines as *in vitro* sources of neural-derived exosomes: one neuroblastoma (IMR-32, ATCC® CCL127™) and one neuroglioma (H4, ATCC® HTB148™). To ensure the validity of these cultures new vials were purchased from ATCC (LGC Standards, Teddington, UK). Information on these cell-lines is detailed in Table 2.1.

Cells were maintained in Opti-MEM® + GlutaMAX™ (Life Technologies, Waltham, MA, USA) supplemented with 4% Foetal Bovine Serum (FBS; Life Technologies, Waltham, MA, USA) for H4 cells and 10% FBS for IMR-32. Antibiotics and other supplements were not added. Every three months, or after recovering frozen cells, cultures were confirmed negative for mycoplasma contamination using the MycoAlert® mycoplasma detection kit (Lonza, Basel, Switzerland).

Where stated, cells were maintained in medium containing exosome-depleted FBS. Bovine exosomes were removed by overnight ultra-centrifugation at 100,000 x g (Optima-LE ultracentrifuge, with 70 Ti rotor, *k*-factor = 44, and Quickseal tubes, Beckman Coulter) and vacuum filtering the supernatant through 0.22 and 0.10 µm filters (Merck, Darmstadt, Germany) as used previously (Webber et al., 2014). Aliquots were stored at -20°C.

Cell line	Organism	Tissue	Disease	Age	Gender	Morphology	Growth properties
H4 (ATCC® HTB148™)	Human	Brain	Neuroglioma	37 years	Male	Epithelial	Adherent
IMR32 (ATCC® CCL127™)	Human	Brain	Neuroblastoma	13 months	Male	Fibroblast, neuroblast	Adherent

Table 2.1: Information on cell-lines used in this study.

2.2.2 Monolayer growth and maintenance of mammalian cell lines

Cells were maintained at 37°C at 95-98% humidity in 75 cm^3 flasks (Sigma-Aldrich Company Ltd., Dorset, UK) and media renewed every two or three days. Cell-lines were sub-cultured before reaching 90% confluence by removal of media, washing with 10 ml PBS (Life Technologies, Waltham, MA, USA) and detached using 0.25% (w/v) Trypsin-EDTA (Life Technologies, Waltham, MA, USA). No more than 20 sub-culturing passages were performed.

2.2.3 Bioreactor culture using Integra CELLine™ flasks

For high yield production of exosomes, H4 and IMR-32 cell-lines were cultured in CELLine AD 1000 Bioreactor flasks (Integra, Zizers, Switzerland). This method was adapted to culture large densities of cells within a small volume of medium allowing the maximum quantity of exosomes to be isolated. However, a caveat to this method is that high density, potentially hypoxic and nutrient-limited conditions are unfavourable for maintaining cells with good viability (Mitchell et al., 2008a). These flasks contain an inner compartment for cells and an outer compartment for nutrient medium (Figure 2.1). Cells within the inner compartment are maintained in a small (15 ml) volume of growth medium and adhere to a woven polyethylene terephtalate (PET) matrix, providing a large surface area. The semi-permeable membrane between compartments allows the exchange of nutrients and waste. The outer compartment contains a large volume of growth medium (500 - 1000 ml) to maintain the high density of cells. The secreted exosomes are retained within the inner compartment, allowing purification from a much smaller volume than monolayer cultures. Therefore cost, labour and time are reduced using this methodology (Mitchell et al., 2008a). Bioreactor cultures were maintained weekly by replacement of media in the outer compartment and collection of exosome-rich media from the inner compartment using 25G blunt needles (BD, Oxford, UK). The collected media was centrifuged twice at 400 x g for 7 min and once at 2000 x g for 15 min to remove cellular debris. Supernatants were then 0.22 μm syringe filtered (Merck, Darmstadt, Germany) and frozen at -80°C.

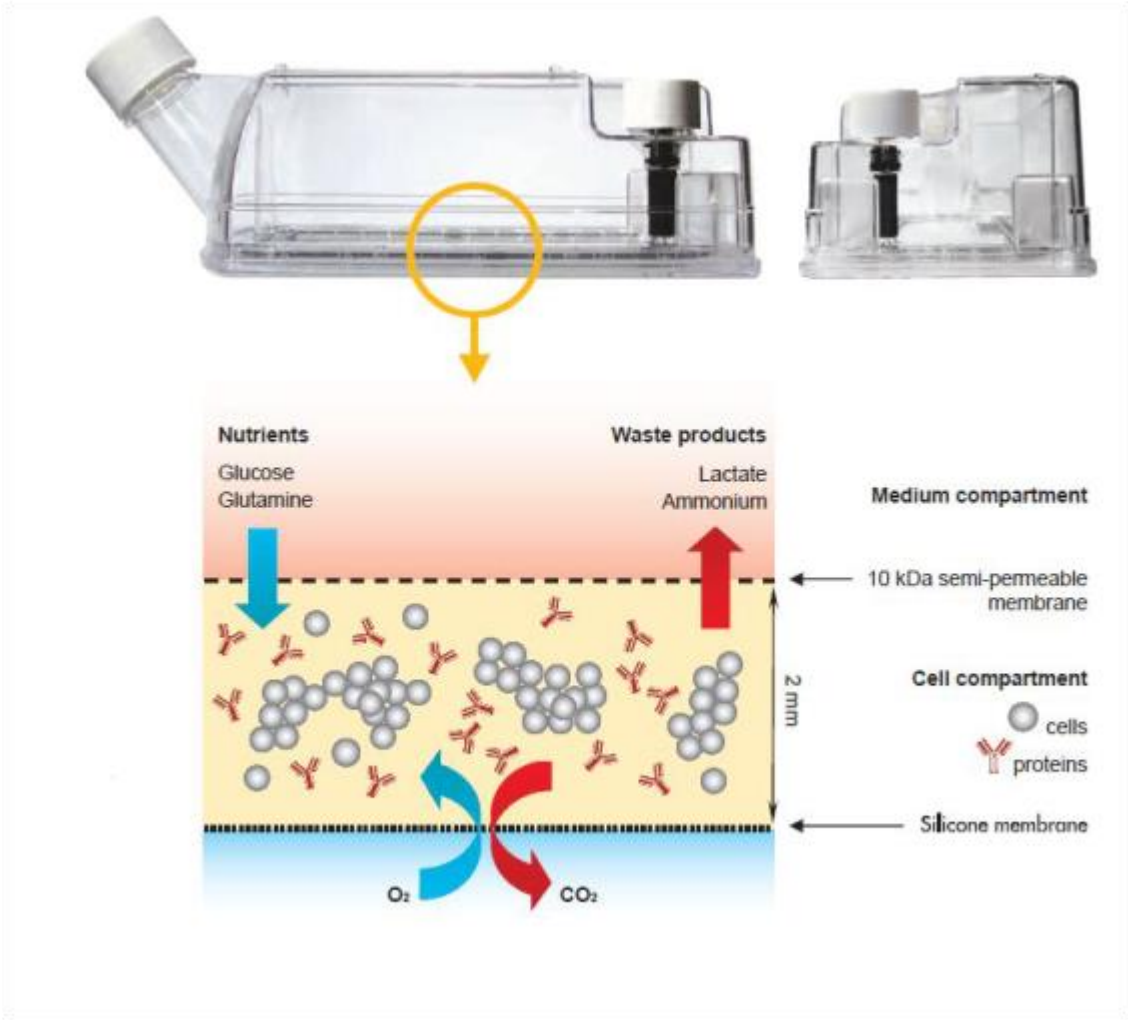

Figure 2.1: Integra CELLine™ AD1000 flask.
Figure adapted from manufacturers handbook (Integra, Zizers, Switzerland). These bioreactor flasks contain an outer compartment that stores up to 1 L of cell culture medium and a cell compartment that stores high densities of adherent cells in 15 ml medium. Nutrients and waste products can pass bi-directionally between the two compartments through a 10 kDa semi-permeable membrane. Gaseous exchange occurs over a silicone membrane. As suggested in the figure, these flasks were originally designed for hybridoma culture and the collection of secreted proteins. However this technique has since been adapted for the culture of other cell-types and the collection of vesicles (Mitchell et al., 2008).

2.2.4 Brightfield microscopy of live cells

Brightfield microscopy was used to assess the general morphology of live cells in standard monolayer culture. 80-100% confluent 75 cm^3 culture flasks were imaged using EVOS FL Cell Imaging System (Life Technologies, Waltham, MA, USA). Brightfield images were taken using both 4x and 10x objective lenses.

2.2.5 Preparation of cell lysates

Live cells, grown by standard 2D cell-culture, were detached from tissue culture plastic using 0.25% (w/v) Trypsin-EDTA (Life Technologies, Waltham, MA, USA), re-suspended in fresh media and counted using a glass haemocytometer and trypan blue staining. Cell lysates were prepared by centrifuging $1x10^6$ cells at 400 x g for 7 min, washing with 1 ml PBS and re-centrifuging. Cells were re-suspended in 100 µl lysis buffer (Cell Signalling Technology, Leiden, The Netherlands), homogenised by vortexing and incubated on ice for 10 minutes. The lysis buffer contained a cocktail of:

20 mM Tris-HCl (pH 7.5)

150 mM NaCl

1 mM Na_2EDTA

1 mM EGTA

1% Triton

2.5 mM sodium pyrophosphate

1 mM β-glycerophosphate

1 mM Na_3VO_4

1 µg/ml leupeptin

The protease inhibitor, phenylmethane sulfonyl fluoride (PMSF, 1 mM), was added to the lysis buffer immediately prior to use. Samples were centrifuged at 14,000 x g for 10 minutes (4°C) and the subsequent supernatant was transferred to a fresh tube and stored at -20°C. Protein concentrations were determined (see section 2.5.2) by Micro-BCA assay (Thermo Fisher Scientific, Inc., Loughborough, UK).

2.3 Human plasma samples

6 – 10 ml blood was drawn into lavender topped potassium-EDTA tubes. Plasma samples were collected for two purposes:

i. Healthy donors were recruited to validate procedures for isolating exosomes.
ii. Alzheimer's disease patients were recruited with age-matched controls for biomarker discovery as part of a larger genetics project in Cardiff University.

Blood samples were collected from healthy donors under informed consent and with ethical approval from Cardiff University, School of Medicine Research Ethics Committee, under the reference number 14/55. Participants voluntarily obtained information regarding the research project and provided informed consent to take part. Blood was drawn by phlebotomists at the Velindre Cancer Centre, Cardiff.

Blood from healthy donors were initially centrifuged at 400 x g for 7 minutes. The top layer of supernatant was collected into 2 ml aliquots and centrifuged again at 6000 x g for 10 min (Welton et al., 2015). Supernatants were then passed through 0.22 µm syringe filters (Merck, Darmstadt, Germany) and stored at -80°C.

Blood samples from AD patients and controls were collected as part of the 'Detecting Susceptibility Genes for Late-onset Alzheimer's disease' study, which has received ethical approval from Wales REC 3 (previously MREC for Wales) (REC reference 04/9/030). All samples were used with the participants' permission, having given their valid informed consent at the time the sample(s) were obtained. Where participants were unable to consent for themselves an appropriate consultee consented on their behalf. Participants and consultees provided their consent, understanding that their sample(s) or information may be used for future or other research studies. After blood was drawn potassium-EDTA tubes were centrifuged at 1600 x g for 15 minutes and 500 µl plasma aliquots stored at -80°C.

2.4 Exosome isolation

2.4.1 Pellet and PBS wash

Where stated exosome preparations were obtained by a simple pellet and PBS-wash procedure (Webber and Clayton, 2013). Cell culture supernatants were pre-cleared of cells and cellular debris by:

Centrifuging at 400 x g for 7 min

Collecting supernatant and centrifuging at 400 x g for 7 min

Collecting supernatant and centrifuging at 2,000 x g for 15 min

Filtering supernatant through 0.22 µm filters

Supernatant was stored at -80°C.

For exosome isolation, these pre-cleared supernatants were centrifuged at 200,000 x g for 2 hours, 4°C (Optima-LE ultracentrifuge, with 70 Ti rotor, *k*-factor = 44, and Quickseal tubes, Beckman Coulter), supernatant removed by aspiration, pellet re-supended in 5 ml PBS and centrifuged again at 200,000 x g for 2 hours, 4°C (Optima-MAX ultracentrifuge, with TLA-110 rotor, *k*-factor = 13, and Optiseal tubes, Beckman Coulter). Exosome pellets were re-suspended in PBS and stored at -80°C.

Plasma samples were similarly prepared by ultra-centrifugation. 0.5 ml plasma was topped up with 1 ml PBS to fill 1.5 ml capped ultra-centrifuge tubes (Beckman Coulter Inc., High Wycombe, UK) and centrifuged at 200,000 x g for 2 hours, 4°C (Optima-MAX ultracentrifuge, with TLA-110 rotor, *k*-factor = 13). Supernatants were aspirated, pellets re-suspended in 100 µl PBS and stored at -80°C.

2.4.2 Continuous sucrose gradient

Sucrose gradients were poured by the bottom fill method using a Hoefer SG15 gradient maker (Hoefer Inc., Holliston, USA). 0.2 M and 2.25 M sucrose solutions were produced and confirmed to be the correct molarity by measuring the refractive index. The 0.2 M measured 1.34277 (n=2) which corresponded to a molarity of 0.1984 M. The 2.25 M solution measured 1.44123 (n=2) which corresponded to a molarity of 2.2413 M. These were calculated using a sucrose standard curve provided by Beckman Coulter (Figure 2.3) and the following equation:

$$y = 2.1398x^2 + 14.792x - 23.522$$

Where y corresponds to the sucrose molarity and x corresponds to the refractive index. Once the gradient maker had been prepared the left hand chamber was filled with 2.25 M sucrose,

the right hand chamber with 0.2 M sucrose and an 18G spinal needle (BD, Oxford, UK) connected the outflow (Figure 2.2) with the bottom of a 4.7 ml open-topped ultra-centrifuge tube (Beckman Coulter Inc., High Wycombe, UK). Gradients were poured and then overlaid with 2.3 mg exosomes collected from a pellet and PBS-wash of bioreactor supernatants. These were centrifuged overnight (Optima-MAX ultracentrifuge, with MLS-50 rotor, *k*-factor = 50) according to the following protocol:

10,000 x g (1 hour)

210,000 x g (15 hours)

10,000 x g (1 hour)

Sixteen fractions of 330 µl were collected and the refractive indices measured. The respective density of each fraction was calculated using a sucrose standard curve provided by the Beckman Coulter (Figure 2.4) and the following equation:

$$y = -0.592x^2 + 4.2944x - 3.6748$$

Where y corresponds to density and x corresponds to refractive index measurement. A simple, linear fit produced the following equation:

$$y = 2.6507x - 2.5345$$

Where, again, y corresponds to density and x corresponds to refractive index measurement. Using either linear or second binomial equations produced the same density values when fractions were analysed. Fractions were topped up to 1.5 ml with PBS in 1.5 ml capped ultra-centrifuge tubes (Beckman Coulter Inc., High Wycombe, UK) and centrifuged at 120,000 x g for 45 minutes, 4°C (Optima-MAX ultracentrifuge, with TLA-110 rotor, *k*-factor = 13). Supernatants were aspirated, pellets re-suspended in 100 µl PBS and stored at -80°C.

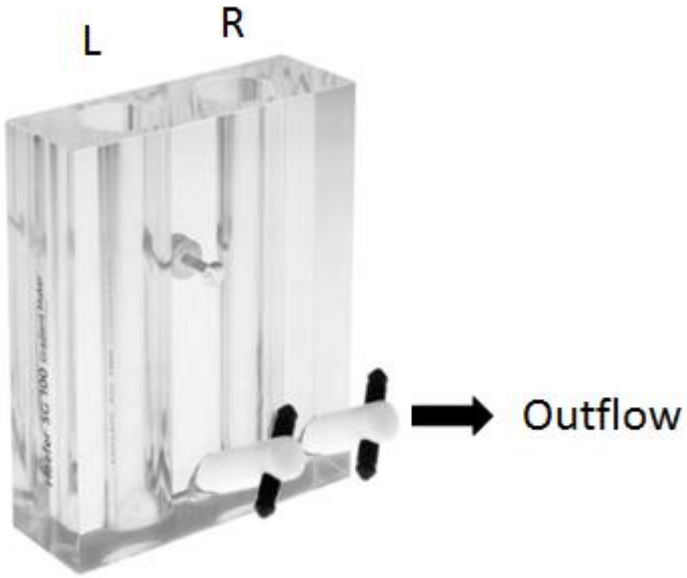

Figure 2.2: A photograph of a Hoefer SG15 gradient maker.
Left (L) and right (R) chambers are marked and were filled with 2.25 M sucrose and 0.2 M sucrose, respectively, for the pouring of sucrose density gradients. An 18G spinal needle was connected to the outflow (labelled).

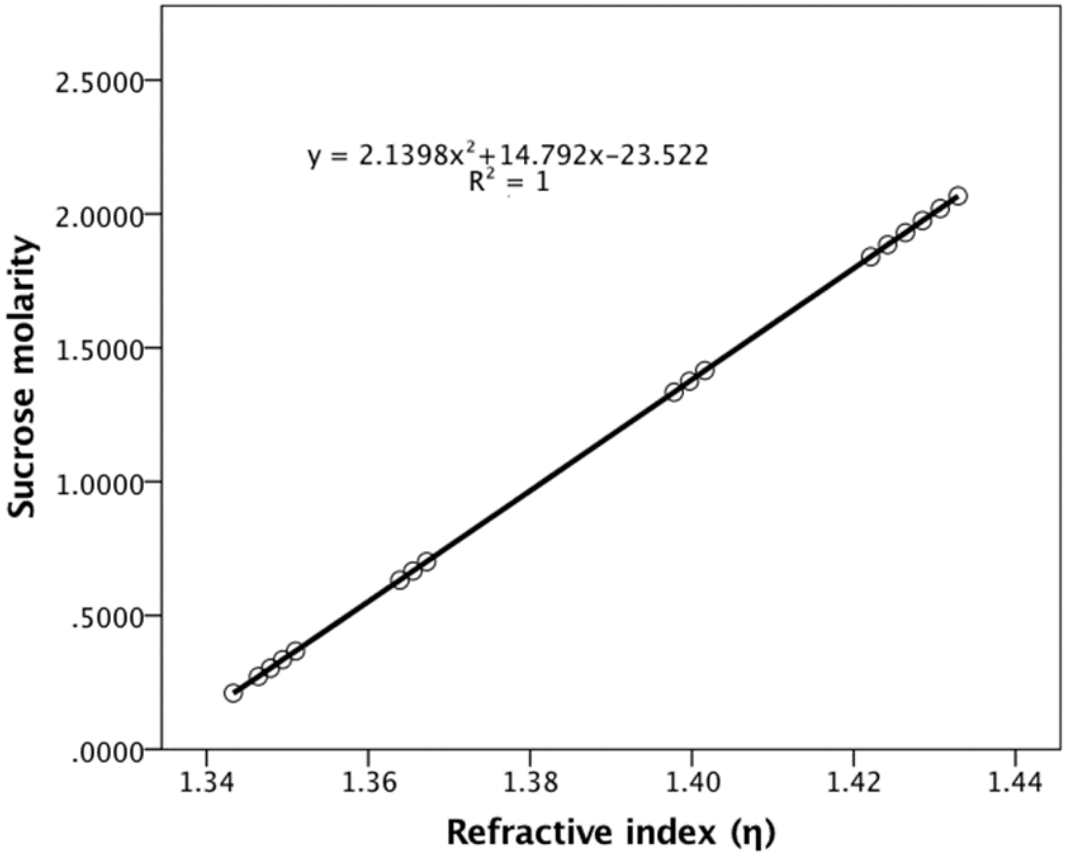

Figure 2.3: Sucrose standard curve showing the relationship of sucrose molarity with refractive index.

Second order polynomial equation is displayed on the graph which was used to calculate the sucrose molarity (y) from refractive index measurements (x).

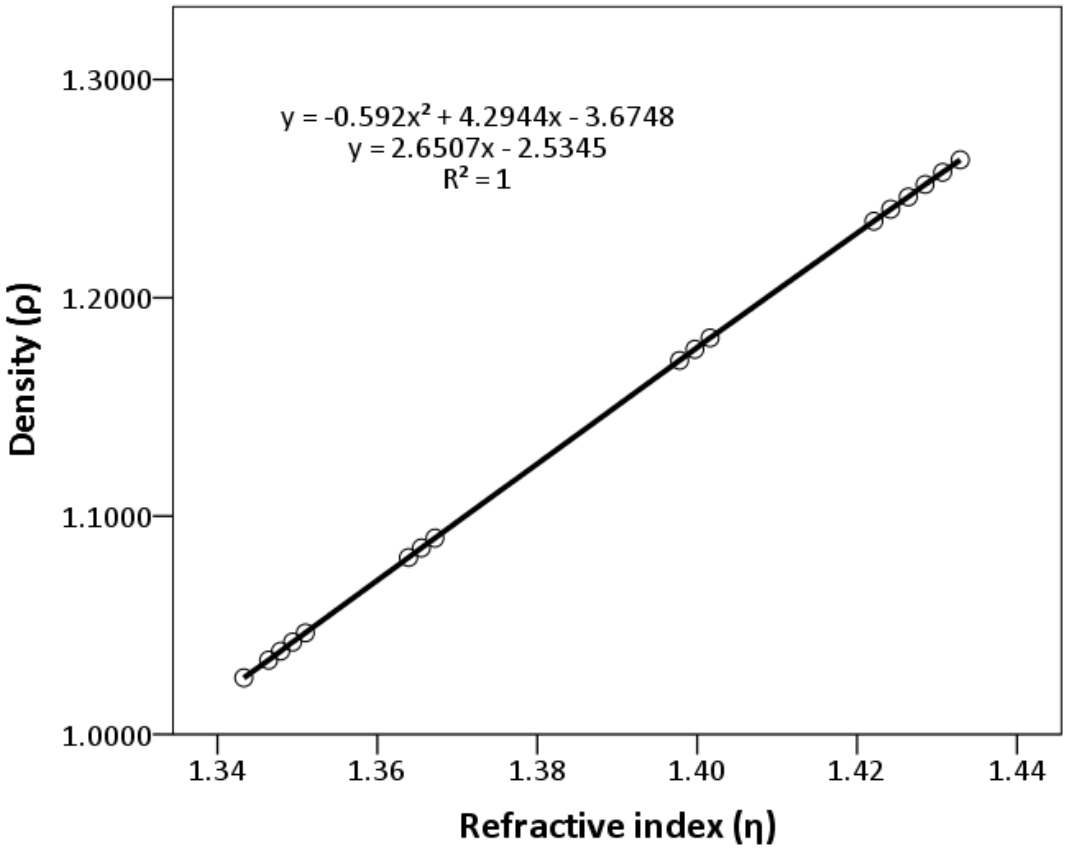

Figure 2.4: Sucrose standard curve showing the relationship of density with refractive index.
Second order polynomial equation and linear equation are displayed on the graph. Both equations were used to calculate the density (y) from refractive index measurements (x).

2.4.3 Sucrose cushion

Exosomes were isolated from the supernatants of bioreactor flasks by centrifugation on a 30% sucrose/D_2O cushion (Thery et al., 2006). Cell culture medium collected from the inner chamber was pre-cleared of cells and cellular debris by differential centrifugation (see section 2.4.1) and supernatants were poured into Quickseal ultra-centrifuge tubes (Beckman Coulter Inc., High Wycombe, UK) through 25G blunt needles (BD, Oxford, UK) under gravity. Sucrose was dissolved in deuterium oxide (D_2O) and 4 ml poured to the bottom using 18G spinal needles (BD, Oxford, UK) under gravity. The tubes were filled, from the top, with PBS until full and sealed. Cell culture supernatants were centrifuged at 100,000 x g for 90 minutes, 4°C in a swing out rotor (SW32, *k*-factor = 204, Optima-LE ultracentrifuge). 2.5 ml sucrose solution was collected from the bottom of the tube, transferred to a fresh Quickseal ultra-centrifuge tube (Beckman Coulter Inc., High Wycombe, UK) and topped up with PBS until filled. A second centrifugation was performed at 100,000 x g for 90 minutes, 4°C in a fixed angle rotor (70 Ti, *k*-factor = 44, Optima-LE ultracentrifuge) to pellet exosomes. Supernatants were removed, pellets re-suspended in PBS and stored at -80°C.

2.4.4 Size exclusion chromatography

Exosomes were isolated from plasma using size exclusion chromatography as previously described (Welton et al., 2015). After the initial draining under gravity, Exo-spin™ columns (Cell Guidance Systems, Cambridge, UK) were washed twice with 10 ml PBS-EDTA. 0.5 ml plasma was diluted to 1 ml in PBS-EDTA and loaded onto the columns before two 0.5 ml fractions were collected. PBS-EDTA was then added at 500 µl intervals for each of the remaining 30 fractions. Fractions were stored at -80°C.

2.5 Exosome analysis

2.5.1 Nanoparticle Tracking Analysis (NTA)

NTA visualises nanometre-sized particles in liquid using laser illumination. A high-intensity laser beam is sent through a chamber containing the sample under fluid flow (Figure 2.5); nanoparticles scatter light that is then detected by a x20 magnification microscope and high-sensitivity camera. Video files are produced that allow nanoparticles to be tracked over multiple frames, the particle velocity to be determined and particle size (diameter) to be calculated using the Stokes Einstein equation:

$$Dt = \frac{TK_B}{3\pi\eta d}$$

Where Dt is the Diffusion constant (product of diffusion coefficient D and time t), T is the temperature, K_B is the Boltzmann's constant, η is the solvent viscosity and d is the diameter of the spherical particle.

NTA allows the detection and tracking of individual particles. The combination of high-intensity laser beams and low-background optical configuration allows, in the case of biological particles such as exosomes, the size of particles to be determined down to a 30 nm resolution.

Particle concentrations and sizes were calculated by NTA with the Nanosight™ NS300 system (Malvern Instruments Ltd., Worcestershire, UK) configured with a high-sensitivity sCMOS Camera System (OrcaFlash 2.8, Hamamatsu C11440, Hamamatsu City, Japan), syringe-pump and temperature regulated 488 nm laser module.

Prior to taking measurements of biological samples the instrument was tested using 100 nm latex beads (Malvern Instruments Ltd., Worcestershire, UK). Three videos, of 30 s duration, were recorded of beads under fluid flow to confirm that size measurements were accurate. Measurements were averaged using the mode. Unless otherwise stated six videos, of 30 s duration, were recorded of vesicles, from biological samples, under fluid flow. Biological samples were diluted in nanoparticle-free water (Fresenius Kabi, Runcorn, UK) and dilution factor recorded by the NTA 3.1 software (version 3.1, build 3.1.54). Before commencing the six-video recording a one-video recording was performed to ensure that less than 100 events were detected per frame. This short video was used to ensure that the correct dilution factor was being used to keep the particle concentration within the linear range of the Nanosight™ instrument.

Samples were run through the sample chamber and the syringe pump set to 50 for a constant flow. The temperature control system was set to 25°C. Particle size distribution plots were determined by batch analysis of videos using the NTA software; the camera sensitivity was set to 14-16 and detection threshold set to 1-3.

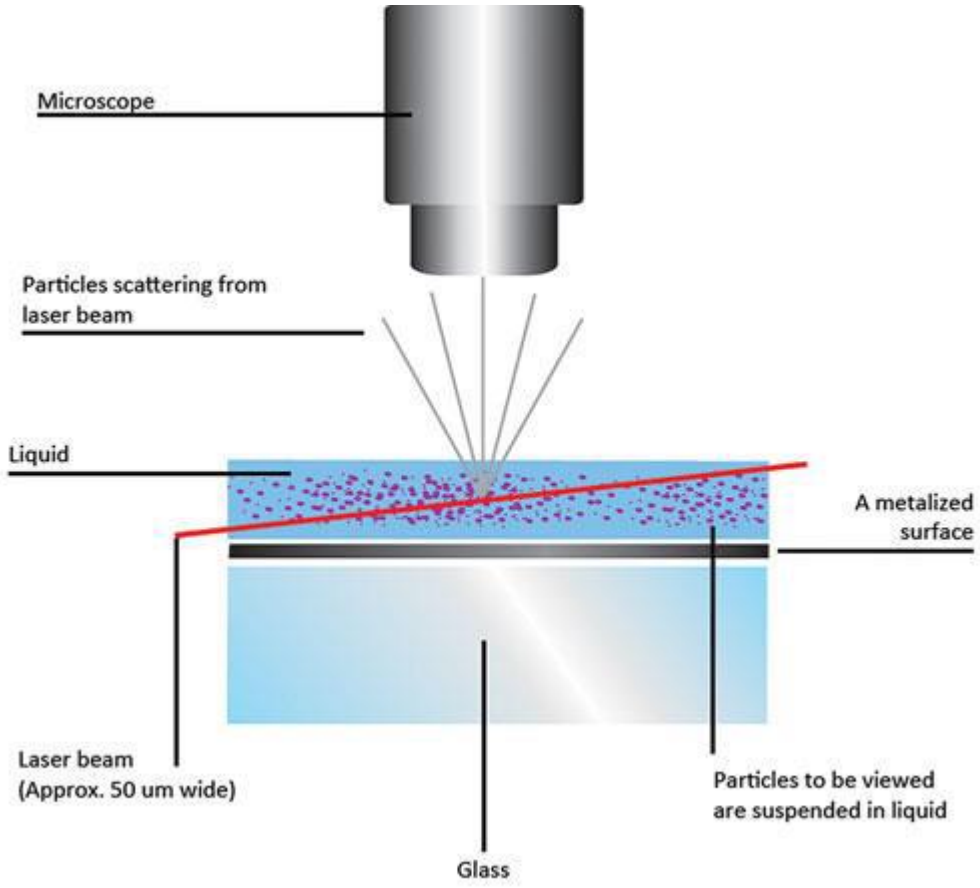

Figure 2.5: The instrumentation for Nanoparticle Tracking Analysis (Malvern Instruments Ltd.).
A high-intensity laser beam passes through the liquid-containing sample chamber and scattered light is detected by a x20 magnification microscope. A high-sensitivity camera captures video files of particles moving under Brownian motion. The Stokes Einstein equation is used to calculate the hydrodynamic diameters of individual particles and provides the user with readouts of particle size and concentration.

2.5.2 Quantification of total exosomal protein

Protein concentrations were calculated using the Micro BCA Protein Assay kit (Thermo Fisher Scientific, Inc., Loughborough, UK). Exosomes were diluted 1 in 8 and compared in duplicate against a serially diluted Bovine Serum Albumin (BSA) standard curve. Protein concentrations were extrapolated from this curve using a second-order polynomial equation:

$$y = ax^2 + bx + c$$

Where y corresponds to protein concentration and x corresponds to colorimetric measurement. The protein concentrations of whole cell lysates were similarly quantified.

2.5.3 Quality check of exosome purity using particle:protein ratio

Vesicle purity was assessed by calculating the particle : protein (P:P) ratio as previously described (Webber and Clayton, 2013). The particle concentration (as calculated by NTA) was divided by the protein concentration (as calculated by BCA assay):

$$P{:}P\ ratio = \frac{Particle\ concentration}{Protein\ concentration}$$

The original study that described this procedure provided guidelines for vesicle purity. Ratios >3 x 10^{10} would be considered highly pure, 2 x 10^{9} – 2 x 10^{10} would be considered low purity and <1.5 x 10^{9} as impure (Webber and Clayton, 2013). Vesicle purity was measured for all exosome preparations in this study and qualified as highly pure if a P:P ratio of >3 x 10^{10} was recorded.

2.5.4 Electron Microscopy

Electron microscopy was performed by David Gil Carton and Juan M. Falcón-Pérez of CIC bioGUNE, Bilboa, Spain. 5 µl of exosome preparation was directly adsorbed onto glow-discharged holey carbon grids (QUANTIFOIL). Grids were blotted at 95% humidity and rapidly plunged into liquid ethane with the aid of VITROBOT (Maastricht Instruments BV). Vitrified samples were imaged at liquid nitrogen temperature using a JEM-2200FS/CR transmission cryo-electron microscope (JEOL), equipped with a field emission gun and operated at an acceleration voltage of 200 kV (Welton et al., 2016).

2.6 Protein analysis

2.6.1 Immunoblotting

20 µg of whole cell lysates/exosome preparations were reduced and loaded onto NuPAGE® Bis-Tris polyacrylamide gels (Life Technologies, Waltham, MA, USA). Electrophoresed gels were transferred onto polyvinylidene difluoride (PVDF) membranes and incubated with primary antibodies in 5% milk-PBS-T for 1 hour at room temperature. Secondary antibodies,

conjugated with horse radish peroxidase (HRP), were applied for 1 hour at room temperature. Chemiluminescence was detected by incubating PVDF membranes with Enhanced Chemiluminescence (ECL) Western Blotting substrate (Thermo Fisher Scientific, Inc., Loughborough, UK) for 5 minutes at room temperature. Blots were read on the C-DiGit® Blot Scanner (LI-COR Inc., Nebraska, USA).

2.6.2 Primary antibodies used in this study

Antibody	Isotype	Size (kDa)	Supplier	Catalogue number
ALIX	IgG_1	95	Santa Cruz Biotechnology	sc-166952
CD63	IgG_1	25	AbD Serotec	MCA2142
CD81	IgG_1	26	BioRad	MCA1847EL
CD9	IgG_{2B}	27	R&D Systems	MAB1880
CD9 (Rabbit)	IgG	27	Santa Cruz Biotechnology	sc-9148
ENO2	IgG	47	Abcam	ab53025
GFAP	IgG	55	Abcam	ab7260
GRIA4	IgG_{2A}	132	Santa Cruz Biotechnology	sc-271894
GRID1	IgG_{2B}	112	Abcam	ab55163
GRP94	IgG_{2B}	94	Santa Cruz Biotechnology	sc-393402
L1CAM	IgG_1	200	Abcam	ab24345
NCAM	IgG_1	140, 160	Abcam	ab9272
NMDAR1	IgG_1	105	Abcam	ab134308
TSG101	IgG_{2A}	43	Santa Cruz Biotechnology	sc-7964

Table 2.2: Primary antibodies used in this study.

2.6.3 Immuno-phenotyping for specific protein targets by time resolved fluorescence

Relative protein concentrations were detected by a plate-based immuno-phenotyping assay with the time-resolved fluorometry method (PerkinElmer, Coventry, UK) using Europium as the fluorophore (Webber et al., 2014). 2 µg whole cell lysate or exosome preparations, in duplicate, were loaded into each well of a high binding enzyme-linked immunosorbent assay (ELISA) plate (Greiner Bio-One Ltd., Stonehouse, UK) and incubated overnight at 4°C. Plates were blocked with 1% BSA at room temperature for 2 hours with agitation. Primary antibodies were prepared in 0.1% BSA and incubated for 2 hours at room temperature with agitation. Secondary antibodies conjugated with biotin were also prepared in 0.1% BSA and incubated for 1 hour at room temperature with agitation. Time resolved fluorescence (TRF) was detected using the lanthanide chelate Europium. Streptavidin-europium conjugate (PerkinElmer, Coventry, UK) was diluted 1 in 1000 in red assay buffer (PerkinElmer, Coventry, UK) and incubated for 45 minutes at room temperature with agitation. Finally, the plates were incubated with enhancer solution (PerkinElmer, Coventry, UK) and read on a PHERAstar plate reader (BMG Labtech, Aylesbury, UK).

Different assay configurations were used and these are detailed in Chapter 4.

2.6.4 Conjugation of biotin to antibodies

Biotin was conjugated to the GRIA4 primary antibody using the Lightning-Link® Biotin Conjugation Kit (Type B) (Innova Biosciences, Cambridge, UK). Manufacturer's procedures were followed. In brief, 10 µl antibody was mixed gently with 1 µl LL-Modifier. This mixture was pipetted onto lyophilised biotin ligand and incubated at room temperature for 3 hours. 1 µl LL-Quencher was added and incubated for a further 30 min before storage at 4°C.

2.7 RNA isolation and quality control

2.7.1 RNA isolation

Ribonucleic acid (RNA) was extracted from cells and exosomes using the mirVana RNA isolation kit (Ambion, Waltham, MA, USA). For cellular-RNA, $1x10^6$ cells were collected, washed with PBS and lysed using lysis solution provided by the manufacturer. Exosome pellets were obtained by pellet and PBS wash (section 2.4.1) and non-vesicular RNA removed by Proteinase K and RNase A digestion (Shelke et al., 2014) detailed in section 2.7.2.

Exosomal-RNA was also isolated directly from plasma samples using exoRNeasy Serum/Plasma Midi Kit (Qiagen, Crawley, UK). Plasma aliquots were thawed and filtered using 0.8 µm syringe filter (Merck, Darmstadt, Germany) to remove any large aggregates. 0.5 ml filtered plasma was mixed with Buffer XBP in a 1:1 ratio and centrifuged in an exoEasy spin column at 500 x g for 5 min. The column was washed with 3.5 ml Buffer XWP and centrifuged at 3500 x g for 5 min. Exosomes were lysed on the column with 700 µl QIAzol and collected by centrifugation at 3500 x g for 5 min. Lysates were mixed by vortexing and allowed to stand at room temperature for 5 min. 90 µl chloroform was added, mixed by vigorous shaking for 15 s and allowed to stand at room temperature for 3 min. Lysates were centrifuged at 12,000 x g for 15 min at 4°C. The upper aqueous phase was transferred to a fresh tube and 100% ethanol added in a 2:1 ratio. Precipitated exosomal-RNA was transferred to an RNeasy MinElute spin column by centrifugation at 12,000 x g for 15 s. Columns were washed with 700 µl Buffer RWT and twice with 500 µl Buffer RPE. Columns were dried and 14 µl RNA eluted using nuclease-free water. RNA was immediately reverse transcribed and remaining eluate stored at -80°C for long term storage.

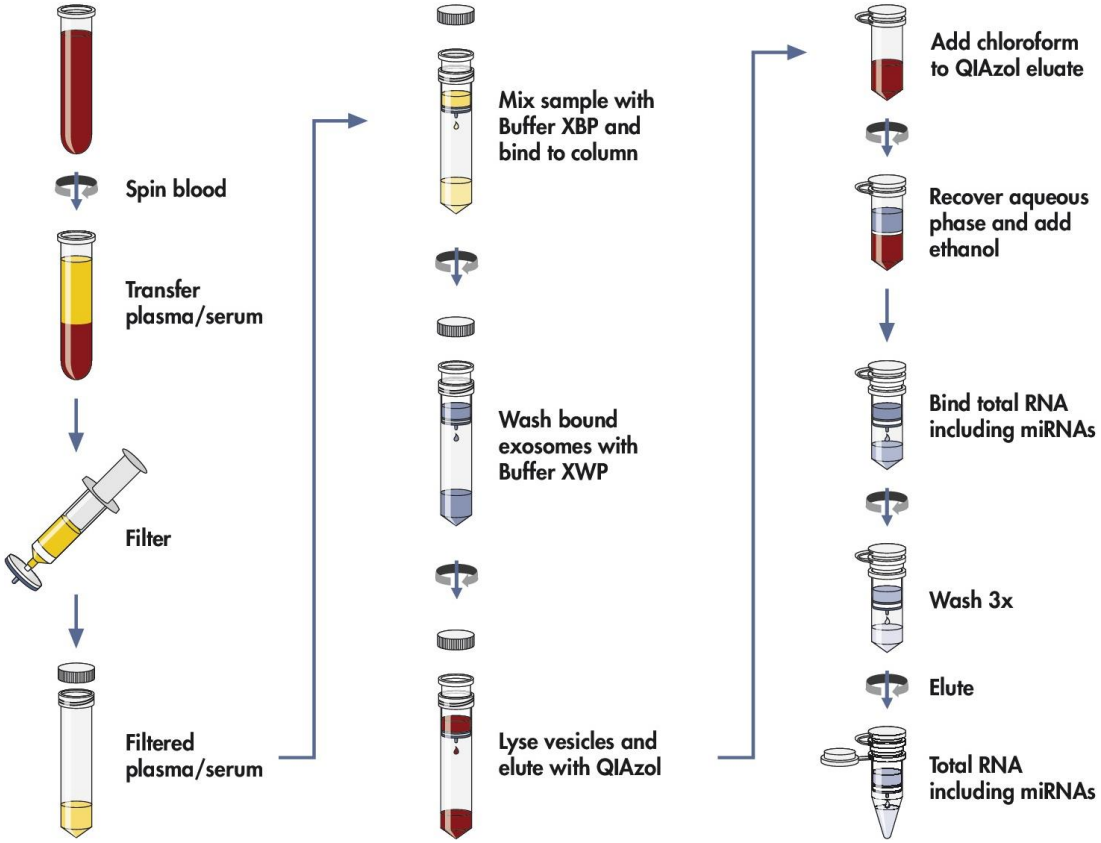

Figure 2.6: Procedure for isolating exosomal-RNA directly from plasma using exoRNeasy Serum/Plasma Midi Kit (Qiagen).
In this study, 0.5 ml human plasma, per individual, was processed using this procedure.

2.7.2 Proteinase K/RNase A digestion of non-vesicular RNA

To dissociate non-vesicular RNA from RNA-binding proteins, such as Argonaute (Arroyo et al., 2011), exosomes were incubated with 0.05 µg/µl Proteinase K (Sigma-Aldrich Co. Ltd., Dorset, UK) for 10 min at 37°C. Proteinase K was inactivated by incubation with 5 mM PMSF (Sigma-Aldrich Co. Ltd., Dorset, UK) for 10 min at room temperature followed by incubation at 90°C for 5 min. These samples were incubated with 0.5 µg/µl RNase A (Thermo Fisher Scientific, Inc., Loughborough, UK) to digest non-vesicular RNA that was liberated in this procedure. The mirVana kit was then used for the isolation of genuine intra-luminal RNA from exosomes (Shelke et al., 2014).

2.7.3 RNA quantification

RNA was quantified using the Qubit® RNA (high sensitivity) assay (Life Technologies, Waltham, MA, USA). In brief Qubit® RNA HS Reagent was diluted 1 in 200 using Qubit® RNA HS Buffer to make a working solution. RNA standards were made by mixing 10 µl RNA

standards with 190 µl working solution. RNA samples were diluted by mixing 1 µl RNA sample with 199 µl working solution, vortexing for 3 s and incubating at room temperature for 2 min. Fluorometric reading of standards and samples were obtained on a Qubit® 3.0 instrument (Life Technologies, Waltham, MA, USA).

Spectrophotometric readings were obtained using Nanodrop™ 8000 instrumentation (Nanodrop, Waltham, MA, USA) to give an assessment of protein and organic compound contamination.

2.7.4 Electrophoretic analysis of RNA

During this study electrophoretic analysis of RNA samples was performed using the Agilent 2100 Bioanalyser system (Agilent Technologies, Santa Clara, CA, USA) with both RNA 6000 Nano and RNA 6000 Pico kits. Manufacturer's instructions were followed. In brief gel matrix was prepared by centrifugation on a spin filter at 1500 x g for 10 min at room temperature. 65 µl filtered gel was mixed with 1 µl RNA dye concentrate and centrifuged at 13000 x g for 10 min at room temperature. 9 µl gel-dye mix was pipetted into the well "G" (Figure 2.7) and dispersed across the chip using the syringe provided. Two additional wells, also marked "G", were filled with 9 µl gel-dye mix. In the case of the Pico chip, 9 µl RNA conditioning solution was added to the well "CS". 5 µl RNA marker was added to each remaining well and 1 µl sample or ladder. Chips were vortexed at 2400 rpm for 1 minute and immediately read on the Bioanalyser instrument. The instrumentation was cleaned before and after use with RNaseZap™ RNase Decontamination Solution (Thermo Fisher Scientific, Inc., Loughborough, UK) and nuclease-free water.

After electrophoresis was completed, data files and reports were exported from the instrumentation. An RNA integrity (RIN) score was automatically calculated and, in the case of cellular-RNA, gave an assessment of degradation within the sample. However this score is calculated by taking into account the 18S and 28S ribosomal RNA (rRNA) peaks on the electropherogram. RNA from exosomes is deplete of rRNA (Shelke et al., 2014) and thus the RIN score was not an accurate assessment of RNA integrity. Therefore, an additional assessment of sample quality was used: the DV_{200} calculation. This calculates the percentage of RNA in the trace of greater length than 200 nucleotides and has been used previously to assess the quality of formalin-fixed paraffin-embedded tissue prior to RNA sequencing (Eikrem et al., 2016). DV_{200} scores were calculated using a Smear Analysis in the advanced settings of the Bioanalyser software. A region from 200 bp to the end of the trace was drawn

and the percentage for that region was displayed underneath the trace for each sample. According to manufacturer's guidelines, the exosomal-RNA samples used in this study were of good quality for sequencing.

Figure 2.7: Photograph of RNA Pico and Nano chips used with the Agilent 2100 Bioanalyser system.

2.8 RNA analysis

2.8.1 Construction of RNA sequencing libraries

Construction of libraries and sequencing on the Illumina HiSeq 2500 were performed at the Wales Gene Park, Cardiff University. Three biological replicates of H4 cellular-RNA and exosomal-RNA were established. 0.1 – 1.0 µg RNA was provided for each sample.

Total RNA libraries were constructed using the TruSeq Stranded Total RNA kit with Ribo-Zero Gold ribosomal RNA depletion step. This was chosen to obtain the fullest reading of the transcriptome without contamination with highly abundant ribosomal RNA (Benes et al., 2011). The final libraries were quantified by Qubit® double-stranded DNA (high sensitivity) assay (Life Technologies, Waltham, MA, USA), sizes measured using Bioanalyser instrumentation (Agilent Technologies, Santa Clara, CA, USA) and normalised to 4 nM before pooling. A small sequencing run was performed on the Illumina MiSeq prior to the main sequencing run to test the sequencing quality of the libraries but data were not used in the analysis.

2.8.2 Sequencing on Illumina HiSeq 2500

Pooled libraries were loaded onto two lanes of an 8-lane flowcell for cluster formation and sequencing, producing >89 gigabases of data. Wales Gene Park performed the initial conversion and de-multiplexing of sequencing files using the bcl2fastq software (Illumina Inc., San Diego, CA, USA) before making .fastq files available for download. In total twenty-four .fastq files were generated: six samples, each sequenced on two lanes, and each lane generating two read files.

2.8.3 Analysis of RNA sequencing

The quality of the sequencing was assessed using FASTQC (v0.11.2; Babraham Bioinformatics, Cambridge, UK). A FASTQC report was generated for each .fastq file providing a plethora of tests (discussed in section 5.3.2) to determine the quality of the sequencing run. These were assessed with the caveat that the software was optimised for whole exome and genome sequencing rather than RNA sequencing.

A modified .gtf gene model annotation file, detailing gene location, was required prior to read alignment and mapping. The original file was downloaded from ensembl (http://ftp.ensembl.org/pub/release-74/gtf/homo_sapiens/; accessed May 2016) and chromosome positions altered to a “chr1” format rather than the original “1” format using an awk script. Raw reads were mapped and aligned to hg19 using TopHat (v2.0.11; Johns Hopkins University, Baltimore, MD, USA). The Bowtie 2 hg19 index was downloaded from http://bowtie-bio.sourceforge.net/bowtie2/manual.shtml (accessed May 2016).

During the analysis the read mapping rate was investigated further by comparison with different alignment software. The Burrows-Wheeler Aligner (BWA, v0.5.9; Cambridge, UK) was used with the same modified gene model annotation file as used for TopHat alignment. The resultant .bam files were analysed for the number of reads using SAMtools (v1.2; Cambridge, UK) flagstat tool and insert sizes using Picard (v2.4.1; Broad Institute, Cambridge, MA, USA) CollectInsertSizeMetrics tool.

The TopHat alignment software was chosen in this study. Resulting .bam files, for each sample in each lane, were sorted by read names using SAMtools (v1.2; Cambridge, UK) sort tool and merged to produce one .bam file per sample using SAMtools merge tool. To obtain a global annotation of the samples the Picard (v2.4.1; Broad Institute, Cambridge, MA, USA)

CollectRnaSeqMetrics tool was used. Thus, the percentage of exonic, intronic, intergenic and untranslated region (UTR) reads was obtained.

Gene count files were obtained from mapped reads using HTSeq (v0.6.1p1; EMBL, Heidelburg). In this study long non-coding RNA (lncRNA) and introns were investigated. The Human lincRNA Catalog (Broad Institute, Cambridge, MA, USA) was used as an annotation file for lncRNAs as it has defined >8000 lncRNAs (Cabili et al., 2011) and has been used independently of the Broad Institute (Huang et al., 2016). A gene model annotation file was also required to itemise introns and their chromosomal positions. To generate this file, the table browser on UCSC (https://genome.ucsc.edu/cgi-bin/hgTables, accessed November 2016) was used to download intron locations, +50 bases flanking sequence, in .bed format (hg19). An awk script was used to process the text into a .gtf format, in particular inserting a third column with "intron" in all rows, which HTSeq requires to perform the count function.

Differential expression analysis of lncRNA and introns was performed using DESeq2 (v1.14.0; Harvard, MA, USA) on R (v3.3.2; open source). In brief, gene count files were read into R and converted to DESeq2 datasets. Rows were removed where no counts were made across all 6 samples to improve computation times. The data were transformed using the regularised-logarithm transformation (rlog) as suggested in the software workflow (Love et al., 2014). This stabilises the variance across the mean making the data approximately homoscedastic. Euclidean distances and Principle Component Analysis (PCA) were used to assess the variance between samples. Individual lncRNA/intron expression differences were visualised by heatmap and Minus-Average (MA) plot. The false discovery rate threshold was reduced to an adjusted Bonferroni p-value of 6.27×10^{-6} for lncRNA analysis and 8.799873×10^{-7} for intron analysis.

To gain functional insight from the lncRNA data, co-expressed coding genes were identified using Co-LncRNA (http://www.bio-bigdata.com/Co-LncRNA/, accessed November 2016). Differentially expressed lncRNAs were sorted by log fold change and the top 10, for cells and exosomes separately, were uploaded into the web interface with coding gene expression profiles from the sequencing data. Genes with correlative expression were identified and functional annotation of genes was performed using the Database for Annotation, Visualisation and Integrated Discovery (DAVID, v6.8; Leidos Biomedical Research, Inc., Frederick, MD, USA). Enrichment maps were drawn using Cytoscape (v3.4.0; open source). The same analysis was performed for differentially expressed introns without the need to identify co-expressed genes.

2.8.4 Validation of RNA sequencing results

A separate method, using independent samples, was used to validate the results of the RNA sequencing. Three biological replicates of the H4 cell-line were established again and RNA isolated from both cells and exosomes. Quantitative polymerase chain reaction (qPCR) using SYBR™ Green was chosen to validate differential lncRNA expression.

Primers were designed for six lncRNAs: three that were up-regulated in cells (XLOC_000670, XLOC_011226 and XLOC_008152) and three that were up-regulated in exosomes (XLOC_009577, XLOC_001047 and XLOC_006043). Chromosomal positions for these lncRNAs were identified from the gene model annotation file and DNA sequences were downloaded from the University of California Santa Cruz (UCSC) genome browser. Exonic regions of three housekeeping genes (GAPDH, TUBA1A and PPIA) were downloaded also. Primers were designed by submitting DNA sequences to Primer3 (Heidelberg, Germany) and requesting amplicons of 80 – 100 bp in length. These primer sets were confirmed to amplify the correct genomic region using the *in silico* PCR tool provided by UCSC and ordered from eurofins (Ebersberg, Germany).

2.8.5 Reverse transcription

RNA samples were reverse-transcribed to complimentary DNA (cDNA) using SuperScript™ IV VILO™ Master Mix with ezDNase™ Enzyme (Thermo Fisher Scientific, Inc., Loughborough, UK). A total of 8 µl RNA was mixed with 1 µl 10X ezDNase buffer, 1 µl exDNase enzyme and incubated at 37°C for two minutes on a BioRad S1000™ Thermal Cycler (Bio-Rad Laboratories, Inc., Watford, UK) to digest any contaminating genomic DNA (gDNA). In the case of quantifiable RNA (H4 cells and cell-derived exosomes), 80 ng RNA was put into this reaction for normalisation. In the case of un-quantifiable RNA (from plasma samples) the volume of sample input provided the normalisation. Reverse transcription was performed by addition of 4 µl SuperScript™ IV VILO™ Master Mix, 6 µl nuclease-free water and incubation with the following protocol:

25°C for 10 min to anneal primers

50°C for 10 min to reverse transcribe RNA to cDNA

65°C for 10 min to reverse transcribe RNA to cDNA

85°C for 5 min to inactivate enzyme

Samples were stored at -80°C for long term storage.

2.8.6 Polymerase chain reaction

Primers were tested by standard polymerase chain reaction (PCR) prior to qPCR. 4 µl cDNA was mixed with the following PCR cocktail:

Reagent	Volume (µl)
Nuclease-free water	4.34
10X Buffer*	1.2
5 mM dNTPs*	1.2
5 ng/µl forward and reverse primers	0.6
5 u/µl Hot start Taq polymerase*	0.06
cDNA	4

*(Thermo Fisher Scientific, Inc., Loughborough, UK)

PCR plates were run on BioRad S1000™ Thermal Cycler (Bio-Rad Laboratories, Inc., Watford, UK) using the following protocol:

95°C for 15 min

35 cycles of:

94°C for 45 s (Denaturation)

58°C for 45 s (Annealing of primers)

72°C for 60s (Extension of double-stranded DNA)

Final extension of 72°C for 10 min

2.8.7 Agarose gel electrophoresis

PCR products were visualised by agarose gel electrophoresis. 1% agarose gels were cast by melting 1 g agarose (Sigma-Aldrich Co. Ltd., Dorset, UK) in 100 ml Tris-Borate-EDTA (TBE) buffer and adding 2 µl ethidium bromide (1% w:v ; Sigma-Aldrich Co. Ltd., Dorset, UK), once cooled. PCR product was mixed in a 1:1 ratio with loading dye (New England BioLabs® Inc., Ipswich, MA, USA) and 10 µl loaded into each well of the agarose gel. 5 µl 100 bp ladder (New England BioLabs® Inc., Ipswich, MA, USA) was loaded in a well for size discrimination. Agarose gels were electrophoresed at 100 V for 30 min or until the dye front had travelled sufficiently far through the gel. PCR products were visualised on the gels using UV exposure on a Gel Doc™ XR+ Gel Documentation System (Bio-Rad Laboratories, Inc., Watford, UK).

2.8.8 qPCR using SYBR™ green

Once suitable primer sets had been confirmed by conventional PCR and gel electrophoresis qPCR was performed. The comparative C_T method (Schmittgen and Livak, 2008) was chosen to assess relative coding gene and lncRNA expression.

2 µl cDNA product was mixed with 2 µl nuclease-free water, 1 µl forward/reverse primers (5 ng/µl) and 5 µl PowerUp™ SYBR™ Green Master Mix (2X). Samples were prepared in duplicate or triplicate. Quantitative PCR was performed using StepOnePlus™ Real-Time PCR System (Thermo Fisher Scientific, Inc., Loughborough, UK) in standard cycling conditions:

50°C for 2 min

95°C for 2 min

40 cycles of:

95°C for 15 s (denaturation)

60 °C for 1 min (primer annealing/extension)

Melt curves were run and analysed for additional PCR products using the following protocol:

95°C for 15 s (1.6°C per s Ramp)

60°C for 1 min (1.6°C per s Ramp)

95°C for 15 s (0.15°C per s Ramp)

Dissociation curves were visualised for each primer set, the number of peaks and melting temperature recorded.

Analysis parameters for amplification plots were set to an automatic baseline and a 0.1 fluorescent units threshold as described elsewhere (Enderle et al., 2015).

2.8.9 qPCR using Taqman® with pre-amplification

In addition to SYBR™ Green qPCR, Taqman® gene expression analysis was performed with an additional step of pre-amplifying selected targets after reverse transcription. 10 µl of 20X TaqMan® gene expression assay, for each target, was pooled with other assays and diluted to 0.2X in Tris-EDTA (TE) buffer. 12.5 µl pooled assay mix (0.2X) was mixed with 12.5 µl cDNA and 25 µl TaqMan® PreAmp Master Mix (2X). The pre-amplification reaction was followed:

95°C for 10 min

10 cycles of:

95°C for 15 s

60°C for 4 min

Samples were diluted 1:5 in TE buffer, aliquoted and frozen at -20°C. Quantitative PCR was performed using StepOnePlus™ Real-Time PCR System (Thermo Fisher Scientific, Inc., Loughborough, UK) in standard cycling conditions:

50°C for 2 min

95°C for 2 min

40 cycles of:

95°C for 15 s (denaturation)

60 °C for 1 min (primer annealing/extension)

No melt curve analysis was required for TaqMan® and the same analysis parameters were applied: automatic baseline and a 0.1 fluorescent unit threshold.

2.9 DNA isolation and quality control

2.9.1 DNA isolation from whole blood

As part of the AD Genetics project whole blood was collected in lavender top EDTA tubes for DNA isolation. Genomic DNA was extracted using Nucleon BACC Genomic DNA Extraction Kits (GE Healthcare, Buckinghamshire, UK). In brief, blood samples were mixed in a 1:4 ratio with Reagent A (1X) for red blood cell lysis. Intact white blood cells were pelleted by centrifugation at 1600 x g for 5 min and supernatant discarded into bleach. Cells were lysed in 2 ml Reagent B. Nucleic acids were separated from proteins by mixing with 500 µl sodium perchlorate, 2 ml chloroform, 300 µl nucleon resin and phases separated by centrifugation at 1600 x g for 3 min. DNA was precipitated from the upper, aqueous phase by mixing with

100% ethanol in a 1:1 ratio. DNA was pelleted by centrifugation at 3500 x g for 5 min. DNA pellets were washed with 2 ml 70% ethanol, centrifuged again and re-suspended in 100 – 650 µl TE buffer dependent on DNA pellet size.

2.9.2 DNA quantification by PicoGreen

Double stranded gDNA was quantified using the Quant-iT PicoGreen dsDNA Assay Kit (Thermo Fisher Scientific, Inc., Loughborough, UK). PicoGreen was diluted to a working concentration in TE buffer and protected from light. 2 µl DNA was diluted in 98 µl working PicoGreen solution in 96-well black, flat-bottom microplates. Fluorescence was measured by excitation at 485 nm and emission at 520 nm using an Infinite® 200 PRO microplate reader (Tecan Group Ltd., Männedorf, Switzerland). DNA quantitations were calculated using a standard curve of λ DNA standard.

2.10 DNA analysis

2.10.1 *APOE* genotyping

APOE genotypes were determined by single nucleotide polymorphism (SNP) genotyping as described previously (Butchart et al., 2015, Ide et al., 2016). TaqMan (Life Technologies, Waltham, MA, USA) genotyping was performed for rs7412 and KASP™ (LGC Ltd., Teddington, UK) genotyping for rs429358. DNA samples were diluted to a working concentration of 2.5 ng/µl.

TaqMan genotyping was performed by mixing 11.25 µl DNA with 12.5 µl TaqMan genotyping mastermix (2X) and 1.25 µl rs7412 primer mix (20X). Standard genotyping procedure was performed using the using StepOnePlus™ Real-Time PCR System (Thermo Fisher Scientific, Inc., Loughborough, UK):

95°C for 10 min

40 cycles of:

95°C for 15 s (denaturation)

60°C for 1 min (primer annealing/extension)

Fluorometric recording of VIC, FAM and ROX dyes was performed by the StepOnePlus™ instrumentation and Allelic Discrimination Plot automatically displayed.

Kompetitive Allele Specific PCR (KASP™) genotyping was performed by mixing 5 µl DNA with 5 µl KASP™ mastermix (2X) and 0.14 µl rs429358 primer mix. Amplification was performed using BioRad S1000™ Thermal Cycler (Bio-Rad Laboratories, Inc., Watford, UK) on a touch-down PCR protocol:

94°C for 15 min

10 cycles of:

94°C for 20 s

68°C for 1 min (reducing -0.5°C each cycle)

26 cycles of:

94°C for 20 s

62°C for 1 min

This was followed by three more cycles to improve clustering of data-points:

3 cycles of:

94°C for 20 s

57°C for 1 min

Fluorescence of FAM, HEX and ROX dyes were measured using an Infinite® 200 PRO microplate reader (Tecan Group Ltd., Männedorf, Switzerland).

Two negative controls and six positive controls, of each *APOE* genotype, were included for both assays to validate correct genotype calling.

2.11 Statistical analyses

Unless otherwise stated, statistical calculations were performed using SPSS Statistics 20 package (IBM). Differential expression analyses were performed using DESeq2 (v1.14.0) on R (v3.3.2).

Where possible, three or more biological and technical replicates were prepared in the experiment design so that the distribution of the resultant data could be analysed. It is acknowledged, by the author, that ideally these numbers of replicates should have been performed in every experiment, however, the limitations of exosome sample and antibody quantity made it necessary for some experiments to be performed with a lower number of repeats. Where this was the case the limitations are discussed and careful interpretation of the results follow.

Prior to performing specific statistical tests, the suitability of each dataset was considered by performing a Shapiro-Wilk test for normality using SPSS Statistic 20 package (IBM). Normally distributed data was subjected to parametric tests, such as t-test or analysis of variance (ANOVA), where the mean of each group is used in the test. When data were not normally distributed, non-parametric tests, such as Mann-Whitney U tests, were performed.

2.12 Experimental design

Throughout this study, general principles of good working practice were followed. For example, exosome stocks were routinely quality checked by BCA and NTA, detailed note-keeping was performed in the laboratory and samples were handled with care to avoid cross-contamination. Chapters 5 and 6, in particular, contained experiments that required additional forethought of experiment design.

In chapter 5, an RNA sequencing experiment was performed and steps were taken to reduce any batch effects. These included: extracting RNA from biological replicates simultaneously with the same extraction kit, handling RNA for quantitation and reverse transcription at the same time for all samples, using central wells of thermal cycler blocks rather than edge wells, performing library preparation of all samples simultaneously and performing sequencing with all libraries pooled and run over 2 lanes.

In chapter 6, a case:control cohort was used to validate a qPCR-based assay. Although cases and controls had been pre-selected, sample IDs were numeric to aid with anonymisation in the laboratory and reduce human bias. Again, steps were taken to reduce batch effects

including: performing all RNA extractions on the same day, handling cases and controls at the same time, performing reverse transcription of all samples on the same day and each gene expression candidate was tested with all samples on one plate at a time. In the future, with larger cohorts for a discovery experiment, these practices would again be adopted with additional steps. Double-blinding would be performed to further reduce any possibility of human bias or batch effects in sample handling. Power calculations will be performed to ensure an adequate cohort size is chosen.

Chapter 3. Establishing and characterising an abundant source of neural-derived exosomes

3.1 Introduction

Multi-vesicular bodies fuse with the plasma membrane to release exosomes into the extracellular space (Thery et al., 2002). Biological fluids are complex tissues containing a heterogeneous pool of cells and particles (Hoog and Lotvall, 2015). This poses significant challenges for the isolation of pure exosomes.

As an alternative to biological fluids, cell culture media gives an opportunity to obtain exquisitely pure exosomes; it is far easier to control for which co-isolates are present. For example, foetal bovine serum (FBS) is a common additive that can introduce bovine exosomes which then mix with those secreted by the cultured cells (Shelke et al., 2014). Bovine exosomes can be depleted with relative efficiency using ultra-centrifugation. Thus, cell cultures can offer an accessible and consistent source of exosomes.

Choosing a cell-line to use is a significant consideration. Primary cells can provide a tissue- or disease-relevant source of exosomes and therefore, representative of what may be found in biological fluids. However, primary cells are susceptible to reaching senescence and can be technically difficult for long-term or high-density cell culture. Alternatively, immortalised cell-lines are less susceptible to reaching senescence and, generally speaking, more robust. Despite being less technically challenging to maintain immortalised cell-lines than primary cells there can be differences between different cell-types. An analysis of a panel of cancer cell-lines found that growth characteristics varied between cell-lines, and indeed, the quantity and size of exosomes differed also (Hurwitz et al., 2016).

The isolation of neural-derived exosomes is an exciting prospect for analysing vesicles relevant to diseases of the CNS, such as Alzheimer's disease. Primarily, an abundant source of neural-derived exosomes was required in this study so immortalised cell-lines were chosen, rather than primary cells. Neuroglioma (H4) and neuroblastoma (IMR-32) cell-lines were chosen as they were cells sourced from the CNS.

Whilst these cell-lines provided a source of neural-derived exosomes, both H4 and IMR-32 had previously been used as cell-models of AD, so provide future potential for AD-relevant analyses. For example, the H4 cell-line has been manipulated to express the Swedish mutant form of *APP* assigned "H4-sw". One study reported that H4-sw exhibited elevated expression of Heme Oxygenase 1, driven by epigenetic alterations in the promoter region of the gene (Sung et al., 2016). This phenomenon was also apparent in the primary T lymphocyte Jurkat cells of AD patients and methylation analyses of the *HMOX1* gene correlated with disease

status and Mini-Mental State Examination. This is a prime example of translating observations from a cell-model into clinical relevance. The *PS1* gene has been knocked-down in the IMR-32 cell-line and this caused decreased Aβ-42 (Kandimalla et al., 2012). Another study reported that *Aloe arborescens* extract protected the IMR-32 cell-line from Aβ-induced toxicity through the reduction of Reactive Oxygen Species (Clementi et al., 2015).

The investigation of exosomes from these cell-lines has only been reported once to date. The H4 cell-line was used to study the PARK9 ATPase in relation to Kufor-Rakeb Syndrome (Tsunemi et al., 2014). PARK9 over-expression promoted the secretion of exosomes and α-synuclein via exosomes. Therefore, the thorough characterisation and study of exosomes from these cell-lines is a novel avenue of research.

A major challenge in collecting exosomes from cell cultures is handling large volumes of media to maximise yields. One example of this is a study that required 3.2 L of media to obtain sufficient protein for one 2D Electrophoresis gel experiment (Staubach et al., 2009). Such work is cumbersome, expensive and inefficient. Unfortunately this is unavoidable with traditional cell culture techniques where the surface area : volume ratio (SA:V) does not allow adherent cells to grow in high densities. However, it is possible with standard cell culture techniques to have ready access to viable cells and their secreted exosomes at the same time. This is a benefit when wanting to study transiently expressed molecules such as RNA (Skog et al., 2008).

To overcome this issue with traditional cell culture, one option is to adopt a 3D culture system and a novel method was developed in the Clayton lab at Cardiff University for exosome production. Bioreactor flasks (Integra CELLine™ flasks) were used to culture adherent cells in a high density but low media volume (Mitchell et al., 2008a). Cells are seeded into the inner chamber of the bioreactor and encapsulated in a matrix of plastic to allow adhesion. The volume of culture medium is typically 10 - 15 ml for the inner chamber and this is maintained by the outer chamber containing 500 – 1000 ml medium. Nutrients and waste products can pass bi-directionally over a membrane that separates the inner and outer chambers to maintain the cells; however, exosomes remain within the inner compartment. This technique allows exosomes from high density cell-culture to be isolated from a small media volume. A caveat of this method is that, by reducing the SA:V ratio, cells are cultured in a more stressful and hypoxic environment, and that cell viability cannot be controlled or monitored easily (Mitchell et al., 2008a).

Once isolated there are a number of characteristics that define exosomes from other extracellular vesicles. One characteristic is size, with exosomes ranging from 40-120 nm diameter (El Andaloussi et al., 2013). The gold standard method for measuring particle size is electron microscopy (EM) as accurately measuring particles smaller than 300 nm using optical methods is technically challenging. Scanning EM (SEM) and Transmission EM (TEM) have both be utilised for the measurement of exosome size (Wu et al., 2015). It has been observed that TEM consistently shows "cup-shaped" vesicles; these structures are not true morphology but artefacts of sample preparation as common fixatives, such as glutaraldehyde, cause sample dehydration and structural collapse. This central depression is not observed with SEM; rather exosomes appear spherical in structure. Despite this difference, TEM offers the well-established utility of immuno-gold labelling of particles, which is not commonplace with SEM, to date. An alternative to these methodologies is cryo-EM that, like SEM, does not have the "cup-shaped" artefact (Xu et al., 2015). Cryo-EM does not involve staining or fixing of samples, instead they are plunge frozen in their native state, which is advantageous for observing true exosome structure (Welton et al., 2016).

Electron microscopy is an expensive, time- and labour-intensive procedure for measuring exosome size. It would be technically challenging to utilise it for routine quality-control of vesicle preparations. Alternative technologies have been developed namely, Tuneable Resistive Pulse Sensing (TRPS) and Nanoparticle Tracking Analysis (NTA). TRPS technology was brought to the market by Izon Science Ltd., with the qNano instrumentation. It can be used to measure exosome size, concentration in solution and electric charge (Akers et al., 2016). In principle, particles in an electrolyte fluid pass through a nanopore and a resistive pulse signal is detected and measured. NTA technology was brought to the market by Malvern Instruments Ltd., with the Nanosight instrumentation. It can be used to measure exosome size and concentration in solution (Livshts et al., 2015). Particles, moving under Brownian motion, scatter light from a laser beam and the velocity and motion is proportional to particle size. This relationship is described by the Stokes-Einstein equation. An additional application of NTA is the measurement of particles fluorescently labelled for an antigen of interest (Stern et al., 2016). Both technologies have been adopted for measuring exosome size to date and offer a far more tractable quality-control step than electron microscopy. The Clayton lab has adopted NTA for routine measurements of exosome size. The dynamic light scattering used in NTA can be applied to measure poly-disperse particles, whereas TRPS requires different pore sizes dependent on the size range of particles being analysed. Therefore, NTA has been used in this study.

A second defining characteristic of exosomes is density: ranging from 1.1 – 1.2 g/ml (Escola et al., 1998, Raposo et al., 1996, Webber et al., 2014). To measure this, vesicle preparations can be under- or over-laid on a continuous sucrose gradient and centrifuged at a high-speed overnight before fractions are collected and analysed. As an alternative to sucrose gradients, iodixanol, an isotonic dense medium marketed as OptiPrep™ and used in medical imaging as an inert contrast reagent, has been used in similar density separation procedures (Konadu et al., 2016). These are useful analytical tools but not widely used as exosome preparation techniques, due to them being time- and labour-intensive. A consequent method was developed, based on trapping vesicles of relevant density, termed the "sucrose cushion method" whereby exosomes are isolated with a sucrose/D_2O solution (Andre et al., 2002, Lamparski et al., 2002, Thery et al., 2006). This can be used as a routine isolation procedure as a single density cushion is prepared far more quickly than a gradient and ultra-centrifugation times are much shorter.

A third characteristic feature of exosomes is protein content. A number of proteins are known to be expressed and enriched in exosomes: the tetraspanins CD63, CD81 and CD9 (Lamparski et al., 2002, Escola et al., 1998, Heijnen et al., 1999); and components of the ESCRT machinery, TSG101 (Stoorvogel et al., 2002) and ALIX (Roucourt et al., 2015, Stoorvogel, 2015). These proteins have been used to validate the isolation of exosomes in the Clayton laboratory at Cardiff University (Clayton et al., 2007, Clayton et al., 2004, Clayton et al., 2005) and elsewhere (Lamparski et al., 2002, Caby et al., 2005). However, the distribution of these typical proteins on different sub-types of EVs, such as those of plasma membrane origin, remains in debate, as discussed previously.

Not only can specific protein markers be analysed but the total protein content of exosome preparations can be used on a global level to assess purity. The Clayton laboratory developed the methodology of combining particle concentration, measured by NTA, and protein concentration, measured by BCA assay, to produce a particle : protein (P:P) ratio (Webber and Clayton, 2013). This gives an assessment of the number of particles in a preparation against the concentration of vesicular, non-vesicular and contaminating proteins. A similar method has been proposed that used a sulfophosphovanilin (SPV) assay to measure total lipid concentration and from that calculate a lipid : protein ratio (Osteikoetxea et al., 2015). Both methods were developed to provide a basic assessment of vesicle purity as a much needed quality control read-out. These reports additionally highlighted the relative difficulty of isolating pure exosomes from biological fluids compared to cell-culture medium. This is likely due to the problem of co-isolating proteins regardless of which isolation method used.

A fourth feature of exosomes is their morphology. With electron microscopy spherical structures with a lipid bilayer are observed (Wu et al., 2015, Xu et al., 2015). As discussed above, TEM can produce "cup-shaped" artefacts that are not observed with SEM or cryo-EM. These techniques also provide an opportunity to assess contamination with other debris. One study recorded approximately 1500 extracellular structures, observed by cryo-EM, from an un-prepared biological fluid (Hoog and Lotvall, 2015). This is in contrast with a pure exosome preparation where heterogeneity is expected but only within a subtype of small, <120nm, size range of bilayer vesicles.

In a 2014 position statement a set of biochemical, biophysical and functional criteria were proposed by the International Society of Extracellular Vesicles (Lotvall et al., 2014). The aim of this was to standardise the minimal experimental requirements to report the genuine isolation of exosomes. With the exception of particle density, this statement lists the same features as mentioned above. The first of these is protein content with the suggestion that 3 or more proteins are reported in at least a semi-quantitative manner. The report suggested the assessment of both transmembrane and intra-luminal proteins that are expected to be present or enriched in exosomes. This requires measuring proteins on exosomes in their native form and within exosomes using a reducing agent. Additionally proteins not expected within exosomes should be measured to rule out cellular contamination. In the case of studies that use cell culture-derived exosomes, these proteins should be evaluated in respect to the source cells. The report also suggested that two techniques are employed to characterise individual exosomes. For example, showing both electron micrographs and size distribution plots by NTA or TRPS. These suggestions provide a helpful guideline and were followed in this study, in combination with the established systems used in the Clayton lab, to provide strong evidence of isolating exosome vesicles of good purity.

Therefore, guidelines have been established for isolating and characterising exosomes secreted from the H4 and IMR-32 cell-lines. Utilising these cell-lines for high-yield production of exosomes would provide an abundant source of neural-derived exosomes. This would provide some of the materials and methodology required for subsequent chapters in this study.

3.2 Aims

The aim of this chapter was to generate a bulk stock of exosomes to be used for the remainder of the thesis, particularly, for developing an affinity capture assay and for RNA analysis. To achieve this aim the following objectives were addressed:

- Establish cell cultures from neural sources
- Establish methods for the isolation of exosomes from these cell cultures
- Characterise exosomes based on their size, protein content, density and structure
- Establish quality control measures for exosome preparations and a stock of exosomes for downstream assay development and RNA analysis

3.3 Results

3.3.1 Cell-line characterisation and validation

Immortalised cell-lines were chosen to allow the scale-up of exosome isolation, as the cells should robustly handle large scale culture. Human cell-lines, from a neural source, were purchased from American Type Culture Collection (ATCC): one neuroglioma (H4, ATCC® HTB148™) and one neuroblastoma (IMR-32, ATCC® CCL127™). Upon receipt of ampoules, cell validation data was requested from the supplier. The H4 cell-line was validated by short tandem repeat (STR) analysis with a unique DNA profile that matched the expected profile (Table 3.1). The IMR-32 cell-line was validated by STR analysis and an isoenzyme analysis that was positive for G6PD type B (Table 3.2). These data, provided by the supplier, confirm that the cells used in this study are from the neural sources as stated.

To avoid cross contamination these cell-lines were handled in isolation from each other. Incubator space was shared with other cell-lines but sub-culturing was performed at different times and safety cabinets decontaminated between uses. Passage counts started at passage 1 upon receipt of the cells. Multiple aliquots of cells were frozen at passage 2 and passage 5 as a banked resource. Sub-culturing never exceeded passage 20. Mycoplasma testing was performed every 3 months if the cells had been in uninterrupted culture or periodically when new ampoules were started. Together these procedures reduced the risk of cross-contamination between cell-lines and with mycoplasma.

Brightfield microscopy was used to routinely assess cell morphology and thus identify a cross-contamination event or fungal/bacterial contamination had it occurred. The H4 cell-line maintained an epithelial morphology (Figure 3.1) and the IMR-32 cell-line was a neuroblast-like morphology (Figure 3.2) as expected from supplier's instructions. Therefore, the cell-lines used were indeed from the neural sources stated and thus suitable for establishing stocks of exosomes and performing further analyses.

Test	Specifications	Results
Post-freeze viability	≥ 50.0%	95.0%
Growth properties	Adherent	Adherent
Morphology	Epithelial-like	Epithelial-like
Test for mycoplasma contamination Hoechst DNA stain (indirect) Agar culture (direct)	None detected None detected	None detected None detected
Species determination: COI assay (interspecies)	Human	Human
Species determination: STR analysis (intraspecies)	**Human (Unique DNA Profile)** D5S818: 10, 12 D13S317: 12 D7S820: 8, 11 D16S539: 11, 12 vWA: 14, 18 THO1: 7, 9 Amelogenin: X, Y TPOX: 8, 11 CSF1PO: 10, 12	**Human (Unique DNA Profile)** D5S818: 10, 12 D13S317: 12 D7S820: 8, 11 D16S539: 11, 12 vWA: 14, 18 THO1: 7, 9 Amelogenin: X, Y TPOX: 8, 11 CSF1PO: 10, 12
Sterility test (BacT/ALERT 3D) iAST bottle (aerobic) at 32°C iNST bottle (anaerobic) at 32°C	No growth No growth	No growth No growth

Table 3.1: Cell validation for the H4 cell-line (ATCC® HTB148™) Lot Number 57637310 (provided by supplier).
Cells were viable after freezing and confirmed to be sterile and free of mycoplasma. STR analysis, performed by the supplier, revealed a DNA profile consistent with expected data to confirm that this lot contained the expected population of cells without cross-contamination. Cell viability and morphology were routinely assessed by the user during sub-culturing.

Test	Specifications	Results
Post-freeze viability	≥ 50.0% average	91.1% average (range of 88.6% to 92.6%)
Morphology	Neuroblast-like and/or rounded	Neuroblast-like
Mycoplasma contamination (Hoechst DNA Stain and Direct Culture Methods)	None detected	None detected
Post-Freeze Cell Growth	Cells are able to be successfully subcultured for two passages post-freeze	Cells are able to be successfully subcultured for two passages post-freeze
Interspecies Determination (Isoenzyme Analysis)	Human, G6PD type B	Human, G6PD type B
Intraspecies Determination (STR Analysis)	Pass (DNA profile is consistent with all other DNA profiles on record for this cell line)	Pass
Bacterial and Fungal Contamination	None detected	None detected

Table 3.2: Cell validation for the IMR-32 cell-line (ATCC® CCL127™) Lot Number 5087900 (provided by supplier).
Cells were viable after freezing and confirmed to be sterile and free of mycoplasma. STR analysis, performed by the supplier, revealed a DNA profile consistent with expected data and isoenzyme analysis was positive for G6PD type B. These data confirm that this lot contained the expected population of cells without cross-contamination. Cell viability and morphology were routinely assessed by the user during sub-culturing.

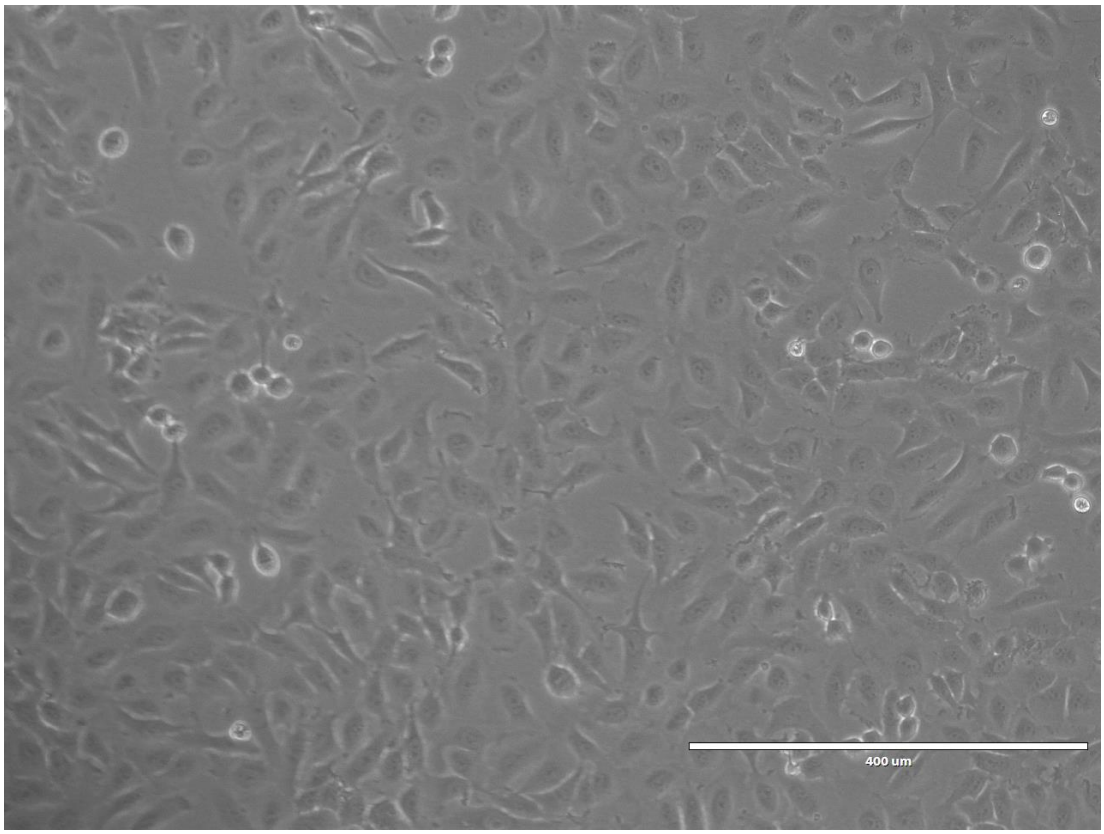

Figure 3.1: Morphology of the H4 cell-line.
Brightfield microscopy images were taken of live cells with 10x magnification. One example is given but representative of routine inspections of cells throughout this study. Cell morphology remained consistent whilst confluency varied during sub-culturing stages. Described as "epithelial-like" these cells showed polygonal shape, were adherent to the cell-culture flask and grew in a monolayer. White bar is representative of 400 µm.

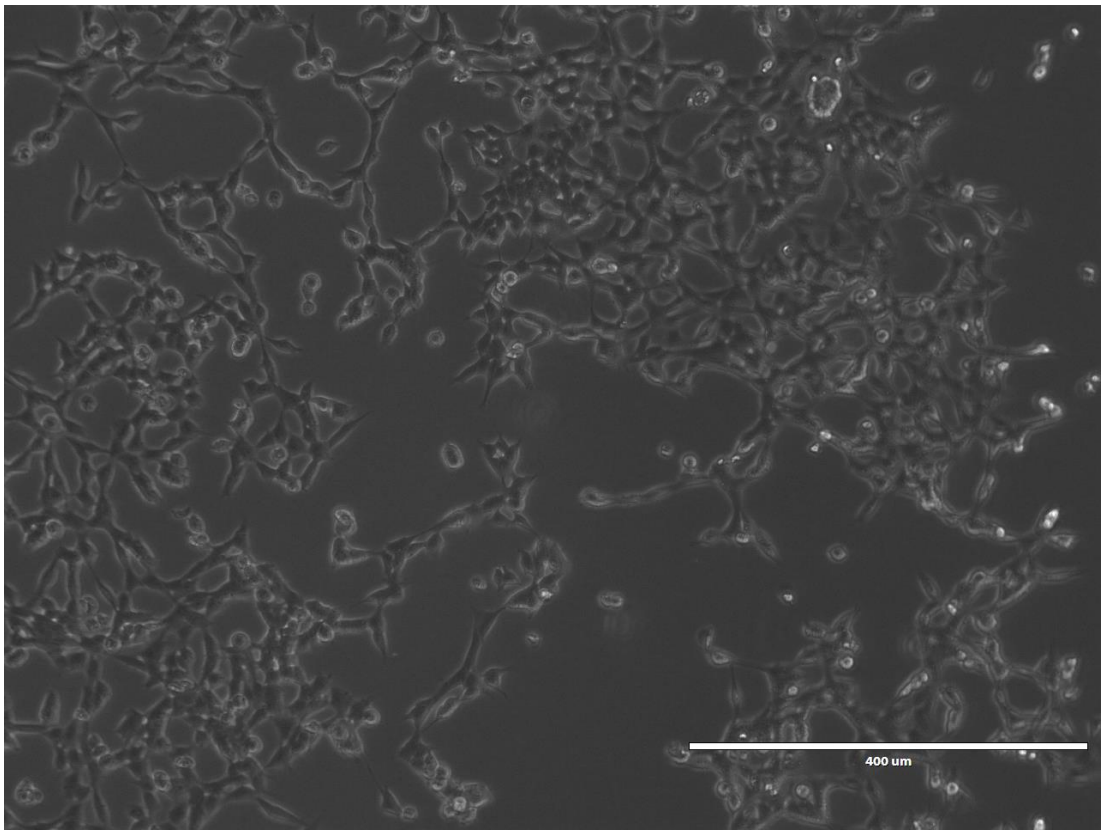

Figure 3.2: Morphology of the IMR-32 cell-line.
Light microscopy images were taken of live cells with 10x magnification. One example is given but representative of routine inspections of cells throughout this study. Cell morphology remained consistent whilst confluency varied during sub-culturing stages. Described as "neuroblast-like" these cells showed elongated shape, were adherent to the cell-culture flask and grew in a monolayer. White bar is representative of 400 µm.

3.3.2 Exosome size

Some researchers suggest that exosomes can be defined by their size: ranging from 40 -120 nm diameter (El Andaloussi et al., 2013). The H4 and IMR-32 cell-lines were tested to see if typically-sized exosomes could be isolated with standard techniques. These cells were grown as monolayers on standard tissue culture plastic with culture medium that was supplemented with exosome-depleted FBS; cell-culture medium was collected for exosome isolation. In the first instance, cell culture supernatants were cleared of cells and cellular debris by differential centrifugation (see chapter 2) and passed through 0.2 µm filters. For exosome preparation, these filtered supernatants were centrifuged at 200,000 x g for 2h, the pellet was washed with PBS and centrifuged again at 200,000 x g for 2h (Webber and Clayton, 2013). These preparations were analysed by NTA for particle size and concentration (Figure 3.3).

The particles had an average size of 81.7 ± 3.5 nm for the H4 cell-line and 62.3 ± 2.3 nm for the IMR-32 cell-line (n=6); both within the accepted range for exosomes. Furthermore, the histograms showed a uniform distribution giving the appearance of a single population of vesicles being isolated. Together these data suggest that the isolation procedure was effective in selecting the appropriate sized vesicles. This technique provided a satisfactory first evaluation of exosome size. All subsequent preparations in this study were assessed in the same way acting as a quality control measure.

A second parameter measured by NTA was particle concentration. The H4 preparation recorded an average concentration of $1.02x10^{14}$ ± $4.25x10^{12}$ particles/ml whilst the IMR-32 preparation recorded $7.02x10^{13}$ ± $2.49x10^{12}$ particles/ml (n=6) (Table 3.3). Taken in conjunction with BCA measurements of total protein these data were used to produce particle : protein ratios as an indication of the purity of the preparation (reported and discussed more fully in section 3.3.4). These ratios were $2.03x10^{10}$ for H4 and $5.06x10^{10}$ for IMR-32 which were close to the approximate $3x10^{10}$ P:P ratio to be considered of high purity (Webber and Clayton, 2013). This quality control measure was also used in all subsequent exosome preparations throughout this study. The particle concentrations were primarily used for calculating P:P ratio, rather than giving an assessment of the relative abundance of vesicles secreted by each cell-line. To do this assessment cell count data prior to exosome isolation would be required.

It is worth noting that NTA measures particles without distinguishing vesicles from other co-isolates of the same size. Therefore, other molecular analyses were also performed to confirm the isolation of exosomes and adhere to the minimal requirement guidelines recommended by ISEV (Lotvall et al., 2014).

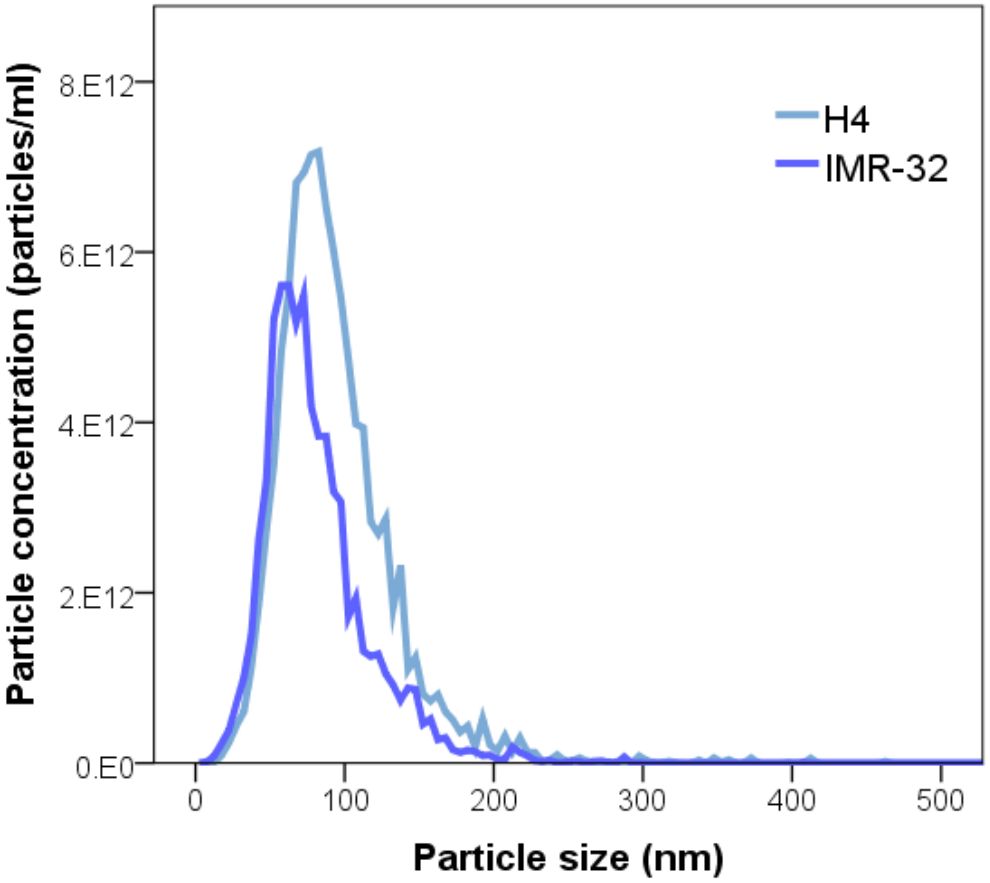

Figure 3.3: A Histogram showing overall size distribution of particles isolated from H4 and IMR-32 cell-lines.

Particle concentrations were calculated by NTA (n=6 videos per cell-line) and averaged to provide a single line for each cell-line. Size distribution plots were drawn for H4 (light blue) and IMR-32 (dark blue) exosome preparations. Average mode size was 81.7 ± 3.5 nm for the H4 cell-line and 62.3 ± 2.3 nm for the IMR-32 cell-line.

3.3.3 Exosome density

Exosomes characteristically float at a sucrose density of 1.1 – 1.2 g/ml (Escola et al., 1998, Raposo et al., 1996, Webber et al., 2014). Density gradients were produced to fractionate either H4 or IMR-32 derived vesicles using sucrose ranging from 0.2 – 2.25 M (n=1, per cell-line); this provided the appropriate density range to carry out this analysis. After an overnight ultra-centrifugation the refractive index (η) of sixteen equal volume fractions from each gradient were measured (Figure 3.4). The densities (ρ) of these fractions were calculated using a second order polynomial equation calculated from a sucrose standard curve provided by the manufacturer (Beckman-Coulter, High Wycombe, UK). The density range was 1.01 – 1.24 g/ml for the H4 gradient and 1.01 – 1.25 g/ml for IMR-32. Both of these gradients were satisfactory for identifying the presence or absence of exosomes floating at the expected density range. Due to exosome sample limitation only one gradient was performed per cell-line, therefore, the following results will be used primarily for confirming the suitability of sucrose cushion isolation which is also based on density. It would be preferable to perform three or more biological replicates to conclusively make these observations but sample limitation did not make this a possibility in this study.

The protein and particle concentration of each of the fractions was calculated by BCA assay and NTA, respectively (Figure 3.5). For the H4 cell-line, these concentrations were below the detectable range of the assays until fraction 12 which corresponded to a density of 1.16 g/ml. This continued for the remainder of the density gradient with a large concentration of particles and protein detected in fraction 16 (1.24 g/ml). This is likely to be caused by deposits of aggregated vesicles, non-vesicular particles and large protein aggregates. However, to fully clarify this, measurements of exosome-specific protein markers needed to be made.

The IMR-32 gradient showed a similar detection of particles and proteins at fraction 10 which corresponded to a density of 1.15 g/ml (Figure 3.5). Again this continued for the remainder of the density gradient before detecting high concentrations of particles and protein in fraction 16 (1.25 g/ml).

From these observations, of both gradients, it can be suggested that an abundance of material was co-isolating with exosomes and therefore being detected in the same fractions. This was particularly noticeable in fraction 16, of both gradients, that contained high concentrations of particles and proteins outside the expected density range for exosomes. NTA and BCA assay are global measures of particle and protein concentrations, respectively,

therefore non-vesicular material could be contributing to the detected signal. Further analyses of specific protein markers were performed to clarify what was being detected in each fraction.

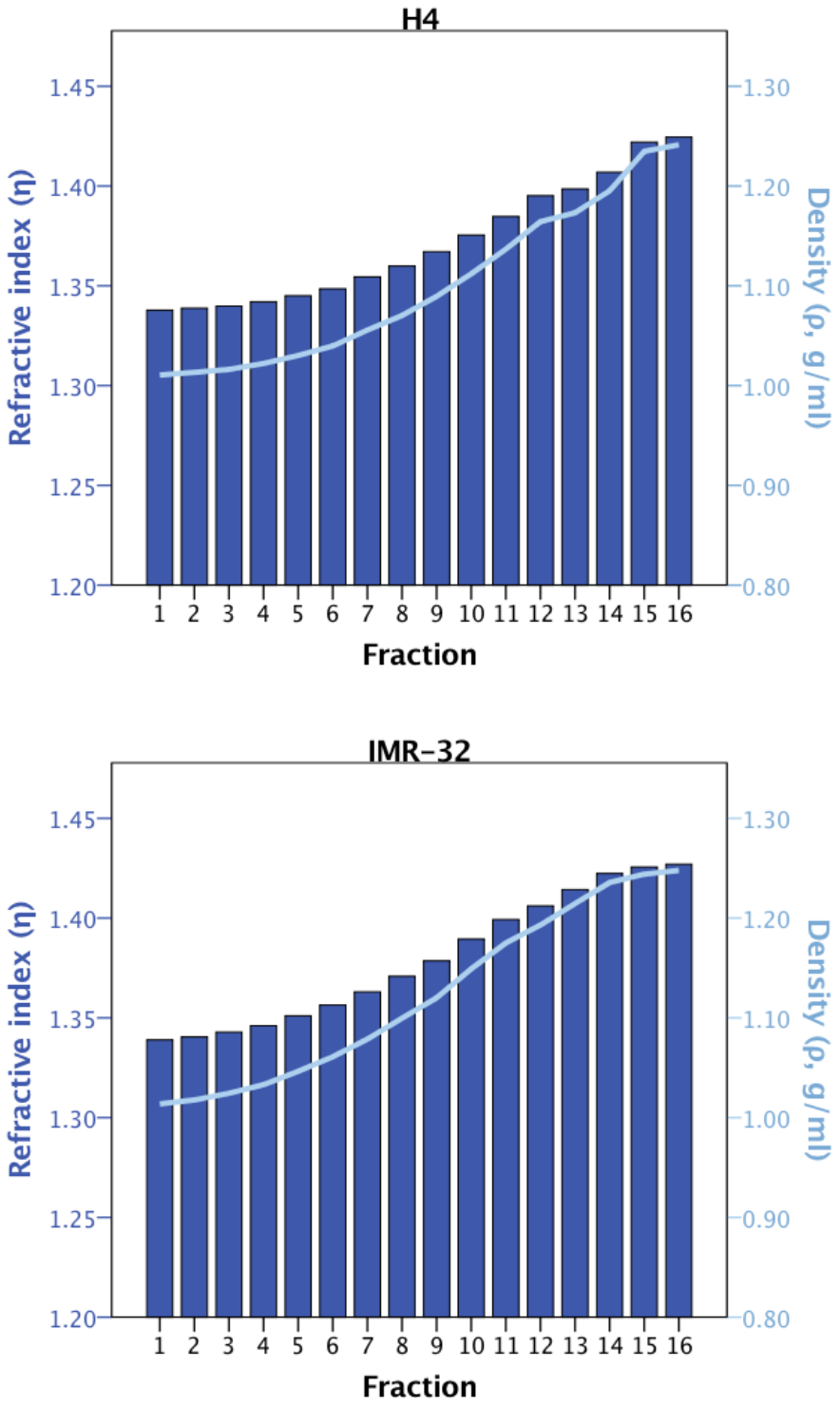

Figure 3.4: The refractive of index of sixteen fractions collected from sucrose density gradients. *Refractive indexes (η, blue bars) were measured in duplicate and the density (ρ, light blue line) of the respective fractions has been overlaid as a line for the H4 (Top) and IMR-32 (Bottom) cell-lines. The density range was 1.01 – 1.24 g/ml for the H4 gradient and 1.01 – 1.25 g/ml for IMR-32. Due to sample limitations, one gradient was run per cell-line.*

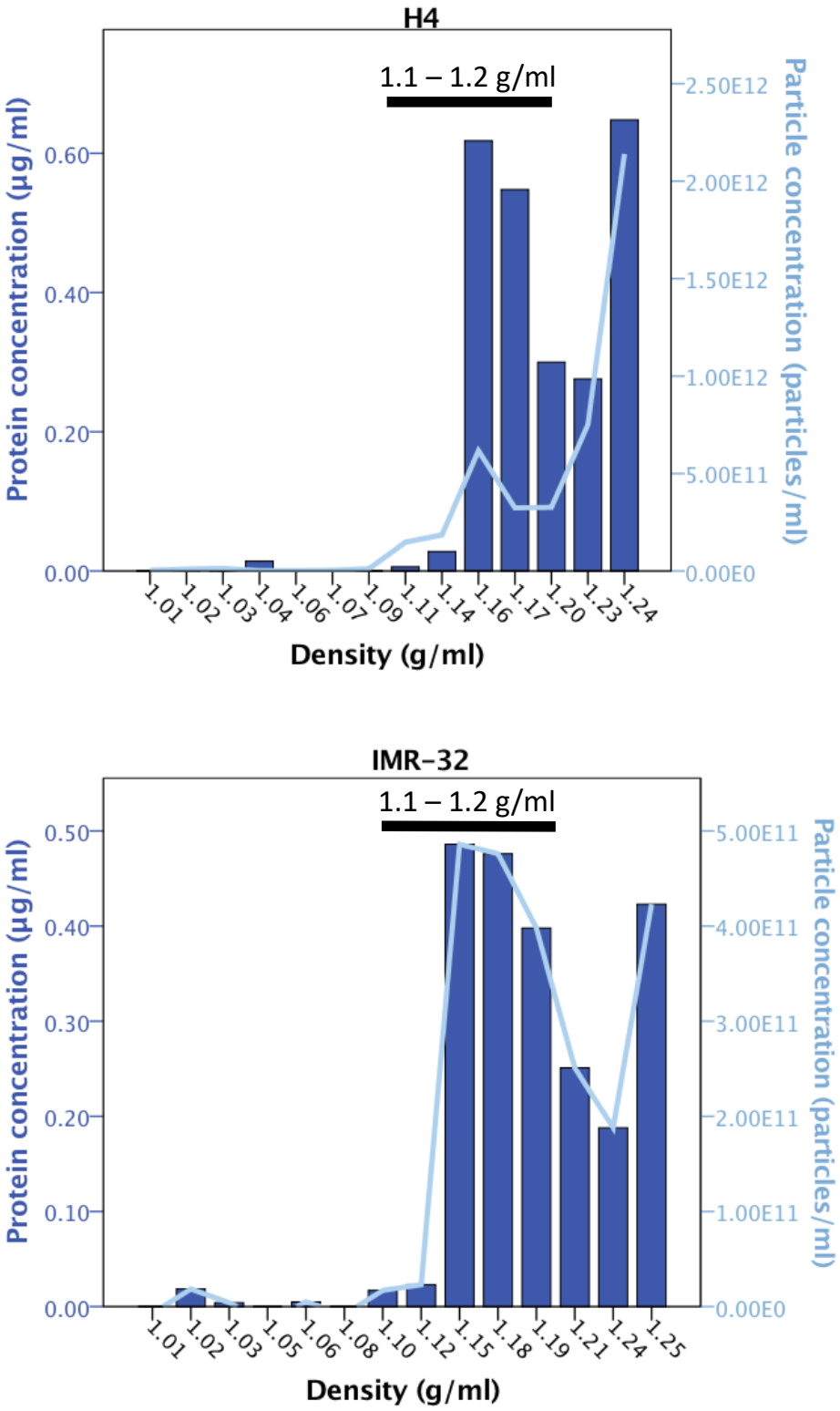

Figure 3.5: The protein and particle concentrations of sixteen fractions collected from sucrose density gradients.
Protein concentration was calculated by BCA assay (n=2) and averaged to be displayed as blue bars. Particle concentration was calculated by NTA (n=6) and averaged to be displayed as light blue lines. Due to sample limitation, one gradient was run each for the H4 (Top) and IMR-32 (Bottom) cell-lines.

To test if the material detected in these density gradient fractions comprised of exosomes, the relative concentrations of tetraspanins CD63, CD81 and CD9 were measured by a plate-based adsorption assay that measured TRF as a readout (see chapter 2).

A sharp peak was detected for all three proteins in fractions 10 and 11 for the H4 cell-line (Figure 3.6). This corresponded to a density range of 1.11 – 1.14 g/ml, as expected for exosomes. A shallow tail extended after these peaks to fraction 16. As a negative control, a mouse IgG1 antibody was used to measure non-specific background signal caused by the primary antibodies; the isotype control signal was less than 5000 TRF units in all fractions indicating minimal background signal and that the tetraspanin measurements were genuine.

These observations clarify that the high protein and particle measurements, made by BCA and NTA, in fraction 16 were not caused by exosomes (Figure 3.5). The material detected in the final fraction did not have a corresponding tetraspanin signal so is likely to have been caused by non-vesicular and large protein aggregates.

To fully determine the presence, or absence, of cellular or non-cellular contaminants direct measurements would need to have been made. For example, lipoproteins or Argonaute proteins may be present in the same fractions as the detected exosomes. Therefore, it cannot be concluded that exosomes were prepared with absolute purity.

It was only possible to perform one sucrose gradient per cell-line due to the availability of exosomes. It would be preferable to have performed additional gradients so that statistical tests could have been performed rather than the qualitative assessment performed here. Nevertheless, this confirms that exosomes can be isolated from H4 cells grown in culture and that the sucrose cushion method of isolation (Andre et al., 2002, Lamparski et al., 2002, Thery et al., 2006) is open to be used for exosome isolation with this cell-line. The advantage of using this cushion technique is that it isolates particles based on their density, yet is more readily scaled up for bulk preparations than gradient techniques. Isolation using the sucrose cushion method is less time-consuming and labour-intensive in terms of sample handling and centrifugation time. Furthermore, it has been included as part of an FDA-approved protocol for exosome isolation from dendritic cells, so a well-tested method for this purpose (Lamparski et al., 2002).

The three tetraspanins were detected in fraction 10 for the IMR-32 cell-line (Figure 3.7). This corresponded to a density of 1.15 g/ml. A broader tail extended after this peak when compared to the sharp peak observed in the H4 cell-line (Figure 3.6). This broader tail

suggests that exosomes were present in later fractions and this was likely caused by the aggregation of vesicles as well as non-vesicular and protein aggregates. It may be a particular feature of this cell-line, compared to H4, that the vesicles are more prone to aggregation. Nevertheless, accepting the caveats of sample size and being unable to rule out other contaminants, exosomes were detected in the expected density range for both cell-lines and thus subsequent preparations were predicted to be compatible with the sucrose cushion method.

These data have shown that other particles were present in the original preparations prior to density gradient separation. Therefore selecting particles based on their density should provide a purer specimen for analysis. From this point onward the sucrose cushion method of isolation was chosen as the preferred and routine method. Quality checks of subsequent exosome preparations confirmed the suitability of this method.

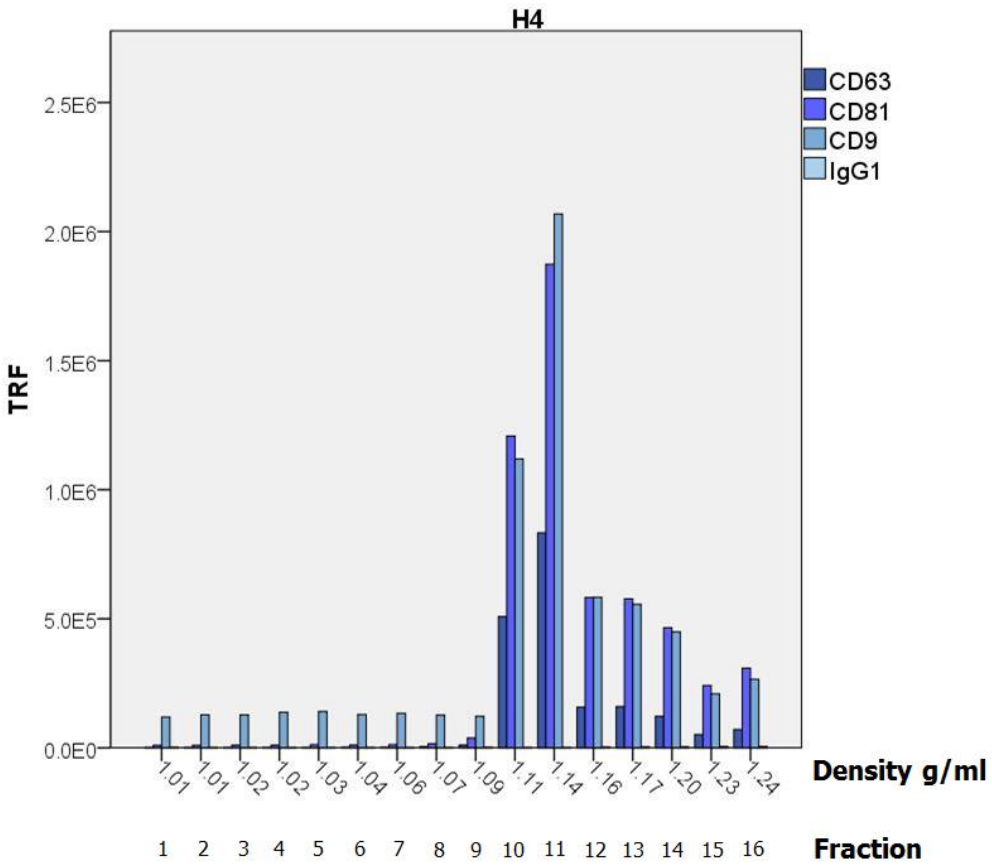

Figure 3.6: Bar chart showing relative levels of the tetraspanins CD63, CD81 and CD9 in fractions from sucrose density gradient (H4 cell-line).

Time-resolved fluorescence (TRF, y-axis) measurements were taken for H4 exosomes overlaid on a sucrose gradient (n=1). The relative levels of CD63 (navy), CD81 (dark blue), CD9 (teal) and IgG1 (turquoise) are represented as bars for each of the sixteen fractions obtained (x-axis). The density (g/ml) of each fraction is also indicated on the x-axis.

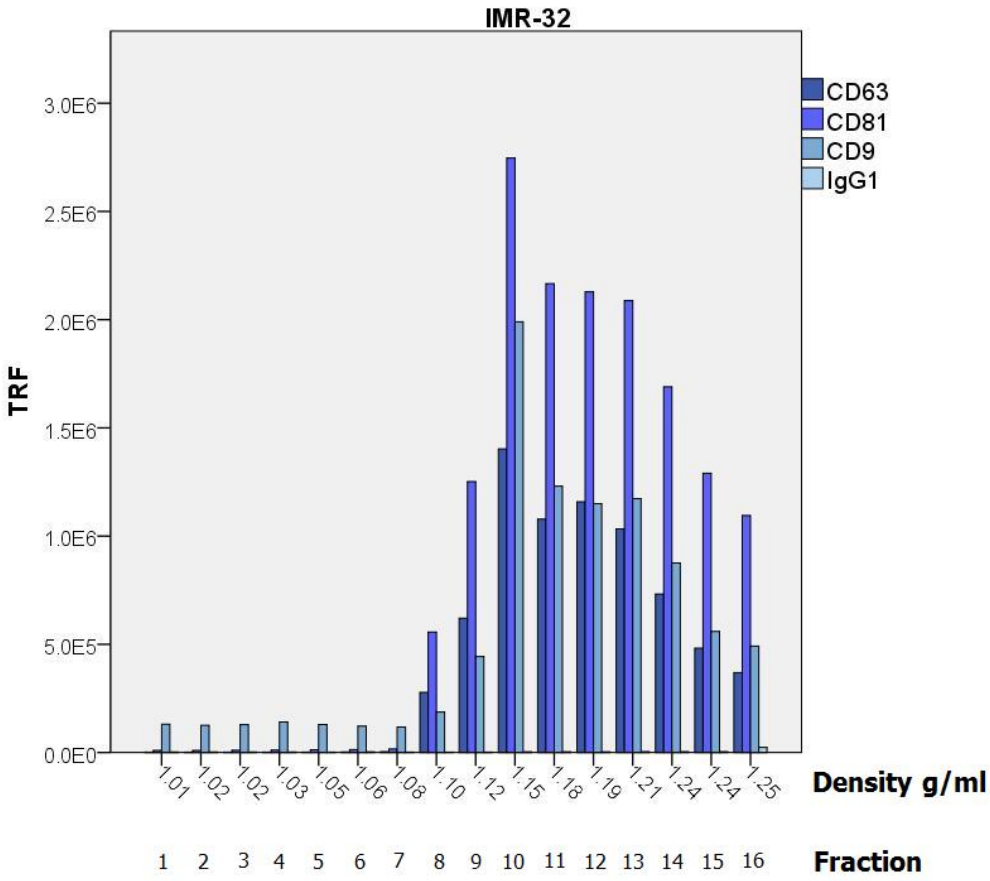

Figure 3.7: Bar chart showing relative levels of the tetraspanins CD63, CD81 and CD9 in fractions from sucrose density gradient (IMR-32 cell-line).

Time-resolved fluorescence (TRF, y-axis) measurements were taken for IMR-32 exosomes overlaid on a sucrose gradient (n=1). The relative levels of CD63 (navy), CD81 (dark blue), CD9 (teal) and IgG1 (turquoise) are represented as bars for each of the sixteen fractions obtained (x-axis). The density (g/ml) of each fraction is also indicated on the x-axis.

3.3.4 Exosome purity and protein content

The purity of exosomes isolated by different preparation techniques was assessed using a P:P ratio (Webber and Clayton, 2013). Bioreactors containing H4 and IMR-32 cell-lines were established to investigate if greater yields of exosomes could be obtained whilst sample purity was maintained by adopting the sucrose cushion method. Exosome preparations were analysed by NTA and BCA.

The media collected from 2D-cultures were subjected to the pellet and PBS wash protocol for exosome isolation whereas the bioreactor supernatants followed the sucrose cushion protocol (Andre et al., 2002, Lamparski et al., 2002, Thery et al., 2006). Particle counts were calculated to be $1.02x10^{14} \pm 4.25x10^{12}$ particles/ml for H4 and $7.02x10^{13} \pm 2.49x10^{12}$ particles/ml for IMR-32 cell-lines cultured two-dimensionally (Table 3.3). This was after 200 ml media was collected from twenty T75 flasks. Exosomes isolated from bioreactor flasks with the sucrose cushion method had particle concentrations of $4.26x10^{13} \pm 1.06x10^{12}$ particles/ml for H4 and $3.07x10^{13} \pm 1.64x10^{12}$ particles/ml for IMR-32 cell-lines. This was after 45 ml supernatant was collected.

As an assessment of the abundancy of particles in the different culture formats ratios of particles/ml media were calculated (Table 3.3). The H4 cell-line was calculated to give $5.61x10^{13}$ particles per ml media for 2D cultures compared with $1.04x10^{14}$ particles per ml media for bioreactor format. Similarly the IMR-32 cell-line produced $3.86x10^{13}$ particles per ml media for 2D cultures and $7.50x10^{13}$ particles per ml media for bioreactor format. Thus approximately double the number of particles per millilitre of media was obtained using the bioreactor format. However, these assessments of particle abundance must be interpreted carefully as the number of cells seeded into each culture format have not been accounted for. The number and viability of the cells was not determined prior to collecting the media so this comparison does not fully determine that the bioreactor format achieves greater exosome yields. Primarily, the NTA measurements were used in conjunction with protein concentrations to calculate the P:P ratio and test if purity was compromised with the bioreactor format.

To determine if purity of preparation was maintained, whilst getting these greater particle yields, protein concentrations were calculated by BCA assay. Protein concentrations were 5023 μg/ml for H4 and 1386 μg/ml for IMR-32 cell-lines cultured two-dimensionally (Table 3.3). From bioreactor flasks these concentrations were 1769 μg/ml for H4 and 1203

µg/ml for IMR-32. To assess the abundance of protein, despite lower media volumes being used in the bioreactor format, ratios of protein/ml media were calculated. The H4 cell-line produced 2.76 µg protein per ml of media in 2D format compared to 4.32 µg protein per ml of media in bioreactors. Therefore, the bioreactor format produced almost double the quantity of protein per millilitre of media compared to the 2D format. The IMR-32 cell-line produced 0.76 µg protein per ml media for 2D format and 2.94 µg protein per ml media for bioreactor. Thus, almost four times the quantity in the bioreactor format compared to 2D format. Again these assessments must be carefully interpreted as the number and viability of the cells had not been determined. Regardless, the bioreactor method was less labour-intensive, as fewer tissue culture flasks were used, and the ultra-centrifugation volumes were lower, giving the potential to scale up the size of exosome preparations. Although the benefits of the bioreactor format have been highlighted the next stage was to determine if the purity of exosome preparations had been compromised.

Using both NTA and BCA assay results, P:P ratios were calculated to assess the purity of the preparations. In 2D cultures these were $2.03x10^{10}$ particles/µg and $5.06x10^{10}$ particles/µg for H4 and IMR-32, respectively (Table 3.3). Similar ratios were observed for bioreactor cultures: $2.41x10^{10}$ particles/µg for H4 and $2.55x10^{10}$ particles/µg for IMR-32. Therefore, purity was consistent across cell-lines and culture methods and all of high purity according to Webber and Clayton (2013) who define "ratios approaching $3x10^{10}$" as being highly pure.

Cell line	Exo-Prep	Prep volume (µl)	Particle concn (particles/ml)	Particle yield (particles)	Protein concn (µg/ml)	Protein yield (µg)	P:P ratio (particles/µg)	Media volume (ml)	Particles/ml media	Protein/ml media (µg/ml)
H4	Pellet & wash	110	$1.02x10^{14}$ $\pm 4.25x10^{12}$	$1.12x10^{16}$	5023 ±804	553	$2.03x10^{10}$	200	$5.61x10^{13}$	2.76
IMR-32	Pellet & wash	110	$7.02x10^{13}$ $\pm 2.49x10^{12}$	$7.72x10^{15}$	1386 ±261	152	$5.06x10^{10}$	200	$3.86x10^{13}$	0.76
H4	Sucrose cushion	110	$4.26x10^{13}$ $\pm 1.06x10^{12}$	$4.69x10^{15}$	1769 ±87	195	$2.41x10^{10}$	45	$1.04x10^{14}$	4.32
IMR-32	Sucrose cushion	110	$3.07x10^{13}$ $\pm 1.64x10^{12}$	$3.38x10^{15}$	1203 ±4	132	$2.55x10^{10}$	45	$7.50x10^{13}$	2.94

Table 3.3: Protein and particle yield of exosomes isolated from H4 and IMR-32 cell-lines.
Protein concentrations were calculated using BCA assay (n=2) and particle concentrations by Nanoparticle Tracking Analysis (n=6). Average concentrations are displayed with standard deviations. Particle:protein (P:P) ratios were calculated for each preparation by dividing the concentration of particles by the protein concentration. Particles isolated by a pellet and wash protocol correspond to 2D-cultures where 200 ml media was collected from twenty T75 flasks for one preparation. Particles isolated by the sucrose cushion method correspond to supernatants collected from bioreactor flasks on three occasions and pooled into one preparation. These volumes were used to calculate yields of particles and proteins per millilitre of media.

To fully validate that exosomes were being isolated, analysis of specific proteins was performed. Immuno-phenotyping of whole cell lysates, exosome preparations and exosome-free supernatants was performed by a plate-based adsorption assay that measured TRF as a readout. The primary assessment was for enrichment of protein markers in exosomes compared to the source cell. Comparison with exosome-free supernatants provided an additional assessment of the concentration of target protein from the culture medium. 1 µg of protein was loaded per well and TRF measurements made in duplicate. Sample sizes were limited by the availability of exosomes so a qualitative assessment of protein enrichment was performed.

Across both cell-lines the tetraspanins CD63, CD81 and CD9 were enriched in exosome preparations over cell lysates and exosome-depleted media (Figure 3.8), as expected (Lotvall et al., 2014). Exosome sample was a limitation in this experiment so only 2 replicates could be performed, however, it would have been ideal to do 3 repeats so that statistical analyses could be applied. With the caveat of sample size highlighted, these observations validated the sucrose cushion method to be used for the isolation of exosomes from these cell-lines. The low measurements, less than 5000 TRF units, observed in the exosome-free supernatant suggest that there was minimal target protein present and that the isolation method was efficient. This TRF method of immuno-phenotyping measures the protein content of exosomes in their non-reduced, native state therefore only proteins present on the vesicle surface were compared.

To investigate the relative concentrations of intra-luminal proteins, exosomes and whole cell lysates were reduced in 20 mM DTT and boiled in SDS-reducing buffer to liberate intra-luminal and intra-cellular proteins for Western Blot analysis. 20 µg of protein was reduced, loaded per well (n=1) and the relative concentrations of ALIX, TSG101 and GRP94 were measured (Figure 3.9). ALIX and TSG101, were enriched in the exosome wells as expected (Stoorvogel et al., 2002, Roucourt et al., 2015, Stoorvogel, 2015). GRP94, primarily found in the endoplasmic reticulum, was present in both cell lysates, had a reduced signal in the IMR-32 exosomes and was undetected in the H4 exosomes. This suggests that there was no cellular contamination in the H4 exosome preparations and minimal contamination in the IMR-32 preparations. However, both exosome preparations were performed identically so another explanation may be that GRP94 is mal-distributed in IMR-32 cells. To conclusively determine the extent of contamination in these samples would require a direct measurement of other proteins.

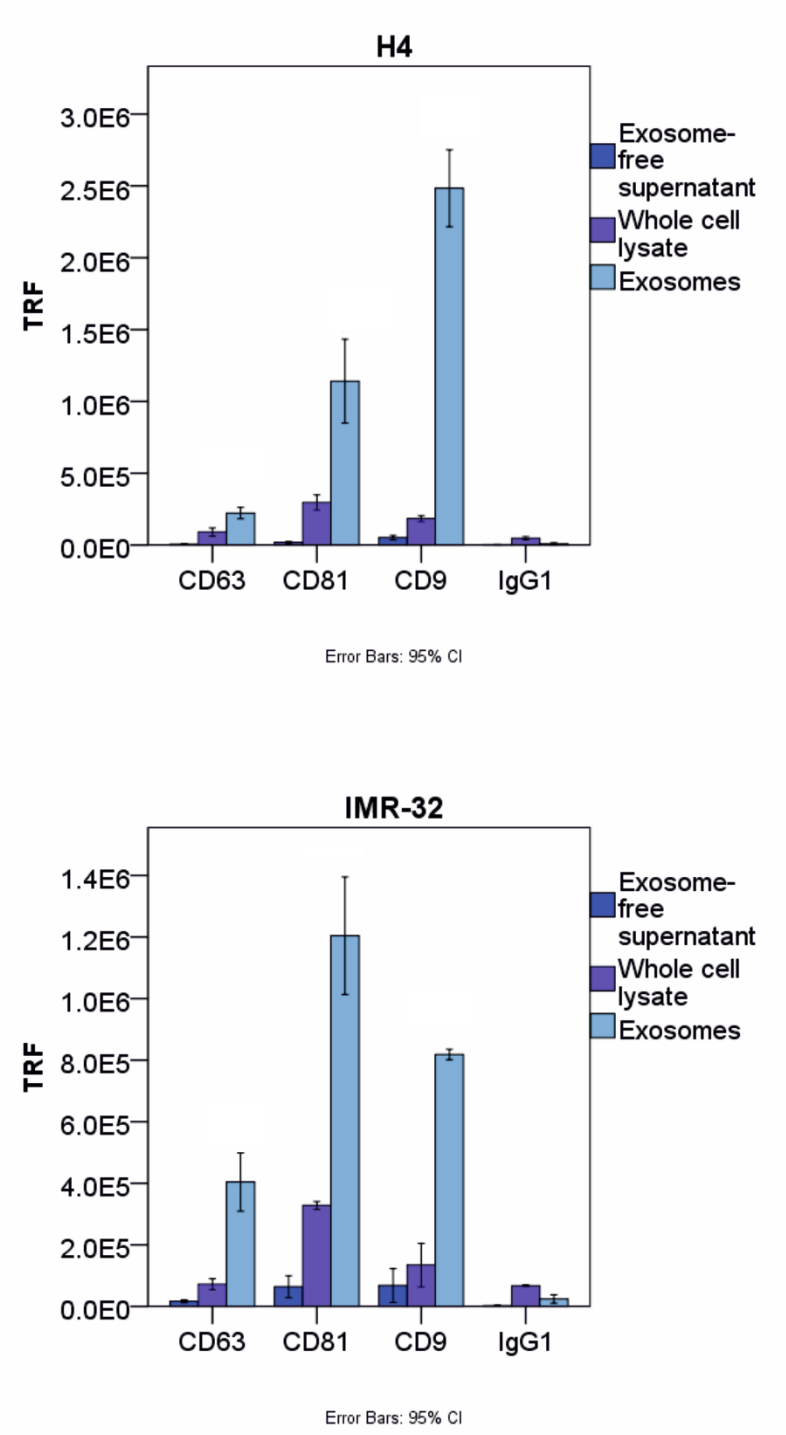

Figure 3.8: Relative concentrations of CD63, CD81 and CD9 tetraspanins in H4 (top) and IMR-32 (bottom) cell-lines.

Exosomes were prepared by the sucrose cushion method of isolation and Time-resolved fluorescence (TRF) measurements recorded with whole cell lysates and supernatants (n=2 per protein). Each bar represents averaged measurements and error bars represent 95% confidence intervals. Navy bars represent exosome-free supernatant, purple bars represent whole cell lysates and light blue bars represent exosomes.

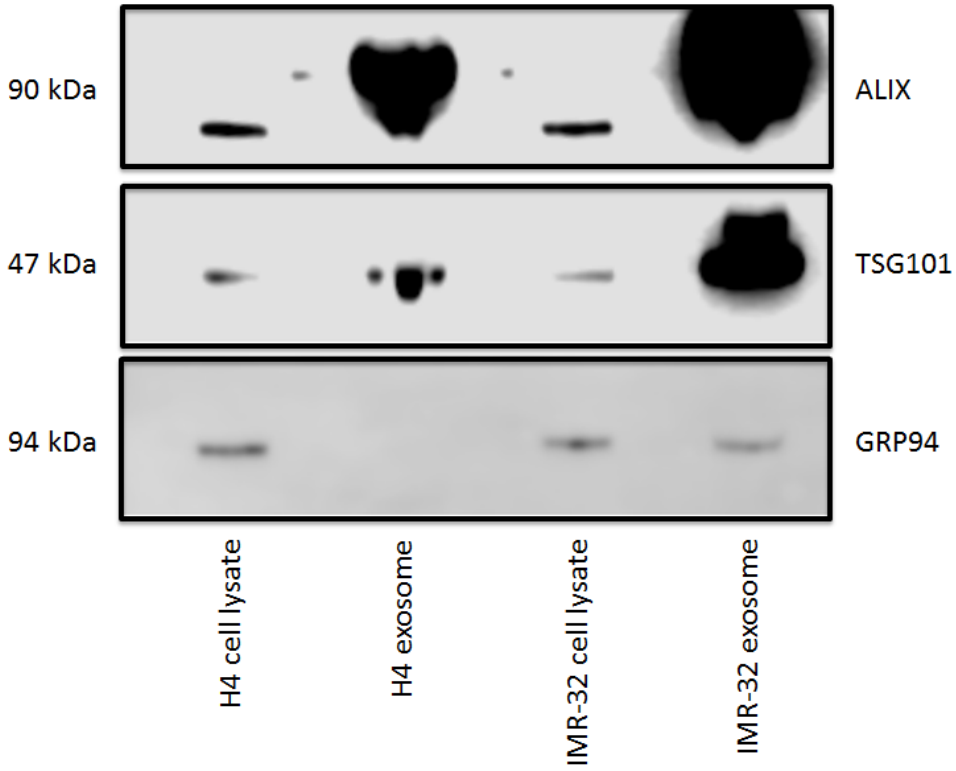

Figure 3.9: Western blots showing relative levels of ALIX, TSG101 and GRP94 with 20 µg total protein loaded into each well.

The relative concentrations of ALIX, TSG101 and GRP94 were visualised by enhanced chemiluminescence. Band sizes are indicated on the left side in kilodaltons (kDa). Cell lysates and exosome preparations were obtained for the H4 (left two lanes) and IMR-32 (right two lanes) cell-lines (n=1).

3.3.5 Exosome structure

NTA has already revealed that exosome preparations from H4 and IMR-32 culture medium were of the correct size. However this method, using light scattering from a laser source, has insufficient resolution to provide any structural detail on the particles present. To provide this detail cryo-EM was performed.

Exosome preparations, for both cell-lines, were transferred to CIC bioGUNE, Bilbao, Spain for cryo-EM, thanks to collaboration with Dr David Gil Carton and Professor Juan M. Falcón-Pérez. 5 µl of each exosome preparation was directly adsorbed onto glow-discharged holey carbon grids (QUANTIFOIL). Grids were blotted at 95% humidity and rapidly plunged into liquid ethane with the aid of VITROBOT (Maastricht Instruments BV). Vitrified samples were imaged at liquid nitrogen temperature using a JEM-2200FS/CR transmission cryo-electron microscope (JEOL), equipped with a field emission gun and operated at an acceleration voltage of 200 kV (Welton et al., 2016). This methodology aims to preserve the native vesicle structure, without the need for fixatives or embedding that may cause dehydration and vesicle collapse. Heterogeneous populations of vesicles of spherical structure with unilaminar lipid bilayers were visualised for both cell-lines (Figure 3.10). No cup-like artefacts were present as previously been seen with TEM (Wu et al., 2015).

There was some heterogeneity in the size and appearance of the structures visualised but little evidence of non-vesicular contamination. A general observation was that H4 exosomes were larger in size than IMR-32 which would be consistent with the NTA data (Figure 3.3). However, a detailed analysis was not performed on a sufficient number of micrographs to confirm this general observation. Overall, these images confirmed that exosomes of the correct structure and size were isolated.

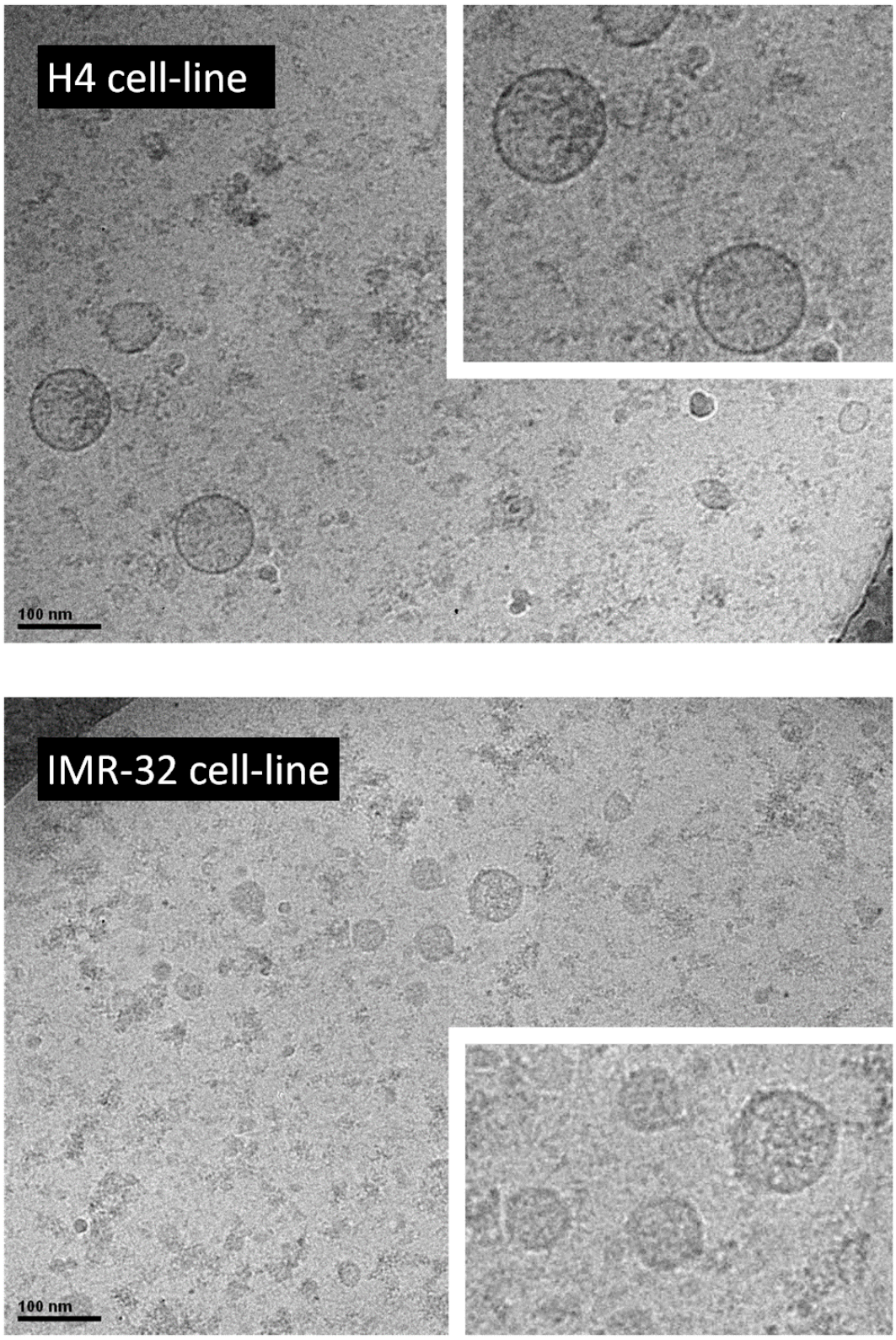

Figure 3.10: Cryo-electron micrographs of H4 and IMR-32 exosomes.
Exosome preparations were made using the sucrose-cushion isolation procedure. A heterogeneous population of vesicles of spherical structure with unilaminar lipid bilayers was observed for both H4 (top) and IMR-32 (bottom) cell-lines. Images are representative of numerous micrographs obtained by the Falcon-Perez group.

.

3.4 Discussion

This chapter aimed to establish cell cultures from neural sources and validate procedures for isolating exosomes from the media. H4 and IMR-32 cell-lines were successfully cultured in traditional 2D and high-density 3D formats. Exosome preparations were thoroughly characterised before upscaling using the bioreactor format of cell culture coupled with sucrose cushion isolation. This has provided the materials and methodology for bulk-exosome collection for subsequent chapters in this study.

Exosomes, from both cell-lines were of the expected size (El Andaloussi et al., 2013) measured by NTA and cryo-EM. The structure of the exosomes was also determined by cryo-EM and, for both cell-lines, spherical shaped vesicles with a unilaminar lipid bilayer were observed. Sucrose density gradients determined that the exosomes were buoyant at the expected density of 1.1 - 1.2 g/ml (Escola et al., 1998, Raposo et al., 1996, Webber et al., 2014). These density data were a pre-requisite for routinely using the sucrose cushion method of isolation (Andre et al., 2002, Lamparski et al., 2002, Thery et al., 2006). The relative expression of different proteins were compared between exosome preparations and whole cell lysates. Exosomes were significantly enriched for the tetraspanins CD63, CD81 and CD9, as expected (Escola et al., 1998) and enriched for intraluminal ALIX and TSG101, as expected (Stoorvogel et al., 2002, Roucourt et al., 2015, Stoorvogel, 2015). Furthermore, GRP94, typically expressed in the endoplasmic reticulum, was less abundant in exosome preparations compared to whole cell lysates indicating that the preparations were relatively devoid of cellular contamination, although, this was more conclusive for H4 exosomes than IMR-32 exosomes (Lotvall et al., 2014).

A comparison has been made between exosomes isolated from 2D cell cultures and bioreactor culture format. Across both cell-lines greater yields of particles and protein were obtained from bioreactor cultures per millilitre of culture medium. These observations should be carefully interpreted as the number and viability of cells was not assessed. Therefore, the particle and protein concentrations were primarily used to produce a P:P ratio and this showed that vesicle purity was not compromised using the bioreactor format.

These observations, of yield and purity, are particularly useful when considering the scalability of the different cell culture options. The limiting step in exosome isolation is the volume of media that can be processed on the ultra-centrifuge. By reducing the volume of media in bioreactor cultures, yet maintaining vesicle purity, there is far more scope to scale

these cell-lines up for high yield isolation of neural-derived exosomes. Other benefits of the bioreactor technique include reduced incubator space and far easier handling of fewer cell-culture vessels.

A caveat of using the bioreactor technique is that the cells are cultured in a high densities. This is likely to cause a more stressful environment than standard 2D-culture and the cells may be hypoxic (Mitchell et al., 2008a). However, the characterisation of exosomes in this study has shown that the benefit of this technique is that increased yields can be produced by scaling up this culture method, without compromising on vesicle purity. Furthermore, the H4 and IMR-32 cell-lines coped in culture as bioreactor flasks were established and maintained for over 6 months.

It is likely that other cell-types may not cope with this culture technique; for example, primary cells may reach senescence within the time frame of 6 months, dependent on the seeding passage and tissue-type. Therefore, whilst accepting the caveats of high density cell culture, this method, of culturing H4 and IMR-32 cells in bioreactor flasks, provided an abundant source of exosomes without compromising on sample purity.

Demonstrating the compatibility of these cell-lines with bioreactor culture, and the methods for isolating exosomes, offers potential for future studies. For example, it may be possible to culture H4 cells, harbouring AD-relevant mutations, in bioreactor vessels for the high yield production of exosomes. The H4 cell-line has been used previously to stably express a mutant form of the *APP* gene (Sung et al., 2016). This may be a particularly relevant line of inquiry if an endocytosis-related gene, such as *CD2AP*, is perturbed; this has been demonstrated in HEK293 cells (Kwon et al., 2016). However, these examples are beyond the scope of this study and, primarily, the aim was to validate the methods of mass-producing neural-derived exosomes.

Procedures have been established for the production and isolation of neural-derived exosomes *en masse*. The exosomes have been thoroughly characterised by size, density, protein content and structure, in keeping with minimal experiment requirements published by Lotval *et al.* (2014). This provided the neural-derived exosome stocks, and methodologies of isolation, required for subsequent chapters.

Chapter 4. Affinity capture of neural-derived exosomes

4.1 Introduction

Exosomes are present in the peripheral circulation (Kalra et al., 2013) but represent a number of sub-populations from different cell-types within perfused tissues/organs. For example, exosomes have reportedly been secreted by hepatocytes (Hirsova et al., 2016), dendritic cells (Kowal et al., 2016), adipocytes (Connolly et al., 2015), cardiomyocytes (Garcia et al., 2015), prostate (Hosseini-Beheshti et al., 2016), myoblasts (Choi et al., 2016), osteoblasts (Cui et al., 2016), keratinocytes (Lo Cicero et al., 2015a), astrocytes (Ipas et al., 2015), platelets (Tan et al., 2016), lymphocytes (Bosque et al., 2016) and endothelial cells (Li et al., 2016b). Exosomes secreted by these cell-types, and others, collect in biological fluids to become a vastly heterogeneous population. Many studies have isolated cell-types of interest to be cultured *in vitro* for the isolation of cell type-specific exosomes. However, the collection of vesicles originating from a particular cell-type directly from complex biological fluids remains a challenging prospect.

The isolation of cell type- or tissue-specific exosomes is desirable for identifying disease-relevant biomarkers. Exosomes have been implicated in a number of different diseases including neuroglioma (Skog et al., 2008), prostate cancer (Royo et al., 2016), pancreatic cancer (Melo et al., 2015), breast cancer (Green et al., 2015), heart disease (Iaconetti et al., 2016), and Alzheimer's disease (Rajendran et al., 2006). It is feasible that by selecting a sub-population of exosomes relevant to the tissue of disease then biomarker studies could be improved by reducing the noise carried by other, unwanted tissue types.

Affinity systems for capturing vesicles based on proteins that are exhibited in high densities on the exosome surface, such as the tetraspanins CD9 or CD63, have already been developed and reported for use with numerous sources including cell-cultures (Wiley and Gummuluru, 2006), urine (Duijvesz et al., 2015) and plasma (Zarovni et al., 2015). Adopting disease-specific ligands has also been reported. For example, an 8-amino-acid peptide aptamer to capture HSP70+ exosomes from multiple cancers (Gobbo et al., 2016) and the A33 protein in colorectal cancer (Mathivanan et al., 2010). Capturing vesicles based on the expression of Neural Cell Adhesion Molecule (NCAM) and L1 Cell Adhesion Molecule (L1CAM) has been used to identify disease biomarkers relevant to the central nervous system (CNS) (Fiandaca et al., 2015, Goetzl et al., 2015b).

A possible utility of capturing vesicles from a sub-population of cells is to then measure a readout that is indicative of a diseased tissue. This has been the case in studies performed at

the Goetzl laboratory where neural-derived exosomes were isolated from plasma for the study of Alzheimer's disease (AD). Using this method, a case-control analysis revealed elevated levels of total tau, P-S396-tau, P-T181-tau and amyloid-β 1-42 in AD (Fiandaca et al., 2015). These proteins represent the state of diseased brain tissue where neurofibrillary tau tangles and amyloid-β (Aβ) plaques are pathological hallmarks (Forman et al., 2004). Furthermore, these proteins are also elevated in patient CSF (Bateman et al., 2012) and it has been suggested that proteins, such as Aβ, are pathologically active in the CNS prior to clinical manifestation (Villemagne et al., 2013). Therefore, it is particularly noteworthy that exosomal Aβ1-42 was significantly elevated in the plasma of both AD and pre-clinical groups over controls (Fiandaca et al., 2015). Thus, the isolation of neural-derived exosomes has the potential for identifying biomarkers of clinical and pre-clinical AD.

Nevertheless, one could argue that selecting a sub-population of exosomes may not be an appropriate route to biomarker discovery. By selecting one population it is possible that only a small fraction of disease-relevant vesicles is isolated and key information can be lost from other relevant, but unexpected, sources. For example, in AD, there is increasing evidence that the immune system could play a pathological role. One such study reported increased *TREM2* expression in peripheral leukocytes for AD patients over controls (Mori et al., 2015). Given that the relationship between exosomes and AD remains largely unknown, it is difficult to be certain of what sub-population(s) is disease-informing. Additionally, the isolation or profiling methods may yield insufficient quantity of the specimen for analysis. Affinity selection can miss the identification of important, pathologically-relevant processes, such as the role of inflammation, and as such a systems-wide examination of disease may be useful. For example, small RNA sequencing of exosomes isolated peripherally, from plasma and serum in different studies, without enrichment of sub-populations, has determined potential miRNA candidates for AD biomarkers (Cheng et al., 2015, Lugli et al., 2015).

Therefore, developing an affinity isolation method for neural-derived exosomes could be of benefit for identifying biomarkers of AD. By enriching for the tissue-type of known relevance to disease it should be easier to discover disease-associated changes in patient samples. However, the relevance of adopting a systems-wide approach should not be disregarded.

4.2 Aim

The aim of this chapter was to develop a means of affinity-isolation of neural-derived exosomes from cell culture medium. To achieve this aim the following objectives were addressed:

- Identify proteins that are selectively expressed in the human brain.
- Identify commercial antibodies that may have utility in capturing neural-derived exosomes.
- Screen cell-cultured exosomes for vesicle surface proteins also expressed in the human brain.
- Using information from the objectives above, establish a micro-titre plate assay for selectively capturing neural-derived exosomes from cultured cell-lines that could be of future use with biological fluids.

4.3 Results

4.3.1 *In silico* selection of protein candidates

To address the aim of isolating neural-derived exosomes, a selective feature of this vesicle population needed to be identified. Proteins present on the surface of exosomes represent the source cell, to a large extent, and thus provide features that could be exploited for affinity capture. The CNS contains a plethora of proteins, such as neurotransmitter receptors and cell surface adhesion molecules, which are selectively expressed in those tissues. Therefore, a number of *in silico* steps were followed to identify a shortlist of candidates that had good potential for the isolation of neural-derived exosomes.

The first pre-requisite for selecting protein candidates was to ensure that they were selectively expressed in tissues of the CNS. The Genotype-Tissue Expression (GTEx) Project (release: 2014-01-17 (dbGaP phs000424.v4.p1)) was accessed to test this. The GTEx project was chosen because it is a publically available dataset that has used microarray and next-generation sequencing to measure global RNA expression across a comprehensive range of tissues. The online browser, http://www.gtexportal.org/home/ (accessed April 2014), was used to search for tissue-specific gene expression of potential protein candidates. The gene expression plots across the tissue range were downloaded and assessed for preferential expression in brain tissues. The tetraspanin *CD9*, an exosome protein marker, showed constitutive expression throughout the tissues analysed and therefore, as expected, would

be a poor candidate for the basis of selective exosomes isolation (Figure 4.1). *CD9* was particularly strongly expressed in the oesophagus, salivary gland, vagina and bladder so particularly representing a feature of mucosal surfaces. Relative to other tissues *CD9* was less abundantly expressed in brain tissues.

Seven candidates, however, showed CNS-enriched expression, namely *ENO2, GFAP, GRIA4, GRID1, L1CAM, NCAM* and *NMDAR1* (Figure 4.1). Of these candidates, *GFAP* and *NMDAR1* showed highly selective expression in brain tissues and undetectable expression in tissues outside of the CNS, therefore ideal for affinity selection. *GFAP* was particularly strongly expressed in the spinal cord and *NMDAR1* was strongly expressed throughout the brain tissues but enriched in cortical regions, which could be particularly relevant for AD as this is a pathological site of degenerating neurons, Aβ plaques and tau tangles (Zilka and Novak, 2006). *GRIA4* and *ENO2* were also highly selectively expressed in brain tissues and had minimal detectable signal in other tissues. *GRIA4* was strongly expressed in cerebral tissues with relatively low expression in mammary tissue of the breast, the pituitary gland, the small intestine and the stomach. *ENO2* also showed enriched expression in cerebral tissues and a relatively low expression across the range of other tissues. Three of the candidates showed less selective expression than the others but, nevertheless, would be good candidates for enriching for exosomes of a CNS source. *L1CAM* showed enriched expression in cerebral tissues and detectable expression in the Tibial nerve, colon and oesophagus. *GRID1* was enriched in brain tissues but had relatively high expression in the cervix and uterus. Similarly, *NCAM* had a good discriminatory signal in the CNS but only a small margin of difference with the expression in the heart. Together, *L1CAM, GRID1* and *NCAM* may be good candidates to enrich for exosomes of a CNS source but may introduce exosomes from other tissues outside of the CNS. Overall, these seven candidates had satisfactory expression profiles to take further into assay development and have also highlighted that different tissues within the CNS could potentially be selected, for example, *GRIA4* was particularly strongly expressed in the cerebellum whilst *NMDAR1* was strongly expressed in the cortex.

The next important feature to be assessed was cellular localisation. The downstream application would be an assay that captures intact exosomes without permeabilisation of the membrane, so suitable protein candidates would need to expose antigens on the exterior surface of the exosome. The cellular localisation of the seven protein candidates was investigated using the UniProt database (www.uniprot.org, accessed April 2014). This was chosen because it is a publically available database that contains protein sequence and functional information. Six of the seven candidates were confirmed to be membrane-bound

or transmembrane and thus potentially could localise to the surface of vesicles (Table 4.1). GFAP was an exception, as it was a cytoskeletal protein and less likely to be present on the exterior surface of the exosome. However, components of the cytoskeleton may well interact in the biogenesis and secretion of exosome (Hurwitz et al., 2016) so GFAP was not excluded at this stage.

To confirm if these candidates had already been identified on the surface of exosomes the ExoCarta database was accessed (http://exocarta.org/, accessed April 2014). ExoCarta is a database of lipids, RNA and proteins associated with exosomes from different species. The seven candidates were searched for by their gene symbol to confirm if they had been previously identified in humans. Five of the seven had entries (ENO2, GFAP, GRID1, L1CAM, and NCAM) on ExoCarta (Table 4.1). However, GRIA4 and NMDAR1 were still included in this study as they may represent novel exosomal proteins.

Finally, commercial retailer websites (for Abcam and Santa Cruz) were accessed to identify antibodies against the human protein orthologue. Antibodies were chosen where the immunogen was situated on an extracellular portion of the protein because these would have a greater potential to bind to the exterior of exosomes in a capture conformation (Table 4.1). Where possible, antibodies were chosen with carrier-protein free buffer, such as GRID1 which only used PBS. However, all antibodies except for GRID1 had some element of carrier protein in the buffer, for example, sodium azide in GFAP buffer and BSA in NCAM buffer. It is foreseeable that these carrier proteins may cause a blocking effect in downstream assay development so are noted as potentially limiting. Unfortunately, carrier proteins are commonly used in antibody buffers so difficult to avoid. Therefore, the assay was developed as systematically as possible using these antibodies.

Where amino acid residues were stated for the immunogen site, UniProt was cross-referenced again for the protein topology. This confirmed that the antibody would target extracellular protein domains for GRIA4, GRID1 and NMDAR1, therefore, likely to be on the exterior surface of exosomes.

Figure 4.1: Gene expression plots accessed from GTEx Project (release: 2014-01-17 (dbGaP phs000424.v4.p1).
Gene expression is reported in Reads Per Kilobase of transcript per Million mapped reads (RPKM, y-axis) for different tissues (x-axis) using the searchable GTEx portal database. Median is displayed with 25th and 75th quartiles, and outliers marked as circles.

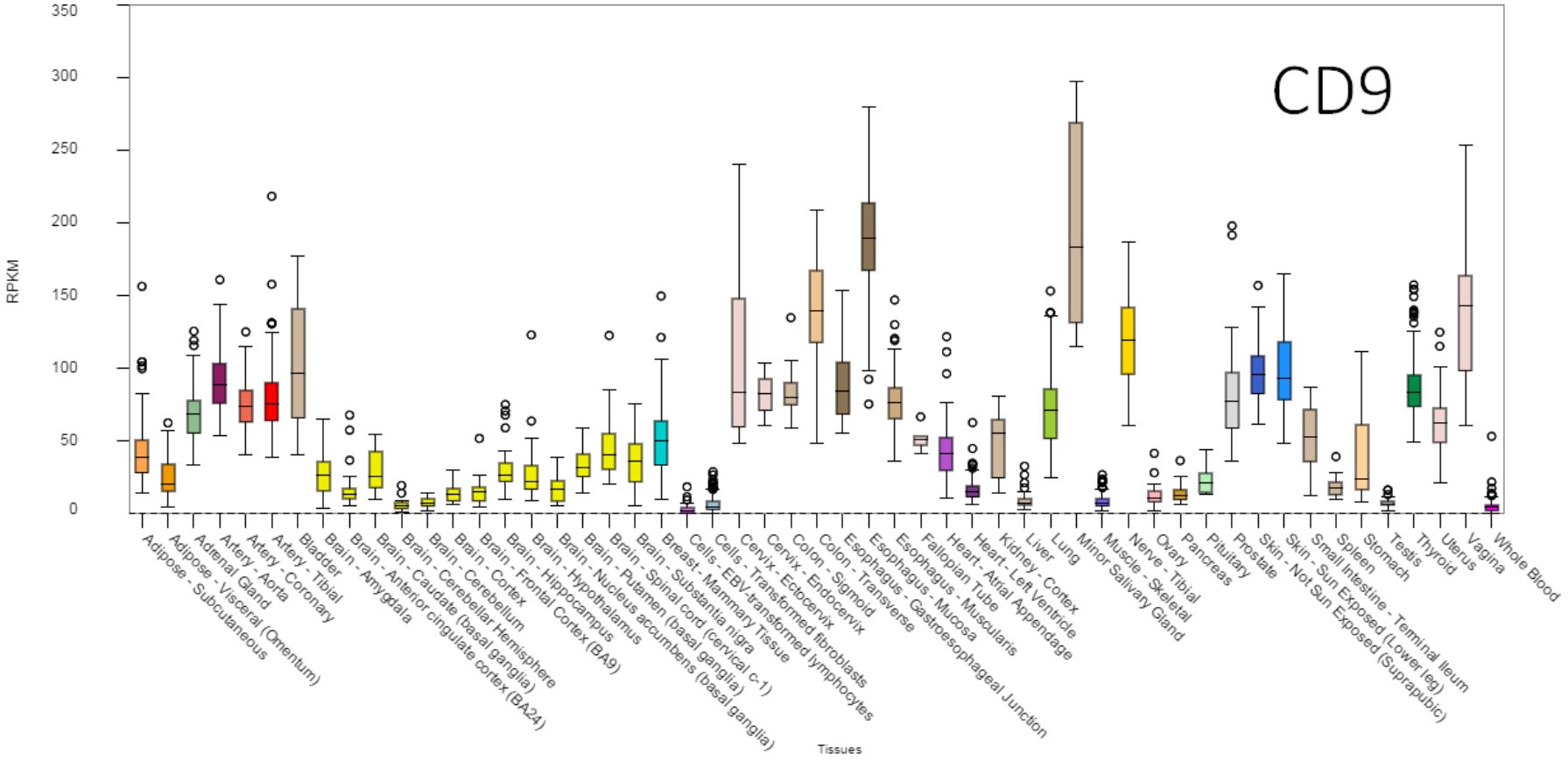

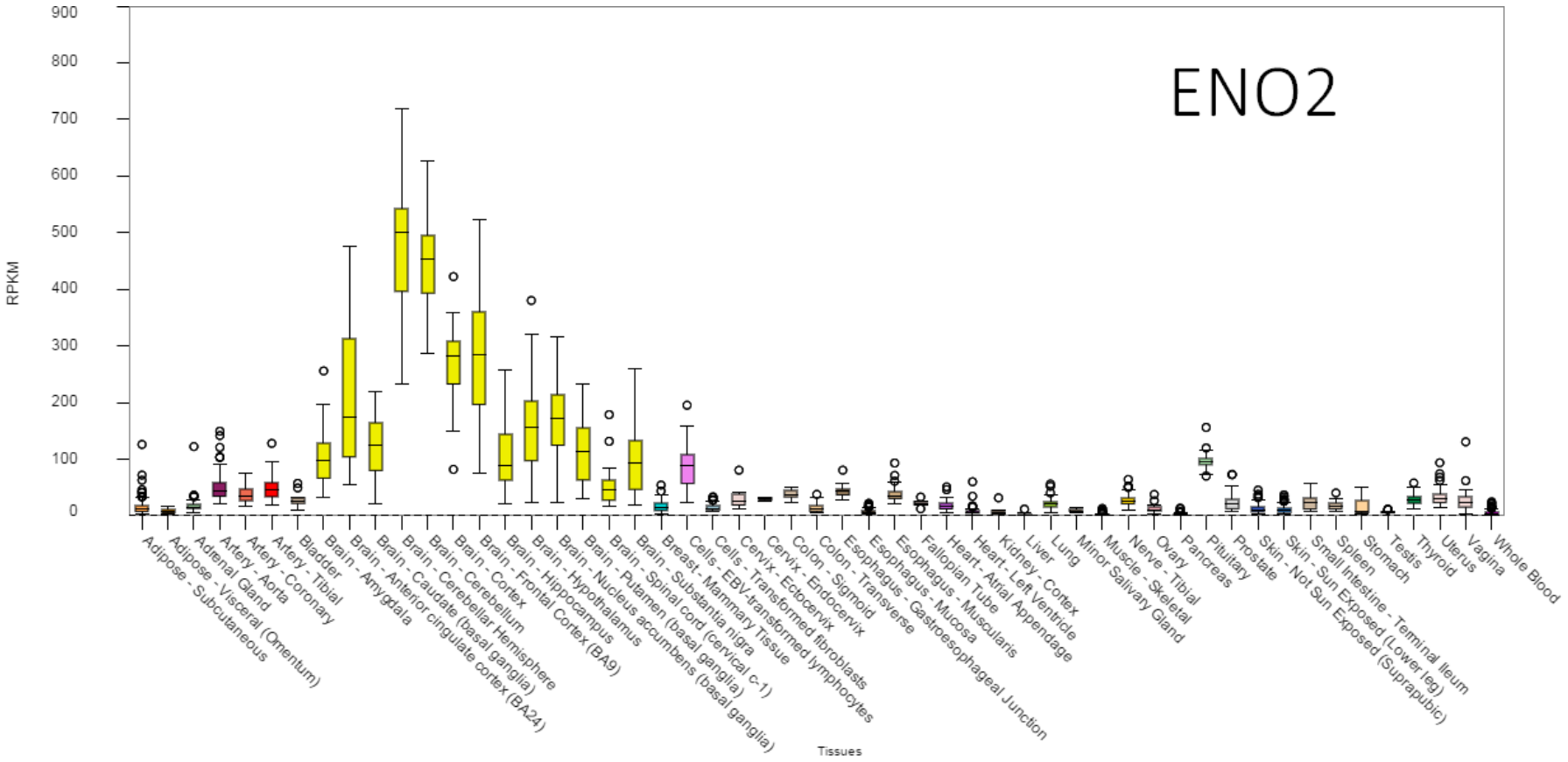
ENO2
RPKM
900
800
700
600
500
400
300
200
100
0
Adipose - Subcutaneous
Adipose - Visceral (Omentum)
Adrenal Gland
Artery - Aorta
Artery - Coronary
Artery - Tibial
Bladder
Brain - Amygdala
Brain - Anterior cingulate cortex (BA24)
Brain - Caudate (basal ganglia)
Brain - Cerebellar Hemisphere
Brain - Cerebellum
Brain - Cortex
Brain - Frontal Cortex (BA9)
Brain - Hippocampus
Brain - Hypothalamus
Brain - Nucleus accumbens (basal ganglia)
Brain - Putamen (basal ganglia)
Brain - Spinal cord (cervical c-1)
Brain - Substantia nigra
Breast - Mammary Tissue
Cells - EBV-transformed lymphocytes
Cells - Transformed fibroblasts
Cervix - Ectocervix
Cervix - Endocervix
Colon - Sigmoid
Colon - Transverse
Esophagus - Gastroesophageal Junction
Esophagus - Mucosa
Esophagus - Muscularis
Fallopian Tube
Heart - Atrial Appendage
Heart - Left Ventricle
Kidney - Cortex
Liver
Lung
Minor Salivary Gland
Muscle - Skeletal
Nerve - Tibial
Ovary
Pancreas
Pituitary
Prostate
Skin - Not Sun Exposed (Suprapubic)
Skin - Sun Exposed (Lower leg)
Small Intestine - Terminal Ileum
Spleen
Stomach
Testis
Thyroid
Uterus
Vagina
Whole Blood
Tissues

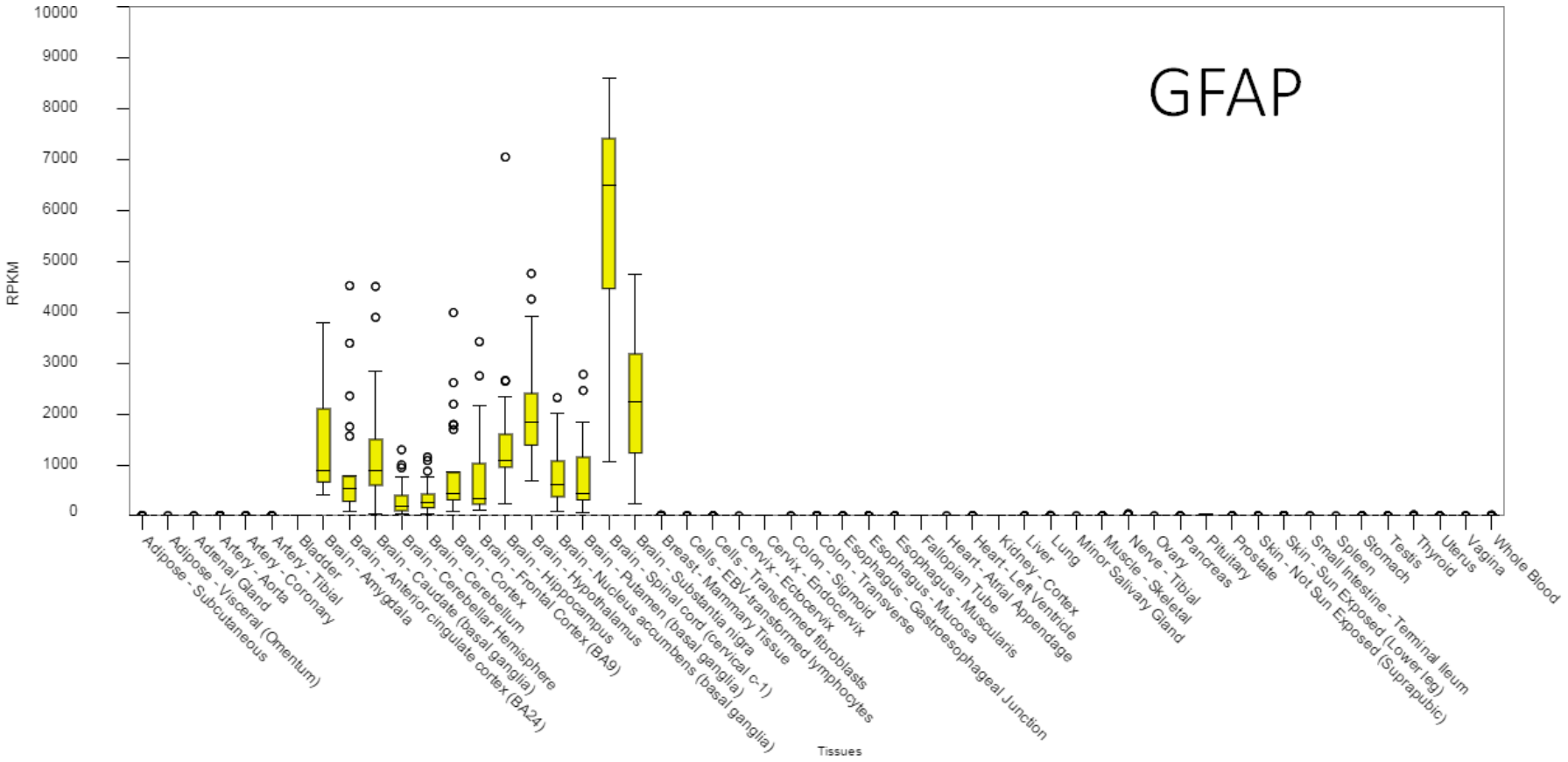
GFAP
RPKM
10000
9000
8000
7000
6000
5000
4000
3000
2000
1000
0
Adipose - Subcutaneous
Adipose - Visceral (Omentum)
Adrenal Gland
Artery - Aorta
Artery - Coronary
Artery - Tibial
Bladder
Brain - Amygdala
Brain - Anterior cingulate cortex (BA24)
Brain - Caudate (basal ganglia)
Brain - Cerebellar Hemisphere
Brain - Cerebellum
Brain - Cortex
Brain - Frontal Cortex (BA9)
Brain - Hippocampus
Brain - Hypothalamus
Brain - Nucleus accumbens (basal ganglia)
Brain - Putamen (basal ganglia)
Brain - Spinal cord (cervical c-1)
Brain - Substantia nigra
Breast - Mammary Tissue
Cells - EBV-transformed lymphocytes
Cells - Transformed fibroblasts
Cervix - Ectocervix
Cervix - Endocervix
Colon - Sigmoid
Colon - Transverse
Esophagus - Gastroesophageal Junction
Esophagus - Mucosa
Esophagus - Muscularis
Fallopian Tube
Heart - Atrial Appendage
Heart - Left Ventricle
Kidney - Cortex
Liver
Lung
Minor Salivary Gland
Muscle - Skeletal
Nerve - Tibial
Ovary
Pancreas
Pituitary
Prostate
Skin - Not Sun Exposed (Suprapubic)
Skin - Sun Exposed (Lower leg)
Small Intestine - Terminal Ileum
Spleen
Stomach
Testis
Thyroid
Uterus
Vagina
Whole Blood
Tissues

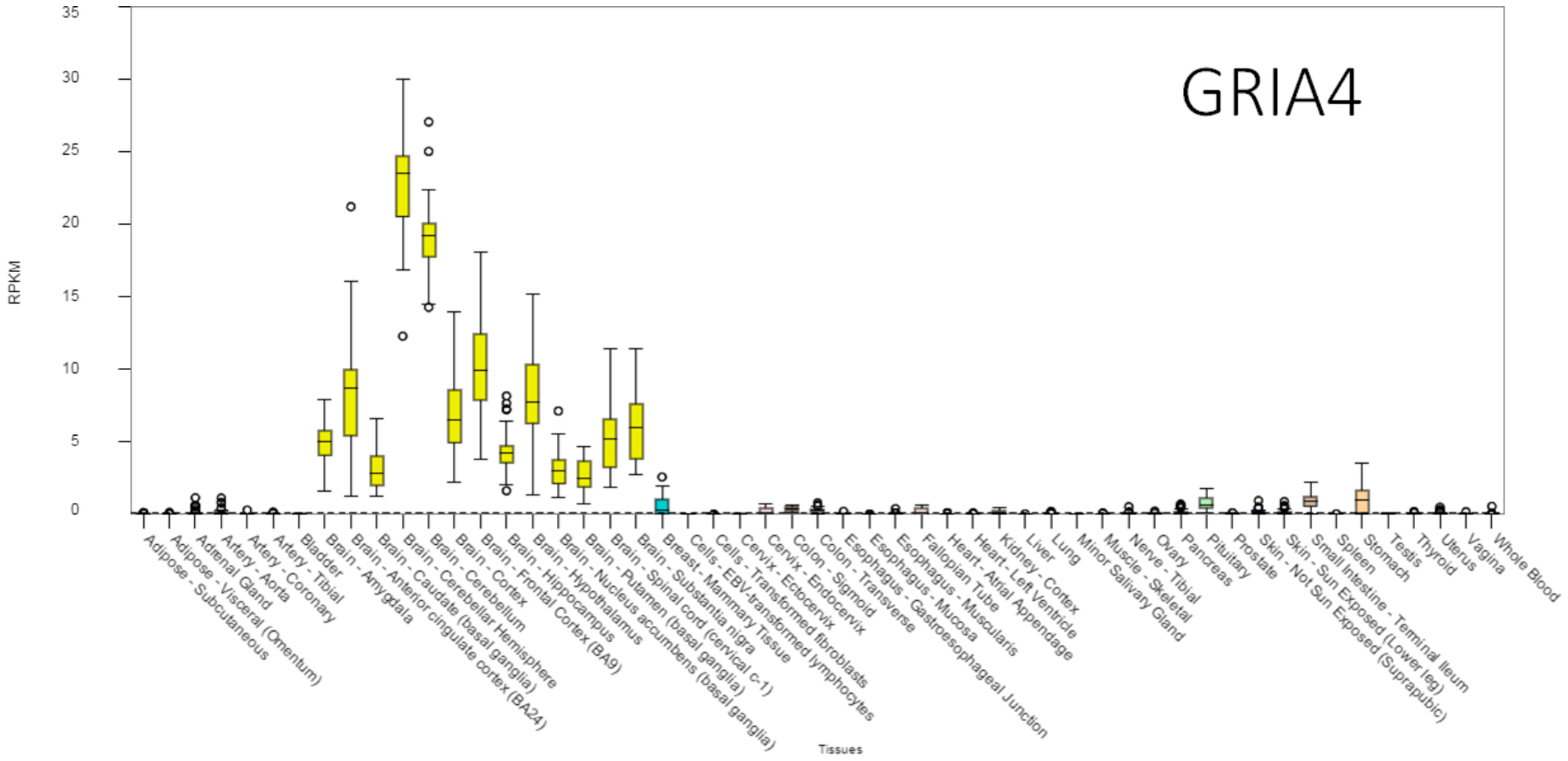
GRIA4
RPKM
35
30
25
20
15
10
5
0
Tissues
Adipose - Subcutaneous
Adipose - Visceral (Omentum)
Adrenal Gland
Artery - Aorta
Artery - Coronary
Artery - Tibial
Bladder
Brain - Amygdala
Brain - Anterior cingulate cortex (BA24)
Brain - Caudate (basal ganglia)
Brain - Cerebellar Hemisphere
Brain - Cerebellum
Brain - Cortex
Brain - Frontal Cortex (BA9)
Brain - Hippocampus
Brain - Hypothalamus
Brain - Nucleus accumbens (basal ganglia)
Brain - Putamen (basal ganglia)
Brain - Spinal cord (cervical c-1)
Brain - Substantia nigra
Breast - Mammary Tissue
Cells - EBV-transformed lymphocytes
Cells - Transformed fibroblasts
Cervix - Ectocervix
Cervix - Endocervix
Colon - Sigmoid
Colon - Transverse
Esophagus - Gastroesophageal Junction
Esophagus - Mucosa
Esophagus - Muscularis
Fallopian Tube
Heart - Atrial Appendage
Heart - Left Ventricle
Kidney - Cortex
Liver
Lung
Minor Salivary Gland
Muscle - Skeletal
Nerve - Tibial
Ovary
Pancreas
Pituitary
Prostate
Skin - Not Sun Exposed (Suprapubic)
Skin - Sun Exposed (Lower leg)
Small Intestine - Terminal Ileum
Spleen
Stomach
Testis
Thyroid
Uterus
Vagina
Whole Blood

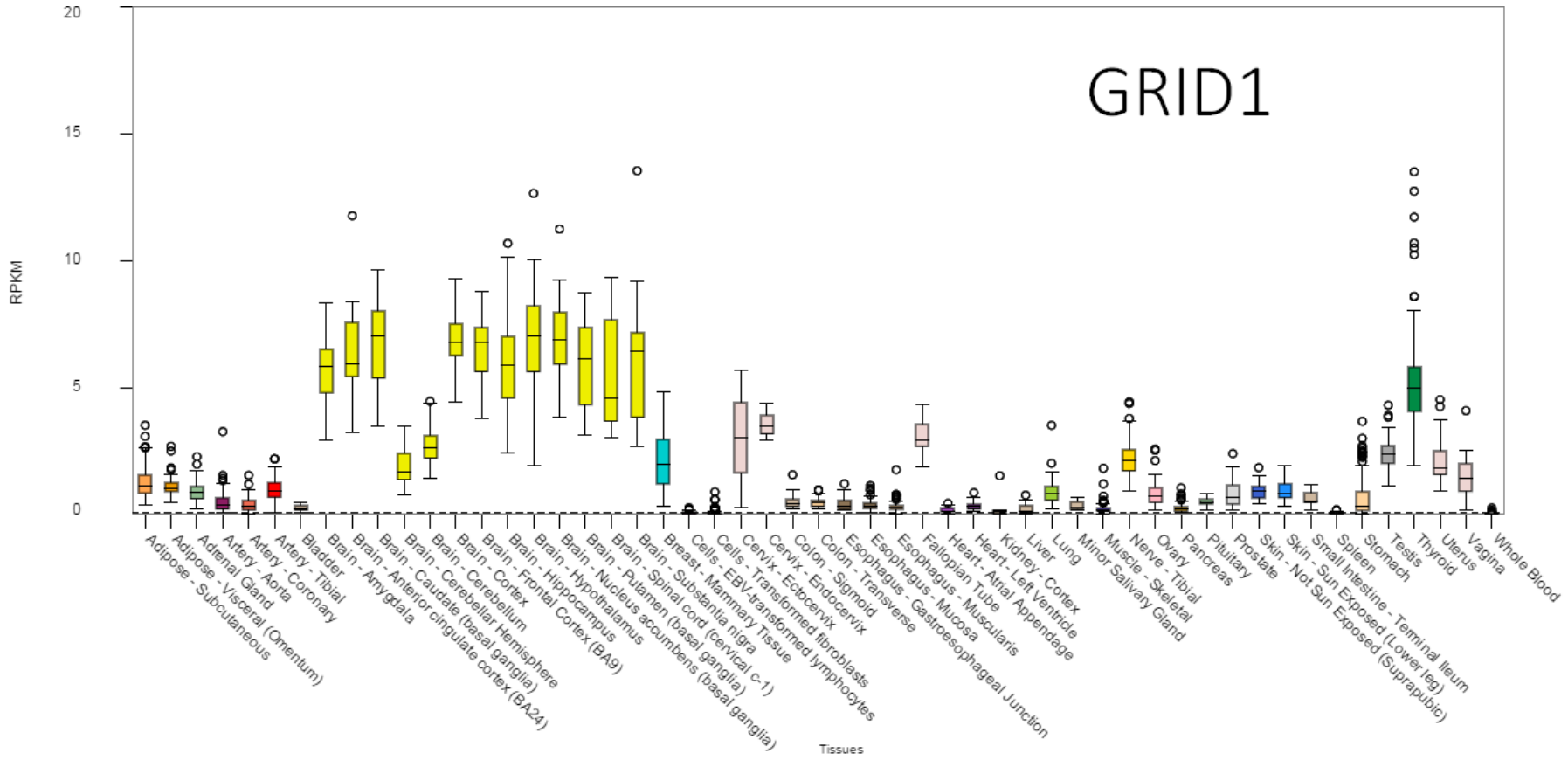
GRID1
RPKM
20
15
10
5
0
Adipose - Subcutaneous
Adipose - Visceral (Omentum)
Adrenal Gland
Artery - Aorta
Artery - Coronary
Artery - Tibial
Bladder
Brain - Amygdala
Brain - Anterior cingulate cortex (BA24)
Brain - Caudate (basal ganglia)
Brain - Cerebellar Hemisphere
Brain - Cerebellum
Brain - Cortex
Brain - Frontal Cortex (BA9)
Brain - Hippocampus
Brain - Hypothalamus
Brain - Nucleus accumbens (basal ganglia)
Brain - Putamen (basal ganglia)
Brain - Spinal cord (cervical c-1)
Brain - Substantia nigra
Breast - Mammary Tissue
Cells - EBV-transformed lymphocytes
Cells - Transformed fibroblasts
Cervix - Ectocervix
Cervix - Endocervix
Colon - Sigmoid
Colon - Transverse
Esophagus - Gastroesophageal Junction
Esophagus - Mucosa
Esophagus - Muscularis
Fallopian Tube
Heart - Atrial Appendage
Heart - Left Ventricle
Kidney - Cortex
Liver
Lung
Minor Salivary Gland
Muscle - Skeletal
Nerve - Tibial
Ovary
Pancreas
Pituitary
Prostate
Skin - Not Sun Exposed (Suprapubic)
Skin - Sun Exposed (Lower leg)
Small Intestine - Terminal Ileum
Spleen
Stomach
Testis
Thyroid
Uterus
Vagina
Whole Blood
Tissues

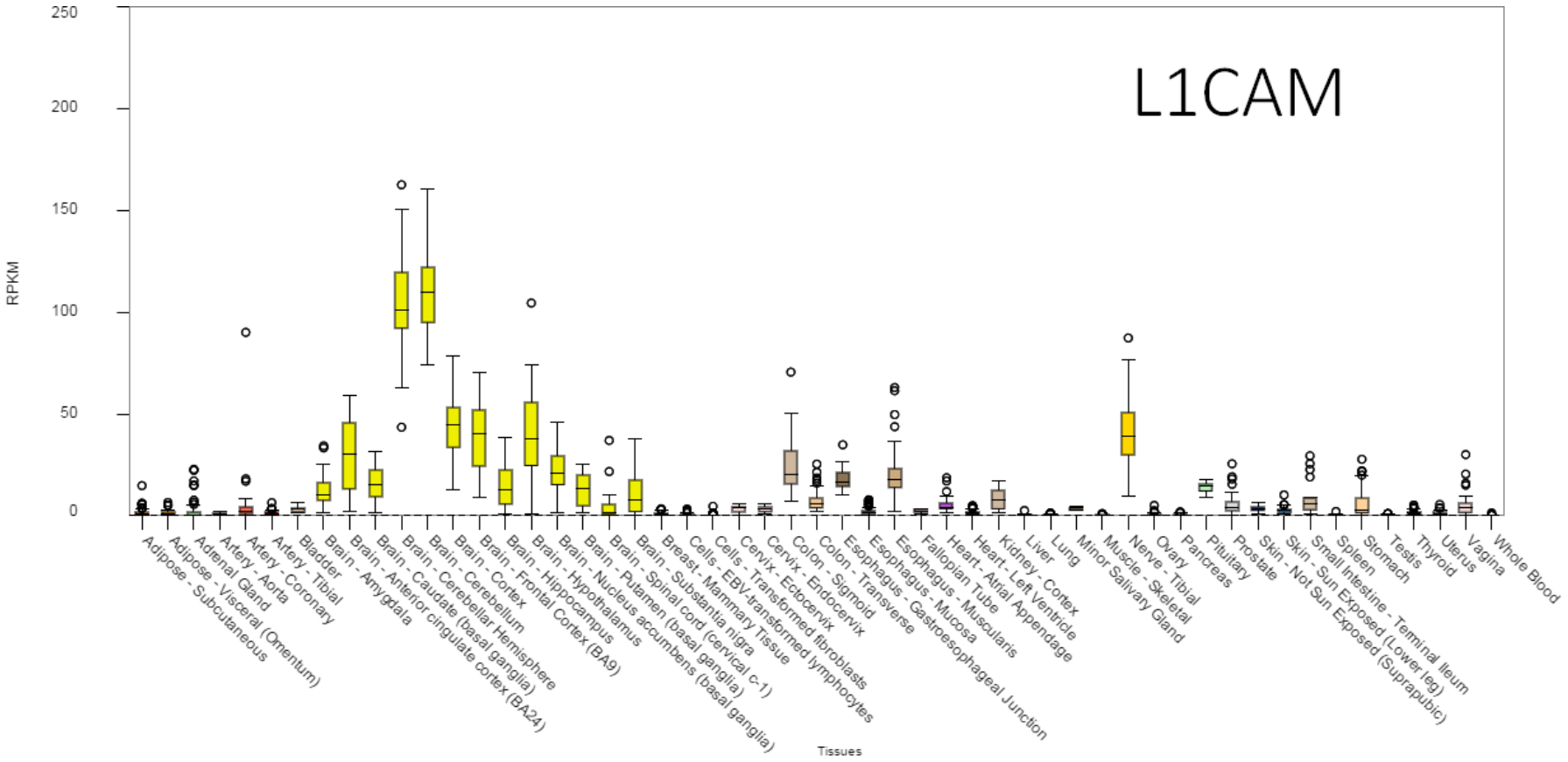
L1CAM
RPKM
250
200
150
100
50
0
Tissues
Adipose - Subcutaneous
Adipose - Visceral (Omentum)
Adrenal Gland
Artery - Aorta
Artery - Coronary
Artery - Tibial
Bladder
Brain - Amygdala
Brain - Anterior cingulate cortex (BA24)
Brain - Caudate (basal ganglia)
Brain - Cerebellar Hemisphere
Brain - Cerebellum
Brain - Cortex
Brain - Frontal Cortex (BA9)
Brain - Hippocampus
Brain - Hypothalamus
Brain - Nucleus accumbens (basal ganglia)
Brain - Putamen (basal ganglia)
Brain - Spinal cord (cervical c-1)
Brain - Substantia nigra
Breast - Mammary Tissue
Cells - EBV-transformed lymphocytes
Cells - Transformed fibroblasts
Cervix - Ectocervix
Cervix - Endocervix
Colon - Sigmoid
Colon - Transverse
Esophagus - Gastroesophageal Junction
Esophagus - Mucosa
Esophagus - Muscularis
Fallopian Tube
Heart - Atrial Appendage
Heart - Left Ventricle
Kidney - Cortex
Liver
Lung
Minor Salivary Gland
Muscle - Skeletal
Nerve - Tibial
Ovary
Pancreas
Pituitary
Prostate
Skin - Not Sun Exposed (Suprapubic)
Skin - Sun Exposed (Lower leg)
Small Intestine - Terminal Ileum
Spleen
Stomach
Testis
Thyroid
Uterus
Vagina
Whole Blood

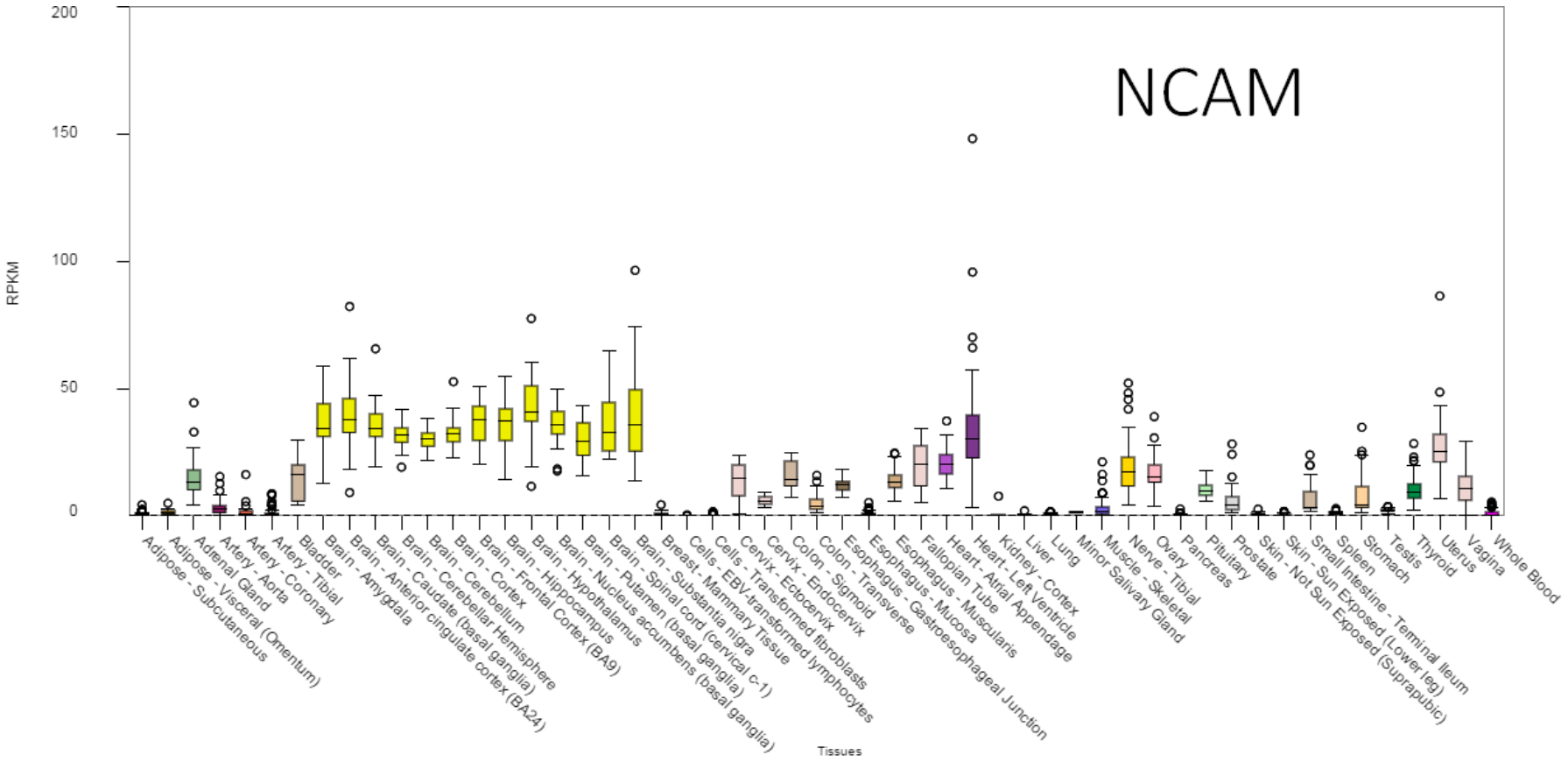
NCAM
RPKM
200
150
100
50
0
Tissues
Adipose - Subcutaneous
Adipose - Visceral (Omentum)
Adrenal Gland
Artery - Aorta
Artery - Coronary
Artery - Tibial
Bladder
Brain - Amygdala
Brain - Anterior cingulate cortex (BA24)
Brain - Caudate (basal ganglia)
Brain - Cerebellar Hemisphere
Brain - Cerebellum
Brain - Cortex
Brain - Frontal Cortex (BA9)
Brain - Hippocampus
Brain - Hypothalamus
Brain - Nucleus accumbens (basal ganglia)
Brain - Putamen (basal ganglia)
Brain - Spinal cord (cervical c-1)
Brain - Substantia nigra
Breast - Mammary Tissue
Cells - EBV-transformed lymphocytes
Cells - Transformed fibroblasts
Cervix - Ectocervix
Cervix - Endocervix
Colon - Sigmoid
Colon - Transverse
Esophagus - Gastroesophageal Junction
Esophagus - Mucosa
Esophagus - Muscularis
Fallopian Tube
Heart - Atrial Appendage
Heart - Left Ventricle
Kidney - Cortex
Liver
Lung
Minor Salivary Gland
Muscle - Skeletal
Nerve - Tibial
Ovary
Pancreas
Pituitary
Prostate
Skin - Not Sun Exposed (Suprapubic)
Skin - Sun Exposed (Lower leg)
Small Intestine - Terminal Ileum
Spleen
Stomach
Testis
Thyroid
Uterus
Vagina
Whole Blood

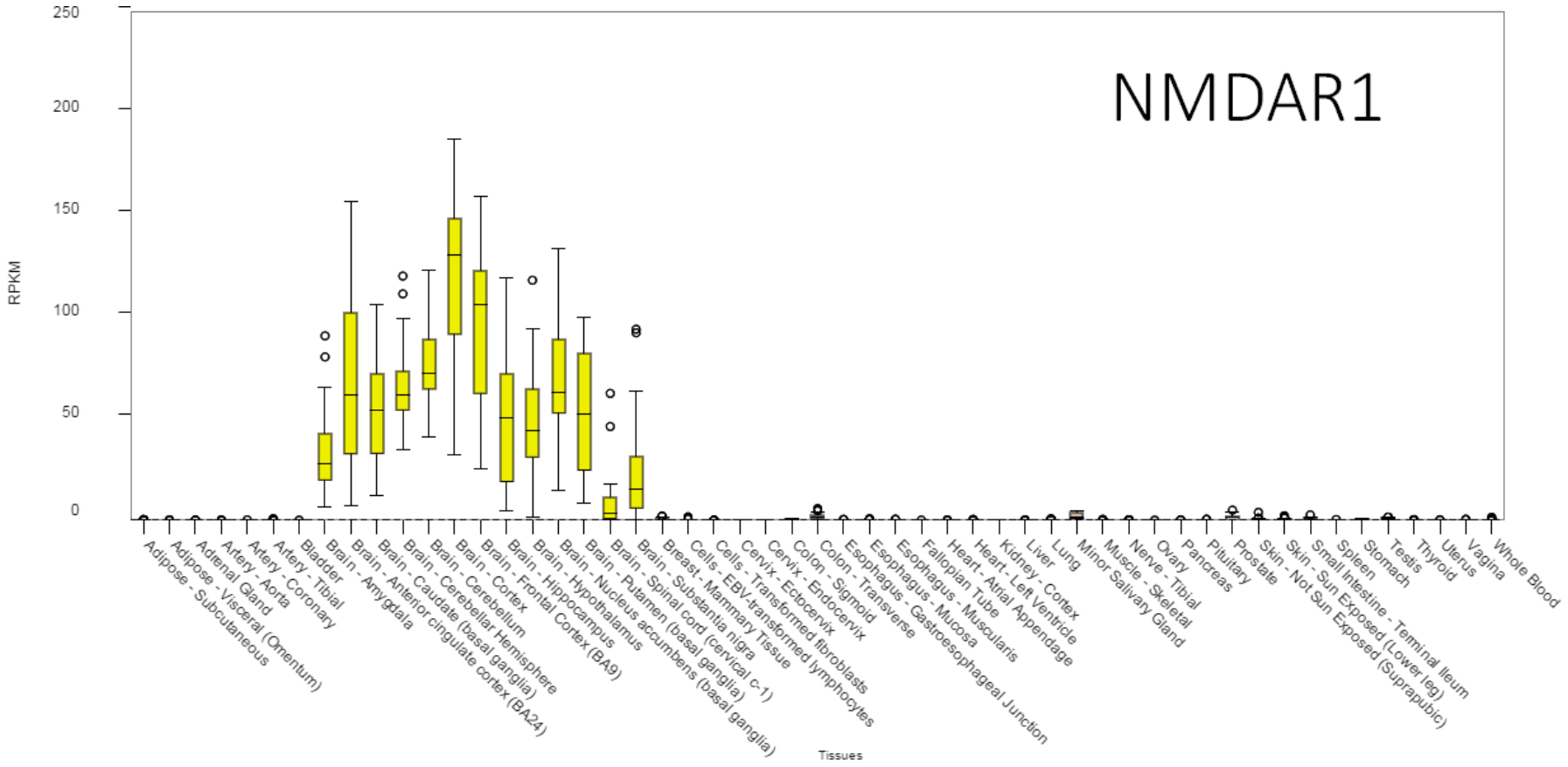
NMDAR1
RPKM
250
200
150
100
50
0
Adipose - Subcutaneous
Adipose - Visceral (Omentum)
Adrenal Gland
Artery - Aorta
Artery - Coronary
Artery - Tibial
Bladder
Brain - Amygdala
Brain - Anterior cingulate cortex (BA24)
Brain - Caudate (basal ganglia)
Brain - Cerebellar Hemisphere
Brain - Cerebellum
Brain - Cortex
Brain - Frontal Cortex (BA9)
Brain - Hippocampus
Brain - Hypothalamus
Brain - Nucleus accumbens (basal ganglia)
Brain - Putamen (basal ganglia)
Brain - Spinal cord (cervical c-1)
Brain - Substantia nigra
Breast - Mammary Tissue
Cells - EBV-transformed lymphocytes
Cells - Transformed fibroblasts
Cervix - Ectocervix
Cervix - Endocervix
Colon - Sigmoid
Colon - Transverse
Esophagus - Gastroesophageal Junction
Esophagus - Mucosa
Esophagus - Muscularis
Fallopian Tube
Heart - Atrial Appendage
Heart - Left Ventricle
Kidney - Cortex
Liver
Lung
Minor Salivary Gland
Muscle - Skeletal
Nerve - Tibial
Ovary
Pancreas
Pituitary
Prostate
Skin - Not Sun Exposed (Suprapubic)
Skin - Sun Exposed (Lower leg)
Small Intestine - Terminal Ileum
Spleen
Stomach
Testis
Thyroid
Uterus
Vagina
Whole Blood
Tissues

Protein	UniProt ID	Cellular localisation	ExoCarta entry	Antibody company	Antibody reference	Immunogen	Buffer
ENO2	P09104	Cytoplasm. Cell membrane.	Y	Abcam	ab53025	Synthetic peptide derived from human ENO2	0.02% Sodium Azide, 50% Glycerol, PBS (w/o Mg^{2+} and Ca^{2+}), 150 mM NaCl
GFAP	P14136	Cytoskeletal.	Y	Abcam	ab7260	Full length human recombinant GFAP	0.01% Sodium Azide
GRIA4	P48058	Cell membrane.	N	Santa Cruz	sc-271894	31-75 (Extracellular)	200 µg IgG2A, PBS, <0.1% sodium azide, 0.1% gelatin
GRID1	Q9ULK0	Cell membrane.	Y	Abcam	ab55163	349-441 (Extracellular)	PBS
L1CAM	P32004	Cell membrane.	Y	Abcam	ab24345	C-terminus	Ascites, Ammonium sulfate, resus and dialyzed in PBS
NCAM	P13591	Secreted and Cell membrane.	Y	Abcam	ab9272	Small cell lung carcinoma specimen	0.02% Sodium Azide, PBS, 0.1% BSA
NMDAR1	Q05586	Cell membrane.	N	Abcam	ab134308	42-361 (Extracellular)	0.09% Sodium Azide, 49% PBS, 50% Glycerol

Table 4.1: Antibodies used for immuno-phenotyping in this chapter and their respective immunogens.
Cellular localisation was determined by functional annotation provided by UniProt. The immunogen and buffer was determined from the website of the antibody supplier and cross-referenced with the protein topology available on UniProt.

4.3.2 Relative expression of protein candidates on cell-cultured exosomes

In order to determine the relative expression of protein candidates, and furthermore attempt to capture and detect exosomes, a number of different europium-linked immunosorbent assay-formats were used in this study (Figure 4.1). Initial immuno-phenotyping of exosomes was performed as previously described (Welton et al., 2015). The use of high-affinity binding microtitre plates allowed for comprehensive adherence of exosomes to the well and probing for antigens of interest. Protein detection was provided using time-resolved fluorometry (TRF, Perkin Elmer) with Europium as the fluorophore.

During assay development, the format of this assay was reconfigured in a number of different ways. For example, the initial immuno-phenotyping was performed with exosomes adhered directly to the microtitre plate but later this format was changed to start with adherence of capture antibodies before exosomes were added. The assay combinations are summarised graphically in Figure 4.2 and adjacent to figures.

The potential suitability of the antibodies detailed above was analysed by probing exosomes from H4, IMR-32 and Du145 cell-lines (Figure 4.3) (n=2). A greater number of replicates would have been preferable so that statistical analyses could have been applied. Instead, with sample and antibody availability limited, a qualitative assessment was performed as a pre-requisite for developing an affinity capture assay.

As expected, CD9 was strongly expressed on exosomes compared to the other, less abundant, protein ligands. For example, TRF ranged from $2.1x10^6$ – $4.5x10^6$ units for CD9 to $0.1x10^6$ – $0.3x10^6$ units for ENO2. Whilst lower TRF units might be caused be poorly working antibodies, these differences are most likely to be caused by the lower ligand densities, as expected.

Based on the gene expression data it was hypothesised that the seven CNS-enriched proteins would be selectively expressed on the neural-derived cell-lines H4 and IMR-32 in preference to Du145, a prostate-derived cell-line. ENO2, GFAP, L1CAM and NCAM were preferentially expressed on IMR-32 exosomes over Du145, thus showing good potential for selectively capturing and enriching for these exosomes later. GRIA4 and GRID1 were preferentially expressed on H4 exosomes over Du145, again showing good potential for affinity capture. None of the candidates showed preferential expression in both H4 and IMR-32 over Du145. Due to sample and antibody limitations only duplicate measures could be recorded so it was not appropriate to perform statistical analyses. This was a limitation in this part of the study

and it was desirable to increase the number of repeats. In this initial immuno-phenotyping screen, the antibodies did not appear to be perturbed by carrier proteins in the buffer and genuine ligand interactions have been measured. In summary, these protein candidates showed good suitability for further assay development based on their relative expression levels on cell culture-derived exosomes.

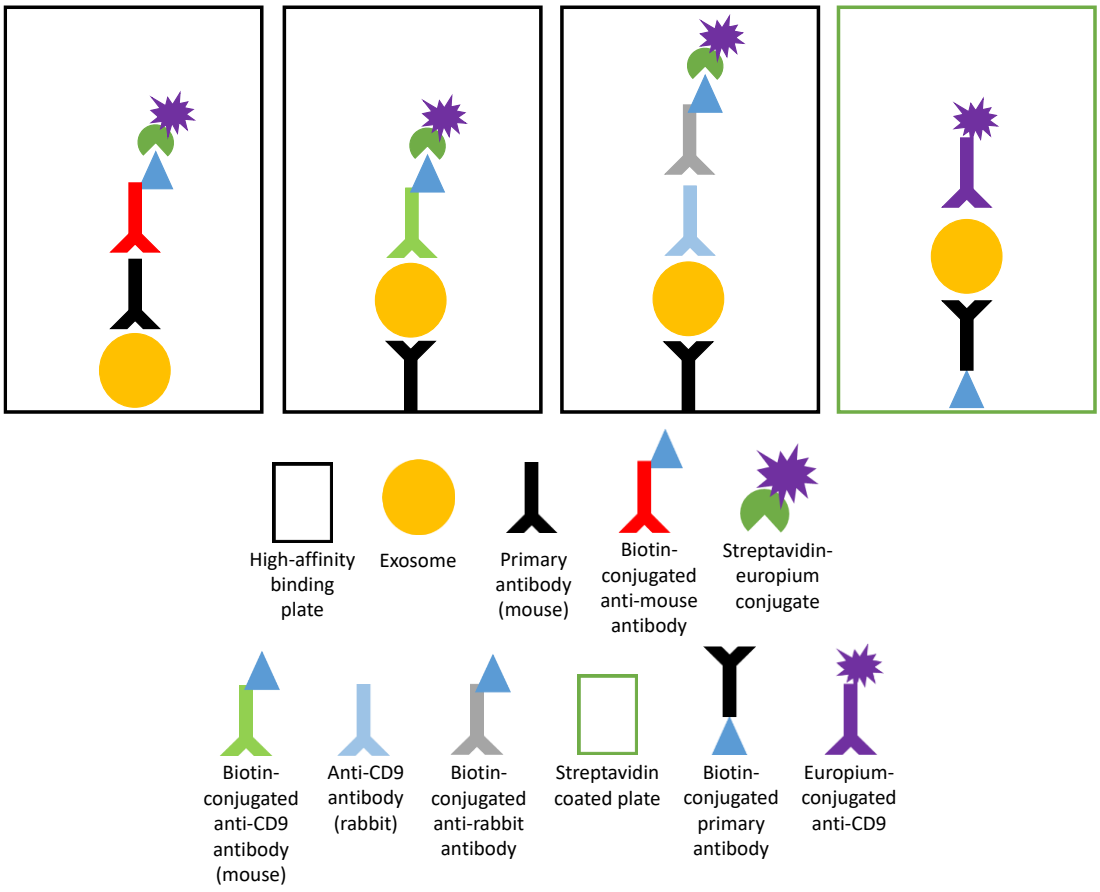

Figure 4.2: Assay conformations used in this study.
From left to right: initial screening format where exosomes were adhered directly to high-affinity binding plate wells; the first capture format where primary antibodies were adhered to high-affinity binding plate wells as capture antibodies; the second capture format where exosomes were detected using a rabbit anti-CD9 antibody; the third capture format where biotin-conjugated capture antibodies were adhered to a streptavidin-coated plate.

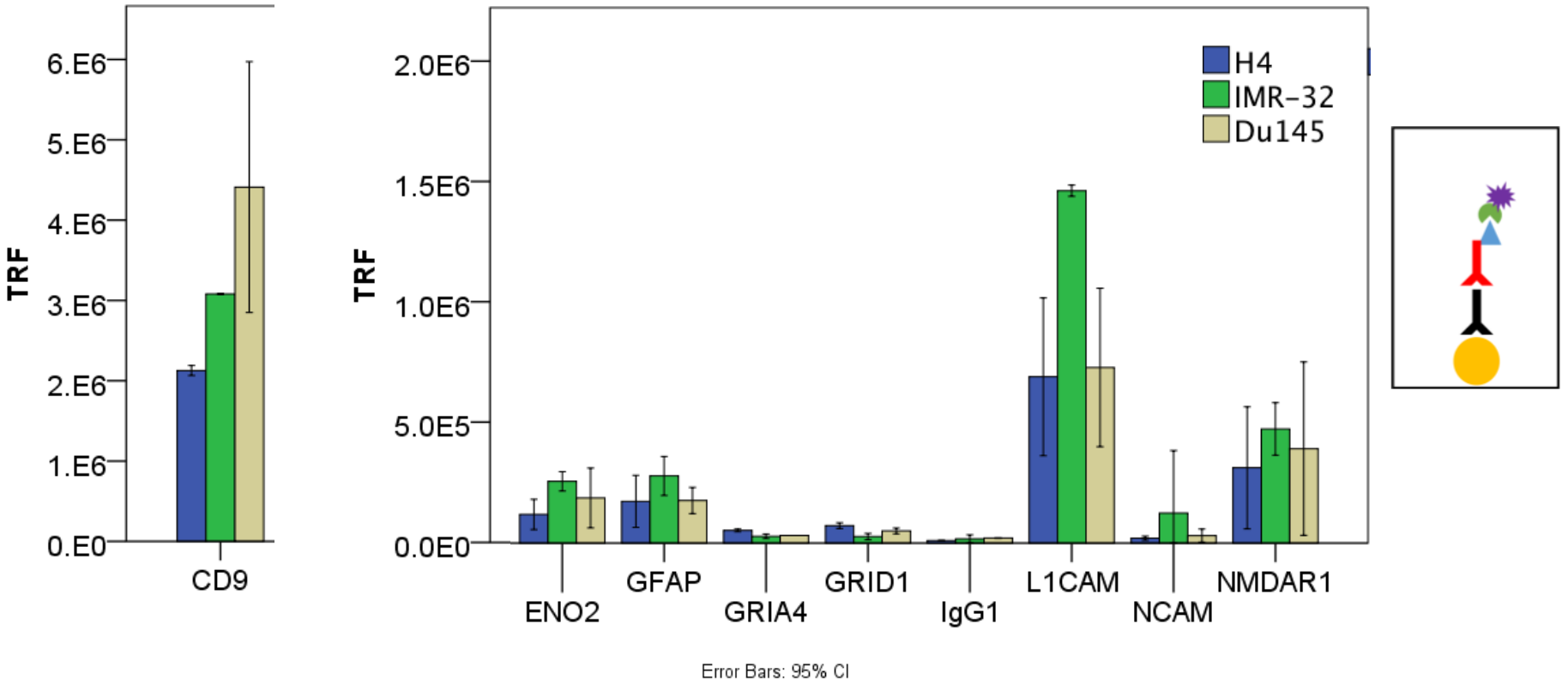

Figure 4.3: Relative expression of seven neural proteins on the surface of cell culture-derived exosomes.
Relative expression is displayed as Time-resolved fluorescence (TRF, y-axis) for the panel of proteins as labelled on the x-axis. Cell-lines are represented by blue bars (H4), green bars (IMR-32) and brown bars (Du145). Exosomes were prepared by sucrose-cushion method and 1 µg loaded per well for immunophenotyping (n=2). Error bars represent 95% confidence intervals. A schematic of the assay format is displayed to the right of the graph.

4.3.3 Affinity capture assays

To test if these protein candidates could selectively capture neural-derived in preference to prostate-derived exosomes a second screen was carried out. The assay format was reconfigured whereby antibodies were coated onto microtitre plates to capture exosomes.

Initially, the optimum antibody dose to fully coat the plate wells was determined by titration. A range of 0 – 1000 ng antibody was coated per well and coverage tested by directly probing with a biotin-conjugated anti-mouse antibody (n=2). TRF was measured and all antibodies tested, except for GRID1, reached a saturation of signal within the concentration range (Figure 4.4). Four of the antibodies reached saturation when 200 ng antibody was coated to the well: ENO2, GFAP, GRIA4 and L1CAM. Four antibodies saturated with 500 ng: CD9, IgG1, NCAM and NMDAR1 but the GRID1 antibody did not reach saturation with 1000 ng coated to the well. It could be that the concentration of antibody provided by the manufacturer was not accurate or, alternatively, GRID1 had more capacity to coat the well of the plate as it was the only antibody in a carrier protein-free buffer. To test if this would be an issue for the downstream assay, the interaction between a bound capture antibody and exosomes would need to be investigated.

The signal strength was strong for all antibodies, reaching 300,000 – 400,000 TRF units, suggesting that genuine coating of the plates had occurred. Thus, the optimum concentrations were determined to fully coat micro-titre plate wells with antibody and provide a surface for antigen-specific adherence of exosomes.

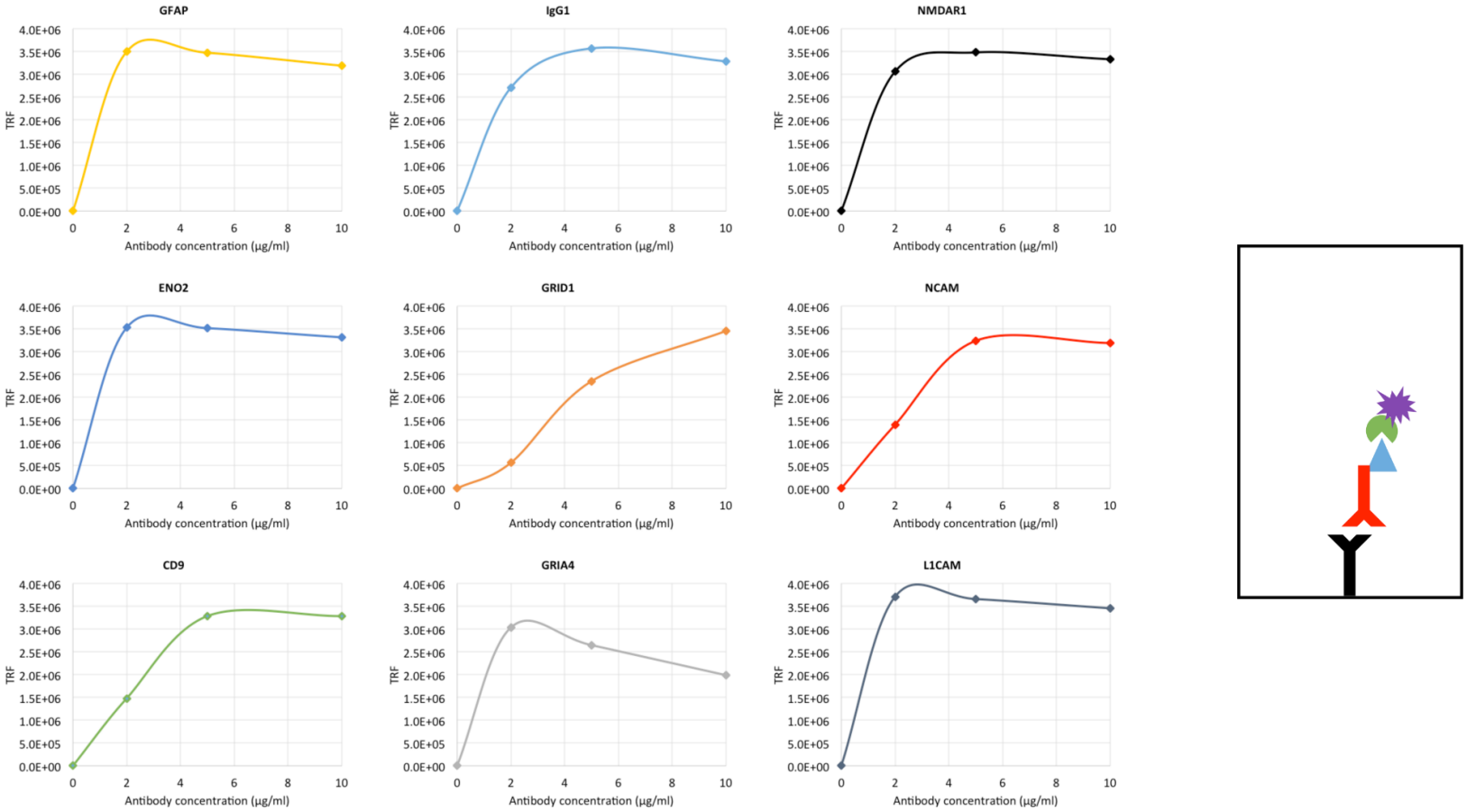

Figure 4.4: Determining the optimum antibody doses to coat high affinity binding wells.
High affinity binding plates were coated with different concentrations of antibodies and measured by Time-resolved fluorescence (TRF, y-axis). Measurements were made in duplicate and averages displayed on the graphs. A schematic of the assay conformation is displayed adjacent to the graphs.

Using these capture antibody concentrations, a second screen was performed to investigate if this assay could capture H4 and/or IMR-32 exosomes in preference to Du145 exosomes (Figure 4.5). Developing an assay that could successfully do this with *in vitro* cell culture-derived exosomes was a pre-requisite before isolation from biological fluids would be attempted.

High-affinity binding plate wells were coated with capture antibody, blocked with 1% BSA, and a fixed concentration of 2 µg/well of exosomes was overlaid (n=2). To detect bound exosomes the assumption was made that neural marker-positive exosomes also presented CD9, so a fixed concentration of 200 ng/well biotin-conjugated anti-CD9 antibody was added. A signal would only be generated if CD9 and the target marker were co-expressed which presented a limitation to the assay as any exosomes that were absent of CD9 would not be detected with this configuration. Only GRIA4 showed selective capture of H4 and IMR32 exosomes in preference to Du145 (Figure 4.5), but insufficient replicates were performed to assess this statistically.

It was particularly noteworthy that TRF values were ~10-fold lower in this screen than the initial candidate screen e.g. <60,000 TRF units compared to >300,000. This suggested that genuine CD9 detection had not taken place. It may be that exosomes had not adhered to the capture antibodies, or alternatively, there was an inherent weakness in detection format. Furthermore, the signal recorded for the isotype control, IgG1, was greater than a number of the neural-specific ligands, suggesting that exosomes were not binding to the plate wells in a ligand-specific manner; if they were binding at all.

It had already been determined that these protein candidates were significantly enriched on H4 or IMR-32 exosomes over Du145 (Figure 4.3) and that the wells of the plates were fully saturated with capture antibody (Figure 4.4). Therefore, it was hypothesised that either the exosomes were not adhering to the antibodies in this altered configuration or there was a weakness in the detection method. To further investigate these issues, the antibody against GRIA4 was chosen to optimise the assay as it had already shown selectivity for H4 exosomes in both screens but had not reached the level of significance in the second.

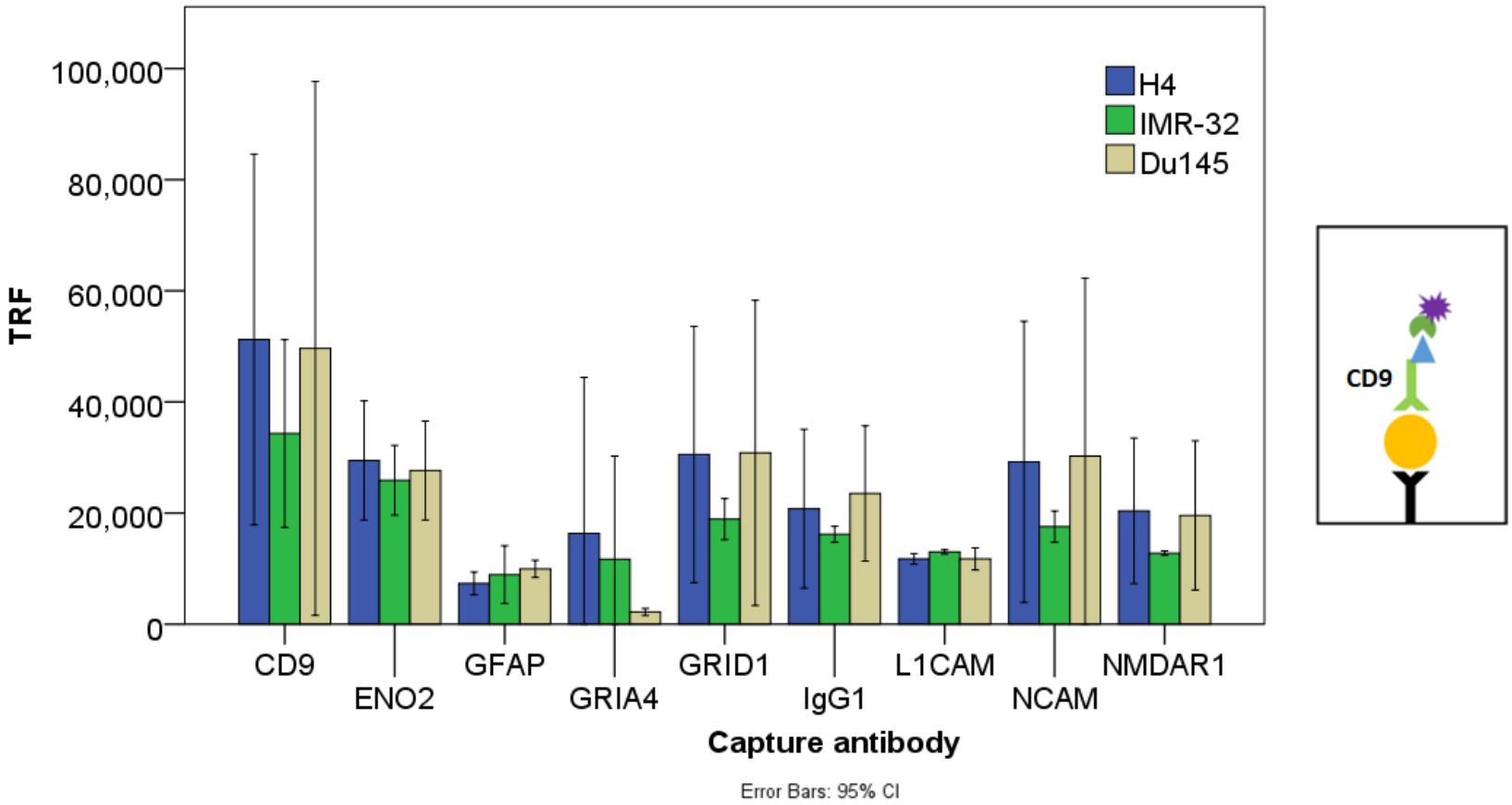

Figure 4.5: Relative CD9 expression on affinity captured exosomes.
Relative expression is displayed as Time-resolved fluorescence (TRF, y-axis) for the panel of proteins as labelled on the x-axis. Cell-lines are represented by blue bars (H4), green bars (IMR-32) and brown bars (Du145) (n=2). Error bars represent 95% confidence intervals. Exosomes were prepared by sucrose-cushion method and 1 µg loaded per well for immunophenotyping (n=2). A schematic of the assay format is displayed to the right of the graph.

4.3.4 Troubleshooting affinity capture assay format

Exosomes dose response curves to test assay limitations

The first problem to address was assessing if H4 exosomes were genuinely adhering to the GRIA4 antibody in this altered configuration. An exosome titration was chosen to test the sensitivity of the assay. It was hypothesised that if the capture antibody had good affinity for exosomes then a dose response would be observed. H4 and Du145 exosome dose curves were run from 0 – 5 µg exosomes/well (Figure 4.6) (n=2).

As expected from the previous screens H4 exosomes were selectively captured over Du145 exosomes in a dose-dependent manner using the GRIA4 antibody. The isotype control (IgG2a), however, matched this signal when 5 µg exosomes were loaded per well. This suggested that when high doses of exosomes were loaded into the assay, non-specific binding to IgG2a had occurred. Thus, the selectivity of the assay to capture exosomes that present the GRIA4 ligand was equivocal.

In addition to this non-specific binding, the signal from this assay format was very poor reaching a maximum of 12,000 TRF units even with 5 µg exosomes in the system. This gave not only a potentially low dynamic range but also a low signal : noise ratio as IgG2a achieved the same signal. So as well as exhibiting non-specific binding, this suggested that there could also be a weakness in the detection method. A strong CD9 signal would be expected for a dose of 5 µg exosomes, albeit that in this case that a subset of those were being selected. It was hoped that a signal exceeding 100,000 TRF units could be achieved to provide a good dynamic range. Therefore, both problems of exosome adherence to the capture antibody and signal strength from the detection antibody still needed to be resolved.

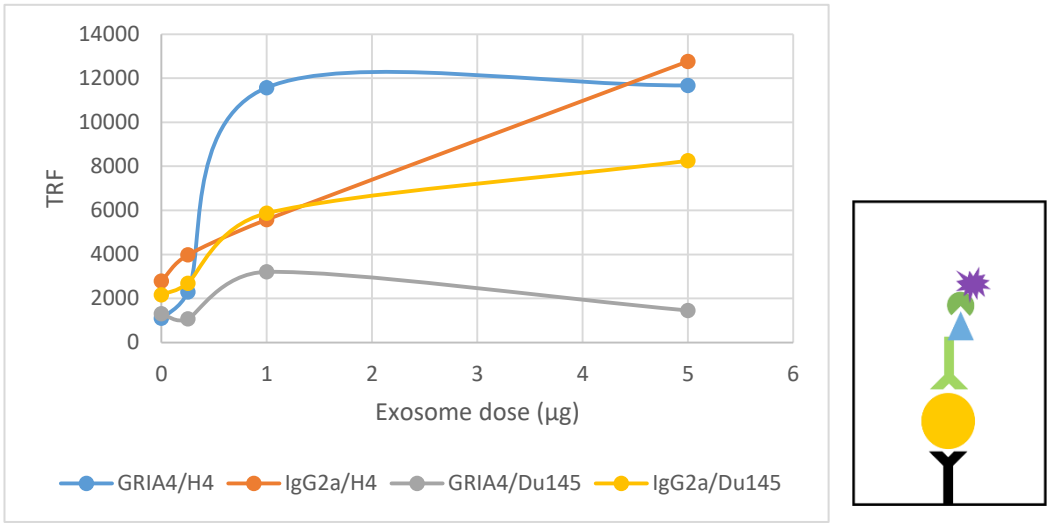

Figure 4.6: Exosome dose curves to test the sensitivity of the assay.
Exosomes were titrated from 0 – 5 µg/well (x-axis) with fixed concentrations of capture and detection antibodies (n=2). Relative expression was averaged and is displayed as Time-resolved fluorescence (TRF, y-axis). A schematic of the assay format is displayed adjacent to the graph.

Titration of mouse anti-CD9 detection antibody

The easier problem to address first was the low signal provided by the detection format. If there was, indeed, a problem using the biotin-conjugated mouse anti-CD9 antibody it would be relatively straightforward to replace this component. Therefore, detection antibody dose curves were run with exosomes adhered directly to the high-affinity binding wells (n=2) (Figure 4.7). This removed the unknown element of exosome adherence to capture antibodies and could thus test the robustness of the detection method.

There was no plateau in the signal within the 0 – 10 µg/ml detection antibody concentration range used. With 100 µl total volume used this equates to 1 µg antibody not providing a saturated signal. This would be considered a high, and costly, dose of antibody so a saturation of signal would have been expected. In addition to not reaching saturation, the TRF signal in general was still low, not exceeding 60,000 units even with 5 µg exosomes in the system. When the initial screen was performed (Figure 4.3) CD9 detection of 2 µg exosomes exceeded 200,000 TRF units for all cell-types using a different detection configuration. Together, these highlight that the detection antibody was a limiting component of the assay.

The background signal observed with no exosomes in the system was barely distinguishable from a dose of 1 µg exosomes and only marginally lower than 2 or 5 µg exosome doses. This suggested insensitivity in the detection system to distinguish a genuine signal caused by exosomes over the background. Therefore, the current assay format had both a low dynamic range and a poor signal : noise ratio.

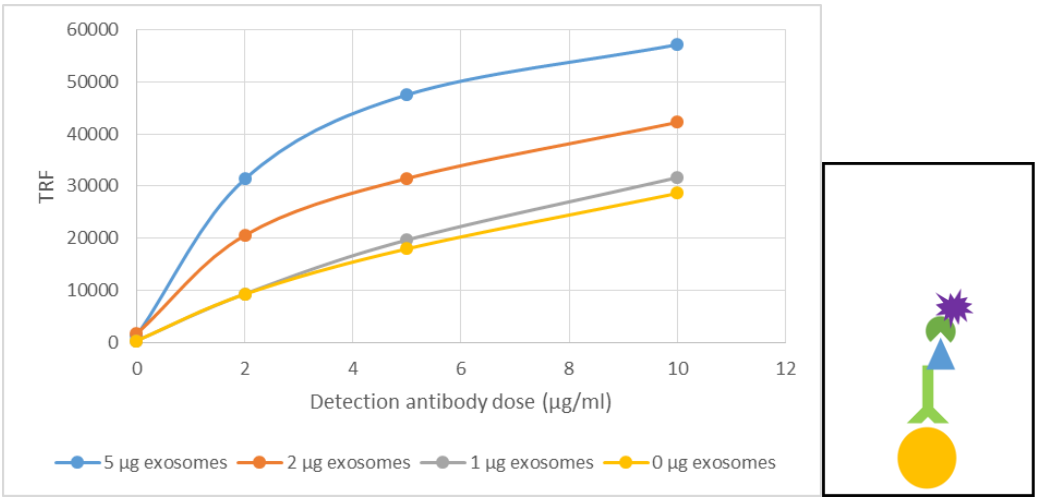

Figure 4.7: Determining the effectiveness of biotin-conjugated mouse anti-CD9 antibody to detect exosomes.
H4 exosomes were directly adhered to high-affinity binding wells at set concentrations of 0, 1, 2 and 5 µg per well (n=2). Detection antibody doses curves were ran from 0 – 1 µg antibody per well (x-axis) and averaged expression displayed as Time-resolved fluorescence (TRF, y-axis). A schematic of the assay format is displayed adjacent to the graph.

Optimising an anti-rabbit secondary antibody to boost detection

In an attempt to boost the signal of the assay, a second detection format was used. The biotin-conjugated mouse anti-CD9 was replaced with a rabbit polyclonal antibody against CD9. This was chosen because the antibody was raised in a different species to the capture antibody which was a mouse GRIA4 antibody. Therefore, the detection signal could be amplified using a secondary biotin-conjugated anti-rabbit antibody.

This secondary antibody had not been used previously in the Clayton laboratory, so the optimal concentration was determined by titration (Figure 4.8). Microtitre plate wells were coated with anti-ENO2 (rabbit) antibody to provide a suitable ligand for the anti-rabbit antibody to bind to. Dose response curves were run from 0 – 5 µg/ml anti-rabbit antibody (n=2). The total volume was 100 µl which equates to 0 – 500 ng antibody per well. Fluorescence signal had not reached saturation with 500 ng in the system suggesting that higher values could be reached. A higher dose would have been too costly so 500 ng was chosen as the dose to be used in this assay.

The TRF values were much higher: exceeding 600,000 TRF units with 500 ng ENO2 and over 1,200,000 TRF units if 1 µg ENO2 was used. This suggested that the use of this secondary antibody amplification had the capacity to produce a stronger signal and improve the dynamic range of the assay compared to the configuration used previously.

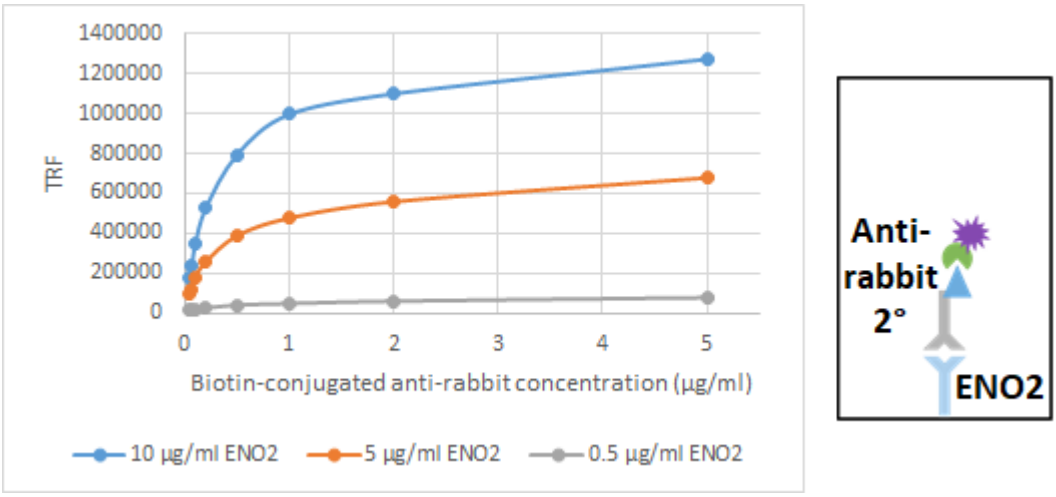

Figure 4.8: Determining the optimum concentration of anti-rabbit secondary antibody.
Microtitre plate wells were coated with rabbit anti-ENO2 antibodies to provide a ligand surface for the secondary antibody to be tested against (n=2). Titrations were run from 0 – 5 µg/ml (x-axis), that is 0 – 500 ng antibody/well. Relative expression was averaged and is displayed as Time-resolved fluorescence (TRF, y-axis). A schematic of the assay format is displayed adjacent to the graph.

Antibody dose response curves to optimise a rabbit anti-CD9 detection

The optimal dose of anti-CD9 was next to be determined by titration. Exosome and anti-rabbit antibody doses were fixed at 2 µg and 500 ng per well, respectively, and anti-CD9 dose curves were run from 0 – 500 ng antibody per well (n=1) (Figure 4.9).

Saturation of the TRF signal was not reached with 500 ng in the system suggesting that greater signals could be achieved. Nevertheless, achieving ~400,000 TRF units was satisfactorily high to achieve a good dynamic range without increasing the costliness of the assay.

There was a high background signal with no anti-CD9 antibody in the system at ~280,000 TRF units. This suggested a non-specific affinity of the anti-rabbit secondary antibody to bind to exosomes without the ligand specific detection antibody. By subtracting the TRF signal of 500 ng anti-CD9 from the background signal, this format produced ~120,000 TRF units of genuine signal achieving a signal : noise ratio of 1.43:1. This highlighted the need to account for background signal. With lower doses of anti-CD9 antibody this signal : noise was reduced, confirming the choice to use of 500 ng anti-CD9 antibody.

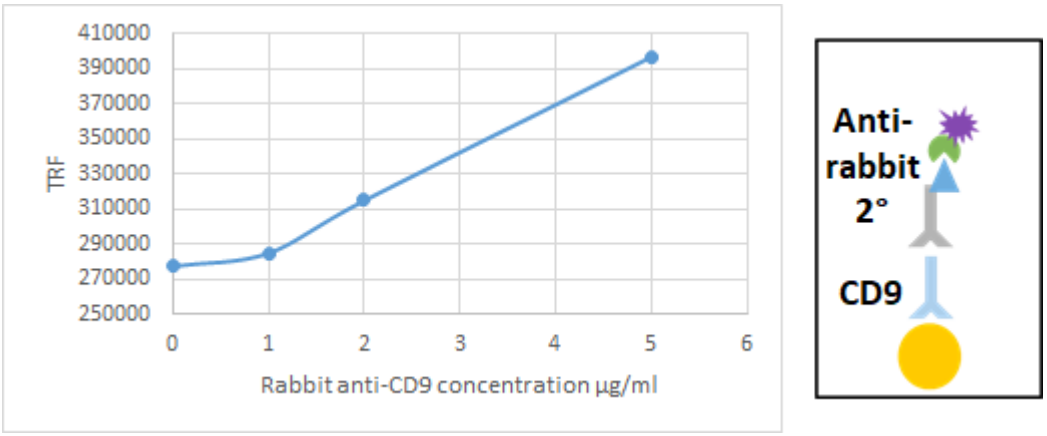

Figure 4.9: Determining the optimum concentration of rabbit anti-CD9 antibody.
Micro-titre plate wells were coated with 2 µg H4 exosomes prior to titration of anti-CD9 antibody from 0 – 500 ng per well (x-axis, n=1). The secondary anti-rabbit antibody was set at a fixed dose of 500 ng per well as previously determined. Relative concentration is displayed as Time-resolved fluorescence (TRF, y-axis). A schematic of the assay conformation is displayed adjacent to the graph.

Exosome dose response curves to test the rabbit anti-CD9 detection format

Up to this point, the optimum doses of capture antibodies, anti-CD9 detection antibody and anti-rabbit secondary antibody had been determined. To test the robustness of this assay, in its entirety, exosome dose response curves were run from 0 – 5 µg per well (n=2) (Figure 4.10). H4 and Du145 exosomes were used to test the selectivity of the assay and an IgG2a isotype control was included to test the specificity of antigen-antibody adherence.

Whilst the dynamic range had successfully improved, exceeding 200,000 TRF units, a number of observations suggested that exosomes were not adhering to the capture antibody. Firstly, there was no increase in signal with exosome dose as would have been expected with this titration. Secondly, there was no selectivity for the GRIA4 antibody to bind H4 exosomes in preference to Du145 exosomes. This is in contrast to both Figure 4.3 and Figure 4.5 that demonstrated that GRIA4 was preferentially expressed on H4 exosomes. Thirdly, the signal produced when an isotype capture antibody was used was almost double that when GRIA4 was used. This suggested that the capture antibody could cause non-specific binding of either exosomes or detection antibodies regardless of ligand. The signal : noise ratio would therefore be a negative value and not suitable for a future assay.

Together, these observations highlighted that whilst the problem of low detection signal had been successfully addressed there was also a fundamental issue with exosomes not adhering to the capture antibody in this format. Indeed, by improving the detection signal and comparing GRIA4 to isotype control it was made clearer that a fundamental problem with this assay was that exosomes were not adhering to the capture antibody.

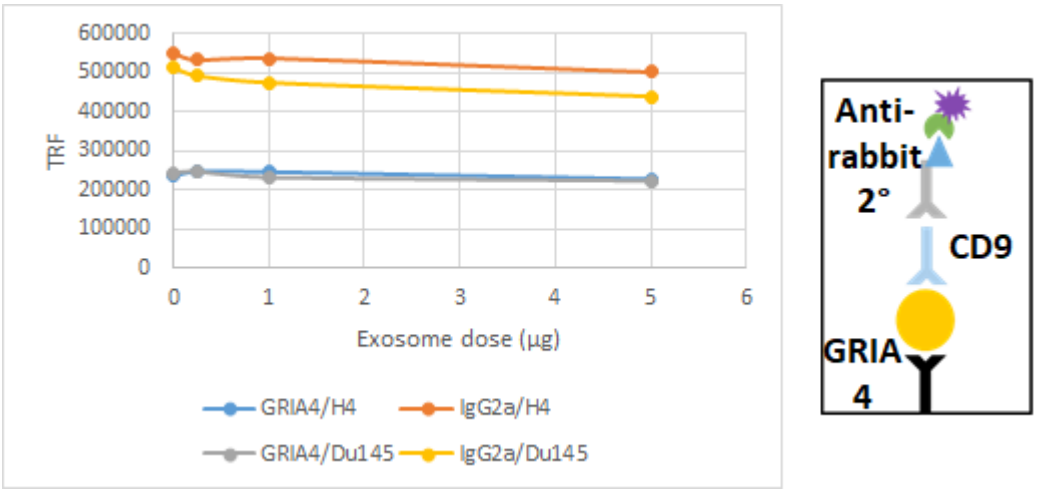

Figure 4.10: Testing the robustness of the second assay format that used rabbit anti-CD9 antibody for the detection of exosomes.
Exosomes were prepared from H4 and Du145 cell-lines using the sucrose cushion method and dose curves were run from 0 – 5 µg per well (x-axis, n=2). Relative CD9 expression of exosomes captured with GRIA4 (blue, grey) or IgG2a (orange, yellow) antibodies were averaged and displayed as Time-resolved fluorescence (TRF, y-axis). A schematic of the assay conformation is displayed adjacent to the graph.

A third assay format that used streptavidin--coated microtitre plates

A robust assay had not been developed by altering the detection format, therefore a third assay was attempted that addressed the issue with exosomes not adhering to the capture antibody. Previously, high-affinity binding plates were coated with capture antibodies, instead, this assay used streptavidin-coated plates that were overlaid with biotin-conjugated capture antibodies. It was hypothesised that this would provide a surface of correctly orientated antibodies for improved exosome adherence. The detection method used was a europium-labelled anti-CD9 antibody.

The use of streptavidin-coated plates limited the number of options to optimise this assay. Therefore, the exosome and detection antibody doses were set at 2 µg/well and 500 ng/well, respectively, and capture antibody dose curves were run from 0 – 1 µg/well (n=1) (Figure 4.11). Biotin was conjugated to the GRIA4 antibody using Lightning-Link® Rapid Antibody Labeling kits (Innova Biosciences). A biotin-conjugated pan-IgG antibody was used as a control. H4 and Du145 exosomes were used to test if the GRIA4 antibody had selectivity for capturing H4 exosomes.

The expected dose response curves were not observed, rather, the signal produced with no GRIA4 capture antibody in the system exceeded that when no antibody was present. This suggested that the capture antibodies themselves had a blocking effect when added to the plate and the signal : noise ratio would be negative. Additionally, the signal produced with Du145 exosomes in the system exceeded that of H4 exosomes suggesting non-selective binding of exosomes regardless of ligand. This was further confirmed when comparing these to the isotype control, which produced a greater signal than the GRIA4 capture antibody. Together, these data suggest that once again the assay was not successfully capturing exosomes to the plate configuration.

Three different assay configurations were attempted in this study but none captured H4 exosomes over Du145 and thus, not suitable for taking further with biological fluids. The dynamic range of the assay could be improved by altering the detection format, but persistently the signal : noise ratio could not be improved. This suggests that an interaction between exosomes and the capture antibodies was not occurring. The same antibodies had worked successfully during the initial immuno-phenotyping screen but could not be re-configured as capture antibodies in this study. Having such technical difficulties when the assay was being developed for cell culture-derived exosomes made for an increasingly challenging prospect of developing an assay that would be compatible with biological fluids.

Therefore, it was decided to stop pursuing an affinity isolation method, although this would be of future interest, and adopt a systems wide approach for the analysis of exosomes from biological fluids.

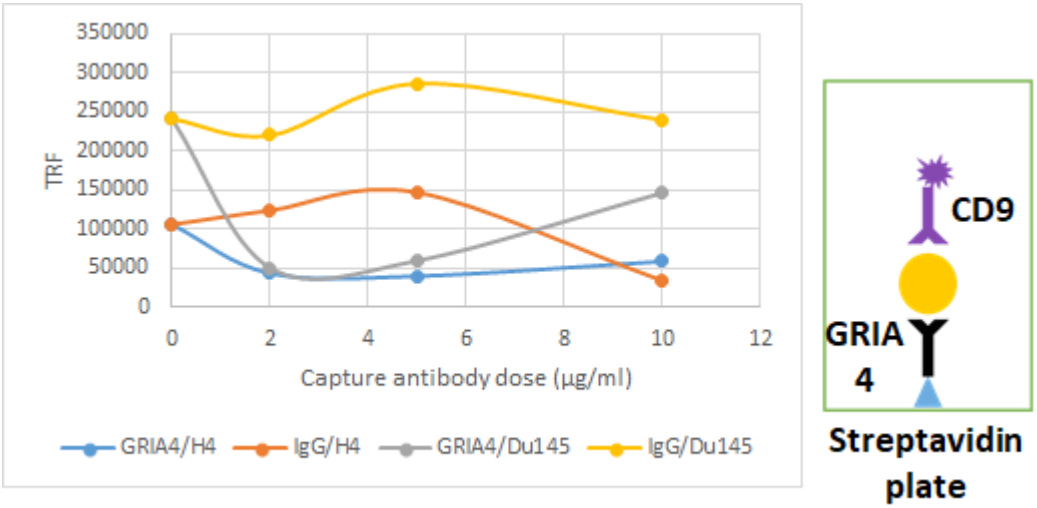

Figure 4.11: Determining the optimum concentration of capture antibody to be used with streptavidin-coated plates.
Capture antibody dose curves were run from 0 – 10 µg/ml (axis) on streptavidin coated plates (n=1); with 100 µl total volume, this is the equivalent of 0 – 1 µg/well. Relative CD9 expression of exosomes captured with GRIA4 (blue, grey) and IgG (orange, yellow) antibodies is displayed as Time-resolved fluorescence (TRF, y-axis). A schematic of the assay format is displayed adjacent to the graph.

4.4 Discussion

It has been reported that neural-derived exosomes can be immuno-precipitated from biofluids such as plasma (Fiandaca et al., 2015, Goetzl et al., 2015b). Such techniques, in theory, will remove high background of non-neural exosomes secreted from other tissue types and allow the investigation of vesicles that are best representative of disease affected cells.

This chapter aimed to identify proteins selectively expressed in the human brain and develop similar micro-titre plate assays for the selective capture of neural derived exosomes. Seven protein candidates were selected, based on promising *in silico* data, and were used to immuno-phenotype cell-cultured derived exosomes. These showed initial promise with six of the seven ligands showing significant preferential expression in H4 and/or IMR-32 exosomes. Unfortunately, the assay format could not be reconfigured to selectively capture H4 exosomes over Du145.

After identifying promising protein ligands a systematic approach was taken to develop an affinity capture assay. An exosomes titration was used with the first assay configuration, which used a mouse anti-CD9 detection antibody, and found that both the dynamic range and signal : noise ratio of the assay was poor. This suggested that there was an inherent weakness in the detection method and, potentially, an issue with exosome adherence to the capture antibody. It was more straightforward to address the detection method so a second assay configuration used a rabbit anti-CD9 antibody. This successfully improved the dynamic range of the assay but, using an exosome titration, it was determined that the signal : noise ratio had not been improved. Therefore, a final assay configuration altered the capture format by coating streptavidin plates with capture antibodies, in the hope that this would correctly orientate the antibodies to efficiently interact with ligands presented on exosomes. Unfortunately, the signal : noise ratio remained poor with this assay configuration when detection antibodies were titrated. It appears that in this study it was not possible to develop a plate-based assay where exosomes could bind to immobilised antibodies although this has been demonstrated elsewhere (Duijvesz et al., 2015, Kaminska et al., 2016).

This study could have been greatly improved by the selection of different antibodies. All of the antibodies used, except for GRID1, contained carrier protein in the buffer. Whilst the initial immuno-phenotyping screen was not adversely affected by these carrier proteins, it is likely that by applying the same antibodies to high-affinity binding plates resulted in carrier

proteins also coating the wells. Titrations of capture antibodies were run and it appeared that the wells were fully coated (Figure 4.4), nevertheless, carrier proteins and the orientation of the antibodies could not be accounted for. In different settings, such as industry, large budgets can be allocated for thoroughly testing or developing new antibodies. This was not an option in this study so commercially available antibodies were used instead and the assay developed as systematically as possible.

A group that has reported successful immuno-absorption of neural-derived exosomes used a streptavidin resin-based enrichment protocol (Fiandaca et al., 2015, Goetzl et al., 2015b) opposed to the micro-titre plate formats employed here. Briefly, this method precipitates exosomes out of plasma or serum, incubates with biotin-conjugated antibodies and uses a streptavidin resin to enrich for NCAM- and L1CAM-positive vesicles (Mustapic et al., 2017). Certainly the choosing of NCAM and L1CAM antibodies is in agreement with the expression data presented in this study (Figure 4.1). Of future interest is to pursue this resin-based approach rather than the microtitre-plate approach used in this study. It may be that by selecting different ligands, such as and *NMDAR1* which is enriched in cortical regions (Figure 4.1), exosomes from different tissues within the brain could be enriched for. Exosomes from different cell-types could also be enriched, for example, astrocytes are enriched for GFAP (Liddelow et al., 2017) so a working assay would enrich for astrocyte-derived vesicles.

The Goetzl laboratory verified their exosomes against the CD81 antigen and, elsewhere, it has been suggested that CD81 is a more specific marker for exosomes than CD9 or CD63 (Kowal et al., 2016). However, the isolation of exosomes in this study was determined by CD9 expression, and it may be that CD81 would have been a better choice. Nevertheless, when the initial immuno-phenotyping screen was performed, CD9 was detected in relatively high abundance on H4 and IMR-32 exosomes, so it appears to have been appropriate with these cell-types.

One assumption that was made was that the captured exosomes would express CD9, but this may not be the case. Exosomes that express a ligand, such as GRIA4, may not co-express CD9 and would not have been detected with this system. The TRIFic™ assay captures and detects exosomes by the same ligand (Duijvesz et al., 2015, Kaminska et al., 2016). Therefore, to fully determine if exosomes were not adhering to the capture antibodies in this study it would have been beneficial to develop detection antibodies with the same ligands.

In summary, it may be that i) the reagents were of low affinity or quality, ii) the ligand density was so low on these exosomes that capturing was difficult with good sensitivity or iii) CD9 was a poor choice for detection. If the assay concept could have been proved with cell-culture derived exosomes it would have potential to be used with biological fluids. Ideally, the capacity to selectively capture neural-derived exosomes present in blood plasma or serum is hugely important; giving a more specific CNS-relevant signature. Options, such as streptavidin resins, or detecting exosome isolation with the same capture ligand are available to continue optimisation of these approaches in the future. This is something likely to be of academic and commercial interest. To continue this present study a system-wide approach of analysing exosomes from AD patients would be pursued instead. Whilst “noise” may be generated from exosomes derived from other, unwanted source tissues it may be that CNS-relevant signals can be teased out of the bulk population or signals from unexpected sources may be of biomarker potential.

Chapter 5. Profiling of cellular and exosomal-RNA from a neuroglioma cell-line

5.1 Introduction

Exosomes contain functionally active RNA molecules: messenger RNA (mRNA) from exosomes can undergo translation into new proteins in recipient cells (Valadi et al., 2007) and micro RNA (miRNA) from exosomes can regulate gene expression and confer a phenotypic response in recipient cells (Narayanan et al., 2013). However, the repertoire of RNA within exosomes appears to differ from the source cells in some studies (Mittelbrunn et al., 2011, Li et al., 2015) but not others (Turchinovich et al., 2011, Tosar et al., 2015). Using electrophoretic analysis it has been determined that exosomes are devoid of rRNA, which is abundant within cells (Shelke et al., 2014). Rather, they are known to contain a variety of different RNA species including mRNA, miRNA, vault RNA, Y RNA, tRNA, siRNA and circRNA (Raposo and Stoorvogel, 2013, Dou et al., 2016, Nolte-'t Hoen et al., 2012). Many of these are not protein coding but instead play a role in gene regulation. Therefore, there appears to be a wide reach of gene regulatory effects that exosomal-RNA may influence.

To the author's knowledge a direct comparison between exosomes and the parent cells has only been performed with microarrays and small RNA-sequencing (Skog et al., 2008, Valadi et al., 2007, Nolte-'t Hoen et al., 2012, Cheng et al., 2014, Royo et al., 2013, Li et al., 2013, Ahadi et al., 2016b). It could be argued that these studies provide only a limited picture as the techniques used pre-select for a subset of the total population. Nevertheless, they have hinted that there is disparity between the RNA cargos of exosomes compared to the source cell.

The investigation of exosomal-RNA, with the aim of identifying biomarkers or functionally active species in disease, has predominantly focussed on small RNA (Bellingham et al., 2012, Burgos et al., 2014, Lugli et al., 2015). By selecting a subset of the total RNA in these studies, there is a limit to how much biological understanding can be obtained. This was reflected in a 2017 position statement by the International Society of Extracellular Vesicles: "This position paper was written […] to clarify that our incomplete knowledge […] currently prohibits the implementation of gold standards in [Extracellular Vesicle]-RNA research" (Mateescu et al., 2017).

The application of next-generation sequencing (NGS) technologies for the identification of non-coding RNAs (ncRNAs) has long been utilised (Jacquier, 2009, Kapranov et al., 2007). Such species do not map to protein coding regions, yet their transcription is pervasive (Carninci et al., 2005) and it has become clear that some species, such as miRNAs, have a

regulatory role in the expression of protein coding genes (Bartel, 2004). The addition of post-transcription modifications may well add to the complexity of RNA within exosomes (Hill et al., 2013) so NGS was chosen here as the best method to deepen the understanding of exosomal-RNA. Not only does NGS provide a non-bias approach to analysing RNA but the depth of data allows superior detection of splice variants and fusions (Haile et al., 2017). In particular, whole-transcriptome sequencing, with rRNA removal only, was chosen here so that the fullest view of the transcriptome could be obtained compared to small RNAseq or microarray analyses.

An emerging species of ncRNA are long non-coding RNAs (lncRNAs) also known as long intergenic non-coding RNAs (lincRNAs). Studies based on individual lncRNAs have previously shown a number of regulatory roles for this species. Such roles include X-chromosome inactivation by the 17 kb-long Xist ncRNA in mammals (Zhao et al., 2008), genomic imprinting and chromatin remodelling by 91 kb-long Kcnq1ot1 antisense ncRNA (Pandey et al., 2008), transcription repression in development by the 2.2 kb-long HOTAIR ncRNA (Rinn et al., 2007), epigenetic regulation of transcription through histone modifications by the 108 kb-long Air ncRNA (Nagano et al., 2008), gene silencing in response to p53 activation by the 3.1 kb-long lincRNA-p21 (Huarte et al., 2010) and regulation of pluripotency genes by the 17.6 kb-long lincRNA-RoR (Loewer et al., 2010). Large screens of lncRNAs have revealed that they can act in *trans* (Guttman et al., 2011), as enhancer RNAs (De Santa et al., 2010), or in *cis* (Orom et al., 2010).

With such a wide variety of functions and mechanisms, lncRNAs are best described as a species of RNA with many sub-families which have yet to be defined. The tools needed for probing deeper into lncRNAs are currently emerging. Catalogues of lncRNA annotations are now being developed (Cabili et al., 2011) and utilised with RNA sequencing datasets. One such study, found differentially expressed lncRNAs in ischemic cardiomyopathy with suggested roles in fibrosis and regulating extracellular matrix synthesis genes (Huang et al., 2016). Another study used this catalogue to find that the anti-cancer drug KR12 did not have an effect in colorectal cancer via lncRNAs (Lin et al., 2016). Directly probing the effects of lncRNAs, by *in vitro* knock-down or knock-up (Loewer et al., 2010), can only be done experimentally on a selected candidate level yet thousands of lncRNAs have now been annotated. Therefore, bioinformatics tools are being established that can link function to lncRNA expression by identifying protein coding-genes that have correlative expression (Huang et al., 2016). Two such publically available tools are lncRNA2function (Jiang et al.,

2015) and Co-LncRNA (Zhao et al., 2015). As such, the tools for investigating lncRNAs are being developed and used to deepen understanding in this emerging field.

Deep –omic profiling of extracellular particles, with similar characteristics to exosomes, released by mast cells showed an enrichment for lncRNAs (Lasser et al., 2016). In a prostate cancer dataset, microarray analysis has revealed the presence, and reported abundance, of lncRNAs in exosomes (Ahadi et al., 2016b). In this dataset, differentially expressed lncRNAs in exosomes were identified across the four different cell-lines investigated. These lncRNAs were enriched for miRNA seed regions and RNA binding protein motifs, suggesting a potential role for these lncRNAs in disease propagation (Ahadi et al., 2016a). Another study performed qPCR analysis of the lncRNAs HOTAIR, MALAT1 and MEG3 in exosomes derived from the cervicovaginal lavage of cervical cancer patients. These lncRNAs were differentially expressed in disease patients (Zhang et al., 2016b) and whilst this was only a small candidate study, it promotes the utility of exosomal lncRNAs as biomarkers of disease.

In this current study, the H4 cell-line was chosen for whole transcriptome sequencing of exosomes and source cells. The aim was to deepen the understanding of exosomal-RNA and how it relates to the source cell and included an analysis of lncRNA expression. A thorough characterisation of exosomes secreted from this cell-line had been performed in Chapter 3 to validate the type of EV being analysed. Furthermore, the cell-culture methods that had been developed could be scaled up to provide an abundant source of exosomes. Whilst this particular study performed first principle sequencing of cellular and exosomal-RNA the choice of the H4 cell-line would pave way for future work with relevance to AD.

The H4 cell-line has previously been used as a cell model of AD due to its neural origin. A number of mechanistic, intracellular trafficking studies have utilised the cell-line to investigate the production of amyloid-β (Aβ). One study demonstrated that amyloid precursor protein (APP) is abundantly expressed in H4 cells and intracellular cleavage to amyloidogenic fragments has been shown to occur in late trans-Golgi network (Kuentzel et al., 1993). Another study adopted the H4 cell-line and found that APP associates with the low-density lipoprotein receptor of APOE (Rebeck et al., 2001).

The cell-line is tolerant to genetic manipulation and has been adopted for numerous studies. One such study introduced a mutated form of presenilin-1 (C92S), discovered in an Italian family with familial Alzheimer's disease, into H4 cells and found this caused increased production of pathogenic Aβ42 (Lewis et al., 2000). Another study introduced three different presenilin-1 mutations (A246E, L286V and deltaE10) and showed that H4 cells with mutated

PS1 were more susceptible to caspase-3 mediated cell death than cells transfected with wild type protein when induced with Staurosporine (Kovacs et al., 1999). Additionally, the H4 cell-line was used to identify novel APP fragments that induce a pathogenic cascade of events which were then replicated in primary cultured neurons (Fiorelli et al., 2013). Thus, the H4 cell-line has proved a useful tool for deepening the understanding of some of the cellular processes underlying AD.

In this chapter, the use of the H4 cell-line has been used primarily as an abundant source of exosomes, to isolate exosomal-RNA, and analyse it in relation to the source cell. However, it has long been adopted to produce cell models of AD, so generation of cellular and exosomal transcriptome data may well complement, or drive, further studies In AD.

5.2 Aim

The aim of this chapter was to comprehensively profile RNA from H4 neuroglioma cells and compare to the RNA of secreted exosomes captured in the culture medium. To achieve this aim the following objectives were addressed:

- Validate procedures for the isolation of RNA from H4 cells and secreted exosomes
- Profile cellular and exosomal-RNA by global measurements of quality and next-generation sequencing
- Identify differentially expressed RNA transcripts and perform a functional annotation of cellular- and exosomal-RNA

5.3 Results

5.3.1 Profiling cellular and exosomal-RNA using global measurements of quality

To address the aim of profiling RNA from H4 cells and exosomes, total RNA was extracted from both. Exosome-rich cell-conditioned media was collected at the same time as cellular RNA isolation. This allowed the most direct comparison between the two sample types as possible.

Prior to isolating RNA from exosomes the procedure for digesting non-vesicular RNA (Shelke et al., 2014) was validated to ensure that downstream extractions and analyses were based on genuine intra-luminal, vesicle cargo. 20 µg exosomes, isolated from bioreactor cultures, was subjected to proteinase K (PK) and RNase A (RA) digestion and compared to a PBS-treated control. Electrophoretic analysis revealed a decrease in measured RNA with PK/RA treatment (Figure 5.1). Measured concentrations were 2.5 and 4.3 ng/µl for treatment and no-treatment, respectively, equating to a 42% digestion of RNA. The electropherograms also showed that a population of RNA with a small nucleotide length was removed with PK/RA digestion. This is reflected in the DV_{200} calculations where 89% of RNA was greater than 200 nucelotides in length for the treated sample compared to 69% for the PBS-treated control (Table 5.1). This suggests that the non-vesicular RNA present in the exosome preparation is enriched for small RNA species, such as miRNAs, and that this population can be removed by PK/RA digestion. The RNA remaining, and extracted for analysis, is resistant to RNase digestion because of its protected location inside the vesicle.

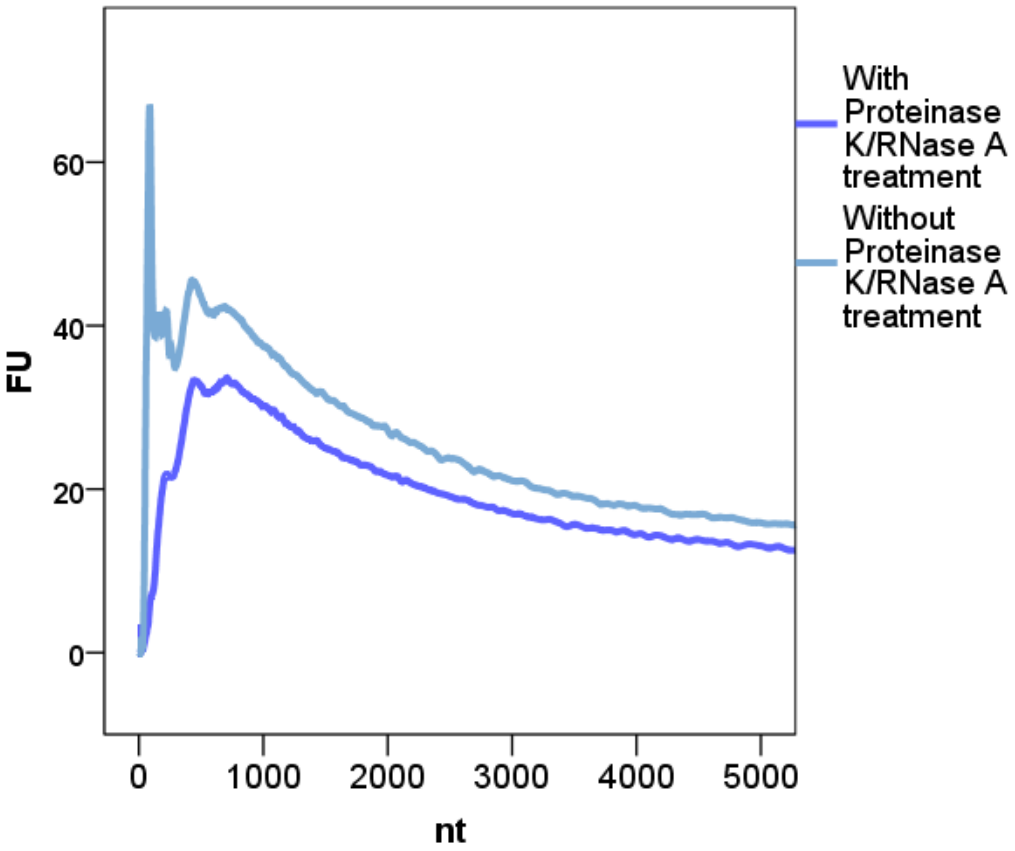

Figure 5.1: Electrophoretic analysis of RNA isolated after Proteinase K and RNase A digestion. *Exosome pellets, obtained by the pellet and PBS wash procedure, were subjected to PK/RA treatment to digest non-vesicular RNA. Agilent Bioanalyser instrumentation was used, with the RNA pico chip, to measure fluorescence units (FU, y-axis) of RNA samples (n=1 per treatment). Concentrations were calculated by the instrumentation as 2.5 and 4.3 ng/µl for PK/RA treatment (dark blue) and no-treatment (light blue), respectively. Nucleotide (nt) length is displayed on the x-axis.*

Treatment	Concentration (pg/µl)	DV_{200}	RIN
With PK/RA	2520	89	n/a
Without PK/RA	4343	69	n/a

Table 5.1: Electrophoretic analysis of RNA isolated after Proteinase K and RNase A digestion. *Agilent Bioanalyser instrumentation was used with the RNA pico chip to evaluate the quality of RNA samples that had been subjected to PK/RA treatment. A Smear analysis was performed to calculate DV_{200}, that is, the proportion of the electropherogram that is >200 nucleotides in length. Without rRNA the RNA Integrity (RIN) score was not calculable from these traces.*

With this validated digestion procedure in place the extraction of cellular- and exosomal-RNA was pursued. Three biological replicates of the H4 cells were established by sub-culturing in separate flasks for 2 passages prior to expansion into ten T75 flasks for each replicate. Once the cells had reached 70% confluency, the conditioned media was replaced with 10 ml fresh media supplemented with exosome-depleted FBS. This ensured that only exosomes from the H4 cells were collected, particularly avoiding bovine exosomes. After 7 days, the conditioned media was collected, spun, filtered and frozen at -80°C whilst the cells were detached, washed in PBS and RNA extracted. Exosomes were prepared from the conditioned media by pelleting at 200,000 x g for 2h with a PBS wash. Exosome pellets were treated with PK/RA to remove non-vesicular RNA prior to extraction. Thus, three biological replicates of H4 cellular-RNA and secreted exosomal-RNA were established.

RNA was initially profiled by two global measurements of quality, namely electrophoretic analysis with Bioanalyser instrumentation and fluorometric quantitation using Qubit instrumentation.

Electrophoretic analysis revealed a stark difference between cellular- and exosomal-RNA (Figure 5.2) consistent with published data (Shelke et al., 2014). Cellular-RNA was replete with ribosomal RNA (rRNA), as observed with the 18S and 28S peaks at ~1800 and ~3800 nucleotides, respectively. The traces for exosomal RNA did not contain such peaks. Instead, the trace for the exosomes was distinct from the respective small nucleotide peak observed in the cell samples. This suggested that there was a distinct population of RNA species within exosomes.

Further evaluation of RIN and DV_{200} scores reflected these visual observations of the electropherograms (Table 5.2). An automatic calculation performed by the instrumentation is the RNA integrity (RIN) score. The cellular-RNA samples all had RIN scores of 10 reflecting intact samples with no RNA degradation. Thus, RNA extraction procedures were of good quality. The exosomal-RNA samples were much lower at ~2 but this can be explained by the absence of 18S and 28S rRNA peaks that RIN is calculated from. Indeed, RIN is an arbitrary measurement if there is no rRNA expected within the sample. Therefore, DV_{200} was chosen as an alternative measure of RNA quality. The DV_{200} scores were lower for the exosome samples with 57-64% of the traces being from species >200 nucleotides in length compared to 81-84% in cells. All of these samples would be considered of high enough quality (>30%, according to manufacturer's specifications) to continue with downstream applications such as sequencing (Eikrem et al., 2016).

Fluorometric quantitation was also performed using Qubit instrumentation (Table 5.2). An abundance of RNA was extracted from cells (225-275 ng/µl) but much lower from exosomes (9.4-13.1 ng/µl). These concentration readings highlight the relative ease of extracting plentiful stocks of RNA from cells compared to exosomes.

Standard quality checks were performed with these exosome preparations, as established in chapter 3, using NTA and BCA assay. The particle concentrations ranged from $9.44x10^{13}$ – $1.20x10^{14}$ and protein concentrations ranged from 2284 – 2986 µg/ml. P:P ratios were calculated to be $4.62x10^{10}$ for Exosome A, $3.31x10^{10}$ for Exosomes B, and $4.13x10^{10}$ for Exosome C, all of which exceed the $3x10^{10}$ ratio to be considered highly pure preparations according to Webber and Clayton, 2013. The quantity of RNA per particle was calculated, using NTA and Qubit values, as a rough estimation of the RNA content of each vesicle, accepting the caveats of NTA, as discussed in chapter 3. Sample Exosome A had $9.7x10^{-14}$ pg RNA/particle, Exosome B had $1.32x10^{-13}$ pg RNA/particle and Exosome C had $9.96x10^{-14}$ pg RNA/vesicle. Whilst NTA provides an overestimation of the number of vesicles, by indiscriminately measuring particles, the values again highlight the technical difficulty of extracting plentiful quantities of RNA from exosomes.

Sufficient material had been obtained for RNA sequencing to further profile both of these sample types. From global quality measurements these samples had already shown remarkable distinction but RNA sequencing would provide a greater depth of data to further understand these differences.

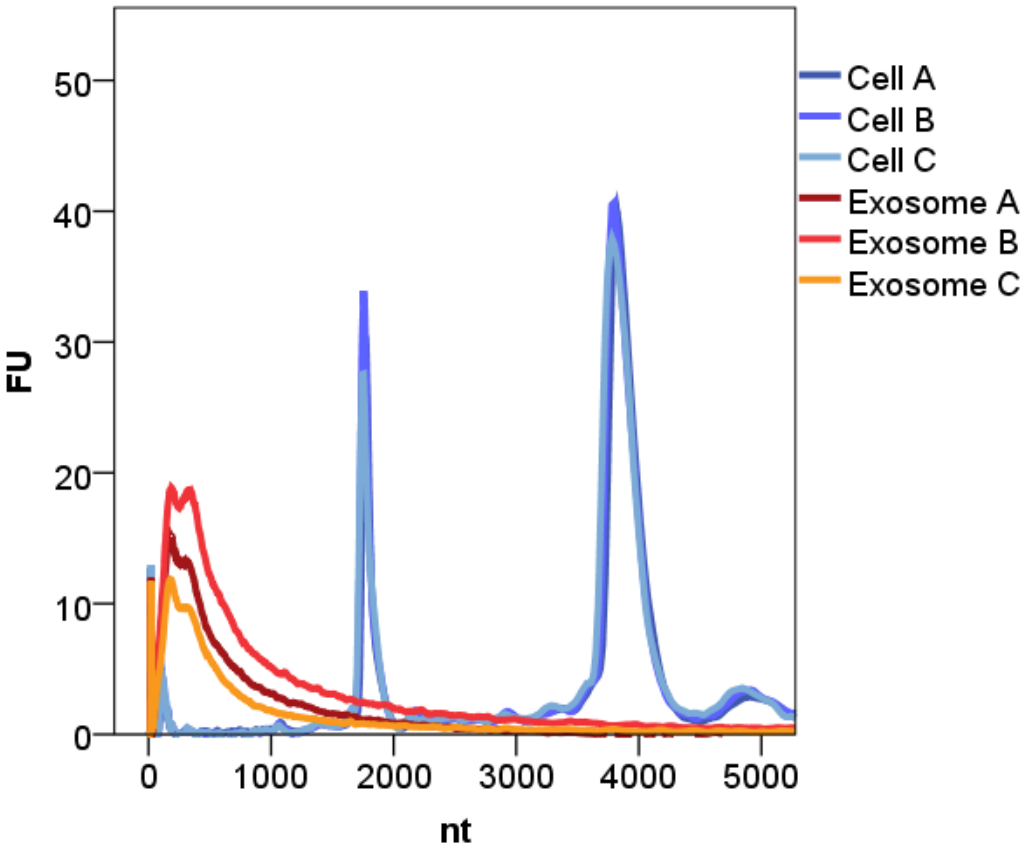

Figure 5.2: Electrophoretic analysis of RNA extracted from H4 cells and secreted exosomes.
Three biological replicates (n=3 each for cells and exosomes) were prepared and processed on the Agilent Bioanalyser using the Nano chip. Fluorescence units (FU) are displayed on the y-axis and nucleotide length (nt) on the x-axis. 18S and 28S peaks, at ~1800 and ~3800 nucleotides respectively, indicated that the cells (blue lines) were replete with ribosomal RNA whilst exosomes (red lines) were deplete of these species. Traces from individual samples are plotted rather than plotting an average.

Sample	Concentration (ng/µl)	RIN	DV_{200} (%)
Cell A	225.0	10	84
Cell B	320.4	10	82
Cell C	275.4	10	81
Exosome A	11.6	2.1	58
Exosome B	13.1	2.1	64
Exosome C	9.4	2.2	57

Table 5.2: Electrophoretic analysis and fluorometric quantitation of RNA extracted from H4 cells and exosomes.

The concentration of RNA extracted from cells and exosomes (n=3 each) was quantified using fluorometric analysis (Qubit instrumentation). RNA integrity (RIN) scores were automatically calculated using the Agilent Bioanalyser instrumentation as one readout of RNA quality. As an alternative assessment of quality, which is less reliant on ribosomal RNA in the sample, the DV_{200} score was calculated manually using a Smear Analysis. DV_{200} is a calculation of the percentage of the trace with nucleotide fragments greater than 200 bp. Individual samples are reported rather than displaying the average.

5.3.2 Profiling cellular and exosomal RNA using next generation sequencing – Quality control

Total RNA sequencing libraries were prepared using TruSeq stranded Total RNA with ribo-zero Gold kit (Illumina) at the Wales Gene Park (Cardiff University). The ribosomal RNA depletion step was chosen to eliminate these species but detect the total remaining RNA. 6 libraries were pooled and sequenced over 2 lanes of a flow cell (HiSeq 2500) generating ~89 gigabases of data. Wales Gene Park performed the initial conversion and de-multiplexing of sequencing files using the bcl2fastq software (Illumina) before making .fastq and insert size metric files available for download.

The distinction between cellular and exosomal RNA, observed by electrophoretic analysis, was observed again with the library insert sizes after preparation (Figure 5.3). The insert size metrics relate to the length of RNA after conversion to barcoded cDNA in the library preparation. With rRNA depleted, a unimodal distribution of insert sizes, around 100 bp, was observed for Cell A-C. This is in contrast with a bimodal distribution for Exosome A-C libraries, which contained a sub-population of larger inserts. Again, this hints of a biological distinction inherent within the samples even before sequencing data was obtained. These libraries were subjected to 100 bp paired-end (PE) sequencing.

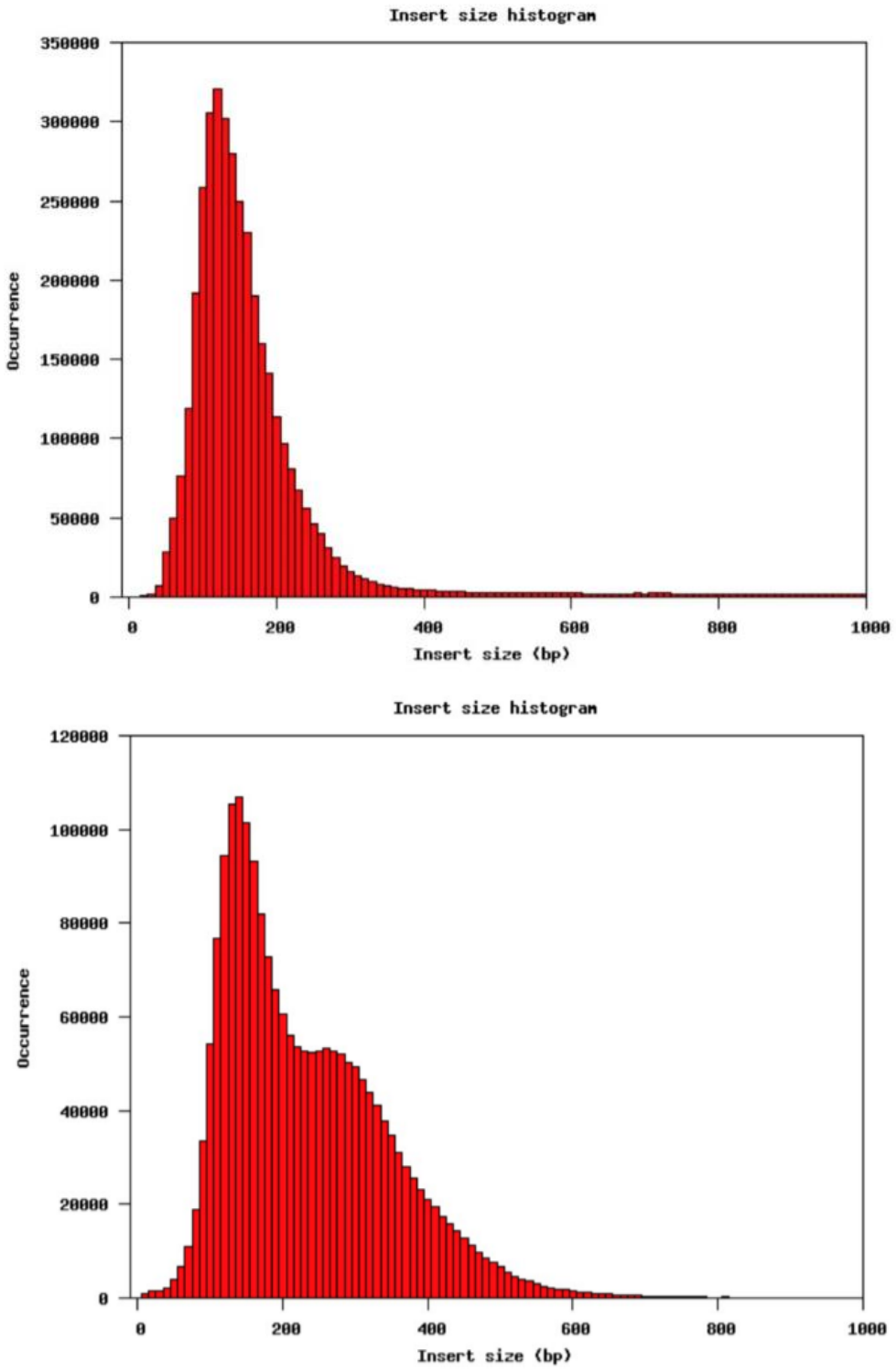

Figure 5.3: Insert size Histograms after total RNA library preparation.
Sequencing libraries were prepared from cellular-RNA (top, 1 library indicative of n=3) and exosomal-RNA (bottom, 1 library indicative of n=3). The insert sizes (measured in base pairs, bp, x-axis) were measured by Bioanalyser instrumentation at Wales Gene Park.

At the Wales Gene Park twenty-four .fastq files were generated from this sequencing run: 2 read files for each library run in duplicate on separate lanes. These were downloaded and the following analyses were performed by the author.

Fastq sequencing files were processed by the software FASTQC (Babraham Bioinformatics) which provided a plethora of tests to determine the quality of the sequencing run. For example: per base sequence quality was reported for each base along the 100 bp read in the .fastq files (Figure 5.4). Typically the first 5 bases of each read had lower scores and quality was slightly poorer after the paired-end turnaround. However, these all remained within the high quality range (28-40 Phred score), so overall the sequencing was performed well. This was observed across all 24 .fastq files indicating that base calling was accurate.

FASTQC provides a traffic light system for a number of other tests that can be informative for evaluating the overall quality of the sequencing run. Two such warnings, at the base level, were for Kmer content and per base sequence content for the first 10 bases (Figure 5.5). According to manufacturer guidelines these are standard, and benign, artefacts of the Nextera transposase that ligates adaptor sequences during library preparation. As these would not have an impact on downstream analyses they were not trimmed out, although there are software packages such as FASTX-Toolkit (Hannon Lab) and Trimmomatic (Usadel Lab) that are able to do this if required.

A second set of warnings were prompted at the sequence level, with per sequence GC content and sequence duplication levels (Figure 5.6). These tests aim to flag up a PCR bias within the library preparation. Such metrics are of concern in the case of DNA sequencing e.g. whole exome or whole genome sequencing. In these techniques, duplicate metrics should be analysed further as a percentage of the total reads, but in the case of RNAseq duplicates are explained and expected with the uneven nature of gene expression. Therefore, duplicates were marked using Picard but not removed as this may distort the expression profile downstream.

Together, these data highlight that FASTQC, whilst a useful tool for identifying issues within the sequencing, is calibrated for whole genome and whole exome data where uniformity is desired. Therefore, careful interpretation of these RNAseq results was required. Overall, the sequencing was of good quality and, other than marking duplicates, no further processing was performed prior to downstream analyses.

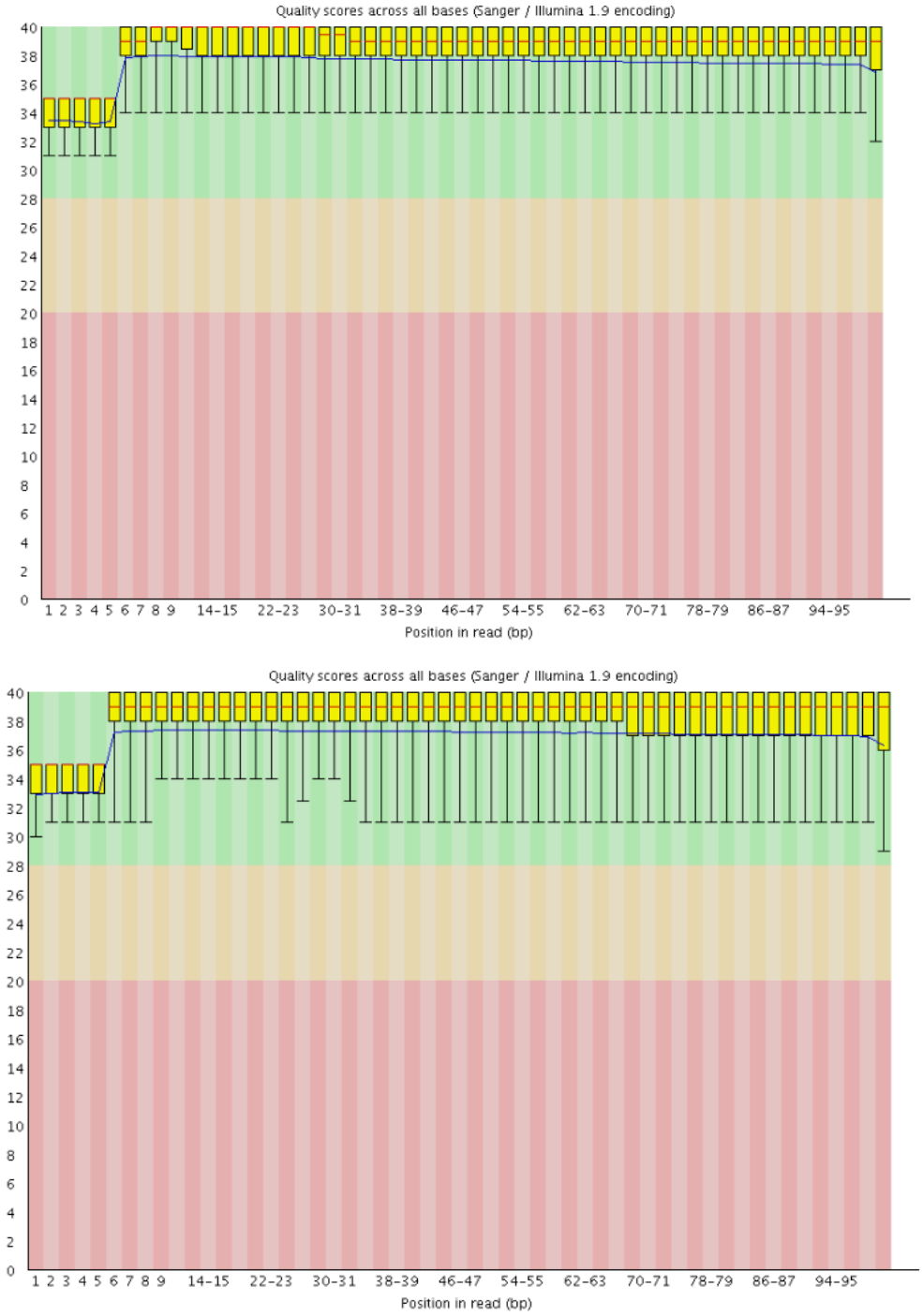

Figure 5.4: Per base sequence quality report for paired-end reads of Cell A sequenced on one flow-cell lane.

Quality scores were recorded by the HiSeq sequencing instrumentation and displayed graphically using the FASTQC software. These graphs are representative of 24 .fastq files. Read 1 is shown on the top and read 2, after the paired-end turnaround, on the bottom. The position in read (x-axis) is measured in base pairs (bp) as the sequencing run was occurring and quality indicated with a Phred score ranging from 0 (poor quality) to 40 (good quality) on the y-axis. FASTQC indicates high, medium and low quality ranges using traffic light colour system. The mean and range of quality across the sample is displayed using box and whiskers.

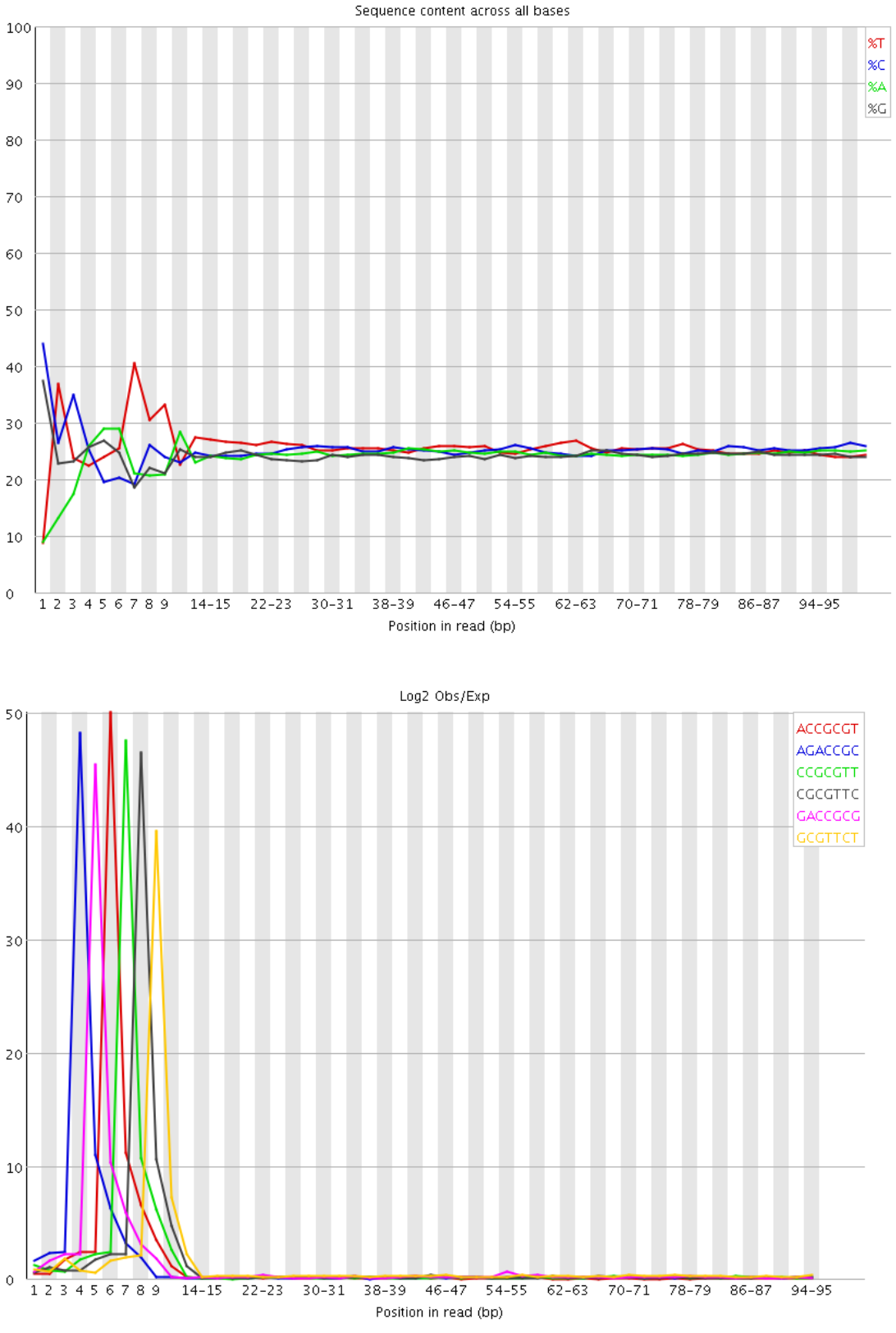

Figure 5.5: FASTQC warnings at the base level.
These reports were produced from Cell Sample A sequenced on one flow-cell lane but representative of all 24 .fastq files. Per base sequence content (top) was flagged up for the first 10 bases (bp, x-axis) with differing percentages (y-axis) of individual bases. Kmer content (bottom) was flagged up for the first 10 bases (bp, x-axis) with higher observations (y-axis) of the sequences indicated in the key.

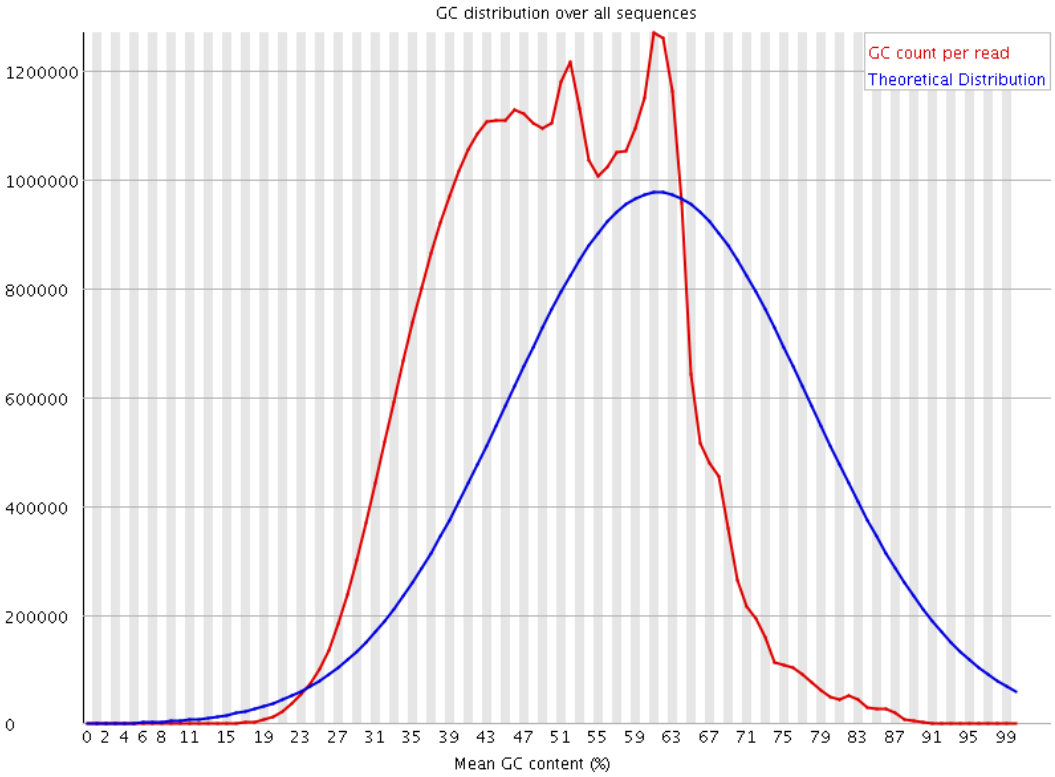

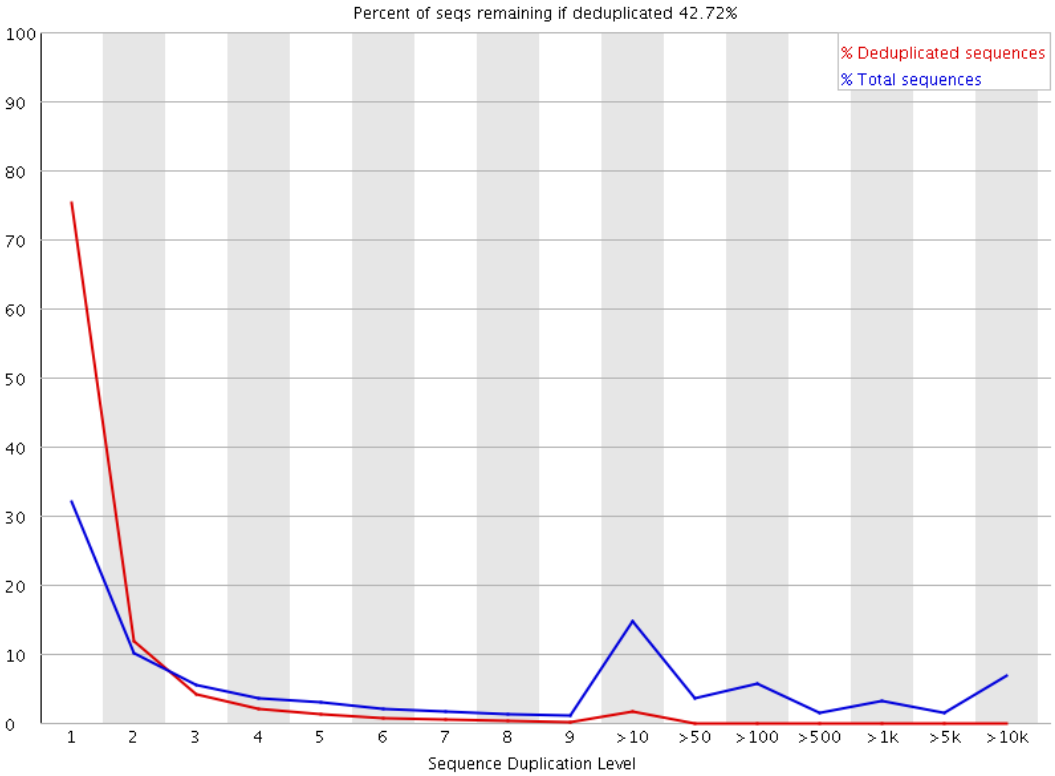

Figure 5.6: FASTQC warnings at the sequence level.
These reports were produced, by FASTQC software, from Cell Sample A sequenced on one flow-cell lane but representative of all 24 .fastq files. GC content (Top) was flagged up as differing from a theoretical distribution expected from the measured reads (y-axis). Duplication (Bottom) was flagged up at the sequence level as a percentages (y-axis) that differed from the deduplicated sequences.

5.3.3 Profiling cellular and exosomal RNA by next generation sequencing – read alignment, mapping and merging .bam files

The next step in the analysis pipeline was to map and align reads to the human genome (hg19). This was performed using the TopHat software (Johns Hopkins University) to generate twelve .bam files (Table 5.3). The Bowtie 2 hg19 index was downloaded from http://bowtie-bio.sourceforge.net/bowtie2/manual.shtml (accessed May 2016) and gene model annotations provided in .gtf format downloaded from http://ftp.ensembl.org/pub/release-74/gtf/homo_sapiens/ (accessed May 2016). All Cell .fastq files mapped well with overall read mapping rates of ~90%. The Exosome files did not map as well with overall read mapping rates of ~70%. Closer inspection of the alignment metrics (Table 5.3) revealed that whilst the left reads mapped fairly close to 90% it was the low mapping rates of right reads that were driving this poor overall mapping rate. This was investigated further to seek an explanation.

The libraries for both cells and exosomes were prepared at the same time suggesting that this disparity of mapping rates is due to a difference inherent in the samples rather than a technical issue. The sequencing quality was good across both right and left reads, as reported above (Figure 5.4), again showing that a technical issue had not arisen in the sequencing run. So with identical preparation procedures, and accurately performed sequencing, there is a suggestion that these poor mapping rates for exosome right reads, is due to a divergence from the reference at the 3' end. Therefore, the insert sizes (Figure 5.3) for exosomes was further investigated.

As previously discussed, distribution plots revealed that exosome libraries had a second population of larger size inserts (Figure 5.3). To investigate if this population mapped poorly at the 3' end, in general, a second mapping software was tested. The Burrows-Wheeler Aligner (BWA) was chosen to compare with TopHat as it typically has a lower threshold for read mapping. Paired-end reads from Exosome 1 (Lane 1) were mapped to hg19 using both pieces of software and the resultant .bam files were analysed using the Samtools flagstat tool (Table 5.4). BWA mapped more reads, particularly right reads, which TopHat did not. This confirmed the threshold differences within these software, whereby, TopHat is more stringent and does not map a proportion of these reads.

Sample	#Left reads	#Left reads mapped	%Left reads mapped	#Right reads	#Right reads mapped	%Right reads mapped	Overall read mapping rate (%)
Cell A (Lane 1)	39906314	36414515	91.3	39906314	35839860	89.8	90.5
Cell A (Lane 2)	39830972	36426648	91.5	39830972	35854738	90.0	90.7
Cell B (Lane 1)	46314074	41928379	90.5	46314074	41150666	88.9	89.7
Cell B (Lane 2)	46487587	42168699	90.7	46487587	41392603	89.0	89.9
Cell C (Lane 1)	45598728	41015278	89.9	45598728	40469754	88.8	89.4
Cell C (Lane 2)	45576114	41072179	90.1	45576114	40534216	88.9	89.5
Exosome A (Lane 1)	35870502	31409777	87.6	35870502	20923299	58.3	72.9
Exosome A (Lane 2)	36162976	31731230	87.7	36162976	21162231	58.5	73.1
Exosome B (Lane 1)	20822237	18440242	88.6	20822237	11084877	53.2	70.9
Exosome B (Lane 2)	20857814	18502700	88.7	20857814	11143441	53.4	71.1
Exosome C (Lane 1)	33243277	28537108	85.8	33243277	20555355	61.8	73.8
Exosome C (Lane 2)	33435182	28752890	86.0	33435182	20741236	62.0	74.0

Table 5.3: Mapping metrics from TopHat.
Sequencing read mapping was performed and mapping rates calculated using TopHat. Individual samples, on individual sequencing lanes, are displayed rather than using the average. Raw read numbers (#) and percentages (%) are reported.

	TopHat	BWA
Total reads mapped and paired in sequencing	67796052	72725273
Read1	40182355	36129350
Read2	27613697	36595923

Table 5.4: Read numbers taken from Samtools flagstat report for TopHat and BWA mapping. *Samtools software was used to compare the read numbers from two mapping softwares, TopHat and BWA. Paired-end reads from Exosome 1 (Lane 1, n=1) were chosen to compare these two software. Raw read numbers are displayed with a breakdown of left reads (Read1) and right reads (Read2).*

Next, the CollectInsertSizeMetrics tool in Picard (Broad Institute) was used to assess the insert sizes of these differently mapped .bam files (Figure 5.7). TopHat mapped reads of relatively uniform size compared to the wider spread of insert sizes in the BWA .bam file. The median insert size in the TopHat file was 178 ± 45 bp compared to 209 ± 73 bp for BWA (Table 5.5). This confirms that BWA, by reducing stringency, did not filter out the reads from larger insert size that TopHat did. This answers the original query about why TopHat had reduced mapping rates for exosomes: the sub-population of larger size inserts (Figure 5.3) map poorly at the 3' end. This is unique to exosomal-RNA and not the cellular-RNA.

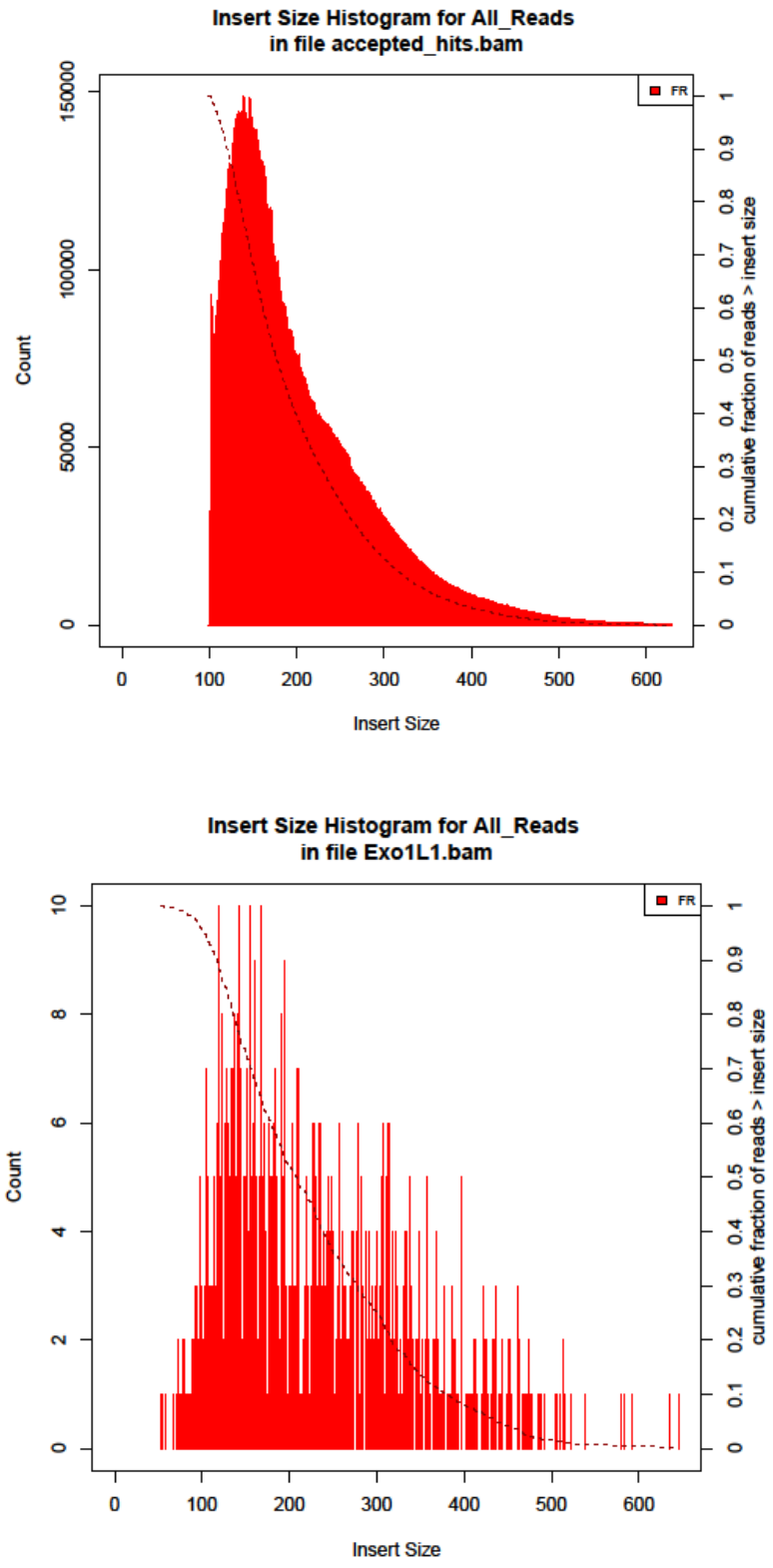

Figure 5.7: Insert size metrics for Exosome 1 (Lane 1) mapped with TopHat (top) and BWA (Bottom). *Histograms were plotted, using the CollectInsertSizeMetrics tool in Picard, to compare .bam files mapped using TopHat and BWA (n=1 per software). Insert sizes were measured in base pairs (x-axis) and read counts displayed on the y-axis.*

	TopHat	BWA
Median size (bp)	178	209
Absolute median deviation	45	73
Mean size (bp)	201	229
SD	82	105

Table 5.5: Insert size metrics for Exosome 1 (Lane 1) mapped with TopHat and BWA.
Insert size metrics were calculated using the CollectInsertSizeMetrics tool in Picard, to compare .bam files mapped using TopHat and BWA (n=1 per software). Both median and mean measurements of insert size are reported with standard deviations (SD).

To assess whether using BWA would be advantageous for a downstream differential gene expression analysis both .bam files were used for a gene count using HTSeq (EMBL, Heidelburg). The TopHat file provided 1053915 gene counts compared to 838121 for BWA (Table 5.6). This suggests that the mapped reads provided by BWA did not reside within standard gene regions and therefore detected by the gene count software. This confirmed that the lower read mapping rate of TopHat was being driven by the larger inserts observed for exosomes diverging from the reference. Furthermore, given the lower gene count and spread of insert size, the BWA mapping tool was not advantageous so TopHat was chosen for this analysis pipeline.

The twelve .bam files output from TopHat were separated by sample and lane. Prior to further analysis, these were merged to produce six .bam files, one for each biological replicate, using the SAMtools merge tool. There were between 169 – 193 million reads in each of the cell files and 77 – 136 million reads in the exosome files (Table 5.7). As expected from the original mapping rates, the second reads mapped poorly for exosome samples when .bam files were merged. It may be that the library preparation procedure for exosome samples could be optimised to improve these but this was beyond the cost and sample limitations of this study. With these data available in .bam format, further analyses were then performed.

	TopHat	BWA
Sum of gene counts	1053915	838121

Table 5.6: Sum of gene counts from Exosome 1 (Lane 1) using HTSeq.
HTSeq was used to assess the number of gene counts possible from the mapping software TopHat and BWA from one sequencing file (n=1). The total sum of gene counts is displayed.

	Mapped	Paired in sequencing	Read 1	Read 2
Cell A	169280297	145232055	73189869	72042186
Cell B	193759301	167473996	84513562	82960434
Cell C	189580918	163865727	82480521	81385206
Exosome A	136320008	105383314	63257700	42125614
Exosome B	77557814	59367811	37067297	22300514
Exosome C	129999401	98911477	57500125	41411352

Table 5.7: Read numbers taken from Samtools flagstat report for merged .bam files.
Samtools was used to merge .bam files from individual sequencing lanes (n=2 per sample) and report the total read numbers in the resultant files. Raw read numbers are reported. Read 1 refers to the left reads and Read 2 to the rights reads of the paired-end sequencing.

5.3.4 Profiling cellular and exosomal-RNA by next generation sequencing – RNAseq metrics

After aligning reads to hg19 and merging .bam files into each biological replicate, the next stage of the analysis pipeline was to evaluate the different species of RNA, on a global level, within the samples. The CollectRnaSeqMetrics tool on Picard was used to annotate reads within the six .bam files with reference to the gene model annotaton file (.gtf) used during the mapping stage (Figure 5.8).

These metrics revealed a distinction between the cells and the exosomes. Reads mapping to coding regions only accounted for ~1% exosomal RNA compared to ~40% in cells. Rather, exosomal RNA was replete with reads that mapped to intronic and intergenic regions of the genome. Thus, the transcriptome of exosomes is fundamentally different to the cells they were secreted from. Binomial exact tests were statistically significant ($p<0.001$) across the coding, intergenic, intronic and UTR annotations.

It should be noted that the extent of this difference may be exaggerated by the library preparation choice. These data would suggest that there is minimal or no coding RNA in exosomes, which is not in keeping with the literature which has demonstrated functionally active coding RNA in exosomes (Valadi et al., 2007). It would be expected that coding RNA would have been sequenced from exosomes if a different library preparation had been used, for example one that used Oligo dT beads to capture poly-A tails. Instead, the Total RNA with Ribo-Zero Gold used here may have caused a preferential sequencing of intronic and intergenic reads which may be exaggerating the observed profiles. Accepting the caveats, this library preparation technique provides the fullest view of the transcriptome possible with currently available techniques and additionally, cell and exosome libraries were prepared simultaneously so can be directly compared. Therefore, the difference in cell and exosome transcriptomes can be accepted, with the caveat that the extent of this difference may be exaggerated by the techniques used in sequencing.

Whilst this observation shed light on an intriguing aspect of cell biology it also posed a problem for downstream analyses. To perform a differential gene expression analysis there is a normalisation step that takes into account the size of the library that gene counts were taken from. In this case, gene counts being based on ~1% of the exosome libraries but ~40% of cell libraries would skew the normalisation step. Indeed, directly comparing such fundamentally different samples in this way would be inappropriate.

So without directly comparing cells to exosomes based on their exonic gene counts two other avenues of investigation were pursued. Firstly, long non-coding RNAs (lncRNA) were chosen as they would come under the intronic and intergenic portions of the reads. The direct function of these molecules is poorly understood but identifying differentially expressed lncRNAs which have co-expressed mRNAs would then allow functional annotation of the samples. Secondly, the intronic reads were directly compared between samples. By linking back to the gene-names, functional annotation was again possible. These analyses are reported below.

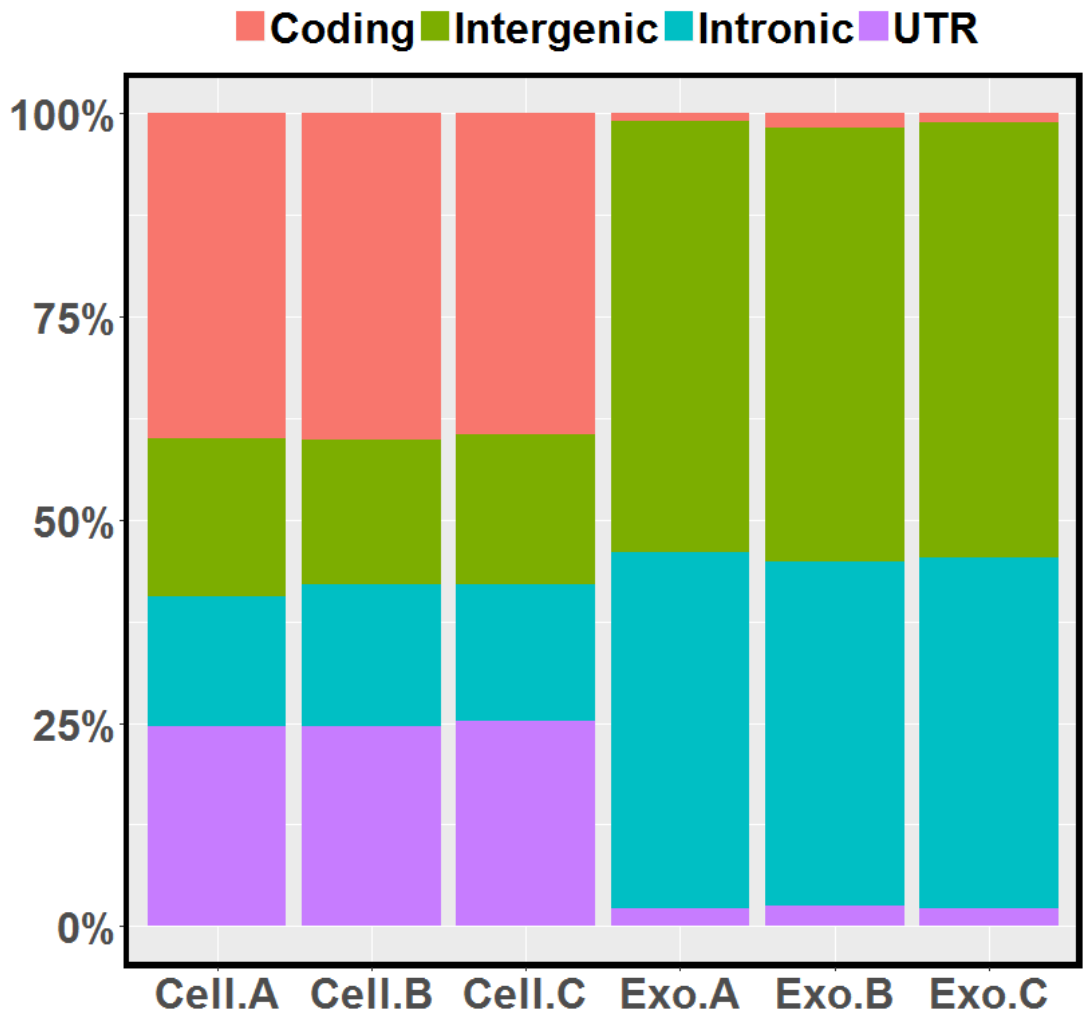

Figure 5.8: RNAseq metrics for cells and exosomes collected using Picard.
Picard was used to assess the content of RNA within the sequencing samples (n=6). Each biological replicate is represented by a bar as indicated on the x-axis. Red colouring represents coding bases, green represents intergenic, blue represents intronic and purple represents untranslated regions. Percentages of each type is indicated on the y-axis.

5.3.5 Differential expression analysis of lncRNAs

Count files give a count of the number of reads that reside within a given annotation, in this case, lncRNAs were counted. The HTSeq software was used to produce count files from the mapped reads using the Human lincRNA Catalog (Broad Institute), in .gtf format, as a reference (http://portals.broadinstitute.org/genome_bio/human_lincrnas/?q=lincRNA_catalog, accessed November 2016). This database was chosen as it has defined >8000 lncRNAs (Cabili et al., 2011) and has been used independently of the Broad Institute (Huang et al., 2016). Differential expression of counted lncRNAs was then performed using DESeq2 (Love et al., 2014).

Prior to directly comparing the samples from merged .bam files, the variability between lanes on the flow cell were assessed (Figure 5.9). Whilst this was only a visual check on variability there was no obvious issue of one lane providing anomalous counts. Therefore, the differential expression pipeline was pursued further with merged .bam files.

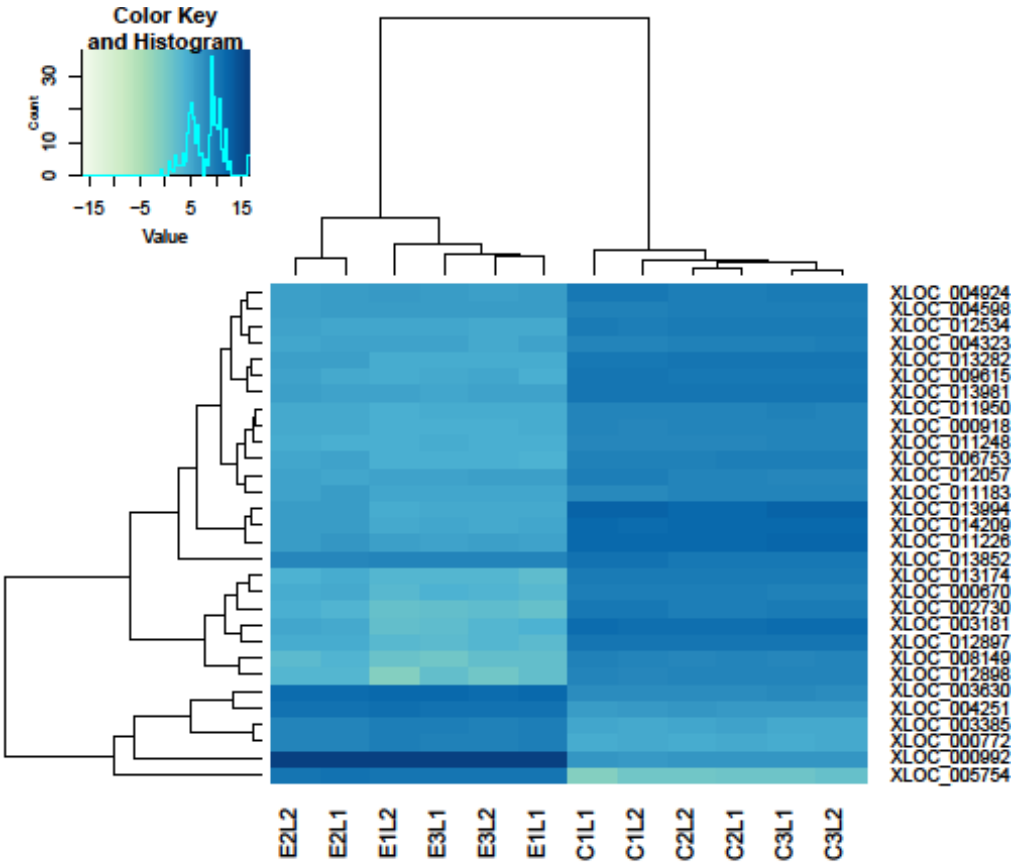

Figure 5.9: Heatmap showing 30 differentially expressed lncRNAs across all sequencing lanes.
DESeq2 was used to assess lncRNA counts (y-axis), as indicated by colour intensity, across six RNA samples (x-axis, C = cell, E = exosome) measured on separate sequencing lanes (L1 = lane 1, L2 = lane 2). Topological similarities were automatically generated by the software and indicated on both axes.

Firstly, sample relationships were explored to investigate the global differences between samples before individual lncRNAs were analysed. The dataset was run into DESeq2 and pre-filtered to remove rows with no counts across the samples. This improved computation times as the number of rows was reduced from 8263 to 7978. Therefore, 285 lncRNAs had no counts across both cell and exosome samples. To allow the calculation of distances between samples the data was transformed using the regularised-logarithm transformation (rlog) as suggested in the software workflow (Love et al., 2014). This stabilises the variance across the mean making the data approximately homoscedastic.

Using rlog transformed data, Euclidean distances between samples were calculated and plotted as a heatmap (Figure 5.10). This emphasised the biological picture that was already emerging: that the RNA profile of cells and the secreted exosomes are distinct. There was separation between cells and exosomes at a sample distance level but good similarity within these two groups. This reproducibility between biological replicates highlights the homogenous characteristics of cell-cultures which would not be expected for patient samples which would likely be highly variable between people.

The sample-to-sample distances were further visualised with a principal component analysis (PCA). Samples were plotted across two dimensions where most of the variance (98%) was explained with the first principle component along the x-axis (Figure 5.11). There was distinction between the cell and exosome sample groups with complete separation along this x-axis. Within these groups, the cell samples showed greatest uniformity between biological replicates. There was variance picked up within the exosome samples where Exosome B (labelled “E2”) did not cluster as tightly with the other 2 biological replicates. However, there was little difference along the first principle component (x-axis). These observations reinforce the sample distances heatmap (Figure 5.10) both of which showed a clear distinction between cells and exosomes.

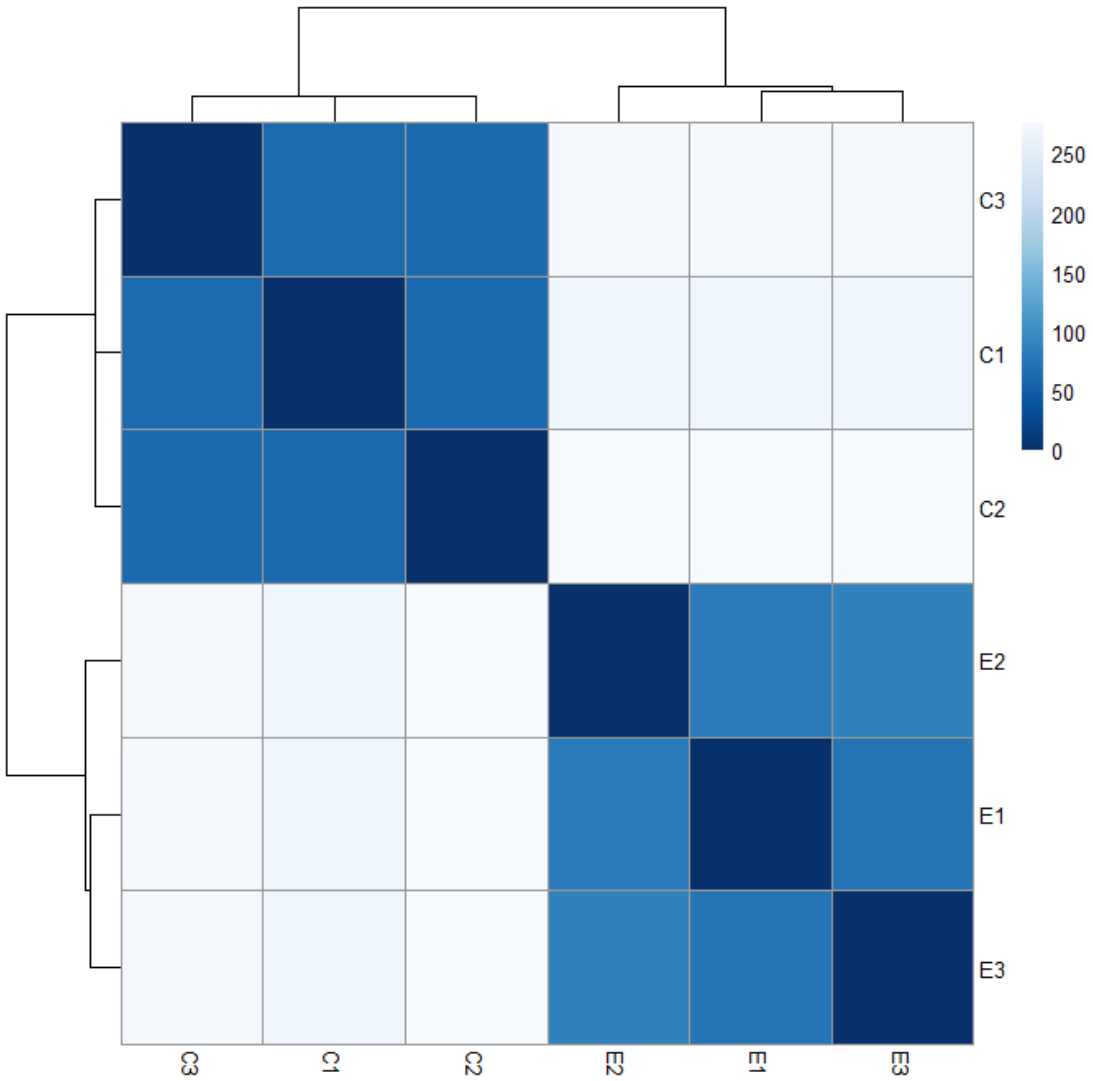

Figure 5.10: Euclidean distances between samples using rlog transformed data.
Euclidean distances between samples in the RNA sequencing data was calculated by DESeq2. C1 – C3 refer to cell samples A – C and E1 – E3 refer to exosome samples A – C. Sample similarity is indicated by colour intensity.

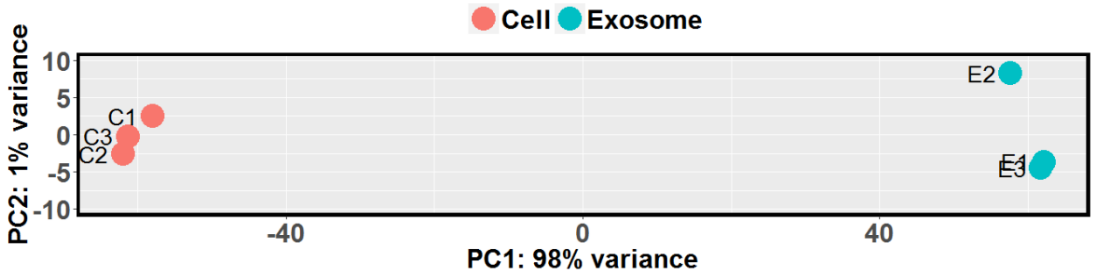

Figure 5.11: Principle component analysis showing variance between samples.
A PCA analysis was performed using DESeq2. The first principle component (PC1, x-axis) describes the majority of variance (98%). The second principle component (PC2) is displayed on the y-axis. C1 – C3 refer to cell samples A – C and E1 – E3 refer to exosome samples A – C.

Secondly, differential expression analysis was performed on raw counts. DESeq2 provided a data frame whereby the lncRNA expression in cells can be compared with exosomes. Of the 7978 lncRNAs tested, with >0 counts, 5325 (67%) showed an increase in log-fold change and 701 (8.8%) showed a decrease in log-fold change (Figure 5.12). This emphasises the distinction between these two sample types; only 24.2% lncRNAs had comparable expression levels between cells and exosomes.

With so many lncRNAs differentially expressed, stricter parameters were set in the analysis. The false discovery rate threshold was reduced to an adjusted Bonferroni p-value of $6.27x10^{-6}$. With this, 1554 lncRNAs passed Bonferroni correction for multiple testing and were found to be differentially expressed between cells and exosomes (Figure 5.13). This Minus-Average (MA) plot demonstrated that those lncRNAs with a higher normalised count required a lower log fold change to reach significance as seen by the narrowing of red dots (where $p<6.27x10^{-6}$) towards 0 along the x-axis.

Next, a subset of these differentially expressed lncRNAs were focused on. DESeq2 offers a function that, using rlog transformed data, calculates the deviation of each lncRNA from the average across all samples and can be plotted for a gene clustering analysis (Figure 5.14). It appeared that an outlier from one sample was not driving the differential expression. Details of log fold change and statistical significance for the top 10 up-regulated in cells and top 10 up-regulated in exosomes are displayed in Table 5.8. For example, *XLOC_000670* had a log2 fold change of -6.32 equating to a ~80 fold change increase in cells. Another example is *XLOC_005754,* which had a log2 fold change of 9.86 equating to a ~900 fold change increase in exosomes. Therefore, there can be large expression differences between cells and exosomes within the lncRNA repertoire.

Together these data, from a sample and individual lncRNA level, revealed that the RNA cargo in exosomes is distinct from the cells they were secreted from. To investigate the nature of the samples they represent, functional annotations needed to be undertaken.

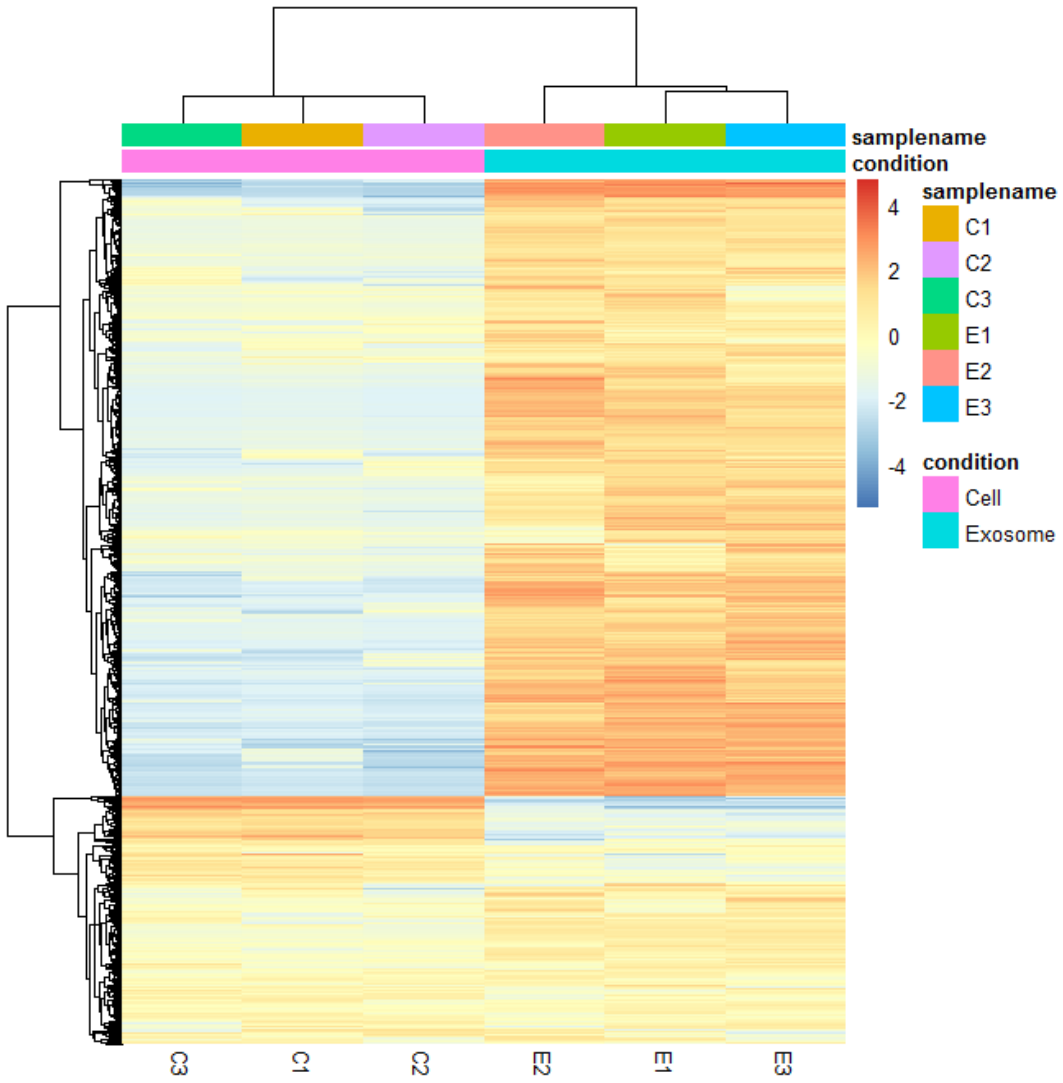

Figure 5.12: Heatmap showing log fold change of 7978 lncRNAs in cells and exosomes.
Heatmaps were generated from sequencing data using DESeq2. Six samples were assessed (C=cell, E=exosome, x-axis) and lncRNA counts indicated by colour intensity. Topological relationships between individual lncRNAs and samples were automatically generated and presented on both axes.

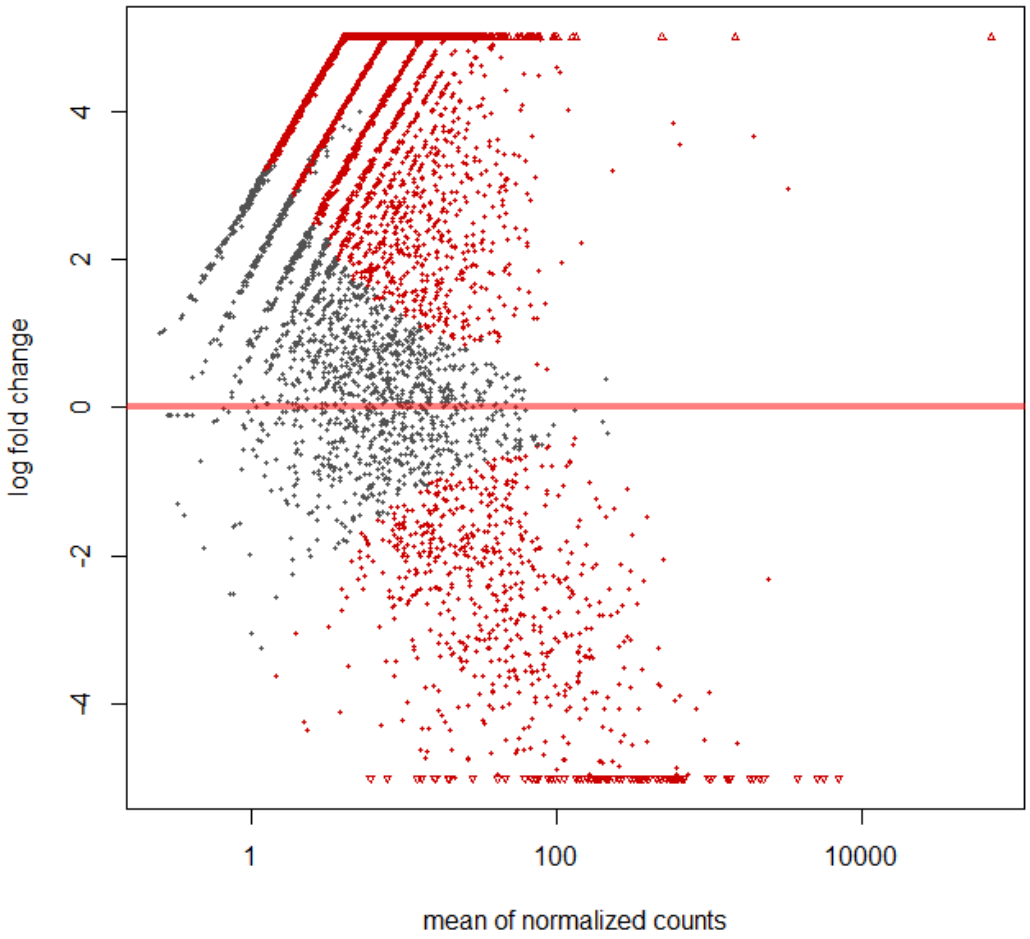

Figure 5.13: An MA plot showing differential lncRNA expression after Bonferroni correction.
A Minus-Average plot was generated from sequencing data using DESeq2. The mean of normalised counts for each lncRNA is displayed on the x-axis and the log fold change between cell and exosome samples (n=3 per type) displayed on the y-axis. Each lncRNA comparison is represented by a dot with 1558 passing Bonferroni correction for multiple testing (red dots) whilst 6424 did not (black dots).

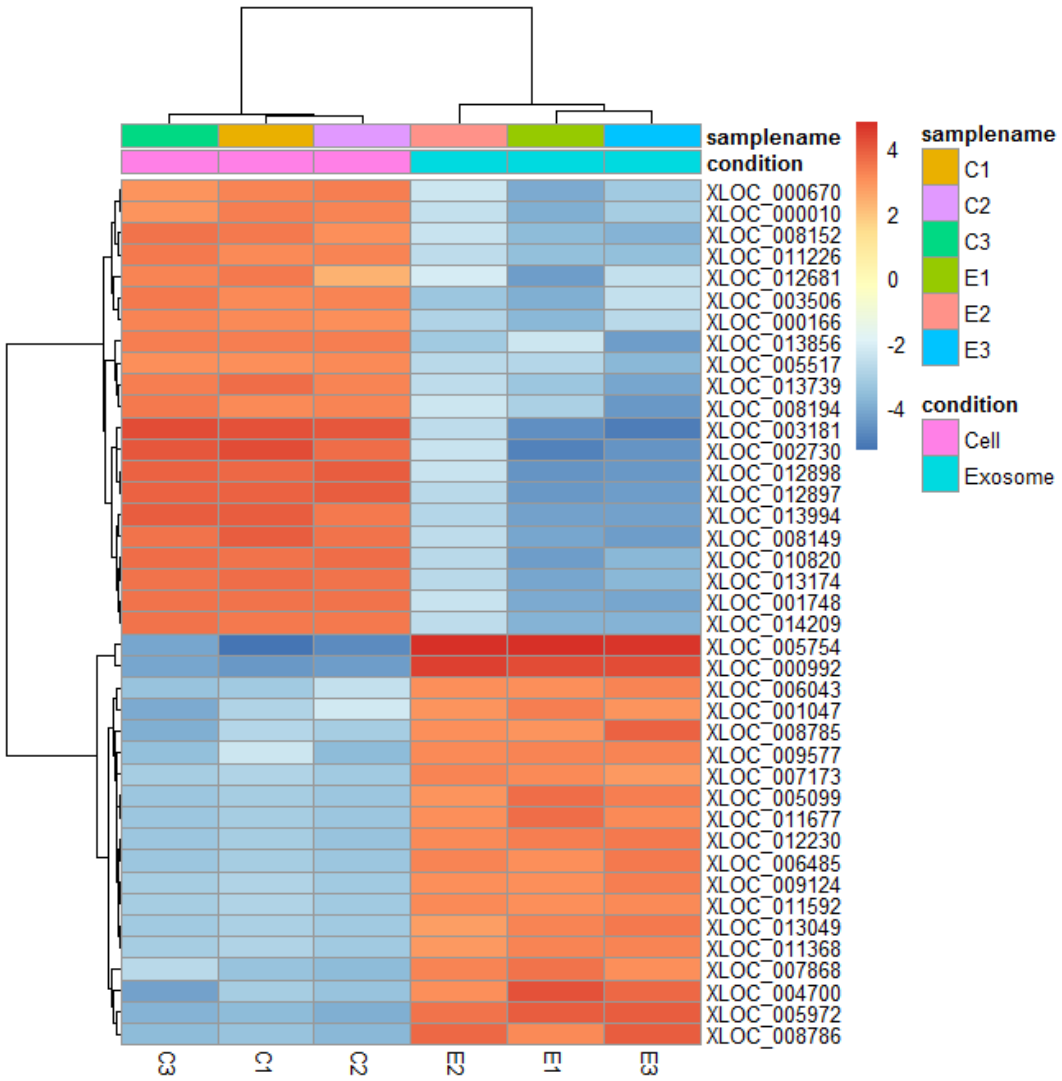

Figure 5.14: Heatmap showing differential expression of the top 40 lncRNAs after rlog transformation.

A function to measure the deviation of each lncRNA from the average across all samples was used in DESeq2 using the sequencing data (n=6). The top 40 of these are plotted and identified on the y-axis and indicated by colour intensity. C1 – C3 refer to cell samples A – C and E1 – E3 refer to exosome samples A – C (x-axis). Topological relationships are automatically generated by DESeq2 and indicated on both axes.

lncRNA_ID	baseMean	log2FoldChange	lfcSE	pvalue	padj
XLOC_000670	1040.25	-6.32	0.28	1.82E-115	8.52E-113
XLOC_000010	159.69	-6.66	0.49	2.29E-41	1.81E-39
XLOC_008152	561.97	-6.77	0.32	1.20E-99	2.99E-97
XLOC_011226	5703.25	-6.55	0.22	1.56E-202	4.14E-199
XLOC_012681	139.81	-6.19	0.50	1.10E-35	6.91E-34
XLOC_003506	178.58	-6.71	0.47	1.49E-45	1.25E-43
XLOC_000166	268.53	-6.45	0.37	7.13E-68	1.03E-65
XLOC_013856	176.02	-6.69	0.47	2.67E-45	2.22E-43
XLOC_005517	134.47	-6.42	0.49	1.52E-38	1.09E-36
XLOC_013739	166.07	-7.21	0.57	3.00E-37	2.03E-35
XLOC_005754	1496.71	9.86	0.49	4.91E-90	1.12E-87
XLOC_000992	71383.36	8.71	0.15	0.00E+00	0.00E+00
XLOC_006043	42.15	7.45	1.15	1.06E-10	1.88E-09
XLOC_001047	69.00	6.53	0.73	3.67E-19	1.25E-17
XLOC_008785	74.48	7.50	0.95	2.49E-15	6.93E-14
XLOC_009577	46.35	7.58	1.15	4.29E-11	8.15E-10
XLOC_007173	31.04	7.93	1.17	1.19E-11	2.40E-10
XLOC_005099	42.26	8.37	1.16	6.13E-13	1.45E-11
XLOC_011677	40.51	8.31	1.16	9.38E-13	2.18E-11
XLOC_012230	42.67	8.38	1.16	4.63E-13	1.10E-11

Table 5.8: Logfold changes of lncRNAs expressed in cells and exosomes.
The top 10 lncRNAs that were up-regulated in cells (XLOC_000670 – XLOC_013739) and up-regulated in exosomes (XLOC_005754 – XLOC_012230) were highlighted from sequencing data using DESeq2. The mean count across samples is displayed in the "baseMean" column followed by log2FoldChange and standard error. All lncRNAs showed a >6 log2 fold expression change between cells and exosomes and p-values passed Bonferroni correction for multiple testing. "lfcSE" refers to the standard error (SE) of the log2FoldChange.

5.3.6 Functional annotation of differentially expressed lncRNAs

To date, not only the annotation onto the genome, but also the functional action of lncRNAs are poorly understood. One known feature is that lncRNAs can show co-expression with neighbouring genes (Cabili et al., 2011). Given this observation, the co-expression of up-regulated lncRNAs in this dataset with mRNAs of known function was investigated further in order to establish a better understanding of possible functional relationships. One bioinformatics tool to perform this analysis is Co-LncRNA (Zhao et al., 2015).

The top 10 differentially expressed lncRNAs for cells and exosomes (Table 5.8), separately, were uploaded into the Co-LncRNA web interface along with expression profiles of differentially expressed mRNAs. Co-LncRNA then provided lists of co-expressed mRNAs with p-value <0.1. These were submitted to the Database for Annotation, Visualisation and Integrated Discovery (DAVID, v6.8) for functional annotation (Huang et al., 2008, Jiao et al., 2012). DAVID was chosen as an appropriate tool to upload large lists of genes (up to 3000) and retrieve biological understanding from them.

Co-expressed mRNAs in the cell samples pointed to numerous general cellular processes (Table 5.9) and enrichment maps were drawn using Cytoscape v3.4.0 (Figure 5.15). These showed enrichment of terms such as protein binding ($p=5.63x10^{-5}$), chromosome ($p=2.06x10^{-4}$), acetylation ($p=2.5x10^{-4}$), phosphoprotein ($p=2.59x10^{-4}$), nucleosome core ($p=5.34x10^{-4}$) and ubiquitin-like protein conjugation ($p=7.92x10^{-4}$). Such terms describe the intracellular functioning of cells in general.

Co-expressed mRNAs in the exosome samples (Table 5.10) provided a very different enrichment profile (Figure 5.16). Here, terms included disulfide bond ($p=3.02x10^{-23}$), Glycoprotein ($p=1.10x10^{-21}$), glycosylation site:N-linked ($p=7.33x10^{-21}$) and topological domain:Extracellular ($p=9.59x10^{-16}$). These terms reflect the molecular structure and composition of exosome vesicles and a number of terms overlap with a previous proteomics study of exosomes (Webber et al., 2014). There were some unexpected terms such as “olfaction” and “Rhodopsin-like 7TM”. Whilst these unexpected terms loosely fit with a cell-line of neural origin it is likely that these are artefacts of the enrichment analysis. A possible explanation is that genes of long length can be overrepresented due to their size, rather than their biological enrichment. Therefore the general observation, of enriched terms reflecting the composition of exosome vesicles, appears genuine.

Thus, by analysing genes that co-express with differentially expressed lncRNAs in these two sample types a biological understanding has been uncovered by enrichment analysis. Despite originating from these cells, the exosomes carry an RNA cargo that is dramatically different. The RNA is enriched for terms such as “glycosylation” and “transmembrane proteins”, which reflects the known molecular structure/composition of exosome vesicles. This suggests that the processes by which RNA has been loaded into exosomes are not random. However, there is a disconnection between the expression of functionally active genes and the abundance of non-coding RNA in exosomes. Translational machinery is absent from exosomes, most notably rRNA, so there is difficulty in understanding how the enrichment of these non-coding RNAs in exosomes can result in functionally relevant terms.

Category	Term	p-value	Genes
GOTERM_MF_DIRECT	GO:0005515~protein binding	5.63E-05	LEPR, PREX1, FAM20C, RORB, MYLIP, SDC4, HOOK3, EPC1, RNF103, MAP1LC3B…
UP_KEYWORDS	Chromosome	2.06E-04	HIST1H2AB, HIST2H2AB, REC8, HIST1H2BN, NSMCE4A, HIST1H2BF, HJURP, HIST1H2BH, HIST1H4D, HMGA1…
UP_KEYWORDS	Acetylation	2.50E-04	ZFAND6, PSMB10, HIST1H2AB, KANSL1L, ZMYND8, HOOK3, HIST2H2AB, HIST1H2BN, PLIN2, VPS13C…
UP_KEYWORDS	Phosphoprotein	2.59E-04	LEPR, PREX1, FAM20C, RASSF8, HOOK3, HIST2H2AB, EPC1, HIST1H2BN, VPS13C, CCDC71L…
UP_KEYWORDS	Nucleosome core	5.34E-04	HIST1H2AB, HIST2H2AB, HIST1H2BN, HIST1H2BF, HIST1H2BH, HIST1H4D
UP_KEYWORDS	Ubl conjugation	7.92E-04	HIST1H2AB, SLC38A2, MYLIP, ZMYND8, ZFP36L1, HIST2H2AB, HIST1H2BN, N4BP1, ETAA1, HIST1H4D…
GOTERM_CC_DIRECT	GO:0000786~nucleosome	8.43E-04	HIST1H2AB, HIST2H2AB, HIST1H2BN, HIST1H2BF, HIST1H2BH, HIST1H4D
GOTERM_BP_DIRECT	GO:0045944~positive regulation of transcription from RNA polymerase II promoter	9.54E-04	PLAG1, MAFF, TBL1XR1, FZD8, LUM, RELB, NCOA7, NR4A3, SIRT1, HMGA1…

Table 5.9: Functional terms associated with mRNAs that co-express with the top 10 lncRNAs differentially expressed in cells over exosomes.
Functional terms were provided by David software after differential lncRNA analysis of sequence data using DESeq2 and co-expression analysis using Co-LncRNA. The top 8 terms (by p-value) are displayed here and where >10 genes are represented in each group the first 10 are listed.

Category	Term	p-value	Genes
UP_SEQ_FEATURE	disulfide bond	3.02E-23	EDN3, MASP1, SCN3B, GDF6, ATP1B4, OR4C5, C1QC, APOB, HTR1A, OR6C3…
UP_KEYWORDS	Glycoprotein	1.10E-21	HCG22, SLC52A1, MASP1, SCN3B, LYPD5, GDF6, OR4C5, C1QC, AQP3, APOB…
UP_SEQ_FEATURE	glycosylation site:N-linked (GlcNAc...)	7.33E-21	RARRES1, MASP1, SCN3B, LYPD5, GDF6, ATP1B4, OR4C5, AQP3, APOB, HTR1A…
UP_KEYWORDS	Disulfide bond	8.94E-21	EDN3, MASP1, SCN3B, GDF6, PTPN22, OR4C5, C1QC, APOB, HTR1A, OR6C3…
UP_SEQ_FEATURE	topological domain:Extracellular	9.59E-16	F2RL3, RARRES1, SCN3B, GRIK4, SLC6A4, ATP1B4, SLC7A9, TNFSF13, OR4C5…
UP_SEQ_FEATURE	signal peptide	7.30E-15	EDN3, SLC52A1, MASP1, LYPD5, SCN3B, GDF6, C1QC, APOB, SBSN, IGLL1…
INTERPRO	IPR017452:GPCR, rhodopsin-like, 7TM	2.44E-13	F2RL3, OR52A1, TACR2, OR4C5, GPR87, GPR88, OR10A7, EDNRA, HTR1A, GALR1…
UP_KEYWORDS	Secreted	2.17E-12	EDN3, HCG22, MASP1, GDF6, TNFSF13, C1QC, IL10, OLFML1, IFNL1, APOB…
INTERPRO	IPR000276:G protein-coupled receptor, rhodopsin-like	2.35E-12	F2RL3, OR52A1, TACR2, GPR87, OR4C5, GPR88, OR10A7, EDNRA, HTR1A, GALR1…
UP_KEYWORDS	G-protein coupled receptor	3.23E-12	TAS2R1, F2RL3, OR52A1, TACR2, OR4C5, GPR87, GPR88, OR10A7, EDNRA, TAS2R60…

Table 5.10: Functional terms associated with mRNAs that co-express with the top 10 lncRNAs differentially expressed in exosomes over cells.
Functional terms were provided by David software after differential lncRNA analysis of sequence data using DESeq2 and co-expression analysis using Co-LncRNA. The top 10 terms (by p-value) are displayed here and the first 10 genes in each group are listed.

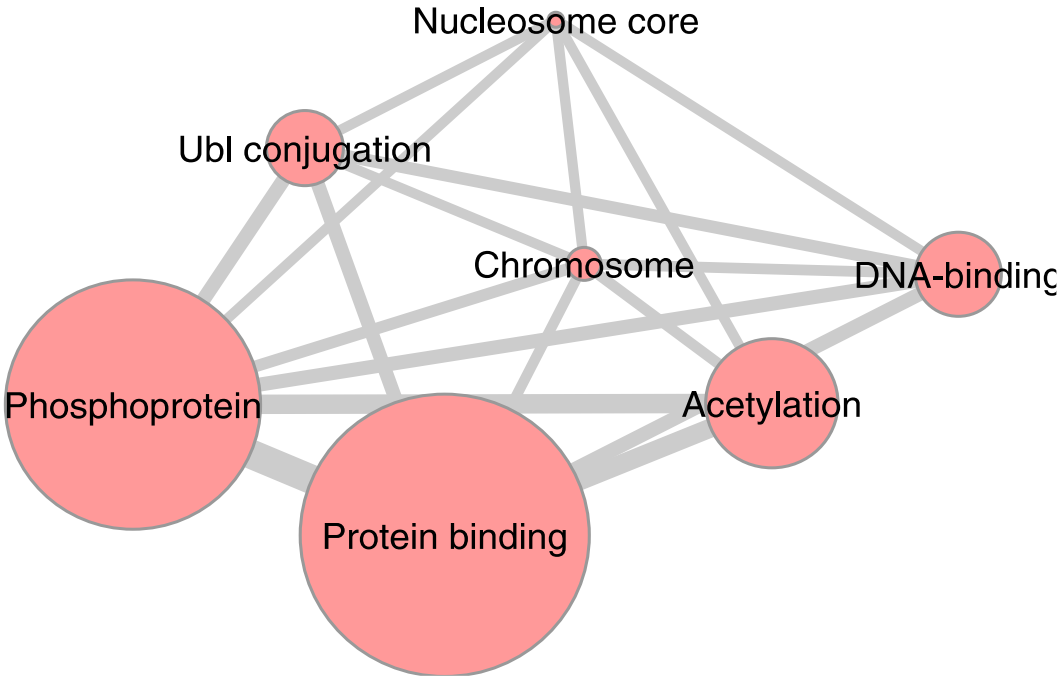

Figure 5.15: Functional annotation of mRNAs that co-express with the top 10 lncRNAs differentially expressed in cells over exosomes.
Functional terms were annotated from sequencing data using DAVID software and plotted using Cytoscape software. Each term is represented by circles with the size of each circle representing the number of genes within the term and the thickness of line represents the number of overlapping genes between terms.

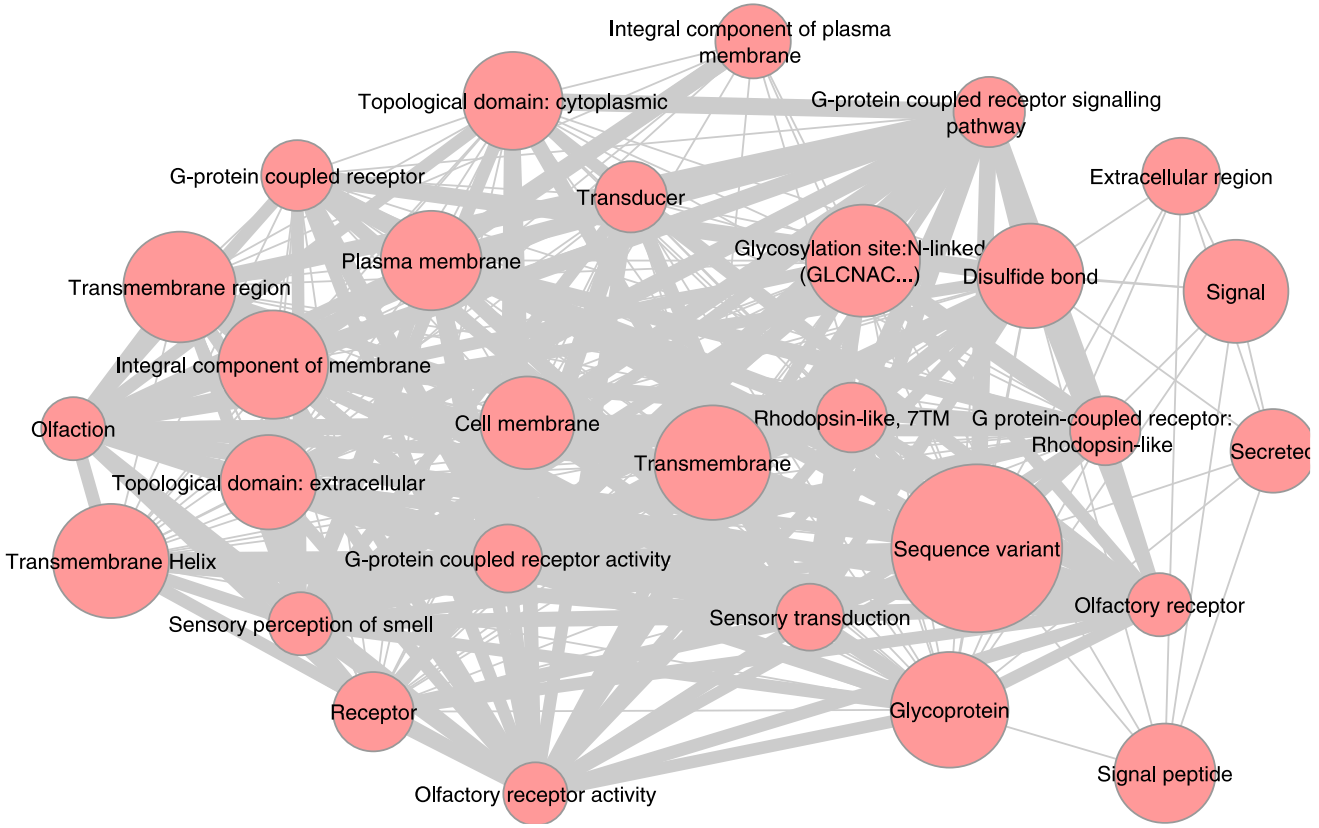

Figure 5.16: Functional annotation of mRNAs that co-express with the top 10 lncRNAs differentially expressed in exosomes over cells.
Functional terms were annotated from sequencing data using DAVID software and plotted using Cytoscape software. Each term is represented by circles with the size of each circle representing the number of genes within the term and the thickness of line represents the number of overlapping genes between terms.

5.3.7 qPCR validation of lncRNA differential expression

So far, differential expression of lncRNAs has been described from RNA sequencing data. To validate these findings, six differentially expressed lncRNAs were tested using quantitative polymerase chain reaction (qPCR): three that had increased expression in cells (*XLOC_000670, XLOC_011226* and *XLOC_008152*) and three that had increased expression in exosomes (*XLOC_009577, XLOC_001047* and *XLOC_006043*). Validation was then performed using an independent technique and with independent samples.

First, reagents and procedures for quantifying these lncRNAs were validated. SYBR green qPCR chemistry was chosen as it provided the most flexibility for self-design of primers. These were designed by downloading DNA sequences from the respective lncRNA regions from the UCSC genome browser (University of California Santa Cruz) and using Primer3 (Untergasser et al., 2012, Koressaar and Remm, 2007) set to produce amplicon sizes of 80-100 bp in length. In the case of housekeeping genes (*GAPDH, PPIA* and *TUBA1A*) DNA from exonic regions were chosen for primer design.

Primers were tested initially by standard PCR using cDNA reverse transcribed from 80 ng cellular- or exosomal-RNA. These samples were extracted on a separate occasion to the RNA sequencing samples to represent an independent sample set for validation. Agarose gels were run (Figure 5.17) after 35 cycles of PCR where 3 ng forward and reverse primers used and 2 µl cDNA template. Three housekeeping genes (*GAPDH, TUBA1A* and *PPIA*) and three lncRNAs (*XLOC_000670, 011226* and *008152*) were tested with cDNA reverse-transcribed from cellular-RNA. Three lncRNAs (*XLOC_009577, 001047* and *006043*) were tested with cDNA reverse-transcribed from exosomal-RNA. All primer sets showed product bands at ~100 bp, as expected, for the three biological replicates tested and no band for the negative control. Therefore, these primer sets were used at a concentration of 3 ng per reaction in quantitative experiments downstream.

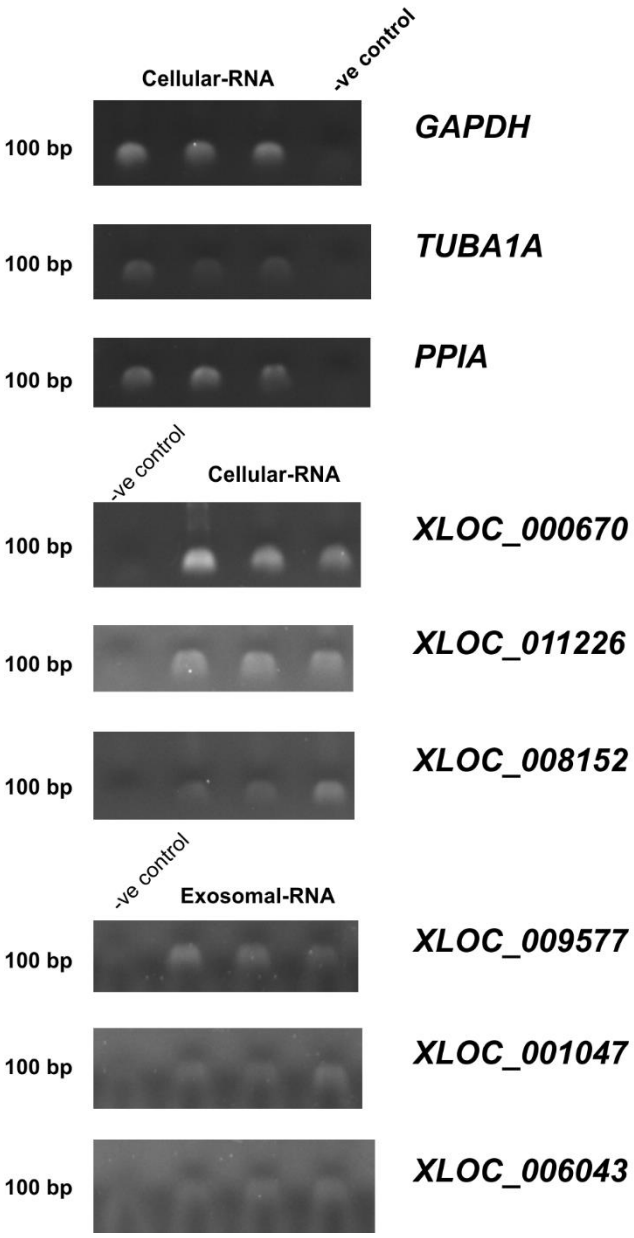

Figure 5.17: Optimisation of primers by standard PCR.
PCR primers were optimised by standard PCR and products visualised by agarose gel electrophoresis. Negative controls are rightmost for GAPDH, TUBA1A and PPIA but leftmost for all six lncRNAs (indicated on y-axis). Three housekeeping genes (GAPDH, TUBA1A and PPIA) and three lncRNAs (XLOC_000670, 011226 and 008152) were optimised by PCR with cDNA reverse-transcribed from cellular-RNA. Three lncRNAs (XLOC_009577, 001047 and 006043) were optimised by PCR with cDNA reverse-transcribed from exosomal-RNA. All primer sets showed product bands at ~100 base pairs (bp) for the three biological replicates tested (n=3) and no band for the negative control.

Next, these primer sets were used to measure relative gene/lncRNA expression in cells and exosomes by qPCR. RNA input was normalised to 80 ng before reverse transcription of cellular- and exosomal-RNA. 3 ng primer-set and 2 µl cDNA template were mixed with SYBR green mastermix (ThermoFisherScientific) and amplified for 40 cycles of Fast qPCR. Three biological replicates were measured in duplicate for each target. Raw C_T values, the cycle at which amplification is detected over a given threshold, were calculated with automated baseline settings and cycle threshold set to 0.1 fluorescence units, as used previously (Enderle et al., 2015).

Raw C_T values were as expected from the RNA sequencing data (Figure 5.18). Three lncRNAs had lower C_T values in cells (*XLOC_000670, 011226* and *008152*), reflecting increased expression, whilst three had lower C_T values in exosomes (*XLOC_009577, 001047* and *006043*). Of the three housekeeping genes tested, two (*GAPDH* and *TUBA1A*) saw higher C_T values in exosomes. However, PPIA showed fairly uniform mean C_T values with 25.18 ± 0.16 cycles in cells and 25.27 ± 0.68 cycles in exosomes (Table 5.11). Melt curves were also analysed to detect any off target amplicons or primer dimers. All replicates showed single peaks (Table 5.11) across the samples showing that only the desired amplicons were contributing to the detected signal.

Based on the Raw C_T values alone, the trends in the data validate what had been observed in the RNA sequencing. However, statistical tests are not appropriate on Raw C_T values as they are a recorded cycle number between 1 and 40 (Schmittgen and Livak, 2008), so further transformation of the data were required. One such transformation is to calculate $2^{-\Delta CT}$ where the raw C_T values are transformed and normalised against a homogenously expressed housekeeping gene. This posed a problem as *GAPDH* and *TUBA1A*, although commonly used as housekeeping genes for cells and tissues, could not be assumed to be appropriate for exosomes and clearly these data showed differentially expression between cells and exosomes. Therefore, *PPIA* was chosen to perform these calculations as the mean C_T values were comparable between samples (Table 5.11).

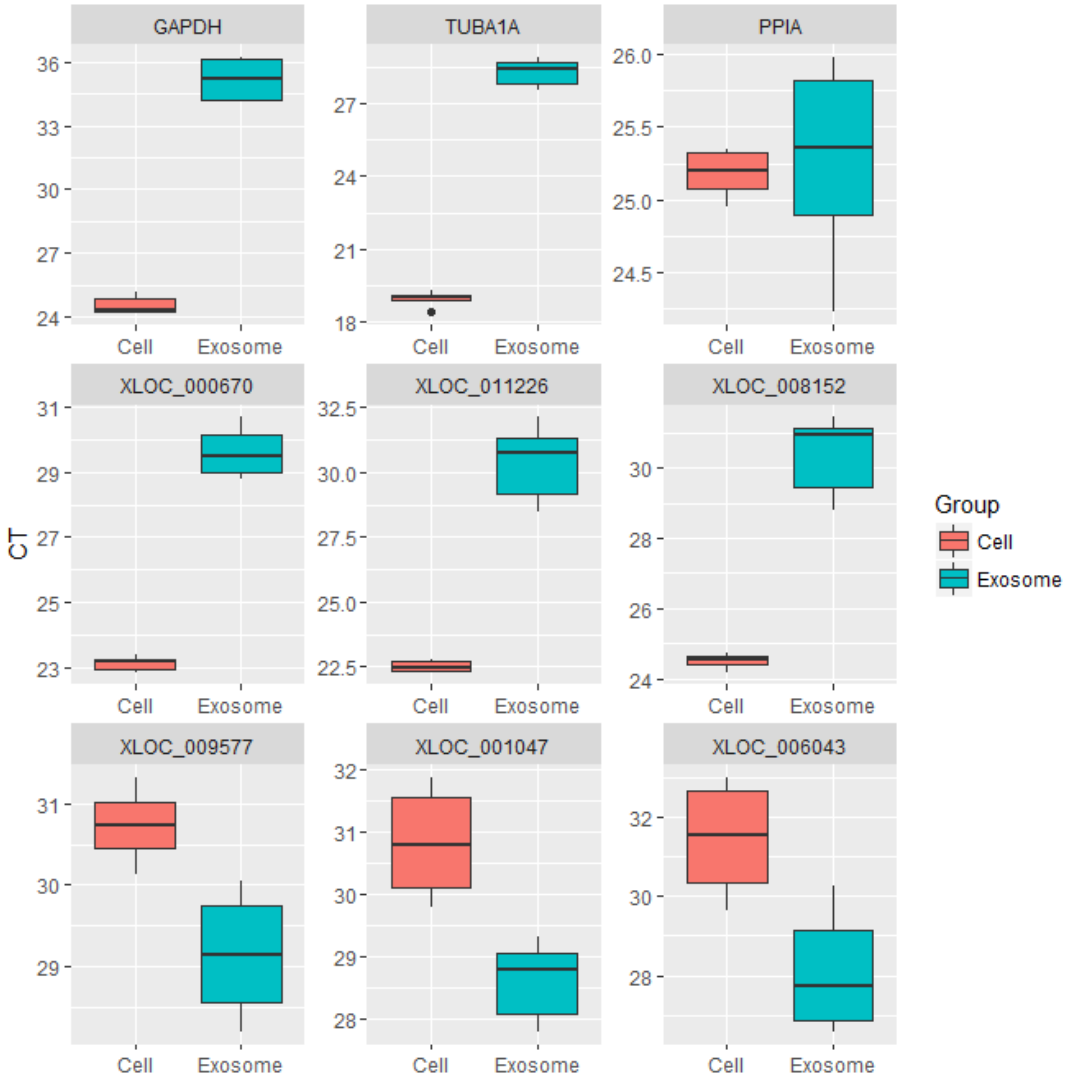

Figure 5.18: Box and whiskers plot to show differential expression of housekeeping genes and lncRNAs measured by qPCR.

Quantitative PCR (qPCR) was used to measure cycle thresholds (CT, y axis) across cellular and exosomal RNA samples (n=3 per group). C_T values reflect the cycle number where fluorescence units exceeded a set threshold of 0.1 FU. The upper and lower "hinges" of the boxes correspond to the first and third quartiles whilst whiskers extend to values within 1.5 x inter-quartile range. Raw C_T values are reported here for 9 targets, as indicated in the title of each graph.

Target	Cell C_T	Cell SD	Exosome C_T	Exosome SD	Melt curve analysis
GAPDH	24.53537	0.408591	35.20336	1.052481	1 peak at 78.27°C
TUBA1A	18.93377	0.316468	28.31364	0.566085	1 peak at 79.91°C
PPIA	25.18366	0.164386	25.2714	0.68322	1 peak at 85.57°C
XLOC_000670	23.12633	0.203302	29.59134	0.781028	1 peak at 80.5°C
XLOC_011226	22.503	0.228325	30.3735	1.494005	1 peak at 89.45°C
XLOC_008152	24.5147	0.198369	30.36	1.176592	1 peak at 76.34°C
XLOC_009577	30.7341	0.446775	29.14086	0.761161	1 peak at 78.56°C
XLOC_001047	30.81294	0.8759	28.60822	0.643157	1 peak at 85.58°C
XLOC_006043	31.44327	1.435735	28.07689	1.50607	1 peak at 81.1°C

Table 5.11: Raw C_T values and melt curve analysis of qPCR data.
Melt curve analysis was performed using qPCR instrumentation on cell and exosome RNA samples (n=3 per group). C_T values reflect the cycle number where fluorescence units exceeded a set threshold of 0.1 FU. Mean C_T values were calculated from three biological replicates measured in duplicate and standard deviation (SD) reported.

Using *PPIA* as an endogenous control, $2^{-\Delta CT}$ were calculated for the six lncRNAs. Box and whisker plots showed differential expression in the correct direction for each (Figure 5.19). Initially, these data were tested for normality using the Shapiro-Wilk test. The significance value for all lncRNA targets was greater than 0.05, therefore, the data was normally distributed. Parametric tests were appropriate for these data so independent t-tests were performed.

Differential expression was statistically significant for the lncRNAs that showed increased expression in cells: *XLOC_000670*, $t(10) = 31.122$, $p < 0.001$; *XLOC_011226*, $t(10) = 12.383$, $p < 0.001$; *XLOC_008152*, $t(10) = 23.376$, $p < 0.001$; and increased expression in exosomes: *XLOC_009577*, $t(10) = -8.198$, $p < 0.001$; *XLOC_001047*, $t(10) = -9.870$, $p < 0.001$; and *XLOC_006043*, $t(10) = -3.398$, $p = 0.007$. Thus, the differential expression of lncRNAs observed by RNA sequencing was validated with an independent method and an independent sample set.

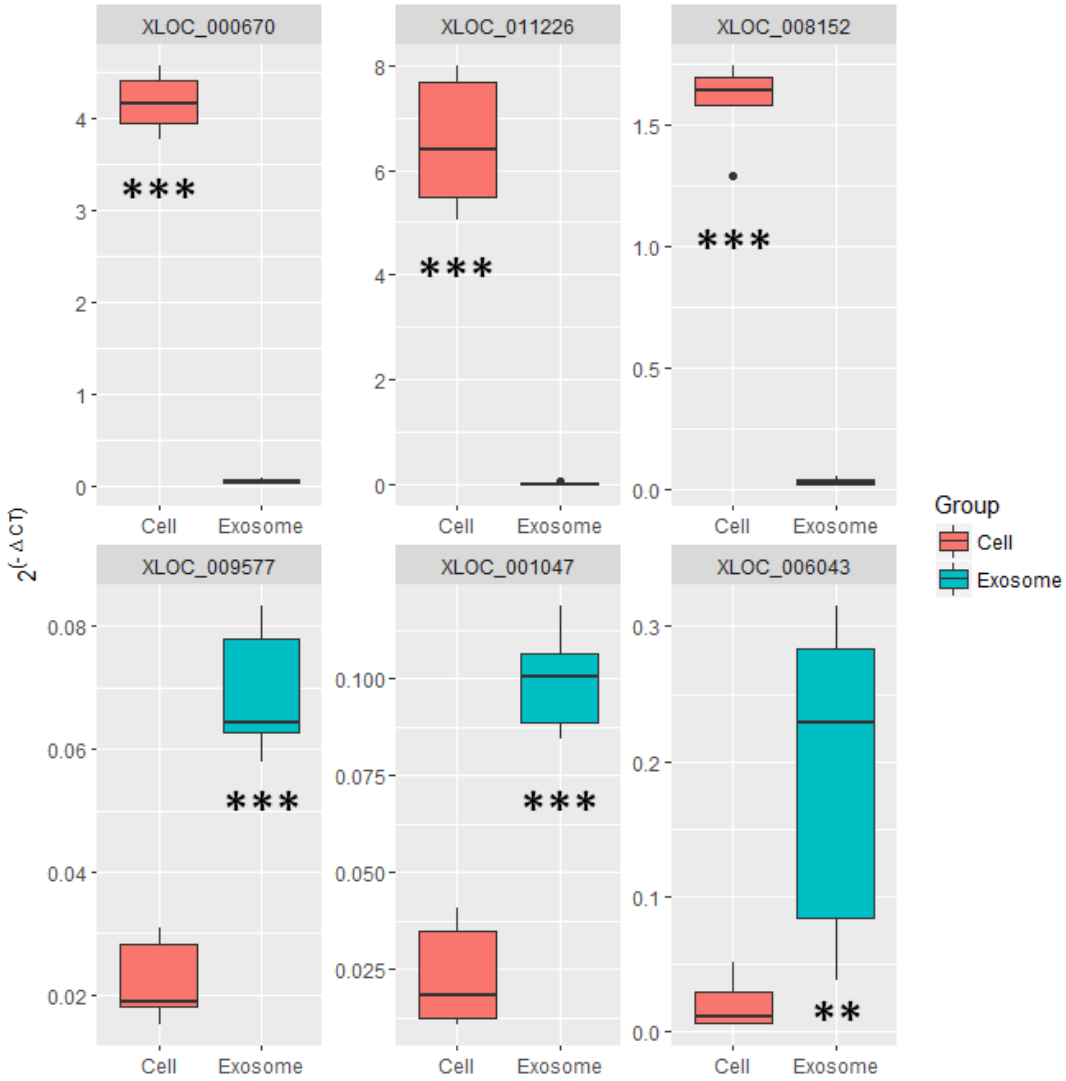

Figure 5.19: Box and whiskers plot to show differential expression of six lncRNAs measured by qPCR. *Quantitative PCR was used to assess gene and lncRNA expression in cell and exosome RNA samples (n=3 per group, measured in duplicate). $2^{-\Delta CT}$ values (y-axis) are reported here by normalisation against PPIA expression. The upper and lower "hinges" of the boxes correspond to the first and third quartiles whilst whiskers extend to values within 1.5 x inter-quartile range. Independent t-tests were performed and p-values <0.05 indicated with *, <0.01 indicated with ** and <0.001 indicated with ***.*

5.3.8 *In silico* confirmation of differential expression by functional annotation of introns

To utilise more of the data available from the RNA sequencing, and to further confirm the findings from differentially expressed lncRNAs, the intronic reads were analysed. To do this, a gene model annotation file (in .gtf format) was required to itemise introns and their chromosomal positions. The table browser on UCSC (https://genome.ucsc.edu/cgi-bin/hgTables, accessed November 2016) was used to download intron locations, +50 bases flanking sequence, in .bed format (hg19). An awk script was used to process the text into a .gtf format, in particular inserting a third column with each row labelled as an intron so that HTSeq could perform the count function. As detailed above, in sections 5.3.5 and 5.3.6, the same analysis pipeline was followed.

HTSeq was used to produce intron count files from the mapped reads and DESeq2 to remove rows with no counts across the samples. 602508 rows were removed from 659327 resulting in a dataset containing 56819 introns. Again, the rlog was calculated to stabilise the variance across the mean and Euclidean distances between samples were plotted as a heatmap (Figure 5.20). There was separation between cells and exosomes at a sample distance level but good similarity within these groups. This plot further confirmed the biological picture that had already emerged from lncRNA analysis: that the RNA profiles of cells and the secreted exosomes are distinct.

The sample-to-sample distances were further visualised with a PCA (Figure 5.21). There was a striking distinction between the cell and exosome sample groups with complete separation along the x-axis. Within these groups the cell samples showed greatest uniformity between biological replicates. There was variance picked up within the exosome samples where Exosome B (“E2”) did not cluster as tightly with the other 2 biological replicates. However, there was little difference along the first principle component (x-axis). These observations reinforce the sample distances heatmap for introns (Figure 5.20) and respective figures for lncRNA (Figure 5.10 & Figure 5.11) all of which showed distinction between cells and exosomes whilst retaining good uniformity between biological replicates.

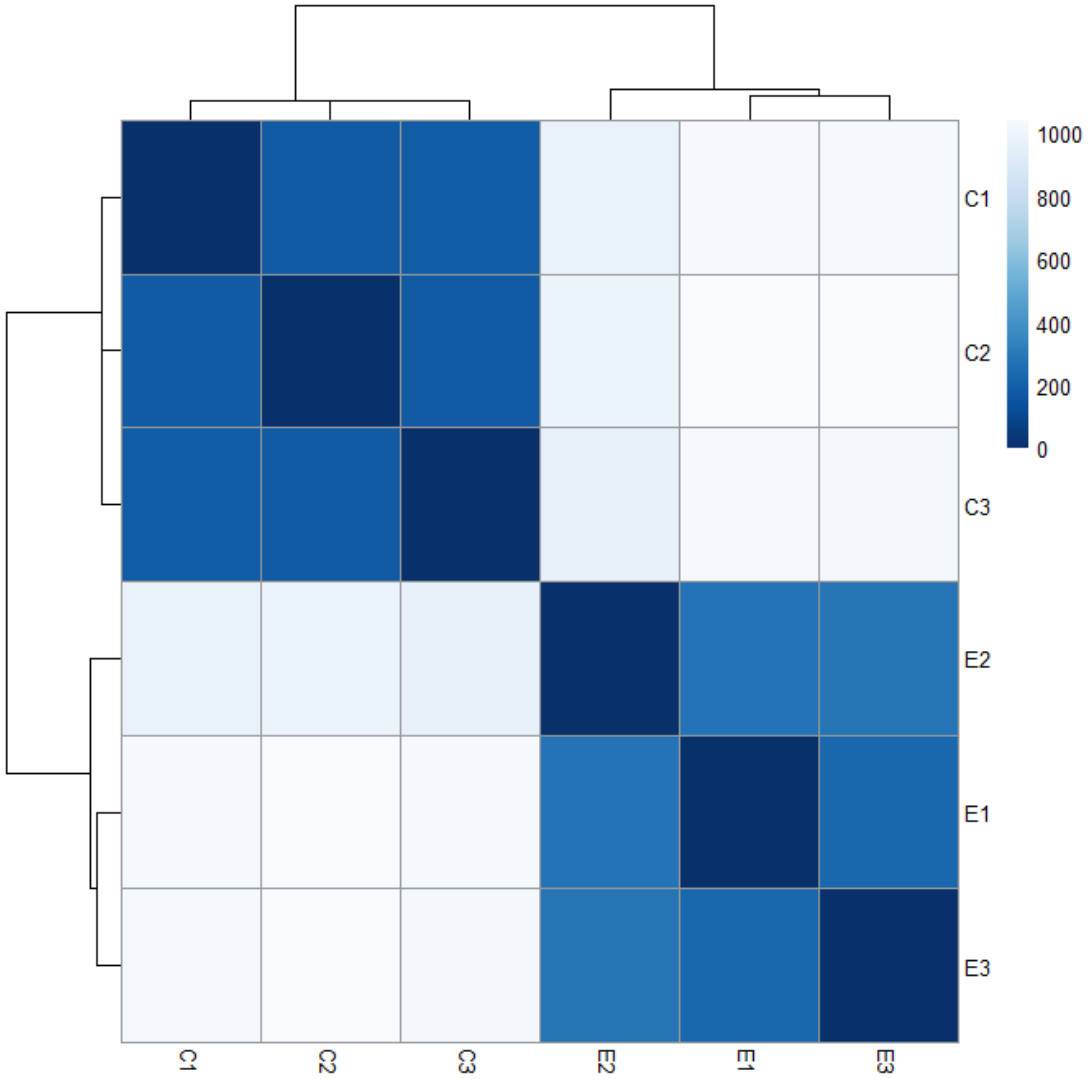

Figure 5.20: Euclidean distances between samples using rlog transformed data.
Euclidean distances between samples in the RNA sequencing data was calculated by DESeq2. C1 – C3 refer to cell samples A – C and E1 – E3 refer to exosome samples A – C. Sample similarity is indicated by colour intensity.

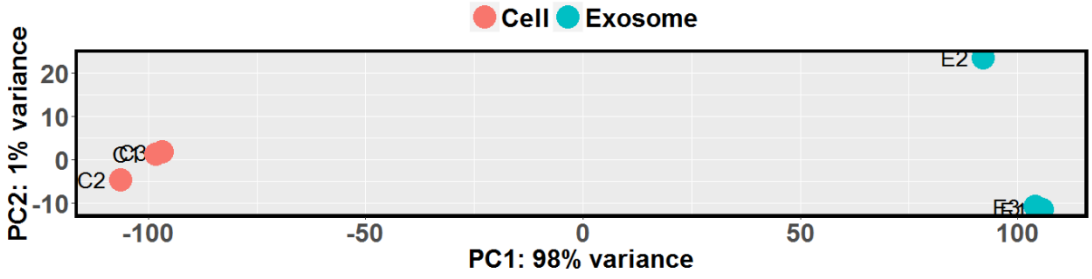

Figure 5.21: Principle component analysis showing variance between samples.
A PCA analysis was performed using DESeq2. The first principle component (PC1, x-axis) describes the majority of variance (98%). The second principle component (PC2) is displayed on the y-axis. C1 – C3 refer to cell samples A – C and E1 – E3 refer to exosome samples A – C.

Of the 56819 introns, with >0 counts, 24972 had increased counts in cells and 31847 had increased counts in exosomes (Figure 5.22). The false discovery rate threshold was reduced to an adjusted Bonferroni p-value of 8.80×10^{-7}. With this, 29919 introns passed Bonferroni correction for multiple testing and were found to be differentially expressed between cells and exosomes (Figure 5.23).

Together these data, from a sample and individual intron level, revealed that the RNA cargo in exosomes is distinct from the cells they were secreted from. The same observations were made when lncRNA expression was analysed. Next, functional annotation of these differentially expressed introns was performed.

In order to perform a functional annotation of these differentially expressed introns the intron names were linked to the gene name and sorted by log fold change. Due to computational capacity the top 3000 gene names were submitted to the functional annotation tool, DAVID, for cells and exosomes separately.

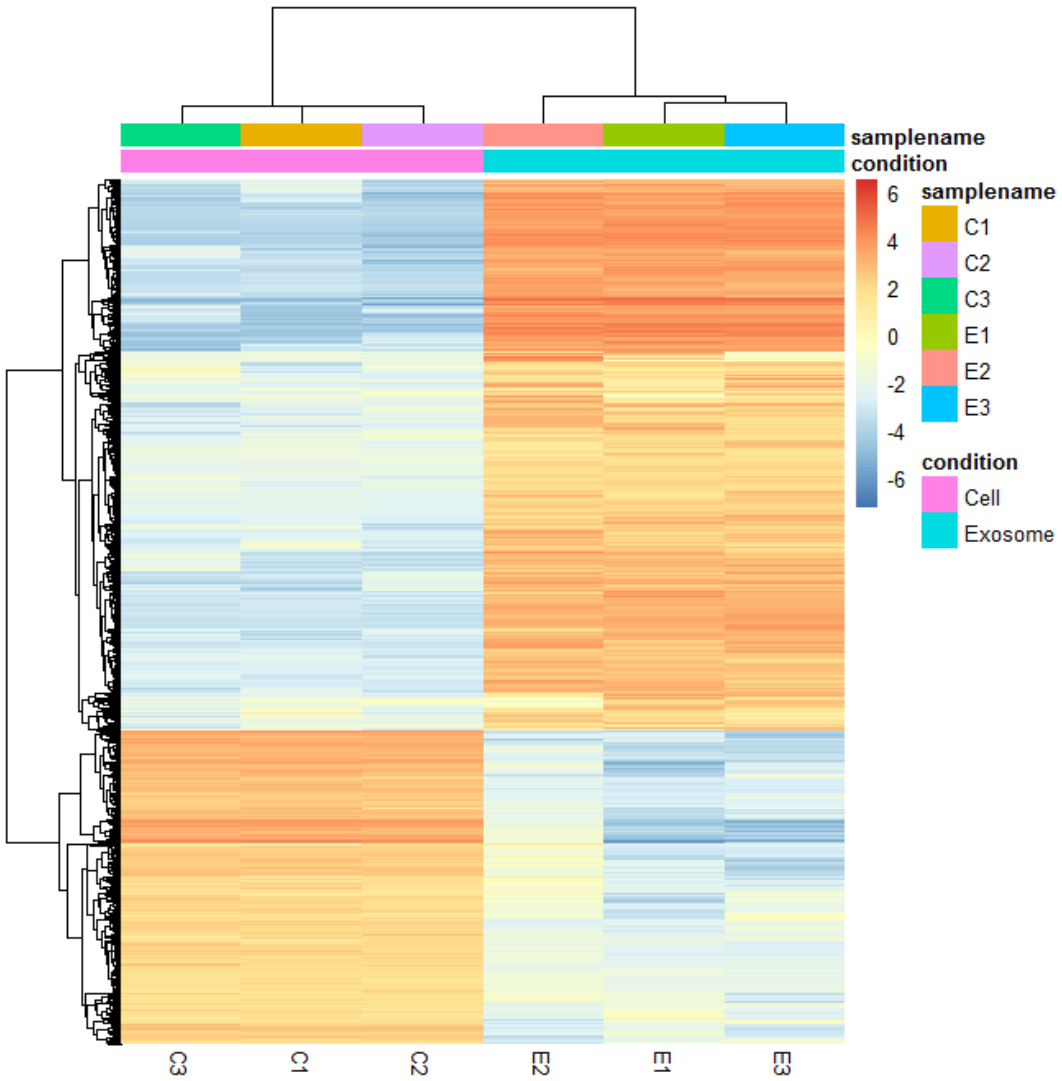

Figure 5.22: Heatmap showing log fold change of 30000 introns in cells and exosomes.
Heatmaps were generated from sequencing data using DESeq2. Due to computational power only 30000 of the 56819 introns could be plotted. Six samples were assessed (C=cell, E=exosome, x-axis) and intron counts indicated by colour intensity. Topological relationships between individual introns and samples were automatically generated and presented on both axes.

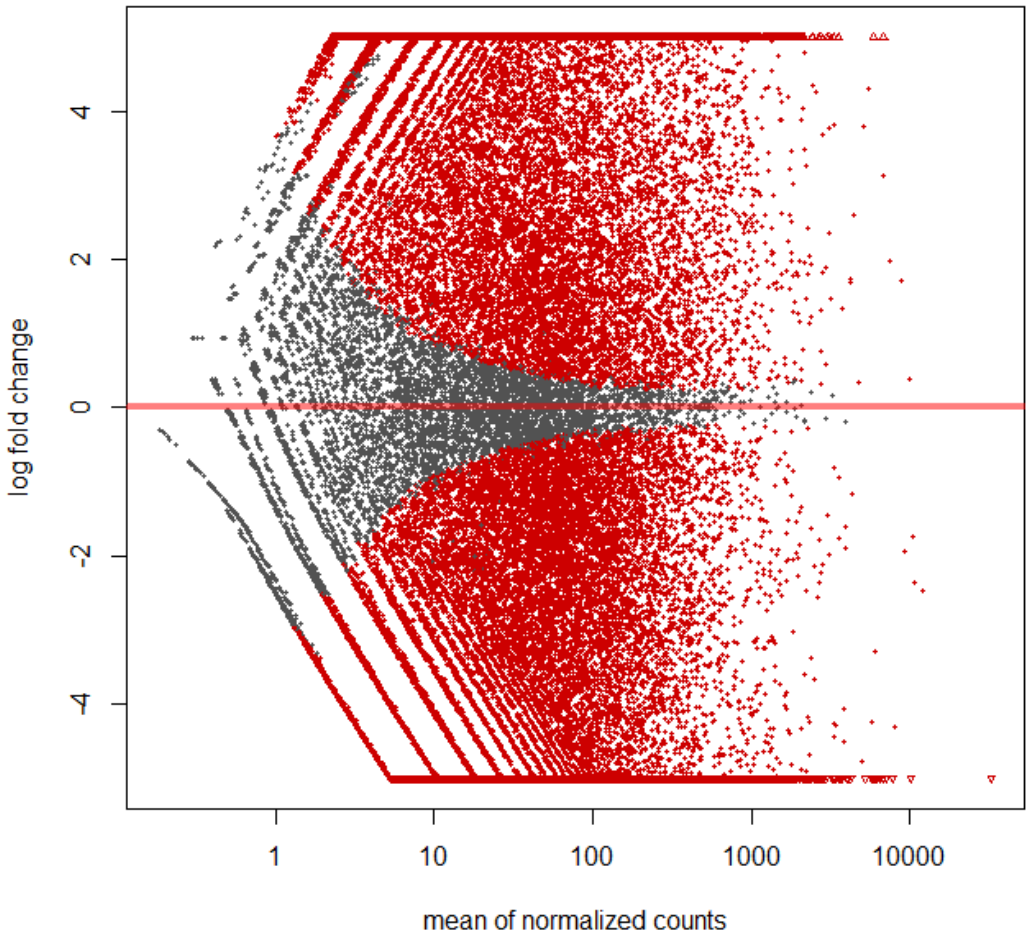

Figure 5.23: An MA plot showing differential intron expression after Bonferroni correction.
A Minus-Average plot was generated from sequencing data using DESeq2. The mean of normalised counts for each intron is displayed on the x-axis and the log fold change between cell and exosome samples (n=3 per type) displayed on the y-axis. Each intron comparison is represented by a dot with 29919 passing Bonferroni correction for multiple testing (red dots) whilst 26900 did not (black dots).

Differentially expressed introns in the cell samples pointed to numerous general cellular processes (Table 5.12) and enrichment maps were drawn using Cytoscape v3.4.0 (Figure 5.24). These included enrichment of terms such as acetylation ($p=3.21x10^{-116}$), phosphoprotein ($p=1.07x10^{-99}$), nucleus ($p=5.16x10^{-44}$), ubiquitin-like protein conjugation ($p=1.74x10^{-38}$), cytoplasm ($p=4.17x10^{-30}$) and ribosomal protein ($p=5.69x10^{-26}$). Such terms describe the intracellular functioning of cells in general. Some terms, such as "Mental retardation" and "Neurodegeneration", reflect that the cell-line was of neural origin, despite being slightly unexpected.

Differentially expressed introns in the exosome samples pointed to the molecular composition of these vesicles (Table 5.13) and enrichment maps were drawn using Cytoscape v3.4.0 (Figure 5.25). These included enrichment of terms such as glycoprotein ($p=7.17x10^{-24}$), secreted ($p=7.49x10^{-18}$), disulphide bond ($p=3.41x10^{-15}$), ion channel ($p=1.97x10^{-7}$) and transmembrane ($p=2.52x10^{-5}$). Some unexpected terms came out of the analysis, such as "Vision", "Hearing" and "Deafness". Whilst these terms may reflect that the cell-line was of neural origin, these are more likely to be explained as artefacts from the enrichment analysis. Overrepresented genes, such as those of long length, can cause unexpected terms as discussed for the lncRNA analysis. For example, *RP1* is a 211 kbp gene that contributed to the enrichment terms "Polymorphism" and "Vision". Therefore, the general observation of enriched terms that describe the molecular composition of exosomes was accepted and confirmed what had been reported in the lncRNA analysis. In both cell and exosome enrichment maps, categories were limited to UP_KEYWORDS only to ensure they were visually interpretable.

Again a strong biological distinction was made between the transcriptome of H4 cells and secreted exosomes. Whilst general processes within the cell are reflected in the transcriptome, terms such as "glycoprotein", "disulphide bond" and "transmembrane" are enriched in the transcriptome of exosomes.

These observations are in agreement with the enrichment maps drawn from lncRNA and co-expressed mRNA. Indeed, a number of the terms were identical in both analyses e.g. "glycoprotein" in exosomes and "acetylation" in cells. Overall, the cell samples were enriched for general intracellular processes and exosomes for molecular features of these vesicles. As such, analysing the intronic data from the RNA sequencing provided a good *in silico* confirmation of the lncRNA differential expression analysis using a separate, although overlapping, part of the RNA sequencing data. These data must be carefully interpreted by

accepting that there is a disconnection between intronic reads in exosomes and enrichment of functional terms.

Category	Term	p-Value	Genes
UP_KEYWORDS	Acetylation	3.21E-116	XRCC5, LDHA, PLEKHM2, RPL14, RPL13, XRCC6, NAA15, STOML2, INTS1, RPLP2…
UP_KEYWORDS	Phosphoprotein	1.07E-99	LDHA, OSMR, VPS54, RPLP2, AMOTL2, SART1, CUL3, MAK16, CUL7, CUL9…
UP_KEYWORDS	Nucleus	5.16E-44	XRCC5, SURF6, XRCC6, NAA15, INTS1, MED23, CIAPIN1, SART1, CTNNB1, CUL3…
UP_KEYWORDS	Ubl conjugation	1.74E-38	XRCC5, ADCY3, LDHA, HMGN2, SLC9A6, RPL19, RPL14, RPL13, U2AF2, XRCC6…
UP_KEYWORDS	Isopeptide bond	1.03E-31	XRCC5, ADCY3, RPL19, HMGN2, SLC9A6, RPL14, RPL13, U2AF2, XRCC6, RNF213…
UP_KEYWORDS	Ribonucleoprotein	1.80E-31	HNRNPA1L2, MRPS36, MRPS34, RPL19, RPL14, RPL13, RPL15, RPLP2, MRPS30, RPS19BP1…
UP_KEYWORDS	Cytoplasm	4.17E-30	KIFC2, LDHA, PLEKHM2, RUSC2, NAA15, STOML2, MYLIP, CIAPIN1, CTNNB1, MAGED1…
UP_KEYWORDS	Ribosomal protein	5.69E-26	MRPS36, MRPS34, RPL19, RPL14, RPL13, RPL15, RPLP2, MRPS30, RPS19BP1, RPS3…
UP_KEYWORDS	RNA-binding	4.30E-25	NCBP2, RNMT, DZIP3, ZC3HAV1, XPO5, SURF6, U2AF2, RBM3, NSUN5P1, NONO…
UP_KEYWORDS	Host-virus interaction	9.21E-19	PVR, DYNC1LI1, TLN1, LDLR, TBK1, COPS6, IL6ST, IDE, ANKRD17, ACOT8…

Table 5.12: Functional terms associated with introns differentially expressed in cells over exosomes.
Functional terms were provided by David software after differential intron expression analysis of sequence data using DESeq2. The top 10 terms (by p-value) are displayed here and the first 10 genes in each group are listed.

Category	Term	p-Value	Genes
UP_KEYWORDS	Glycoprotein	7.17E-24	TEX101, GDF3, SLC52A1, SERPINA13P, MASP1, ATP1B2, LYPD5, SLC9A4, CRHBP, LHCGR…
UP_KEYWORDS	Signal	4.55E-21	TEX101, GDF3, SLC52A1, SERPINA13P, MASP1, LYPD5, CRHBP, LHCGR, GDF5, FSTL4…
UP_KEYWORDS	Secreted	7.49E-18	GDF3, SERPINA13P, MASP1, CRHBP, GDF5, FSTL4, SHH, APOB, SOSTDC1, CCBE1…
UP_KEYWORDS	Disulfide bond	3.41E-15	GDF3, MASP1, ATP1B2, CRHBP, GDF5, LHCGR, SYT9, FSTL4, CD48, APOB…
UP_KEYWORDS	Polymorphism	5.69E-14	RP1, SLC52A1, MASP1, SLC9A4, FSTL4, KIFC3, C16ORF78, TBPL2, TMEM145, GRIN2D…
UP_KEYWORDS	Ion transport	1.75E-08	SLC5A5, SLC5A4, GABRB3, ATP1B2, SLC9A4, SLC5A1, KCNK18, KCNJ10, KCNK12, CNGB3…
UP_KEYWORDS	Ion channel	1.97E-07	GABRB3, KCNK18, PANX3, KCNJ10, KCNK12, KCNA7, CNGB3, FXYD7, KCNMB2, PKD1L3…
UP_KEYWORDS	Vision	9.34E-06	RP1, GUCY2F, NDP, RP1L1, C2ORF71, BFSP2, RCVRN, RPGRIP1, VSX2, CNGB3…
UP_KEYWORDS	Serine protease inhibitor	9.99E-06	WFDC10A, HMSD, SERPINA13P, SERPINA11, SERPINA12, SPINK4, A2ML1, SPINK8, SERPINB9, CPAMD8…
UP_KEYWORDS	Transmembrane	2.52E-05	HIGD1C, SLC52A1, RARRES1, SERTM1, ATP1B2, SLC9A4, LHCGR, AQP4, SYT9, CD52…

Table 5.13: Functional terms associated with introns differentially expressed in exosomes over cells.
Functional terms were provided by David software after differential intron expression analysis of sequence data using DESeq2. The top 10 terms (by p-value) are displayed here and the first 10 genes in each group are listed.

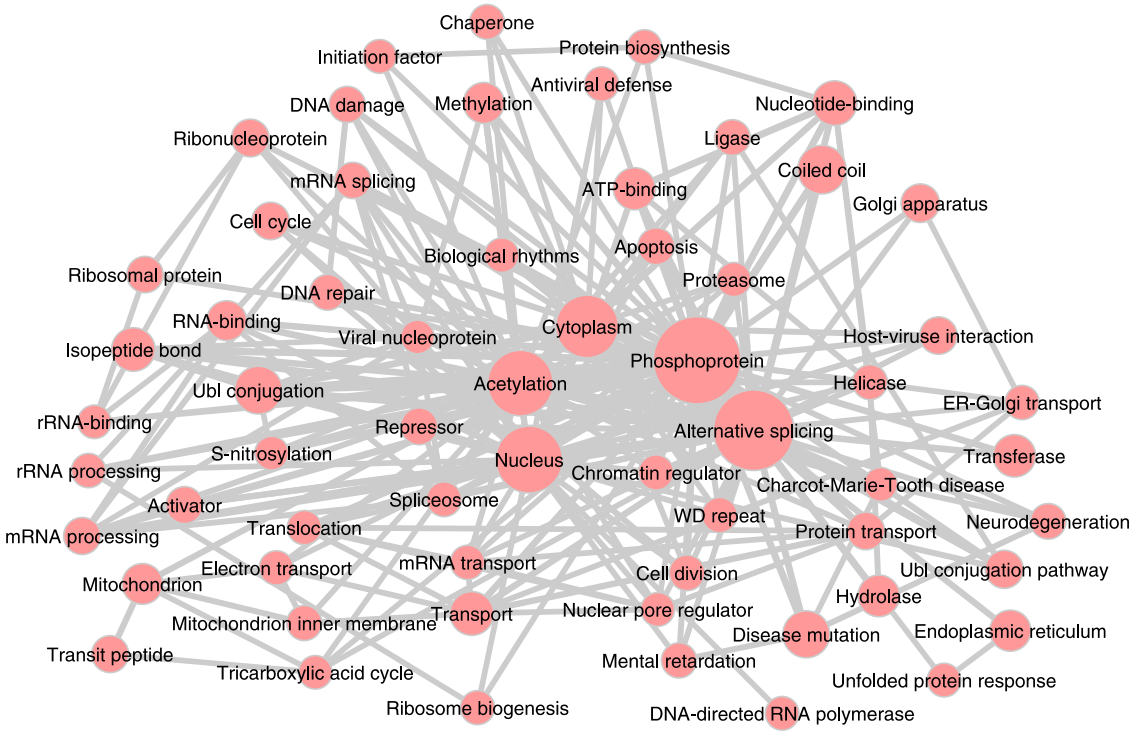

Figure 5.24: Functional annotation of the top 3000 introns differentially expressed in cells over exosomes.
Functional terms were annotated from sequencing data using DAVID software, limited to UP_KEYWORDS only, and plotted using Cytoscape software. Each term is represented by circles with the size of each circle representing the number of genes within the term and the thickness of line represents the number of overlapping genes between terms.

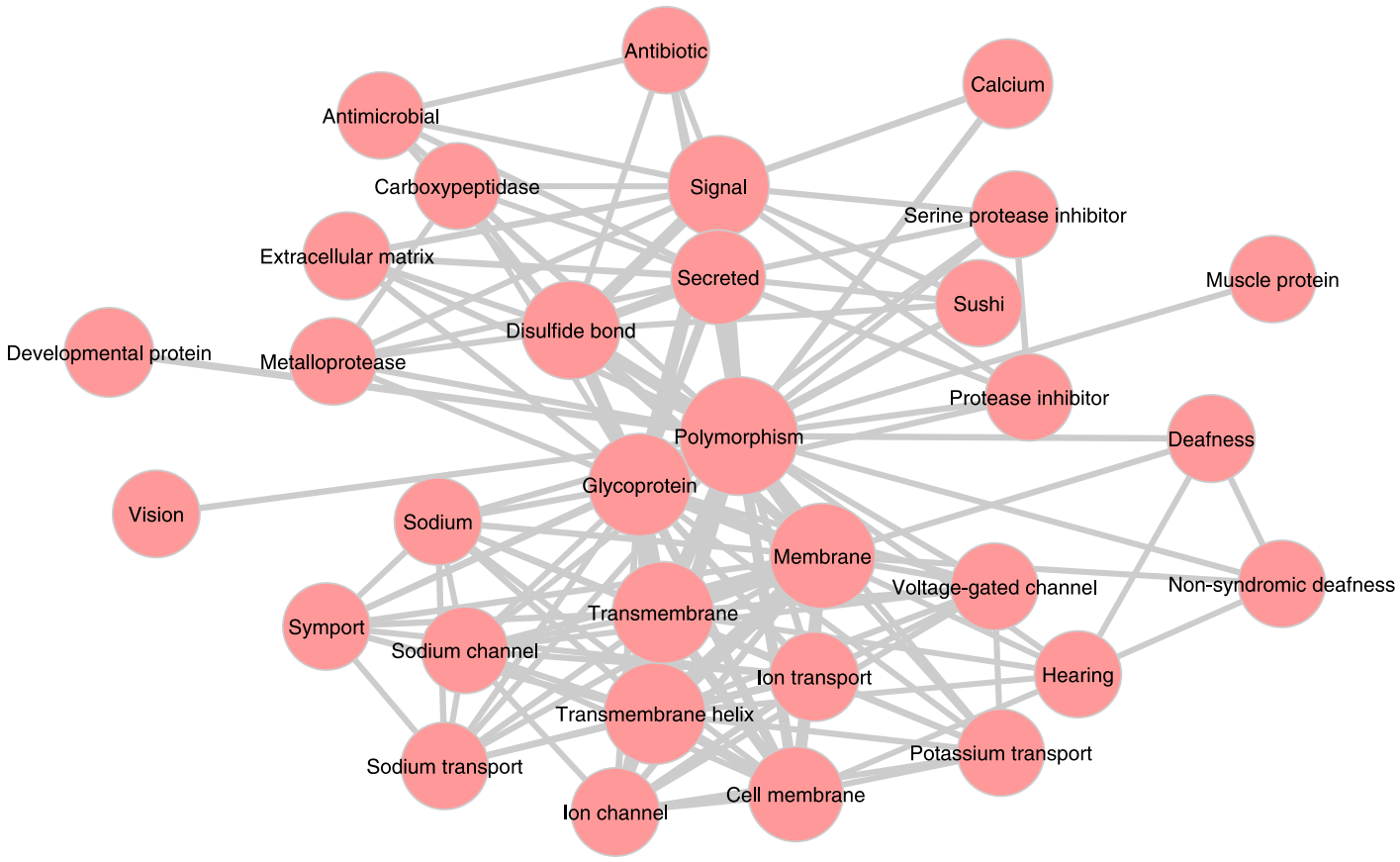

Figure 5.25: Functional annotation of the top 3000 introns differentially expressed in exosomes over cells.
Functional terms were annotated from sequencing data using DAVID software, limited to UP_KEYWORDS only, and plotted using Cytoscape software. Each term is represented by circles with the size of each circle representing the number of genes within the term and the thickness of line represents the number of overlapping genes between terms.

5.4 Discussion

This chapter aimed to validate procedures for isolating exosomal-RNA and to profile RNA from exosomes and the parent cell. It has previously been described that nuclease treatment should be used to ensure the analysis of genuine intra-luminal RNA (Hill et al., 2013) and procedures have been reported (Shelke et al., 2014). This PK/RA digestion was validated in-house and showed a 42% digestion of RNA in the exosome preparation (Figure 5.1). Notably, the population of small RNAs was removed which was reflected in the DV_{200} calculations of 89% for the treated sample, compared to 69% for the PBS-treated control (Table 5.1). This suggests that the non-vesicular RNA present in these preparations is enriched for small RNA species, such as miRNAs, and that this population can be removed by PK/RA digestion. This is in concordance with a previous study that showed Argonaute2 forms a complex with miRNA and is present in the circulation *in vivo* separately from vesicle-derived RNA (Arroyo et al., 2011). Based on these observations it was considered of great importance to include the PK/RA digestion in this study. Not all studies include this digestion step and subsequently analyse a mixed population of vesicular and non-vesicular RNA. It is questionable if the functional conclusions of such studies are overstated. Thus, the PK/RA procedure was validated and used in this study for extracting RNAse-resistant, intra-luminal RNA, which was protected by being located inside the exosomes.

Three biological replicates of H4 cells and secreted exosomes were established for RNA analysis. Cellular-RNA was extracted at the same time as exosome isolation to allow the most direct comparison between the two sample types. Electrophoretic analysis revealed a difference between cellular- and exosomal-RNA, consistent with published data (Shelke et al., 2014). Cellular-RNA was replete with rRNA as observed with the 18S and 28S peaks whilst the traces for exosomal-RNA lacked such peaks (Figure 5.2). These observations were reflected in the RNA integrity (RIN) and DV_{200} scores (Table 5.2). The RIN scores were a maximum of 10 for cell samples indicating no degradation of RNA. These were much lower at 2.1-2.2 for exosome samples but this is an unsuitable measurement of RNA quality in exosomes as they lack rRNA which the score is calculated from. Instead, here proposed for the first time, the use of the DV_{200} calculation as an indication of RNA integrity in exosomes. This score calculates the percentage of fragments >200 nucleotides in length and has been used previously to assess the suitability of formalin-fixed paraffin-embedded tissue for RNA sequencing (Eikrem et al., 2016). In consensus with manufacturer guidelines, the exosome samples, ranging from 57-64% DV_{200}, were of good quality for downstream sequencing. Thus

the DV_{200} calculation is of utility for assessing exosomal-RNA quality and worth incorporating into future workflows.

Whole transcriptome sequencing was performed on the HiSeq 2500, where only rRNA was depleted in the library preparation stage (Benes et al., 2011). Thus, the most comprehensive RNA profiling that was possible for this study was performed; an approach that would be suitable for others in the field to follow. The sequencing was of high quality but the exosome reads did not map and align as efficiently as cell samples. This was investigated further and deemed to be an intrinsic property of exosomal-RNA, whereby longer inserts in the prepared libraries (Figure 5.3) caused a divergence from the reference. Therefore, it could be advantageous, prior to future work, to refine the library preparation procedure for exosomes, but this was beyond the time and cost limitations of this project. This divergence from the reference caused by long inserts was the first of many observations that revealed that the repertoire of exosomal-RNA is fundamentally different from the source cell. This was investigated further by analysis of the RNA sequencing data. GATK guidelines and a recent survey of RNAseq data analysis best practices (Conesa et al., 2016) where referred to in the establishment of the pipeline described here.

The Picard tool CollectRnaSeqMetrics was used to get a global view of the cell and exosomes transcriptomes (Figure 5.8). An unprecedented difference between exosomal-RNA and the source cell was revealed. Over 96% of reads measured from exosomes were non-coding and thus, a completely different profile to cellular-RNA which contained a large proportion of coding RNA. It has been noted that the library preparation technique may have driven a preferential sequencing of intronic and intergenic reads which may have led to the difference between sample types being exaggerated. Considering the literature, which has demonstrated functionally active coding RNA in exosomes (Valadi et al., 2007), it should not be concluded that exosomes are devoid of coding RNA completely. Even if this library preparation technique has exaggerated the difference between cellular- and exosomal-RNA, the libraries were prepared simultaneously and the samples can be directly compared. It can be concluded then that the difference between transcriptomes is genuine.

To date, different techniques have been used to analyse exosomes compared to the source cell (Skog et al., 2008, Valadi et al., 2007, Nolte-'t Hoen et al., 2012, Cheng et al., 2014, Royo et al., 2013, Li et al., 2013, Ahadi et al., 2016b). Microarray analysis has revealed non-correlation between cells and exosomes (Skog et al., 2008) and small RNA sequencing

showed different profiles of small RNA species (Cheng et al., 2014), but not to this extent, as described with whole transcriptome sequencing.

Functional enrichment analyses were then performed to investigate if RNA was randomly packaged into exosomes. However, the vastly different profiles of cells and exosomes posed a problem for such analyses. A differential gene expression analysis would be skewed by the normalisation step that takes into account the size of the library. Indeed, directly comparing exonic reads from such fundamentally different samples in this way would be inappropriate. So without directly comparing cells to exosomes based on their exonic gene counts, two other avenues of investigation were pursued. Firstly, long non-coding RNAs (lncRNA) were chosen as they would come under the intronic and intergenic portions of the reads. Secondly, the intronic reads were directly compared between samples. By linking back to the associated gene-names, functional annotation was possible.

The analysis of differentially expressed lncRNAs and co-expressed mRNAs allowed the first functional analysis. Terms enriched in cells included “protein binding”, “chromosome”, “acetylation”, “phosphoprotein”, “nucleosome core” and “ubiquitin-like protein conjugation”. Such terms, in general, describe the dominant structures and processes within cells. Equivalent terms in exosomes included “disulfide bond”, “Glycoprotein”, “glycosylation site:N-linked”, “topological domain:Extracellular” and “Secreted”. With striking specificity these terms reflect the known protein composition of exosomes and appear similar to several proteomics based analysis of vesicles (Webber et al., 2014, Kalra et al., 2012, Simpson et al., 2012). Indeed, it has been described that glycosylation is one of the processes by which exosomal proteins are regulated (Kore and Abraham, 2016) and glycoproteins on the surface of exosomes play important physiological roles such as the binding of activated platelets in the coagulation cascade (Del Conde et al., 2005). Tetraspanins such as CD63, CD81 and CD9 and tetraspanin webs are proteins that are characteristic of exosomes, as described in chapter 3, and are based on disulphide bonds to keep the structural integrity and stability of vesicles. One study demonstrated that most of the exosomal proteins, from B-cells, were insoluble in CHAPS-containing buffers and thus, extensively include tetraspanins to be detergent-resistant vesicles (Wubbolts et al., 2003).

It is remarkable that by analysing lncRNA expression, and intron expression as discussed below, an enrichment of such functionally relevant terms has been demonstrated. LncRNA and intronic reads do not represent coding RNA so there is a disconnection between their presence in exosomes and their functional role. Most notably, there is no translation

machinery, such as rRNA, in exosomes so there is currently no apparent reason for why these species should be enriched. It is also notoriously difficult to interpret enrichment maps with absolute certainty. To provide further weight behind these observations qPCR replication of 6 of the lncRNA candidates was performed and a differential expression analysis of introns, which did not require the co-expression step, retrieved similar results.

One conclusion that can be drawn from these data, accepting the caveat of the disconnection between non-coding RNA and functional activity in exosomes, is that the sorting of RNA into exosomes is not an entirely random process. This is in concordance with other studies which have shown that the exosomal-RNA profile is altered when cells are subject to hypoxia (Li et al., 2016a, Gray et al., 2015, Yang et al., 2016) and oxidative stress (de Jong et al., 2012, Eldh et al., 2010). The observation here, using whole transcriptome RNAseq analysis, suggests that there are intracellular processes for sorting RNA into exosomes. According to the literature these processes appear to be sensitive to the state of the cell and, together with this current study, implies that the dynamics of vesicular RNA is functionally important.

These processes, underlying the sorting of RNA into extracellular vesicles, are unknown but hypotheses were made in a 2017 position statement from ISEV (Mateescu et al., 2017). Leading this discussion was the observation that miRNA is prone to rapid degradation by nucleases (Mitchell et al., 2008b) but dramatically more stable when bound to RNA-binding proteins such as the Argonaute (AGO) family (Olejniczak et al., 2013). Thus, sorting RNA into vesicles is fundamentally a discussion on the interaction with RNA-binding proteins. Studies have shown that AGO2, and other miRNA-interacting proteins, can interact with components of the endocytic tracts such as multi-vesicular bodies (Gibbings et al., 2009, Lee et al., 2009), endoplasmic reticulum (Stalder et al., 2013) and endogenous prion protein which is a transmembrane protein in the endolysosomal network (Gibbings et al., 2012). Currently it is inconclusive if AGO proteins are generally associated with extracellular vesicles but it is likely that post-translational modification of the protein, and modulation of miRNA transcripts, would play a role in the incorporation into EVs (Mateescu et al., 2017). Indeed, a number of RNA motifs have been associated with incorporation into EVs (Szostak et al., 2014, Batagov et al., 2011) including a GGAG motif on miRNAs that binds to sumoylated heterogeneous nuclear ribonucleoprotein A2B1 for loading into exosomes (Villarroya-Beltri et al., 2013). Thus, it has been proposed that there may be active and passive loading of RNAs into EVs, such as exosomes, based on the interaction of RNAs with RNA-binding proteins, but as yet these processes have not been thoroughly investigated (Mateescu et al., 2017).

Here, it has been observed that the RNA packaged into exosomes and secreted out of the cell are indicative of the known protein composition of these vesicles and thus not packaged by random. This was not a phenomenon that might have been expected, yet is in agreement with, and provides additional evidence for, the current opinion in the field (Mateescu et al., 2017).

To ensure the validity of these observations two lines of inquiry were followed. First, differential expression of six of the lncRNAs was replicated with separately prepared samples and using qPCR as an independent method (Figure 5.19). Second, the equivalent differential expression analysis was performed with introns. Functional annotation and enrichment analysis of introns revealed similar and overlapping terms as described for the lncRNA analysis. These observations confirmed the original lncRNA analysis.

In the future it would be beneficial to directly investigate the function of these differentially expressed lncRNAs. It has been demonstrated that exosomal miRNAs can be pharmacologically inhibited leading to physiological changes, for example, pathological changes in cardiac hypertrophy (Bang et al., 2014). It is also possible to target lncRNAs for overexpression and silencing. One study showed that expression of the lncRNA, Chast, can be altered *in vivo* and in an *in vitro* cell model of cardiac remodelling (Viereck et al., 2016). Another study showed differential expression of lncRNAs as a response to hypoxia in endothelial cells and experimental validation that two of these drove angiogenic defects (Fiedler et al., 2015). Thus, the tools are available to further the work in this study and more deeply investigate the roles of lncRNAs in exosomes.

It can be concluded that the sorting of RNA into exosomes does not occur entirely by random. The processes that underlie this phenomenon are unknown and would require a different avenue of investigation to unearth. The whole transcriptome sequencing approach, used here, has also revealed an unprecedented distinction in the repertoire of RNA in exosomes compared to the source cell. Exosomes appear to be a route for ncRNAs, non-randomly sorted, to be eliminated from the cell and into the extracellular *milieu*. This affirms the direction of investigation in this thesis: that exosomes, and their encapsulated, nuclease-resistant, stable RNA, have potential to be utilised for biomarkers of AD. Therefore, the direction of the final chapter was to move from cell culture-derived exosomes to patient-derived exosomes. The challenges of isolating exosomes from biological fluids were addressed next.

Chapter 6. Isolating exosomal-RNA from peripheral blood for biomarkers of Alzheimer's disease

6.1 Introduction

Exosomes are of growing interest for biomarkers of AD, given the recent findings in the field of cancer. For example, the proteoglycan, glypican-1, was measured on exosomes isolated from pancreatic cancer patient serum and showed absolute specificity and sensitivity for identifying patients over healthy controls (Melo et al., 2015); although for many reasons, including image manipulation, this publication has questionable credibility. In the field of neurological diseases, such as AD, exosomes have good potential as a biomarker as they are known to pass bi-directionally over the blood-brain barrier. In one study, a glioblastoma specific mRNA, EGFRvIII, was detected peripherally in exosomes isolated from patient serum (Skog et al., 2008). Another study detected myelin proteins on serum-derived exosomes from patients with multiple sclerosis (Galazka et al., 2017). Exosomes passing the opposite direction has also been observed in a murine model. Exosomes loaded with siRNA were able to achieve knockdown of *BACE1* in mouse brain (Alvarez-Erviti et al., 2011). In essence, exosomes from peripheral blood hold potential for use as a non-invasive "liquid biopsy" of processes occurring in the brain.

Peripheral exosomes have been investigated for a number of neurological diseases. One technique, that has been adopted for multiple diseases, is to enrich for exosomes of neural origin and analyse protein expression in patients and healthy controls (Goetzl et al., 2015b, Fiandaca et al., 2015, Hamlett et al., 2016, Mullins et al., 2017, Goetzl et al., 2015a, Mustapic et al., 2017).

Using this technique it has been demonstrated that the expression of a number of proteins are significantly altered in AD. These include: LRP6, HSF, REST, cathepsin D, LAMP-1, ubiquitin, HSP70, total tau, P-T181-tau, P-S396-tau and Aβ1–42 (Goetzl et al., 2015a, Goetzl et al., 2015b, Fiandaca et al., 2015). In these studies, similar observations were also made for frontotemporal dementia (FTD) (Goetzl et al., 2015a, Goetzl et al., 2015b, Fiandaca et al., 2015). The same technique was used with Down's syndrome (DS) patients to measure the AD-related proteins Aβ1–42, P-T181-tau and P-S396-tau for the early detection of AD pathology, which is often masked by intellectual disability (Hamlett et al., 2016).

In the case of Parkinson's disease (PD), plasma-derived exosomes have shown elevated protein concentrations of α-synuclein over healthy controls in a large cohort (Shi et al., 2014). Interestingly, this observation was in contrast to what was known previously: that α-synuclein was consistently lower in patient CSF. Cells can transmit toxic forms of prion

protein (PrPsc) in association with exosomes as a potential route of propagating neurodegenerative Prion disease (Fevrier et al., 2004). In the case of Amyotrophic lateral sclerosis (ALS), exosomes have been shown to harbour misfolded forms of superoxide dismutase 1 (SOD1) (Grad et al., 2014) and TAR DNA-binding protein-43 (TDP-43) (Nonaka et al., 2013) and thus, a potential route of intercellular transfer. Observed using a cell culture model, polyglutamine huntingtin protein and RNA containing the expanded CAG repeat were transferred between cells, via exosomes, as a potential route of propagating Huntington's disease (HD) (Zhang et al., 2016c). Thus, exosomes have been implicated in a number of neurodegenerative diseases and investigating the potential of utilising them as biomarkers has already begun in a number of these diseases.

Isolating exosomes from peripheral blood comes with some difficulties. An issue for proteomic analyses, in particular, is the contamination of abundant proteins such as Human Serum Albumin (HSA) that can co-isolate with exosomes (Welton et al., 2015). Within the total population of exosomes there are many sub-populations representing different tissues, as discussed in Chapter 4. Solutions are available to select sub-populations of relevance to disease (Mustapic et al., 2017) which should enrich for the signal under investigation. However, this reduces the yield of material obtained in the isolation procedure which is likely to be a particular problem for isolating RNA which is present in low quantities in exosomes (Enderle et al., 2015). Not enriching for exosomes from disease-relevant tissue provides a larger amount of material to analyse but may be littered with "noise" from other, unwanted, tissue types.

The availability of material to analyse is a limiting factor in exosome research. For example, RNA extracted from blood-derived exosomes is measured in the picogram range (Enderle et al., 2015). Nevertheless, a benefit of utilising exosomes from biological fluids is that they provide a source of nuclease-resistant RNA (Cheng et al., 2014). Exosomal-RNA is encapsulated in a lipid-bounded vesicle and this study demonstrated, in chapter 5 using cell culture-derived neuroglioma exosomes, that this provides protection from enzymes such as RNase A compared to circulating, free RNA which is susceptible to such degradation.

A number of considerations have so far been highlighted for isolating exosomes from biological fluids. These considerations include overcoming the contamination of highly abundant proteins in a complex fluid, such as blood, and achieving a balance between selecting a sub-population of disease/tissue-relevant exosomes whilst maintaining sufficient yield for RNA analysis. It is worth noting that the scalability of the isolation method is also an

important consideration. In chapters 3 and 5, highly pure exosomes were isolated from the conditioned media of neuroglioma cell cultures by ultra-centrifugation, non-vesicular RNA was removed by PK/RA digestion and a sufficient yield of exosomal-RNA was obtained for sequencing. This workflow provided pure samples but was time- and labour-intensive. Therefore, the same methods of exosomal-RNA isolation may not be directly applicable to a biomarker study with patients where handling biological fluids have inherent technical challenges and large sample numbers are required. This chapter aimed to address these challenges whilst developing a scalable workflow for analysing exosomal-RNA from patient plasma.

There have been two studies that have undertaken RNA sequencing of blood-derived exosomes for biomarker discovery in AD, to date. The first of these reported the use of 4 ml plasma to obtain less than 100 pg RNA (Lugli et al., 2015). Despite being below manufacturer's guidelines for input, cDNA libraries were successfully prepared and small RNA sequencing performed. Screening of AD cases unveiled 20 miRNAs associated with disease, 7 of which worked well in a machine-learning model of predicting disease. The second of these studies reported the use of 1 ml serum to isolate exosomal RNA but did not report the yield of RNA (Cheng et al., 2015). Nevertheless, sequencing and qPCR replication was performed and a panel of 16 miRNAs showed sensitivity and specificity for AD prediction in combination with other risk factors. Both studies performed small RNA sequencing but there was little overlap in the results (Kumar and Reddy, 2016). However, one miRNA, miR-342-3p, was down-regulated in AD across both studies. These results highlight the difficulty in finding consensus across biomarkers of AD and the capabilities of the sequencing platforms were stretched by the input material. Therefore, a challenge remains in isolating sufficient exosomal material from blood for such biomarker discovery studies.

An added complication is that often a clean and conclusive diagnosis of AD is not possible until *post-mortem*. Yet the pre-clinical and symptomatic phases of disease, during which biomarkers are needed, occurs over decades (Villemagne et al., 2013). Whilst collecting stocks of biological fluids from probable AD cases is relatively easy, collecting biological fluids collected from definitively diagnosed AD cases can be difficult. These stocks can be easily depleted as participants may have deceased before a conclusive diagnosis had been made. This means that high volumes, such as the 4 ml plasma used by Lugli *et al.*, are not readily available if the original collection was performed years previously. To address this complication, an assay to investigate exosomes from minute volumes of plasma is much needed so that easily-depleted, archived materials can be used to obtain meaningful data.

6.2 Aim

The aim of this chapter was to identify and overcome the obstacles of isolating exosomal-RNA from minute volumes of blood and develop an assay for the detection of AD biomarkers. To achieve this aim the following objectives were addressed:

- Prior to accessing archived material, use Nanoparticle Tracking Analysis to assess the effects of freezing plasma samples over time and detect any gross aggregation or loss of particles
- Assess the efficacy of ultra-centrifugation, size exclusion chromatography and spin-column based isolation as techniques for obtaining sufficient yields of plasma exosomal-RNA for downstream analysis
- Develop a scalable workflow for extracting exosomal-RNA from 0.5 ml plasma
- Investigate a selection of candidate exosomal-RNA targets for their potential to be disease discriminating in a case:control cohort

6.3 Results

6.3.1 Effect of freezing plasma over time on exosome size and concentration

The first aim addressed was assessing the effect of freezing plasma samples over time on the size and concentration of exosomes. Blood was collected into potassium-EDTA tubes from four healthy donors and processed for the isolation of plasma. In short, these were centrifuged at 400 x g for 7 min, re-centrifuged at 6000 x g for 10 min, passed through 0.2 µm filters and aliquoted before freezing. This procedure allowed for the assessment of exosomes and particles of similar size by NTA measurements. These were performed at Day 0 (non-frozen plasma), Day 2, Day 7, Day 14 and Day 30. For the sake of clarity, NTA measurements will be referred to as "particles" due to the co-detection of other, non-vesicular, particles of similar size.

A histogram showing particle size against particle concentration is displayed in Figure 6.1A based on six NTA measurements of one donor, at Day 0, but indicative of the whole dataset. A sharp peak was observed at 64 nm. Alternatively, the mean can be averaged and in this instance would result in a size of 75.21 ± 1.66 nm compared to averaging the mode to give a size of 64.33 ± 0.84 nm. Due to the size distribution observed in the raw data (Figure 6.1A), averaged mode size was chosen as the standard measurement of particle size.

Particle size was determined for each donor over the time course (Figure 6.1). There was a general trend for particles to increase in size over the time course reaching a peak on Day 14 of ~100 nm. Assessing the donors individually (Figure 6.1C), this appears to be driven by a large spike in Donor 4. Such readings can occur if particles aggregate and are therefore detected as one larger particle by the system. It is important that this phenomenon is counteracted by taking repeated video measurements or increasing the time of recording. In this study, six videos of 30 s duration were taken as used elsewhere (Webber and Clayton, 2013). By Day 30, this trend had plateaued and the size range over the time course was 70-100 nm which was within the expected size range for exosomes (El Andaloussi et al., 2013). Shapiro-Wilk tests confirmed that data were normally distributed on each day, except day 14. The Q-Q plot for day 14 was visualised and it was apparent that this lack of normality was driven by the outlying data point. Therefore, it was deemed that a parametric test was most appropriate for the whole dataset. A repeated measures ANOVA, using SPSS statistics software, determined that there was no statistically significant difference in particle size over 30 days of freezing $F(1.344, 4.032) = 2.441$, $p = 0.198$.

Overall, these data suggest that there may be a small element of vesicle aggregation over time frozen. This phenomenon does not cause a statistically significant change in particle size and stayed within the range expected for exosomes. Therefore, it appears that the vesicles within plasma are stable at -80°C, however, the limitations of NTA must be considered. Firstly, NTA measure particles without discriminating between exosomes and non-vesicular particles of the same size, such as high-density lipoproteins. Secondly, NTA gives no indication of vesicle structure. In chapter 3, cryo-EM was performed on cell culture-derived exosomes that had been previously frozen at -80°C and detected intact vesicles of spherical structure with unilaminar lipid bilayers. Such methods would be required to conclusively determine that vesicle structure is not degraded by freezing plasma over time but this was beyond the scope of this thesis. However, cryo-EM has been performed on exosomes isolated from frozen plasma elsewhere, and similar structures were observed (Welton et al., 2016). Thirdly, NTA gives no indication of molecular degradation caused by the freezing process. Enzymatic assays would need to be performed for the activity of proteins such as acetylcholinesterase (Lotvall et al., 2014) but particularly, for this study, there is no indication of the integrity of the exosomal-RNA. These assessments were performed with archived, frozen plasma samples in sections 6.3.5 and 6.3.7. Overall, this approach has given an indication that there is no gross aggregation of vesicles caused by the freezing process.

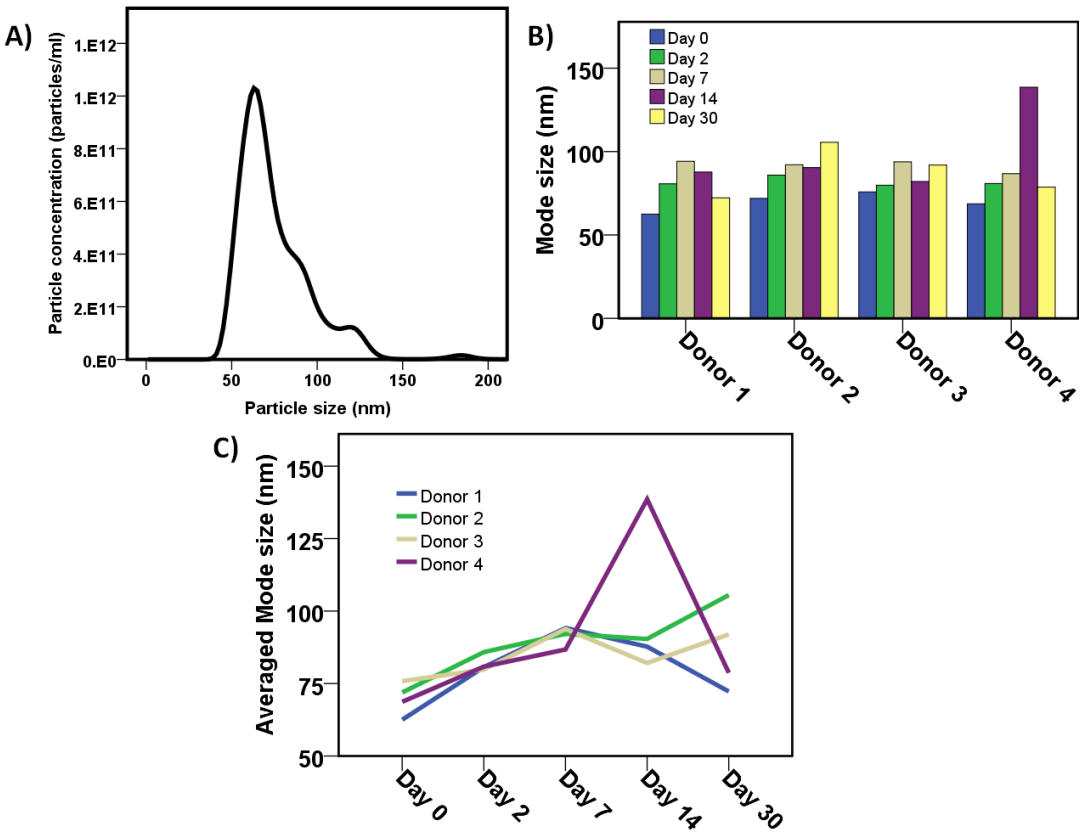

Figure 6.1: The effect of freezing plasma on particle size over time.
Plasma samples were obtained from four donors, frozen over a 30 day period an assessed by Nanoparticle Tracking Analysis. A) *A histogram showing particle size (x-axis) and concentration (y-axis) measured by NTA (n=6) for one sample but indicative of the whole dataset. B) A bar chart showing mode particle size for each donor separated (n=6 videos per donor at each time point). C) A line graph showing averaged mode size across all donors.*

Next, the effect of freezing on particle concentration was assessed. NTA provided an output of concentration and size so the same sets of videos were used as above.

Particle concentration for each donor, over the 30 day time course, were obtained (Figure 6.2). The concentration of particles remained stable over the time course with no overall trend showing an increase or decrease. Shapiro-Wilk tests confirmed that data were normally distributed on each day so parametric statistical tests were appropriate. A repeated measures ANOVA determined that there was no statistically significant difference in particle concentration over 30 days of freezing $F(1.986, 5.959) = 2.674$, $p = 0.148$. Particle concentrations stayed within a range of ~$2.5x10^{13}$ particles/ml and ~$4.5x10^{13}$ particles/ml.

Overall these data suggest that there was no overall fluctuation in particle concentration over the time course. This confirmed that the process of freezing and storing plasma at -80°C caused no gross aggregation (determined by size) or gross loss of particles (determined by concentration) over the course of 30 days.

The limitations of using NTA to draw these conclusions has been highlighted above, namely, that non-discriminate particles are measured in this technique with no indication of changes in structural or molecular degradation. Nevertheless, these observations bolster support for using frozen, archived plasma. The time course studied here was for plasma stored for up to 30 days which may be a shorter time than archived material, however, no significant trends where observed for particle concentration or size. Therefore, there has been some indication that plasma samples are stable at -80°C and consequently frozen, archived plasma was used next for the isolation of exosomal-RNA.

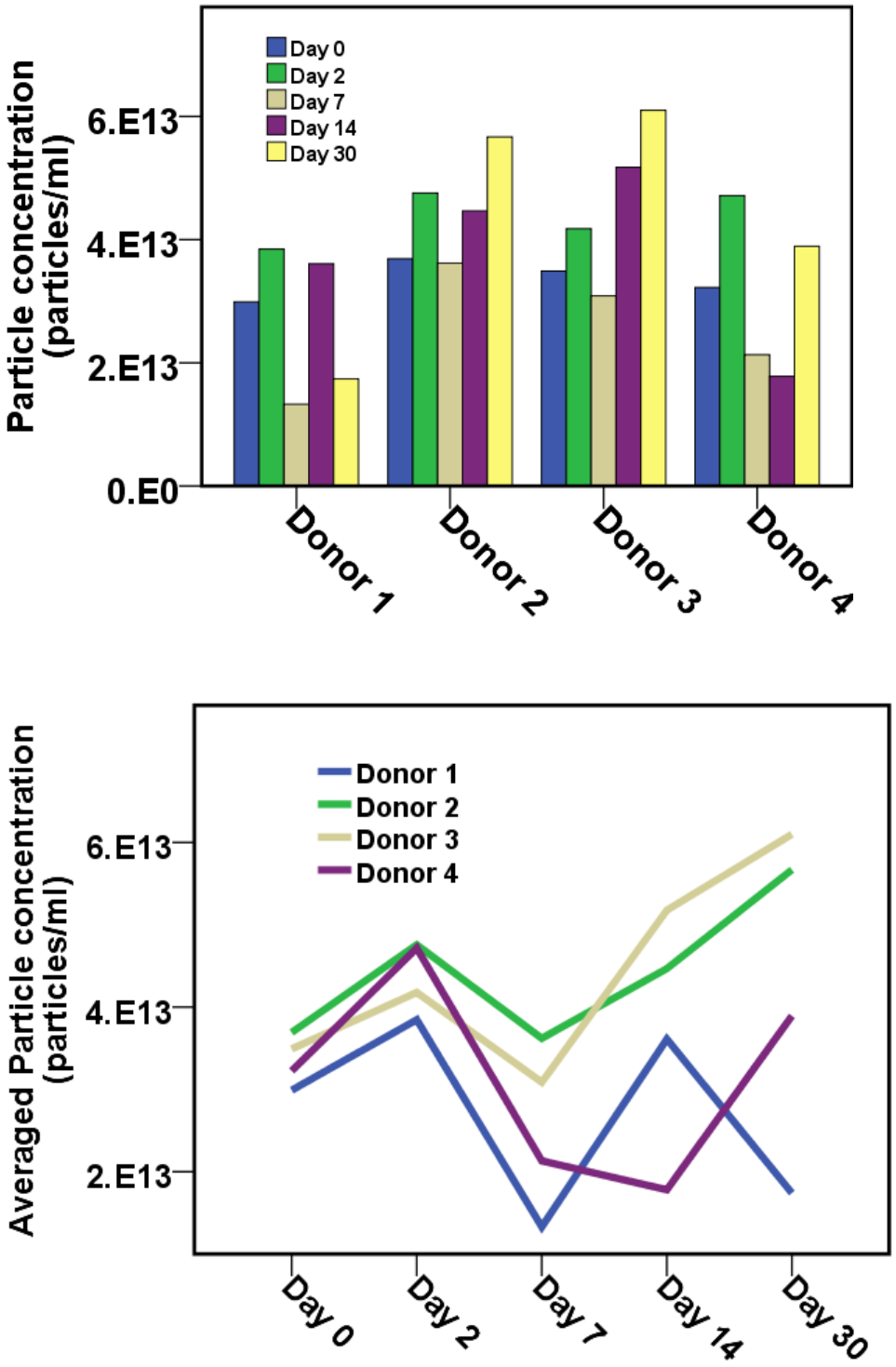

Figure 6.2: The effect of freezing plasma on particle concentration over time.
Plasma samples were obtained from four donors, frozen over a 30 day period an assessed by Nanoparticle Tracking Analysis. *Top: a bar chart showing averaged particle concentration for each donor separated (n=6 per donor at each time point). Bottom: a line graph showing averaged particle concentration across all donors.*

6.3.2 Isolating exosomes and exosomal-RNA from human plasma

Different methods of isolating exosomes from plasma were compared with an aim to identify obstacles prior to the isolation and analysis of exosomal-RNA. Different solutions have been proposed for this including differential ultra-centrifugation (Thery et al., 2006), size-exclusion chromatography (Welton et al., 2015), density gradients or cushions (Thery et al., 2006), immuno-precipitation (Mustapic et al., 2017) and spin column-based isolation (Enderle et al., 2015). Here ultra-centrifugation, size-exclusion chromatography using ExoSpin™ (Cell Guidance Systems) and spin column-based exoRNeasy™ (Qiagen) were compared.

These three methods were selected as they provided a range of principally different isolation techniques. Ultra-centrifugation was used in chapter 5 to pellet exosomes from cell-conditioned media and, in combination with PK/RA digestion, exosomal-RNA isolated for sequencing. It was expected that, when applied to plasma, this technique would indiscriminately pellet non-vesicular particles and soluble proteins with exosomes so would again require the PK/RA digestion step to ensure genuine vesicular RNA was isolated. Provided that the pelleting efficiency of exosomes in plasma is similar to cell-conditioned media, reported to be greater than 90% efficiency in the Clayton laboratory, this technique should pellet the majority of exosomes in the sample without preferentially selecting a sub-population. However, a disadvantage of this technique is that ultra-centrifugation is time- and labour-intensive so technically challenging to scale up for numerous samples. Size-exclusion chromatography allows exosome-containing fractions to be separated from human serum albumin (HSA). This provides a purer sample but increases the volume of exosome-containing liquid that requires ultra-centrifugation (Welton et al., 2015). Again, this combination of steps is time- and labour-intensive and the pellet would again require PK/RA treatment. As an alternative method, a spin-based column does not require ultra-centrifugation or PK/RA treatment. It has been reported that the exoRNeasy™ columns have high specificity for vesicular- over non-vesicular RNA and only requires standard centrifuge equipment. Therefore, this technique is principally different from ultra-centrifugation and size-exclusion chromatography, however, the commercial kit increases the cost of sample preparation.

It is vital to strike the right balance between sample purity, cost and scalability for an isolation method to be tractable. This balance is considered and discussed below as exosomal-RNA was extracted using the three different isolation techniques.

6.3.3 Isolating plasma exosomes by ultra-centrifugation

The plasma samples, used in section 6.3.1 above, were ultra-centrifuged at 200,000 x g for 2 hours to obtain a pellet (Optima-MAX ultracentrifuge, with TLA-110 rotor, *k*-factor = 13). To assess the efficiency of ultra-centrifugation, NTA was used to measure particle concentration pre- and post-ultracentrifugation in the supernatant (Figure 6.3). Particle concentration was reduced from $3.67x10^{13} \pm 2.88x10^{12}$ particles/ml before ultracentrifugation to $2.79x10^{13} \pm 2.58x10^{12}$ particles/ml in the supernatant afterwards. A Shapiro-Wilk test confirmed that data were normally distributed so parametric statistical tests were appropriate. Whilst a paired t-test showed a statistically significant difference in particle concentration, $t(19) = 3.328$, $p = 0.004$, this corresponded to a pelleting efficiency of 24%.

Analysing individual NTA traces more closely revealed that this pelleting efficiency was not uniform across the range of particles in these samples. There was a rightward shift in the trace that suggested that the smaller particles had pelleted more successfully than larger. The averaged mode size, across the dataset, increased from 86 ± 16 nm to 101 ± 20 nm (n=20). Whether these correspond to exosomes or other non-vesicular particles cannot be teased out of NTA data.

Overall it appears that the pelleting of exosomes, and other non-vesicular particles, by ultra-centrifugation is an inefficient process. However, the observation that smaller particles appeared to pellet more efficiency than larger particles may reassure that the efficiency for exosomes may be higher than reported. It is possible that by increasing ultra-centrifugation time, speed and rotor may well increase this efficiency. A thorough development of this method was beyond the scope of this thesis as it would require a large quantity of archived plasma to do so. Furthermore, changing the method in these ways would make it increasingly time- and labour-intensive and thus, less suitable for larger biomarker discovery studies. The isolation of exosomal-RNA was performed on the pellet (reported later in sections 6.3.5 and 6.3.7) and would provide the best evaluation of this method compared to others.

A consideration, prior to RNA extraction, is that ultra-centrifugation does not discriminate between vesicular and non-vesicular particles. Therefore, within the pellet there is likely to be co-isolation of exosomes and RNA-binding proteins such as Argonaute (Arroyo et al., 2011) or high-density lipoproteins (Vickers et al., 2011). Nucleases can be used on pellets, prior to RNA extraction, to ensure the isolation of genuine intra-luminal RNA (Hill et al., 2013). Procedures for doing so have been established (Shelke et al., 2014) and shown to be

important in chapter 5. The exosome pellet was similarly treated here prior to extraction using the mirVana RNA isolation kit (Ambion).

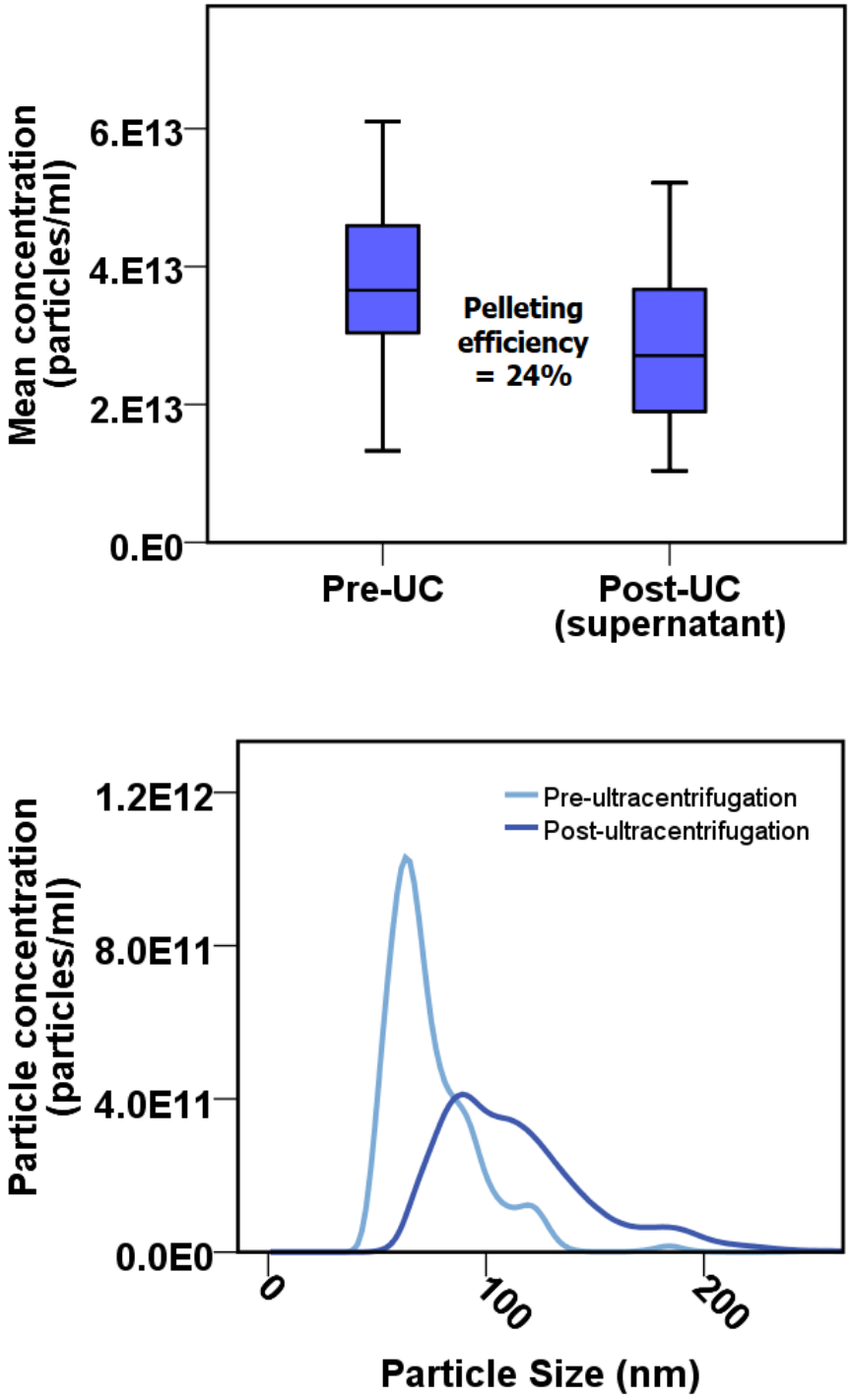

Figure 6.3: Pelleting efficiency of ultra-centrifugation.
Plasma samples were obtained from four donors and assessed by Nanoparticle Tracking Analysis before and after ultra-centrifugation. Top: a box-plot showing particle concentration pre-and post-ultracentrifugation in the supernatant (n=20). The upper and lower "hinges" of the boxes correspond to the first and third quartiles whilst whiskers extend to values within 1.5 x inter-quartile range. Bottom: A histogram of one sample, pre- and post-ultracentrifugation (light blue and purple lines, respectively), measured by NTA indicative of the dataset.

6.3.4 Isolating plasma exosomes by size exclusion chromatography

A major obstacle in proteomic analysis of exosomes from human plasma is the co-isolation of Human Serum Albumin (HSA). One solution to overcome this has been the use of size exclusion chromatography (Welton et al., 2015). Using this method, fractions enriched for exosome protein markers can be separated from proteins otherwise abundunt in blood, such as HSA.

This method, now available as the commercial product Exo-spin™ (Cell Guidance Systems Ltd.), was validated for this study using 0.5 ml plasma isolated from two human donors. Thirty equal volume fractions were collected and relative protein expression of CD81, IgG1 and HSA were quantified by TRF (Figure 6.4). The exosome marker, CD81, was enriched in fractions 8-14 whilst HSA was detected in high concentrations from fractions 18-30. These data are reflective of what is expected in the literature (Welton et al., 2015) and demonstrates the separation of exosome-enriched fractions from HSA and the bulk of plasma proteins.

This very simple approach therefore, provides a useful tool to isolate exosomes from plasma. However, the exosome-enriched fractions equated to 3.5 ml of liquid which is a larger, but purer, volume than the original 0.5 ml plasma and would require concentration prior to RNA isolation. Welton *et al.,* discuss concentration efficiency in the original publication for Exo-spin™ and reported a 9.6% protein recovery and 5% particle recovery after ultra-centrifugation. Particle recovery was similar using a precipitation technique but less pure in terms of protein content. This highlights a potential problem for isolating exosomal-RNA.

In sections 6.3.6 and 6.3.7 exosomal-RNA was isolated using this method and compared to ultra-centrifugation and spin-column based methods. For size-exclusion chromatography samples, the exosome-enriched fractions were concentrated by ultra-centrifugation to obtain a pellet. 3.5 ml of exosome-enriched fractions were poured into Quickseal ultra-centrifuge tubes and topped up to 4.8 ml with PBS before ultra-centrifugation at 200,000 x g for 2 hours (Optima-LE ultracentrifuge, 70 Ti rotor, *k*-factor = 44). PK/RA digestion was performed on the pellet prior to RNA extraction using the mirVana RNA isolation kit (Ambion).

Therefore, the same obstacles described for ultra-centrifugation, in section 6.3.3, are likely to pose a problem for exosomal-RNA yield and assay scalability with size exclusion chromatography. Whilst it has been demonstrated that this method successfully removed

HSA as a contaminant, the ultra-centrifugation volumes were greater and so increased the time- and labour-intensity. PK/RA digestion was still a necessary step as there was no indication if non-vesicular RNA would be present in the exosome-enriched fractions. Running plasma through the columns added additional financial and time cost which again reduces the potential to scale this method up for numerous samples. In summary, this method gives a purer sample by separating exosome-enriched fractions from abundant plasma proteins but comes at a cost of reducing exosome yield and increasing the time-, labour- and financial-cost.

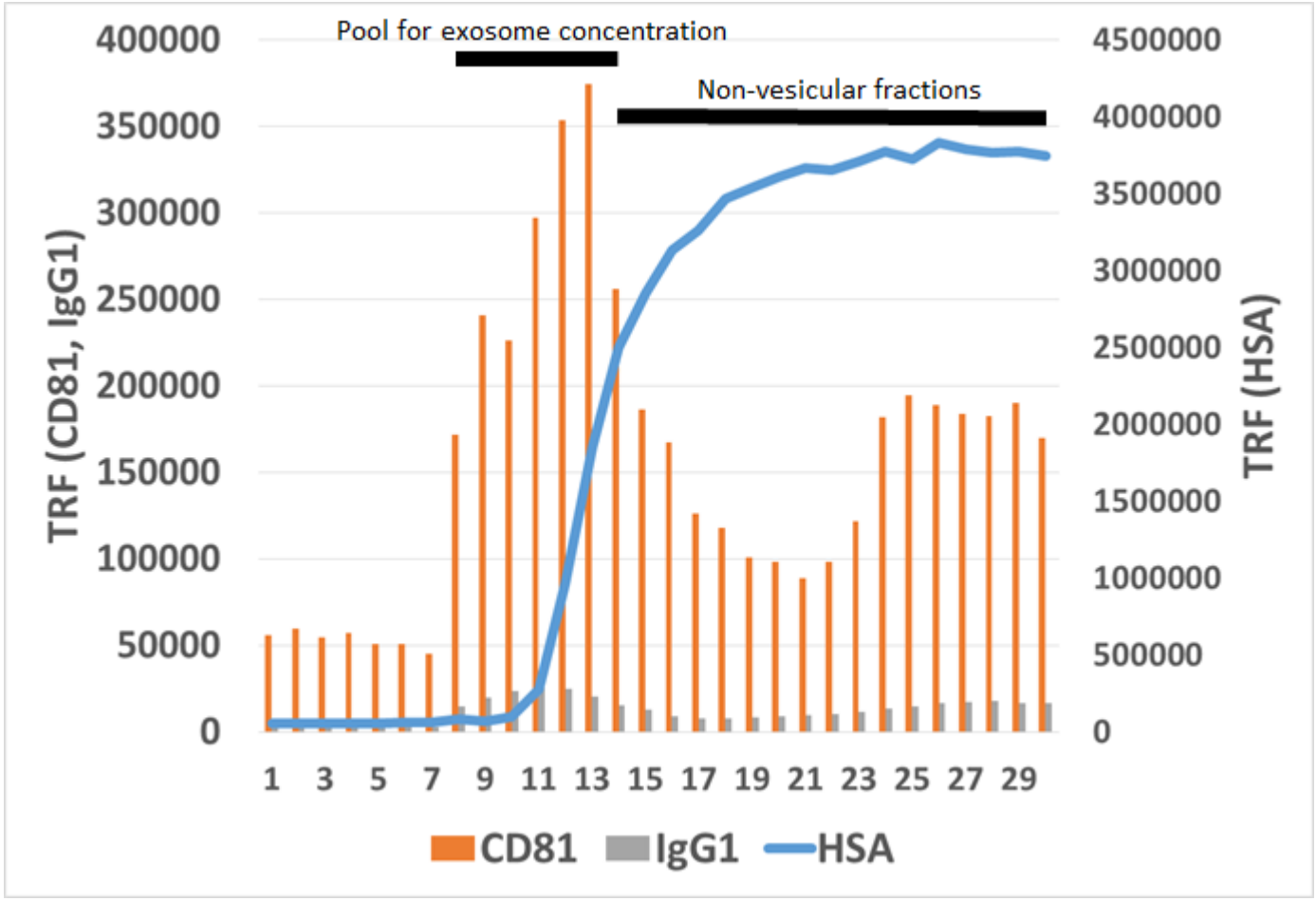

Figure 6.4: Relative levels of CD81, IgG1 and HSA in size exclusion chromatography fractions (Donor 1).
Plasma samples from two donors were subjected to size exclusion chromatography, thirty fractions collected and relative protein levels measured by Time Resolved Fluorescence (TRF). The exosome marker, CD81, is represented with orange bars, IgG1 control with grey bars and Human Serum Albumin (HSA) with blue line.

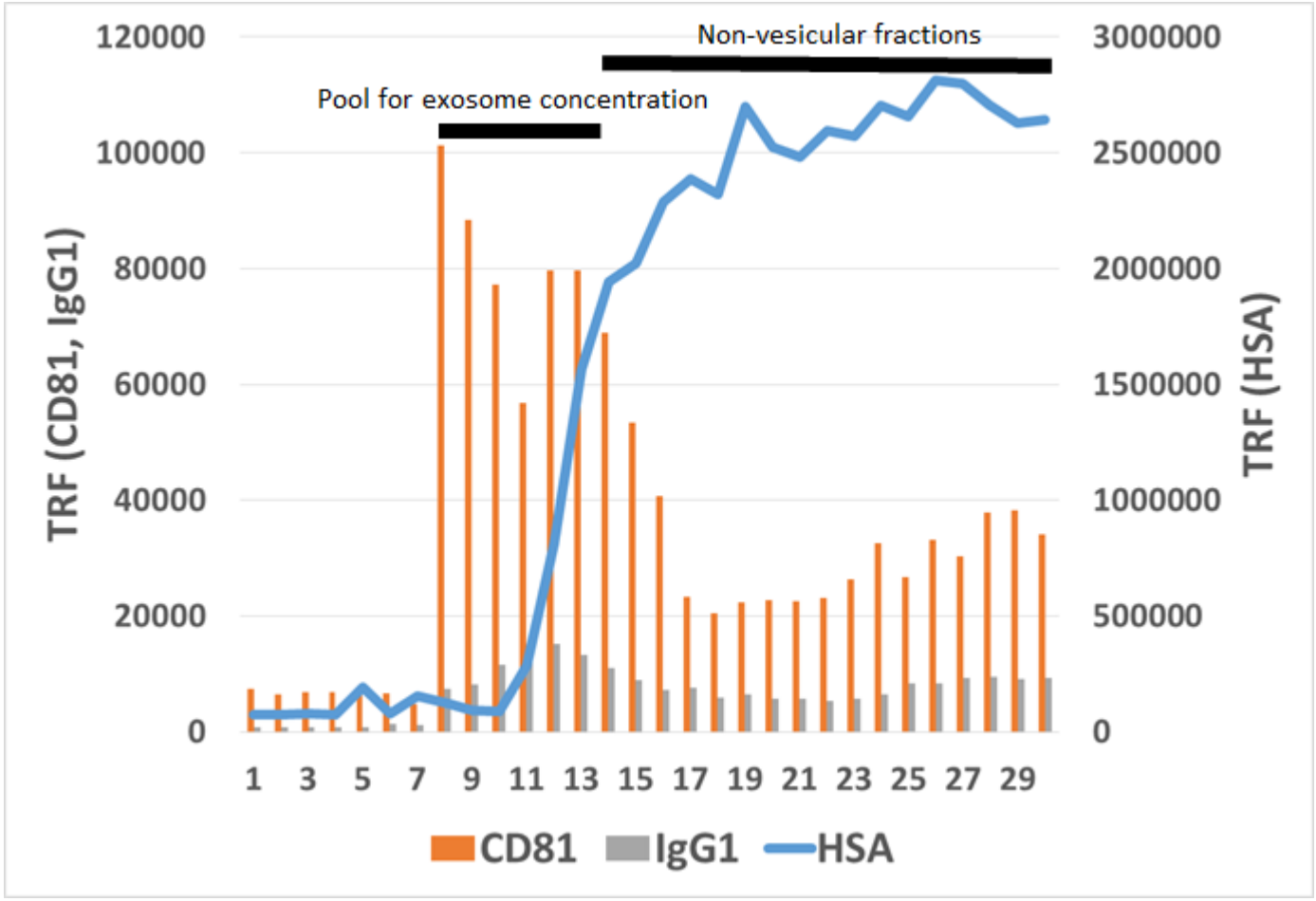

Relative concentrations of CD81, IgG1 and HSA in size exclusion chromatography fractions (Donor 2).
Plasma samples from two donors were subjected to size exclusion chromatography, thirty fractions collected and relative protein levels measured by Time Resolved Fluorescence (TRF). The exosome marker, CD81, is represented with orange bars, IgG1 control with grey bars and Human Serum Albumin (HSA) with blue line.

6.3.5 Isolating plasma exosomal-RNA using exoRNeasy™ spin-columns

As a principally different isolation method, which does not require ultra-centrifugation or PK/RA treatment, a spin-column based method was evaluated. The exoRNeasy™ (Qiagen) workflow was chosen as it has demonstrated the isolation of RNA from extracellular vesicles with high specificity over non-vesicular RNA (Enderle et al., 2015).

This technique required no ultra-centrifugation step, which removed the potential issue of pelleting efficiency and a major time and labour obstacle for scaling up the assay for numerous samples. However, intact exosomes are not typically eluted using this method, rather, RNA extraction is performed by direct lysis of vesicles bound to the spin-column. Therefore, routine characterisation assays and quality checks of the exosomes would not feature in a scaled-up assay. However, the original publication eluted vesicles off the spin-column and performed characterisation (Enderle et al., 2015).

The original study used SEM to visualise vesicles of the correct structure and WB analysis confirmed that TSG101 was present in the preparations. NTA measurements revealed an averaged mode particle size of 160 ± 15 nm which is slightly larger than typical exosomes but, similarly, ultra-centrifuged samples recorded an averaged mode particle size of 173 ± 29 nm (Enderle et al., 2015). These size distributions give an indication that other vesicle subtypes may adhere to the exoRNeasy™ spin-columns, as may be the case with ultra-centrifugation also, so that the isolation of RNA specifically from exosomes over other EV subtypes cannot be guaranteed. Recovery of particles from the original plasma sample were 1% for both techniques highlighting the general difficulty of isolating exosomes from biological fluids.

The original study also reported selectivity for isolating membrane-bound RNA on the columns, which removes the need of a PK/RA step. Non-vesicular RNA is detectable in the flow-through of the spin-column which is normally discarded. The removal of the digestion step, coupled with not requiring ultra-centrifugation, improves the scalability of the assay compared to ultra-centrifugation and size-exclusion chromatography. Large aggregates were removed from 0.5 ml plasma using 0.8 μm filters (Millipore) and the exoRNeasy™ workflow was followed, as per manufacturer's guidelines, to obtain exosomal-RNA.

6.3.6 Electrophoretic analysis of exosomal-RNA extracted from 0.5 ml plasma using three different methodologies

With the caveats of each of the three isolation methods now highlighted, exosomal-RNA was extracted, using all three methods, from 0.5 ml donor plasma and evaluated by electrophoretic analysis (Figure 6.5). The volume of 0.5 ml was chosen to assess if a method could be developed that produced meaningful data from low volume, easily-depleted, archival material.

Electrophoretic analysis was chosen as a first evaluation of the three different exosomal-RNA isolation techniques. To ensure the isolation and analysis of genuine intra-luminal RNA, the ultra-centrifugation and size-exclusion chromatography samples were treated with proteinase K and RNase A. This treatment has been described elsewhere (Shelke et al., 2014) and validated in the previous chapter. An optional step in the Qiagen exoRNeasy workflow was the 0.8 µm filtering of plasma prior to isolation on the column. Whilst the plasma samples had been filtered before freezing this additional filtering step was included.

Electrophoretic analysis was performed using the Agilent Bioanalyser with the Pico chip as minute RNA concentrations were expected. Plasma from three human donors were processed using each of the 3 isolation techniques (Figure 6.6). Ultra-centrifugation and size-exclusion chromatography samples did not produce decent RNA yields, with concentrations ranging from 17-24 pg/µl and 8-17 pg/µl, respectively (Table 6.1). The exoRNeasy samples, however, did show traceable RNA and this was reflected in concentrations ranging from 11-275 pg/µl. There was a wide range of concentrations using this technique which may be explained by donor variability or the dubious concentration estimates of the Agilent system (Mateescu et al., 2017). No rRNA was detected in these samples, as visualised by the absence of 18S and 28S peaks in the electropherograms and reflected in low RIN scores ranging from N/A (not calculable) to 1.5. Therefore, it appears that there was little or no cellular RNA contamination in the samples.

Overall, these data give a hint that the exoRNeasy method was more effective at isolating RNA from 0.5 ml plasma. However, a more robust method, such as qPCR, would be required to conclusively compare the three techniques. The minute concentrations detected in these samples, in the picogram range, rules out the possibility of performing conventional sequencing, as would have been desirable to explore, so an amplification-based method was chosen next.

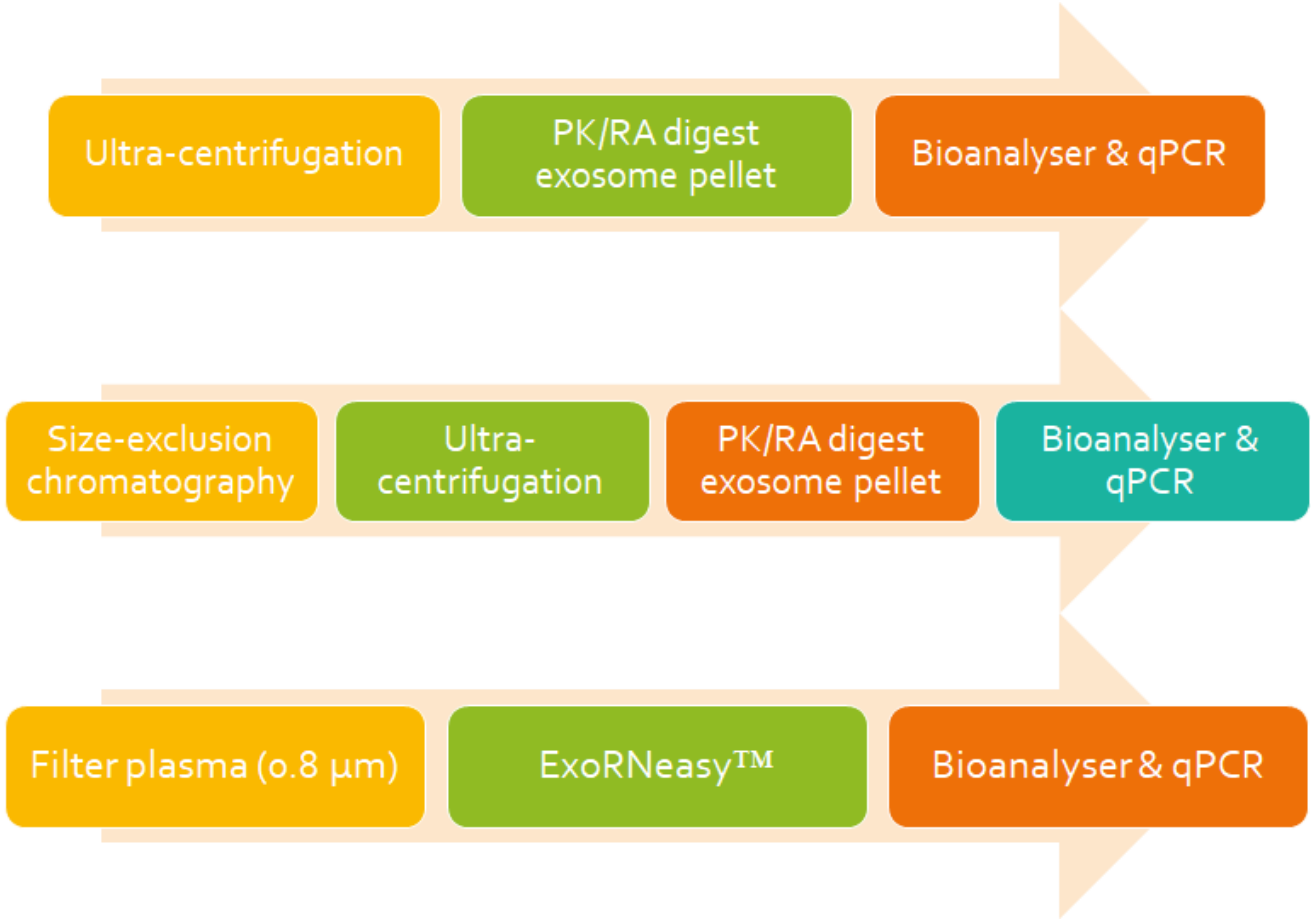

Figure 6.5: Workflows of three methods used to isolate exosomal-RNA from 0.5 ml plasma.
Ultra-centrifugation, size-exclusion chromatography and exoRNeasy™ techniques were used to isolate exosomal-RNA from three donor plasma samples. These were evaluated by electrophoretic analysis (Bioanalyser) and quantitative polymerase chain reaction (qPCR).

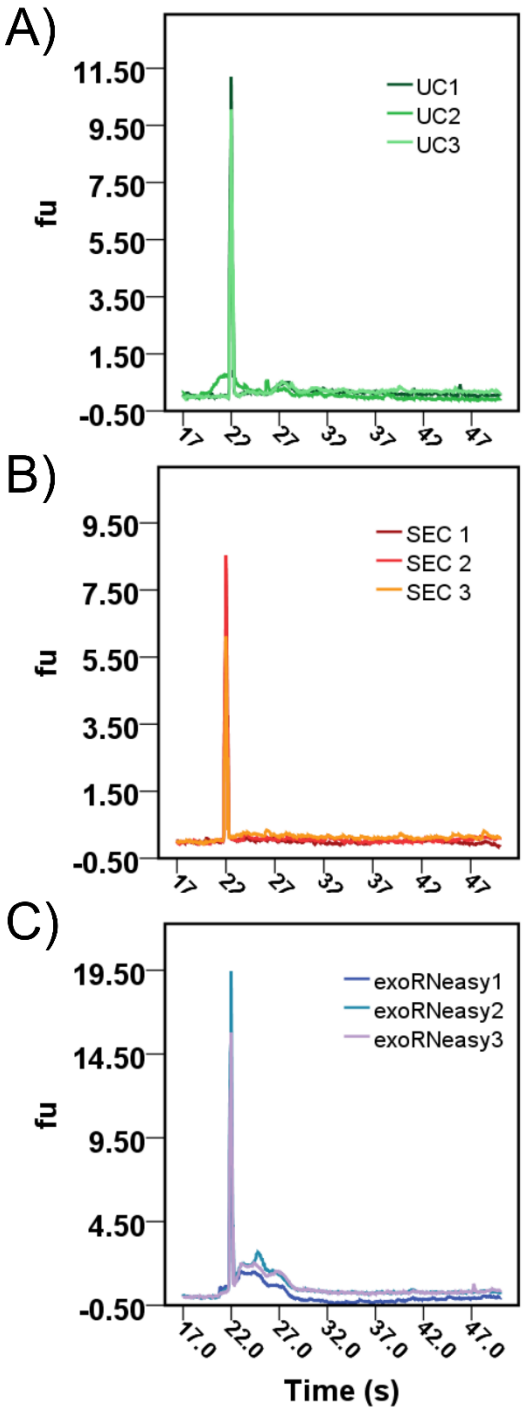

Figure 6.6: Electropherograms of exosomal-RNA extracted from 0.5 ml plasma.
Exosomal-RNA was extracted from plasma using three different techniques (n=3 per technique) and assessed using Bioanlayser instrumentation with the pico chip. RNA in the samples is indicated by fluorescence units (fu, y-axis) over time (x-axis) as the trace was obtained. A) RNA extracted from ultra-centrifuged (UC) plasma. B) RNA extracted from plasma subjected to size-exclusion chromatography (SEC) and ultra-centrifugation. C) RNA extracted from plasma using exoRNeasy™ (Qiagen) spin-column method.

Sample	Concentration (pg/µl)	RIN
Ultra-centrifugation 1	24	1
Ultra-centrifugation 2	27	1.1
Ultra-centrifugation 3	17	1
Size-exclusion chromatography 1	8	N/A
Size-exclusion chromatography 2	11	N/A
Size-exclusion chromatography 3	17	1
ExoRNeasy 1	11	1.5
ExoRNeasy 2	142	1.1
ExoRNeasy 3	275	1

Table 6.1: Concentrations of RNA extracted from 0.5 ml plasma.
Three techniques were used to isolate RNA from healthy donor plasma (n=3 per technique) and measured using Agilent Bioanalyser instrumentation. Concentrations and RNA Integrity scores (RIN) are automatically generated by the instrumentation. Individual values for each sample is presented here rather than averages.

6.3.7 Quantitative polymerase chain reaction of exosomal-RNA extracted from 0.5 ml plasma using three different methodologies

In the previous chapter reverse transcription and qPCR of cell culture-derived exosomal-RNA was described. The procedure was repeated here for the detection of *TUBA1A*, a house-keeping gene and therefore most likely to be detectable, in plasma-derived exosomal-RNA.

The three techniques for isolating exosomal-RNA were compared using 0.5 ml plasma from three separate donors. As the RNA could not be reliably quantified using electrophoretic analysis, equal volumes were reverse transcribed from each sample for qPCR analysis. Raw CT values were obtained, in duplicate, by SYBR green qPCR (Figure 6.7). Cell culture-derived exosomal-RNA was used as a positive control and non-template controls showed no amplification. Melt-curve analyses were performed and confirmed that only one amplicon was measured.

Ultra-centrifugation (UC) and size exclusion-chromatography (SEC) samples did not reliably amplify *TUBA1A*. Raw CT values were not obtained across all biological and technical replicates, with two out of the 3 biological replicates not amplifying *TUBA1A* above the cycle threshold. Gene expression would be considered very low with CT values greater than 35 cycles. For exoRNeasy samples, all 3 biological replicates showed *TUBA1A* expression, across duplicate technical replicates. These CT values were lower at 30.9-31.4 cycles, compared to >35.0 for UC and SEC samples, indicating greater detection of gene expression.

Overall these data, coupled with electrophoretic analysis, highlights that the exoRNeasy technique was far more reliable for isolating exosomal-RNA from plasma and certainly easier to do so in terms of time- and labour-intensity. The methodology could be more easily be scaled up to obtain exosomal-RNA from numerous samples as there were no ultra-centrifugation or PK/RA steps required. However, two problems can be highlighted. First, the CT values of 30.9-31.4 cycles indicate fairly weak detection of *TUBA1A*. Considering this is a house-keeping gene it would be preferable to observe CTs <30 cycles (Enderle et al., 2015) if less abundant targets, as expected for a disease biomarker, were to be detected in the future. Second, only a small volume of cDNA was obtained with this workflow; only enough volume was obtained to perform four qPCR reactions per sample. Therefore, in its current form this workflow could not be scaled up to investigate multiple targets or even to perform replicated experiments if a technical problem occurred.

To address these problems the qPCR chemistry was changed from SYBR green to Taqman. A pre-amplification step can be adopted into this workflow which allows for a higher sample volume prior to qPCR. Samples undergo 10-14 cycles of amplification with gene expression probes to obtain pre-amplified samples with which comparative CT values can be obtained. Pre-amplification requires pre-selection of gene targets and thus a limited number, up to 50, can be chosen. This step increases the sample volume to be large enough for multiple technical measurements.

It was not known whether this would improve the detection of *TUBA1A* or if the starting quantity in the sample was a limiting factor. The Taqman quantitation chemistry differs to SYBR green. Taqman is based on the release of fluorescent dyes from primers that probe the gene of interest whilst SYBR green is based on non-discriminant fluorescent detection of double-stranded DNA. This difference may lead to different efficiencies in detecting the gene of interest. The pre-amplification step would also have an unknown effect on final CT. Therefore, this change of qPCR chemistry was pursued with potential to improve the performance of the workflow and to investigate the potential to scale up to larger sample sets.

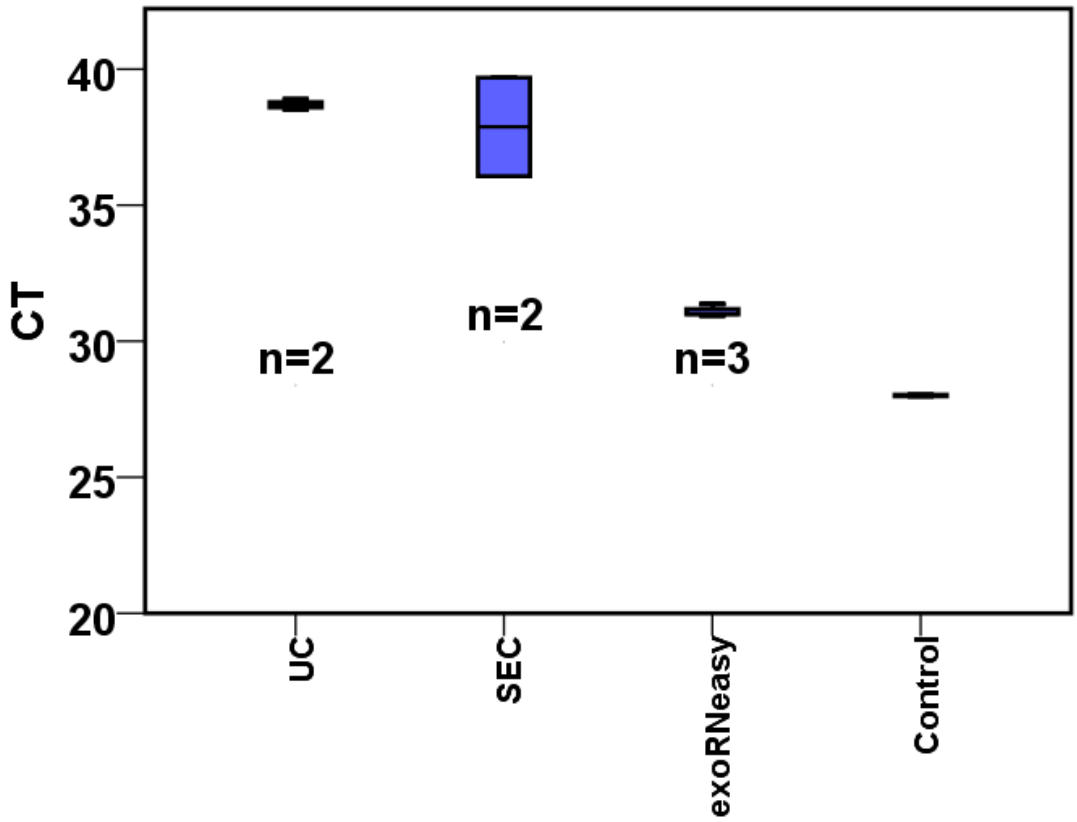

Figure 6.7: Raw CT values comparing TUBA1A expression in ultra-centrifugation (UC), size-exclusion chromatography (SEC) and exoRNeasy samples.

TUBA1A expression in three sets of RNA samples (n=3 per technique, measured in duplicate) was measured by qPCR and cycle thresholds (CT reported). C_T values reflect the cycle number where fluorescence units exceeded a set threshold of 0.1 FU. The upper and lower "hinges" of the boxes correspond to the first and third quartiles whilst whiskers extend to values within 1.5 x inter-quartile range. UC and SEC samples did not reliably amplify TUBA1A with undetermined CTs for one of the biological replicates (n=2). All 3 biological replicates showed TUBA1A expression, across duplicate technical replicates, for exoRNeasy samples (n=3). Melt curve analysis was performed and confirmed the presence of only one amplicon.

6.3.8 Testing the suitability of the exoRNeasy™ workflow with a pre-amplification step

It has been determined that the exoRNeasy™ workflow was the most tractable, and practical, technique for extracting good yields of exosomal-RNA from 0.5 ml plasma. However, a pre-amplification step would be needed to address limitations, namely signal strength and sample volume, with this workflow.

To test if the pre-amplification step would provide the desired improvements, 0.5 ml plasma from three human donors was spiked with either 0, 1, 10 or 100 µg of previously purified H4 exosomes. Not only would this provide an assessment of the detection range of the assay in itself but also, give an insight into the sensitivity of the assay to detect gene expression changes in reference to different concentrations of target exosomes. The latter would be a particularly beneficial readout as the secretion of exosomes has previously been shown to be altered in disease (Zhang et al., 2015).

After exosomal-RNA isolation, electropherograms were obtained using the Agilent Bioanalyser with the Pico chip (Figure 6.8). The quantity of RNA in each sample increased in a dose-dependent manner with exosomes spiked-in. Concentrations ranged from 11-275 pg/µl with no spike in, 570 – 802 pg/µl with 1 µg spiked exosomes, 1430 -3820 with 10 µg spiked exosomes and 2639 – 4496 pg/µl with 100 µg spiked exosomes (Table 6.2). The working range of the Pico chip is 50 – 5000 pg/µl so it is likely that the signal was saturated in some of these samples and the concentration may be higher.

This analysis has confirmed that dosing the plasma with exosomes does contribute to higher concentrations of RNA in the resultant sample. This is reassuring that the capacity of the spin-column to isolate vesicular-RNA is not limited even up to high, artificial doses of exosomes. Indeed this can be considered direct evidence, in addition to the original publication, that exosome vesicles adhere to the spin-column (Enderle et al., 2015). Using a global measure of RNA quantity, it has been determined that the method has sensitivity for differing doses of exosomes but qPCR would be used next to measure gene expression of candidate gene targets. Exosomal-RNA samples were reverse transcribed and cDNA samples pre-amplified with selected gene expression assays as detailed later.

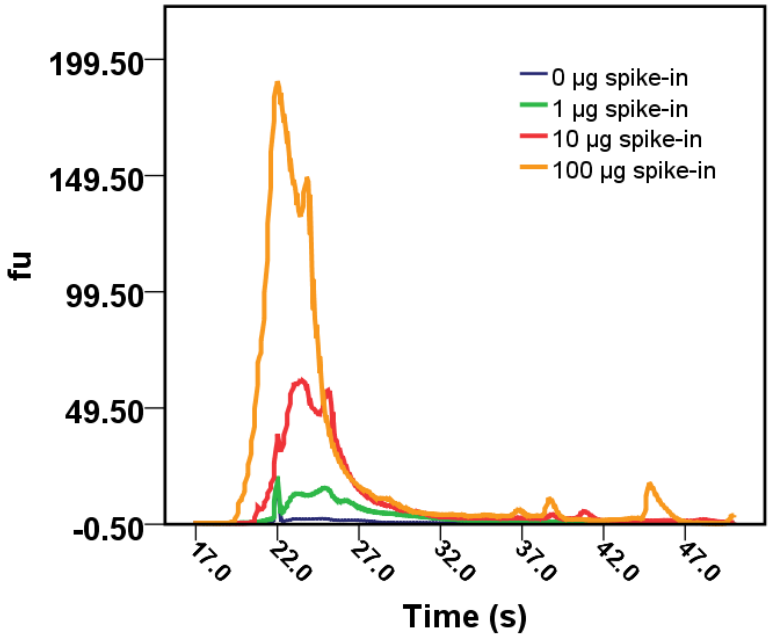

Figure 6.8: Electropherograms of RNA extracted from 0.5 ml plasma with spiked-in H4 exosomes. *Plasma samples were spiked with different quantities of H4 exosomes (see colours in key, n=3 per dose) and assessed using Bioanalyser instrumentation. RNA was detected using fluorescence units (fu, y-axis) over time (x-axis) as the trace was obtained. Traces were averaged across three biological replicates (n=3) and individual concentration reported in Table 6.2.*

Sample	Concentration (pg/µl)
0 µg spike-in 1	11
0 µg spike-in 2	142
0 µg spike-in 3	275
1 µg spike-in 1	802
1 µg spike-in 2	570
1 µg spike-in 3	642
10 µg spike-in 1	1430
10 µg spike-in 2	1598
10 µg spike-in 3	3820
100 µg spike-in 1	4496
100 µg spike-in 2	2639
100 µg spike-in 3	4406

Table 6.2: Concentrations of RNA extracted from 0.5 ml plasma with spiked-in H4 exosomes. *Plasma samples were spiked with different quantities of H4 exosomes and assessed using Bioanalyser instrumentation. Concentration was automatically calculated by the instrumentation*

Twelve targets were selected for qPCR as the pre-amplification step allows multiple targets to be amplified: *GAPDH*, *PPIA, TUBA1A, BLOC1S6*, *TBC1D8B*, *SHISA9, XLOC_000992*, *XLOC_003630*, *XLOC_004251*, *APOE*, *APP* and *BACE1*. These twelve targets were chosen to provide an assessment of:

i) House-keeping genes (*GAPDH*, *PPIA* and *TUBA1A*) which would be expected in relatively high abundance compared to other gene targets.

ii) Genes that showed high expression in H4 exosomes from RNA sequencing data presented in the previous chapter (*BLOC1S6*, *TBC1D8B* and *SHISA9*) and therefore expected to be detectable in the spiked-in samples.

iii) LncRNAs that showed high expression in H4 exosomes from RNA sequencing data presented in the previous chapter (*XLOC_000992, XLOC_003630* and *XLOC_004251*), and therefore, expected to be detectable in the spiked-in samples. The primers for these had to be designed for this study so had not been previously validated.

iv) Candidate gene targets with well-established relevance to Alzheimer's disease (*APOE*, *APP* and *BACE1*) which would be expected in less abundance than house-keeping genes.

The pre-amplification step provided higher sample volumes for qPCR so a greater number of technical replicates could be performed. Therefore, three biological replicates were measured, in triplicate, for each target at each concentration of spike-in.

Raw CT values were obtained for 10 of the 12 targets measured (Figure 6.9). *TUBA1A* recorded lower CT values in this assay than with SYBR green qPCR chemistry indicating greater detection of gene expression. Therefore, both problems of boosting signal for greater detection and increasing sample volume to allow multiple measurements had been addressed with this refined workflow.

Dose-dependent responses to exosome spike-in were observed for *GAPDH, PPIA, TUBA1A, BLOC1S6, TBC1D8B, APOE, APP* and *BACE1*. Changes were detectable even with 1 µg of exosomes spiked-in compared to native, untouched plasma. This is equivalent to 2 µg of exosomes per ml plasma *in vivo* causing a detectable change. It would be inappropriate to calculate $2^{-\Delta CT}$ in these samples as there was no suitable, unchanging housekeeping target to normalise to. The house-keeping genes *GAPDH, PPIA* and *TUBA1A* recorded decreasing CT values with addition of spiked-in exosomes (Figure 6.9A). Therefore, no statistics were applied to these measurements.

Of particular note are the dose response curves for *GAPDH, PPIA, TUBA1A, APP* and *BACE1* (Figure 6.9A and B). These 5 targets saw considerable differences between the CT values for un-spiked and 1 µg spiked samples, for example, a difference of ~4 cycles for *GAPDH* between un-spiked and 1 µg spiked. There is certainly scope, for these targets in particular, that exosomes doses of 0.1 µg or perhaps 0.01 µg could be discriminated. This observation highlights a good, inherent sensitivity within the assay.

Reassuringly amplification was observed for gene targets with an expected lower abundance than the house-keeping genes. Of these *APOE, APP* and *BACE1* are Alzheimer's disease-relevant genes (Figure 6.9B). Whilst not necessarily drivers of pathology in all cases, detection of these genes suggests there is potential to utilise this assay for AD biomarkers. Furthermore, this has demonstrated that low-abundant targets can be measured despite the technical difficulties of using 0.5 ml plasma and obtaining low yields of exosomal-RNA.

CT values could not be determined for *SHISA9* across any of the samples including the cell culture-derived exosome only control. This suggested a technical problem with the assay itself. Dose-response curves for *BLOC1S6* and *TBC1D8B* were observed, as expected from the RNA sequencing data reported in chapter 5.

CT values were detected for the lncRNA, *XLOC_000992,* in non-template controls (NTC). These results were therefore disregarded as the gene expression assay was producing false positives. NTCs produced CT values of 36 cycles - undetermined for *XLOC_003630.* This observation again suggested that there was a small amount of self-amplification within the assay. This self-amplification may account for the relatively high detection (CT values 25 – 27.5 cycles) for this target or these may be genuine. All NTCs were undetermined for *XLOC_004251* so the gene expression assay was working as expected. Typical dose response curves were not observed for both *XLOC_003630* and *XLOC_004251* as it took 100 µg spiked-in exosomes to produce a stronger signal. A puzzling observation from these curves were increasing CT values, suggesting weaker detection of gene expression, with 1 µg and 10µg exosomes spiked-in. A possible explanation is that the efficiency of the PCR was not well optimised and better primers needed to be designed. Nevertheless, these assays were novel designs used first in this study, and had not been previously validated, so it was reassuring to be able to demonstrate the detection of lncRNAs in plasma-derived exosomes. Further optimisation and designing of additional primers would be required to take this further, which is of future interest as chapter 5 demonstrated that meaningful data can be obtained from the lncRNA cargo of exosomes.

Overall, an assay has been developed that can measure RNA expression in vesicles from only 0.5 ml plasma. The assay has capacity to measure multiple targets, 12 reported here but can be scaled up to 50, with multiple replications without exhausting the sample. Gene expression is measurable in targets that are less abundant than constitutively expressed house-keeping genes such as *GAPDH, PPIA* and *TUBA1A* giving reassurance that changes in some targets that are less abundant should be possible. Furthermore, this assay shows excellent sensitivity to small changes in exosome dose with changes in CT values observed when 1 µg of H4 exosomes spiked-in and some samples appeared to have scope for discriminating even lower doses than that. This sensitivity is likely to be of good utility for investigating diseases where exosome secretion is altered, for example, the increased secretion of tumours (Zhang et al., 2015).

Figure 6.9: Raw CT values for RNA extracted from 0.5 ml plasma with spiked-in exosomes.
Exosomal-RNA was extracted from 0.5 ml plasma with different doses of H4 exosomes spiked in (see colours in key, n=3 per dose, measured in triplicate). Cycle thresholds (CT, y-axis) are reported for each target as indicated in the title of each graph.
A. House-keeping genes: GAPDH, PPIA and TUBA1A.

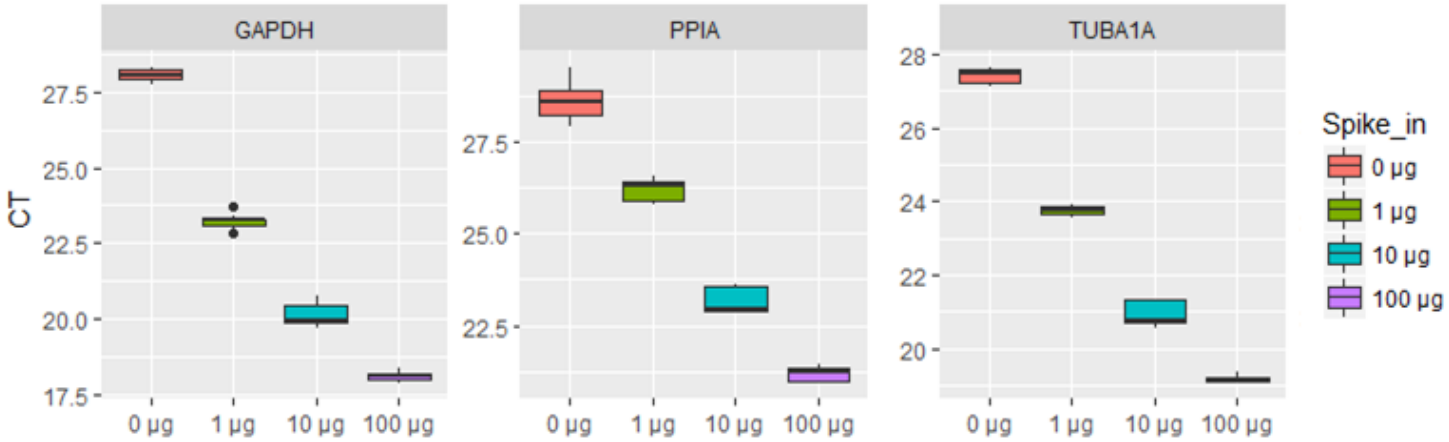

B. Alzheimer's disease-relevant genes.

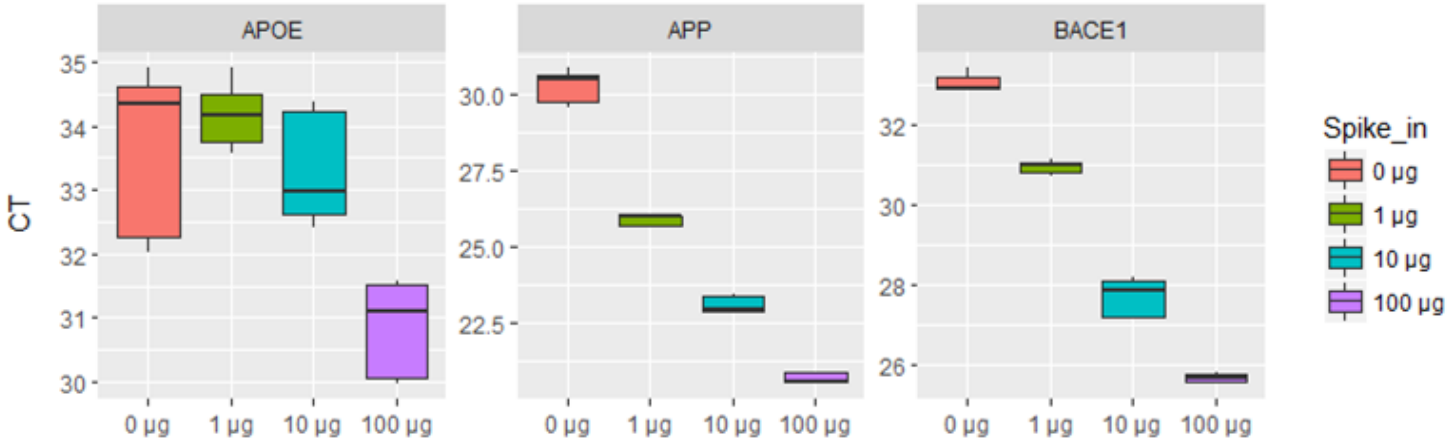

C. Genes that have previously shown high expression in H4 exosomes: BLOC1S6 and TBC1D8B.

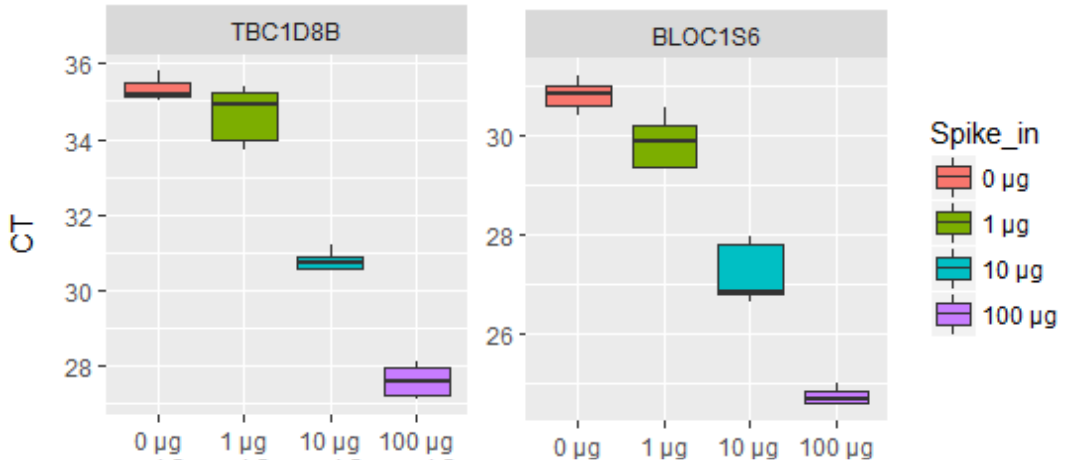

D. LncRNAs that have previously shown high expression in H4 exosomes: XLOC_003630 and XLOC_004251.

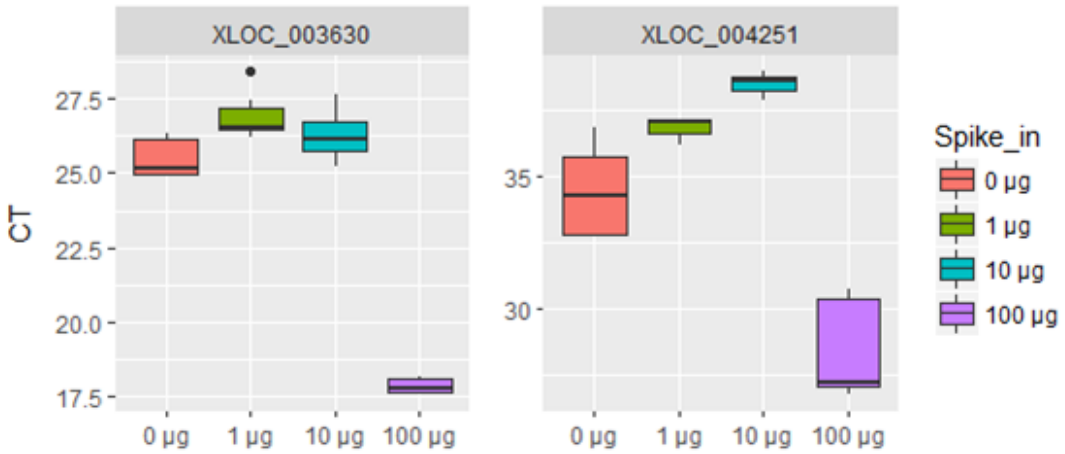

6.3.9 Participant selection in an Alzheimer's disease case:control cohort

Next, a small Alzheimer's disease case:control cohort was used to test if this assay could detect any gene expression changes associated with disease. At this early stage of assay development, and with only a small cohort to measure, the aim was to validate the method by looking for trends towards significance in candidate genes and to test the sensitivity of the assay to detect low-abundant, CNS-enriched candidates.

Plasma samples were available for 582 research participants with corresponding *APOE* genotypes: 211 Late-Onset AD (LOAD), 293 Early-Onset AD (EOAD) and 78 Controls. DNA was extracted from whole blood and *APOE* genotypes were determined by Taqman genotyping of SNP rs7412 and KASP genotyping of SNP rs429358 as shown previously (Butchart et al., 2015, Ide et al., 2016). Distribution of *APOE* genotypes are shown in Figure 6.10. The rarity of the e2/e2 genotype is reflected in the observation of only one control sample with this genotype in the entire collection. Instead, there is a relative abundance of participants with the e3/e3 genotype.

Carrying an e4 allele of the *APOE* gene confers a greater genetic risk of Alzheimer's disease (Mahley et al., 2006). With so many e3/e3 samples available it was decided that this study should be a case:control analysis where *APOE* genotype was controlled for rather than investigated. Furthermore, the pathology of Late and Early Onset forms of AD vary greatly so the group was narrowed down to LOAD cases only.

The gender and age distributions of both case and control groups was evaluated (Figure 6.11). There were more females than males in both parts of the cohort. Participant and next-of-kin interviews were used to determine the age at which the onset of symptoms took place. Age of AD onset ranged from 66-90 years old in cases. Age-matched controls with no cognitive deficits were recruited to the study. The age at their latest interview was recorded and ranged from 68-92 years old. In the final cohort for this study, gender was controlled for by choosing fairly equal numbers of males and females and matching these between cases and controls. Controls would be prioritised by their age at latest interview. Further cognitive data, rather than just age of AD onset, would be used to select cases.

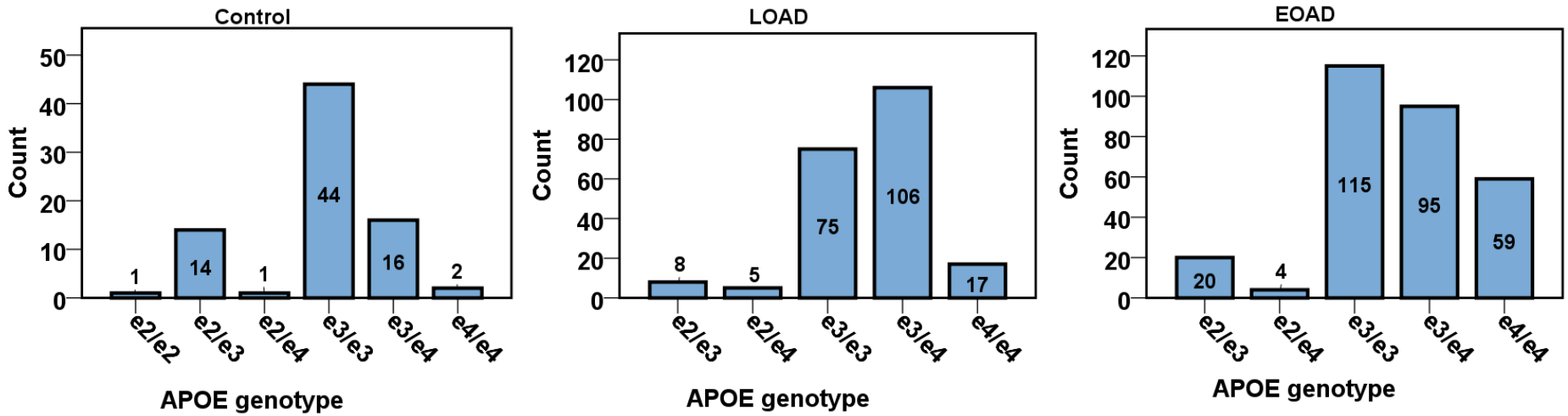

Figure 6.10: Histograms showing distribution of APOE genotypes across research participants.
Whole blood had been collected from LOAD, EOAD and Control participants and genotypes determined by single SNP genotyping of rs7412 and rs429358. Genotypes are indicated on the x-axis.

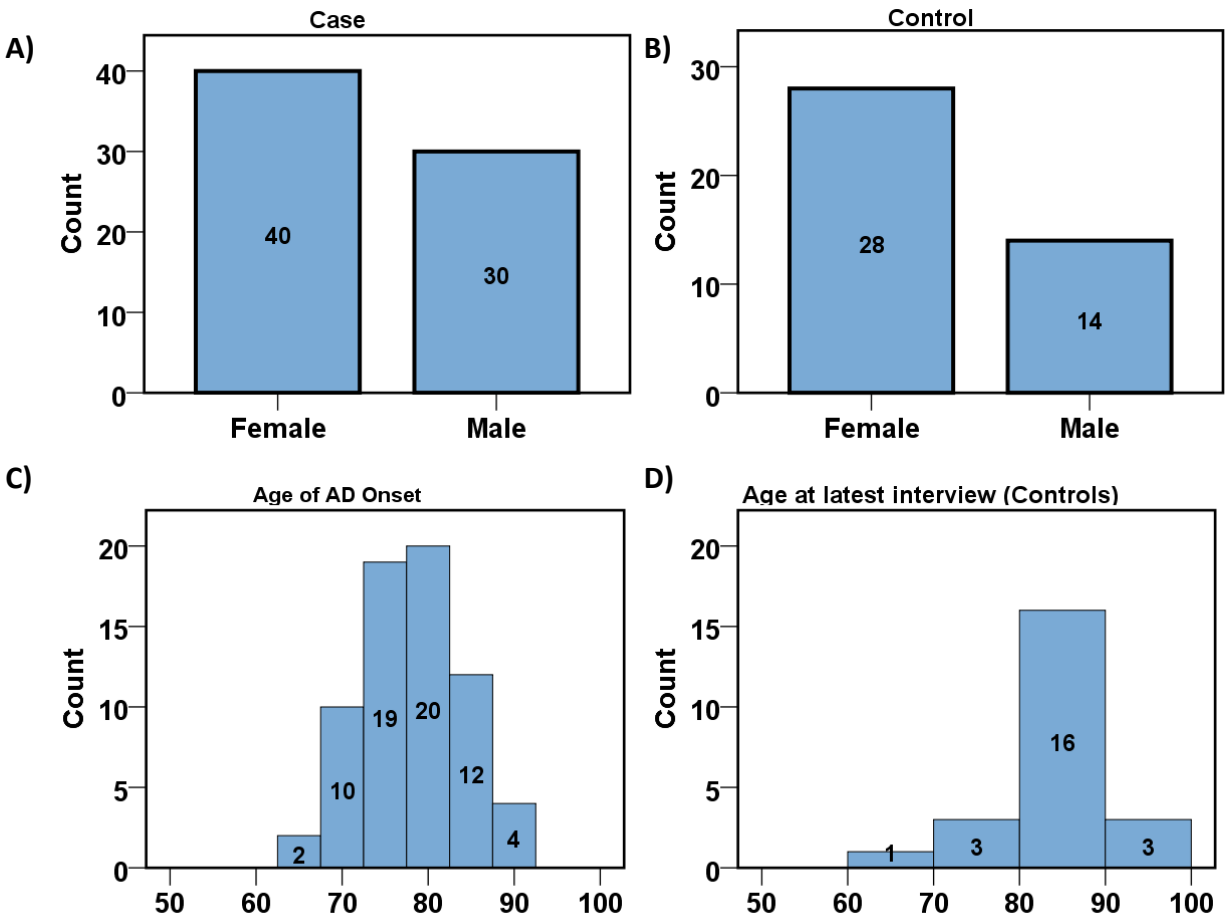

Figure 6.11: Histograms showing age and gender distributions across LOAD cases and controls.
Age of AD onset (cases), age at interview (controls) and gender were determined at interview when entering the study. A) and B) Gender distributions for cases and controls. C) Age of AD onset was recorded for cases ranging from 66-90 years old. D) The age at their latest interview was recorded for controls and ranged from 68-92 years old.

A suite of cognitive and memory tests are performed with research participants by field team members of the research group at Cardiff University. These tests include Mini-Mental State Examination (MMSE) and Addenbrooke's Cognitive Examination (ACE). From these tests, a research diagnosis of probable AD can be determined and a certainty rating (%) was calculated (Figure 6.12). A number of the research participants volunteer to donate their brain after death through the Brains for Dementia Research project (http://www.brainsfordementiaresearch.org.uk/). From this project, the top AD certainty score was 99% as an autopsy report confirmed "Alzheimer's disease with some TDP-43 pathology" (Wilson et al., 2013). There were 18 individuals with an AD certainty score greater than 75%. The certainty of diagnosis was chosen as a priority in patient selection because AD is difficult to cleanly diagnose using cognitive measures and often relies on autopsy to reveal co-morbidities and other dementia pathologies.

The case:control cohort was chosen based on the priorities highlighted thus far:

i. An *APOE* genotype of e3/e3
ii. Males and females would be chosen equally and matched in case and control groups
iii. Controls would be prioritised by individuals with latest age at interview
iv. Cases would be prioritised by individuals with a higher certainty of diagnosis

The final cohort consisted of 15 cases (6 male and 9 female) and 15 controls (6 male and 9 female) and all *APOE* e3/e3 homozygotes. The controls were chosen by eldest at interview. The cases had a range of AD diagnosis certainty from 75 – 99%.

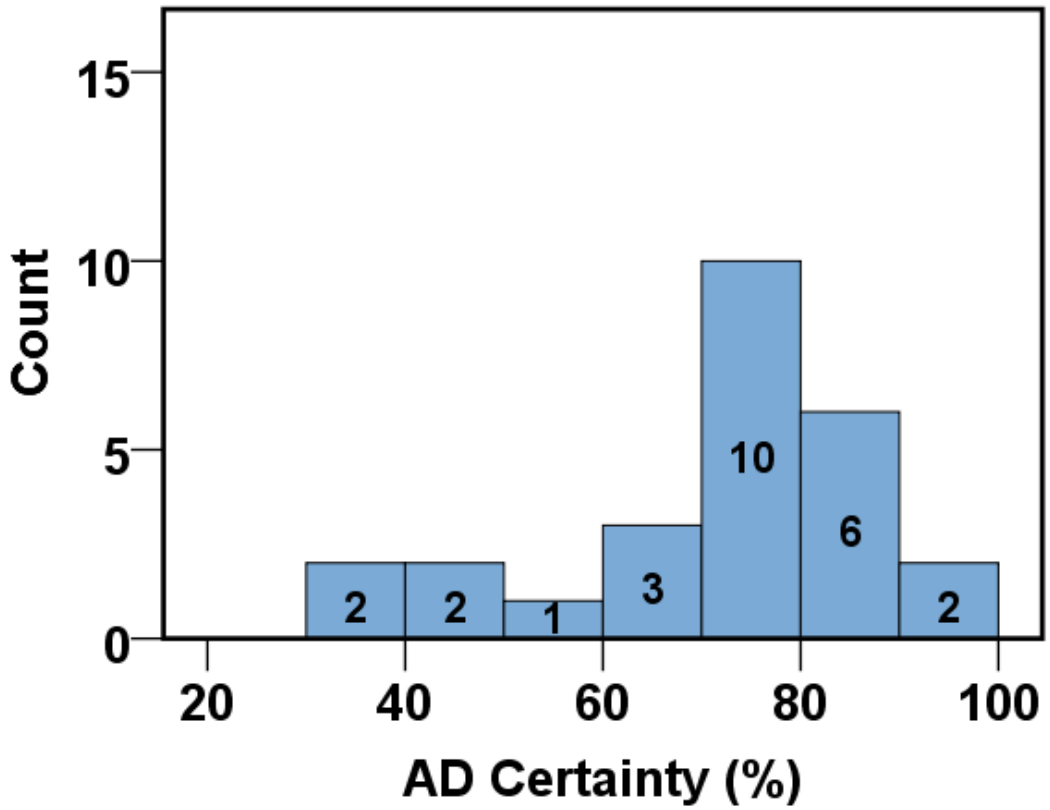

Figure 6.12: A Histogram showing distribution of AD Certainty across LOAD cases.
AD certainty score was determined from phenotypic data collected in this study. The top AD certainty score was 99% as an autopsy report confirmed "Alzheimer's disease with some TDP-43 pathology". 18 individuals had an AD certainty score greater than 75%.

6.3.10 Selecting targets for gene expression profiling

The gene expression assay has already been demonstrated with ten gene and lncRNA targets (Figure 6.9) but this was extended to sixteen for the final study. Sixteen targets were chosen as it balanced a sufficient number of targets to validate the assay, but not too many that the number of participants had to be reduced. An additional six gene targets needed to be identified. One aim of adding the additional gene candidates was to identify any targets that showed potential for being a biomarker of disease. A second aim was to test if the assay could detect CNS-enriched gene targets and therefore the suitability to apply this method to neurological disorders in general. The assay had already successfully been used for the detection of constitutively expressed, housekeeping targets despite using a small plasma volume to start with, so choosing CNS-enriched genes would further test the robustness of this assay. Therefore, gene candidates that could address both of these aims were identified and selected.

There have been numerous studies into gene expression in Alzheimer's disease brains which were reviewed in 2014 (Feng et al., 2014). In this review, 12 genes showed consistent expression changes with disease progression and were validated in independent datasets. Six showed higher expression throughout disease progression and six were lower. It was predicted that these genes would have good potential to discriminate disease in plasma exosomes as they had previously been implicated in AD brains. There was scope to select 6 of the 12 targets.

To address the second aim, the GTEx Portal (https://gtexportal.org/home/) was accessed to narrow the list to 6 genes ensuring that these were preferentially expressed in the CNS (Figure 6.13). All six showed enrichment in brain tissues: three that were upregulated in disease (*ITPKB, GFAP* and *FAM107A*) and three that were downregulated (*GNG3, CDK5* and *RGS4*). It was not known whether the RNA transcripts of these genes would be loaded onto exosomes and transported into peripheral circulation, and indeed if the change in expression would be in the same direction as observed from the tissue-based analyses (Feng et al., 2014). Therefore, half of the candidates chosen were upregulated and the other half were downregulated in disease.

GFAP and *GNG3*, in particular, were almost entirely selectively expressed in brain tissues; other non-CNS tissues recorded no gene expression except a low detection of *GNG3* in the testis (Figure 6.13). *FAM107A, CDK5* and *RGS4* had enriched signals in brain tissues with a wider spread of gene expression detected in other tissues. Interestingly, *RGS4*, is

preferentially expressed with particularly strong expression in cortical regions, namely, the anterior cingulate cortex, cortex and frontal cortex tissues. These tissues are known to be sites of degenerating neurons and the neuropathological hallmarks of AD, Aβ plaques and neurofibrillary tangles (Zilka and Novak, 2006). Of the six genes evaluated, *ITPKB* had the most widespread expression in other tissues but an enrichment in brain tissues, particularly the substantia nigra.

These 6 genes were chosen to expand the list of targets to test in the case:control cohort. They fulfilled both criteria of i) being previously identified as differentially expressed in AD brain so have a stronger likelihood of being differentially expressed in peripherally-available exosomes and ii) showing enriched expression in brain tissues so able to test the sensitivity of the assay to measure lower abundant, CNS-specific candidates.

Figure 6.13: Gene expression profiles for six brain-enriched genes.
Gene expression is reported in Reads Per Kilobase of transcript per Million mapped reads (RPKM, y-axis) for different tissues (x-axis) using the searchable GTEx portal database. Median is displayed with 25th and 75th quartiles, and outliers marked as circles.

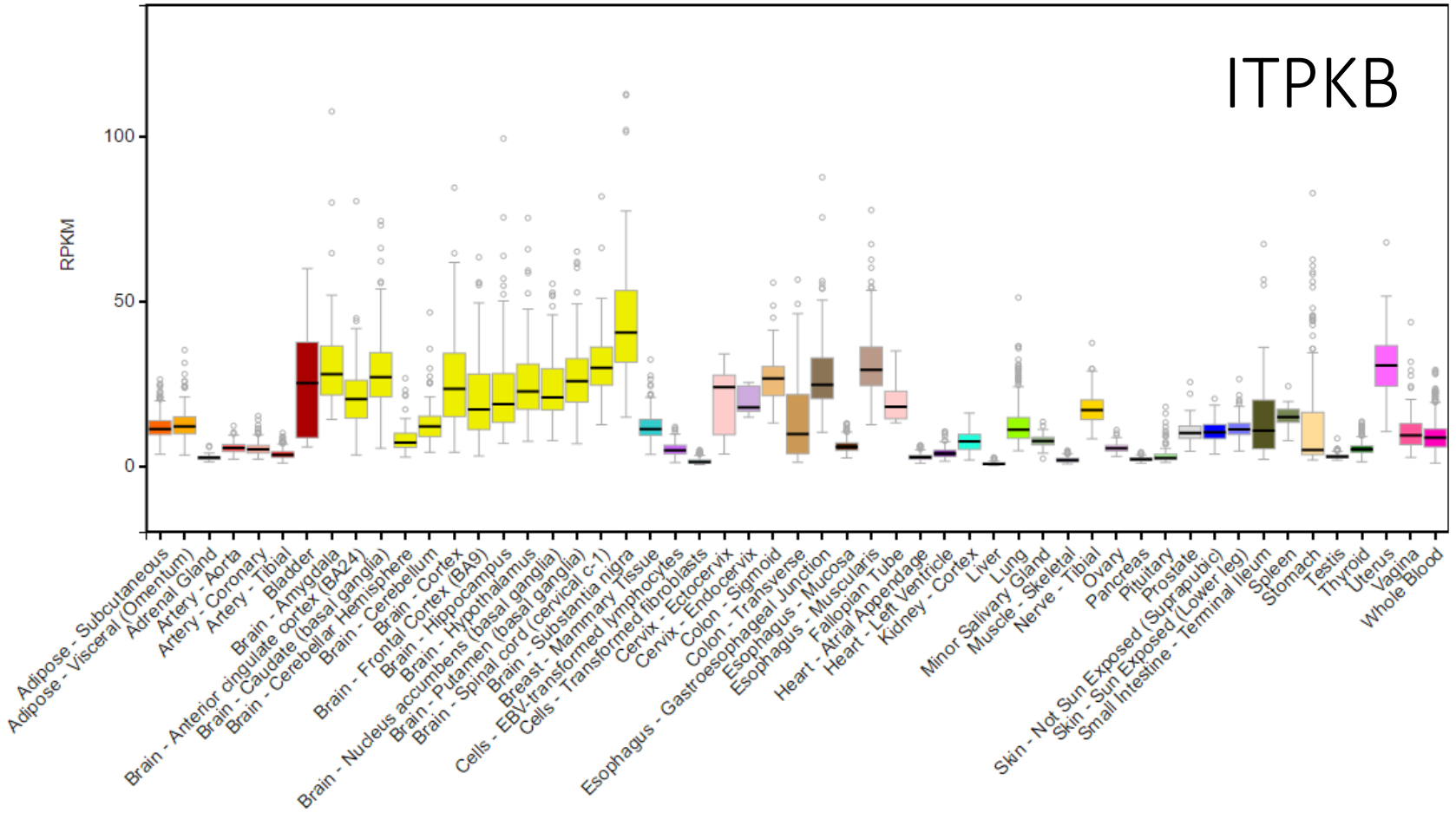

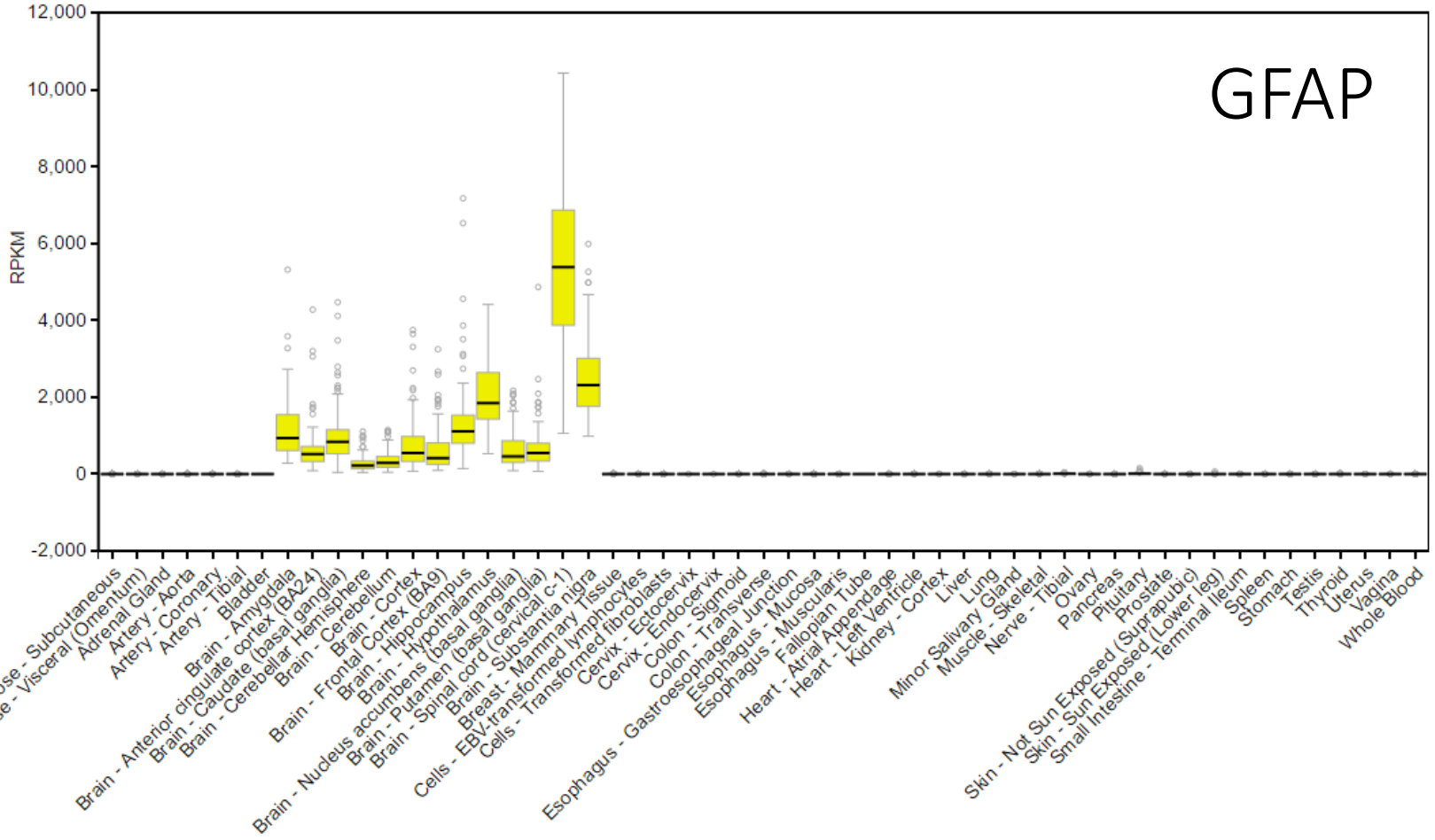
GFAP
RPKM
12,000
10,000
8,000
6,000
4,000
2,000
0
-2,000
Adipose - Subcutaneous
Adipose - Visceral (Omentum)
Adrenal Gland
Artery - Aorta
Artery - Coronary
Artery - Tibial
Bladder
Brain - Amygdala
Brain - Anterior cingulate cortex (BA24)
Brain - Caudate (basal ganglia)
Brain - Cerebellar Hemisphere
Brain - Cerebellum
Brain - Cortex
Brain - Frontal Cortex (BA9)
Brain - Hippocampus
Brain - Hypothalamus
Brain - Nucleus accumbens (basal ganglia)
Brain - Putamen (basal ganglia)
Brain - Spinal cord (cervical c-1)
Brain - Substantia nigra
Breast - Mammary Tissue
Cells - EBV-transformed lymphocytes
Cells - Transformed fibroblasts
Cervix - Ectocervix
Cervix - Endocervix
Colon - Sigmoid
Colon - Transverse
Esophagus - Gastroesophageal Junction
Esophagus - Mucosa
Esophagus - Muscularis
Fallopian Tube
Heart - Atrial Appendage
Heart - Left Ventricle
Kidney - Cortex
Liver
Lung
Minor Salivary Gland
Muscle - Skeletal
Nerve - Tibial
Ovary
Pancreas
Pituitary
Prostate
Skin - Not Sun Exposed (Suprapubic)
Skin - Sun Exposed (Lower leg)
Small Intestine - Terminal Ileum
Spleen
Stomach
Testis
Thyroid
Uterus
Vagina
Whole Blood

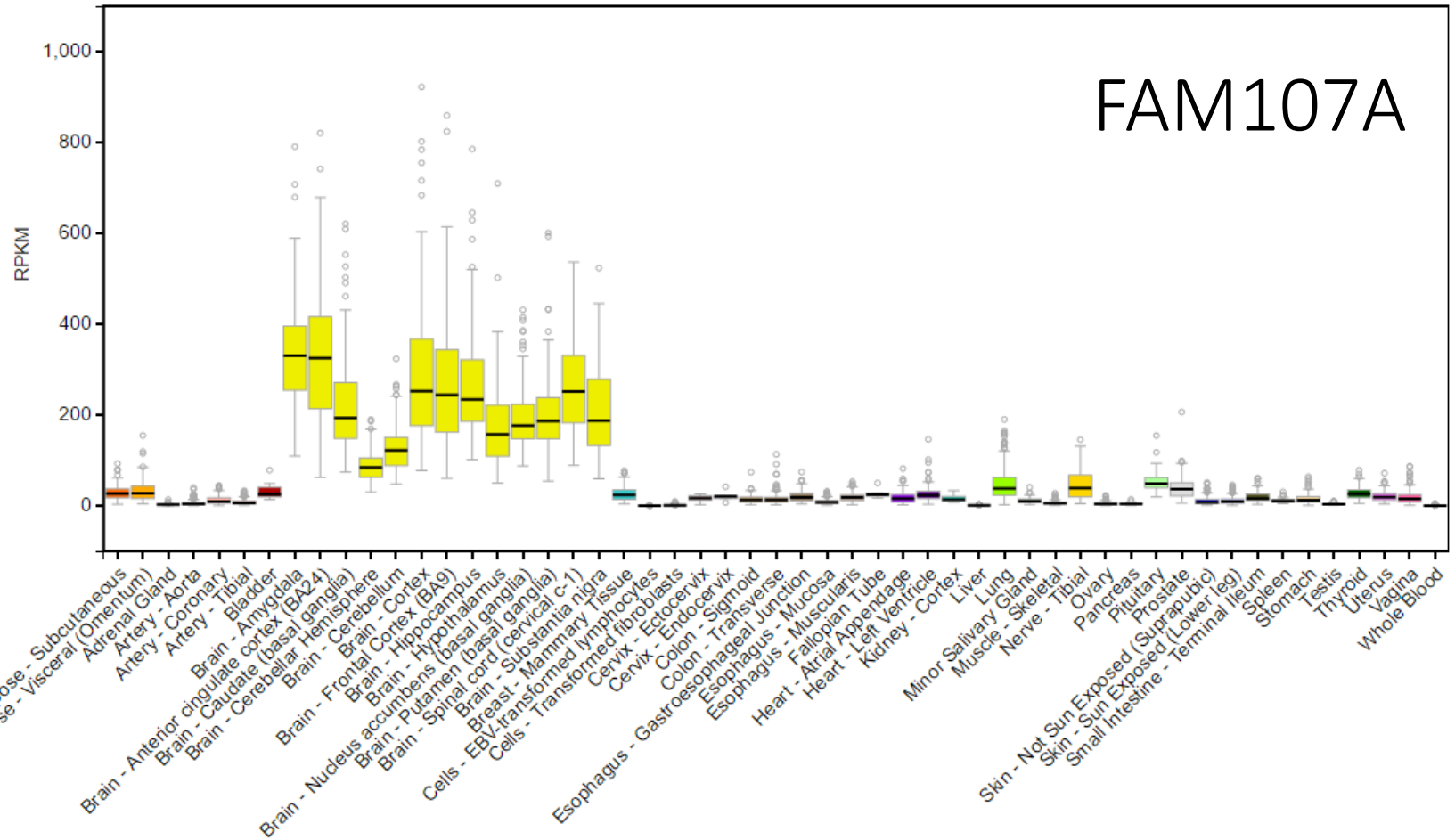
FAM107A
RPKM
1,000
800
600
400
200
0
Adipose - Subcutaneous
Adipose - Visceral (Omentum)
Adrenal Gland
Artery - Aorta
Artery - Coronary
Artery - Tibial
Bladder
Brain - Amygdala
Brain - Anterior cingulate cortex (BA24)
Brain - Caudate (basal ganglia)
Brain - Cerebellar Hemisphere
Brain - Cerebellum
Brain - Cortex
Brain - Frontal Cortex (BA9)
Brain - Hippocampus
Brain - Hypothalamus
Brain - Nucleus accumbens (basal ganglia)
Brain - Putamen (basal ganglia)
Brain - Spinal cord (cervical c-1)
Brain - Substantia nigra
Breast - Mammary Tissue
Cells - EBV-transformed lymphocytes
Cells - Transformed fibroblasts
Cervix - Ectocervix
Cervix - Endocervix
Colon - Sigmoid
Colon - Transverse
Esophagus - Gastroesophageal Junction
Esophagus - Mucosa
Esophagus - Muscularis
Fallopian Tube
Heart - Atrial Appendage
Heart - Left Ventricle
Kidney - Cortex
Liver
Lung
Minor Salivary Gland
Muscle - Skeletal
Nerve - Tibial
Ovary
Pancreas
Pituitary
Prostate
Skin - Not Sun Exposed (Suprapubic)
Skin - Sun Exposed (Lower leg)
Small Intestine - Terminal Ileum
Spleen
Stomach
Testis
Thyroid
Uterus
Vagina
Whole Blood

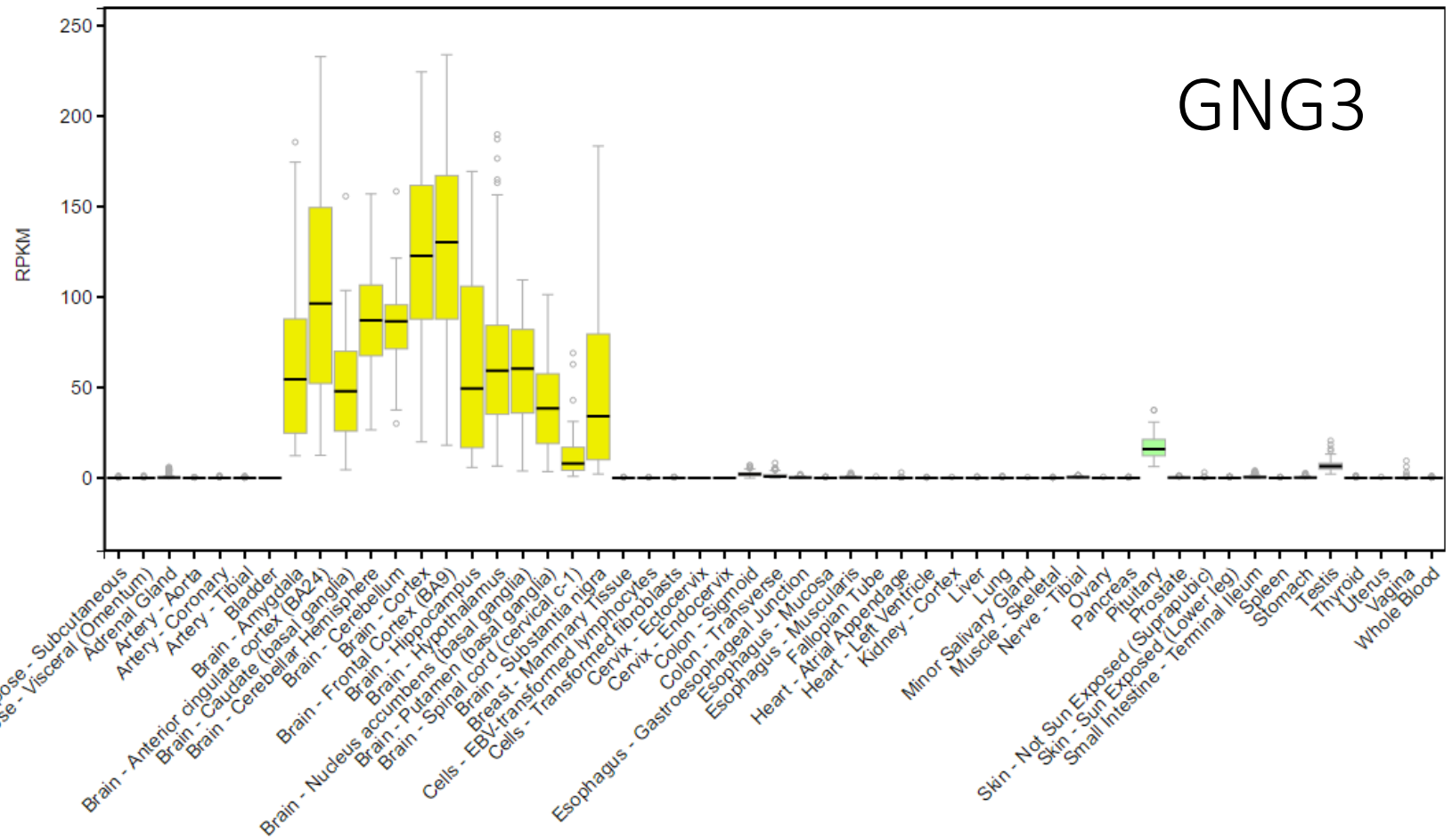
GNG3
RPKM
250
200
150
100
50
0
Adipose - Subcutaneous
Adipose - Visceral (Omentum)
Adrenal Gland
Artery - Aorta
Artery - Coronary
Artery - Tibial
Bladder
Brain - Amygdala
Brain - Anterior cingulate cortex (BA24)
Brain - Caudate (basal ganglia)
Brain - Cerebellar Hemisphere
Brain - Cerebellum
Brain - Cortex
Brain - Frontal Cortex (BA9)
Brain - Hippocampus
Brain - Hypothalamus
Brain - Nucleus accumbens (basal ganglia)
Brain - Putamen (basal ganglia)
Brain - Spinal cord (cervical c-1)
Brain - Substantia nigra
Breast - Mammary Tissue
Cells - EBV-transformed lymphocytes
Cells - Transformed fibroblasts
Cervix - Ectocervix
Cervix - Endocervix
Colon - Sigmoid
Colon - Transverse
Esophagus - Gastroesophageal Junction
Esophagus - Mucosa
Esophagus - Muscularis
Fallopian Tube
Heart - Atrial Appendage
Heart - Left Ventricle
Kidney - Cortex
Liver
Lung
Minor Salivary Gland
Muscle - Skeletal
Nerve - Tibial
Ovary
Pancreas
Pituitary
Prostate
Skin - Not Sun Exposed (Suprapubic)
Skin - Sun Exposed (Lower leg)
Small Intestine - Terminal Ileum
Spleen
Stomach
Testis
Thyroid
Uterus
Vagina
Whole Blood

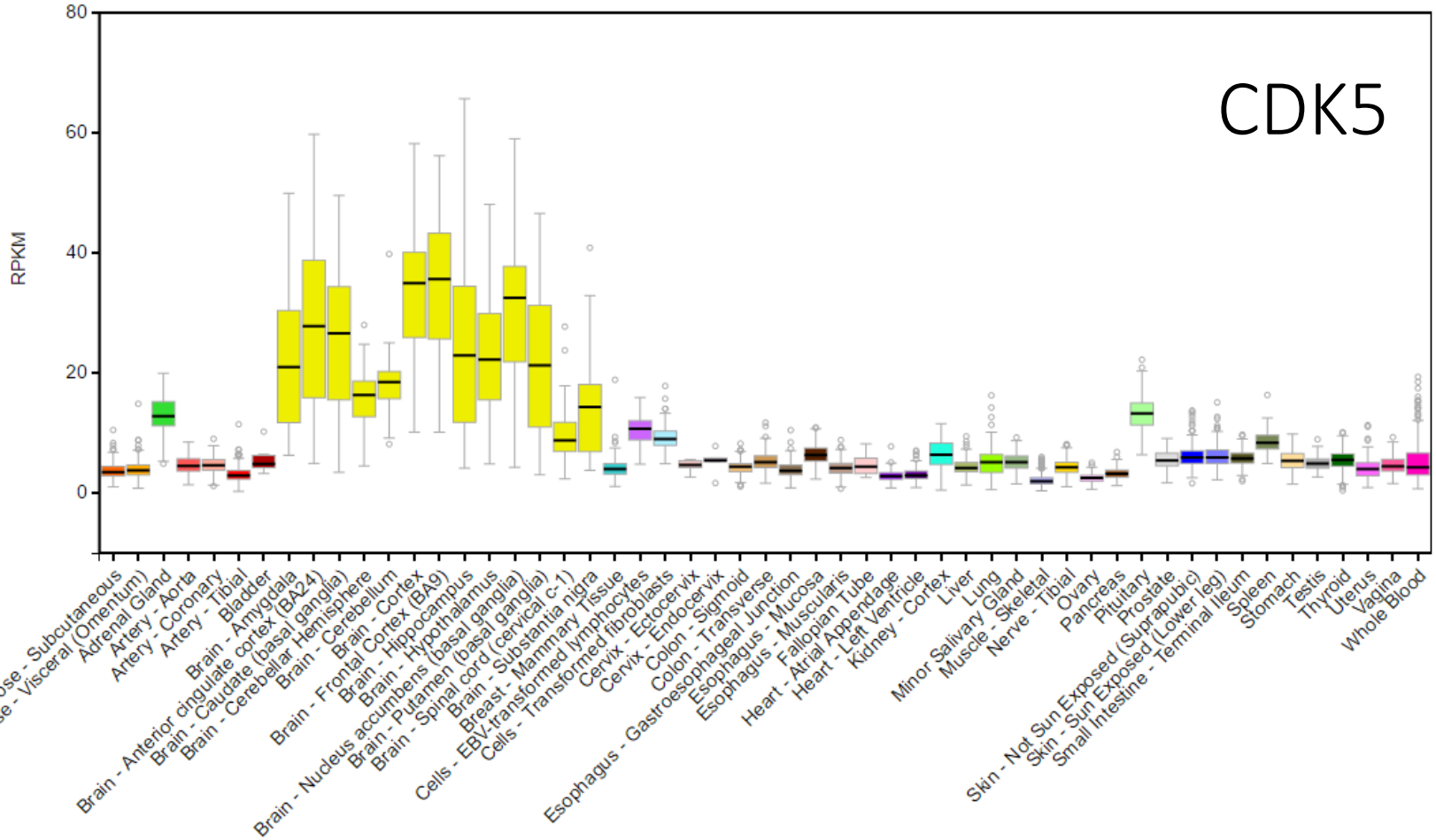
CDK5
RPKM
80
60
40
20
0
Adipose - Subcutaneous
Adipose - Visceral (Omentum)
Adrenal Gland
Artery - Aorta
Artery - Coronary
Artery - Tibial
Bladder
Brain - Amygdala
Brain - Anterior cingulate cortex (BA24)
Brain - Caudate (basal ganglia)
Brain - Cerebellar Hemisphere
Brain - Cerebellum
Brain - Cortex
Brain - Frontal Cortex (BA9)
Brain - Hippocampus
Brain - Hypothalamus
Brain - Nucleus accumbens (basal ganglia)
Brain - Putamen (basal ganglia)
Brain - Spinal cord (cervical c-1)
Brain - Substantia nigra
Breast - Mammary Tissue
Cells - EBV-transformed lymphocytes
Cells - Transformed fibroblasts
Cervix - Ectocervix
Cervix - Endocervix
Colon - Sigmoid
Colon - Transverse
Esophagus - Gastroesophageal Junction
Esophagus - Mucosa
Esophagus - Muscularis
Fallopian Tube
Heart - Atrial Appendage
Heart - Left Ventricle
Kidney - Cortex
Liver
Lung
Minor Salivary Gland
Muscle - Skeletal
Nerve - Tibial
Ovary
Pancreas
Pituitary
Prostate
Skin - Not Sun Exposed (Suprapubic)
Skin - Sun Exposed (Lower leg)
Small Intestine - Terminal Ileum
Spleen
Stomach
Testis
Thyroid
Uterus
Vagina
Whole Blood

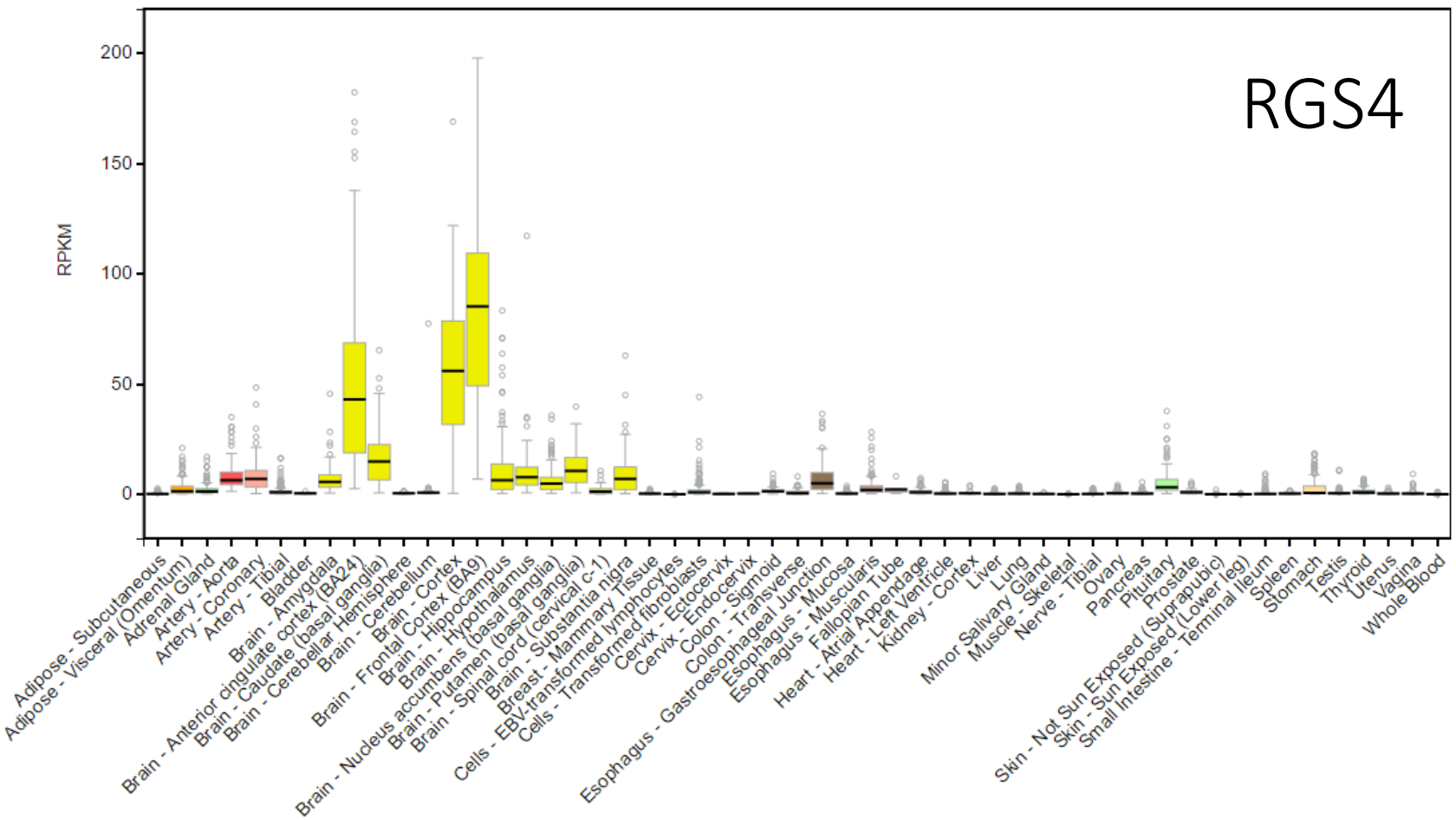
RGS4
RPKM
200
150
100
50
0
Adipose - Subcutaneous
Adipose - Visceral (Omentum)
Adrenal Gland
Artery - Aorta
Artery - Coronary
Artery - Tibial
Bladder
Brain - Amygdala
Brain - Anterior cingulate cortex (BA24)
Brain - Caudate (basal ganglia)
Brain - Cerebellar Hemisphere
Brain - Cerebellum
Brain - Cortex
Brain - Frontal Cortex (BA9)
Brain - Hippocampus
Brain - Hypothalamus
Brain - Nucleus accumbens (basal ganglia)
Brain - Putamen (basal ganglia)
Brain - Spinal cord (cervical c-1)
Brain - Substantia nigra
Breast - Mammary Tissue
Cells - EBV-transformed lymphocytes
Cells - Transformed fibroblasts
Cervix - Ectocervix
Cervix - Endocervix
Colon - Sigmoid
Colon - Transverse
Esophagus - Gastroesophageal Junction
Esophagus - Mucosa
Esophagus - Muscularis
Fallopian Tube
Heart - Atrial Appendage
Heart - Left Ventricle
Kidney - Cortex
Liver
Lung
Minor Salivary Gland
Muscle - Skeletal
Nerve - Tibial
Ovary
Pancreas
Pituitary
Prostate
Skin - Not Sun Exposed (Suprapubic)
Skin - Sun Exposed (Lower leg)
Small Intestine - Terminal Ileum
Spleen
Stomach
Testis
Thyroid
Uterus
Vagina
Whole Blood

6.3.11 Quantitative polymerase chain reaction in a case:control cohort

Analysis of Raw CT values

Exosomal-RNA was isolated from 0.5 ml plasma in the case:control cohort (detailed in section 6.3.9). The selection of sixteen targets (detailed in section 6.3.10) were pre-amplified from reverse-transcribed cDNA. Relative expression was measured by qPCR and cases were compared to controls with the comparative CT method (Schmittgen and Livak, 2008).

Raw CT values were plotted comparing cases against controls (Figure 6.14). This analysis was normalised by input volume with 0.5 ml plasma used per sample. The three housekeeping genes were detected in every sample and showed increased expression in controls. For example, *GAPDH* had an average CT of 27.19 cycles in cases and 26.15 cycles in controls (n=15 per group, measured in triplicate).

The gene *CDK5* was detected in all samples, except one case, and had previously shown to be downregulated throughout disease progression (Feng et al., 2014). This observation was also reflected in this study, with cases showing a higher average CT of 31.66 cycles compared to 30.68 in controls. Two other genes from the Feng *et al*. study were measured in similar numbers across this cohort: *ITPKB* (n=14 cases, n=15 controls) and *FAM107A* (n=15 cases, n=15 controls). However, the direction of expression differed from what had been demonstrated previously in *post-mortem* brain. One explanation for this may be that biomarkers of AD, associated with exosomes, differ in levels over the course of disease progression or with severity of condition. For example, phosphorylated tau is significantly increased on CSF-derived exosomes in mild cases of AD and not moderate or severe (Saman et al., 2012). The Feng *et al*. study had demonstrated consistent dysregulation of *CDK5, ITPKB* and *FAM107A* in the brain during disease progression but there may be an added complexity here of the unknown regulatory role of packing these transcripts into exosomes and their subsequent transport into peripheral blood (Feng et al., 2014). Indeed, in the case of Parkinson's disease, toxic α-synuclein is reduced in patient CSF but increased in association with plasma exosomes (Shi et al., 2014). This suggests that elimination of certain factors from the CNS, into peripheral circulation, may go hand-in-hand with disease processes.

Of the six genes chosen from the Feng *et al*. review three were not strongly detected (Feng et al., 2014). Firstly, *GFAP* did not produce a detectable signal in any samples (Figure 6.14). According to the gene expression data, obtained from the GTEx portal (Figure 6.13), *GFAP* is selectively expressed in the brain and so would be a highly specific tissue-discriminating

signal if detected in exosomes. It may be that plasma-derived exosomes contain an abundance of non-coding RNAs, as demonstrated for H4 exosomes in chapter 5, and of the proportion of remaining coding RNA, *GFAP* is in too low abundance to be detected from such low volumes of plasma. Alternatively, it may be that the gene expression assay itself was not working robustly. Secondly, *GNG3* was detected in 9 samples (n=2 cases, n=7 controls). The GTEx portal expression plot was similar to *GFAP* as *GNG3* was highly selectively expressed in brain tissues. As this worked in a number of the samples this is probably explained by a low abundance of the transcript in plasma-derived exosomes, rather than a technical problem with the assay. It may be that *GNG3* is down-regulated in peripheral exosomes in AD as 2 cases produced a detectable signal and 7 controls. This would need further experiments, likely with a higher volume of plasma to boost the signal, to be conclusive. Thirdly, *RGS4* was detected in only two samples (n=1 case, n=1 control). As with the previous two candidates, *RGS4* is highly selectively expressed in brain tissues so maybe a low abundant target in peripherally available exosomes or the assay itself may not be well optimised.

Therefore, it is difficult to come to meaningful conclusions from *GFAP, GNG3* and *RGS4*. However, the other three brain-enriched genes, *CDK5, ITPKB* and *FAM107A* (Figure 6.13), showed good detection across the cohort. Indeed, the detectable signal was good at below 30 cycles for *ITPKB* and *FAM107A* and on the threshold of good detection at 29 – 34 cycles for *CDK5*. These observations meant that the aim producing an assay that could detect CNS-enriched signals in peripheral exosomes had been achieved. To further test if the gene expression changes in *CDK5, ITPKB* and *FAM107A* were statistically significant between cases and controls, these data would need to be transformed from the raw CTs (Schmittgen and Livak, 2008) which has been reported later.

Detection of gene expression in *APOE* and *APP* was achieved across the cohort with all 30 samples detected for these targets and CT values ranging from 22 to 36 cycles. Both candidates were downregulated in disease. *APOE* had an average CT of 34.47 in cases and 33.53 in controls whilst *APP* was 27.42 in cases and 26.03 in controls, suggesting down-regulation in disease. *BACE1* was less well detected across the cohort (n=10 cases, n=13 controls) and showed the same direction of gene expression change with average CTs of 34.16 in cases and 33.66 in controls. As LOAD does not typically have an *APP* or *BACE1* genetic component, and as the cohort has been normalised by *APOE* genotype, it is not expected that these differences between cases and controls would be statistically significant when the data are transformed later.

Of the candidates identified as having strong expression in H4 exosomes, in the previous chapter, *BLOC1S6* and *XLOC_003630* were detected across the entire cohort (n=30, Figure 6.14). It must again be noted that NTCs in the *XLOC_003630* assay did produce measurable CTs which suggested contamination or, more likely as this has occurred in a separate experiment, self-amplification inherent in the assay. Threshold detection in these NTCs was achieved late in the qPCR, after 37 cycles, so the patient data was still analysed.

Both *BLOC1S6* and *XLOC_003630* appeared to be down-regulated in disease with *BLOC1S6* recording average CTs of 29.82 in cases and 28.29 in controls whilst *XLOC_003630* recorded 29.80 in cases and 29.04 in controls. Only 3 samples produced a detectable signal for *XLOC_004251* (n=2 cases, n=1 controls) and 23 samples for *TBC1D8B* (n=9 cases, n=14 controls). Of these 23 samples producing a detectable signal, 14 were controls so there may be a genuine down-regulation of *TBC1D8B* in disease, to the extent that cases became undetectable. This would require more samples, with a better detection rate, to be fully conclusive.

Overall, these data demonstrated that detection was achieved across 12 of the 16 targets tested. Reassuringly, 3 of these were targets are preferentially expressed in brain tissues, according to the GTEx portal, which confirms an added utility of this assay: to detect CNS-enriched signals from a small volume of peripheral blood. Using raw CT values, however, is not compatible with statistical tests so these results cannot currently be used to determine if any of the candidates are significantly dysregulated in AD.

Figure 6.14: Relative gene expression shown with raw CT values.
Quantitative PCR (qPCR) was used to measure cycle thresholds (CT, y axis) in exosomal-RNA collected from plasma in a case:control cohort (n=30). C_T values reflect the cycle number where fluorescence units exceeded a set threshold of 0.1 FU. The upper and lower "hinges" of the boxes correspond to the first and third quartiles whilst each circle represents a technical replicate data point. Raw C_T values are reported here for 16 targets, as indicated in the title of each graph. Eight of the targets were detected in every sample (n=30): GAPDH, TUBA1A, PPIA, FAM107A, APOE, APP, BLOC1S6 and XLOC_003630. Four more targets were also detected in similar numbers: ITPKB (n=14 cases, n=15 controls), CDK5 (n=14 cases, n=15 controls), BACE1 (n=10 cases, n=13 controls) and TBC1D8B (n=9 cases, n=14 controls). Four of the targets were not detected in high numbers and were thus not included in further analyses: GFAP (n=0), GNG3 (n=2 cases, n=7 controls), RGS4 (n=1 cases, n=1 control) and XLOC_004251 (n=2 cases, n=1 control).

A. *Three housekeeping genes: GAPDH, TUBA1A and PPIA*

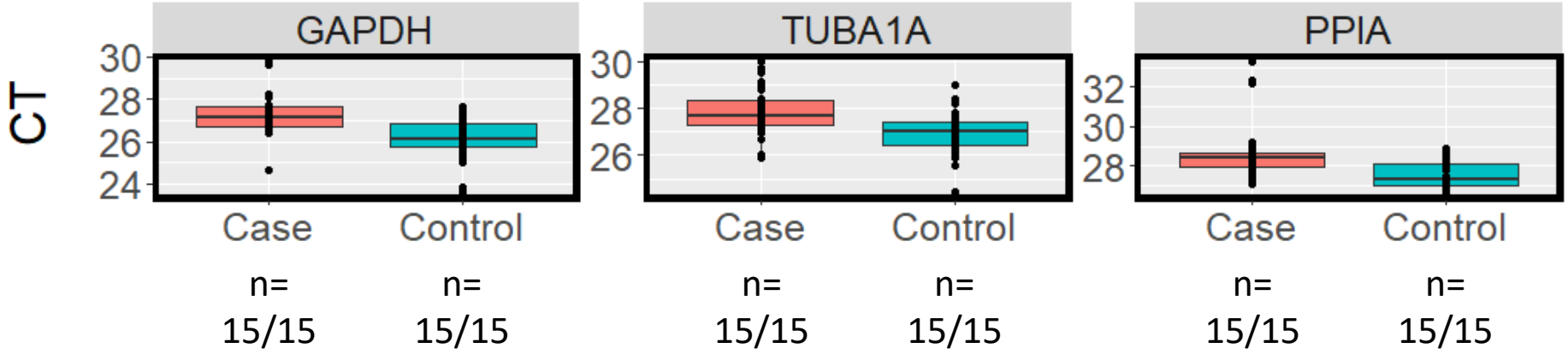

B. Six brain-enriched genes: ITPKB, GFAP, FAM107A, GNG3, CDK5 and RGS4

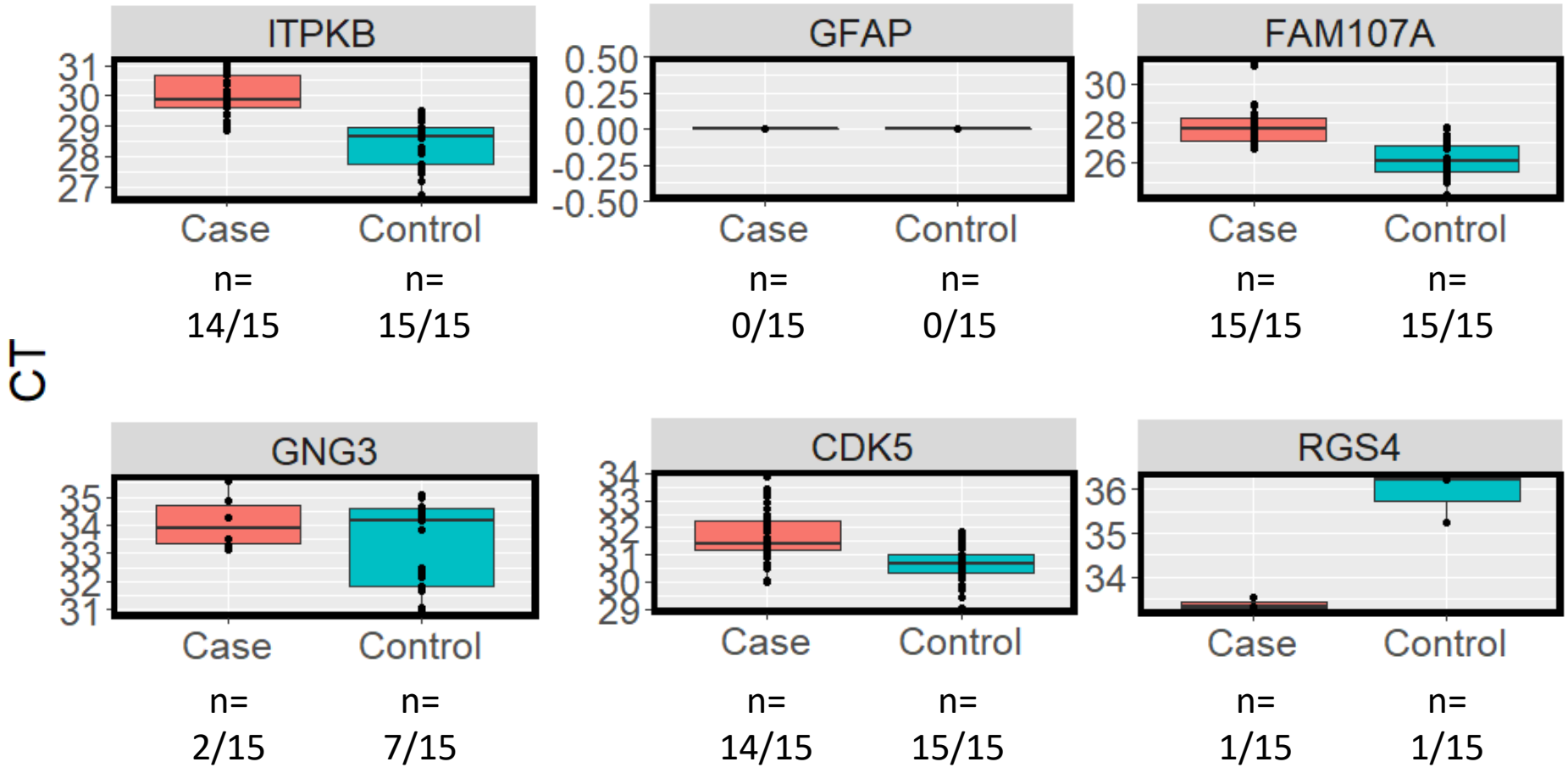

C. Three AD-relevant genes: APOE, APP and BACE1

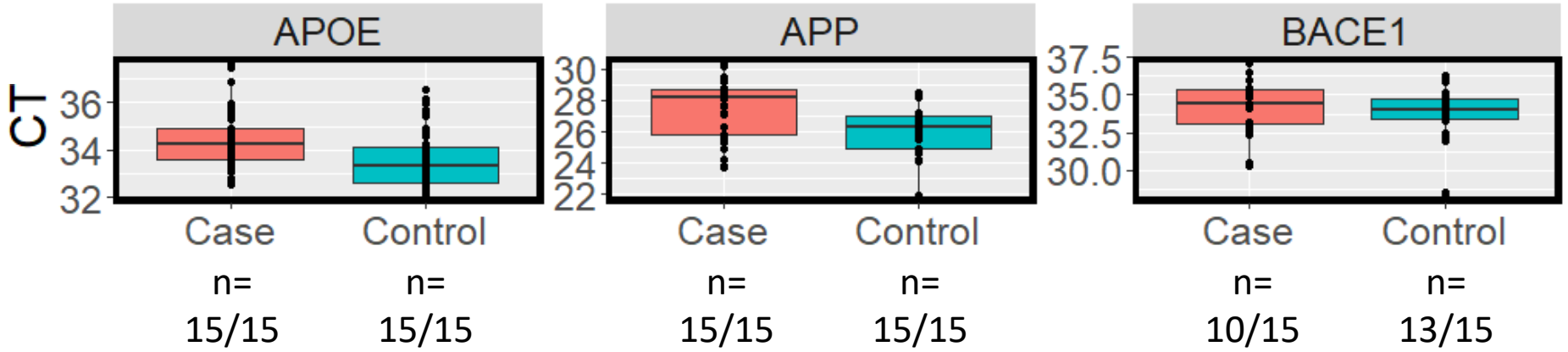

D. Four candidates previously shown to be strongly expressed in H4 exosomes: BLOC1S6, TBC1D8B, XLOC_003630, XLOC_004251

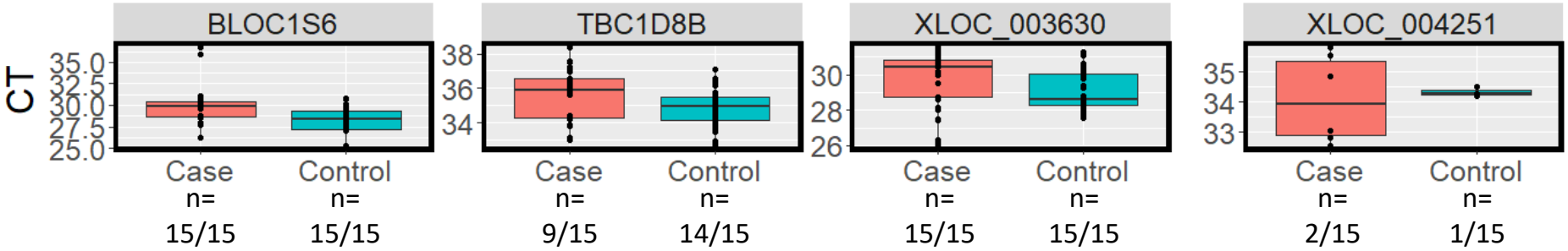

Analysis of transformed CT values (2^{-CT})

Transformation of these data from the raw CTs was performed next so that statistical tests could be applied. Four of the candidates were not detectable across many of the samples so were excluded and the following twelve taken further: *GAPDH, TUBA1A, PPIA, FAM107A, APOE, APP, BLOC1S6, XLOC_003630, ITPKB, CDK5, BACE1* and *TBC1D8B*. Raw CT values were transformed to $2^{(-CT)}$ as a numeric transformation of the number of cycles required to reach the threshold of detection (Figure 6.15). This meant that the data were still being normalised against sample input volume (0.5 ml plasma). This transformation allowed statistical analyses to be applied and thus indicate if a difference in CT value between cases and controls was significant. Shapiro-Wilk tests indicated that these data were not normally distributed so non-parametric tests were adopted. Mann-Whitney U tests were applied to the data using SPSS statistics software.

Of the three targets previously shown to be dysregulated in disease, *CDK5, ITPKB* and *FAM107A* (Feng et al., 2014), all reached the threshold of significance ($p<0.001$) (Figure 6.15). This indicated that the difference in CT values between cases and controls was statistically significant, an indication that each of the three genes were down-regulated in AD. Being down-regulated in disease was expected for *CDK5* but not *ITPKB* and *FAM107A* which had previously been reported as upregulated in AD brain. However, gene expression changes in brain may not correlate well with the RNA that is packaged into exosomes and transported into the periphery. For example, it has been demonstrated that the α-synuclein protein is present in lower concentrations in CSF but higher in plasma-derived exosomes in Parkinson's disease (Shi et al., 2014). A similar phenomenon may be occurring here with *ITPKB* and *FAM107A* RNA in AD.

In this analysis statistically significant changes in CT values were also detected for *APOE*, *APP* and *BLOC1S6* ($p<0.001$) (Figure 6.15). Each of these were down-regulated in disease but this was not expected, particularly, for *APOE* and *APP*. However, an important consideration must be made of the house-keeping genes. Statistically significant changes in CT value were detected for *GAPDH*, *TUBA1A* and *PPIA* ($p<0.001$). These house-keeping genes were measured with the aim to either confirm uniform expression across the sample-set or, if that was not the case, to be used for data normalisation.

These samples had been normalised by plasma volume prior to RNA extraction, so the observation of non-uniform expression of house-keeping genes suggests that uneven quantities of RNA where in the original samples. Therefore, normalising the data by sample

volume was not sufficient to draw meaningful conclusions. This variation between plasma samples was not entirely unexpected as person-to-person variation can be subject to disease status and many other factors, such as how recently the participant had drunk before venepuncture.

In summary, it would not be appropriate to draw conclusions from these data after the 2^{-CT} transformation. Rather, this analysis has highlighted that there is likely to be uneven starting quantities of RNA in the samples because there was statistically significant changes in the CT values of house-keeping genes. Whilst it is not necessarily the case that *GAPDH, PPIA* and *TUBA1A* are constitutively expressed in exosomes, and thus suitably used as house-keeping genes for normalisation, it would be most appropriate to account for these expression differences in another analysis.

Figure 6.15: Relative gene expression shown with $2^{(-CT)}$ values.
Quantitative PCR (qPCR) was used to measure cycle thresholds in exosomal-RNA collected from plasma in a case:control cohort (n=30). C_T values were transformed to $2^{(-CT)}$ for this analysis (y-axis)*. The upper and lower "hinges" of the boxes correspond to the first and third quartiles whilst each circle represents a technical replicate data point. Gene targets are indicated in the title of each graph. Mann-Whitney U tests were performed where * donates p<0.05, ** donates p<0.01 and *** donates p<0.001.*

A. *Three housekeeping genes: GAPDH, PPIA and TUBA1A.*

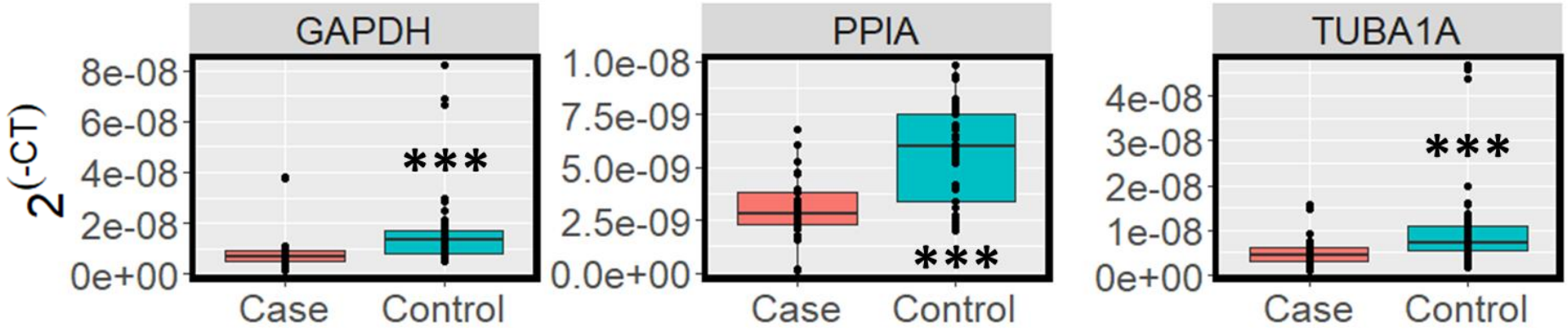

B. *Three brain-enriched genes: ITPKB, FAM107A and CDK5.*

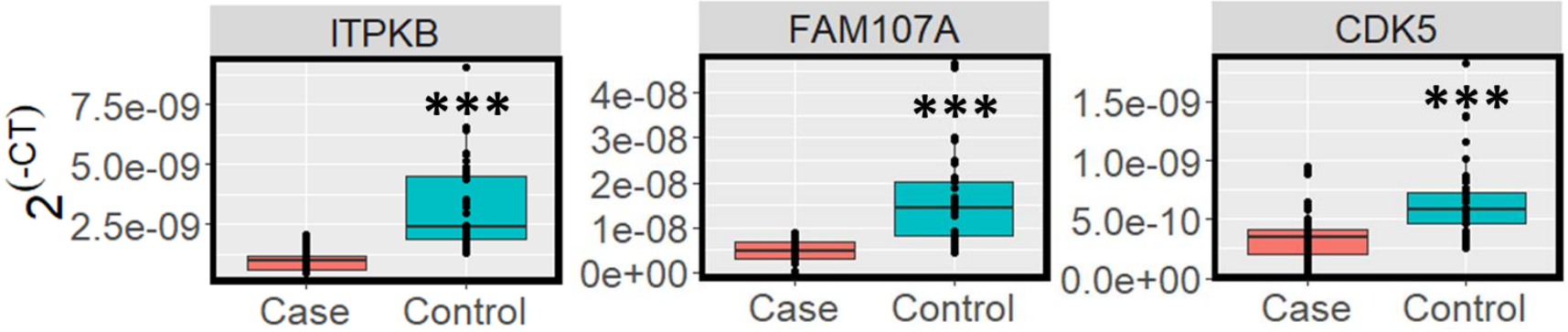

C. Three AD-relevant genes: APOE, APP and BACE1.

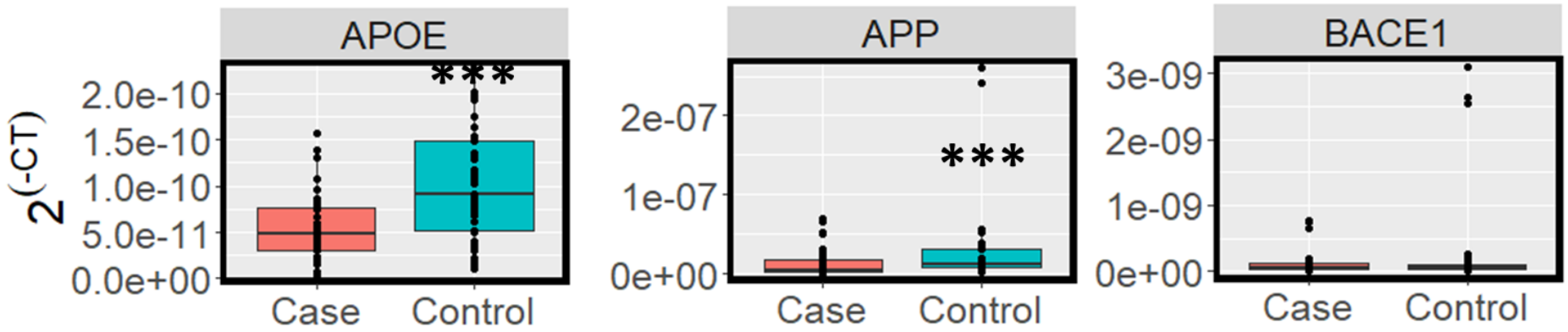

D. Three candidates that were enriched in H4 exosomes: BLOC1S6, TBC1D8B and XLOC_003630

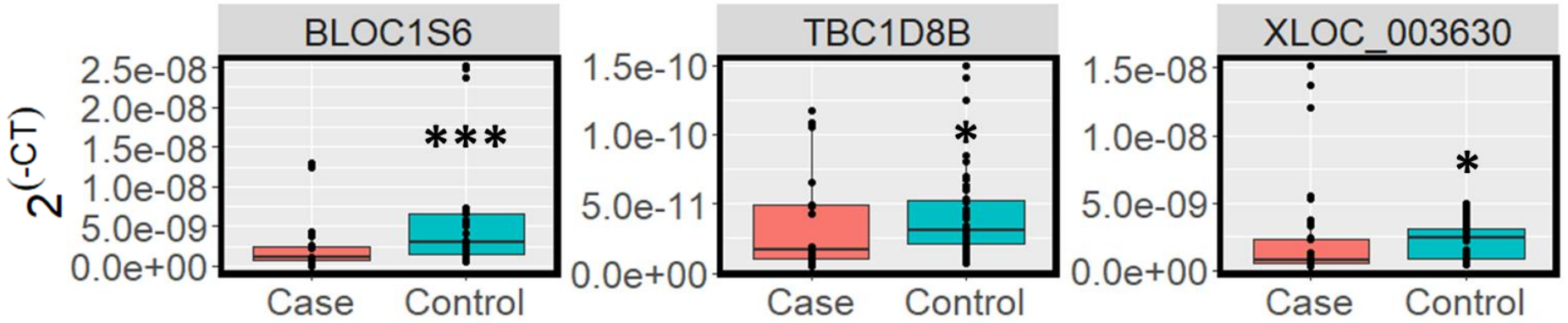

Analysis of CT values normalised to GAPDH expression ($2^{-\Delta CT}$)

Calculating 2^{-CT} values and observing statistically significant changes in the CT values of housekeeping genes had suggested that there was not uniform quantities of RNA in the plasma samples despite normalising by input volume. *GAPDH, PPIA* and *TUBA1A* are typically used housekeeping genes (Eisenberg and Levanon, 2013) so uniform expression would be expected if there were similar quantities of starting RNA. It is possible to normalise qPCR data by house-keeping gene expression by calculating the $2^{-\Delta CT}$ (Schmittgen and Livak, 2008). This is a similar numeric transformation of the CT as used in the previous section but this time the CT value of the candidate is subtracted from the CT value of the housekeeping gene before transformation. This accounts for the differences in starting material prior to qPCR. However, whilst *GAPDH, PPIA* and *TUBA1A* are typical housekeeping genes in cells and tissues (Eisenberg and Levanon, 2013), it is unknown which of these would be expected to have uniform RNA quantities in exosomes so the average across all three house-keeping genes was used in this calculation.

The qPCR data for each candidate was transformed to account for *GAPDH, TUBA1A* and *PPIA* expression (averaged) by calculating $2^{-\Delta CT}$ (Figure 6.16). Shapiro-Wilk tests indicated that data were not normally distributed so non-parametric tests would be most appropriate.

Mann-Whitney U tests confirmed statistically significant changes in the normalised CT values of *ITPKB* (*p<0.001*) and *FAM107A* (*p=0.001*). Both candidates were down-regulated in cases and, as discussed earlier, these were not in the expected direction of effect based on *post-mortem* brain tissue datasets (Feng et al., 2014). The meaning of this is unclear but currently little is known about the sorting and packaging of specific RNA molecules into exosomes prior to secretion (Mateescu et al., 2017). There may be a regulatory reason why these particular RNAs are less-abundantly packaged into exosomes in AD, or alternatively, it may be that the passage of exosomes out of the CNS is perturbed in AD. The down-regulation of *ITPKB* and *FAM107A* in the peripheral exosomes of AD patients may prove of future utility as biomarkers of AD. Certainly, by reaching the threshold of significance in this small case:control cohort, the assay method is validated and the argument for utilising exosomal-RNA as biomarkers of AD has been bolstered.

Two other targets reached statistical significance in this analysis: *BACE1* (*p=0.*041) and *BLOC1S6* (*p=0.044*). *BACE1* is the β-secretase enzyme that cleaves APP to pathogenic Aβ. It is difficult to make a biological inference from this having a lower expression in the RNA of exosomes without repeating in a larger sample set to confirm this observation. *BLOC1S6* had

been identified as enriched in exosomes by RNA sequencing in the previous chapter and, independently, has been associated with human gliomas (Meyer, 2014). The gene-product plays a role in intracellular vesicle trafficking, which is intriguing when this observation has been made analysing exosomes. Mutations in the *BLOC1S6* gene have been found to cause Hermansky-Pudlak Syndrome (Gahl and Huizing, 1993). Here, it was significantly down-regulated in the exosomes of AD cases. Genetic variations of endocytosis genes have previously been associated with Alzheimer's disease (Lambert et al., 2013, Karch and Goate, 2015) including *BIN1, PICALM, CD2AP, EPHA1* and *SORL1*. Pathological variations may not regulate expression of these genes but, in principle, there is a growing case for investigating endocytosis in Alzheimer's disease from a biomarker and pathology perspective.

Overall, this study has demonstrated a tractable method for detecting gene expression in exosomal-RNA isolated from small volumes of plasma. It has sensitivity to detect CNS-specific transcripts such as *CDK5, ITPKB* and *FAM107A* which are preferentially expressed in the brain. Furthermore, it has been demonstrated that this assay has potential to identify biomarkers of AD but larger cohorts would need to be tested to confirm the utility of candidates identified here. A non-hypothesis driven, RNA-sequencing approach would be preferable but with the limitations of RNA input described, this could not be performed in this study but would be of future interest. Nevertheless, these observations bolster the argument for analysing exosomal-RNA from peripheral blood for the future discovery of AD biomarkers.

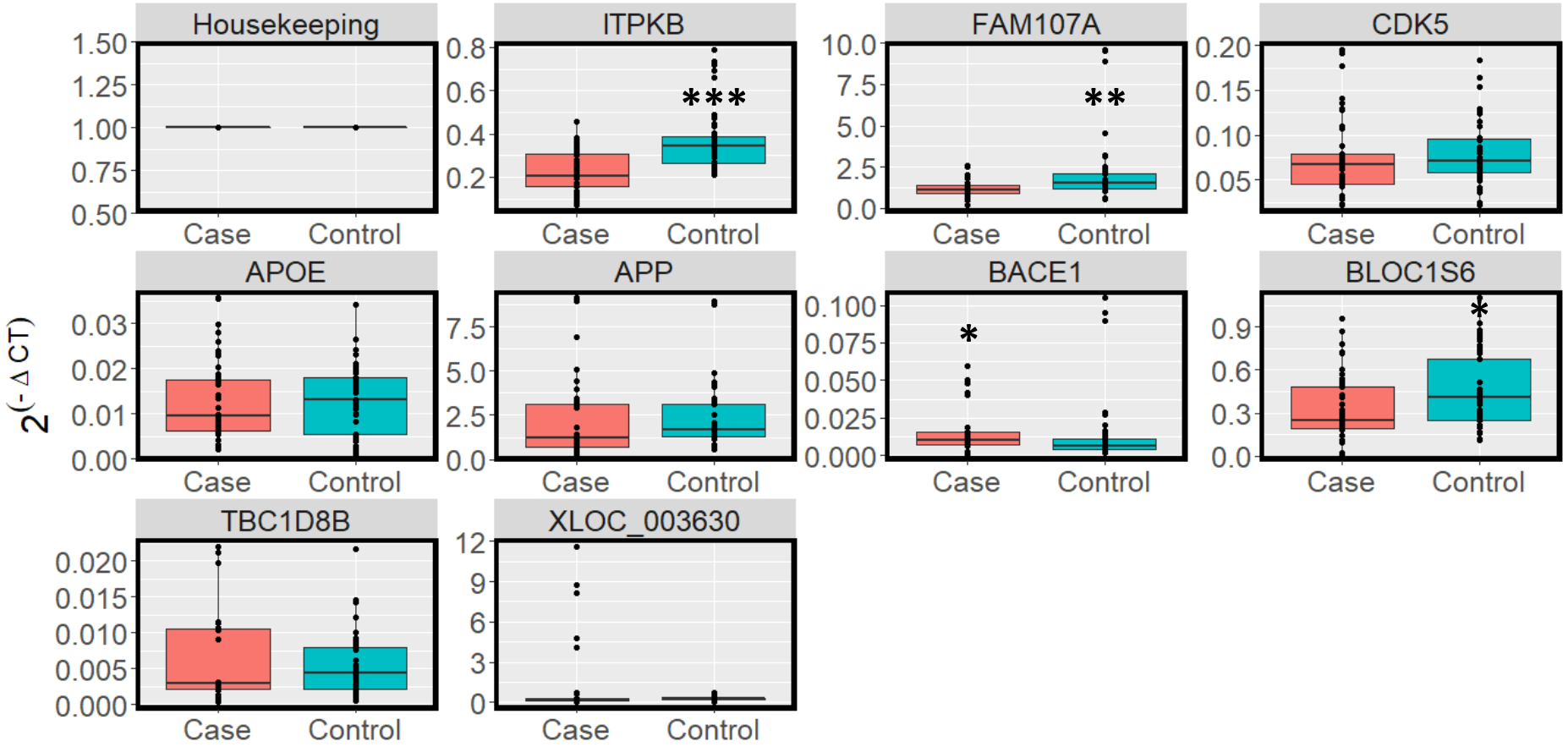

Figure 6.16: Relative gene expression shown with $2^{(-\Delta CT)}$ values calculated from three housekeeping genes.
*Quantitative PCR (qPCR) was used to measure cycle thresholds in exosomal-RNA collected from plasma in a case:control cohort (n=30). GAPDH, TUBA1A and PPIA expression was averaged and used in the calculation of $2^{(-\Delta CT)}$ values (y-axis). The upper and lower "hinges" of the boxes correspond to the first and third quartiles whilst each circle represents a technical replicate data point. Gene targets are indicated in the title of each graph. Mann-Whitney U tests were performed where * donates p<0.05, ** donates p<0.01 and *** donates p<0.001.*

6.4 Discussion

The aims of this chapter were to assess the feasibility of isolating exosomes from frozen plasma, develop an optimised workflow for analysing exosomal-RNA and investigate the expression of multiple candidate genes in an AD case:control cohort.

For the development and testing of any biomarker it is imperative that the assay is compatible with archival material. A brief analysis, by NTA, showed that storing plasma at -80°C for extended periods of 30 days did not cause any gross changes in the concentration or size of particles.

Three different techniques were evaluated for isolating exosomal-RNA from frozen plasma. Ultra-centrifugation appeared to be inefficient for pelleting exosomes from plasma, as has been reported elsewhere (Enderle et al., 2015). This inefficiency may be a peculiarity of plasma as pelleting exosomes from cell culture medium has been reported to be far more efficient, up to 90% recovery of particles, in the Clayton laboratory. This may be due to the relative viscosity of plasma compared to cell culture medium or the high protein content. The question remains: is it possible to alter the ultra-centrifugation procedure to improve this inefficiency? Solutions include testing rotors with more efficient *k*-factors, centrifuging at faster speeds, centrifuging for longer time or to pre-diluting the sample to decrease the viscosity. To test these options, and thereby hopefully improve the efficiency of ultra-centrifugation, significantly more blood and time would be required and this could not be fully achieved in the scope of this current thesis.

Size-exclusion chromatography was demonstrated to be effective at separating exosomes from the highly abundant blood protein HSA, as has been reported elsewhere (Welton et al., 2015). However, low efficiency of recovering exosomes from enriched fractions has been reported in the original publication whether ultra-centrifugation or precipitation is used. Therefore, the third isolation method evaluated was the spin-column based exoRNeasy™ procedure (Enderle et al., 2015) which had no requirements for ultra-centrifugation.

These three techniques were principally different from each other but a major difference with the spin-column based method is not requiring ultra-centrifugation which could have posed a potential bottleneck for a future assay. The process of ultra-centrifugation is time-consuming; in this study plasma samples were centrifuged for 2 hours yet did not efficiently recover particles. It is also labour-intensive as samples must be carefully prepared to cope with the sheer forces applied in pelleting exosomes. Furthermore, indiscriminately pelleting

exosomes with other particulates requires an addition PK/RA digestion step to ensure that intra-luminal RNA is extracted. These features would make it technically difficult to scale up an assay for numerous samples, as would be needed for a large-scale biomarker discovery study. Therefore, the spin-column based method was technically easier and quicker to perform and so had greater potential for being scaled up for multiple samples.

To fully evaluate these procedures, the yield of exosomal-RNA extracted from 0.5 ml plasma was investigated. RNA was extracted from 3 donors for each technique and evaluated by electrophoretic analysis and SYBR-green qPCR of *TUBA1A.* It was clear that the spin-column technique not only provided a simpler workflow, which could be scaled up for multiple samples, but that the quantity of RNA isolated was far greater allowing more flexibility in the PCR-based analysis later on. However, the assay had to be refined to improve the measurable signal and increase sample volume so that multiple targets and replicates could be analysed.

The qPCR chemistry as changed from SYBR-green to Taqman so that a pre-amplification step could be included. This addition addressed both the issues of increasing signal and sample volume. A drawback to using this pre-amplification step is that gene candidates have to be pre-selected and qPCR analysis is then limited to these. Amplification bias is an issue with sequencing studies but the relative expression of each gene candidate was measured independently of others in this study. The sensitivity of the assay was very good, being able to detect gene expression differences with 1 µg of H4 exosomes spiked-in. For a number of the targets there was a wide separation between the CT values suggesting that the exosome dose could have been much lower. For example, there was a difference in ~4 cycles for *GAPDH* between 0 and 1 µg of exosomes spiked-in so it is highly likely that lower titrations of 0.1 or 0.01 µg may also show differences in CT values. This means that there is very good sensitivity in the assay to detect minute changes in exosome dose, which is desirable for biomarker discovery. Thus, a workflow has been developed for the effective isolation of exosomal-RNA from 0.5 ml plasma, detection of multiple gene-targets and with very good sensitivity to changes in exosome concentration.

With the workflow established the assay was tested on an AD case:control cohort. AD is a complex, progressive disorder with multiple genetic and environmental factors so deciding on a cohort is not simple. In this study, as much additional information as possible was sought to inform these decisions. 15 AD cases (6 male, 9 female) were selected with a diagnosis certainty score of 75-99% based on cognitive assessments and autopsy report. 15 controls (6 male, 9 female) were selected with a priority of eldest at interview. Therefore, these

individuals were as well-defined as possible with the information available. All participants were tested for their *APOE* genotype and e3/e3 homozygotes were chosen to remove this strong genetic effect that could bias the results if not accounted for.

The gene target list was increased to sixteen by the addition of six targets that are dysregulated throughout disease progression in AD (Feng et al., 2014) and showed preferential expression in the brain over other tissue types. Primarily, these candidates were chosen as, by previously showing dysregulation in AD brain over the course of disease, they would be most likely detected in plasma exosomes. Additionally, by demonstrating that the targets were preferentially expressed in brain tissues they provided an opportunity to test the sensitivity of the assay to detect CNS-enriched signals, despite the technical difficulties of analysing peripheral blood, only using 0.5 ml plasma and only having picograms of RNA available.

The case-control cohort was analysed by Taqman qPCR but, despite plasma input volume being normalised to 0.5 ml, it became apparent that normalisation would have to be performed based on house-keeping gene expression. In future studies, quantitation of exosomes in the samples could be made by NTA and/or BCA. However, this would introduce additional assays that would increase the time taken to process the samples when house-keeping gene expression is relatively simple to include in the qPCR. Therefore, gene expression was measured using the comparative CT method (Schmittgen and Livak, 2008) and $2^{-\Delta CT}$ values calculated against *GAPDH* expression.

With these data, *ITPKB* and *FAM107A* showed significant down-regulation of expression in disease. This was contrary to the expected direction that showed up-regulation of these genes in *post-mortem* AD brain (Feng et al., 2014). These unexpected results may be a genuine insight into disease. In the case of Parkinson's disease, toxic α-synuclein is present in lower concentrations in CSF but higher in plasma-derived exosomes (Shi et al., 2014). A similar phenomenon appears to be occurring here, whereby *ITPKB* and *FAM107A* are up-regulated in diseased brain tissue but down-regulated in the peripheral exosomes. It may be that there is a disturbance in the mechanisms for packaging these transcripts into exosomes and so they remain within disease cells or, alternatively, the passage of exosomes out of the CNS is perturbed in AD. These hypotheses would need to be determined mechanistically.

The ideal analysis to perform would have been RNA-sequencing as it would have been non-hypothesis driven, rather than selecting gene candidates as done here. Unfortunately, the sequencing of plasma-derived exosomes was not possible as the RNA quantities obtained

were limiting. This could be increased if larger volumes of plasma were acquired but, based on the quantities of RNA extracted in this study, volumes greater than 1 ml would certainly be required. Indeed, one study reported using 4 ml plasma and still not isolating sufficient material for the technical requirements of RNA sequencing (Lugli et al., 2015). Such volumes could be achieved in new sample collections but would likely prove difficult when obtaining archived material which could be lower than those requirements. Therefore, the aim of this chapter was purposefully to develop a workflow with minute volume samples. Another option would have been to perform a pre-amplification with random decamer and oligo-dT primers and then perform RNA sequencing. Such an approach would certainly introduce amplification bias so was not pursued. Pre-amplification of selected targets was chosen as relative gene expression changes of each candidate, independently of others, could be performed using the comparative CT method.

Producing meaningful data by pre-amplification and qPCR does give some suggestion that this isolation method may be compatible with sequencing despite the low RNA quantities isolated. By performing 10 cycles of pre-amplification and 40 cycles of qPCR the exponential phase of amplification was achieved for a number of the candidates. The same level of amplification is not performed during sequencing library preparations but there is an element of amplification which may bring some transcripts into the detectable range. Alternatively, library preparations based on oligo-dT capture have lower sample input requirements than other methods. It is foreseeable that, with low RNA input, amplification bias will feature in these sorts of studies but, in principle, low volume samples isolated using the spin-column based method may be compatible with RNA sequencing.

Another future approach is to isolate and sequence exosomal-RNA from a cell model, which can provide the quantities of RNA needed, and follow up potential disease-discriminating candidates in biological fluids using the qPCR method described in this study. An appropriate cell model for AD would be difficult to identify as the cells undergoing pathological damage *in vivo* are unobtainable without major invasive surgery. The advent of induced-pluripotent stem cells (iPSCs) allows the culture of cells, readily obtainable from patients, derived from a known phenotypic background and with potential to be differentiated to disease-relevant cell types. Even so it is not known how relatable this cell model is to disease.

Rather than refining the choice of gene candidates, it may be beneficial to refine the case:control sample set in future. A larger sample set would of course provide more evidence for genuine gene expression changes by altering the statistical significance. However, there

is the added complexity that gene expression changes over time. A sample set from a longitudinal study would give more scope for assessing this phenomenon. It is known that symptomatic phase of AD covers a timeline of years but that a pre-clinical state of pathology maybe occurring over decades (Villemagne et al., 2013). Therefore, plasma samples collected at different points in this time-course may well have different expression patterns and this could not be dissected out of the dataset produced here. Furthermore, disease severity can lead to different protein profiles, for example, it has been observed that phosphorylated Tau is elevated in CSF exosomes only in mild AD, not moderate or severe (Saman et al., 2012). These observations highlight the challenge of using generalised sample sets to discover biomarkers of AD due to it being complex and progressive.

Another future approach is to alter the workflow described her for the detection of exosome-associated miRNAs. This would be a fundamental change to the workflow at the reverse transcription stage (Enderle et al., 2015). However, the success of measuring house-keeping genes, less-abundant targets, CNS-specific targets and the limited success of measuring lncRNAs suggests that such a change would be feasible. It was beyond the scope and resources of this study to develop this workflow as it would have to have been developed in parallel and thus require double the sample volumes.

Exosomal miRNAs have been associated with Alzheimer's disease by sequencing analysis (Cheng et al., 2015, Lugli et al., 2015) but have not shown any consensus across datasets yet (Kumar and Reddy, 2016). By altering the workflow described here for miRNA it would be possible to follow up some of these candidates to assess if they replicate in a separate cohort, even with minute volumes of plasma. The inconsistencies observed in these studies may be a general feature that again highlights the difficulty of identifying biomarkers of a complex and progressive disease.

An additional gene target that showed significant down-regulation in AD cases in this study was *BLOC1S6*. This target had shown enrichment in exosomes over cells based on RNA sequencing in the previous chapter. As a regulator of intra-cellular vesicle trafficking it is intriguing that this target was down-regulated in cases, given the recent observations of the endocytic tracts being implicated in AD. There is growing evidence that exosomes (Rajendran et al., 2006) and the endo-lysosomal system (Lambert et al., 2013, Karch and Goate, 2015) are implicated in the pathology of AD. Therefore, the observation here, that the expression of a vesicle trafficking regulator is dysregulated in disease, adds to this mounting evidence.

Sixteen gene targets were analysed in this study but manufacturer's guidelines report that up to 50 targets can used and so the assay can be expanded to a wider target panel. If this is done it would be worthwhile to refine a list based on a specific hypothesis. This could be replicating candidates from other datasets, as discussed above, or alternatively, be informed by other genetic analyses. It is through genome wide association studies (Harold et al., 2009, Hollingworth et al., 2011, Lambert et al., 2013) that unexpected associations with AD were discovered, including cholesterol metabolism, endocytosis and immunity (Karch and Goate, 2015). From these datasets, gene lists could be populated and the workflow adapted to investigate a narrower area of disease pathology, which is beneficial if a hypothesis-driven study is performed.

Of particular success in this study was demonstrating the detection of CNS-enriched gene targets despite the technical limitations of using peripheral blood and obtaining picograms of RNA. It was not known whether low abundant targets, such as those from specific tissues, would be measurable with this workflow but three of the six attempted were detected in this dataset. This was reassuring after an assay was not developed for the isolation of neural-derived exosomes in Chapter 4. Instead, an assay has been developed with sensitivity to measure neural-derived gene targets in a pool of exosomes derived from multiple tissues; in essence, finding the needle in the haystack. It is also worth noting that two of these CNS-enriched genes, *ITPKB* and *FAM107A*, were significantly down-regulated in disease and thus have good biomarker potential.

An alternative methodology, which also measures exosomal-RNA from small volumes of plasma is the use of molecular beacons for specific mRNAs of interest (Lee et al., 2016b, Wu et al., 2013). This allows the capture of EVs and measurement of gene expression from small sample volumes and can be scaled up for multiple targets using a tethered lipoplex nanoparticle (TLN) biochip. This technology has been utilised in a small number of studies including detection of mRNAs in lung adenocarcinomas (Lee et al., 2016b) and viral infection (Wu et al., 2013). This methodology provides an alternative to standard qPCR and, similarly to this study, can be utilised with small volumes of plasma.

This chapter has shown that, using commercially available products, it is possible to detect disease-discriminating gene expression changes in exosomal-RNA, even for CNS-specific targets, from volumes as low as 0.5 ml peripheral plasma. The biomarker field in AD is complex but the tools here described can be used, and potentially improved, to help utilise exosomes as non-invasive biomarkers of AD and other disease of the CNS.

Chapter 7. General discussion

7.1 Summarising discussion

Alzheimer's disease (AD) is the most common form of dementia (Imtiaz et al., 2014). The prevalence of dementias, including AD, is a rapidly growing, global problem estimated to rise to 81.1 million people worldwide by 2040 (Prince et al., 2013). Definitive diagnosis of AD is only possible *post mortem* by identifying senile plaques and neurofibrillary tangles present in brain tissue (Knopman et al., 2003). During life, the disease manifests itself with cognitive deficits and decline over time (McKhann et al., 1984, McKhann et al., 2011). A "probable AD" diagnosis can be determined by cognitive and physical examinations coupled with patient history and has proved reliable and valid (O'Connor et al., 1996, Becker et al., 1994, Foy et al., 2007, Gearing et al., 1995, Holmes et al., 1999). To complement these assessments, a small number of biomarkers have been developed with robustness for the clinic (Jack and Holtzman, 2013). These biomarkers measure either amyloid-β deposition or neurodegeneration by the analysis of proteins in cerebrospinal fluid (CSF) or by neuroimaging techniques. As yet, there are no clinically used peripheral biomarkers for AD. The research presented in this thesis assessed the potential of utilising exosomes in plasma to this end. It has been demonstrated that RNA appears to be actively packaged into exosomes, therefore functionally important, and a workflow for isolating exosomal-RNA from minute volumes of plasma was developed as a research tool that could be taken further with larger patient cohorts. Given the invasive nature of current biomarker analyses, it is of vital importance that new, peripherally-available, biomarkers are identified for better and earlier diagnosis of AD.

Exosomes provide an ideal source material for biomarkers of disease and have already shown potential in diagnosing cancers (Duijvesz et al., 2011, Duijvesz et al., 2015, Melo et al., 2015). Exosomes are derived from multi-vesicular bodies fusing with the plasma membrane (Harding et al., 1983, Harding et al., 1984, Harding et al., 2013), with proteins, lipids and nucleic acids non-randomly incorporated into the vesicle, and represent many aspects of the source cell (Colombo et al., 2014, Hugel et al., 2005, Mateescu et al., 2017). This study focused on the RNA cargo within exosomes, as it has been demonstrated that this becomes altered in the cases of hypoxia (Li et al., 2016a, Gray et al., 2015, Yang et al., 2016) and oxidative stress (de Jong et al., 2012, Eldh et al., 2010). Therefore, if the RNA present within exosomes is indicative of the disease status of the source cell it is likely that it can be used to identify AD patients. With the knowledge that exosomes can pass bi-directionally over the blood-brain barrier (Skog et al., 2008, Alvarez-Erviti et al., 2011) and myelin protein can be

present on serum-derived exosomes from patients with multiple sclerosis (Galazka et al., 2017), there is great potential that they can be utilised as peripherally-available biomarkers for neurological and neurodegenerative disorders, in general.

A variety of methods are available for the isolation of exosomes which vary greatly in the yield and purity of preparations, as well as ease of use and time demands (Thery et al., 2006). It is also worth noting that isolating exosomes from cell-culture supernatant or from biological-fluids are vastly different disciplines, due to the complex nature of the latter (Welton et al., 2015). From the outset of this study, a large stock of neural-derived exosomes were required to establish and test methods, so the bioreactor method (Mitchell et al., 2008a) of culturing H4 and IMR-32 cells, coupled with the sucrose cushion method of exosome isolation, were initially employed (Andre et al., 2002, Thery et al., 2006).

In 2014, a position statement from the International Society of Extracellular Vesicles (ISEV) gave a minimum set of biochemical, biophysical and functional requirements for reporting the genuine isolation of exosomes (Lotvall et al., 2014). These guidelines are important as exosomes are technically difficult to isolate, so sufficient evidence should be supplied before biological inferences made from data. The research presented in this thesis took heed of these guidelines. Multiple proteins, both intra-luminal and transmembrane, were analysed with different techniques and intact exosomes were analysed by NTA and cryo-electron microscopy. Furthermore, running sucrose density gradients was not merely a pre-requisite for the sucrose cushion method, but also confirmed that the exosomes were buoyant at the expected density (Escola et al., 1998, Raposo et al., 1996, Webber et al., 2014).

By using these methods, the exosomes secreted from H4 and IMR-32 cell-lines were thoroughly characterised in chapter 3 and, thereafter, the sucrose cushion method of exosome isolation was used to increase the yield of exosomes for bulk stocks, without compromising purity, as measured by P:P ratio (Webber and Clayton, 2013). Stocks of neural-derived exosomes were established and used for assay development; particularly in chapter 4, an immunocapture assay was attempted for the selective isolation of exosomes.

It is a desirable prospect to isolate exosomes from a particular tissue sub-type, so that a more disease-relevant population can be analysed. However, narrowing the analysis for biomarker discovery in this way may well exclude a population of interest. In this study, an assay that would selectively capture H4 or IMR-32 exosomes, over prostate-derived Du145 exosomes, was attempted in chapter 4. The use of cell-culture derived exosomes was chosen to develop this assay in principle, prior to testing in biological fluids, due to the foreseen technical

difficulties of handling complex specimens, such as plasma (Welton et al., 2015). Good ligand candidates, which were preferentially expressed in CNS tissues, for immunocapture were identified bioinformatically, and experimentally found to be enriched on H4 or IMR-32 exosomes over Du145. Reconfiguring the assay format to capture exosomes, based on these ligands, proved technically difficult. Detection methods were refined which improved the dynamic range of the assay. However, it appeared that exosomes were not efficiently adhering to capture antibodies because the signal : noise ratio could not be improved. These difficulties forced a change in direction for this study; as a result, exosomes were isolated *en masse,* rather than as a subset of the total population. Mounting evidence implicates not only neurons but also microglia and astrocytes in the pathology of AD (Sims et al., 2017, Askew and Gomez-Nicola, 2017, Liddelow et al., 2017). Depending on the ligand chosen, isolating a subset of exosomes may well exclude exosomes harbouring clinically useful information. So, for the scope of this study, and given the early stage of peripheral biomarker discovery in AD, analysing the total population of exosomes was considered an appropriate approach.

This thesis has a particular focus on the RNA content of exosomes. Methods for isolating and analysing exosomal-RNA needed to be developed in-house. Therefore, the H4 cell-line was chosen to begin this work. The methods for cell-culture and exosome isolation had been established and verified for this. Not only did this cell-line provide technical benefits, such as coping well with high density culture, but it also gave a unique opportunity to analyse the RNA of the source cell in comparison to the RNA within exosomes. This is of particular interest as there is considerable need for a better understanding of the packaging of RNA into exosomes (Mateescu et al., 2017). In order to have access to culture H4 cells, at the same time as isolating exosomes, the standard 2D culture method was reverted to because harvesting cells from bioreactor flasks is not straightforward (Mitchell et al., 2008a). The pellet and PBS wash method was required to obtain a high enough yield of exosomes from this culture method to facilitate the analysis of RNA. Whilst this had the potential to reduce the purity of exosome preparation (Webber and Clayton, 2013), nuclease digestion was used to ensure that intra-luminal RNA was analysed and co-isolated extracellular RNA was degraded, and hence eliminated from the analysis (Shelke et al., 2014, Hill et al., 2013). Thus, there was a dual-benefit of beginning with cell cultured-derived exosomes rather than biological fluids: it gave an opportunity to develop methods without the complexities of biological fluids and to gain significant new insights by comparing exosomal-RNA with the source cell.

Previous observations suggest that RNA is both passively and actively packaged into exosomes prior to secretion (Colombo et al., 2014, Hugel et al., 2005). It has not been thoroughly determined yet but RNA-binding proteins appear to play a role in actively packaging miRNAs into exosomes (Villarroya-Beltri et al., 2013). There have been a number of studies that have used microarray and small RNA sequencing to compare exosomal-RNA with the source cell but these methods fail to provide a comprehensive picture of the RNA as they preselect for a sub-selection of RNA (Skog et al., 2008, Valadi et al., 2007, Nolte-'t Hoen et al., 2012, Cheng et al., 2014, Royo et al., 2013, Li et al., 2013, Ahadi et al., 2016b). In this thesis, whole transcriptome sequencing was performed, with only ribosomal RNA (rRNA) removed (Benes et al., 2011), in chapter 5. This unbiased approach is hitherto unused, so was chosen to provide novel insights into the entire RNA of exosomes compared to the source cell.

RNA sequencing data were generated from H4 cells and exosomes, using TruSeq Stranded Total RNA with Ribo-Zero Gold library preparation kits (Illumina), sequenced on a HiSeq 2500 (Illumina) at Wales Gene Park and analysed, by the author, using standard bioinformatics tools and best practices (Conesa et al., 2016, Mercken et al., 2013). The first novel and striking observation from these data came from annotating coding and non-coding RNA bases. Over 96% of reads measured from exosomes were non-coding, and thus, a completely different profile to cellular-RNA, which contained a large proportion (40%) of coding RNA. Disparity between the RNA of cells and exosomes has been reported before (Mittelbrunn et al., 2011, Li et al., 2015); however, other reports have shown good correlation between intracellular and exosomal RNA (Turchinovich et al., 2011, Tosar et al., 2015). In this thesis, an unprecedented difference between the RNA within cells and exosomes was shown. The profile of RNA within exosomes is mostly non-coding, demonstrating that the particular transcriptome of exosomes is fundamentally different from the source cell. On one hand, it may be that exosomes exist to eliminate junk RNA, such as spliced introns, from cells, as suggested from the relative abundance of intronic reads (43%) in this dataset. However, the non-coding transcriptome has not been well annotated and novel species, such as lncRNAs, are continually being identified and annotated. In this dataset, lncRNAs and introns were analysed and found to be informative, as discussed below, so it is likely that exosomes function as more than a route for eliminating junk RNA.

A second observation from the sequencing data was that the functional annotation of differentially-expressed RNA found enrichment of terms in exosomes, which reflected the known protein composition of these vesicles (Webber et al., 2014, Kalra et al., 2012, Simpson

et al., 2012). Exosomes are secreted lipid-bounded vesicle structures often replete with intra-luminal proteins and tetraspanins that are known to cross-link with other tetraspanins and membrane proteins to for tetraspanin-webs. The enrichment of terms such as “disulfide bond”, “topological domain:Extracellular”, “Secreted” and “transmembrane” are strikingly similar to the known molecular composition of exosomes and to the GO enrichment terms that have arisen from proteomic profiling. Protein array methods have identified enrichment of terms such as “Disulfide Bond”, “Transmembrane” and “Topological domain:Extracellular” (Webber et al., 2014). Additionally, in the RNA sequencing dataset, there was enrichment of terms such as “Glycoprotein” and “glycosylation site:N-linked”. It has previously been described that glycosylation is one of the processes by which exosomal proteins are regulated (Kore and Abraham, 2016) and glycoproteins on the surface of exosomes play important physiological roles, such as the binding of activated platelets in the coagulation cascade (Del Conde et al., 2005) and many other functions. Terms, such as “Glycosylation site:N-linked” and “Glycoprotein” were also identified by proteomic profiling (Webber et al., 2014). Therefore, overlapping terms have been identified using both proteomic analysis and RNA sequencing, despite the technically different approaches.

If RNA is non-randomly sorted into exosomes, they are representative of the cell they were derived from and functionally important. As a result, the analysis of exosomal-RNA is of great potential for biomarker discovery, as they will harbour select transcripts from diseased cells, as has been demonstrated in neuroglioma (Skog et al., 2008). The apparent disparity between cellular and exosomal-RNA suggests that unique biomarkers may well reside in these vesicles and not always be readily detected by pathological analyses in cells or tissues.

A small number of studies, to date, have investigated the utility of peripherally available exosomes as biomarkers of AD. These include the analysis of proteins found on neural-enriched plasma exosomes (Goetzl et al., 2015b, Fiandaca et al., 2015, Hamlett et al., 2016, Mullins et al., 2017, Goetzl et al., 2015a, Mustapic et al., 2017), and small RNA sequencing of plasma (Lugli et al., 2015) and serum-derived (Cheng et al., 2015) exosomes. These latter two studies used 1 – 4 ml volume of biological fluid and yet struggled to obtain the manufacturer’s requirements of RNA input for sequencing. This highlighted a challenge that had to be considered in the design of this study. A small yield of RNA, in the picogram range, is available from biological fluids and this problem is exaggerated in the context of AD where elderly subjects can be difficult to obtain blood from and banks of samples soon become exhaustible resources as patients become deceased. This study investigated the possibility of using a small volume of 0.5 ml plasma to address this challenge.

Whilst methods had been validated for isolating RNA from cell culture medium, the final section of this thesis addressed the challenge of isolating exosomal-RNA from biological fluids. Three techniques for isolating exosomal-RNA from plasma were investigated in chapter 6: ultra-centrifugation, size-exclusion chromatography (Cell Guidance Systems) and exoRNeasy spin-columns (Qiagen). Using qPCR, it was determined that the exoRNeasy technique yielded greater concentrations of exosomal-RNA than the other two techniques, and more reliably. Furthermore, this technique did not require a centrifugation step which greatly increased the scalability of the assay to be increased for larger studies.

The exoRNeasy method of RNA isolation was combined with Taqman qPCR chemistry and pre-amplification to refine and validate a workflow for analysing exosomal-RNA from plasma. This refined workflow was adopted in an AD case : control cohort, with the aims of measuring low-expressed gene targets and detecting significant differential gene expression changes to validate the assay.

This approach required the selection of gene candidates prior to qPCR. According to a review of studies with *post mortem* brain tissue, twelve genes were consistently up- or down-regulated in AD (Feng et al., 2014). Six of these were chosen, as they were ideal candidates to use in validating the workflow: the genes are preferentially expressed in the brain so would validate the detection of low-expressed, CNS-specific signals that have passed over the blood brain barrier via exosomes. By measuring gene expression in plasma-derived exosomes, the genes *ITPKB* and *FAM107A* were found to be significantly down-regulated in cases compared to controls. This was the opposite direction as had been reported in *post mortem* brain (Feng et al., 2014). It is difficult to make a biological inference from these observations. It has been observed, in Parkinson's disease, that concentrations of the protein α-synuclein can be reduced in patient CSF, but increased in association with plasma exosomes (Shi et al., 2014). It can be hypothesised, therefore, that exosomes can serve as a route for eliminating harmful products from the brain. In the case of AD, it may be that the elimination of *ITPKB* and *FAM107A* is perturbed in disease. This idea is complemented still further with the observation that *BLOC1S6* was differentially expressed. This gene plays a role in intracellular vesicle trafficking which hints at an already intriguing role for endocytosis and exosomes in AD. Regardless of these hypotheses, observing significant changes in gene expression, especially with brain-derived targets, was a good validation of the chosen approach and this workflow.

In summary, the research presented in this thesis showed a characterisation of neural-derived exosomes which were used as bulk stocks in an attempt to develop an immunocapture assay, and to develop methodologies for isolating and analysing exosomal-RNA. The latter revealed intriguing features of exosome biology: the profile of RNA within exosomes is vastly different from its source cell and the sorting of RNA into exosomes is not an entirely random process. These observations, coupled with current literature, suggest that exosomes are a prime candidate for developing peripheral biomarkers of AD. In light of this, a tractable workflow was developed to isolate exosomal-RNA from only 0.5 ml archival, frozen plasma. This technique was validated by qPCR and showed sufficient sensitivity to detect small changes in exosome dose and also to measure low-expressed, brain-enriched genes that have passed over the blood-brain barrier via exosomes. Thus, the potential utility of exosomes as peripheral biomarkers of AD has been confirmed, as well as a methodology, which can be used for the analysis of RNA from small volumes of plasma, has been developed.

7.2 Future directions

7.2.1 Future directions of analysing the RNA sequencing dataset

In the RNA sequencing dataset, the profile of RNA in exosomes was fundamentally different from that of the source cell. A global annotation of the data found more than 96% RNA within exosomes to be either intronic or intergenic. This proved problematic for performing a standard differential gene expression analysis, so long non-coding RNAs and introns were analysed to provide functional annotations. However, the data could have been mined much further.

One analysis that has been performed with small RNA sequencing data is to annotate the proportion of different RNA species in exosomes (Cheng et al., 2014). Using annotation files, the proportions of micro RNA, lncRNA, small nucleolar RNA, rRNA, transfer RNA and other RNA species was determined. It has since been determined that other species of RNA are also present in exosomes, including: mRNA, vault RNA, Y RNA, small interfering RNA and circular RNA (Raposo and Stoorvogel, 2013, Dou et al., 2016, Nolte-'t Hoen et al., 2012). A comprehensive annotation file that can capture these different species needs to be developed but this is not a trivial undertaking as the field is constantly changing with new species and novel annotations being reported. Indeed, it is possible to identify novel transcripts using RNA sequencing data (Mercken et al., 2013), which could be performed

with this current dataset. Given the disparity between cellular and exosomal-RNA, reported here and in the literature (Mittelbrunn et al., 2011, Li et al., 2015), this may well be a fruitful avenue of research. Of particular note, with the dataset produced here, is the novelty of performing whole transcriptome sequencing with exosomes and source cells, only rRNA was removed. There is good potential to identify an array of RNA species and perform *de novo* annotation that is not possible with microarray data and limited in small RNA sequencing datasets. However, it must be conceded that small RNA sequencing is technically more suitable for measuring the expression of miRNAs and other small RNA species, as the library preparation protocols enrich for these species, based on their size.

This dataset has the potential to be mined further: RNA sequencing data can be used for the investigation of the structure of transcripts and, in particular, detecting splice variants and fusions (Haile et al., 2017). An additional analysis could be performed with this dataset if DNA sequencing data was available for the H4 cell-line. It has been shown that RNA sequencing data can be integrated with whole-exome DNA sequencing for the enhanced detection of somatic mutations in lung and breast cancer (Wilkerson et al., 2014). This method, termed UNCeqR, improved mutation detection, particularly in low purity tumours. To apply this method to the dataset developed in this thesis may be problematic given the dominance of non-coding RNA in exosomes. However, it would give a flavour of the possibilities of integrating different datasets and deepen the understanding of the nature of exosomal-RNA.

The RNA sequencing also provided additional evidence that RNA is non-randomly sorted into exosomes (Mateescu et al., 2017). Despite this, direct mechanistic evidence is required. It has been shown that AGO2, and other miRNA-interacting proteins, can interact with components of the endocytic tracts such as MVBs (Gibbings et al., 2009, Lee et al., 2009), endoplasmic reticulum (Stalder et al., 2013) and endogenous prion protein in the endolysosomal network (Gibbings et al., 2012). Currently, it is inconclusive if AGO proteins are generally associated with extracellular vesicles, but it is likely that post-translational modification of the protein, and modulation of miRNA transcripts, would play a role in the incorporation into EVs (Mateescu et al., 2017). A number of RNA motifs have been associated with incorporation into EVs (Szostak et al., 2014, Batagov et al., 2011), including a GGAG motif on miRNAs that binds to sumoylated heterogeneous nuclear ribonucleoprotein A2B1 for loading into exosomes (Villarroya-Beltri et al., 2013). As a result of this, further experimental work is required to provide mechanistic evidence.

The differential expression of lncRNAs was performed in this study and future work in this area may well increase the understanding of RNA packaging into exosomes. LncRNAs have been reported as enriched in exosome-like particles secreted by mast cells (Lasser et al., 2016) and abundant in prostate cancer-derived exosomes (Ahadi et al., 2016b). The same group reported an enrichment of miRNA seed regions and RNA binding protein motifs on the lncRNAs being studied (Ahadi et al., 2016a). Whilst this was linked to disease propagation in the study, it should not be overlooked that the enrichment of these motifs in exosome lncRNAs may well point to the general mechanisms involved in loading these RNAs into exosomes, as reported for miRNAs (Villarroya-Beltri et al., 2013). Here, common sequence motifs present within sets of exosomal-enriched lncRNAs could be identified, pointing to a likely role in directing these towards a vesicle secretion fate.

It would be beneficial to directly investigate the functional role of the lncRNAs identified as differentially expressed in exosomes. It has been demonstrated that viral induction can be used to alter the expression of the lncRNA Chast (Viereck et al., 2016). A similar study used a pharmacological agent to knock down cellular miR-21*, which would otherwise be enriched in exosomes in models of cardiomyocyte hypertrophy (Bang et al., 2014). Such techniques could be adopted to follow up on some of the lncRNA candidates reported as enriched in this study. However, it is unclear whether these would address questions about the packaging of RNA into exosomes in general or specifically for the H4 cell-line used.

7.2.2 Future directions of RNA sequencing with cell culture-derived exosomes

The H4 cell-line was chosen for this study for a number of reasons. Primarily, the cell-line proved useful for the bulk production of neural-derived exosomes as it did not reach senescence as a primary cell-line might, especially when using bioreactor culture methods. In addition, the H4 cell-line has been routinely manipulated to create cell-models of AD (Asai et al., 2007, Sung et al., 2016), yet there has only been one report of studying the exosomes secreted from it to date (Tsunemi et al., 2014). Therefore, it proved useful and reliable for the first principle investigations reported here and has the potential to be taken further by introducing genetic mutations.

An immediate extension of the RNA sequencing work with the H4 cell-line and secreted exosomes, is to do similar analyses after introducing AD-relevant gene expression changes or mutations. For example, the H4 cell-line has been, and can relatively easily be manipulated

to stably express the Swedish mutated form of *APP* (Asai et al., 2007). More recently, *CD2AP*, which encodes for an adaptor protein implicated by GWAS, has been linked to exosome trafficking in HEK293 cells (Kwon et al., 2016). There is scope to take this cell-line further using gene manipulation. This thesis has demonstrated a number of techniques for measuring exosome secretion, protein composition and RNA analysis that could easily be adopted when introducing the Swedish mutation of *APP* or knocking in/out *CD2AP,* and other AD risk genes, in H4 cells.

There are numerous options and careful considerations that should be made prior to gene manipulation experiments as a number of risk genes have been implicated in AD (Robinson et al., 2017). It is far more likely to achieve measurable changes in exosome secretion, or composition, if endocytosis related risk genes are perturbed (Lambert et al., 2013). Yet, the development of CRISPR-Cas9 genome editing allows far more subtle changes in gene expression such as the introduction of point mutations (Hockemeyer and Jaenisch, 2016). It also requires a careful choice of gene to perturb, or single nucleotide polymorphism to alter, as the genes reported in GWAS studies are determined by proximity to the SNP probe in the study. This means that the disease causing SNP or gene may not be the one reported to have statistical association. Indeed, many are situated in intronic or intergenic genomic regions. Deeper mining of GWAS data, such as the use of conditional analyses (Hoffmann et al., 2015), may narrow down to one SNP of interest or even highlight multiple SNPs with independent signals. The long range effects, such as chromatin remodelling, of these disease variants are also unknown. There are numerous options for manipulating the H4 cell-line with AD-relevant gene changes and to monitor the impact of these on exosome number, protein and RNA.

However, a primary, diseased cell type from AD patients would provide an ideal candidate for culture and for collection of exosomes for sequencing analysis. As AD is a disease of the brain, the cell types in question are not readily obtainable from patients. Alternatively, peripheral blood monocytes (PBMCs) are primary cells that are relatively easy to obtain non-invasively. With the aid of Epstein Barr Virus transformation, it is also possible to immortalise B-lymphocytes, within PBMCs, to lymphoblastoid cell-lines (LCLs) for long term use (Gallo et al., 2017). Such cells can be expanded readily and maintained at high densities to yield plentiful stocks of exosomes. Whilst these cell-types are more readily obtainable from patients, the relevance to disease is questionable for both.

Alternatively, to transforming PBMCs to LCLs, it has been demonstrated that primary cells, such as fibroblasts, PBMCs and keratinocytes, can be modulated to a pluripotent cell-type known as induced pluripotent stem cells (iPSCs) (Takahashi and Yamanaka, 2006, Lee et al., 2016a, Khazaei et al., 2016). These can be differentiated to the cell type of interest, including neurons (Hayakawa et al., 2017, Takahashi, 2017), microglia (Muffat et al., 2016) and astrocytes (Yamamizu et al., 2017). Protocols are now being developed that allow direct induction to neurons (Broccoli, 2017). It is an exciting prospect to obtain a primary cell from an AD patient, reprogram to iPSCs (Lee et al., 2016a) and derive a cell-type of relevance for further study. In theory, a suitable cell-type with the correct genetic background for disease is available this way, but it should be considered that the epigenetic background, either from the original cell or from the induction process, may not give the exact mimicry required (Khazaei et al., 2016). Nevertheless, exosomes from iPSC-derived cells can be of utility in disease therapeutics (Liu et al., 2017) and may have wider applications, including the identification of disease-discriminating RNA profiles, in the future.

The use of iPSC-derived neurons comes with an additional complexity of trying to physiologically replicate the aged brain *in vitro* (Arber et al., 2017). For example, it can take up to 100 days of culture to generate functionally and electrically active neurons (Gaspard et al., 2008, Shi et al., 2012). Furthermore, a foetal form of the tau protein is predominately expressed in IPSC-derived neurons and can take up to 365 days of culture before multiple isoforms are present (Sposito et al., 2015, Wren et al., 2015, Iovino et al., 2015, Imamura et al., 2016). Even with such caveats highlighted, iPSCs provide a unique avenue to probe into the pathology and therapeutics of AD. The development of CRISPR-Cas9 genome editing technology has coincided with the growing use of iPSCs and shows promise in being used together (Hockemeyer and Jaenisch, 2016). As such, the possibilities are numerous for designing studies and, as discussed, careful consideration of the relevance of cell types and epigenetic background must be made.

This thesis has described the first principle work of whole transcriptome sequencing using H4 cells and exosomes. The methods could be adopted for more complex, yet closer to disease relevance, research questions through the adoption of iPSC and CRISPR-Cas9 technologies. This was beyond the scope of this study, but the sequencing data provided evidence that RNA is non-randomly sorted into exosomes and is a gold-mine for future explorations of the nature of exosomal-encapsulated transcriptomics.

7.2.3 Future directions of analysing RNA isolated from peripherally available exosomes

A biomarker of disease is an objectively measured biochemical, physiological or anatomical change (Jack and Holtzman, 2013). A probable diagnosis of AD can be determined by cognitive and physical examinations coupled with patient history (McKhann et al., 1984, McKhann et al., 2011). Currently, clinical biomarkers of AD rely on lumbar puncture or neuroimaging which are prohibitively invasive and expensive, respectively, for routine use (Jack and Holtzman, 2013). Therefore, a blood test for AD would be of great utility. Until 2017, consistent measurements of amyloid-β (Aβ) in the blood, using antibodies, proved difficult until the announcement of a mass spectroscopy-based method (Ovod et al., 2017). As an alternative, exosomes are showing promise of carrying protein and RNA biomarkers of AD (Fiandaca et al., 2015, Goetzl et al., 2015b, Goetzl et al., 2015a, Hamlett et al., 2016, Mullins et al., 2017, Mustapic et al., 2017, Cheng et al., 2015, Lugli et al., 2015). In this thesis, a method of extracting exosomal-RNA from 0.5 ml plasma was validated by qPCR. This method has great potential to be taken much further.

So far, the method has been used to measure gene expression of pre-selected targets by qPCR. According to manufacturer's guidelines, the pre-amplification step allows up to 50 targets to be measured so a natural extension of this work is to simply investigate additional genes.

A hypothesis-driven approach gives numerous options. One option is to measure the gene expression of targets implicated by GWAS (Lambert et al., 2013). However, the functional, disease-causing variants have not necessarily been identified with such studies. Furthermore, they individually have weak effect sizes that required large genetic studies to reach a genome-wide significant association and so the likelihood of detecting significant changes in gene expression is dubious without large sample sets. The hypothesis could be narrowed by changing the sample set or target set. For example, familial, early onset AD is driven by causal mutations in *APP, PSEN1* or *PSEN2* (Tanzi and Bertram, 2005) and whilst these primarily affect amyloidogenesis, the strong genetic component may be more likely to affect gene expression than a hypothesis involving common variants. Mutations in *TREM2, PLCG2* and *ABI3* have been implicated by exome studies so coding variants have been identified (Sims et al., 2017). Alternatively, the sample set could be narrowed by accounting for genetic background such as *APOE* genotype (Robinson et al., 2017) or polygenic risk score (Escott-Price et al., 2015, Escott-Price et al., 2017); or a clinical measurement of disease state

(Mendez and Cummings, 2003); or a grouping by clinically-used biomarkers (Jack and Holtzman, 2013). A combination of these could be to narrow the study down to individuals with a polygenic risk score calculated for a particular biological pathway, for example, endocytosis, cholesterol metabolism or immunity, and then measuring gene expression for targets relevant to that pathway.

Perhaps a better approach, with a view of discovering novel biomarkers, would be to adopt this method in a non-hypothesis driven study. Despite the challenge of a small quantity of starting material, this method has shown sensitivity to small exosomes dose changes and was able to detect gene expression changes in brain-enriched targets. The methodology of detecting gene expression was qPCR, which involves exponential amplification of the target (Harbison and Nguyen, 2017). Whilst there is an element of amplification in RNA sequencing library preparation, it is not to the same extent as qPCR. However, technologies have emerged for sequencing based on low sample input such as single cell genome (Navin et al., 2011, Nawy, 2014), chromatin capture (Ulianov et al., 2017) and transcriptome (See et al., 2017, Papalexi and Satija, 2017) sequencing. Whilst these studies are challenging, it has been reported that RNA sequencing data, of good quality, can be collected with as low an input as 50 pg (Shanker et al., 2015). This was within the input range of the RNA yields in this study that used 0.5 ml plasma to isolate exosomal-RNA. Therefore, with the technical limitations of sequencing low input samples having been lessened, this method, already validated by qPCR, should be used in the future for RNA sequencing. An unbiased, non-hypothesis driven study based on sequencing should prove to be a fruitful avenue of research, even with 0.5 ml plasma, as has been reported for higher volumes previously (Cheng et al., 2015, Lugli et al., 2015).

Currently, the identification of peripheral biomarkers of AD is very much in the early stages. As such, studies have largely aimed to distinguish AD cases from controls and occasionally included patients with Mild Cognitive Impairment (MCI). The ultimate aim must be to identify biomarkers of pre-clinical AD pathology, as it has been determined that the harmful events of Aβ deposition occur years before the cognitive deficits present in the clinic (Villemagne et al., 2013). Using neuro-imaging techniques, differences in scene perception and short-term memory have been observed in young, healthy adults who carry the *APOE* e4 allele, compared to non-carriers (Shine et al., 2015). Exosomes, as discussed previously, carry an RNA cargo that is sensitive to the state of the source cell and, consequently, would be suitable candidates for harbouring biomarkers in these pre-clinical stages. Therefore, the

future work described could well drive forward the pursuit of a peripherally available, pre-clinical biomarker of AD.

7.3 Concluding comments

This thesis has demonstrated the isolation and analysis of exosomal-RNA derived from cell cultures and biological fluids. The limitations and technical difficulties of both have been highlighted as methodologies have been developed. By analysing RNA enriched in exosomes, compared to source cells, it can be inferred that RNA is not entirely randomly sorted into exosomes. Indeed, this observation, with others in the literature, that exosomal-RNA is sensitive to the state of the source cell, makes exosomes excellent candidates for carrying biomarkers of AD.

Follow up studies using cultured cells could further illuminate the mechanisms involved in sorting RNA into exosomes, or the mechanisms perturbed in disease by AD-associated mutations, particularly, the exosome biogenesis/secretion pathway. It would not be a trivial undertaking, but adopting the method for isolating exosomal-RNA from biological fluids and applying it to RNA sequencing technologies is a potential broad route to identifying novel biomarkers of AD, and other diseases.

Bibliography

(HTTPS://WWW.ALZHEIMERS.ORG.UK/STATISTICS), A. S. S. 2015. *Statistics* [Online]. [Accessed October 15th 2015].

ABIEGA, O., BECCARI, S., DIAZ-APARICIO, I., NADJAR, A., LAYE, S., LEYROLLE, Q., GOMEZ-NICOLA, D., DOMERCQ, M., PEREZ-SAMARTIN, A., SANCHEZ-ZAFRA, V., PARIS, I., VALERO, J., SAVAGE, J. C., HUI, C. W., TREMBLAY, M. E., DEUDERO, J. J., BREWSTER, A. L., ANDERSON, A. E., ZALDUMBIDE, L., GALBARRIATU, L., MARINAS, A., VIVANCO, M., MATUTE, C., MALETIC-SAVATIC, M., ENCINAS, J. M. & SIERRA, A. 2016. Neuronal Hyperactivity Disturbs ATP Microgradients, Impairs Microglial Motility, and Reduces Phagocytic Receptor Expression Triggering Apoptosis/Microglial Phagocytosis Uncoupling. *PLoS Biol,* 14**,** e1002466.

ABRAMI, L., BRANDI, L., MOAYERI, M., BROWN, M. J., KRANTZ, B. A., LEPPLA, S. H. & VAN DER GOOT, F. G. 2013. Hijacking multivesicular bodies enables long-term and exosome-mediated long-distance action of anthrax toxin. *Cell Rep,* 5**,** 986-96.

ADMYRE, C., GRUNEWALD, J., THYBERG, J., GRIPENBACK, S., TORNLING, G., EKLUND, A., SCHEYNIUS, A. & GABRIELSSON, S. 2003. Exosomes with major histocompatibility complex class II and co-stimulatory molecules are present in human BAL fluid. *Eur Respir J,* 22**,** 578-83.

AHADI, A., BRENNAN, S., KENNEDY, P. J., HUTVAGNER, G. & TRAN, N. 2016a. Long non-coding RNAs harboring miRNA seed regions are enriched in prostate cancer exosomes. *Sci Rep,* 6**,** 24922.

AHADI, A., KHOURY, S., LOSSEVA, M. & TRAN, N. 2016b. A comparative analysis of lncRNAs in prostate cancer exosomes and their parental cell lines. *Genom Data,* 9**,** 7-9.

AKERS, J. C., RAMAKRISHNAN, V., NOLAN, J. P., DUGGAN, E., FU, C. C., HOCHBERG, F. H., CHEN, C. C. & CARTER, B. S. 2016. Comparative Analysis of Technologies for Quantifying Extracellular Vesicles (EVs) in Clinical Cerebrospinal Fluids (CSF). *PLoS One,* 11**,** e0149866.

AL-NEDAWI, K., MEEHAN, B., KERBEL, R. S., ALLISON, A. C. & RAK, J. 2009. Endothelial expression of autocrine VEGF upon the uptake of tumor-derived microvesicles containing oncogenic EGFR. *Proc Natl Acad Sci U S A,* 106**,** 3794-9.

AL-NEDAWI, K., MEEHAN, B., MICALLEF, J., LHOTAK, V., MAY, L., GUHA, A. & RAK, J. 2008. Intercellular transfer of the oncogenic receptor EGFRvIII by microvesicles derived from tumour cells. *Nat Cell Biol,* 10**,** 619-24.

ALVAREZ-ERVITI, L., SEOW, Y., YIN, H., BETTS, C., LAKHAL, S. & WOOD, M. J. A. 2011. Delivery of siRNA to the mouse brain by systemic injection of targeted exosomes. *Nat Biotech,* 29**,** 341-345.

ALZHEIMER, A., STELZMANN, R. A., SCHNITZLEIN, H. N. & MURTAGH, F. R. 1995. An English translation of Alzheimer's 1907 paper, "Uber eine eigenartige Erkankung der Hirnrinde". *Clin Anat,* 8**,** 429-31.

ANDRE, F., SCHARTZ, N. E., MOVASSAGH, M., FLAMENT, C., PAUTIER, P., MORICE, P., POMEL, C., LHOMME, C., ESCUDIER, B., LE CHEVALIER, T., TURSZ, T., AMIGORENA, S., RAPOSO, G., ANGEVIN, E. & ZITVOGEL, L. 2002. Malignant effusions and immunogenic tumour-derived exosomes. *Lancet,* 360**,** 295-305.

ARBER, C., LOVEJOY, C. & WRAY, S. 2017. Stem cell models of Alzheimer's disease: progress and challenges. *Alzheimers Res Ther,* 9**,** 42.

ARROYO, J. D., CHEVILLET, J. R., KROH, E. M., RUF, I. K., PRITCHARD, C. C., GIBSON, D. F., MITCHELL, P. S., BENNETT, C. F., POGOSOVA-AGADJANYAN, E. L., STIREWALT, D. L., TAIT, J. F. & TEWARI, M. 2011. Argonaute2 complexes carry a population of

circulating microRNAs independent of vesicles in human plasma. *Proc Natl Acad Sci U S A,* 108**,** 5003-8.

ASAI, H., IKEZU, S., TSUNODA, S., MEDALLA, M., LUEBKE, J., HAYDAR, T., WOLOZIN, B., BUTOVSKY, O., KUGLER, S. & IKEZU, T. 2015. Depletion of microglia and inhibition of exosome synthesis halt tau propagation. *Nat Neurosci,* 18**,** 1584-93.

ASAI, M., IWATA, N., YOSHIKAWA, A., AIZAKI, Y., ISHIURA, S., SAIDO, T. C. & MARUYAMA, K. 2007. Berberine alters the processing of Alzheimer's amyloid precursor protein to decrease Abeta secretion. *Biochem Biophys Res Commun,* 352**,** 498-502.

ASKEW, K. & GOMEZ-NICOLA, D. 2017. A story of birth and death: Insights into the formation and dynamics of the microglial population. *Brain Behav Immun*.

BABST, M. 2005. A protein's final ESCRT. *Traffic,* 6**,** 2-9.

BAJ-KRZYWORZEKA, M., SZATANEK, R., WEGLARCZYK, K., BARAN, J., URBANOWICZ, B., BRANSKI, P., RATAJCZAK, M. Z. & ZEMBALA, M. 2006. Tumour-derived microvesicles carry several surface determinants and mRNA of tumour cells and transfer some of these determinants to monocytes. *Cancer Immunol Immunother,* 55**,** 808-18.

BAJ-KRZYWORZEKA, M., SZATANEK, R., WEGLARCZYK, K., BARAN, J. & ZEMBALA, M. 2007. Tumour-derived microvesicles modulate biological activity of human monocytes. *Immunol Lett,* 113**,** 76-82.

BANG, C., BATKAI, S., DANGWAL, S., GUPTA, S. K., FOINQUINOS, A., HOLZMANN, A., JUST, A., REMKE, J., ZIMMER, K., ZEUG, A., PONIMASKIN, E., SCHMIEDL, A., YIN, X., MAYR, M., HALDER, R., FISCHER, A., ENGELHARDT, S., WEI, Y., SCHOBER, A., FIEDLER, J. & THUM, T. 2014. Cardiac fibroblast-derived microRNA passenger strand-enriched exosomes mediate cardiomyocyte hypertrophy. *J Clin Invest,* 124**,** 2136-46.

BARBERGER-GATEAU, P., RAFFAITIN, C., LETENNEUR, L., BERR, C., TZOURIO, C., DARTIGUES, J. F. & ALPEROVITCH, A. 2007. Dietary patterns and risk of dementia: the Three-City cohort study. *Neurology,* 69**,** 1921-30.

BARTEL, D. P. 2004. MicroRNAs: genomics, biogenesis, mechanism, and function. *Cell,* 116**,** 281-97.

BATAGOV, A. O., KUZNETSOV, V. A. & KUROCHKIN, I. V. 2011. Identification of nucleotide patterns enriched in secreted RNAs as putative cis-acting elements targeting them to exosome nano-vesicles. *BMC Genomics,* 12 Suppl 3**,** S18.

BATEMAN, R. J., XIONG, C., BENZINGER, T. L. S., FAGAN, A. M., GOATE, A., FOX, N. C., MARCUS, D. S., CAIRNS, N. J., XIE, X., BLAZEY, T. M., HOLTZMAN, D. M., SANTACRUZ, A., BUCKLES, V., OLIVER, A., MOULDER, K., AISEN, P. S., GHETTI, B., KLUNK, W. E., MCDADE, E., MARTINS, R. N., MASTERS, C. L., MAYEUX, R., RINGMAN, J. M., ROSSOR, M. N., SCHOFIELD, P. R., SPERLING, R. A., SALLOWAY, S. & MORRIS, J. C. 2012. Clinical and Biomarker Changes in Dominantly Inherited Alzheimer's Disease. *New England Journal of Medicine,* 367**,** 795-804.

BAUDIC, S., BARBA, G. D., THIBAUDET, M. C., SMAGGHE, A., REMY, P. & TRAYKOV, L. 2006. Executive function deficits in early Alzheimer's disease and their relations with episodic memory. *Arch Clin Neuropsychol,* 21**,** 15-21.

BAYER, T. A., CAPPAI, R., MASTERS, C. L., BEYREUTHER, K. & MULTHAUP, G. 1999. It all sticks together--the APP-related family of proteins and Alzheimer's disease. *Mol Psychiatry,* 4**,** 524-8.

BECKER, J. T., BOLLER, F., LOPEZ, O. L., SAXTON, J. & MCGONIGLE, K. L. 1994. The natural history of Alzheimer's disease. Description of study cohort and accuracy of diagnosis. *Arch Neurol,* 51**,** 585-94.

BECKETT, K., MONIER, S., PALMER, L., ALEXANDRE, C., GREEN, H., BONNEIL, E., RAPOSO, G., THIBAULT, P., LE BORGNE, R. & VINCENT, J. P. 2013. Drosophila S2 cells secrete wingless on exosome-like vesicles but the wingless gradient forms independently of exosomes. *Traffic,* 14**,** 82-96.

BEHRENDT, R. P. 1998. Underconstrained perception: a theoretical approach to the nature and function of verbal hallucinations. *Compr Psychiatry,* 39**,** 236-48.

BELLINGHAM, S. A., COLEMAN, B. M. & HILL, A. F. 2012. Small RNA deep sequencing reveals a distinct miRNA signature released in exosomes from prion-infected neuronal cells. *Nucleic Acids Res,* 40**,** 10937-49.

BENES, V., BLAKE, J. & DOYLE, K. 2011. Ribo-Zero Gold Kit: improved RNA-seq results after removal of cytoplasmic and mitochondrial ribosomal RNA. *Nat Meth,* 8.

BISHT, K., SHARMA, K. P., LECOURS, C., SANCHEZ, M. G., EL HAJJ, H., MILIOR, G., OLMOS-ALONSO, A., GOMEZ-NICOLA, D., LUHESHI, G., VALLIERES, L., BRANCHI, I., MAGGI, L., LIMATOLA, C., BUTOVSKY, O. & TREMBLAY, M. E. 2016. Dark microglia: A new phenotype predominantly associated with pathological states. *Glia,* 64**,** 826-39.

BLESSED, G., TOMLINSON, B. E. & ROTH, M. 1968. The association between quantitative measures of dementia and of senile change in the cerebral grey matter of elderly subjects. *Br J Psychiatry,* 114**,** 797-811.

BOBINSKI, M., DE LEON, M. J., CONVIT, A., DE SANTI, S., WEGIEL, J., TARSHISH, C. Y., SAINT LOUIS, L. A. & WISNIEWSKI, H. M. 1999. MRI of entorhinal cortex in mild Alzheimer's disease. *Lancet,* 353**,** 38-40.

BOBINSKI, M., DE LEON, M. J., WEGIEL, J., DESANTI, S., CONVIT, A., SAINT LOUIS, L. A., RUSINEK, H. & WISNIEWSKI, H. M. 2000. The histological validation of post mortem magnetic resonance imaging-determined hippocampal volume in Alzheimer's disease. *Neuroscience,* 95**,** 721-5.

BOBRIE, A., COLOMBO, M., KRUMEICH, S., RAPOSO, G. & THERY, C. 2012a. Diverse subpopulations of vesicles secreted by different intracellular mechanisms are present in exosome preparations obtained by differential ultracentrifugation. *J Extracell Vesicles,* 1.

BOBRIE, A., KRUMEICH, S., REYAL, F., RECCHI, C., MOITA, L. F., SEABRA, M. C., OSTROWSKI, M. & THERY, C. 2012b. Rab27a supports exosome-dependent and -independent mechanisms that modify the tumor microenvironment and can promote tumor progression. *Cancer Res,* 72**,** 4920-30.

BOSQUE, A., DIETZ, L., GALLEGO-LLEYDA, A., SANCLEMENTE, M., ITURRALDE, M., NAVAL, J., ALAVA, M. A., MARTINEZ-LOSTAO, L., THIERSE, H. J. & ANEL, A. 2016. Comparative proteomics of exosomes secreted by tumoral Jurkat T cells and normal human T cell blasts unravels a potential tumorigenic role for valosin-containing protein. *Oncotarget*.

BOUWMAN, F. H., SCHOONENBOOM, N. S., VERWEY, N. A., VAN ELK, E. J., KOK, A., BLANKENSTEIN, M. A., SCHELTENS, P. & VAN DER FLIER, W. M. 2009. CSF biomarker levels in early and late onset Alzheimer's disease. *Neurobiol Aging,* 30**,** 1895-901.

BOWERS, K., LOTTRIDGE, J., HELLIWELL, S. B., GOLDTHWAITE, L. M., LUZIO, J. P. & STEVENS, T. H. 2004. Protein-protein interactions of ESCRT complexes in the yeast Saccharomyces cerevisiae. *Traffic,* 5**,** 194-210.

BRACCO, L., GALLATO, R., GRIGOLETTO, F., LIPPI, A., LEPORE, V., BINO, G., LAZZARO, M. P., CARELLA, F., PICCOLO, T., POZZILLI, C. & ET AL. 1994. Factors affecting course and survival in Alzheimer's disease. A 9-year longitudinal study. *Arch Neurol,* 51**,** 1213-9.

BREWIS, I. A. & GADELLA, B. M. 2010. Sperm surface proteomics: from protein lists to biological function. *Mol Hum Reprod,* 16**,** 68-79.

BRITES, D. & VAZ, A. R. 2014. Microglia centered pathogenesis in ALS: insights in cell interconnectivity. *Frontiers in Cellular Neuroscience,* 8**,** 117.

BROCCOLI, V. 2017. Reprogramming of somatic cells: iPS and iN cells. *Prog Brain Res,* 230**,** 53-68.

BUERGER, K., EWERS, M., PIRTTILA, T., ZINKOWSKI, R., ALAFUZOFF, I., TEIPEL, S. J., DEBERNARDIS, J., KERKMAN, D., MCCULLOCH, C., SOININEN, H. & HAMPEL, H. 2006.

CSF phosphorylated tau protein correlates with neocortical neurofibrillary pathology in Alzheimer's disease. *Brain,* 129**,** 3035-41.

BURGOS, K., MALENICA, I., METPALLY, R., COURTRIGHT, A., RAKELA, B., BEACH, T., SHILL, H., ADLER, C., SABBAGH, M., VILLA, S., TEMBE, W., CRAIG, D. & VAN KEUREN-JENSEN, K. 2014. Profiles of extracellular miRNA in cerebrospinal fluid and serum from patients with Alzheimer's and Parkinson's diseases correlate with disease status and features of pathology. *PLoS One,* 9**,** e94839.

BURNS, A. 1992. Psychiatric phenomena in dementia of the Alzheimer type. *Int Psychogeriatr,* 4 Suppl 1**,** 43-54.

BURNS, A., JACOBY, R. & LEVY, R. 1990a. Psychiatric phenomena in Alzheimer's disease. I: Disorders of thought content. *Br J Psychiatry,* 157**,** 72-6, 92-4.

BURNS, A., JACOBY, R. & LEVY, R. 1990b. Psychiatric phenomena in Alzheimer's disease. II: Disorders of perception. *Br J Psychiatry,* 157**,** 76-81, 92-4.

BURNS, A., JACOBY, R. & LEVY, R. 1990c. Psychiatric phenomena in Alzheimer's disease. III: Disorders of mood. *Br J Psychiatry,* 157**,** 81-6, 92-4.

BURNS, A., JACOBY, R. & LEVY, R. 1990d. Psychiatric phenomena in Alzheimer's disease. IV: Disorders of behaviour. *Br J Psychiatry,* 157**,** 86-94.

BUTCHART, J., BROOK, L., HOPKINS, V., TEELING, J., PUNTENER, U., CULLIFORD, D., SHARPLES, R., SHARIF, S., MCFARLANE, B., RAYBOULD, R., THOMAS, R., PASSMORE, P., PERRY, V. H. & HOLMES, C. 2015. Etanercept in Alzheimer disease: A randomized, placebo-controlled, double-blind, phase 2 trial. *Neurology,* 84**,** 2161-8.

CABILI, M. N., TRAPNELL, C., GOFF, L., KOZIOL, M., TAZON-VEGA, B., REGEV, A. & RINN, J. L. 2011. Integrative annotation of human large intergenic noncoding RNAs reveals global properties and specific subclasses. *Genes Dev,* 25**,** 1915-27.

CABY, M. P., LANKAR, D., VINCENDEAU-SCHERRER, C., RAPOSO, G. & BONNEROT, C. 2005. Exosomal-like vesicles are present in human blood plasma. *Int Immunol,* 17**,** 879-87.

CAI, Z., YANG, F., YU, L., YU, Z., JIANG, L., WANG, Q., YANG, Y., WANG, L., CAO, X. & WANG, J. 2012. Activated T cell exosomes promote tumor invasion via Fas signaling pathway. *J Immunol,* 188**,** 5954-61.

CAMUSSI, G., DEREGIBUS, M. C., BRUNO, S., GRANGE, C., FONSATO, V. & TETTA, C. 2011. Exosome/microvesicle-mediated epigenetic reprogramming of cells. *Am J Cancer Res,* 1**,** 98-110.

CARAYON, K., CHAOUI, K., RONZIER, E., LAZAR, I., BERTRAND-MICHEL, J., ROQUES, V., BALOR, S., TERCE, F., LOPEZ, A., SALOME, L. & JOLY, E. 2011. Proteolipidic composition of exosomes changes during reticulocyte maturation. *J Biol Chem,* 286**,** 34426-39.

CARNINCI, P., KASUKAWA, T., KATAYAMA, S., GOUGH, J., FRITH, M. C., MAEDA, N., OYAMA, R., RAVASI, T., LENHARD, B., WELLS, C., KODZIUS, R., SHIMOKAWA, K., BAJIC, V. B., BRENNER, S. E., BATALOV, S., FORREST, A. R., ZAVOLAN, M., DAVIS, M. J., WILMING, L. G., AIDINIS, V., ALLEN, J. E., AMBESI-IMPIOMBATO, A., APWEILER, R., ATURALIYA, R. N., BAILEY, T. L., BANSAL, M., BAXTER, L., BEISEL, K. W., BERSANO, T., BONO, H., CHALK, A. M., CHIU, K. P., CHOUDHARY, V., CHRISTOFFELS, A., CLUTTERBUCK, D. R., CROWE, M. L., DALLA, E., DALRYMPLE, B. P., DE BONO, B., DELLA GATTA, G., DI BERNARDO, D., DOWN, T., ENGSTROM, P., FAGIOLINI, M., FAULKNER, G., FLETCHER, C. F., FUKUSHIMA, T., FURUNO, M., FUTAKI, S., GARIBOLDI, M., GEORGII-HEMMING, P., GINGERAS, T. R., GOJOBORI, T., GREEN, R. E., GUSTINCICH, S., HARBERS, M., HAYASHI, Y., HENSCH, T. K., HIROKAWA, N., HILL, D., HUMINIECKI, L., IACONO, M., IKEO, K., IWAMA, A., ISHIKAWA, T., JAKT, M., KANAPIN, A., KATOH, M., KAWASAWA, Y., KELSO, J., KITAMURA, H., KITANO, H., KOLLIAS, G., KRISHNAN, S. P., KRUGER, A., KUMMERFELD, S. K., KUROCHKIN, I. V., LAREAU, L. F., LAZAREVIC, D., LIPOVICH, L., LIU, J., LIUNI, S., MCWILLIAM, S., MADAN BABU, M., MADERA, M., MARCHIONNI, L., MATSUDA, H., MATSUZAWA, S., MIKI, H., MIGNONE, F., MIYAKE, S., MORRIS, K.,

MOTTAGUI-TABAR, S., MULDER, N., NAKANO, N., NAKAUCHI, H., NG, P., NILSSON, R., NISHIGUCHI, S., NISHIKAWA, S., et al. 2005. The transcriptional landscape of the mammalian genome. *Science,* 309**,** 1559-63.

CHANG, M., JONSSON, P. V., SNAEDAL, J., BJORNSSON, S., SACZYNSKI, J. S., ASPELUND, T., EIRIKSDOTTIR, G., JONSDOTTIR, M. K., LOPEZ, O. L., HARRIS, T. B., GUDNASON, V. & LAUNER, L. J. 2010. The effect of midlife physical activity on cognitive function among older adults: AGES--Reykjavik Study. *J Gerontol A Biol Sci Med Sci,* 65**,** 1369-74.

CHAPMAN, P. F., FALINSKA, A. M., KNEVETT, S. G. & RAMSAY, M. F. 2001. Genes, models and Alzheimer's disease. *Trends Genet,* 17**,** 254-61.

CHENG, L., DOECKE, J. D., SHARPLES, R. A., VILLEMAGNE, V. L., FOWLER, C. J., REMBACH, A., MARTINS, R. N., ROWE, C. C., MACAULAY, S. L., MASTERS, C. L. & HILL, A. F. 2015. Prognostic serum miRNA biomarkers associated with Alzheimer's disease shows concordance with neuropsychological and neuroimaging assessment. *Mol Psychiatry,* 20**,** 1188-96.

CHENG, L., QUEK, C. Y., SUN, X., BELLINGHAM, S. A. & HILL, A. F. 2013. The detection of microRNA associated with Alzheimer's disease in biological fluids using next-generation sequencing technologies. *Front Genet,* 4**,** 150.

CHENG, L., SHARPLES, R. A., SCICLUNA, B. J. & HILL, A. F. 2014. Exosomes provide a protective and enriched source of miRNA for biomarker profiling compared to intracellular and cell-free blood. *J Extracell Vesicles,* 3.

CHIVET, M., HEMMING, F., PERNET-GALLAY, K., FRABOULET, S. & SADOUL, R. 2012. Emerging role of neuronal exosomes in the central nervous system. *Front Physiol,* 3**,** 145.

CHOI, J. S., YOON, H. I., LEE, K. S., CHOI, Y. C., YANG, S. H., KIM, I. S. & CHO, Y. W. 2016. Exosomes from differentiating human skeletal muscle cells trigger myogenesis of stem cells and provide biochemical cues for skeletal muscle regeneration. *J Control Release,* 222**,** 107-15.

CLARK, C. M., SCHNEIDER, J. A., BEDELL, B. J., BEACH, T. G., BILKER, W. B., MINTUN, M. A., PONTECORVO, M. J., HEFTI, F., CARPENTER, A. P., FLITTER, M. L., KRAUTKRAMER, M. J., KUNG, H. F., COLEMAN, R. E., DORAISWAMY, P. M., FLEISHER, A. S., SABBAGH, M. N., SADOWSKY, C. H., REIMAN, E. P., ZEHNTNER, S. P. & SKOVRONSKY, D. M. 2011. Use of florbetapir-PET for imaging beta-amyloid pathology. *Jama,* 305**,** 275-83.

CLARK, C. M., TROJANOWSKI, J. Q. & LEE, M.-Y. L. 1997. Pharmacological treatment of Alzheimer's Disease: Molecular and Neurobiological Foundations. New York: Wiley-Liss.

CLAYTON, A., COURT, J., NAVABI, H., ADAMS, M., MASON, M. D., HOBOT, J. A., NEWMAN, G. R. & JASANI, B. 2001. Analysis of antigen presenting cell derived exosomes, based on immuno-magnetic isolation and flow cytometry. *J Immunol Methods,* 247**,** 163-74.

CLAYTON, A., MITCHELL, J. P., COURT, J., LINNANE, S., MASON, M. D. & TABI, Z. 2008. Human tumor-derived exosomes down-modulate NKG2D expression. *J Immunol,* 180**,** 7249-58.

CLAYTON, A., MITCHELL, J. P., COURT, J., MASON, M. D. & TABI, Z. 2007. Human tumor-derived exosomes selectively impair lymphocyte responses to interleukin-2. *Cancer Res,* 67**,** 7458-66.

CLAYTON, A., TURKES, A., DEWITT, S., STEADMAN, R., MASON, M. D. & HALLETT, M. B. 2004. Adhesion and signaling by B cell-derived exosomes: the role of integrins. *Faseb j,* 18**,** 977-9.

CLAYTON, A., TURKES, A., NAVABI, H., MASON, M. D. & TABI, Z. 2005. Induction of heat shock proteins in B-cell exosomes. *J Cell Sci,* 118**,** 3631-8.

CLEMENTI, M. E., TRINGALI, G., TRIGGIANI, D. & GIARDINA, B. 2015. Aloe arborescens Extract Protects IMR-32 Cells against Alzheimer Amyloid Beta Peptide via Inhibition of Radical Peroxide Production. *Nat Prod Commun,* 10**,** 1993-5.

COLEMAN, P., FEDEROFF, H. & KURLAN, R. 2004. A focus on the synapse for neuroprotection in Alzheimer disease and other dementias. *Neurology,* 63**,** 1155-62.

COLOMBO, M., MOITA, C., VAN NIEL, G., KOWAL, J., VIGNERON, J., BENAROCH, P., MANEL, N., MOITA, L. F., THERY, C. & RAPOSO, G. 2013. Analysis of ESCRT functions in exosome biogenesis, composition and secretion highlights the heterogeneity of extracellular vesicles. *J Cell Sci,* 126**,** 5553-65.

COLOMBO, M., RAPOSO, G. & THERY, C. 2014. Biogenesis, secretion, and intercellular interactions of exosomes and other extracellular vesicles. *Annu Rev Cell Dev Biol,* 30**,** 255-89.

COMAS-HERRERA, A., WITTENBERG, R., PICKARD, L. & KNAPP, M. 2007. Cognitive impairment in older people: future demand for long-term care services and the associated costs. *Int J Geriatr Psychiatry,* 22**,** 1037-45.

CONESA, A., MADRIGAL, P., TARAZONA, S., GOMEZ-CABRERO, D., CERVERA, A., MCPHERSON, A., SZCZESNIAK, M. W., GAFFNEY, D. J., ELO, L. L., ZHANG, X. & MORTAZAVI, A. 2016. A survey of best practices for RNA-seq data analysis. *Genome Biol,* 17**,** 13.

CONNOLLY, K. D., GUSCHINA, I. A., YEUNG, V., CLAYTON, A., DRAMAN, M. S., VON RUHLAND, C., LUDGATE, M., JAMES, P. E. & REES, D. A. 2015. Characterisation of adipocyte-derived extracellular vesicles released pre- and post-adipogenesis. *J Extracell Vesicles,* 4**,** 29159.

CORDER, E. H., SAUNDERS, A. M., STRITTMATTER, W. J., SCHMECHEL, D. E., GASKELL, P. C., SMALL, G. W., ROSES, A. D., HAINES, J. L. & PERICAK-VANCE, M. A. 1993. Gene dose of apolipoprotein E type 4 allele and the risk of Alzheimer's disease in late onset families. *Science,* 261**,** 921-3.

COSSETTI, C., SMITH, J. A., IRACI, N., LEONARDI, T., ALFARO-CERVELLO, C. & PLUCHINO, S. 2012. Extracellular membrane vesicles and immune regulation in the brain. *Front Physiol,* 3**,** 117.

CRESCITELLI, R., LASSER, C., SZABO, T. G., KITTEL, A., ELDH, M., DIANZANI, I., BUZAS, E. I. & LOTVALL, J. 2013. Distinct RNA profiles in subpopulations of extracellular vesicles: apoptotic bodies, microvesicles and exosomes. *J Extracell Vesicles,* 2.

CUI, Y., LUAN, J., LI, H., ZHOU, X. & HAN, J. 2016. Exosomes derived from mineralizing osteoblasts promote ST2 cell osteogenic differentiation by alteration of microRNA expression. *FEBS Lett,* 590**,** 185-92.

CUMMINGS, J. L. 2003. Alzheimer's disease: from molecular biology to neuropsychiatry. *Semin Clin Neuropsychiatry,* 8**,** 31-6.

CUMMINGS, J. L. & COLE, G. 2002. Alzheimer disease. *Jama,* 287**,** 2335-8.

CUMMINGS, J. L., VINTERS, H. V., COLE, G. M. & KHACHATURIAN, Z. S. 1998. Alzheimer's disease: etiologies, pathophysiology, cognitive reserve, and treatment opportunities. *Neurology,* 51**,** S2-17; discussion S65-7.

CUNHA, S., AMARAL, M. H., LOBO, J. M. & SILVA, A. C. 2016. Therapeutic Strategies for Alzheimer's and Parkinson's Diseases by Means of Drug Delivery Systems. *Curr Med Chem,* 23**,** 3618-3631.

DACHARY-PRIGENT, J., FREYSSINET, J. M., PASQUET, J. M., CARRON, J. C. & NURDEN, A. T. 1993. Annexin V as a probe of aminophospholipid exposure and platelet membrane vesiculation: a flow cytometry study showing a role for free sulfhydryl groups. *Blood,* 81**,** 2554-65.

DAS, U., SCOTT, D. A., GANGULY, A., KOO, E. H., TANG, Y. & ROY, S. 2013. Activity-induced convergence of APP and BACE-1 in acidic microdomains via an endocytosis-dependent pathway. *Neuron,* 79**,** 447-60.

DAW, E. W., PAYAMI, H., NEMENS, E. J., NOCHLIN, D., BIRD, T. D., SCHELLENBERG, G. D. & WIJSMAN, E. M. 2000. The number of trait loci in late-onset Alzheimer disease. *Am J Hum Genet,* 66**,** 196-204.

DE GASSART, A., GEMINARD, C., HOEKSTRA, D. & VIDAL, M. 2004. Exosome secretion: the art of reutilizing nonrecycled proteins? *Traffic,* 5**,** 896-903.

DE JONG, O. G., VERHAAR, M. C., CHEN, Y., VADER, P., GREMMELS, H., POSTHUMA, G., SCHIFFELERS, R. M., GUCEK, M. & VAN BALKOM, B. W. 2012. Cellular stress conditions are reflected in the protein and RNA content of endothelial cell-derived exosomes. *J Extracell Vesicles,* 1.

DE LEON, M. J., CONVIT, A., DESANTI, S., BOBINSKI, M., GEORGE, A. E., WISNIEWSKI, H. M., RUSINEK, H., CARROLL, R. & SAINT LOUIS, L. A. 1997. Contribution of structural neuroimaging to the early diagnosis of Alzheimer's disease. *Int Psychogeriatr,* 9 Suppl 1**,** 183-90; discussion 247-52.

DE ROECK, A., VAN DEN BOSSCHE, T., VAN DER ZEE, J., VERHEIJEN, J., DE COSTER, W., VAN DONGEN, J., DILLEN, L., BARADARAN-HERAVI, Y., HEEMAN, B., SANCHEZ-VALLE, R., LLADO, A., NACMIAS, B., SORBI, S., GELPI, E., GRAU-RIVERA, O., GOMEZ-TORTOSA, E., PASTOR, P., ORTEGA-CUBERO, S., PASTOR, M. A., GRAFF, C., THONBERG, H., BENUSSI, L., GHIDONI, R., BINETTI, G., DE MENDONCA, A., MARTINS, M., BORRONI, B., PADOVANI, A., ALMEIDA, M. R., SANTANA, I., DIEHL-SCHMID, J., ALEXOPOULOS, P., CLARIMON, J., LLEO, A., FORTEA, J., TSOLAKI, M., KOUTROUMANI, M., MATEJ, R., ROHAN, Z., DE DEYN, P., ENGELBORGHS, S., CRAS, P., VAN BROECKHOVEN, C. & SLEEGERS, K. 2017. Deleterious ABCA7 mutations and transcript rescue mechanisms in early onset Alzheimer's disease. *Acta Neuropathol*.

DE SANTA, F., BAROZZI, I., MIETTON, F., GHISLETTI, S., POLLETTI, S., TUSI, B. K., MULLER, H., RAGOUSSIS, J., WEI, C. L. & NATOLI, G. 2010. A large fraction of extragenic RNA pol II transcription sites overlap enhancers. *PLoS Biol,* 8**,** e1000384.

DEDDENS, J. C., VRIJSEN, K. R., COLIJN, J. M., OERLEMANS, M. I., METZ, C. H., VAN DER VLIST, E. J., NOLTE-'T HOEN, E. N., DEN OUDEN, K., JANSEN OF LORKEERS, S. J., VAN DER SPOEL, T. I., KOUDSTAAL, S., ARKESTEIJN, G. J., WAUBEN, M. H., VAN LAAKE, L. W., DOEVENDANS, P. A., CHAMULEAU, S. A. & SLUIJTER, J. P. 2016. Circulating Extracellular Vesicles Contain miRNAs and are Released as Early Biomarkers for Cardiac Injury. *J Cardiovasc Transl Res,* 9**,** 291-301.

DEL CONDE, I., SHRIMPTON, C. N., THIAGARAJAN, P. & LOPEZ, J. A. 2005. Tissue-factor-bearing microvesicles arise from lipid rafts and fuse with activated platelets to initiate coagulation. *Blood,* 106**,** 1604-11.

DESAI, A. K. & GROSSBERG, G. T. 2005. Diagnosis and treatment of Alzheimer's disease. *Neurology,* 64**,** S34-9.

DESIKAN, R. S., CABRAL, H. J., HESS, C. P., DILLON, W. P., GLASTONBURY, C. M., WEINER, M. W., SCHMANSKY, N. J., GREVE, D. N., SALAT, D. H., BUCKNER, R. L. & FISCHL, B. 2009. Automated MRI measures identify individuals with mild cognitive impairment and Alzheimer's disease. *Brain,* 132**,** 2048-57.

DEVORE, E. E., GRODSTEIN, F., VAN ROOIJ, F. J., HOFMAN, A., STAMPFER, M. J., WITTEMAN, J. C. & BRETELER, M. M. 2010. Dietary antioxidants and long-term risk of dementia. *Arch Neurol,* 67**,** 819-25.

DICKERSON, B. C. & WOLK, D. A. 2012. MRI cortical thickness biomarker predicts AD-like CSF and cognitive decline in normal adults. *Neurology,* 78**,** 84-90.

DONG, H., LI, J., HUANG, L., CHEN, X., LI, D., WANG, T., HU, C., XU, J., ZHANG, C., ZEN, K., XIAO, S., YAN, Q., WANG, C. & ZHANG, C. Y. 2015. Serum MicroRNA Profiles Serve as Novel Biomarkers for the Diagnosis of Alzheimer's Disease. *Dis Markers,* 2015**,** 625659.

DOU, Y., CHA, D. J., FRANKLIN, J. L., HIGGINBOTHAM, J. N., JEPPESEN, D. K., WEAVER, A. M., PRASAD, N., LEVY, S., COFFEY, R. J., PATTON, J. G. & ZHANG, B. 2016. Circular RNAs are down-regulated in KRAS mutant colon cancer cells and can be transferred to exosomes. *Sci Rep,* 6**,** 37982.

DRZEZGA, A. 2010. Amyloid-plaque imaging in early and differential diagnosis of dementia. *Ann Nucl Med,* 24**,** 55-66.

DUIJVESZ, D., LUIDER, T., BANGMA, C. H. & JENSTER, G. 2011. Exosomes as biomarker treasure chests for prostate cancer. *Eur Urol,* 59**,** 823-31.

DUIJVESZ, D., VERSLUIS, C. Y., VAN DER FELS, C. A., VREDENBREGT-VAN DEN BERG, M. S., LEIVO, J., PELTOLA, M. T., BANGMA, C. H., PETTERSSON, K. S. & JENSTER, G. 2015. Immuno-based detection of extracellular vesicles in urine as diagnostic marker for prostate cancer. *Int J Cancer*.

EIKREM, O., BEISLAND, C., HJELLE, K., FLATBERG, A., SCHERER, A., LANDOLT, L., SKOGSTRAND, T., LEH, S., BEISVAG, V. & MARTI, H.-P. 2016. Transcriptome Sequencing (RNAseq) Enables Utilization of Formalin-Fixed, Paraffin-Embedded Biopsies with Clear Cell Renal Cell Carcinoma for Exploration of Disease Biology and Biomarker Development. *PLoS ONE,* 11**,** e0149743.

EISENBERG, E. & LEVANON, E. Y. 2013. Human housekeeping genes, revisited. *Trends Genet,* 29**,** 569-74.

EL ANDALOUSSI, S., MAGER, I., BREAKEFIELD, X. O. & WOOD, M. J. A. 2013. Extracellular vesicles: biology and emerging therapeutic opportunities. *Nat Rev Drug Discov,* 12**,** 347-357.

ELDH, M., EKSTROM, K., VALADI, H., SJOSTRAND, M., OLSSON, B., JERNAS, M. & LOTVALL, J. 2010. Exosomes communicate protective messages during oxidative stress; possible role of exosomal shuttle RNA. *PLoS One,* 5**,** e15353.

ENDERLE, D., SPIEL, A., COTICCHIA, C. M., BERGHOFF, E., MUELLER, R., SCHLUMPBERGER, M., SPRENGER-HAUSSELS, M., SHAFFER, J. M., LADER, E., SKOG, J. & NOERHOLM, M. 2015. Characterization of RNA from Exosomes and Other Extracellular Vesicles Isolated by a Novel Spin Column-Based Method. *PLoS One,* 10**,** e0136133.

ESCOLA, J. M., KLEIJMEER, M. J., STOORVOGEL, W., GRIFFITH, J. M., YOSHIE, O. & GEUZE, H. J. 1998. Selective enrichment of tetraspan proteins on the internal vesicles of multivesicular endosomes and on exosomes secreted by human B-lymphocytes. *J Biol Chem,* 273**,** 20121-7.

ESCOTT-PRICE, V., MYERS, A. J., HUENTELMAN, M. & HARDY, J. 2017. Polygenic Risk Score Analysis of Pathologically Confirmed Alzheimer's Disease. *Ann Neurol*.

ESCOTT-PRICE, V., SIMS, R., BANNISTER, C., HAROLD, D., VRONSKAYA, M., MAJOUNIE, E., BADARINARAYAN, N., MORGAN, K., PASSMORE, P., HOLMES, C., POWELL, J., BRAYNE, C., GILL, M., MEAD, S., GOATE, A., CRUCHAGA, C., LAMBERT, J. C., VAN DUIJN, C., MAIER, W., RAMIREZ, A., HOLMANS, P., JONES, L., HARDY, J., SESHADRI, S., SCHELLENBERG, G. D., AMOUYEL, P. & WILLIAMS, J. 2015. Common polygenic variation enhances risk prediction for Alzheimer's disease. *Brain,* 138**,** 3673-84.

FADER, C. M., SANCHEZ, D. G., MESTRE, M. B. & COLOMBO, M. I. 2009. TI-VAMP/VAMP7 and VAMP3/cellubrevin: two v-SNARE proteins involved in specific steps of the autophagy/multivesicular body pathways. *Biochim Biophys Acta,* 1793**,** 1901-16.

FAGAN, A. M., HEAD, D., SHAH, A. R., MARCUS, D., MINTUN, M., MORRIS, J. C. & HOLTZMAN, D. M. 2009. Decreased cerebrospinal fluid Abeta(42) correlates with brain atrophy in cognitively normal elderly. *Ann Neurol,* 65**,** 176-83.

FAGAN, A. M., MINTUN, M. A., MACH, R. H., LEE, S. Y., DENCE, C. S., SHAH, A. R., LAROSSA, G. N., SPINNER, M. L., KLUNK, W. E., MATHIS, C. A., DEKOSKY, S. T., MORRIS, J. C. & HOLTZMAN, D. M. 2006. Inverse relation between in vivo amyloid imaging load and cerebrospinal fluid Abeta42 in humans. *Ann Neurol,* 59**,** 512-9.

FAGAN, A. M., ROE, C. M., XIONG, C., MINTUN, M. A., MORRIS, J. C. & HOLTZMAN, D. M. 2007. Cerebrospinal fluid tau/beta-amyloid(42) ratio as a prediction of cognitive decline in nondemented older adults. *Arch Neurol,* 64**,** 343-9.

FAISON, W. E. 2005. Formulating a clinical practice care plan for the diagnosis and assessment of Alzheimer's disease. *CNS Spectr,* 10**,** 10-2.

FENG, X., BAI, Z., WANG, J., XIE, B., SUN, J., HAN, G., SONG, F., CRACK, P. J., DUAN, Y. & LEI, H. 2014. Robust gene dysregulation in Alzheimer's disease brains. *J Alzheimers Dis,* 41**,** 587-97.

FEVRIER, B., VILETTE, D., ARCHER, F., LOEW, D., FAIGLE, W., VIDAL, M., LAUDE, H. & RAPOSO, G. 2004. Cells release prions in association with exosomes. *Proc Natl Acad Sci U S A,* 101**,** 9683-8.

FIANDACA, M. S., KAPOGIANNIS, D., MAPSTONE, M., BOXER, A., EITAN, E., SCHWARTZ, J. B., ABNER, E. L., PETERSEN, R. C., FEDEROFF, H. J., MILLER, B. L. & GOETZL, E. J. 2015. Identification of preclinical Alzheimer's disease by a profile of pathogenic proteins in neurally derived blood exosomes: A case-control study. *Alzheimer's & Dementia,* 11**,** 600-607.e1.

FIEDLER, J., BRECKWOLDT, K., REMMELE, C. W., HARTMANN, D., DITTRICH, M., PFANNE, A., JUST, A., XIAO, K., KUNZ, M., MULLER, T., HANSEN, A., GEFFERS, R., DANDEKAR, T., ESCHENHAGEN, T. & THUM, T. 2015. Development of Long Noncoding RNA-Based Strategies to Modulate Tissue Vascularization. *J Am Coll Cardiol,* 66**,** 2005-15.

FIORELLI, T., KIROUAC, L. & PADMANABHAN, J. 2013. Altered processing of amyloid precursor protein in cells undergoing apoptosis. *PLoS One,* 8**,** e57979.

FLEISHER, A. S., CHEN, K., LIU, X., ROONTIVA, A., THIYYAGURA, P., AYUTYANONT, N., JOSHI, A. D., CLARK, C. M., MINTUN, M. A., PONTECORVO, M. J., DORAISWAMY, P. M., JOHNSON, K. A., SKOVRONSKY, D. M. & REIMAN, E. M. 2011. Using positron emission tomography and florbetapir F18 to image cortical amyloid in patients with mild cognitive impairment or dementia due to Alzheimer disease. *Arch Neurol,* 68**,** 1404-11.

FORMAN, M. S., TROJANOWSKI, J. Q. & LEE, V. M. 2004. Neurodegenerative diseases: a decade of discoveries paves the way for therapeutic breakthroughs. *Nat Med,* 10**,** 1055-63.

FOY, C. M., NICHOLAS, H., HOLLINGWORTH, P., BOOTHBY, H., WILLAMS, J., BROWN, R. G., AL-SARRAJ, S. & LOVESTONE, S. 2007. Diagnosing Alzheimer's disease--non-clinicians and computerised algorithms together are as accurate as the best clinical practice. *Int J Geriatr Psychiatry,* 22**,** 1154-63.

FRENETTE, G., LESSARD, C. & SULLIVAN, R. 2002. Selected proteins of "prostasome-like particles" from epididymal cauda fluid are transferred to epididymal caput spermatozoa in bull. *Biol Reprod,* 67**,** 308-13.

FRUHBEIS, C., FROHLICH, D. & KRAMER-ALBERS, E. M. 2012. Emerging roles of exosomes in neuron-glia communication. *Front Physiol,* 3**,** 119.

FRUHBEIS, C., FROHLICH, D., KUO, W. P., AMPHORNRAT, J., THILEMANN, S., SAAB, A. S., KIRCHHOFF, F., MOBIUS, W., GOEBBELS, S., NAVE, K. A., SCHNEIDER, A., SIMONS, M., KLUGMANN, M., TROTTER, J. & KRAMER-ALBERS, E. M. 2013. Neurotransmitter-triggered transfer of exosomes mediates oligodendrocyte-neuron communication. *PLoS Biol,* 11**,** e1001604.

GAHL, W. A. & HUIZING, M. 1993. Hermansky-Pudlak Syndrome. *In: GeneReviews.* Seattle (WA).

GALAZKA, G., MYCKO, M. P., SELMAJ, I., RAINE, C. S. & SELMAJ, K. W. 2017. Multiple sclerosis: Serum-derived exosomes express myelin proteins. *Mult Scler***,** 1352458517696597.

GALIMBERTI, D., VILLA, C., FENOGLIO, C., SERPENTE, M., GHEZZI, L., CIOFFI, S. M., ARIGHI, A., FUMAGALLI, G. & SCARPINI, E. 2014. Circulating miRNAs as potential biomarkers in Alzheimer's disease. *J Alzheimers Dis,* 42**,** 1261-7.

GALLO, A., VELLA, S., MIELE, M., TIMONERI, F., DI BELLA, M., BOSI, S., SCIVERES, M. & CONALDI, P. G. 2017. Global profiling of viral and cellular non-coding RNAs in Epstein-

Barr virus-induced lymphoblastoid cell lines and released exosome cargos. *Cancer Lett,* 388**,** 334-343.

GARCIA, N. A., MONCAYO-ARLANDI, J., SEPULVEDA, P. & DIEZ-JUAN, A. 2015. Cardiomyocyte exosomes regulate glycolytic flux in endothelium by direct transfer of GLUT transporters and glycolytic enzymes. *Cardiovasc Res*.

GASPARD, N., BOUSCHET, T., HOUREZ, R., DIMIDSCHSTEIN, J., NAEIJE, G., VAN DEN AMEELE, J., ESPUNY-CAMACHO, I., HERPOEL, A., PASSANTE, L., SCHIFFMANN, S. N., GAILLARD, A. & VANDERHAEGHEN, P. 2008. An intrinsic mechanism of corticogenesis from embryonic stem cells. *Nature,* 455**,** 351-7.

GATTI, S., BRUNO, S., DEREGIBUS, M. C., SORDI, A., CANTALUPPI, V., TETTA, C. & CAMUSSI, G. 2011. Microvesicles derived from human adult mesenchymal stem cells protect against ischaemia-reperfusion-induced acute and chronic kidney injury. *Nephrol Dial Transplant,* 26**,** 1474-83.

GEARING, M., MIRRA, S. S., HEDREEN, J. C., SUMI, S. M., HANSEN, L. A. & HEYMAN, A. 1995. The Consortium to Establish a Registry for Alzheimer's Disease (CERAD). Part X. Neuropathology confirmation of the clinical diagnosis of Alzheimer's disease. *Neurology,* 45**,** 461-6.

GEEKIYANAGE, H., JICHA, G. A., NELSON, P. T. & CHAN, C. 2012. Blood serum miRNA: non-invasive biomarkers for Alzheimer's disease. *Exp Neurol,* 235**,** 491-6.

GIBBINGS, D., LEBLANC, P., JAY, F., PONTIER, D., MICHEL, F., SCHWAB, Y., ALAIS, S., LAGRANGE, T. & VOINNET, O. 2012. Human prion protein binds Argonaute and promotes accumulation of microRNA effector complexes. *Nat Struct Mol Biol,* 19**,** 517-24, s1.

GIBBINGS, D. J., CIAUDO, C., ERHARDT, M. & VOINNET, O. 2009. Multivesicular bodies associate with components of miRNA effector complexes and modulate miRNA activity. *Nat Cell Biol,* 11**,** 1143-9.

GOATE, A., CHARTIER-HARLIN, M. C., MULLAN, M., BROWN, J., CRAWFORD, F., FIDANI, L., GIUFFRA, L., HAYNES, A., IRVING, N., JAMES, L. & ET AL. 1991. Segregation of a missense mutation in the amyloid precursor protein gene with familial Alzheimer's disease. *Nature,* 349**,** 704-6.

GOBBO, J., MARCION, G., CORDONNIER, M., DIAS, A. M., PERNET, N., HAMMANN, A., RICHAUD, S., MJAHED, H., ISAMBERT, N., CLAUSSE, V., REBE, C., BERTAUT, A., GOUSSOT, V., LIRUSSI, F., GHIRINGHELLI, F., DE THONEL, A., FUMOLEAU, P., SEIGNEURIC, R. & GARRIDO, C. 2016. Restoring Anticancer Immune Response by Targeting Tumor-Derived Exosomes With a HSP70 Peptide Aptamer. *J Natl Cancer Inst,* 108.

GOETZL, E. J., BOXER, A., SCHWARTZ, J. B., ABNER, E. L., PETERSEN, R. C., MILLER, B. L., CARLSON, O. D., MUSTAPIC, M. & KAPOGIANNIS, D. 2015a. Low neural exosomal levels of cellular survival factors in Alzheimer's disease. *Ann Clin Transl Neurol,* 2**,** 769-73.

GOETZL, E. J., BOXER, A., SCHWARTZ, J. B., ABNER, E. L., PETERSEN, R. C., MILLER, B. L. & KAPOGIANNIS, D. 2015b. Altered lysosomal proteins in neural-derived plasma exosomes in preclinical Alzheimer disease. *Neurology,* 85**,** 40-7.

GOMEZ-NICOLA, D. & PERRY, V. H. 2014. Microglial Dynamics and Role in the Healthy and Diseased Brain. *The Neuroscientist,* 21**,** 169-184.

GOURAS, G. K., XU, H., JOVANOVIC, J. N., BUXBAUM, J. D., WANG, R., GREENGARD, P., RELKIN, N. R. & GANDY, S. 1998. Generation and regulation of beta-amyloid peptide variants by neurons. *J Neurochem,* 71**,** 1920-5.

GRAD, L. I., POKRISHEVSKY, E., SILVERMAN, J. M. & CASHMAN, N. R. 2014. Exosome-dependent and independent mechanisms are involved in prion-like transmission of propagated Cu/Zn superoxide dismutase misfolding. *Prion,* 8**,** 331-335.

GRAY, W. D., FRENCH, K. M., GHOSH-CHOUDHARY, S., MAXWELL, J. T., BROWN, M. E., PLATT, M. O., SEARLES, C. D. & DAVIS, M. E. 2015. Identification of therapeutic covariant microRNA clusters in hypoxia-treated cardiac progenitor cell exosomes using systems biology. *Circ Res,* 116**,** 255-63.

GREEN, T. M., ALPAUGH, M. L., BARSKY, S. H., RAPPA, G. & LORICO, A. 2015. Breast Cancer-Derived Extracellular Vesicles: Characterization and Contribution to the Metastatic Phenotype. *Biomed Res Int,* 2015**,** 634865.

GUERREIRO, R., WOJTAS, A., BRAS, J., CARRASQUILLO, M., ROGAEVA, E., MAJOUNIE, E., CRUCHAGA, C., SASSI, C., KAUWE, J. S., YOUNKIN, S., HAZRATI, L., COLLINGE, J., POCOCK, J., LASHLEY, T., WILLIAMS, J., LAMBERT, J. C., AMOUYEL, P., GOATE, A., RADEMAKERS, R., MORGAN, K., POWELL, J., ST GEORGE-HYSLOP, P., SINGLETON, A. & HARDY, J. 2013. TREM2 variants in Alzheimer's disease. *N Engl J Med,* 368**,** 117-27.

GUPTA, A. & PULLIAM, L. 2014. Exosomes as mediators of neuroinflammation. *J Neuroinflammation,* 11**,** 68.

GUTTMAN, M., DONAGHEY, J., CAREY, B. W., GARBER, M., GRENIER, J. K., MUNSON, G., YOUNG, G., LUCAS, A. B., ACH, R., BRUHN, L., YANG, X., AMIT, I., MEISSNER, A., REGEV, A., RINN, J. L., ROOT, D. E. & LANDER, E. S. 2011. lincRNAs act in the circuitry controlling pluripotency and differentiation. *Nature,* 477**,** 295-300.

GÓMEZ-NICOLA, D., FRANSEN, N. L., SUZZI, S. & PERRY, V. H. 2013. Regulation of Microglial Proliferation during Chronic Neurodegeneration. *The Journal of Neuroscience,* 33**,** 2481.

HAASS, C., SCHLOSSMACHER, M. G., HUNG, A. Y., VIGO-PELFREY, C., MELLON, A., OSTASZEWSKI, B. L., LIEBERBURG, I., KOO, E. H., SCHENK, D., TEPLOW, D. B. & ET AL. 1992. Amyloid beta-peptide is produced by cultured cells during normal metabolism. *Nature,* 359**,** 322-5.

HAILE, S., CORBETT, R. D., MACLEOD, T., BILOBRAM, S., SMAILUS, D., TSAO, P., KIRK, H., MCDONALD, H., PANDOH, P., BALA, M., HIRST, M., MILLER, D., MOORE, R. A., MUNGALL, A. J., SCHEIN, J., COOPE, R. J., MA, Y., ZHAO, Y., HOLT, R. A., JONES, S. J. & MARRA, M. A. 2017. Increasing quality, throughput and speed of sample preparation for strand-specific messenger RNA sequencing. *BMC Genomics,* 18**,** 515.

HAMLETT, E. D., GOETZL, E. J., LEDREUX, A., VASILEVKO, V., BOGER, H. A., LAROSA, A., CLARK, D., CARROLL, S. L., CARMONA IRAGUI, M., FORTEA, J., MUFSON, E. J., SABBAGH, M., MOHAMMED, A. H., HARTLEY, D., DORAN, E., LOTT, I. T. & GRANHOLM, A. C. 2016. Neuronal exosomes reveal Alzheimer's disease biomarkers in Down syndrome. *Alzheimers Dement*.

HARBISON, A. M. & NGUYEN, J. N. T. 2017. PCR: Identification of Genetic Polymorphisms. *Methods Mol Biol,* 1606**,** 193-203.

HARDING, C., HEUSER, J. & STAHL, P. 1983. Receptor-mediated endocytosis of transferrin and recycling of the transferrin receptor in rat reticulocytes. *J Cell Biol,* 97**,** 329-39.

HARDING, C., HEUSER, J. & STAHL, P. 1984. Endocytosis and intracellular processing of transferrin and colloidal gold-transferrin in rat reticulocytes: demonstration of a pathway for receptor shedding. *Eur J Cell Biol,* 35**,** 256-63.

HARDING, C. V., COLLINS, D. S., SLOT, J. W., GEUZE, H. J. & UNANUE, E. R. 1991. Liposome-encapsulated antigens are processed in lysosomes, recycled, and presented to T cells. *Cell,* 64**,** 393-401.

HARDING, C. V., HEUSER, J. E. & STAHL, P. D. 2013. Exosomes: Looking back three decades and into the future. *The Journal of Cell Biology,* 200**,** 367-371.

HAROLD, D., ABRAHAM, R., HOLLINGWORTH, P., SIMS, R., GERRISH, A., HAMSHERE, M. L., PAHWA, J. S., MOSKVINA, V., DOWZELL, K., WILLIAMS, A., JONES, N., THOMAS, C., STRETTON, A., MORGAN, A. R., LOVESTONE, S., POWELL, J., PROITSI, P., LUPTON, M. K., BRAYNE, C., RUBINSZTEIN, D. C., GILL, M., LAWLOR, B., LYNCH, A., MORGAN, K.,

BROWN, K. S., PASSMORE, P. A., CRAIG, D., MCGUINNESS, B., TODD, S., HOLMES, C., MANN, D., SMITH, A. D., LOVE, S., KEHOE, P. G., HARDY, J., MEAD, S., FOX, N., ROSSOR, M., COLLINGE, J., MAIER, W., JESSEN, F., SCHURMANN, B., HEUN, R., VAN DEN BUSSCHE, H., HEUSER, I., KORNHUBER, J., WILTFANG, J., DICHGANS, M., FROLICH, L., HAMPEL, H., HULL, M., RUJESCU, D., GOATE, A. M., KAUWE, J. S., CRUCHAGA, C., NOWOTNY, P., MORRIS, J. C., MAYO, K., SLEEGERS, K., BETTENS, K., ENGELBORGHS, S., DE DEYN, P. P., VAN BROECKHOVEN, C., LIVINGSTON, G., BASS, N. J., GURLING, H., MCQUILLIN, A., GWILLIAM, R., DELOUKAS, P., AL-CHALABI, A., SHAW, C. E., TSOLAKI, M., SINGLETON, A. B., GUERREIRO, R., MUHLEISEN, T. W., NOTHEN, M. M., MOEBUS, S., JOCKEL, K. H., KLOPP, N., WICHMANN, H. E., CARRASQUILLO, M. M., PANKRATZ, V. S., YOUNKIN, S. G., HOLMANS, P. A., O'DONOVAN, M., OWEN, M. J. & WILLIAMS, J. 2009. Genome-wide association study identifies variants at CLU and PICALM associated with Alzheimer's disease. *Nat Genet,* 41**,** 1088-93.

HAUW, J. & DUYCKAERTS, C. 2001. Pathology of the Aging Human Nervous System. New York: Oxford University Press.

HAYAKAWA, K., SAKAMOTO, Y., KANIE, O., OHTAKE, A., DAIKOKU, S., ITO, Y. & SHIOTA, K. 2017. Reactivation of hyperglycemia-induced hypocretin (HCRT) gene silencing by N-acetyl-d-mannosamine in the orexin neurons derived from human iPS cells. *Epigenetics***,** 0.

HEIJNEN, H. F., SCHIEL, A. E., FIJNHEER, R., GEUZE, H. J. & SIXMA, J. J. 1999. Activated platelets release two types of membrane vesicles: microvesicles by surface shedding and exosomes derived from exocytosis of multivesicular bodies and alpha-granules. *Blood,* 94**,** 3791-9.

HICKMAN, S. E., KINGERY, N. D., OHSUMI, T. K., BOROWSKY, M. L., WANG, L.-C., MEANS, T. K. & EL KHOURY, J. 2013. The microglial sensome revealed by direct RNA sequencing. *Nat Neurosci,* 16**,** 1896-1905.

HILL, A. F., PEGTEL, D. M., LAMBERTZ, U., LEONARDI, T., O'DRISCOLL, L., PLUCHINO, S., TER-OVANESYAN, D. & NOLTE-'T HOEN, E. N. 2013. ISEV position paper: extracellular vesicle RNA analysis and bioinformatics. *J Extracell Vesicles,* 2.

HIRSOVA, P., IBRAHIM, S. H., KRISHNAN, A., VERMA, V. K., BRONK, S. F., WERNEBURG, N. W., CHARLTON, M. R., SHAH, V. H., MALHI, H. & GORES, G. J. 2016. Lipid-induced Signaling Causes Release of Inflammatory Extracellular Vesicles from Hepatocytes. *Gastroenterology*.

HOCKEMEYER, D. & JAENISCH, R. 2016. Induced Pluripotent Stem Cells Meet Genome Editing. *Cell Stem Cell,* 18**,** 573-86.

HOFFMANN, T. J., VAN DEN EEDEN, S. K., SAKODA, L. C., JORGENSON, E., HABEL, L. A., GRAFF, R. E., PASSARELLI, M. N., CARIO, C. L., EMAMI, N. C., CHAO, C. R., GHAI, N. R., SHAN, J., RANATUNGA, D. K., QUESENBERRY, C. P., AARONSON, D., PRESTI, J., ZHAOMING, W., BERNDT, S. I., CHANOCK, S. J., MCDONNELL, S. K., FRENCH, A. J., SCHAID, D. J., THIBODEAU, S. N., LI, Q., FREEDMAN, M. L., PENNEY, K. L., MUCCI, L. A., HAIMAN, C. A., HENDERSON, B. E., SEMINARA, D., KVALE, M. N., KWOK, P.-Y., SCHAEFER, C., RISCH, N. & WITTE, J. S. 2015. A large multi-ethnic genome-wide association study of prostate cancer identifies novel risk variants and substantial ethnic differences. *Cancer discovery,* 5**,** 878-891.

HOLLINGWORTH, P., HAROLD, D., SIMS, R., GERRISH, A., LAMBERT, J. C., CARRASQUILLO, M. M., ABRAHAM, R., HAMSHERE, M. L., PAHWA, J. S., MOSKVINA, V., DOWZELL, K., JONES, N., STRETTON, A., THOMAS, C., RICHARDS, A., IVANOV, D., WIDDOWSON, C., CHAPMAN, J., LOVESTONE, S., POWELL, J., PROITSI, P., LUPTON, M. K., BRAYNE, C., RUBINSZTEIN, D. C., GILL, M., LAWLOR, B., LYNCH, A., BROWN, K. S., PASSMORE, P. A., CRAIG, D., MCGUINNESS, B., TODD, S., HOLMES, C., MANN, D., SMITH, A. D.,

BEAUMONT, H., WARDEN, D., WILCOCK, G., LOVE, S., KEHOE, P. G., HOOPER, N. M., VARDY, E. R., HARDY, J., MEAD, S., FOX, N. C., ROSSOR, M., COLLINGE, J., MAIER, W., JESSEN, F., RUTHER, E., SCHURMANN, B., HEUN, R., KOLSCH, H., VAN DEN BUSSCHE, H., HEUSER, I., KORNHUBER, J., WILTFANG, J., DICHGANS, M., FROLICH, L., HAMPEL, H., GALLACHER, J., HULL, M., RUJESCU, D., GIEGLING, I., GOATE, A. M., KAUWE, J. S., CRUCHAGA, C., NOWOTNY, P., MORRIS, J. C., MAYO, K., SLEEGERS, K., BETTENS, K., ENGELBORGHS, S., DE DEYN, P. P., VAN BROECKHOVEN, C., LIVINGSTON, G., BASS, N. J., GURLING, H., MCQUILLIN, A., GWILLIAM, R., DELOUKAS, P., AL-CHALABI, A., SHAW, C. E., TSOLAKI, M., SINGLETON, A. B., GUERREIRO, R., MUHLEISEN, T. W., NOTHEN, M. M., MOEBUS, S., JOCKEL, K. H., KLOPP, N., WICHMANN, H. E., PANKRATZ, V. S., SANDO, S. B., AASLY, J. O., BARCIKOWSKA, M., WSZOLEK, Z. K., DICKSON, D. W., GRAFF-RADFORD, N. R., PETERSEN, R. C., et al. 2011. Common variants at ABCA7, MS4A6A/MS4A4E, EPHA1, CD33 and CD2AP are associated with Alzheimer's disease. *Nat Genet,* 43**,** 429-35.

HOLMANS, P., GREEN, E. K., PAHWA, J. S., FERREIRA, M. A., PURCELL, S. M., SKLAR, P., OWEN, M. J., O'DONOVAN, M. C. & CRADDOCK, N. 2009. Gene ontology analysis of GWA study data sets provides insights into the biology of bipolar disorder. *Am J Hum Genet,* 85**,** 13-24.

HOLMES, C., CAIRNS, N., LANTOS, P. & MANN, A. 1999. Validity of current clinical criteria for Alzheimer's disease, vascular dementia and dementia with Lewy bodies. *Br J Psychiatry,* 174**,** 45-50.

HOOG, J. L. & LOTVALL, J. 2015. Diversity of extracellular vesicles in human ejaculates revealed by cryo-electron microscopy. *J Extracell Vesicles,* 4**,** 28680.

HOSHINO, D., KIRKBRIDE, K. C., COSTELLO, K., CLARK, E. S., SINHA, S., GREGA-LARSON, N., TYSKA, M. J. & WEAVER, A. M. 2013. Exosome secretion is enhanced by invadopodia and drives invasive behavior. *Cell Rep,* 5**,** 1159-68.

HOSSEINI-BEHESHTI, E., CHOI, W., WEISWALD, L. B., KHARMATE, G., GHAFFARI, M., ROSHAN-MONIRI, M., HASSONA, M. D., CHAN, L., CHIN, M. Y., TAI, I. T., RENNIE, P. S., FAZLI, L. & TOMLINSON GUNS, E. S. 2016. Exosomes confer pro-survival signals to alter the phenotype of prostate cells in their surrounding environment. *Oncotarget*.

HSU, C., MOROHASHI, Y., YOSHIMURA, S., MANRIQUE-HOYOS, N., JUNG, S., LAUTERBACH, M. A., BAKHTI, M., GRONBORG, M., MOBIUS, W., RHEE, J., BARR, F. A. & SIMONS, M. 2010. Regulation of exosome secretion by Rab35 and its GTPase-activating proteins TBC1D10A-C. *J Cell Biol,* 189**,** 223-32.

HUA, X., LEOW, A. D., LEE, S., KLUNDER, A. D., TOGA, A. W., LEPORE, N., CHOU, Y. Y., BRUN, C., CHIANG, M. C., BARYSHEVA, M., JACK, C. R., JR., BERNSTEIN, M. A., BRITSON, P. J., WARD, C. P., WHITWELL, J. L., BOROWSKI, B., FLEISHER, A. S., FOX, N. C., BOYES, R. G., BARNES, J., HARVEY, D., KORNAK, J., SCHUFF, N., BORETA, L., ALEXANDER, G. E., WEINER, M. W. & THOMPSON, P. M. 2008. 3D characterization of brain atrophy in Alzheimer's disease and mild cognitive impairment using tensor-based morphometry. *Neuroimage,* 41**,** 19-34.

HUANG, D. W., SHERMAN, B. T. & LEMPICKI, R. A. 2008. Systematic and integrative analysis of large gene lists using DAVID bioinformatics resources. *Nat. Protocols,* 4**,** 44-57.

HUANG, Z. P., DING, Y., CHEN, J., WU, G., KATAOKA, M., HU, Y., YANG, J. H., LIU, J., DRAKOS, S. G., SELZMAN, C. H., KYSELOVIC, J., QU, L. H., DOS REMEDIOS, C. G., PU, W. T. & WANG, D. Z. 2016. Long non-coding RNAs link extracellular matrix gene expression to ischemic cardiomyopathy. *Cardiovasc Res*.

HUARTE, M., GUTTMAN, M., FELDSER, D., GARBER, M., KOZIOL, M. J., KENZELMANN-BROZ, D., KHALIL, A. M., ZUK, O., AMIT, I., RABANI, M., ATTARDI, L. D., REGEV, A., LANDER, E. S., JACKS, T. & RINN, J. L. 2010. A large intergenic noncoding RNA induced by p53 mediates global gene repression in the p53 response. *Cell,* 142**,** 409-19.

HUGEL, B., MARTINEZ, M. C., KUNZELMANN, C. & FREYSSINET, J. M. 2005. Membrane microparticles: two sides of the coin. *Physiology (Bethesda),* 20**,** 22-7.

HURWITZ, S. N., CONLON, M. M., RIDER, M. A., BROWNSTEIN, N. C. & MECKES, D. G., JR. 2016. Nanoparticle analysis sheds budding insights into genetic drivers of extracellular vesicle biogenesis. *J Extracell Vesicles,* 5**,** 31295.

HUSSAIN, I., POWELL, D., HOWLETT, D. R., TEW, D. G., MEEK, T. D., CHAPMAN, C., GLOGER, I. S., MURPHY, K. E., SOUTHAN, C. D., RYAN, D. M., SMITH, T. S., SIMMONS, D. L., WALSH, F. S., DINGWALL, C. & CHRISTIE, G. 1999. Identification of a novel aspartic protease (Asp 2) as beta-secretase. *Mol Cell Neurosci,* 14**,** 419-27.

IACONETTI, C., SORRENTINO, S., DE ROSA, S. & INDOLFI, C. 2016. Exosomal miRNAs in Heart Disease. *Physiology (Bethesda),* 31**,** 16-24.

IDE, M., HARRIS, M., STEVENS, A., SUSSAMS, R., HOPKINS, V., CULLIFORD, D., FULLER, J., IBBETT, P., RAYBOULD, R., THOMAS, R., PUENTER, U., TEELING, J., PERRY, V. H. & HOLMES, C. 2016. Periodontitis and Cognitive Decline in Alzheimer's Disease. *PLoS One,* 11**,** e0151081.

IKONEN, E. 2001. Roles of lipid rafts in membrane transport. *Curr Opin Cell Biol,* 13**,** 470-7.

IKONOMOVIC, M. D., KLUNK, W. E., ABRAHAMSON, E. E., MATHIS, C. A., PRICE, J. C., TSOPELAS, N. D., LOPRESTI, B. J., ZIOLKO, S., BI, W., PALJUG, W. R., DEBNATH, M. L., HOPE, C. E., ISANSKI, B. A., HAMILTON, R. L. & DEKOSKY, S. T. 2008. Post-mortem correlates of in vivo PiB-PET amyloid imaging in a typical case of Alzheimer's disease. *Brain,* 131**,** 1630-45.

IMAMURA, K., SAHARA, N., KANAAN, N. M., TSUKITA, K., KONDO, T., KUTOKU, Y., OHSAWA, Y., SUNADA, Y., KAWAKAMI, K., HOTTA, A., YAWATA, S., WATANABE, D., HASEGAWA, M., TROJANOWSKI, J. Q., LEE, V. M., SUHARA, T., HIGUCHI, M. & INOUE, H. 2016. Calcium dysregulation contributes to neurodegeneration in FTLD patient iPSC-derived neurons. *Sci Rep,* 6**,** 34904.

IMTIAZ, B., TOLPPANEN, A. M., KIVIPELTO, M. & SOININEN, H. 2014. Future directions in Alzheimer's disease from risk factors to prevention. *Biochem Pharmacol,* 88**,** 661-70.

IOVINO, M., AGATHOU, S., GONZALEZ-RUEDA, A., DEL CASTILLO VELASCO-HERRERA, M., BORRONI, B., ALBERICI, A., LYNCH, T., O'DOWD, S., GETI, I., GAFFNEY, D., VALLIER, L., PAULSEN, O., KARADOTTIR, R. T. & SPILLANTINI, M. G. 2015. Early maturation and distinct tau pathology in induced pluripotent stem cell-derived neurons from patients with MAPT mutations. *Brain,* 138**,** 3345-59.

IPAS, H., GUTTIN, A. & ISSARTEL, J. P. 2015. Exosomal MicroRNAs in Tumoral U87 MG Versus Normal Astrocyte Cells. *Microrna,* 4**,** 131-45.

JACK, C. R., JR., DICKSON, D. W., PARISI, J. E., XU, Y. C., CHA, R. H., O'BRIEN, P. C., EDLAND, S. D., SMITH, G. E., BOEVE, B. F., TANGALOS, E. G., KOKMEN, E. & PETERSEN, R. C. 2002. Antemortem MRI findings correlate with hippocampal neuropathology in typical aging and dementia. *Neurology,* 58**,** 750-7.

JACK, C. R., JR. & HOLTZMAN, D. M. 2013. Biomarker modeling of Alzheimer's disease. *Neuron,* 80**,** 1347-58.

JACQUIER, A. 2009. The complex eukaryotic transcriptome: unexpected pervasive transcription and novel small RNAs. *Nat Rev Genet,* 10**,** 833-44.

JAGUST, W. J., BANDY, D., CHEN, K., FOSTER, N. L., LANDAU, S. M., MATHIS, C. A., PRICE, J. C., REIMAN, E. M., SKOVRONSKY, D. & KOEPPE, R. A. 2010. The Alzheimer's Disease Neuroimaging Initiative positron emission tomography core. *Alzheimers Dement,* 6**,** 221-9.

JAGUST, W. J., LANDAU, S. M., SHAW, L. M., TROJANOWSKI, J. Q., KOEPPE, R. A., REIMAN, E. M., FOSTER, N. L., PETERSEN, R. C., WEINER, M. W., PRICE, J. C. & MATHIS, C. A. 2009. Relationships between biomarkers in aging and dementia. *Neurology,* 73**,** 1193-9.

JARRETT, J. T., BERGER, E. P. & LANSBURY, P. T., JR. 1993. The carboxy terminus of the beta amyloid protein is critical for the seeding of amyloid formation: implications for the pathogenesis of Alzheimer's disease. *Biochemistry,* 32**,** 4693-7.

JESTE, D. V., WRAGG, R. E., SALMON, D. P., HARRIS, M. J. & THAL, L. J. 1992. Cognitive deficits of patients with Alzheimer's disease with and without delusions. *Am J Psychiatry,* 149**,** 184-9.

JI, H., ERFANI, N., TAURO, B. J., KAPP, E. A., ZHU, H. J., MORITZ, R. L., LIM, J. W. & SIMPSON, R. J. 2008. Difference gel electrophoresis analysis of Ras-transformed fibroblast cell-derived exosomes. *Electrophoresis,* 29**,** 2660-71.

JIANG, Q., MA, R., WANG, J., WU, X., JIN, S., PENG, J., TAN, R., ZHANG, T., LI, Y. & WANG, Y. 2015. LncRNA2Function: a comprehensive resource for functional investigation of human lncRNAs based on RNA-seq data. *BMC Genomics,* 16**,** S2.

JIAO, X., SHERMAN, B. T., HUANG, D. W., STEPHENS, R., BASELER, M. W., LANE, H. C. & LEMPICKI, R. A. 2012. DAVID-WS: a stateful web service to facilitate gene/protein list analysis. *Bioinformatics,* 28**,** 1805-1806.

JONES, L., HOLMANS, P. A., HAMSHERE, M. L., HAROLD, D., MOSKVINA, V., IVANOV, D., POCKLINGTON, A., ABRAHAM, R., HOLLINGWORTH, P., SIMS, R., GERRISH, A., PAHWA, J. S., JONES, N., STRETTON, A., MORGAN, A. R., LOVESTONE, S., POWELL, J., PROITSI, P., LUPTON, M. K., BRAYNE, C., RUBINSZTEIN, D. C., GILL, M., LAWLOR, B., LYNCH, A., MORGAN, K., BROWN, K. S., PASSMORE, P. A., CRAIG, D., MCGUINNESS, B., TODD, S., HOLMES, C., MANN, D., SMITH, A. D., LOVE, S., KEHOE, P. G., MEAD, S., FOX, N., ROSSOR, M., COLLINGE, J., MAIER, W., JESSEN, F., SCHURMANN, B., HEUN, R., KOLSCH, H., VAN DEN BUSSCHE, H., HEUSER, I., PETERS, O., KORNHUBER, J., WILTFANG, J., DICHGANS, M., FROLICH, L., HAMPEL, H., HULL, M., RUJESCU, D., GOATE, A. M., KAUWE, J. S., CRUCHAGA, C., NOWOTNY, P., MORRIS, J. C., MAYO, K., LIVINGSTON, G., BASS, N. J., GURLING, H., MCQUILLIN, A., GWILLIAM, R., DELOUKAS, P., AL-CHALABI, A., SHAW, C. E., SINGLETON, A. B., GUERREIRO, R., MUHLEISEN, T. W., NOTHEN, M. M., MOEBUS, S., JOCKEL, K. H., KLOPP, N., WICHMANN, H. E., RUTHER, E., CARRASQUILLO, M. M., PANKRATZ, V. S., YOUNKIN, S. G., HARDY, J., O'DONOVAN, M. C., OWEN, M. J. & WILLIAMS, J. 2010. Genetic evidence implicates the immune system and cholesterol metabolism in the aetiology of Alzheimer's disease. *PLoS One,* 5**,** e13950.

JONSSON, T., ATWAL, J. K., STEINBERG, S., SNAEDAL, J., JONSSON, P. V., BJORNSSON, S., STEFANSSON, H., SULEM, P., GUDBJARTSSON, D., MALONEY, J., HOYTE, K., GUSTAFSON, A., LIU, Y., LU, Y., BHANGALE, T., GRAHAM, R. R., HUTTENLOCHER, J., BJORNSDOTTIR, G., ANDREASSEN, O. A., JONSSON, E. G., PALOTIE, A., BEHRENS, T. W., MAGNUSSON, O. T., KONG, A., THORSTEINSDOTTIR, U., WATTS, R. J. & STEFANSSON, K. 2012. A mutation in APP protects against Alzheimer's disease and age-related cognitive decline. *Nature,* 488**,** 96-9.

JONSSON, T., STEFANSSON, H., STEINBERG, S., JONSDOTTIR, I., JONSSON, P. V., SNAEDAL, J., BJORNSSON, S., HUTTENLOCHER, J., LEVEY, A. I., LAH, J. J., RUJESCU, D., HAMPEL, H., GIEGLING, I., ANDREASSEN, O. A., ENGEDAL, K., ULSTEIN, I., DJUROVIC, S., IBRAHIM-VERBAAS, C., HOFMAN, A., IKRAM, M. A., VAN DUIJN, C. M., THORSTEINSDOTTIR, U., KONG, A. & STEFANSSON, K. 2013. Variant of TREM2 associated with the risk of Alzheimer's disease. *N Engl J Med,* 368**,** 107-16.

KALRA, H., ADDA, C. G., LIEM, M., ANG, C. S., MECHLER, A., SIMPSON, R. J., HULETT, M. D. & MATHIVANAN, S. 2013. Comparative proteomics evaluation of plasma exosome isolation techniques and assessment of the stability of exosomes in normal human blood plasma. *Proteomics,* 13**,** 3354-64.

KALRA, H., SIMPSON, R. J., JI, H., AIKAWA, E., ALTEVOGT, P., ASKENASE, P., BOND, V. C., BORRAS, F. E., BREAKEFIELD, X., BUDNIK, V., BUZAS, E., CAMUSSI, G., CLAYTON, A.,

COCUCCI, E., FALCON-PEREZ, J. M., GABRIELSSON, S., GHO, Y. S., GUPTA, D., HARSHA, H. C., HENDRIX, A., HILL, A. F., INAL, J. M., JENSTER, G., KRAMER-ALBERS, E. M., LIM, S. K., LLORENTE, A., LOTVALL, J., MARCILLA, A., MINCHEVA-NILSSON, L., NAZARENKO, I., NIEUWLAND, R., NOLTE-'T HOEN, E. N., PANDEY, A., PATEL, T., PIPER, M. G., PLUCHINO, S., PRASAD, T. S., RAJENDRAN, L., RAPOSO, G., RECORD, M., REID, G. E., SANCHEZ-MADRID, F., SCHIFFELERS, R. M., SILJANDER, P., STENSBALLE, A., STOORVOGEL, W., TAYLOR, D., THERY, C., VALADI, H., VAN BALKOM, B. W., VAZQUEZ, J., VIDAL, M., WAUBEN, M. H., YANEZ-MO, M., ZOELLER, M. & MATHIVANAN, S. 2012. Vesiclepedia: a compendium for extracellular vesicles with continuous community annotation. *PLoS Biol,* 10**,** e1001450.

KAMINSKA, A., PLATT, M., KASPRZYK, J., KUSNIERZ-CABALA, B., GALA-BLADZINSKA, A., WOZNICKA, O., JANY, B. R., KROK, F., PIEKOSZEWSKI, W., KUZNIEWSKI, M. & STEPIEN, E. L. 2016. Urinary Extracellular Vesicles: Potential Biomarkers of Renal Function in Diabetic Patients. *J Diabetes Res,* 2016**,** 5741518.

KANDIMALLA, R. J., WANI, W. Y., BINUKUMAR, B. K. & GILL, K. D. 2012. siRNA against presenilin 1 (PS1) down regulates amyloid beta42 production in IMR-32 cells. *J Biomed Sci,* 19**,** 2.

KANG, J., LEMAIRE, H. G., UNTERBECK, A., SALBAUM, J. M., MASTERS, C. L., GRZESCHIK, K. H., MULTHAUP, G., BEYREUTHER, K. & MULLER-HILL, B. 1987. The precursor of Alzheimer's disease amyloid A4 protein resembles a cell-surface receptor. *Nature,* 325**,** 733-6.

KAPRANOV, P., CHENG, J., DIKE, S., NIX, D. A., DUTTAGUPTA, R., WILLINGHAM, A. T., STADLER, P. F., HERTEL, J., HACKERMULLER, J., HOFACKER, I. L., BELL, I., CHEUNG, E., DRENKOW, J., DUMAIS, E., PATEL, S., HELT, G., GANESH, M., GHOSH, S., PICCOLBONI, A., SEMENTCHENKO, V., TAMMANA, H. & GINGERAS, T. R. 2007. RNA maps reveal new RNA classes and a possible function for pervasive transcription. *Science,* 316**,** 1484-8.

KARCH, C. M. & GOATE, A. M. 2015. Alzheimer's disease risk genes and mechanisms of disease pathogenesis. *Biol Psychiatry,* 77**,** 43-51.

KATSUDA, T., OKI, K. & OCHIYA, T. 2015. Potential application of extracellular vesicles of human adipose tissue-derived mesenchymal stem cells in Alzheimer's disease therapeutics. *Methods Mol Biol,* 1212**,** 171-81.

KHAZAEI, M., AHUJA, C. S. & FEHLINGS, M. G. 2016. Induced Pluripotent Stem Cells for Traumatic Spinal Cord Injury. *Front Cell Dev Biol,* 4**,** 152.

KIM, D.-K., KANG, B., KIM, O. Y., CHOI, D.-S., LEE, J., KIM, S. R., GO, G., YOON, Y. J., KIM, J. H., JANG, S. C., PARK, K.-S., CHOI, E.-J., KIM, K. P., DESIDERIO, D. M., KIM, Y.-K., LÖTVALL, J., HWANG, D. & GHO, Y. S. 2013. EVpedia: an integrated database of high-throughput data for systemic analyses of extracellular vesicles. *Journal of Extracellular Vesicles,* 2**,** 10.3402/jev.v2i0.20384.

KIM, J. W., LEE, D. Y., LEE, B. C., JUNG, M. H., KIM, H., CHOI, Y. S. & CHOI, I. G. 2012. Alcohol and cognition in the elderly: a review. *Psychiatry Investig,* 9**,** 8-16.

KIM, J. W., WIECKOWSKI, E., TAYLOR, D. D., REICHERT, T. E., WATKINS, S. & WHITESIDE, T. L. 2005. Fas ligand-positive membranous vesicles isolated from sera of patients with oral cancer induce apoptosis of activated T lymphocytes. *Clin Cancer Res,* 11**,** 1010-20.

KIVIPELTO, M., HELKALA, E. L., LAAKSO, M. P., HANNINEN, T., HALLIKAINEN, M., ALHAINEN, K., SOININEN, H., TUOMILEHTO, J. & NISSINEN, A. 2001. Midlife vascular risk factors and Alzheimer's disease in later life: longitudinal, population based study. *Bmj,* 322**,** 1447-51.

KIVIPELTO, M., NGANDU, T., FRATIGLIONI, L., VIITANEN, M., KAREHOLT, I., WINBLAD, B., HELKALA, E. L., TUOMILEHTO, J., SOININEN, H. & NISSINEN, A. 2005. Obesity and

vascular risk factors at midlife and the risk of dementia and Alzheimer disease. *Arch Neurol,* 62**,** 1556-60.

KLUNK, W. E., ENGLER, H., NORDBERG, A., WANG, Y., BLOMQVIST, G., HOLT, D. P., BERGSTROM, M., SAVITCHEVA, I., HUANG, G. F., ESTRADA, S., AUSEN, B., DEBNATH, M. L., BARLETTA, J., PRICE, J. C., SANDELL, J., LOPRESTI, B. J., WALL, A., KOIVISTO, P., ANTONI, G., MATHIS, C. A. & LANGSTROM, B. 2004. Imaging brain amyloid in Alzheimer's disease with Pittsburgh Compound-B. *Ann Neurol,* 55**,** 306-19.

KNOPMAN, D. S., BOEVE, B. F. & PETERSEN, R. C. 2003. Essentials of the proper diagnoses of mild cognitive impairment, dementia, and major subtypes of dementia. *Mayo Clin Proc,* 78**,** 1290-308.

KOGA, K., MATSUMOTO, K., AKIYOSHI, T., KUBO, M., YAMANAKA, N., TASAKI, A., NAKASHIMA, H., NAKAMURA, M., KUROKI, S., TANAKA, M. & KATANO, M. 2005. Purification, characterization and biological significance of tumor-derived exosomes. *Anticancer Res,* 25**,** 3703-7.

KOLES, K., NUNNARI, J., KORKUT, C., BARRIA, R., BREWER, C., LI, Y., LESZYK, J., ZHANG, B. & BUDNIK, V. 2012. Mechanism of evenness interrupted (Evi)-exosome release at synaptic boutons. *J Biol Chem,* 287**,** 16820-34.

KONADU, K. A., HUANG, M. B., ROTH, W., ARMSTRONG, W., POWELL, M., VILLINGER, F. & BOND, V. 2016. Isolation of Exosomes from the Plasma of HIV-1 Positive Individuals. *J Vis Exp*.

KORE, R. A. & ABRAHAM, E. C. 2016. Phosphorylation negatively regulates exosome mediated secretion of cryAB in glioma cells. *Biochim Biophys Acta,* 1863**,** 368-77.

KORESSAAR, T. & REMM, M. 2007. Enhancements and modifications of primer design program Primer3. *Bioinformatics,* 23**,** 1289-91.

KORF, E. S., WHITE, L. R., SCHELTENS, P. & LAUNER, L. J. 2004. Midlife blood pressure and the risk of hippocampal atrophy: the Honolulu Asia Aging Study. *Hypertension,* 44**,** 29-34.

KOSS, E., EDLAND, S., FILLENBAUM, G., MOHS, R., CLARK, C., GALASKO, D. & MORRIS, J. C. 1996. Clinical and neuropsychological differences between patients with earlier and later onset of Alzheimer's disease: A CERAD analysis, Part XII. *Neurology,* 46**,** 136-41.

KOVACS, D. M., MANCINI, R., HENDERSON, J., NA, S. J., SCHMIDT, S. D., KIM, T. W. & TANZI, R. E. 1999. Staurosporine-induced activation of caspase-3 is potentiated by presenilin 1 familial Alzheimer's disease mutations in human neuroglioma cells. *J Neurochem,* 73**,** 2278-85.

KOWAL, J., ARRAS, G., COLOMBO, M., JOUVE, M., MORATH, J. P., PRIMDAL-BENGTSON, B., DINGLI, F., LOEW, D., TKACH, M. & THERY, C. 2016. Proteomic comparison defines novel markers to characterize heterogeneous populations of extracellular vesicle subtypes. *Proc Natl Acad Sci U S A*.

KUENTZEL, S. L., ALI, S. M., ALTMAN, R. A., GREENBERG, B. D. & RAUB, T. J. 1993. The Alzheimer beta-amyloid protein precursor/protease nexin-II is cleaved by secretase in a trans-Golgi secretory compartment in human neuroglioma cells. *Biochem J,* 295 (Pt 2)**,** 367-78.

KUMAR, P., DEZSO, Z., MACKENZIE, C., OESTREICHER, J., AGOULNIK, S., BYRNE, M., BERNIER, F., YANAGIMACHI, M., AOSHIMA, K. & ODA, Y. 2013. Circulating miRNA biomarkers for Alzheimer's disease. *PLoS One,* 8**,** e69807.

KUMAR, S. & REDDY, P. H. 2016. Are circulating microRNAs peripheral biomarkers for Alzheimer's disease? *Biochim Biophys Acta,* 1862**,** 1617-1627.

KWON, S. H., OH, S., NACKE, M., MOSTOV, K. E. & LIPSCHUTZ, J. H. 2016. Adaptor Protein CD2AP and L-type Lectin LMAN2 Regulate Exosome Cargo Protein Trafficking through the Golgi Complex. *J Biol Chem,* 291**,** 25462-25475.

LACHENAL, G., PERNET-GALLAY, K., CHIVET, M., HEMMING, F. J., BELLY, A., BODON, G., BLOT, B., HAASE, G., GOLDBERG, Y. & SADOUL, R. 2011. Release of exosomes from differentiated neurons and its regulation by synaptic glutamatergic activity. *Mol Cell Neurosci,* 46**,** 409-18.

LAI, R. C., CHEN, T. S. & LIM, S. K. 2011. Mesenchymal stem cell exosome: a novel stem cell-based therapy for cardiovascular disease. *Regen Med,* 6**,** 481-92.

LAMBERT, J. C., HEATH, S., EVEN, G., CAMPION, D., SLEEGERS, K., HILTUNEN, M., COMBARROS, O., ZELENIKA, D., BULLIDO, M. J., TAVERNIER, B., LETENNEUR, L., BETTENS, K., BERR, C., PASQUIER, F., FIEVET, N., BARBERGER-GATEAU, P., ENGELBORGHS, S., DE DEYN, P., MATEO, I., FRANCK, A., HELISALMI, S., PORCELLINI, E., HANON, O., DE PANCORBO, M. M., LENDON, C., DUFOUIL, C., JAILLARD, C., LEVEILLARD, T., ALVAREZ, V., BOSCO, P., MANCUSO, M., PANZA, F., NACMIAS, B., BOSSU, P., PICCARDI, P., ANNONI, G., SERIPA, D., GALIMBERTI, D., HANNEQUIN, D., LICASTRO, F., SOININEN, H., RITCHIE, K., BLANCHE, H., DARTIGUES, J. F., TZOURIO, C., GUT, I., VAN BROECKHOVEN, C., ALPEROVITCH, A., LATHROP, M. & AMOUYEL, P. 2009. Genome-wide association study identifies variants at CLU and CR1 associated with Alzheimer's disease. *Nat Genet,* 41**,** 1094-9.

LAMBERT, J. C., IBRAHIM-VERBAAS, C. A., HAROLD, D., NAJ, A. C., SIMS, R., BELLENGUEZ, C., DESTAFANO, A. L., BIS, J. C., BEECHAM, G. W., GRENIER-BOLEY, B., RUSSO, G., THORTON-WELLS, T. A., JONES, N., SMITH, A. V., CHOURAKI, V., THOMAS, C., IKRAM, M. A., ZELENIKA, D., VARDARAJAN, B. N., KAMATANI, Y., LIN, C. F., GERRISH, A., SCHMIDT, H., KUNKLE, B., DUNSTAN, M. L., RUIZ, A., BIHOREAU, M. T., CHOI, S. H., REITZ, C., PASQUIER, F., CRUCHAGA, C., CRAIG, D., AMIN, N., BERR, C., LOPEZ, O. L., DE JAGER, P. L., DERAMECOURT, V., JOHNSTON, J. A., EVANS, D., LOVESTONE, S., LETENNEUR, L., MORON, F. J., RUBINSZTEIN, D. C., EIRIKSDOTTIR, G., SLEEGERS, K., GOATE, A. M., FIEVET, N., HUENTELMAN, M. W., GILL, M., BROWN, K., KAMBOH, M. I., KELLER, L., BARBERGER-GATEAU, P., MCGUINESS, B., LARSON, E. B., GREEN, R., MYERS, A. J., DUFOUIL, C., TODD, S., WALLON, D., LOVE, S., ROGAEVA, E., GALLACHER, J., ST GEORGE-HYSLOP, P., CLARIMON, J., LLEO, A., BAYER, A., TSUANG, D. W., YU, L., TSOLAKI, M., BOSSU, P., SPALLETTA, G., PROITSI, P., COLLINGE, J., SORBI, S., SANCHEZ-GARCIA, F., FOX, N. C., HARDY, J., DENIZ NARANJO, M. C., BOSCO, P., CLARKE, R., BRAYNE, C., GALIMBERTI, D., MANCUSO, M., MATTHEWS, F., MOEBUS, S., MECOCCI, P., DEL ZOMPO, M., MAIER, W., HAMPEL, H., PILOTTO, A., BULLIDO, M., PANZA, F., CAFFARRA, P., NACMIAS, B., GILBERT, J. R., MAYHAUS, M., LANNEFELT, L., HAKONARSON, H., PICHLER, S., et al. 2013. Meta-analysis of 74,046 individuals identifies 11 new susceptibility loci for Alzheimer's disease. *Nat Genet,* 45**,** 1452-8.

LAMPARSKI, H. G., METHA-DAMANI, A., YAO, J. Y., PATEL, S., HSU, D. H., RUEGG, C. & LE PECQ, J. B. 2002. Production and characterization of clinical grade exosomes derived from dendritic cells. *J Immunol Methods,* 270**,** 211-26.

LANTOS, P. & CAIRNS, N. 2000. Dementia. 2nd ed. London: Arnold.

LARSON, E. B., SHADLEN, M. F., WANG, L., MCCORMICK, W. C., BOWEN, J. D., TERI, L. & KUKULL, W. A. 2004. Survival after initial diagnosis of Alzheimer disease. *Ann Intern Med,* 140**,** 501-9.

LASSER, C., SHELKE, G. V., YERI, A., KIM, D. K., CRESCITELLI, R., RAIMONDO, S., SJOSTRAND, M., GHO, Y. S., VAN KEUREN JENSEN, K. & LOTVALL, J. 2016. Two distinct extracellular RNA signatures released by a single cell type identified by microarray and next-generation sequencing. *RNA Biol***,** 0.

LAULAGNIER, K., MOTTA, C., HAMDI, S., ROY, S., FAUVELLE, F., PAGEAUX, J. F., KOBAYASHI, T., SALLES, J. P., PERRET, B., BONNEROT, C. & RECORD, M. 2004. Mast cell- and

dendritic cell-derived exosomes display a specific lipid composition and an unusual membrane organization. *Biochem J,* 380**,** 161-71.

LEE, H. K., MORIN, P. & XIA, W. 2016a. Peripheral blood mononuclear cell-converted induced pluripotent stem cells (iPSCs) from an early onset Alzheimer's patient. *Stem Cell Res,* 16**,** 213-5.

LEE, L. J., YANG, Z., RAHMAN, M., MA, J., KWAK, K. J., MCELROY, J., SHILO, K., GOPARAJU, C., YU, L., ROM, W., KIM, T. K., WU, X., HE, Y., WANG, K., PASS, H. I. & NANA-SINKAM, S. P. 2016b. Extracellular mRNA Detected by Tethered Lipoplex Nanoparticle Biochip for Lung Adenocarcinoma Detection. *Am J Respir Crit Care Med,* 193**,** 1431-3.

LEE, V. M., BALIN, B. J., OTVOS, L., JR. & TROJANOWSKI, J. Q. 1991. A68: a major subunit of paired helical filaments and derivatized forms of normal Tau. *Science,* 251**,** 675-8.

LEE, Y. S., PRESSMAN, S., ANDRESS, A. P., KIM, K., WHITE, J. L., CASSIDY, J. J., LI, X., LUBELL, K., LIM, D. H., CHO, I. S., NAKAHARA, K., PREALL, J. B., BELLARE, P., SONTHEIMER, E. J. & CARTHEW, R. W. 2009. Silencing by small RNAs is linked to endosomal trafficking. *Nat Cell Biol,* 11**,** 1150-6.

LEVY-LAHAD, E., WASCO, W., POORKAJ, P., ROMANO, D. M., OSHIMA, J., PETTINGELL, W. H., YU, C. E., JONDRO, P. D., SCHMIDT, S. D., WANG, K. & ET AL. 1995a. Candidate gene for the chromosome 1 familial Alzheimer's disease locus. *Science,* 269**,** 973-7.

LEVY-LAHAD, E., WIJSMAN, E. M., NEMENS, E., ANDERSON, L., GODDARD, K. A., WEBER, J. L., BIRD, T. D. & SCHELLENBERG, G. D. 1995b. A familial Alzheimer's disease locus on chromosome 1. *Science,* 269**,** 970-3.

LEWIS, P. A., PEREZ-TUR, J., GOLDE, T. E. & HARDY, J. 2000. The presenilin 1 C92S mutation increases abeta 42 production. *Biochem Biophys Res Commun,* 277**,** 261-3.

LI, C. C., EATON, S. A., YOUNG, P. E., LEE, M., SHUTTLEWORTH, R., HUMPHREYS, D. T., GRAU, G. E., COMBES, V., BEBAWY, M., GONG, J., BRAMMAH, S., BUCKLAND, M. E. & SUTER, C. M. 2013. Glioma microvesicles carry selectively packaged coding and non-coding RNAs which alter gene expression in recipient cells. *RNA Biol,* 10**,** 1333-44.

LI, L., LI, C., WANG, S., WANG, Z., JIANG, J., WANG, W., LI, X., CHEN, J., LIU, K. & ZHU, G. 2016a. Exosomes Derived from Hypoxic Oral Squamous Cell Carcinoma Cells Deliver miR-21 to Normoxic Cells to Elicit a Prometastatic Phenotype. *Cancer Res,* 76**,** 1770-80.

LI, X., JIANG, C. & ZHAO, J. 2016b. Human endothelial progenitor cells-derived exosomes accelerate cutaneous wound healing in diabetic rats by promoting endothelial function. *J Diabetes Complications*.

LI, Y., ZHENG, Q., BAO, C., LI, S., GUO, W., ZHAO, J., CHEN, D., GU, J., HE, X. & HUANG, S. 2015. Circular RNA is enriched and stable in exosomes: a promising biomarker for cancer diagnosis. *Cell Res,* 25**,** 981-4.

LIDDELOW, S. A., GUTTENPLAN, K. A., CLARKE, L. E., BENNETT, F. C., BOHLEN, C. J., SCHIRMER, L., BENNETT, M. L., MUNCH, A. E., CHUNG, W. S., PETERSON, T. C., WILTON, D. K., FROUIN, A., NAPIER, B. A., PANICKER, N., KUMAR, M., BUCKWALTER, M. S., ROWITCH, D. H., DAWSON, V. L., DAWSON, T. M., STEVENS, B. & BARRES, B. A. 2017. Neurotoxic reactive astrocytes are induced by activated microglia. *Nature,* 541**,** 481-487.

LIN, J., HIRAOKA, K., WATANABE, T., KUO, T., SHINOZAKI, Y., TAKATORI, A., KOSHIKAWA, N., CHANDRAN, A., OTSUKI, J., SUGIYAMA, H., HORTON, P. & NAGASE, H. 2016. Identification of Binding Targets of a Pyrrole-Imidazole Polyamide KR12 in the LS180 Colorectal Cancer Genome. *PLoS One,* 11**,** e0165581.

LIN, X., KOELSCH, G., WU, S., DOWNS, D., DASHTI, A. & TANG, J. 2000. Human aspartic protease memapsin 2 cleaves the beta-secretase site of beta-amyloid precursor protein. *Proc Natl Acad Sci U S A,* 97**,** 1456-60.

LIPPINCOTT-SCHWARTZ, J. & FAMBROUGH, D. M. 1987. Cycling of the integral membrane glycoprotein, LEP100, between plasma membrane and lysosomes: Kinetic and morphological analysis. *Cell,* 49**,** 669-677.

LIU, X., LI, Q., NIU, X., HU, B., CHEN, S., SONG, W., DING, J., ZHANG, C. & WANG, Y. 2017. Exosomes Secreted from Human-Induced Pluripotent Stem Cell-Derived Mesenchymal Stem Cells Prevent Osteonecrosis of the Femoral Head by Promoting Angiogenesis. *Int J Biol Sci,* 13**,** 232-244.

LIVSHTS, M. A., KHOMYAKOVA, E., EVTUSHENKO, E. G., LAZAREV, V. N., KULEMIN, N. A., SEMINA, S. E., GENEROZOV, E. V. & GOVORUN, V. M. 2015. Isolation of exosomes by differential centrifugation: Theoretical analysis of a commonly used protocol. *Sci Rep,* 5**,** 17319.

LLORENTE, A., SKOTLAND, T., SYLVANNE, T., KAUHANEN, D., ROG, T., ORLOWSKI, A., VATTULAINEN, I., EKROOS, K. & SANDVIG, K. 2013. Molecular lipidomics of exosomes released by PC-3 prostate cancer cells. *Biochim Biophys Acta,* 1831**,** 1302-9.

LO CICERO, A., DELEVOYE, C., GILLES-MARSENS, F., LOEW, D., DINGLI, F., GUERE, C., ANDRE, N., VIE, K., VAN NIEL, G. & RAPOSO, G. 2015a. Exosomes released by keratinocytes modulate melanocyte pigmentation. *Nat Commun,* 6**,** 7506.

LO CICERO, A., STAHL, P. D. & RAPOSO, G. 2015b. Extracellular vesicles shuffling intercellular messages: for good or for bad. *Curr Opin Cell Biol,* 35**,** 69-77.

LOEWER, S., CABILI, M. N., GUTTMAN, M., LOH, Y. H., THOMAS, K., PARK, I. H., GARBER, M., CURRAN, M., ONDER, T., AGARWAL, S., MANOS, P. D., DATTA, S., LANDER, E. S., SCHLAEGER, T. M., DALEY, G. Q. & RINN, J. L. 2010. Large intergenic non-coding RNA-RoR modulates reprogramming of human induced pluripotent stem cells. *Nat Genet,* 42**,** 1113-7.

LOGAN, M. R., LACY, P., ODEMUYIWA, S. O., STEWARD, M., DAVOINE, F., KITA, H. & MOQBEL, R. 2006. A critical role for vesicle-associated membrane protein-7 in exocytosis from human eosinophils and neutrophils. *Allergy,* 61**,** 777-84.

LOTVALL, J., HILL, A. F., HOCHBERG, F., BUZAS, E. I., DI VIZIO, D., GARDINER, C., GHO, Y. S., KUROCHKIN, I. V., MATHIVANAN, S., QUESENBERRY, P., SAHOO, S., TAHARA, H., WAUBEN, M. H., WITWER, K. W. & THERY, C. 2014. Minimal experimental requirements for definition of extracellular vesicles and their functions: a position statement from the International Society for Extracellular Vesicles. *J Extracell Vesicles,* 3**,** 26913.

LOVE, M. I., HUBER, W. & ANDERS, S. 2014. Moderated estimation of fold change and dispersion for RNA-seq data with DESeq2. *Genome Biology,* 15**,** 550.

LOWIN, A., KNAPP, M. & MCCRONE, P. 2001. Alzheimer's disease in the UK: comparative evidence on cost of illness and volume of health services research funding. *Int J Geriatr Psychiatry,* 16**,** 1143-8.

LUGLI, G., COHEN, A. M., BENNETT, D. A., SHAH, R. C., FIELDS, C. J., HERNANDEZ, A. G. & SMALHEISER, N. R. 2015. Plasma Exosomal miRNAs in Persons with and without Alzheimer Disease: Altered Expression and Prospects for Biomarkers. *PLoS One,* 10**,** e0139233.

MACK, M., KLEINSCHMIDT, A., BRUHL, H., KLIER, C., NELSON, P. J., CIHAK, J., PLACHY, J., STANGASSINGER, M., ERFLE, V. & SCHLONDORFF, D. 2000. Transfer of the chemokine receptor CCR5 between cells by membrane-derived microparticles: a mechanism for cellular human immunodeficiency virus 1 infection. *Nat Med,* 6**,** 769-75.

MAHLEY, R. W., WEISGRABER, K. H. & HUANG, Y. 2006. Apolipoprotein E4: a causative factor and therapeutic target in neuropathology, including Alzheimer's disease. *Proc Natl Acad Sci U S A,* 103**,** 5644-51.

MANN, D. M. 1988a. Alzheimer's disease and Down's syndrome. *Histopathology,* 13**,** 125-37.

MANN, D. M. 1988b. The pathological association between Down syndrome and Alzheimer disease. *Mech Ageing Dev,* 43**,** 99-136.

MANN, U. M., MOHR, E., GEARING, M. & CHASE, T. N. 1992. Heterogeneity in Alzheimer's disease: progression rate segregated by distinct neuropsychological and cerebral metabolic profiles. *J Neurol Neurosurg Psychiatry,* 55**,** 956-9.

MANSCHRECK, T. C. & KHAN, N. L. 2006. Recent advances in the treatment of delusional disorder. *Can J Psychiatry,* 51**,** 114-9.

MARTIN-SERRANO, J., YAROVOY, A., PEREZ-CABALLERO, D. & BIENIASZ, P. D. 2003. Divergent retroviral late-budding domains recruit vacuolar protein sorting factors by using alternative adaptor proteins. *Proc Natl Acad Sci U S A,* 100**,** 12414-9.

MATEESCU, B., KOWAL, E. J., VAN BALKOM, B. W., BARTEL, S., BHATTACHARYYA, S. N., BUZAS, E. I., BUCK, A. H., DE CANDIA, P., CHOW, F. W., DAS, S., DRIEDONKS, T. A., FERNANDEZ-MESSINA, L., HADERK, F., HILL, A. F., JONES, J. C., VAN KEUREN-JENSEN, K. R., LAI, C. P., LASSER, C., LIEGRO, I. D., LUNAVAT, T. R., LORENOWICZ, M. J., MAAS, S. L., MAGER, I., MITTELBRUNN, M., MOMMA, S., MUKHERJEE, K., NAWAZ, M., PEGTEL, D. M., PFAFFL, M. W., SCHIFFELERS, R. M., TAHARA, H., THERY, C., TOSAR, J. P., WAUBEN, M. H., WITWER, K. W. & NOLTE-'T HOEN, E. N. 2017. Obstacles and opportunities in the functional analysis of extracellular vesicle RNA - an ISEV position paper. *J Extracell Vesicles,* 6**,** 1286095.

MATHIVANAN, S., FAHNER, C. J., REID, G. E. & SIMPSON, R. J. 2012. ExoCarta 2012: database of exosomal proteins, RNA and lipids. *Nucleic Acids Res,* 40**,** D1241-4.

MATHIVANAN, S., LIM, J. W., TAURO, B. J., JI, H., MORITZ, R. L. & SIMPSON, R. J. 2010. Proteomics analysis of A33 immunoaffinity-purified exosomes released from the human colon tumor cell line LIM1215 reveals a tissue-specific protein signature. *Mol Cell Proteomics,* 9**,** 197-208.

MATTSSON, N., ZETTERBERG, H., HANSSON, O., ANDREASEN, N., PARNETTI, L., JONSSON, M., HERUKKA, S. K., VAN DER FLIER, W. M., BLANKENSTEIN, M. A., EWERS, M., RICH, K., KAISER, E., VERBEEK, M., TSOLAKI, M., MULUGETA, E., ROSEN, E., AARSLAND, D., VISSER, P. J., SCHRODER, J., MARCUSSON, J., DE LEON, M., HAMPEL, H., SCHELTENS, P., PIRTTILA, T., WALLIN, A., JONHAGEN, M. E., MINTHON, L., WINBLAD, B. & BLENNOW, K. 2009. CSF biomarkers and incipient Alzheimer disease in patients with mild cognitive impairment. *Jama,* 302**,** 385-93.

MCKHANN, G., DRACHMAN, D., FOLSTEIN, M., KATZMAN, R., PRICE, D. & STADLAN, E. M. 1984. Clinical diagnosis of Alzheimer's disease: report of the NINCDS-ADRDA Work Group under the auspices of Department of Health and Human Services Task Force on Alzheimer's Disease. *Neurology,* 34**,** 939-44.

MCKHANN, G. M., KNOPMAN, D. S., CHERTKOW, H., HYMAN, B. T., JACK, C. R., JR., KAWAS, C. H., KLUNK, W. E., KOROSHETZ, W. J., MANLY, J. J., MAYEUX, R., MOHS, R. C., MORRIS, J. C., ROSSOR, M. N., SCHELTENS, P., CARRILLO, M. C., THIES, B., WEINTRAUB, S. & PHELPS, C. H. 2011. The diagnosis of dementia due to Alzheimer's disease: recommendations from the National Institute on Aging-Alzheimer's Association workgroups on diagnostic guidelines for Alzheimer's disease. *Alzheimers Dement,* 7**,** 263-9.

MEDWAY, C. & MORGAN, K. 2014. Review: The genetics of Alzheimer's disease; putting flesh on the bones. *Neuropathology and Applied Neurobiology,* 40**,** 97-105.

MELO, S. A., LUECKE, L. B., KAHLERT, C., FERNANDEZ, A. F., GAMMON, S. T., KAYE, J., LEBLEU, V. S., MITTENDORF, E. A., WEITZ, J., RAHBARI, N., REISSFELDER, C., PILARSKY, C., FRAGA, M. F., PIWNICA-WORMS, D. & KALLURI, R. 2015. Glypican-1 identifies cancer exosomes and detects early pancreatic cancer. *Nature,* 523**,** 177-182.

MENDEZ, A. M. F. 2000. Comprehensive geriatric assessment. New York McGraw-Hill

MENDEZ, M. F. & CUMMINGS, J. L. 2003. Dementia: a clinical approach. 3rd ed.: Butterworth Heinemann.

MERCKEN, E. M., MAJOUNIE, E., DING, J., GUO, R., KIM, J., BERNIER, M., MATTISON, J., COOKSON, M. R., GOROSPE, M., DE CABO, R. & ABDELMOHSEN, K. 2013. Age-associated miRNA alterations in skeletal muscle from rhesus monkeys reversed by caloric restriction. *Aging (Albany NY),* 5**,** 692-703.

MEYER, M. A. 2014. Highly expressed genes in human high grade gliomas: immunohistochemical analysis of data from the human protein atlas. *Neurol Int,* 6**,** 5348.

MITCHELL, J. P., COURT, J., MASON, M. D., TABI, Z. & CLAYTON, A. 2008a. Increased exosome production from tumour cell cultures using the Integra CELLine Culture System. *J Immunol Methods,* 335**,** 98-105.

MITCHELL, P. S., PARKIN, R. K., KROH, E. M., FRITZ, B. R., WYMAN, S. K., POGOSOVA-AGADJANYAN, E. L., PETERSON, A., NOTEBOOM, J., O'BRIANT, K. C., ALLEN, A., LIN, D. W., URBAN, N., DRESCHER, C. W., KNUDSEN, B. S., STIREWALT, D. L., GENTLEMAN, R., VESSELLA, R. L., NELSON, P. S., MARTIN, D. B. & TEWARI, M. 2008b. Circulating microRNAs as stable blood-based markers for cancer detection. *Proc Natl Acad Sci U S A,* 105**,** 10513-8.

MITTELBRUNN, M., GUTIERREZ-VAZQUEZ, C., VILLARROYA-BELTRI, C., GONZALEZ, S., SANCHEZ-CABO, F., GONZALEZ, M. A., BERNAD, A. & SANCHEZ-MADRID, F. 2011. Unidirectional transfer of microRNA-loaded exosomes from T cells to antigen-presenting cells. *Nat Commun,* 2**,** 282.

MOREL, E., CHAMOUN, Z., LASIECKA, Z. M., CHAN, R. B., WILLIAMSON, R. L., VETANOVETZ, C., DALL'ARMI, C., SIMOES, S., POINT DU JOUR, K. S., MCCABE, B. D., SMALL, S. A. & DI PAOLO, G. 2013. Phosphatidylinositol-3-phosphate regulates sorting and processing of amyloid precursor protein through the endosomal system. *Nat Commun,* 4**,** 2250.

MORI, Y., YOSHINO, Y., OCHI, S., YAMAZAKI, K., KAWABE, K., ABE, M., KITANO, T., OZAKI, Y., YOSHIDA, T., NUMATA, S., MORI, T., IGA, J., KURODA, N., OHMORI, T. & UENO, S. 2015. TREM2 mRNA Expression in Leukocytes Is Increased in Alzheimer's Disease and Schizophrenia. *PLoS One,* 10**,** e0136835.

MORRA, J. H., TU, Z., APOSTOLOVA, L. G., GREEN, A. E., AVEDISSIAN, C., MADSEN, S. K., PARIKSHAK, N., TOGA, A. W., JACK, C. R., JR., SCHUFF, N., WEINER, M. W. & THOMPSON, P. M. 2009. Automated mapping of hippocampal atrophy in 1-year repeat MRI data from 490 subjects with Alzheimer's disease, mild cognitive impairment, and elderly controls. *Neuroimage,* 45**,** S3-15.

MORRIS, M. C., EVANS, D. A., BIENIAS, J. L., TANGNEY, C. C., BENNETT, D. A., AGGARWAL, N., SCHNEIDER, J. & WILSON, R. S. 2003. Dietary fats and the risk of incident Alzheimer disease. *Arch Neurol,* 60**,** 194-200.

MUFFAT, J., LI, Y., YUAN, B., MITALIPOVA, M., OMER, A., CORCORAN, S., BAKIASI, G., TSAI, L. H., AUBOURG, P., RANSOHOFF, R. M. & JAENISCH, R. 2016. Efficient derivation of microglia-like cells from human pluripotent stem cells. *Nat Med,* 22**,** 1358-1367.

MULLINS, R. J., MUSTAPIC, M., GOETZL, E. J. & KAPOGIANNIS, D. 2017. Exosomal biomarkers of brain insulin resistance associated with regional atrophy in Alzheimer's disease. *Hum Brain Mapp*.

MURRAY, C. J. L. & LOPEZ, A. D. 1996. The Global Burden of Disease. A comprehensive assessment of mortality and disability from diseases, injuries, and risk factors in 1990 and projected to 2020.

MUSTAPIC, M., EITAN, E., WERNER, J. K., JR., BERKOWITZ, S. T., LAZAROPOULOS, M. P., TRAN, J., GOETZL, E. J. & KAPOGIANNIS, D. 2017. Plasma Extracellular Vesicles Enriched for

Neuronal Origin: A Potential Window into Brain Pathologic Processes. *Front Neurosci,* 11**,** 278.

NAGANO, T., MITCHELL, J. A., SANZ, L. A., PAULER, F. M., FERGUSON-SMITH, A. C., FEIL, R. & FRASER, P. 2008. The Air noncoding RNA epigenetically silences transcription by targeting G9a to chromatin. *Science,* 322**,** 1717-20.

NAJ, A. C., JUN, G., BEECHAM, G. W., WANG, L.-S., VARDARAJAN, B. N., BUROS, J., GALLINS, P. J., BUXBAUM, J. D., JARVIK, G. P., CRANE, P. K., LARSON, E. B., BIRD, T. D., BOEVE, B. F., GRAFF-RADFORD, N. R., DE JAGER, P. L., EVANS, D., SCHNEIDER, J. A., CARRASQUILLO, M. M., ERTEKIN-TANER, N., YOUNKIN, S. G., CRUCHAGA, C., KAUWE, J. S. K., NOWOTNY, P., KRAMER, P., HARDY, J., HUENTELMAN, M. J., MYERS, A. J., BARMADA, M. M., DEMIRCI, F. Y., BALDWIN, C. T., GREEN, R. C., ROGAEVA, E., GEORGE-HYSLOP, P. S., ARNOLD, S. E., BARBER, R., BEACH, T., BIGIO, E. H., BOWEN, J. D., BOXER, A., BURKE, J. R., CAIRNS, N. J., CARLSON, C. S., CARNEY, R. M., CARROLL, S. L., CHUI, H. C., CLARK, D. G., CORNEVEAUX, J., COTMAN, C. W., CUMMINGS, J. L., DECARLI, C., DEKOSKY, S. T., DIAZ-ARRASTIA, R., DICK, M., DICKSON, D. W., ELLIS, W. G., FABER, K. M., FALLON, K. B., FARLOW, M. R., FERRIS, S., FROSCH, M. P., GALASKO, D. R., GANGULI, M., GEARING, M., GESCHWIND, D. H., GHETTI, B., GILBERT, J. R., GILMAN, S., GIORDANI, B., GLASS, J. D., GROWDON, J. H., HAMILTON, R. L., HARRELL, L. E., HEAD, E., HONIG, L. S., HULETTE, C. M., HYMAN, B. T., JICHA, G. A., JIN, L.-W., JOHNSON, N., KARLAWISH, J., KARYDAS, A., KAYE, J. A., KIM, R., KOO, E. H., KOWALL, N. W., LAH, J. J., LEVEY, A. I., LIEBERMAN, A. P., LOPEZ, O. L., MACK, W. J., MARSON, D. C., MARTINIUK, F., MASH, D. C., MASLIAH, E., MCCORMICK, W. C., MCCURRY, S. M., MCDAVID, A. N., MCKEE, A. C., MESULAM, M., MILLER, B. L., et al. 2011. Common variants at MS4A4/MS4A6E, CD2AP, CD33 and EPHA1 are associated with late-onset Alzheimer's disease. *Nat Genet,* 43**,** 436-441.

NARAYANAN, A., IORDANSKIY, S., DAS, R., VAN DUYNE, R., SANTOS, S., JAWORSKI, E., GUENDEL, I., SAMPEY, G., DALBY, E., IGLESIAS-USSEL, M., POPRATILOFF, A., HAKAMI, R., KEHN-HALL, K., YOUNG, M., SUBRA, C., GILBERT, C., BAILEY, C., ROMERIO, F. & KASHANCHI, F. 2013. Exosomes derived from HIV-1-infected cells contain trans-activation response element RNA. *J Biol Chem,* 288**,** 20014-33.

NAVIN, N., KENDALL, J., TROGE, J., ANDREWS, P., RODGERS, L., MCINDOO, J., COOK, K., STEPANSKY, A., LEVY, D., ESPOSITO, D., MUTHUSWAMY, L., KRASNITZ, A., MCCOMBIE, R., HICKS, J. & WIGLER, M. 2011. Tumor Evolution Inferred by Single Cell Sequencing. *Nature,* 472**,** 90-94.

NAWY, T. 2014. Single-cell sequencing. *Nat Meth,* 11**,** 18-18.

NELSON, M. R., TIPNEY, H., PAINTER, J. L., SHEN, J., NICOLETTI, P., SHEN, Y., FLORATOS, A., SHAM, P. C., LI, M. J., WANG, J., CARDON, L. R., WHITTAKER, J. C. & SANSEAU, P. 2015. The support of human genetic evidence for approved drug indications. *Nat Genet,* 47**,** 856-60.

NGANDU, T., HELKALA, E. L., SOININEN, H., WINBLAD, B., TUOMILEHTO, J., NISSINEN, A. & KIVIPELTO, M. 2007a. Alcohol drinking and cognitive functions: findings from the Cardiovascular Risk Factors Aging and Dementia (CAIDE) Study. *Dement Geriatr Cogn Disord,* 23**,** 140-9.

NGANDU, T., VON STRAUSS, E., HELKALA, E. L., WINBLAD, B., NISSINEN, A., TUOMILEHTO, J., SOININEN, H. & KIVIPELTO, M. 2007b. Education and dementia: what lies behind the association? *Neurology,* 69**,** 1442-50.

NIMMERJAHN, A., KIRCHHOFF, F. & HELMCHEN, F. 2005. Resting Microglial Cells Are Highly Dynamic Surveillants of Brain Parenchyma in Vivo. *Science,* 308**,** 1314.

NITSCH, R. M., SLACK, B. E., WURTMAN, R. J. & GROWDON, J. H. 1992. Release of Alzheimer amyloid precursor derivatives stimulated by activation of muscarinic acetylcholine receptors. *Science,* 258**,** 304-7.

NOLTE-'T HOEN, E. N., BUERMANS, H. P., WAASDORP, M., STOORVOGEL, W., WAUBEN, M. H. & T HOEN, P. A. 2012. Deep sequencing of RNA from immune cell-derived vesicles uncovers the selective incorporation of small non-coding RNA biotypes with potential regulatory functions. *Nucleic Acids Res,* 40**,** 9272-85.

NONAKA, T., MASUDA-SUZUKAKE, M., ARAI, T., HASEGAWA, Y., AKATSU, H., OBI, T., YOSHIDA, M., MURAYAMA, S., MANN, D. M., AKIYAMA, H. & HASEGAWA, M. 2013. Prion-like properties of pathological TDP-43 aggregates from diseased brains. *Cell Rep,* 4**,** 124-34.

NORDBERG, A., CARTER, S. F., RINNE, J., DRZEZGA, A., BROOKS, D. J., VANDENBERGHE, R., PERANI, D., FORSBERG, A., LANGSTROM, B., SCHEININ, N., KARRASCH, M., NAGREN, K., GRIMMER, T., MIEDERER, I., EDISON, P., OKELLO, A., VAN LAERE, K., NELISSEN, N., VANDENBULCKE, M., GARIBOTTO, V., ALMKVIST, O., KALBE, E., HINZ, R. & HERHOLZ, K. 2013. A European multicentre PET study of fibrillar amyloid in Alzheimer's disease. *Eur J Nucl Med Mol Imaging,* 40**,** 104-14.

O'CONNOR, D. W., BLESSED, G., COOPER, B., JONKER, C., MORRIS, J. C., PRESNELL, I. B., AMES, D., KAY, D. W., BICKEL, H., SCHAUFELE, M., WIND, A., COATS, M. & BERG, L. 1996. Cross-national interrater reliability of dementia diagnosis in the elderly and factors associated with disagreement. *Neurology,* 47**,** 1194-9.

OLEJNICZAK, S. H., LA ROCCA, G., GRUBER, J. J. & THOMPSON, C. B. 2013. Long-lived microRNA-Argonaute complexes in quiescent cells can be activated to regulate mitogenic responses. *Proc Natl Acad Sci U S A,* 110**,** 157-62.

OLMOS-ALONSO, A., SCHETTERS, S. T. T., SRI, S., ASKEW, K., MANCUSO, R., VARGAS-CABALLERO, M., HOLSCHER, C., PERRY, V. H. & GOMEZ-NICOLA, D. 2016. Pharmacological targeting of CSF1R inhibits microglial proliferation and prevents the progression of Alzheimer's-like pathology. *Brain,* 139**,** 891-907.

OROM, U. A., DERRIEN, T., BERINGER, M., GUMIREDDY, K., GARDINI, A., BUSSOTTI, G., LAI, F., ZYTNICKI, M., NOTREDAME, C., HUANG, Q., GUIGO, R. & SHIEKHATTAR, R. 2010. Long noncoding RNAs with enhancer-like function in human cells. *Cell,* 143**,** 46-58.

OSTEIKOETXEA, X., BALOGH, A., SZABO-TAYLOR, K., NEMETH, A., SZABO, T. G., PALOCZI, K., SODAR, B., KITTEL, A., GYORGY, B., PALLINGER, E., MATKO, J. & BUZAS, E. I. 2015. Improved characterization of EV preparations based on protein to lipid ratio and lipid properties. *PLoS One,* 10**,** e0121184.

OSTROWSKI, M., CARMO, N. B., KRUMEICH, S., FANGET, I., RAPOSO, G., SAVINA, A., MOITA, C. F., SCHAUER, K., HUME, A. N., FREITAS, R. P., GOUD, B., BENAROCH, P., HACOHEN, N., FUKUDA, M., DESNOS, C., SEABRA, M. C., DARCHEN, F., AMIGORENA, S., MOITA, L. F. & THERY, C. 2010. Rab27a and Rab27b control different steps of the exosome secretion pathway. *Nat Cell Biol,* 12**,** 19-30; sup pp 1-13.

OVOD, V., RAMSEY, K. N., MAWUENYEGA, K. G., BOLLINGER, J. G., HICKS, T., SCHNEIDER, T., SULLIVAN, M., PAUMIER, K., HOLTZMAN, D. M., MORRIS, J. C., BENZINGER, T., FAGAN, A. M., PATTERSON, B. W. & BATEMAN, R. J. 2017. Amyloid beta concentrations and stable isotope labeling kinetics of human plasma specific to central nervous system amyloidosis. *Alzheimers Dement*.

PAN, B.-T. & JOHNSTONE, R. M. 1983. Fate of the transferrin receptor during maturation of sheep reticulocytes in vitro: Selective externalization of the receptor. *Cell,* 33**,** 967-978.

PAN, B. T., TENG, K., WU, C., ADAM, M. & JOHNSTONE, R. M. 1985. Electron microscopic evidence for externalization of the transferrin receptor in vesicular form in sheep reticulocytes. *J Cell Biol,* 101**,** 942-8.

PANDEY, R. R., MONDAL, T., MOHAMMAD, F., ENROTH, S., REDRUP, L., KOMOROWSKI, J., NAGANO, T., MANCINI-DINARDO, D. & KANDURI, C. 2008. Kcnq1ot1 antisense

noncoding RNA mediates lineage-specific transcriptional silencing through chromatin-level regulation. *Mol Cell,* 32**,** 232-46.

PANZA, F., FRISARDI, V., SERIPA, D., LOGROSCINO, G., SANTAMATO, A., IMBIMBO, B. P., SCAFATO, E., PILOTTO, A. & SOLFRIZZI, V. 2012. Alcohol consumption in mild cognitive impairment and dementia: harmful or neuroprotective? *Int J Geriatr Psychiatry,* 27**,** 1218-38.

PAPALEXI, E. & SATIJA, R. 2017. Single-cell RNA sequencing to explore immune cell heterogeneity. *Nat Rev Immunol*.

PEGTEL, D. M., COSMOPOULOS, K., THORLEY-LAWSON, D. A., VAN EIJNDHOVEN, M. A., HOPMANS, E. S., LINDENBERG, J. L., DE GRUIJL, T. D., WURDINGER, T. & MIDDELDORP, J. M. 2010. Functional delivery of viral miRNAs via exosomes. *Proc Natl Acad Sci U S A,* 107**,** 6328-33.

PEINADO, H., ALECKOVIC, M., LAVOTSHKIN, S., MATEI, I., COSTA-SILVA, B., MORENO-BUENO, G., HERGUETA-REDONDO, M., WILLIAMS, C., GARCIA-SANTOS, G., GHAJAR, C., NITADORI-HOSHINO, A., HOFFMAN, C., BADAL, K., GARCIA, B. A., CALLAHAN, M. K., YUAN, J., MARTINS, V. R., SKOG, J., KAPLAN, R. N., BRADY, M. S., WOLCHOK, J. D., CHAPMAN, P. B., KANG, Y., BROMBERG, J. & LYDEN, D. 2012. Melanoma exosomes educate bone marrow progenitor cells toward a pro-metastatic phenotype through MET. *Nat Med,* 18**,** 883-91.

PERICAK-VANCE, M. A., BEBOUT, J. L., GASKELL, P. C., JR., YAMAOKA, L. H., HUNG, W. Y., ALBERTS, M. J., WALKER, A. P., BARTLETT, R. J., HAYNES, C. A., WELSH, K. A. & ET AL. 1991. Linkage studies in familial Alzheimer disease: evidence for chromosome 19 linkage. *Am J Hum Genet,* 48**,** 1034-50.

PIAZZA-GARDNER, A. K., GAFFUD, T. J. & BARRY, A. E. 2013. The impact of alcohol on Alzheimer's disease: a systematic review. *Aging Ment Health,* 17**,** 133-46.

POLANCO, J. C., SCICLUNA, B. J., HILL, A. F. & GOTZ, J. 2016. Extracellular Vesicles Isolated from the Brains of rTg4510 Mice Seed Tau Protein Aggregation in a Threshold-dependent Manner. *J Biol Chem,* 291**,** 12445-66.

PRINCE, M., BRYCE, R., ALBANESE, E., WIMO, A., RIBEIRO, W. & FERRI, C. P. 2013. The global prevalence of dementia: a systematic review and metaanalysis. *Alzheimers Dement,* 9**,** 63-75.e2.

PRINCE, M., KNAPP, M., GUERCHET, M., MCCRONE, P., PRINA, M., COMAS-HERRERA, A., WITTENBERG, R., ADELAJA, B., HU, B., KING, D., REHILL, A. & SALIMKUMAR, D. 2014. Dementia UK: Update. Second edition.

PURI, N. & ROCHE, P. A. 2008. Mast cells possess distinct secretory granule subsets whose exocytosis is regulated by different SNARE isoforms. *Proc Natl Acad Sci U S A,* 105**,** 2580-5.

QIAN, J., HYMAN, B. T. & BETENSKY, R. A. 2017. Neurofibrillary Tangle Stage and the Rate of Progression of Alzheimer Symptoms: Modeling Using an Autopsy Cohort and Application to Clinical Trial Design. *JAMA Neurol,* 74**,** 540-548.

RABINOWITS, G., GERCEL-TAYLOR, C., DAY, J. M., TAYLOR, D. D. & KLOECKER, G. H. 2009. Exosomal microRNA: a diagnostic marker for lung cancer. *Clin Lung Cancer,* 10**,** 42-6.

RAINVILLE, C., AMIEVA, H., LAFONT, S., DARTIGUES, J. F., ORGOGOZO, J. M. & FABRIGOULE, C. 2002. Executive function deficits in patients with dementia of the Alzheimer's type: a study with a Tower of London task. *Arch Clin Neuropsychol,* 17**,** 513-30.

RAJENDRAN, L. & ANNAERT, W. 2012. Membrane Trafficking Pathways in Alzheimer's Disease. *Traffic,* 13**,** 759-770.

RAJENDRAN, L., HONSHO, M., ZAHN, T. R., KELLER, P., GEIGER, K. D., VERKADE, P. & SIMONS, K. 2006. Alzheimer's disease beta-amyloid peptides are released in association with exosomes. *Proc Natl Acad Sci U S A,* 103**,** 11172-7.

RAK, J. & GUHA, A. 2012. Extracellular vesicles--vehicles that spread cancer genes. *Bioessays,* 34**,** 489-97.

RAO, S. K., HUYNH, C., PROUX-GILLARDEAUX, V., GALLI, T. & ANDREWS, N. W. 2004. Identification of SNAREs involved in synaptotagmin VII-regulated lysosomal exocytosis. *J Biol Chem,* 279**,** 20471-9.

RAPOSO, G., NIJMAN, H. W., STOORVOGEL, W., LIEJENDEKKER, R., HARDING, C. V., MELIEF, C. J. & GEUZE, H. J. 1996. B lymphocytes secrete antigen-presenting vesicles. *The Journal of Experimental Medicine,* 183**,** 1161-1172.

RAPOSO, G. & STOORVOGEL, W. 2013. Extracellular vesicles: exosomes, microvesicles, and friends. *J Cell Biol,* 200**,** 373-83.

RATAJCZAK, J., MIEKUS, K., KUCIA, M., ZHANG, J., RECA, R., DVORAK, P. & RATAJCZAK, M. Z. 2006a. Embryonic stem cell-derived microvesicles reprogram hematopoietic progenitors: evidence for horizontal transfer of mRNA and protein delivery. *Leukemia,* 20**,** 847-56.

RATAJCZAK, J., WYSOCZYNSKI, M., HAYEK, F., JANOWSKA-WIECZOREK, A. & RATAJCZAK, M. Z. 2006b. Membrane-derived microvesicles: important and underappreciated mediators of cell-to-cell communication. *Leukemia,* 20**,** 1487-95.

RATAJCZAK, M. Z., KUCIA, M., JADCZYK, T., GRECO, N. J., WOJAKOWSKI, W., TENDERA, M. & RATAJCZAK, J. 2012. Pivotal role of paracrine effects in stem cell therapies in regenerative medicine: can we translate stem cell-secreted paracrine factors and microvesicles into better therapeutic strategies? *Leukemia,* 26**,** 1166-73.

REBECK, G. W., MOIR, R. D., MUI, S., STRICKLAND, D. K., TANZI, R. E. & HYMAN, B. T. 2001. Association of membrane-bound amyloid precursor protein APP with the apolipoprotein E receptor LRP. *Brain Res Mol Brain Res,* 87**,** 238-45.

REIJMER, Y. D., VAN DEN BERG, E., DEKKER, J. M., NIJPELS, G., STEHOUWER, C. D., KAPPELLE, L. J. & BIESSELS, G. J. 2012. Development of vascular risk factors over 15 years in relation to cognition: the Hoorn Study. *J Am Geriatr Soc,* 60**,** 1426-33.

RINN, J. L., KERTESZ, M., WANG, J. K., SQUAZZO, S. L., XU, X., BRUGMANN, S. A., GOODNOUGH, L. H., HELMS, J. A., FARNHAM, P. J., SEGAL, E. & CHANG, H. Y. 2007. Functional demarcation of active and silent chromatin domains in human HOX loci by noncoding RNAs. *Cell,* 129**,** 1311-23.

ROBINSON, M., LEE, B. Y. & HANE, F. T. 2017. Recent Progress in Alzheimer's Disease Research, Part 2: Genetics and Epidemiology. *J Alzheimers Dis,* 57**,** 317-330.

RODRIGUE, K. M., KENNEDY, K. M., DEVOUS, M. D., SR., RIECK, J. R., HEBRANK, A. C., DIAZ-ARRASTIA, R., MATHEWS, D. & PARK, D. C. 2012. beta-Amyloid burden in healthy aging: regional distribution and cognitive consequences. *Neurology,* 78**,** 387-95.

ROGAEV, E. I., SHERRINGTON, R., ROGAEVA, E. A., LEVESQUE, G., IKEDA, M., LIANG, Y., CHI, H., LIN, C., HOLMAN, K., TSUDA, T. & ET AL. 1995. Familial Alzheimer's disease in kindreds with missense mutations in a gene on chromosome 1 related to the Alzheimer's disease type 3 gene. *Nature,* 376**,** 775-8.

ROUCOURT, B., MEEUSSEN, S., BAO, J., ZIMMERMANN, P. & DAVID, G. 2015. Heparanase activates the syndecan-syntenin-ALIX exosome pathway. *Cell Res,* 25**,** 412-28.

ROWE, C. C., ELLIS, K. A., RIMAJOVA, M., BOURGEAT, P., PIKE, K. E., JONES, G., FRIPP, J., TOCHON-DANGUY, H., MORANDEAU, L., O'KEEFE, G., PRICE, R., RANIGA, P., ROBINS, P., ACOSTA, O., LENZO, N., SZOEKE, C., SALVADO, O., HEAD, R., MARTINS, R., MASTERS, C. L., AMES, D. & VILLEMAGNE, V. L. 2010. Amyloid imaging results from the Australian Imaging, Biomarkers and Lifestyle (AIBL) study of aging. *Neurobiol Aging,* 31**,** 1275-83.

ROYO, F., SCHLANGEN, K., PALOMO, L., GONZALEZ, E., CONDE-VANCELLS, J., BERISA, A., ARANSAY, A. M. & FALCON-PEREZ, J. M. 2013. Transcriptome of extracellular vesicles released by hepatocytes. *PLoS One,* 8**,** e68693.

ROYO, F., ZUNIGA-GARCIA, P., TORRANO, V., LOIZAGA, A., SANCHEZ-MOSQUERA, P., UGALDE-OLANO, A., GONZALEZ, E., CORTAZAR, A. R., PALOMO, L., FERNANDEZ-RUIZ, S., LACASA-VISCASILLAS, I., BERDASCO, M., SUTHERLAND, J. D., BARRIO, R., ZABALA-LETONA, A., MARTIN-MARTIN, N., ARRUABARRENA-ARISTORENA, A., VALCARCEL-JIMENEZ, L., CARO-MALDONADO, A., GONZALEZ-TAMPAN, J., CACHI-FUENTES, G., ESTELLER, M., ARANSAY, A. M., UNDA, M., FALCON-PEREZ, J. M. & CARRACEDO, A. 2016. Transcriptomic profiling of urine extracellular vesicles reveals alterations of CDH3 in prostate cancer. *Oncotarget*.

RUIZ, A., HEILMANN, S., BECKER, T., HERNANDEZ, I., WAGNER, H., THELEN, M., MAULEON, A., ROSENDE-ROCA, M., BELLENGUEZ, C., BIS, J. C., HAROLD, D., GERRISH, A., SIMS, R., SOTOLONGO-GRAU, O., ESPINOSA, A., ALEGRET, M., ARRIETA, J. L., LACOUR, A., LEBER, M., BECKER, J., LAFUENTE, A., RUIZ, S., VARGAS, L., RODRIGUEZ, O., ORTEGA, G., DOMINGUEZ, M. A., MAYEUX, R., HAINES, J. L., PERICAK-VANCE, M. A., FARRER, L. A., SCHELLENBERG, G. D., CHOURAKI, V., LAUNER, L. J., VAN DUIJN, C., SESHADRI, S., ANTUNEZ, C., BRETELER, M. M., SERRANO-RIOS, M., JESSEN, F., TARRAGA, L., NOTHEN, M. M., MAIER, W., BOADA, M. & RAMIREZ, A. 2014. Follow-up of loci from the International Genomics of Alzheimer's Disease Project identifies TRIP4 as a novel susceptibility gene. *Transl Psychiatry,* 4**,** e358.

RUSANEN, M., ROVIO, S., NGANDU, T., NISSINEN, A., TUOMILEHTO, J., SOININEN, H. & KIVIPELTO, M. 2010. Midlife smoking, apolipoprotein E and risk of dementia and Alzheimer's disease: a population-based cardiovascular risk factors, aging and dementia study. *Dement Geriatr Cogn Disord,* 30**,** 277-84.

RUSSO, C., SALIS, S., DOLCINI, V., VENEZIA, V., SONG, X. H., TELLER, J. K. & SCHETTINI, G. 2001. Amino-terminal modification and tyrosine phosphorylation of [corrected] carboxy-terminal fragments of the amyloid precursor protein in Alzheimer's disease and Down's syndrome brain. *Neurobiol Dis,* 8**,** 173-80.

SACKS, C. A., AVORN, J. & KESSELHEIM, A. S. 2017. The Failure of Solanezumab - How the FDA Saved Taxpayers Billions. *N Engl J Med,* 376**,** 1706-1708.

SAEZ, F., FRENETTE, G. & SULLIVAN, R. 2003. Epididymosomes and prostasomes: their roles in posttesticular maturation of the sperm cells. *J Androl,* 24**,** 149-54.

SAMAN, S., KIM, W., RAYA, M., VISNICK, Y., MIRO, S., SAMAN, S., JACKSON, B., MCKEE, A. C., ALVAREZ, V. E., LEE, N. C. Y. & HALL, G. F. 2012. Exosome-associated Tau Is Secreted in Tauopathy Models and Is Selectively Phosphorylated in Cerebrospinal Fluid in Early Alzheimer Disease. *Journal of Biological Chemistry,* 287**,** 3842-3849.

SANNERUD, R., DECLERCK, I., PERIC, A., RAEMAEKERS, T., MENENDEZ, G., ZHOU, L., VEERLE, B., COEN, K., MUNCK, S., DE STROOPER, B., SCHIAVO, G. & ANNAERT, W. 2011. ADP ribosylation factor 6 (ARF6) controls amyloid precursor protein (APP) processing by mediating the endosomal sorting of BACE1. *Proc Natl Acad Sci U S A,* 108**,** E559-68.

SATOH, J., KINO, Y. & NIIDA, S. 2015. MicroRNA-Seq Data Analysis Pipeline to Identify Blood Biomarkers for Alzheimer's Disease from Public Data. *Biomark Insights,* 10**,** 21-31.

SAVINA, A., VIDAL, M. & COLOMBO, M. I. 2002. The exosome pathway in K562 cells is regulated by Rab11. *J Cell Sci,* 115**,** 2505-15.

SCARMEAS, N., STERN, Y., TANG, M. X., MAYEUX, R. & LUCHSINGER, J. A. 2006. Mediterranean diet and risk for Alzheimer's disease. *Ann Neurol,* 59**,** 912-21.

SCHMITTGEN, T. D. & LIVAK, K. J. 2008. Analyzing real-time PCR data by the comparative C(T) method. *Nat Protoc,* 3**,** 1101-8.

SCOURFIELD, E. J. & MARTIN-SERRANO, J. 2017. Growing functions of the ESCRT machinery in cell biology and viral replication. *Biochem Soc Trans,* 45**,** 613-634.

SEE, K., TAN, W. L. W., LIM, E. H., TIANG, Z., LEE, L. T., LI, P. Y. Q., LUU, T. D. A., ACKERS-JOHNSON, M. & FOO, R. S. 2017. Single cardiomyocyte nuclear transcriptomes reveal

a lincRNA-regulated de-differentiation and cell cycle stress-response in vivo. *Nat Commun,* 8**,** 225.

SESHADRI, S., FITZPATRICK, A. L., IKRAM, M. A., DESTEFANO, A. L., GUDNASON, V., BOADA, M., BIS, J. C., SMITH, A. V., CARASSQUILLO, M. M., LAMBERT, J. C., HAROLD, D., SCHRIJVERS, E. M., RAMIREZ-LORCA, R., DEBETTE, S., LONGSTRETH, W. T., JR., JANSSENS, A. C., PANKRATZ, V. S., DARTIGUES, J. F., HOLLINGWORTH, P., ASPELUND, T., HERNANDEZ, I., BEISER, A., KULLER, L. H., KOUDSTAAL, P. J., DICKSON, D. W., TZOURIO, C., ABRAHAM, R., ANTUNEZ, C., DU, Y., ROTTER, J. I., AULCHENKO, Y. S., HARRIS, T. B., PETERSEN, R. C., BERR, C., OWEN, M. J., LOPEZ-ARRIETA, J., VARADARAJAN, B. N., BECKER, J. T., RIVADENEIRA, F., NALLS, M. A., GRAFF-RADFORD, N. R., CAMPION, D., AUERBACH, S., RICE, K., HOFMAN, A., JONSSON, P. V., SCHMIDT, H., LATHROP, M., MOSLEY, T. H., AU, R., PSATY, B. M., UITTERLINDEN, A. G., FARRER, L. A., LUMLEY, T., RUIZ, A., WILLIAMS, J., AMOUYEL, P., YOUNKIN, S. G., WOLF, P. A., LAUNER, L. J., LOPEZ, O. L., VAN DUIJN, C. M. & BRETELER, M. M. 2010. Genome-wide analysis of genetic loci associated with Alzheimer disease. *Jama,* 303**,** 1832-40.

SEUBERT, P., VIGO-PELFREY, C., ESCH, F., LEE, M., DOVEY, H., DAVIS, D., SINHA, S., SCHLOSSMACHER, M., WHALEY, J., SWINDLEHURST, C. & ET AL. 1992. Isolation and quantification of soluble Alzheimer's beta-peptide from biological fluids. *Nature,* 359**,** 325-7.

SEVUSH, S., LEVE, N. & BRICKMAN, A. 1993. Age at disease onset and pattern of cognitive impairment in probable Alzheimer's disease. *J Neuropsychiatry Clin Neurosci,* 5**,** 66-72.

SHANKER, S., PAULSON, A., EDENBERG, H. J., PEAK, A., PERERA, A., ALEKSEYEV, Y. O., BECKLOFF, N., BIVENS, N. J., DONNELLY, R., GILLASPY, A. F., GROVE, D., GU, W., JAFARI, N., KERLEY-HAMILTON, J. S., LYONS, R. H., TEPPER, C. & NICOLET, C. M. 2015. Evaluation of commercially available RNA amplification kits for RNA sequencing using very low input amounts of total RNA. *J Biomol Tech,* 26**,** 4-18.

SHASTRY, B. S. & GIBLIN, F. J. 1999. Genes and susceptible loci of Alzheimer's disease. *Brain Res Bull,* 48**,** 121-7.

SHAW, L. M., VANDERSTICHELE, H., KNAPIK-CZAJKA, M., CLARK, C. M., AISEN, P. S., PETERSEN, R. C., BLENNOW, K., SOARES, H., SIMON, A., LEWCZUK, P., DEAN, R., SIEMERS, E., POTTER, W., LEE, V. M. & TROJANOWSKI, J. Q. 2009. Cerebrospinal fluid biomarker signature in Alzheimer's disease neuroimaging initiative subjects. *Ann Neurol,* 65**,** 403-13.

SHELKE, G. V., LASSER, C., GHO, Y. S. & LOTVALL, J. 2014. Importance of exosome depletion protocols to eliminate functional and RNA-containing extracellular vesicles from fetal bovine serum. *J Extracell Vesicles,* 3.

SHERRINGTON, R., ROGAEV, E. I., LIANG, Y., ROGAEVA, E. A., LEVESQUE, G., IKEDA, M., CHI, H., LIN, C., LI, G., HOLMAN, K., TSUDA, T., MAR, L., FONCIN, J. F., BRUNI, A. C., MONTESI, M. P., SORBI, S., RAINERO, I., PINESSI, L., NEE, L., CHUMAKOV, I., POLLEN, D., BROOKES, A., SANSEAU, P., POLINSKY, R. J., WASCO, W., DA SILVA, H. A., HAINES, J. L., PERKICAK-VANCE, M. A., TANZI, R. E., ROSES, A. D., FRASER, P. E., ROMMENS, J. M. & ST GEORGE-HYSLOP, P. H. 1995. Cloning of a gene bearing missense mutations in early-onset familial Alzheimer's disease. *Nature,* 375**,** 754-60.

SHI, M., LIU, C., COOK, T. J., BULLOCK, K. M., ZHAO, Y., GINGHINA, C., LI, Y., ARO, P., DATOR, R., HE, C., HIPP, M. J., ZABETIAN, C. P., PESKIND, E. R., HU, S. C., QUINN, J. F., GALASKO, D. R., BANKS, W. A. & ZHANG, J. 2014. Plasma exosomal alpha-synuclein is likely CNS-derived and increased in Parkinson's disease. *Acta Neuropathol,* 128**,** 639-50.

SHI, Y., KIRWAN, P., SMITH, J., ROBINSON, H. P. & LIVESEY, F. J. 2012. Human cerebral cortex development from pluripotent stem cells to functional excitatory synapses. *Nat Neurosci,* 15**,** 477-86, s1.

SHINE, J. P., HODGETTS, C. J., POSTANS, M., LAWRENCE, A. D. & GRAHAM, K. S. 2015. APOE-epsilon4 selectively modulates posteromedial cortex activity during scene perception and short-term memory in young healthy adults. *Sci Rep,* 5**,** 16322.

SHIOI, J., ANDERSON, J. P., RIPELLINO, J. A. & ROBAKIS, N. K. 1992. Chondroitin sulfate proteoglycan form of the Alzheimer's beta-amyloid precursor. *J Biol Chem,* 267**,** 13819-22.

SHIOI, J., REFOLO, L. M., EFTHIMIOPOULOS, S. & ROBAKIS, N. K. 1993. Chondroitin sulfate proteoglycan form of cellular and cell-surface Alzheimer amyloid precursor. *Neurosci Lett,* 154**,** 121-4.

SIDHU, S. S., MENGISTAB, A. T., TAUSCHER, A. N., LAVAIL, J. & BASBAUM, C. 2004. The microvesicle as a vehicle for EMMPRIN in tumor-stromal interactions. *Oncogene,* 23**,** 956-63.

SIMPSON, R. J., KALRA, H. & MATHIVANAN, S. 2012. ExoCarta as a resource for exosomal research. *J Extracell Vesicles,* 1.

SIMS, R., VAN DER LEE, S. J., NAJ, A. C., BELLENGUEZ, C., BADARINARAYAN, N., JAKOBSDOTTIR, J., KUNKLE, B. W., BOLAND, A., RAYBOULD, R., BIS, J. C., MARTIN, E. R., GRENIER-BOLEY, B., HEILMANN-HEIMBACH, S., CHOURAKI, V., KUZMA, A. B., SLEEGERS, K., VRONSKAYA, M., RUIZ, A., GRAHAM, R. R., OLASO, R., HOFFMANN, P., GROVE, M. L., VARDARAJAN, B. N., HILTUNEN, M., NOTHEN, M. M., WHITE, C. C., HAMILTON-NELSON, K. L., EPELBAUM, J., MAIER, W., CHOI, S. H., BEECHAM, G. W., DULARY, C., HERMS, S., SMITH, A. V., FUNK, C. C., DERBOIS, C., FORSTNER, A. J., AHMAD, S., LI, H., BACQ, D., HAROLD, D., SATIZABAL, C. L., VALLADARES, O., SQUASSINA, A., THOMAS, R., BRODY, J. A., QU, L., SANCHEZ-JUAN, P., MORGAN, T., WOLTERS, F. J., ZHAO, Y., GARCIA, F. S., DENNING, N., FORNAGE, M., MALAMON, J., NARANJO, M. C. D., MAJOUNIE, E., MOSLEY, T. H., DOMBROSKI, B., WALLON, D., LUPTON, M. K., DUPUIS, J., WHITEHEAD, P., FRATIGLIONI, L., MEDWAY, C., JIAN, X., MUKHERJEE, S., KELLER, L., BROWN, K., LIN, H., CANTWELL, L. B., PANZA, F., MCGUINNESS, B., MORENO-GRAU, S., BURGESS, J. D., SOLFRIZZI, V., PROITSI, P., ADAMS, H. H., ALLEN, M., SERIPA, D., PASTOR, P., CUPPLES, L. A., PRICE, N. D., HANNEQUIN, D., FRANK-GARCIA, A., LEVY, D., CHAKRABARTY, P., CAFFARRA, P., GIEGLING, I., BEISER, A. S., GIEDRAITIS, V., HAMPEL, H., GARCIA, M. E., WANG, X., LANNFELT, L., MECOCCI, P., EIRIKSDOTTIR, G., CRANE, P. K., PASQUIER, F., BOCCARDI, V., et al. 2017. Rare coding variants in PLCG2, ABI3, and TREM2 implicate microglial-mediated innate immunity in Alzheimer's disease. *Nat Genet*.

SINFORIANI, E., ZUCCHELLA, C., PASOTTI, C., CASONI, F., BINI, P. & COSTA, A. 2011. The effects of alcohol on cognition in the elderly: from protection to neurodegeneration. *Funct Neurol,* 26**,** 103-6.

SINHA, S., ANDERSON, J. P., BARBOUR, R., BASI, G. S., CACCAVELLO, R., DAVIS, D., DOAN, M., DOVEY, H. F., FRIGON, N., HONG, J., JACOBSON-CROAK, K., JEWETT, N., KEIM, P., KNOPS, J., LIEBERBURG, I., POWER, M., TAN, H., TATSUNO, G., TUNG, J., SCHENK, D., SEUBERT, P., SUOMENSAARI, S. M., WANG, S., WALKER, D., ZHAO, J., MCCONLOGUE, L. & JOHN, V. 1999. Purification and cloning of amyloid precursor protein beta-secretase from human brain. *Nature,* 402**,** 537-40.

SKOG, J., WURDINGER, T., VAN RIJN, S., MEIJER, D. H., GAINCHE, L., SENA-ESTEVES, M., CURRY, W. T., JR., CARTER, B. S., KRICHEVSKY, A. M. & BREAKEFIELD, X. O. 2008. Glioblastoma microvesicles transport RNA and proteins that promote tumour growth and provide diagnostic biomarkers. *Nat Cell Biol,* 10**,** 1470-6.

SKOOG, I., LERNFELT, B., LANDAHL, S., PALMERTZ, B., ANDREASSON, L. A., NILSSON, L., PERSSON, G., ODEN, A. & SVANBORG, A. 1996. 15-year longitudinal study of blood pressure and dementia. *Lancet,* 347**,** 1141-5.

SOFI, F., VALECCHI, D., BACCI, D., ABBATE, R., GENSINI, G. F., CASINI, A. & MACCHI, C. 2011. Physical activity and risk of cognitive decline: a meta-analysis of prospective studies. *J Intern Med,* 269**,** 107-17.

SOJKOVA, J., DRISCOLL, I., IACONO, D., ZHOU, Y., CODISPOTI, K. E., KRAUT, M. A., FERRUCCI, L., PLETNIKOVA, O., MATHIS, C. A., KLUNK, W. E., O'BRIEN, R. J., WONG, D. F., TRONCOSO, J. C. & RESNICK, S. M. 2011. In vivo fibrillar beta-amyloid detected using [11C]PiB positron emission tomography and neuropathologic assessment in older adults. *Arch Neurol,* 68**,** 232-40.

SOLOMON, A., KAREHOLT, I., NGANDU, T., WINBLAD, B., NISSINEN, A., TUOMILEHTO, J., SOININEN, H. & KIVIPELTO, M. 2007. Serum cholesterol changes after midlife and late-life cognition: twenty-one-year follow-up study. *Neurology,* 68**,** 751-6.

SPOSITO, T., PREZA, E., MAHONEY, C. J., SETO-SALVIA, N., RYAN, N. S., MORRIS, H. R., ARBER, C., DEVINE, M. J., HOULDEN, H., WARNER, T. T., BUSHELL, T. J., ZAGNONI, M., KUNATH, T., LIVESEY, F. J., FOX, N. C., ROSSOR, M. N., HARDY, J. & WRAY, S. 2015. Developmental regulation of tau splicing is disrupted in stem cell-derived neurons from frontotemporal dementia patients with the 10 + 16 splice-site mutation in MAPT. *Hum Mol Genet,* 24**,** 5260-9.

ST GEORGE-HYSLOP, P. H., TANZI, R. E., POLINSKY, R. J., HAINES, J. L., NEE, L., WATKINS, P. C., MYERS, R. H., FELDMAN, R. G., POLLEN, D., DRACHMAN, D. & ET AL. 1987. The genetic defect causing familial Alzheimer's disease maps on chromosome 21. *Science,* 235**,** 885-90.

STALDER, L., HEUSERMANN, W., SOKOL, L., TROJER, D., WIRZ, J., HEAN, J., FRITZSCHE, A., AESCHIMANN, F., PFANZAGL, V., BASSELET, P., WEILER, J., HINTERSTEINER, M., MORRISSEY, D. V. & MEISNER-KOBER, N. C. 2013. The rough endoplasmatic reticulum is a central nucleation site of siRNA-mediated RNA silencing. *Embo j,* 32**,** 1115-27.

STAUBACH, S., RAZAWI, H. & HANISCH, F. G. 2009. Proteomics of MUC1-containing lipid rafts from plasma membranes and exosomes of human breast carcinoma cells MCF-7. *Proteomics,* 9**,** 2820-35.

STERN, R. A., TRIPODIS, Y., BAUGH, C. M., FRITTS, N. G., MARTIN, B. M., CHAISSON, C., CANTU, R. C., JOYCE, J. A., SHAH, S., IKEZU, T., ZHANG, J., GERCEL-TAYLOR, C. & TAYLOR, D. D. 2016. Preliminary Study of Plasma Exosomal Tau as a Potential Biomarker for Chronic Traumatic Encephalopathy. *J Alzheimers Dis*.

STERN, Y., ALBERT, M., BRANDT, J., JACOBS, D. M., TANG, M. X., MARDER, K., BELL, K., SANO, M., DEVANAND, D. P., BYLSMA, F. & ET AL. 1994a. Utility of extrapyramidal signs and psychosis as predictors of cognitive and functional decline, nursing home admission, and death in Alzheimer's disease: prospective analyses from the Predictors Study. *Neurology,* 44**,** 2300-7.

STERN, Y., GURLAND, B., TATEMICHI, T. K., TANG, M. X., WILDER, D. & MAYEUX, R. 1994b. Influence of education and occupation on the incidence of Alzheimer's disease. *Jama,* 271**,** 1004-10.

STOORVOGEL, W. 2015. Resolving sorting mechanisms into exosomes. *Cell Res,* 25**,** 531-2.

STOORVOGEL, W., KLEIJMEER, M. J., GEUZE, H. J. & RAPOSO, G. 2002. The biogenesis and functions of exosomes. *Traffic,* 3**,** 321-30.

STROZYK, D., BLENNOW, K., WHITE, L. R. & LAUNER, L. J. 2003. CSF Abeta 42 levels correlate with amyloid-neuropathology in a population-based autopsy study. *Neurology,* 60**,** 652-6.

SULLIVAN, R., SAEZ, F., GIROUARD, J. & FRENETTE, G. 2005. Role of exosomes in sperm maturation during the transit along the male reproductive tract. *Blood Cells Mol Dis,* 35**,** 1-10.

SUNG, H. Y., CHOI, B. O., JEONG, J. H., KONG, K. A., HWANG, J. & AHN, J. H. 2016. Amyloid Beta-Mediated Hypomethylation of Heme Oxygenase 1 Correlates with Cognitive Impairment in Alzheimer's Disease. *PLoS One,* 11**,** e0153156.

SUZUKI, N., IWATSUBO, T., ODAKA, A., ISHIBASHI, Y., KITADA, C. & IHARA, Y. 1994a. High tissue content of soluble beta 1-40 is linked to cerebral amyloid angiopathy. *Am J Pathol,* 145**,** 452-60.

SUZUKI, T., OISHI, M., MARSHAK, D. R., CZERNIK, A. J., NAIRN, A. C. & GREENGARD, P. 1994b. Cell cycle-dependent regulation of the phosphorylation and metabolism of the Alzheimer amyloid precursor protein. *Embo j,* 13**,** 1114-22.

SZOSTAK, N., ROYO, F., RYBARCZYK, A., SZACHNIUK, M., BLAZEWICZ, J., DEL SOL, A. & FALCON-PEREZ, J. M. 2014. Sorting signal targeting mRNA into hepatic extracellular vesicles. *RNA Biol,* 11**,** 836-44.

TAKAHASHI, J. 2017. Strategies for bringing stem cell-derived dopamine neurons to the clinic: The Kyoto trial. *Prog Brain Res,* 230**,** 213-226.

TAKAHASHI, K., ROCHFORD, C. D. & NEUMANN, H. 2005. Clearance of apoptotic neurons without inflammation by microglial triggering receptor expressed on myeloid cells-2. *J Exp Med,* 201**,** 647-57.

TAKAHASHI, K. & YAMANAKA, S. 2006. Induction of pluripotent stem cells from mouse embryonic and adult fibroblast cultures by defined factors. *Cell,* 126**,** 663-76.

TAMBOLI, I. Y., BARTH, E., CHRISTIAN, L., SIEPMANN, M., KUMAR, S., SINGH, S., TOLKSDORF, K., HENEKA, M. T., LUTJOHANN, D., WUNDERLICH, P. & WALTER, J. 2010. Statins promote the degradation of extracellular amyloid {beta}-peptide by microglia via stimulation of exosome-associated insulin-degrading enzyme (IDE) secretion. *J Biol Chem,* 285**,** 37405-14.

TAN, L., YU, J. T., LIU, Q. Y., TAN, M. S., ZHANG, W., HU, N., WANG, Y. L., SUN, L. & JIANG, T. 2014a. Circulating miR-125b as a biomarker of Alzheimer's disease. *J Neurol Sci,* 336**,** 52-6.

TAN, L., YU, J. T., TAN, M. S., LIU, Q. Y., WANG, H. F., ZHANG, W. & JIANG, T. 2014b. Genome-wide serum microRNA expression profiling identifies serum biomarkers for Alzheimer's disease. *J Alzheimers Dis,* 40**,** 1017-27.

TAN, M., YAN, H. B., LI, J. N., LI, W. K., FU, Y. Y., CHEN, W. & ZHOU, Z. 2016. Thrombin Stimulated Platelet-Derived Exosomes Inhibit Platelet-Derived Growth Factor Receptor-Beta Expression in Vascular Smooth Muscle Cells. *Cell Physiol Biochem,* 38**,** 2348-65.

TANZI, R. E. & BERTRAM, L. 2005. Twenty years of the Alzheimer's disease amyloid hypothesis: a genetic perspective. *Cell,* 120**,** 545-55.

TAPIOLA, T., ALAFUZOFF, I., HERUKKA, S. K., PARKKINEN, L., HARTIKAINEN, P., SOININEN, H. & PIRTTILA, T. 2009. Cerebrospinal fluid {beta}-amyloid 42 and tau proteins as biomarkers of Alzheimer-type pathologic changes in the brain. *Arch Neurol,* 66**,** 382-9.

TAYLOR, D. D., GERCEL-TAYLOR, C. & PARKER, L. P. 2009. Patient-derived tumor-reactive antibodies as diagnostic markers for ovarian cancer. *Gynecol Oncol,* 115**,** 112-20.

THERY, C., AMIGORENA, S., RAPOSO, G. & CLAYTON, A. 2006. Isolation and characterization of exosomes from cell culture supernatants and biological fluids. *Curr Protoc Cell Biol,* Chapter 3**,** Unit 3.22.

THERY, C., BOUSSAC, M., VERON, P., RICCIARDI-CASTAGNOLI, P., RAPOSO, G., GARIN, J. & AMIGORENA, S. 2001. Proteomic analysis of dendritic cell-derived exosomes: a

secreted subcellular compartment distinct from apoptotic vesicles. *J Immunol,* 166**,** 7309-18.

THERY, C., REGNAULT, A., GARIN, J., WOLFERS, J., ZITVOGEL, L., RICCIARDI-CASTAGNOLI, P., RAPOSO, G. & AMIGORENA, S. 1999. Molecular characterization of dendritic cell-derived exosomes. Selective accumulation of the heat shock protein hsc73. *J Cell Biol,* 147**,** 599-610.

THERY, C., ZITVOGEL, L. & AMIGORENA, S. 2002. Exosomes: composition, biogenesis and function. *Nat Rev Immunol,* 2**,** 569-79.

THINAKARAN, G. & KOO, E. H. 2008. Amyloid precursor protein trafficking, processing, and function. *J Biol Chem,* 283**,** 29615-9.

THINAKARAN, G., SLUNT, H. H. & SISODIA, S. S. 1995. Novel regulation of chondroitin sulfate glycosaminoglycan modification of amyloid precursor protein and its homologue, APLP2. *J Biol Chem,* 270**,** 16522-5.

THINAKARAN, G., TEPLOW, D. B., SIMAN, R., GREENBERG, B. & SISODIA, S. S. 1996. Metabolism of the "Swedish" amyloid precursor protein variant in neuro2a (N2a) cells. Evidence that cleavage at the "beta-secretase" site occurs in the golgi apparatus. *J Biol Chem,* 271**,** 9390-7.

TIWARI, N., WANG, C. C., BROCHETTA, C., KE, G., VITA, F., QI, Z., RIVERA, J., SORANZO, M. R., ZABUCCHI, G., HONG, W. & BLANK, U. 2008. VAMP-8 segregates mast cell-preformed mediator exocytosis from cytokine trafficking pathways. *Blood,* 111**,** 3665-74.

TOLBOOM, N., VAN DER FLIER, W. M., YAQUB, M., BOELLAARD, R., VERWEY, N. A., BLANKENSTEIN, M. A., WINDHORST, A. D., SCHELTENS, P., LAMMERTSMA, A. A. & VAN BERCKEL, B. N. 2009. Relationship of cerebrospinal fluid markers to 11C-PiB and 18F-FDDNP binding. *J Nucl Med,* 50**,** 1464-70.

TOLPPANEN, A. M., LAVIKAINEN, P., SOLOMON, A., KIVIPELTO, M., UUSITUPA, M., SOININEN, H. & HARTIKAINEN, S. 2013. History of medically treated diabetes and risk of Alzheimer disease in a nationwide case-control study. *Diabetes Care,* 36**,** 2015-9.

TOLPPANEN, A. M., NGANDU, T., KAREHOLT, I., LAATIKAINEN, T., RUSANEN, M., SOININEN, H. & KIVIPELTO, M. 2014. Midlife and late-life body mass index and late-life dementia: results from a prospective population-based cohort. *J Alzheimers Dis,* 38**,** 201-9.

TOSAR, J. P., GAMBARO, F., SANGUINETTI, J., BONILLA, B., WITWER, K. W. & CAYOTA, A. 2015. Assessment of small RNA sorting into different extracellular fractions revealed by high-throughput sequencing of breast cell lines. *Nucleic Acids Res,* 43**,** 5601-16.

TOSTO, G. & REITZ, C. 2013. Genome-wide association studies in Alzheimer's disease: a review. *Curr Neurol Neurosci Rep,* 13**,** 381.

TRAJKOVIC, K., HSU, C., CHIANTIA, S., RAJENDRAN, L., WENZEL, D., WIELAND, F., SCHWILLE, P., BRUGGER, B. & SIMONS, M. 2008. Ceramide triggers budding of exosome vesicles into multivesicular endosomes. *Science,* 319**,** 1244-7.

TRAMS, E. G., LAUTER, C. J., NORMAN SALEM, JR. & HEINE, U. 1981. Exfoliation of membrane ecto-enzymes in the form of micro-vesicles. *Biochimica et Biophysica Acta (BBA) - Biomembranes,* 645**,** 63-70.

TSUNEMI, T., HAMADA, K. & KRAINC, D. 2014. ATP13A2/PARK9 regulates secretion of exosomes and alpha-synuclein. *J Neurosci,* 34**,** 15281-7.

TURCHINOVICH, A., WEIZ, L., LANGHEINZ, A. & BURWINKEL, B. 2011. Characterization of extracellular circulating microRNA. *Nucleic Acids Res,* 39**,** 7223-33.

TURIAK, L., MISJAK, P., SZABO, T. G., ARADI, B., PALOCZI, K., OZOHANICS, O., DRAHOS, L., KITTEL, A., FALUS, A., BUZAS, E. I. & VEKEY, K. 2011. Proteomic characterization of thymocyte-derived microvesicles and apoptotic bodies in BALB/c mice. *J Proteomics,* 74**,** 2025-33.

UDAYAR, V., BUGGIA-PREVOT, V., GUERREIRO, R. L., SIEGEL, G., RAMBABU, N., SOOHOO, A. L., PONNUSAMY, M., SIEGENTHALER, B., BALI, J., SIMONS, M., RIES, J., PUTHENVEEDU, M. A., HARDY, J., THINAKARAN, G. & RAJENDRAN, L. 2013. A paired RNAi and RabGAP overexpression screen identifies Rab11 as a regulator of beta-amyloid production. *Cell Rep,* 5**,** 1536-51.

ULIANOV, S. V., TACHIBANA-KONWALSKI, K. & RAZIN, S. V. 2017. Single-cell Hi-C bridges microscopy and genome-wide sequencing approaches to study 3D chromatin organization. *Bioessays*.

UNTERGASSER, A., CUTCUTACHE, I., KORESSAAR, T., YE, J., FAIRCLOTH, B. C., REMM, M. & ROZEN, S. G. 2012. Primer3--new capabilities and interfaces. *Nucleic Acids Res,* 40**,** e115.

VALADI, H., EKSTROM, K., BOSSIOS, A., SJOSTRAND, M., LEE, J. J. & LOTVALL, J. O. 2007. Exosome-mediated transfer of mRNAs and microRNAs is a novel mechanism of genetic exchange between cells. *Nat Cell Biol,* 9**,** 654-9.

VAN BROECKHOVEN, C., BACKHOVENS, H., CRUTS, M., DE WINTER, G., BRUYLAND, M., CRAS, P. & MARTIN, J. J. 1992. Mapping of a gene predisposing to early-onset Alzheimer's disease to chromosome 14q24.3. *Nat Genet,* 2**,** 335-9.

VAN DEUN, J., MESTDAGH, P., AGOSTINIS, P., AKAY, O., ANAND, S., ANCKAERT, J., MARTINEZ, Z. A., BAETENS, T., BEGHEIN, E., BERTIER, L., BERX, G., BOERE, J., BOUKOURIS, S., BREMER, M., BUSCHMANN, D., BYRD, J. B., CASERT, C., CHENG, L., CMOCH, A., DAVELOOSE, D., DE SMEDT, E., DEMIRSOY, S., DEPOORTER, V., DHONDT, B., DRIEDONKS, T. A., DUDEK, A., ELSHARAWY, A., FLORIS, I., FOERS, A. D., GARTNER, K., GARG, A. D., GEEURICKX, E., GETTEMANS, J., GHAZAVI, F., GIEBEL, B., KORMELINK, T. G., HANCOCK, G., HELSMOORTEL, H., HILL, A. F., HYENNE, V., KALRA, H., KIM, D., KOWAL, J., KRAEMER, S., LEIDINGER, P., LEONELLI, C., LIANG, Y., LIPPENS, L., LIU, S., LO CICERO, A., MARTIN, S., MATHIVANAN, S., MATHIYALAGAN, P., MATUSEK, T., MILANI, G., MONGUIO-TORTAJADA, M., MUS, L. M., MUTH, D. C., NEMETH, A., NOLTE-'T HOEN, E. N., O'DRISCOLL, L., PALMULLI, R., PFAFFL, M. W., PRIMDAL-BENGTSON, B., ROMANO, E., ROUSSEAU, Q., SAHOO, S., SAMPAIO, N., SAMUEL, M., SCICLUNA, B., SOEN, B., STEELS, A., SWINNEN, J. V., TAKATALO, M., THAMINY, S., THERY, C., TULKENS, J., VAN AUDENHOVE, I., VAN DER GREIN, S., VAN GOETHEM, A., VAN HERWIJNEN, M. J., VAN NIEL, G., VAN ROY, N., VAN VLIET, A. R., VANDAMME, N., VANHAUWAERT, S., VERGAUWEN, G., VERWEIJ, F., WALLAERT, A., WAUBEN, M., WITWER, K. W., ZONNEVELD, M. I., DE WEVER, O., VANDESOMPELE, J. & HENDRIX, A. 2017. EV-TRACK: transparent reporting and centralizing knowledge in extracellular vesicle research. *Nat Methods,* 14**,** 228-232.

VAN HERWIJNEN, M. J., ZONNEVELD, M. I., GOERDAYAL, S., NOLTE-'T HOEN, E. N., GARSSEN, J., STAHL, B., MAARTEN ALTELAAR, A. F., REDEGELD, F. A. & WAUBEN, M. H. 2016. Comprehensive Proteomic Analysis of Human Milk-derived Extracellular Vesicles Unveils a Novel Functional Proteome Distinct from Other Milk Components. *Mol Cell Proteomics,* 15**,** 3412-3423.

VAN NIEL, G. 2016. Study of Exosomes Shed New Light on Physiology of Amyloidogenesis. *Cell Mol Neurobiol,* 36**,** 327-42.

VAN NIEL, G., WUBBOLTS, R. & STOORVOGEL, W. 2008. Endosomal sorting of MHC class II determines antigen presentation by dendritic cells. *Curr Opin Cell Biol,* 20**,** 437-44.

VAN NIEL, G., WUBBOLTS, R., TEN BROEKE, T., BUSCHOW, S. I., OSSENDORP, F. A., MELIEF, C. J., RAPOSO, G., VAN BALKOM, B. W. & STOORVOGEL, W. 2006. Dendritic cells regulate exposure of MHC class II at their plasma membrane by oligoubiquitination. *Immunity,* 25**,** 885-94.

VAN VLIET, P., VAN DE WATER, W., DE CRAEN, A. J. & WESTENDORP, R. G. 2009. The influence of age on the association between cholesterol and cognitive function. *Exp Gerontol,* 44**,** 112-22.

VASSAR, R. 2001. The beta-secretase, BACE: a prime drug target for Alzheimer's disease. *J Mol Neurosci,* 17**,** 157-70.

VASSAR, R., BENNETT, B. D., BABU-KHAN, S., KAHN, S., MENDIAZ, E. A., DENIS, P., TEPLOW, D. B., ROSS, S., AMARANTE, P., LOELOFF, R., LUO, Y., FISHER, S., FULLER, J., EDENSON, S., LILE, J., JAROSINSKI, M. A., BIERE, A. L., CURRAN, E., BURGESS, T., LOUIS, J. C., COLLINS, F., TREANOR, J., ROGERS, G. & CITRON, M. 1999. Beta-secretase cleavage of Alzheimer's amyloid precursor protein by the transmembrane aspartic protease BACE. *Science,* 286**,** 735-41.

VELLA, L. J., SHARPLES, R. A., LAWSON, V. A., MASTERS, C. L., CAPPAI, R. & HILL, A. F. 2007. Packaging of prions into exosomes is associated with a novel pathway of PrP processing. *J Pathol,* 211**,** 582-90.

VEMURI, P., WHITWELL, J. L., KANTARCI, K., JOSEPHS, K. A., PARISI, J. E., SHIUNG, M. S., KNOPMAN, D. S., BOEVE, B. F., PETERSEN, R. C., DICKSON, D. W. & JACK, C. R., JR. 2008. Antemortem MRI based STructural Abnormality iNDex (STAND)-scores correlate with postmortem Braak neurofibrillary tangle stage. *Neuroimage,* 42**,** 559-67.

VEMURI, P., WISTE, H. J., WEIGAND, S. D., SHAW, L. M., TROJANOWSKI, J. Q., WEINER, M. W., KNOPMAN, D. S., PETERSEN, R. C. & JACK, C. R., JR. 2009. MRI and CSF biomarkers in normal, MCI, and AD subjects: diagnostic discrimination and cognitive correlations. *Neurology,* 73**,** 287-93.

VICKERS, K. C., PALMISANO, B. T., SHOUCRI, B. M., SHAMBUREK, R. D. & REMALEY, A. T. 2011. MicroRNAs are transported in plasma and delivered to recipient cells by high-density lipoproteins. *Nat Cell Biol,* 13**,** 423-33.

VIERECK, J., KUMARSWAMY, R., FOINQUINOS, A., XIAO, K., AVRAMOPOULOS, P., KUNZ, M., DITTRICH, M., MAETZIG, T., ZIMMER, K., REMKE, J., JUST, A., FENDRICH, J., SCHERF, K., BOLESANI, E., SCHAMBACH, A., WEIDEMANN, F., ZWEIGERDT, R., DE WINDT, L. J., ENGELHARDT, S., DANDEKAR, T., BATKAI, S. & THUM, T. 2016. Long noncoding RNA Chast promotes cardiac remodeling. *Sci Transl Med,* 8**,** 326ra22.

VILLAREAL, D. T. & MORRIS, J. C. 1999. The diagnosis of Alzheimer's disease. *J Alzheimers Dis,* 1**,** 249-63.

VILLARROYA-BELTRI, C., GUTIERREZ-VAZQUEZ, C., SANCHEZ-CABO, F., PEREZ-HERNANDEZ, D., VAZQUEZ, J., MARTIN-COFRECES, N., MARTINEZ-HERRERA, D. J., PASCUAL-MONTANO, A., MITTELBRUNN, M. & SANCHEZ-MADRID, F. 2013. Sumoylated hnRNPA2B1 controls the sorting of miRNAs into exosomes through binding to specific motifs. *Nat Commun,* 4**,** 2980.

VILLEMAGNE, V. L., BURNHAM, S., BOURGEAT, P., BROWN, B., ELLIS, K. A., SALVADO, O., SZOEKE, C., MACAULAY, S. L., MARTINS, R., MARUFF, P., AMES, D., ROWE, C. C. & MASTERS, C. L. 2013. Amyloid beta deposition, neurodegeneration, and cognitive decline in sporadic Alzheimer's disease: a prospective cohort study. *Lancet Neurol,* 12**,** 357-67.

VILLEMAGNE, V. L., PIKE, K. E., CHETELAT, G., ELLIS, K. A., MULLIGAN, R. S., BOURGEAT, P., ACKERMANN, U., JONES, G., SZOEKE, C., SALVADO, O., MARTINS, R., O'KEEFE, G., MATHIS, C. A., KLUNK, W. E., AMES, D., MASTERS, C. L. & ROWE, C. C. 2011. Longitudinal assessment of Abeta and cognition in aging and Alzheimer disease. *Ann Neurol,* 69**,** 181-92.

VIRTA, J. J., HEIKKILA, K., PEROLA, M., KOSKENVUO, M., RAIHA, I., RINNE, J. O. & KAPRIO, J. 2013. Midlife cardiovascular risk factors and late cognitive impairment. *Eur J Epidemiol,* 28**,** 405-16.

VISSER, P. J., VERHEY, F., KNOL, D. L., SCHELTENS, P., WAHLUND, L. O., FREUND-LEVI, Y., TSOLAKI, M., MINTHON, L., WALLIN, A. K., HAMPEL, H., BURGER, K., PIRTTILA, T., SOININEN, H., RIKKERT, M. O., VERBEEK, M. M., SPIRU, L. & BLENNOW, K. 2009. Prevalence and prognostic value of CSF markers of Alzheimer's disease pathology in patients with subjective cognitive impairment or mild cognitive impairment in the DESCRIPA study: a prospective cohort study. *Lancet Neurol,* 8**,** 619-27.

VON SCHWEDLER, U. K., STUCHELL, M., MULLER, B., WARD, D. M., CHUNG, H. Y., MORITA, E., WANG, H. E., DAVIS, T., HE, G. P., CIMBORA, D. M., SCOTT, A., KRAUSSLICH, H. G., KAPLAN, J., MORHAM, S. G. & SUNDQUIST, W. I. 2003. The protein network of HIV budding. *Cell,* 114**,** 701-13.

WEBBER, J. & CLAYTON, A. 2013. How pure are your vesicles? *Journal of Extracellular Vesicles; Vol 2 (2013) incl Supplements*.

WEBBER, J., STEADMAN, R., MASON, M. D., TABI, Z. & CLAYTON, A. 2010. Cancer exosomes trigger fibroblast to myofibroblast differentiation. *Cancer Res,* 70**,** 9621-30.

WEBBER, J., STONE, T. C., KATILIUS, E., SMITH, B. C., GORDON, B., MASON, M. D., TABI, Z., BREWIS, I. A. & CLAYTON, A. 2014. Proteomics analysis of cancer exosomes using a novel modified aptamer-based array (SOMAscan) platform. *Mol Cell Proteomics,* 13**,** 1050-64.

WEBBER, J. P., SPARY, L. K., SANDERS, A. J., CHOWDHURY, R., JIANG, W. G., STEADMAN, R., WYMANT, J., JONES, A. T., KYNASTON, H., MASON, M. D., TABI, Z. & CLAYTON, A. 2015. Differentiation of tumour-promoting stromal myofibroblasts by cancer exosomes. *Oncogene,* 34**,** 290-302.

WEGGEN, S. & BEHER, D. 2012. Molecular consequences of amyloid precursor protein and presenilin mutations causing autosomal-dominant Alzheimer's disease. *Alzheimer's Research & Therapy,* 4**,** 9-9.

WEIGAND, S. D., VEMURI, P., WISTE, H. J., SENJEM, M. L., PANKRATZ, V. S., AISEN, P. S., WEINER, M. W., PETERSEN, R. C., SHAW, L. M., TROJANOWSKI, J. Q., KNOPMAN, D. S. & JACK, C. R., JR. 2011. Transforming cerebrospinal fluid Abeta42 measures into calculated Pittsburgh Compound B units of brain Abeta amyloid. *Alzheimers Dement,* 7**,** 133-41.

WELTON, J. L., BRENNAN, P., GURNEY, M., WEBBER, J. P., SPARY, L. K., CARTON, D. G., FALCON-PEREZ, J. M., WALTON, S. P., MASON, M. D., TABI, Z. & CLAYTON, A. 2016. Proteomics analysis of vesicles isolated from plasma and urine of prostate cancer patients using a multiplex, aptamer-based protein array. *J Extracell Vesicles,* 5**,** 31209.

WELTON, J. L., WEBBER, J. P., BOTOS, L. A., JONES, M. & CLAYTON, A. 2015. Ready-made chromatography columns for extracellular vesicle isolation from plasma. *J Extracell Vesicles,* 4**,** 27269.

WHITE, P. & CLARE, A. 2002. Clinical Medicine. Edinburgh: WB Saunders.

WHITMER, R. A., GUNDERSON, E. P., QUESENBERRY, C. P., JR., ZHOU, J. & YAFFE, K. 2007. Body mass index in midlife and risk of Alzheimer disease and vascular dementia. *Curr Alzheimer Res,* 4**,** 103-9.

WHITMER, R. A., SIDNEY, S., SELBY, J., JOHNSTON, S. C. & YAFFE, K. 2005. Midlife cardiovascular risk factors and risk of dementia in late life. *Neurology,* 64**,** 277-81.

WHITWELL, J. L., JOSEPHS, K. A., MURRAY, M. E., KANTARCI, K., PRZYBELSKI, S. A., WEIGAND, S. D., VEMURI, P., SENJEM, M. L., PARISI, J. E., KNOPMAN, D. S., BOEVE, B. F., PETERSEN, R. C., DICKSON, D. W. & JACK, C. R., JR. 2008. MRI correlates of neurofibrillary tangle pathology at autopsy: a voxel-based morphometry study. *Neurology,* 71**,** 743-9.

WIECKOWSKI, E. U., VISUS, C., SZAJNIK, M., SZCZEPANSKI, M. J., STORKUS, W. J. & WHITESIDE, T. L. 2009. Tumor-derived microvesicles promote regulatory T cell

expansion and induce apoptosis in tumor-reactive activated CD8+ T lymphocytes. *J Immunol,* 183**,** 3720-30.

WILEY, R. D. & GUMMULURU, S. 2006. Immature dendritic cell-derived exosomes can mediate HIV-1 trans infection. *Proc Natl Acad Sci U S A,* 103**,** 738-43.

WILKERSON, M. D., CABANSKI, C. R., SUN, W., HOADLEY, K. A., WALTER, V., MOSE, L. E., TROESTER, M. A., HAMMERMAN, P. S., PARKER, J. S., PEROU, C. M. & HAYES, D. N. 2014. Integrated RNA and DNA sequencing improves mutation detection in low purity tumors. *Nucleic Acids Res,* 42**,** e107.

WILKINS, R. H. & BRODY, I. A. 1969. Alzheimer's disease. *Arch Neurol,* 21**,** 109-10.

WILSON, R. S., YU, L., TROJANOWSKI, J. Q., CHEN, E. Y., BOYLE, P. A., BENNETT, D. A. & SCHNEIDER, J. A. 2013. TDP-43 pathology, cognitive decline, and dementia in old age. *JAMA Neurol,* 70**,** 1418-24.

WOLFERS, J., LOZIER, A., RAPOSO, G., REGNAULT, A., THERY, C., MASURIER, C., FLAMENT, C., POUZIEUX, S., FAURE, F., TURSZ, T., ANGEVIN, E., AMIGORENA, S. & ZITVOGEL, L. 2001. Tumor-derived exosomes are a source of shared tumor rejection antigens for CTL cross-priming. *Nat Med,* 7**,** 297-303.

WREN, M. C., ZHAO, J., LIU, C. C., MURRAY, M. E., ATAGI, Y., DAVIS, M. D., FU, Y., OKANO, H. J., OGAKI, K., STRONGOSKY, A. J., TACIK, P., RADEMAKERS, R., ROSS, O. A., DICKSON, D. W., WSZOLEK, Z. K., KANEKIYO, T. & BU, G. 2015. Frontotemporal dementia-associated N279K tau mutant disrupts subcellular vesicle trafficking and induces cellular stress in iPSC-derived neural stem cells. *Mol Neurodegener,* 10**,** 46.

WU, Y., DENG, W. & KLINKE, D. J., 2ND 2015. Exosomes: improved methods to characterize their morphology, RNA content, and surface protein biomarkers. *Analyst,* 140**,** 6631-42.

WU, Y., KWAK, K. J., AGARWAL, K., MARRAS, A., WANG, C., MAO, Y., HUANG, X., MA, J., YU, B., LEE, R., VACHANI, A., MARCUCCI, G., BYRD, J. C., MUTHUSAMY, N., OTTERSON, G., HUANG, K., CASTRO, C. E., PAULAITIS, M., NANA-SINKAM, S. P. & LEE, L. J. 2013. Detection of extracellular RNAs in cancer and viral infection via tethered cationic lipoplex nanoparticles containing molecular beacons. *Anal Chem,* 85**,** 11265-74.

WUBBOLTS, R., LECKIE, R. S., VEENHUIZEN, P. T., SCHWARZMANN, G., MOBIUS, W., HOERNSCHEMEYER, J., SLOT, J. W., GEUZE, H. J. & STOORVOGEL, W. 2003. Proteomic and biochemical analyses of human B cell-derived exosomes. Potential implications for their function and multivesicular body formation. *J Biol Chem,* 278**,** 10963-72.

XIAO, T., ZHANG, W., JIAO, B., PAN, C. Z., LIU, X. & SHEN, L. 2017. The role of exosomes in the pathogenesis of Alzheimer' disease. *Transl Neurodegener,* 6**,** 3.

XU, R., GREENING, D. W., RAI, A., JI, H. & SIMPSON, R. J. 2015. Highly-purified exosomes and shed microvesicles isolated from the human colon cancer cell line LIM1863 by sequential centrifugal ultrafiltration are biochemically and functionally distinct. *Methods,* 87**,** 11-25.

YAMAMIZU, K., IWASAKI, M., TAKAKUBO, H., SAKAMOTO, T., IKUNO, T., MIYOSHI, M., KONDO, T., NAKAO, Y., NAKAGAWA, M., INOUE, H. & YAMASHITA, J. K. 2017. In Vitro Modeling of Blood-Brain Barrier with Human iPSC-Derived Endothelial Cells, Pericytes, Neurons, and Astrocytes via Notch Signaling. *Stem Cell Reports,* 8**,** 634-647.

YAN, R., BIENKOWSKI, M. J., SHUCK, M. E., MIAO, H., TORY, M. C., PAULEY, A. M., BRASHIER, J. R., STRATMAN, N. C., MATHEWS, W. R., BUHL, A. E., CARTER, D. B., TOMASSELLI, A. G., PARODI, L. A., HEINRIKSON, R. L. & GURNEY, M. E. 1999. Membrane-anchored aspartyl protease with Alzheimer's disease beta-secretase activity. *Nature,* 402**,** 533-7.

YANG, Y., LI, Y., CHEN, X., CHENG, X., LIAO, Y. & YU, X. 2016. Exosomal transfer of miR-30a between cardiomyocytes regulates autophagy after hypoxia. *J Mol Med (Berl),* 94**,** 711-24.

YUYAMA, K. & IGARASHI, Y. 2017. Exosomes as Carriers of Alzheimer's Amyloid-ss. *Front Neurosci,* 11**,** 229.

YUYAMA, K., SUN, H., MITSUTAKE, S. & IGARASHI, Y. 2012. Sphingolipid-modulated exosome secretion promotes clearance of amyloid-beta by microglia. *J Biol Chem,* 287**,** 10977-89.

YUYAMA, K., SUN, H., SAKAI, S., MITSUTAKE, S., OKADA, M., TAHARA, H., FURUKAWA, J., FUJITANI, N., SHINOHARA, Y. & IGARASHI, Y. 2014. Decreased amyloid-beta pathologies by intracerebral loading of glycosphingolipid-enriched exosomes in Alzheimer model mice. *J Biol Chem,* 289**,** 24488-98.

YUYAMA, K., SUN, H., USUKI, S., SAKAI, S., HANAMATSU, H., MIOKA, T., KIMURA, N., OKADA, M., TAHARA, H., FURUKAWA, J., FUJITANI, N., SHINOHARA, Y. & IGARASHI, Y. 2015. A potential function for neuronal exosomes: sequestering intracerebral amyloid-beta peptide. *FEBS Lett,* 589**,** 84-8.

ZAROVNI, N., CORRADO, A., GUAZZI, P., ZOCCO, D., LARI, E., RADANO, G., MUHHINA, J., FONDELLI, C., GAVRILOVA, J. & CHIESI, A. 2015. Integrated isolation and quantitative analysis of exosome shuttled proteins and nucleic acids using immunocapture approaches. *Methods,* 87**,** 46-58.

ZAROW, C., VINTERS, H. V., ELLIS, W. G., WEINER, M. W., MUNGAS, D., WHITE, L. & CHUI, H. C. 2005. Correlates of hippocampal neuron number in Alzheimer's disease and ischemic vascular dementia. *Ann Neurol,* 57**,** 896-903.

ZHANG, B., YEO, R. W., TAN, K. H. & LIM, S. K. 2016a. Focus on Extracellular Vesicles: Therapeutic Potential of Stem Cell-Derived Extracellular Vesicles. *Int J Mol Sci,* 17**,** 174.

ZHANG, J., LIU, S. C., LUO, X. H., TAO, G. X., GUAN, M., YUAN, H. & HU, D. K. 2016b. Exosomal Long Noncoding RNAs are Differentially Expressed in the Cervicovaginal Lavage Samples of Cervical Cancer Patients. *J Clin Lab Anal,* 30**,** 1116-1121.

ZHANG, X., ABELS, E. R., REDZIC, J. S., MARGULIS, J., FINKBEINER, S. & BREAKEFIELD, X. O. 2016c. Potential Transfer of Polyglutamine and CAG-Repeat RNA in Extracellular Vesicles in Huntington's Disease: Background and Evaluation in Cell Culture. *Cell Mol Neurobiol,* 36**,** 459-70.

ZHANG, X., YUAN, X., SHI, H., WU, L., QIAN, H. & XU, W. 2015. Exosomes in cancer: small particle, big player. *Journal of Hematology & Oncology,* 8**,** 83.

ZHAO, J., SUN, B. K., ERWIN, J. A., SONG, J. J. & LEE, J. T. 2008. Polycomb proteins targeted by a short repeat RNA to the mouse X chromosome. *Science,* 322**,** 750-6.

ZHAO, Z., BAI, J., WU, A., WANG, Y., ZHANG, J., WANG, Z., LI, Y., XU, J. & LI, X. 2015. Co-LncRNA: investigating the lncRNA combinatorial effects in GO annotations and KEGG pathways based on human RNA-Seq data. *Database (Oxford),* 2015.

ZILKA, N. & NOVAK, M. 2006. The tangled story of Alois Alzheimer. *Bratisl Lek Listy,* 107**,** 343-5.

ZITVOGEL, L., REGNAULT, A., LOZIER, A., WOLFERS, J., FLAMENT, C., TENZA, D., RICCIARDI-CASTAGNOLI, P., RAPOSO, G. & AMIGORENA, S. 1998. Eradication of established murine tumors using a novel cell-free vaccine: dendritic cell-derived exosomes. *Nat Med,* 4**,** 594-600.

ZONNEVELD, M. I., BRISSON, A. R., VAN HERWIJNEN, M. J., TAN, S., VAN DE LEST, C. H., REDEGELD, F. A., GARSSEN, J., WAUBEN, M. H. & NOLTE-'T HOEN, E. N. 2014. Recovery of extracellular vesicles from human breast milk is influenced by sample collection and vesicle isolation procedures. *J Extracell Vesicles,* 3.

ZYLBERSZTEJN, K. & GALLI, T. 2011. Vesicular traffic in cell navigation. *Febs j,* 278**,** 4497-505.